



FRIEDRICH-SCHILLER- UNIVERSITÄT JENA

Guanidinium containing Poly(methacrylamide)s for Non-viral Gene Delivery

**Dissertation
(kumulativ)**

zur Erlangung des akademischen Grades doctor rerum naturalium

(Dr. rer. nat.)

vorlegt dem Rat der Chemisch-Geowissenschaftliche Fakultät der
Friedrich-Schiller-Universität Jena

von M.Sc. Ceren Cokca

geboren am 20.01.1986 in Adana/Türkei

Gutachter:

1. Prof. Dr. Kalina Peneva, FSU Jena
2. Prof. Dr. Dagmar Fischer, FAU Erlangen-Nürnberg

Tag der Verteidigung: 10.07.2023

Table of Contents

Table of Contents.....	i
Declaration on Authorship.....	iii
Attachment to the Declaration on Authorship.....	iv
List of Figures.....	vii
List of Schemes.....	xi
List of Tables.....	xiii
List of Abbreviations.....	xv
1. Introduction.....	1
1.1 Viral Gene Delivery.....	1
1.2 Non-viral Gene Delivery.....	2
1.2.1 Lipid-based non-viral gene delivery.....	3
1.2.2 Polymer-based non-viral gene delivery.....	3
1.3 Guanidinium Group and its Role in Cell Penetration and Interactions with Nucleic Acids.....	6
1.3.1 History of guanidinium group.....	7
1.3.2 ‘Guanidinium magic’: special non-covalent interactions.....	9
1.4 Guanidinium Containing Polymers for Non-viral Gene Delivery.....	15
1.4.1 Structure-activity investigations on guanidinium containing polymers.....	16
1.4.2 Strategies improving the nucleic acid delivery efficiency of guanidinium containing polymers.....	20
1.5 The Synthetic Approaches for Guanidinium Containing Polymers.....	25
1.5.1 RAFT polymerization.....	28
2. Motivation.....	37
3. Impact of Comonomer Distribution on DNA Binding.....	41
3.1 Preparation and Physicochemical Characterization of the Polymer Library.....	42
3.2 Biological Investigations on the Prepared Copolymers.....	50
4. Impact of Indole Bearing Comonomer on DNA Delivery Efficiency.....	55
4.1 Preparation and Physicochemical Characterization of Amphipathic Terpolymer.....	56
4.2 Biological Investigations on P(HPMA- <i>co</i> -GPMA- <i>co</i> -IEMA) Terpolymer and P(HPMA- <i>co</i> -GPMA) copolymer.....	58
5. The Impact of Hydrophobic Group Origin on DNA Delivery Efficiency.....	63
5.1 Preparation and Physicochemical Characterization of Amphipathic Terpolymers.....	64
5.2 Biological Investigations on the Prepared Amphipathic Terpolymers.....	65
6. Improving the Biocompatibility of Guanidinium and Indole Containing Terpolymers.....	71

6.1 Synthesis and Physicochemical Characterizations of Diblock Copolymers	72
6.1.1 Synthesis and physicochemical characterization of P(MEO ₉ MA) macro-RAFT agents.....	73
6.1.2 Synthesis and Physicochemical Characterization of Fluorescently Labeled P(MEO ₉ MA- <i>co</i> -PMIM) Macro-RAFT Agents	74
6.1.3 The preparation and physicochemical characterization of diblock copolymers....	76
6.2 Structured Illumination Microscopy Investigation on Fluorescently Labeled P(MEO ₉ MA- <i>co</i> -PMIM)- <i>b</i> -P(HGI) Diblock Copolymer	78
6.3 Biological Investigations on P(MEO ₉ MA- <i>co</i> -PMIM)- <i>b</i> -P(HGI) Diblock Copolymers	80
7. Guanidinium Containing Poly(methacrylamide) Copolymer for Ultrasensitive Arsenic Detection.....	85
7.1 Synthesis and Physicochemical Characterization of P(HPMA- <i>co</i> -GPMA) Copolymer	86
7.2 Optimization, Selectivity Analysis, and Application of the Developed Aptasensor	87
8. Summary and Outlook	93
9. Zusammenfassung und Ausblick	99
10. References	105
Selbständigkeitserklärung	131
Acknowledgement.....	133
Curriculum vitae.....	135

Attachment to the Declaration on Authorship

Publication P1: Tabujew, I. ¹ ; Cokca, C. ² ; Zartner, L. ³ ; Schubert, U. S. ⁴ ; Nischang, I. ⁵ ; Fischer, D. ⁶ ; Peneva, K. ⁷ , The influence of gradient and statistical arrangements of guanidinium or primary amine groups in poly(methacrylate) copolymers on their DNA binding affinity. <i>J. Mater. Chem. B</i> 2019 , 7 (39), 5889-6066.							
Involved in	Author						
	1	2	3	4	5	6	7
Conceptual research design	X	X					X
Synthesis of monomer and polymer	X	X					
Physicochemical characterization	X	X			X		
Analytical ultracentrifugation					X		
Data analysis and interpretation	X	X	X		X		
Biological investigation			X				
Manuscript preparation	X	X					
Manuscript correction	X	X	X	X	X	X	X
Suggested publication equivalence value		1.00					

Publication P2: Cokca, C. ¹ ; Zartner, L. ² ; Tabujew, I. ³ ; Fischer, D. ⁴ ; Peneva, K. ⁵ , Incorporation of Indole Significantly Improves the Transfection Efficiency of Guanidinium-Containing Poly(Methacrylamide)s. <i>Macromol. Rapid Commun.</i> 2020 , 41 (6), 1900668.					
Involved in	Author				
	1	2	3	4	5
Conceptual research design	X	X	X	X	X
Synthesis monomer and polymer	X				
Physicochemical characterization	X				
Data analysis and interpretation	X	X			
Biological investigation		X			
Manuscript preparation	X	X			
Manuscript correction	X	X	X	X	X
Suggested publication equivalence value	1.00				

Publication P3: Hack, F. J.¹; Cokca, C.²; Städter, S.³; Hülsmann, J.⁴; Peneva, K.⁵; Fischer, D.⁶, Indole, Phenyl, and Phenol Groups: The Role of the Comonomer on Gene Delivery in Guanidinium Containing Methacrylamide Terpolymers.
Macromol. Rapid Commun. **2020**, *42* (8), 2000580.

Involved in	Author					
	1	2	3	4	5	6
Conceptual research design	X	X	X		X	X
Synthesis of monomer and polymer		X	X			
Physicochemical characterization		X	X			
Data analysis and interpretation	X	X	X			
Biological investigation	X			X		
Manuscript preparation	X	X				
Manuscript correction	X	X			X	X
Suggested publication equivalence value		1.00				

Publication P4: Cokca, C.¹; Hack, F. J.²; Costabel, D.³; Herwig, K.⁴; Hülsmann, J.⁵; Then, P.⁶; Heintzmann, R.⁷; Fischer, D.⁸; Peneva, K.⁹, PEGylation of Guanidinium and Indole Bearing Poly(methacrylamide)s - Biocompatible Terpolymers for pDNA Delivery.
Macromol. Biosci. **2021**, *21* (10), 2100146.

Involved in	Author								
	1	2	3	4	5	6	7	8	9
Conceptual research design	X	X						X	X
Synthesis of monomer and polymer	X								
Synthesis of fluorescent monomer			X	X					
Physicochemical characterization	X								
Data analysis and interpretation	X	X				X			
Biological investigation		X			X				
SIM investigation						X			
Manuscript preparation	X	X							
Manuscript correction	X	X	X			X	X	X	X
Suggested publication equivalence value	1.00								

Publication P5: Soni, G. K. ¹ ; Wangoo, N. ² ; Cokca, C. ³ ; Peneva, K. ⁴ ; Sharma, R. K. ⁵ , Ultrasensitive aptasensor for arsenic detection using quantum dots and guanylated Poly(methacrylamide). <i>Anal. Chim. Acta</i> 2022 , <i>1209</i> , 339854.					
Involved in	Author				
	1	2	3	4	5
Conceptual research design	X	X	X	X	X
Synthesis of monomer and polymer			X		
Physicochemical characterization			X		
Synthesis of QDs	X				
Preparation of aptasensor	X				
Tests on aptasensor	X				
Data analysis and interpretation	X		X		
Manuscript preparation	X		X		
Manuscript correction	X		X	X	X
Suggested publication equivalence value			0.25		

List of Figures

Figure 1.1 Summary of formulation, extra- and intracellular barriers for polymeric vectors	4
Figure 1.2 The breakthrough chemical and biological discoveries on guanidinium ..	7
Figure 1.3 Schematic diagram for special non-covalent interactions of guanidinium	10
Figure 1.4 General chemical structures of commonly studied guanidinium containing polymers in non-viral gene delivery.....	16
Figure 1.5 General structural properties of thiocarbonylthio RAFT agent.....	31
Figure 1.6 General classes of RAFT agents and their advantages/disadvantages	31
Figure 2.1 Innovative designs of guanidinium containing poly(methacrylamide)s..	39
Figure 3.1 The general concept described in Chapter 3	42
Figure 3.2 Schematic illustration of the synthetic approaches for statistical and gradient copolymers.....	44
Figure 3.3 Example differential distributions of sedimentation coefficients, (<i>s</i>), of (A) P(HPMA- <i>stat</i> -APMA) copolymers (B) P(HPMA- <i>grad</i> -APMA) copolymers, (C) P(HPMA- <i>stat</i> -GPMA) copolymers, and (D) P(HPMA- <i>grad</i> -GPMA) copolymers. Trace color assignment: black Copolymers with 5 mol% cationic comonomer content; red Copolymers with 10 mol% cationic comonomer content; green Copolymers with 20 mol% cationic comonomer content; blue Copolymers with 40 mol% cationic comonomer content; magenta Copolymers with 50 mol% cationic comonomer content; wine Copolymers with 60 mol% cationic comonomer content; orange Copolymers with 75 mol% cationic comonomer content; gray Copolymers with 90 mol% cationic comonomer content.....	50
Figure 3.4 pGL3 DNA binding affinity of (A) P(HPMA-APMA) (B) and P(HPMA-GPMA) copolymers depending on the degree of substitution and N/P ratio ($n = 4$, mean \pm SD). The comparison of DNA binding affinity regarding the cationic comonomer content (C) APMA and (D) GPMA contents. The binding efficiency was calculated by subtracting the mean relative fluorescence unit (RFU) derived from the binding experiments from 100% binding efficiency. The efficiency of statistical copolymers was then subtracted from the binding efficiency of the gradient copolymers, leading to positive (superiority of gradient copolymers) or negative (superiority of statistical counterparts) values. The comparison of DNA binding affinity for (E) gradient and (F) statistical comonomer distribution. Positive values demonstrate a higher binding efficiency for P(HPMA-APMA) copolymers, negative values represent a more efficient binding of the P(HPMA-GPMA) copolymer counterparts. The binding efficiency was calculated by subtracting the mean RFU derived from the binding experiments from 100% binding efficiency. The efficiency of P(HPMA-GPMA) copolymers was then subtracted from the binding efficiency of the P(HPMA-APMA) copolymers, leading to positive (superiority of P(HPMA-APMA)) or negative (superiority of P(HPMA-GPMA)) values.....	51
Figure 3.5 (A) <i>In vitro</i> luciferase reporter gene expression of pGL3 DNA/copolymer polyplexes at N/P ratio 20 in CHO-K1 cells compared to the negative controls; free DNA and sodium chloride (NaCl) (mean \pm SD). (B) Cationic comonomer content-dependent <i>in vitro</i> cell viability assay of P(HPMA-APMA) and P(HPMA-GPMA) copolymers in L-929 mouse fibroblasts (mean \pm SD).	53

Figure 4.1 The general concept described in Chapter 4	56
Figure 4.2 (A) Cell viability assay on L-929 mouse fibroblasts with increasing polymer concentrations ($n = 7 \pm \text{SD}$). Apoptosis versus necrosis and viability (B) for P(HPMA- <i>co</i> -GPMA) copolymer and (C) for P(HPMA- <i>co</i> -GPMA- <i>co</i> -IEMA) terpolymer determined by caspase activity Caspase-Glo 3/7 assay ($n = 3 \pm \text{SD}$).....	59
Figure 4.3 (A) Quantitative DNA binding assessment for P(HPMA- <i>co</i> -GPMA) copolymer and P(HPMA- <i>co</i> -GPMA- <i>co</i> -IEMA) terpolymer by AccuBlue™ assay including free polymers (P) and IPEI/DNA polyplexes (PEI) ($M_{\text{nIPEI}} \sim 2\,500 \text{ g mol}^{-1}$, N/P 20) ($n = 4 \pm \text{SD}$) (B) Hydrodynamic diameters (HD) and zeta potentials (ZP) of P(HPMA- <i>co</i> -GPMA)/DNA and P(HPMA- <i>co</i> -GPMA- <i>co</i> -IEMA)/DNA polyplexes with a cumulative analysis of HD and ZP ($n = 4 \pm \text{SD}$).....	60
Figure 4.4 Transfection studies of (A) P(HPMA- <i>co</i> -GPMA) copolymer (B) P(HPMA- <i>co</i> -GPMA- <i>co</i> -IEMA) terpolymer in CHO-K1 cells (DNA: 4 $\mu\text{g pGL3}$ plasmid, PEI: $M_{\text{nIPEI}} \sim 2\,500 \text{ g mol}^{-1}$, N/P 20).....	61
Figure 5.1 The general concept described in Chapter 5	63
Figure 5.2 (A) Concentration-dependent <i>in vitro</i> cell viability assay of the terpolymers (named according to the pendant groups of the hydrophobic comonomers) in L-929 mouse fibroblasts after 24 h incubation by the CellTiter-Glo® luminescent cell viability assay ($n = 8$, mean \pm SD). (B) Dependency of hemolysis after 1 h incubation and (C) Polymer concentration dependent sheep erythrocyte aggregation after 2 h incubation induced by the terpolymers in comparison to 15 $\mu\text{g mL}^{-1}$ bPEI ($M_{\text{n}} \sim 25\,000 \text{ g mol}^{-1}$) (PC) ($n = 6$, mean \pm SD).....	66
Figure 5.3 (A) N/P ratio dependent DNA binding capacity [%] of the terpolymers (named according to the pendant groups of the hydrophobic comonomers) determined by AccuBlue™ assay in comparison to DNA/IPEI polyplexes (LPEI) ($M_{\text{nIPEI}} \sim 2\,500 \text{ g mol}^{-1}$, N/P ratio 20) and free polymers (P) ($n = 8$, mean \pm SD). (B) N/P ratio dependent particle size measurements of DNA/terpolymer polyplexes by nanoparticle tracking analysis (mean \pm SD measured in triplicates). (C) N/P ratio dependent zeta potential measurements of polyplexes by LDA (mean \pm SD measured in triplicates).....	67
Figure 5.4 <i>In vitro</i> luciferase reporter gene expression of pGL3 plasmid DNA/terpolymer polyplexes at different N/P ratios in CHO-K1 cells compared to the positive control (PC) ($M_{\text{nIPEI}} \sim 2\,500 \text{ g mol}^{-1}$, N/P ratio 20). Experiments were performed in quadruplicates and free DNA served as the negative control (NC) (mean \pm SD).	69
Figure 6.1 The general concept described in Chapter 6	72
Figure 6.2 Photophysical characterization of P(MEO ₉ MA- <i>co</i> -PMIM) macro-RAFT agent and P(MEO ₉ MA- <i>co</i> -PMIM)- <i>b</i> -P(HGI) diblock copolymer at the polymer concentration of 10 mg mL^{-1} in water (A) Normalized absorbance spectra and (B) Emission spectra of labelled polymers.....	78
Figure 6.3 SIM live images of Hela cells treated with P(MEO ₉ MA- <i>co</i> -PMIM) ₂₀ - <i>b</i> -P(HGI)/DNA polyplexes at N/P ratio 10 (A) after 1 h incubation and (B) after 4 h incubation. Optical magnification of the system in normal widefield fluorescence mode is $\sim 100\times$ (63x Objective + 1.6x Optovar for a total of 100.8x). The total area in the SIM-images is 76 x 76 μm , for a pixel size of 40 μm . The scalebar is 10 μm	79

Figure 6.4 Concentration dependent <i>in vitro</i> cell viability assay of diblock copolymers and P(HGI) terpolymer in L-929 mouse fibroblasts after 24 h incubation using the CellTiter-Glo® luminescent cell viability assay (<i>eightfold</i> , mean ± SD). .	80
Figure 6.5 N/P ratio dependent pGL3 DNA binding capacity [%] of the diblock copolymers determined by the AccuBlue™ assay in comparison to lPEI/DNA polyplexes (lPEI) ($M_{n_{lPEI}} \sim 2\,500\text{ g mol}^{-1}$, N/P ratio 20) and the free polymers (P) (<i>eightfold</i> , mean ± SD).	81
Figure 6.6 Stability of diblock copolymer/DNA polyplexes at different N/P ratios against enzymatic DNase I degradation (controls: untreated free DNA (U), free DNA treated in the same way as polyplexes but without enzyme (-), free DNA treated with enzyme (+))	82
Figure 6.7 <i>In vitro</i> luciferase reporter gene expression of diblock copolymer/DNA polyplexes at different N/P ratios in CHO-K1 cells. Experiments were performed in quadruplicates with free DNA serving as negative control (NC) and lPEI/DNA polyplexes ($M_{n_{lPEI}} \sim 2\,500\text{ g mol}^{-1}$, N/P ratio 20) as positive control (PC) (mean ± SD).	83
Figure 7.1 General description of Chapter 7	86
Figure 7.2 (a) Emission spectra of CdTe and CdTe@CdS QDs upon excitation at 365 nm and 357 nm, respectively, (b) Absorbance spectra of CdTe and CdTe@CdS QDs, (c) HR-TEM image of CdTe@CdS QDs at scale bar of 20 nm (inset HR-TEM image at the scale bar of 10 nm).	88
Figure 7.3 Influence of (a) the copolymer concentrations, (b) volume of the copolymer solution at 0.06 mg mL ⁻¹ copolymer concentration and (c) incubation time at 0.06 mg mL ⁻¹ copolymer concentration with 25 µL copolymer solution on the fluorescence signal of MPA-CdTe@CdS QDs. The excitation wavelength was 357 nm with excitation and emission slit width 5 and 10, respectively. All the samples were incubated in 1 M Tris buffer (pH 7.0) at R.T.	89
Figure 7.4 Influence of (a) aptamer concentration, (b) volume, and (c) incubation time on fluorescence intensity of MPA-CdTe@CdS QDs in the presence of P(HPMA- <i>co</i> -GPMA) copolymer solution (0.06 mg mL ⁻¹ , 25 µL). All the samples were incubated in 1 M Tris buffer (pH 7.0) at R.T.	89
Figure 7.5 (a) Influence of As ³⁺ ion concentration on the fluorescence signal of MPA-CdTe@CdS QDs in the presence of aptamer (3 µM) and copolymer (0.06 mg mL ⁻¹), (b) Calibration curve of the aptasensor, where F ₀ and F represent the fluorescence intensities in the absence and presence of As ³⁺ ions, respectively. Inset shows the naked eye quenching of MPA-CdTe@CdS QDs in the presence of As ³⁺ under a UV illuminator. For the detection of As ³⁺ , the samples were incubated in 1 M Tris buffer (pH 7.0) at R.T.	90
Figure 7.6 Fluorescence response of the aptasensor towards different non-target metal ions: 1 µM As ³⁺ ions and 1000 µM non-target metal ions at the 0.06 mg mL ⁻¹ copolymer concentration and 3 µM aptasensor concentration, where F ₀ and F represent the fluorescence intensities in the absence and presence of As ³⁺ ions.	91
Figure 8.1 Evolutionary process of guanidinium containing poly(methacrylamide)s presented in this thesis	94
Figure 8.2 Guanidinium containing poly(methacrylamide)s for non-viral gene delivery illustrated by cover pictures of publications represented in this thesis: P1	

Journal of Materials Chemistry B, **P2**) Macromolecular Rapid Communications-
selected as 'Best of Healthcare', and **P3**) Macromolecular Rapid Communications 97

List of Schemes

Scheme 1.1 The generally accepted reaction mechanism of RAFT polymerization.	30
Scheme 3.1 RAFT polymerization of A) P(HPMA- <i>co</i> -GPMA) and B) P(HPMA- <i>co</i> -APMA) copolymers	43
Scheme 4.1 RAFT polymerization of P(HPMA- <i>co</i> -GPMA- <i>co</i> -IEMA) amphipathic terpolymers.....	58
Scheme 5.1 RAFT polymerization of P(HPMA- <i>co</i> -GPMA- <i>co</i> -PhEMA) amphipathic terpolymer	64
Scheme 5.2 RAFT polymerization of P(HPMA- <i>co</i> -GPMA- <i>co</i> -PhOHEMA) amphipathic terpolymer	64
Scheme 6.1 RAFT polymerization of P(MEO ₉ MA) macro-RAFT agent	73
Scheme 6.2 Fluorescent labeling on P(HPMA- <i>co</i> -GPMA- <i>co</i> -IEMA) terpolymer by postpolymerization modification	74
Scheme 6.3 RAFT polymerization of P(MEO ₉ MA- <i>co</i> -PMIM) macro-RAFT agent	75
Scheme 6.4 RAFT polymerization of P(MEO ₉ MA)- <i>b</i> -P(HGI) diblock copolymers	77
Scheme 6.5 RAFT polymerization of P(MEO ₉ MA- <i>co</i> -PMIM)- <i>b</i> -P(HGI) diblock copolymers	77
Scheme 7.1 RAFT polymerization of P(HPMA- <i>co</i> -GPMA) copolymer	87

List of Tables

Table 1.1 Nucleic acids commonly utilized for non-viral gene delivery	2
Table 1.2 Guanidinium containing polymer classes for non-viral gene delivery regarding their advantages and disadvantages	27
Table 3.1 Preliminary investigations on comonomer content of P(HPMA- <i>stat</i> -APMA) and P(HPMA- <i>stat</i> -GPMA) copolymers at low monomer conversion (<15%)	44
Table 3.2 Investigations on comonomer contents of P(HPMA- <i>stat</i> -APMA) and P(HPMA- <i>stat</i> -GPMA) copolymers during the polymerization timescale of 5 hours	44
Table 3.3 Cationic comonomer addition rate in semi-batch copolymerization.....	45
Table 3.4 Molar mass (in g mol ⁻¹) and dispersity index (<i>D</i>) for each P(HPMA-APMA) copolymer sample	46
Table 3.5 Molar mass (in g mol ⁻¹) and dispersity index (<i>D</i>) for each P(HPMA-GPMA) copolymer sample	46
Table 3.6 The values of intrinsic viscosity (η), Huggins constants (<i>kH</i>), and partial specific volume (<i>v</i>) for P(HPMA-APMA) and P(HPMA-GPMA) copolymers.....	49
Table 4.1 Preliminary studies on polymerization of HPMA, GPMA, and IEMA comonomers	57
Table 4.2 Overview of the selected physicochemical characteristics for P(HPMA- <i>co</i> -GPMA- <i>co</i> -IEMA) terpolymer and P(HPMA- <i>co</i> -GPMA) copolymer	58
Table 5.1 Overview of the selected physicochemical characteristics for the prepared terpolymers.....	65
Table 6.1 Overview of reaction conditions and the selected physicochemical characteristics of P(MEO ₉ MA) macro-RAFT agents	73
Table 6.2 Overview of reaction conditions and the selected physicochemical characteristics of P(MEO ₉ MA- <i>co</i> -PMIM) macro-RAFT agents	76
Table 6.3 Overview of selected physicochemical characteristics for the prepared diblock copolymers and terpolymer.....	77
Table 7.1 Overview of selected physicochemical characteristics for P(HPMA- <i>co</i> -GPMA) copolymer.....	87
Table 7.2 LOD values for As ³⁺ detection based on previously reported sensing methods	91
Table 7.3 Percentage recovery for detection of As ³⁺ ions in spiked water, soil and food samples using the proposed assay.....	92

List of Abbreviations

[CTA] ₀	initial concentration of RAFT agent
[M] ₀	initial concentration of monomer
[η]	intrinsic viscosity
AAV	adeno-associated virus
APMA	<i>N</i> -(3-aminopropyl)methacrylamide
aq	aqueous
As ³⁺	arsenite
ATRP	atom transfer radical polymerization
AUC	analytical ultracentrifugation
BBB	blood brain barrier
bPEI	branched polyethyleneimine
<i>c</i>	concentration
CD	circular dichroism
cLSM	confocal laser scanning microscopy
CPP	cell penetrating peptide
CRISPR	clustered regularly interspaced short palindromic repeats
CTA	chain transfer agent
CTA1	4-(((2-carboxyethyl)thio)carbonothioylthio)-4-cyanopentanoic acid
CTA2	4-cyano-4-(phenylcarbonothioylthio)pentanoic acid
<i>D</i>	dispersity index
DEAE-dextran	diethylaminoethyl dextran
δ	chemical shift
DLS	dynamic light scattering
DMAc	dimethylacetamide
DMF	dimethylformamide
DMSO	dimethyl sulfoxide
DNA	deoxyribonucleic acid

DP	degree of polymerization
DSC	differential scanning calorimetry
ECM	extracellular matrix
EMA	European Medicines Agency
et al.	et alia
etc.	et cetera
F	fluorescence intensity
FDA	US Food and Drug Administration
fM	femtomolar
g	gram
GAGs	glycosaminoglycans
GCP	guanidinium containing polymers
GPMA	<i>N</i> -(3-guanidinopropyl)methacrylamide
GSH	glutathione
HC	hydrodynamic characterization
HD	hydrodynamic diameter
HR-TEM	high-resolution transmission electron microscopy
η_r	relative viscosity
HIV-1 Tat	human immunodeficiency virus encoded trans-activator
HPMA	<i>N</i> -(2-hydroxypropyl)methacrylamide
IC ₅₀	half-maximal inhibitory concentration
K	lysine
kg	kilogram
k_H	Huggins constant
KOH	potassium hydroxide
λ	wavelength
LAMs	less activated monomers
LDA	laser Doppler anemometry
LiCl	lithium chloride

LOD	limit of detection
IPEI	linear polyethyleneimine
LPL	lipoprotein lipase
M	molar
MALDI-TOF flight	matrix-assisted laser desorption/ionization coupled to time-of-flight
MAMs	more activated monomers
MD	molecular dynamics
MEO ₉ MA	nona(ethylene glycol)methyl ether methacrylate
miRNA	microRNA
mL	milliliter
mM	millimolar
M_n	number average molar mass
$M_{n,theory}$	theoretical number average molar mass
mol	mole
mol%	mole percent
mPa.s	millipascal second
MTT	3-(4,5-dimethylthiazol-2-yl)-2,5-diphenyltetrazolium bromide
μ	micro
μm	micrometer
mV	millivolt
n.d.	not determined
NaBH ₄	sodium borohydride
NaCl	sodium chloride
ncRNA	non-coding ribonucleic acids
NDIS	neutron diffraction with isotropic substitution
nm	nanometer
NMP	nitroxide-mediated polymerization
NMR	Nuclear magnetic resonance
N/P ratio	nitrogen to phosphate ratio

P2VP	poly(2-vinylpyridine)
PBS	phosphate-buffered saline
PC	phosphatidylcholine
pM	picomolar
pDAMA	poly(2-methyl-acrylic acid 2-[(2-(dimethylamino)-ethyl)-methyl-amino]-ethyl ester
pDNA	plasmid DNA
PEG	polyethylene glycol
PEI	polyethyleneimine
PG	phosphatidylglycerol
pH	power of hydrogen
P(HGI)	P(HPMA- <i>co</i> -GPMA- <i>co</i> -IEMA) terpolymer
pKa	acid dissociation constant
PLO	poly-L-ornithine
PLL	poly-L-lysine
P(MEO ₉ MA)	poly(nona(ethylene glycol)methyl ether methacrylate)
PMIM	perylene monodiimide derivative
PMMA	poly(methyl methacrylate)
ppb	parts per billion
Q	glutamine
QDs	quantum dots
R	arginine
RAFT	reversible addition-fragmentation chain transfer
RDRP	reversible deactivation radical polymerization
RES	reticuloendothelial system
RFU	relative fluorescence unit
RLU	relative light units
RNA	ribonucleic acid
ROMP	ring-opening metathesis polymerization
ROP	ring-opening polymerization

ROS	reactive oxygen species
SAXS	synchrotron X-ray scattering
SEC	size exclusion chromatography
shRNA	short hairpin RNA
SIM	structured illumination microscopy
siRNA	short interfering ribonucleic acid
ssDNA	single-stranded DNA
TCEP	tris(2-carboxyethyl)phosphine hydrochloride
TPP	triphenylphosphonium
TPDPI maleimide	maleimide functionalized perylene diimide derivative
UV-Vis	ultraviolet-visible
v	partial specific volume
w%	weight percent
ZP	zeta potential

1. Introduction

The discovery of deoxyribonucleic acid (DNA) is one of the most fascinating scientific breakthroughs in human history.¹⁻³ Later on, the advancement on the field accelerated by pioneering studies such as recombinant DNA technology⁴, Sanger sequencing for determination of DNA sequence⁵, the human genome project⁶⁻⁷, the discovery of non-coding ribonucleic acids (ncRNAs) and their therapeutical potential⁸⁻¹⁰, and lately genome editing by (CRISPR)–Cas-associated nucleases¹¹. The deeper knowledge on nucleic acids and the further advancement in technology allowed the interpretation of diseases at the nucleic acids level, which opened a new field: gene therapy. The aim of gene therapy is the treatment of various diseases *via* the replacement of faulty genes with the functional counterparts or inactivation of disease related genes.¹² As a result, a selective and long-term treatment with a single application can be obtained. In addition, personalized therapies for patients can be offered for challenging diseases (e.g., cancer, cardiovascular, infectious, and inflammatory diseases).¹³

Despite of its high potential, over the course of time, gene therapy has faced critical points that negatively affects the implementation. These critical points are mainly dictated by the extra- and intracellular barriers, which drastically influence the treatment efficiency.¹⁴ First of all, the systemic administration of nucleic acids causes immature degradation of them by nucleases, which are present in physiological fluids, before arrival to their target sites. Hence, the success chance of gene therapy drops dramatically.¹⁵ Afterwards, the limited amount of surviving nucleic acids, which can reach to target cells, faces with cellular uptake barrier due to their large size, hydrophilicity and negative charge at physiological pH. Therefore, a limited cellular uptake of naked nucleic acids occur through the hydrophobic and negatively charged cellular membrane.¹⁶ After facing nucleases and cell membrane barriers, very low amount of nucleic acids can survive and enter to cells. Following cellular uptake, the survivals end up in endosomes and lysosomes where they are digested by lysosomal enzymes.¹⁷ If there is still any functional nucleic acids left, the intracellular translocation of them is poor. As a result, limited amount of gene expression takes place. To overcome above-mentioned barriers, viral and non-viral gene delivery systems were proposed.

1.1 Viral Gene Delivery





Originally, viral vectors were considered to be the best carriers since viruses are programmed to protect and transfer their nucleic acid to the host cells.¹⁸ Different from naturally occurring viruses, nonetheless, viral vectors are defective regarding their replication capability yet they keep effective target recognition, cell penetration, intracellular translocation, and gene expression in target cells. In light of these facts, a seminal clinical study on gene therapy was conducted by Anderson and co-workers in 1990.¹⁹ This study proved the first safe utilization of a retroviral vector to modify tumor-infiltrating lymphocytes to improve antitumor activity. Afterwards, the research

on viral gene delivery accelerated significantly. Various clinical trial examples were performed by utilizing retroviruses and adenoviruses mainly.²⁰ In 2012, the first product of viral gene therapy, Glybera®, was approved by European Medicines Agency (EMA) for the treatment of lipoprotein lipase (LPL) deficiency by means of adeno-associated virus (AAV) vector.²¹ Despite of further clinical achievements, viral vectors have not fulfilled all the initial expectations except their high transfection efficiency with long-term gene expression.^{18, 22} The safety issue is one of the major drawbacks because viral vectors are prone to create inflammatory and immune reactions. Moreover, their low cargo capacity leads to the demand of higher application dose, which also increases the probability of immune reactions occurrence. The last but not the least, they have high production cost and hurdle in translation to large-scale production. For overcoming these disadvantages, the utilization of biomaterials was inevitable. Consequently, the idea of non-viral gene delivery came to life.

1.2 Non-viral Gene Delivery

Non-viral gene delivery can be divided into three major branches: physical methods, organic delivery systems and inorganic nanoparticles.²¹ Due to the scope of this thesis, this chapter focuses only on organic delivery systems, particularly polymer-based non-viral gene delivery systems. For organic delivery systems, cationic biomaterials can be designed and produced by elegant synthetic methods to fulfill the needs that are high cargo capacity, lower risk of immunogenicity, low-cost production, and easier industrial translation.¹⁷ The utilized biomaterials can be lipid- or polymer-based materials with cationic nature. Cationic charge is required for the binding and condensation of nucleic acids into nano-sized particles by creating electrostatic interactions with the phosphate groups of nucleic acids. Thus, the protected nucleic acid cannot be targetable by serum nucleases. Moreover, the reduced size and steric hinderance of negative charge for nucleic acids improve the cellular uptake and cytosolic mobility. Commonly utilized nucleic acids for non-viral gene are summarized in **Table 1.1**.

Table 1.1 Nucleic acids commonly utilized for non-viral gene delivery

	Plasmid DNA (pDNA) 	Small interfering RNA (siRNA) 	Short hairpin RNA (shRNA) 	Micro RNA (miRNA) 
Molecular Weight	~1.5-20 kilobase	19-25 base pair	Stem: 25-29 base pair Loop: 4-23 nucleotides	21-24 nucleotides
Target Site	Nucleus	Cytosol		
Mechanism of Activity	After nuclear localization, transgene expression		Inhibition of translation for the target gene	

1.2.1 Lipid-based non-viral gene delivery

DNA delivery *via* the vectors made of cationic lipids was performed for the first time by Danielsen and co-workers in 1987.²³ After this study, more and more lipid formulations were explored for non-viral gene delivery. The working principle of lipidic vectors is based on the interaction between anionic nucleic acids and cationic head groups of lipids. The formed nucleic acid/lipid complexes are called lipoplexes. The cationic head groups of the lipids affect gene binding and transfection efficiency because charge density, particle stability, cellular uptake, and endosomal escape efficiency are regulated by them.²⁴ The source of positive charge on head groups mostly arises from nitrogen based functional groups (e.g., primary, secondary, and tertiary amines, quaternary ammonium, imidazole, and guanidinium).²⁵⁻²⁶ Small linkers in lipidic vectors attached to the head groups can tune the lipoplex stability, biodegradability, cytotoxicity, and transfection efficiency.²⁷ The hydrophobic tails of lipids, which is composed of aliphatic chains or steroid domains, are often utilized for supramolecular assembly for the formation of micellar or bilayer structures around the nucleic acids.²⁸⁻²⁹ Similar to heads and linkers, structural variations in tail groups affect particle stability, transfection efficiency, and toxicity. Moreover, they dictate phase transition temperature and fluidity of bilayer.¹⁷ Apart from the chemical structure of utilized lipids, lipoplex formulation and manufacturing methods significantly influence the delivery performance. In long term, detailed structure-activity studies on lipidic vectors led to the evolution of lipoplexes.^{25, 30} Hence, more adaptive lipidic vectors are designed regarding extra- and intracellular barriers. For instance, the new generation designs aim for a positive net charge before nucleic acid binding, a neutral net charge after complex formation for longer blood circulation, and regaining a net positive charge in the endosomes of target cells for endosomal escape of lipoplexes.²⁷ In 2018, the first lipid-based short interfering ribonucleic acid (siRNA) formulation, Patisiran, was approved by US Food and Drug Administration (FDA) to treat transthyretin-mediated amyloidosis which is a hereditary disease with high mortality.³¹

1.2.2 Polymer-based non-viral gene delivery

Another approach for organic-based non-viral gene delivery is the utilization of cationic polymers. The working principle of polymeric vectors is same as cationic lipids. Cationic polymers efficiently bind to nucleic acids by electrostatic interactions and create nano-sized particles in solution. These particles are called as polyplexes. Polymeric vectors bear a great potential for non-viral gene delivery by offering some advantages over lipidic vectors such as feasible chemical modifications, structural and functional diversity, and precise control of particle features.³²⁻³³ However, similar to lipoplexes, polyplexes face extra- and intracellular barriers in addition to nanoparticle formulation challenge (**Figure 1.1**). Therefore, the strategical evolution of polymeric vectors has been going for five decades step-by-step in parallel to the developments in macromolecular chemistry.

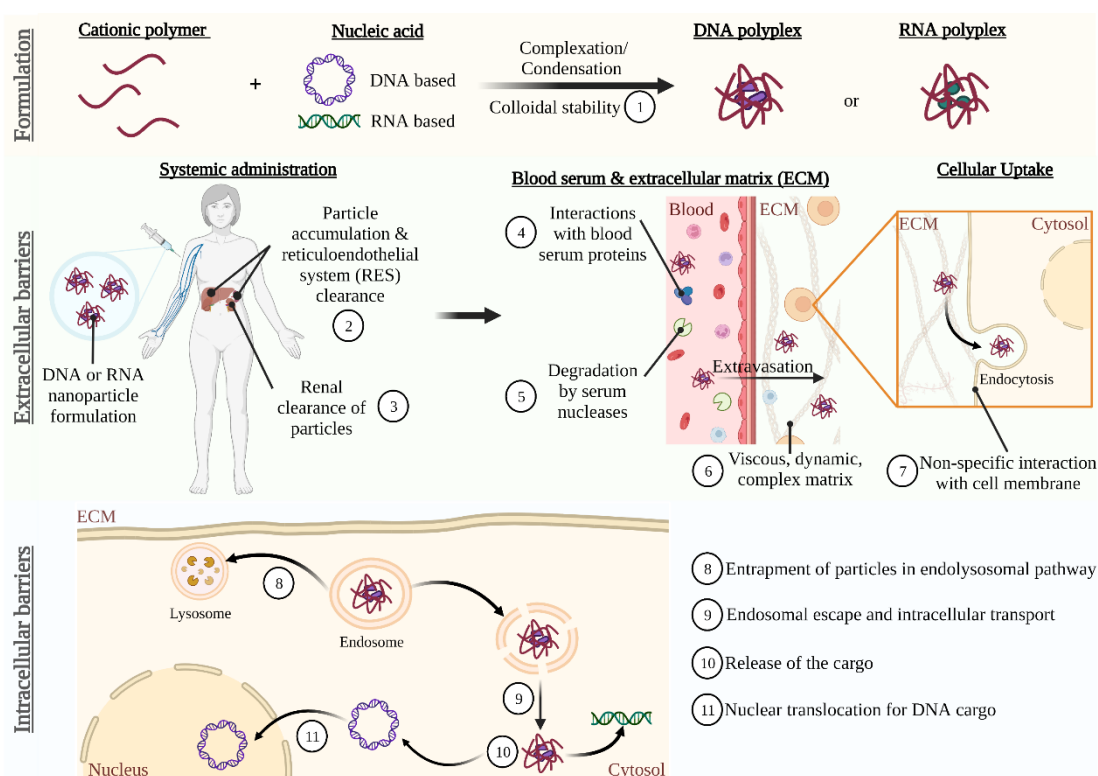


Figure 1.1 Summary of formulation, extra- and intracellular barriers for polymeric vectors

The adventure of polymeric vectors began with the cationic linear homopolymers. The first polyplex formulation was achieved by Vaehri and Pagano in 1965.³⁴ The utilization of diethylaminoethyl (DEAE) dextran for the complexation with poliovirus originated (ribonucleic acid) RNA improved the transfection efficiency. The reason of higher transfection was proposed as the stabilization and protection functions of the polymer for RNA. Afterwards, most of the investigations focused on poly-L-lysine (PLL) originated polyplexes and the strategies to improve their transfection efficiency. For example, Wu and Wu introduced the concept of receptor mediated gene delivery to hepatocytes both *in vitro* and *in vivo*.³⁵⁻³⁶ The covalent attachment of asialoglycoprotein to PLL improved the cellular uptake and transfection efficiency. The first clinical study on polyplexes was also based on PLL polymeric vectors.³⁷ On the contrary to promising findings, the first-generation polymeric vectors could show only moderate transfection efficiency.

Deeper knowledge on the intracellular pathway of polyplexes helped to understand the importance of endosomal escape for efficient transfection. Afterwards, various strategies were proposed to improve endosomal escape such as the treatment of the cells with chloroquine³⁸⁻³⁹, dimethyl sulfoxide (DMSO) or glycerol shock application on the cells⁴⁰⁻⁴¹. Nevertheless, these strategies were not feasible for *in vivo* applications. For example, Fabre and co-workers performed a systemic administration of PLL-DNA polyplexes with the combination of chloroquine in rats.⁴² After multiple-

dose application, chloroquine caused the systemic toxicity. Hence, the researchers focused on simple and efficient formulations by taking the advantage of macromolecular chemistry, which led to the birth of second-generation polymeric vectors.

Polyamidoamine (PMAM) dendrimers are one of the first examples for the second-generation of polymeric vectors.⁴³ DNA/PMAM polyplexes led to better transfection efficiency without employing chloroquine in comparison to the first-generation polyplexes. It was speculated that the improved transfection efficiency was due to the buffering capacity of amine groups (pKa ~6) in PMAM structure leading to the pH change in endosomes, which originally has pH ranging from 5.3 to 6.3.⁴⁴ Subsequently, the polymers with buffering capacity below physiological pH such as polyethyleneimine (PEI) were utilized. In 1995, PEI was applied in non-viral gene delivery by Behr and co-workers for the first time.⁴⁵ Pronounced DNA transfection was achieved both *in vitro* and *in vivo* studies by using branched polyethyleneimine (bPEI). In addition, the same group proposed the debatable hypothesis “proton sponge effect”. This hypothesis suggested endosomal membrane burst due to an enhanced influx of chloride ions into the endosome upon further protonation of free amine groups in PEI at the acidic pH. Over the course of time, PEI has become one of the gold standards for non-viral gene delivery investigations.⁴⁶⁻⁴⁷ However, proton sponge hypothesis has remained controversial based on several studies. For instance, Hennink and co-workers designed a methacrylate based polymer, poly(2-methyl-acrylic acid 2-[(2-(dimethylamino)-ethyl)-methyl-amino]-ethyl ester) (pDAMA), with a repeating unit of two tertiary amine groups.⁴⁸ The system relied on two different pKa values, which were pH ~9 for DNA binding and pH ~5 for proton sponge effect. However, *in vitro* transfection efficiency of resulted polyplexes was insignificant. In another study, Andresen and co-workers estimated a critical membrane tension of lysosome.⁴⁹ The osmotic pressure created by free amine groups of PEI did not lead to the burst of endolysosomal membranes. Based on the electron microscopy images investigated by Elsasser and co-workers, another endosomal escape mechanism ‘the enhanced membrane permeabilization’ was proposed for PEI polyplexes.⁵⁰ The interaction between PEI and the membrane increased the osmotic pressure and membrane tension of endosomes created enlarged pores on the endolysosomal membranes. Nevertheless, the discussion on the endosomal escape mechanism of cationic polymers is still ongoing.⁵¹ Beside above-mentioned polymers, many other cationic polymers bearing primary, secondary and/or tertiary amine groups such as β -Cyclodextrin, chitosan, and poly(amino ester) were also investigated in respect of non-viral gene delivery efficiency.⁵² Nevertheless, PEI is still considered as one of the gold standards.

Parallel to these investigations, a watershed event occurred. The reason for the excellent cellular uptake and endosomal escape capability of human immunodeficiency virus encoded trans-activator (HIV-1 Tat) protein was finally revealed. Guanidinium moieties of the HIV-1 Tat protein were responsible for this excellent performance.⁵³ Hence, the question arrived: Can guanidinium containing transporters be efficient non-viral vectors?

1.3 Guanidinium Group and its Role in Cell Penetration and Interactions with Nucleic Acids

1988 was a turning point for understanding how evolutionary process gave viruses the power of penetration through cellular and nuclear membranes. Two independent studies conducted by Green & Loewenstein⁵⁴ and Frankel & Pabo⁵⁵ proved the cell penetration ability of HIV-1 Tat protein, which was not possible for the other known proteins⁵⁶. Lebleu and co-workers revealed the responsible cationic peptide sequence, which is called as Tat₄₉₋₅₇ or Tat 9-mer (RKKRRQRRR).⁵⁷ Rothbar and co-workers narrowed down the investigation by introducing analogues of Tat₄₉₋₅₇ and examined their cellular uptake potential in Jurkat cells.⁵⁸ Cellular uptake of 9-mer L-arginine was 20-fold higher in comparison to Tat₄₉₋₅₇. The same group also examined arginine, lysine, ornithine, and histidine homopeptide counterparts.⁵³ Oligoarginine depicted the highest cellular uptake in Jurkat cells. The presence of guanidinium group in arginine was given as the reason for high cell penetration capability. These remarkable findings led to the development of guanidinium-rich transporters. Guanidinium containing cell penetrating peptides (CPP)s, polyarginine, peptoids, oligocarbamates, dendrimers, and carbohydrates can be considered as the first-generation of guanidinium-rich transporters.⁵⁹ Among them, guanidinium-rich CPPs were explored the most extensively.

A plethora of studies was conducted on revealing the exact mechanism for cellular uptake and the impact of guanidinium group.⁶⁰⁻⁶¹ Most of the studies was conducted on guanidinium-rich CPPs by utilizing simulations, simplified model systems like artificial lipid bilayers, and/or *in vitro* cellular uptake studies.⁶² The direct translocation of these hydrophilic CPPs through the hydrophobic phospholipid membranes was a fascinating observation, which was called 'arginine magic'.⁶³ In fact, guanidinium as a side chain of arginine was the source of this magical power. However, it was shown that not every guanidinium-rich transporter follows the direct translocation mechanism.⁶⁴ These transporters can also follow endocytosis depending on morphology of the transporter, type of the cargo, the target cell, and the method used for uptake analysis.

The first non-viral gene delivery application of guanidinium-rich vectors was achieved in the form of CPPs. Khavari, Wender and co-workers observed an enhanced plasmid DNA transfection *in vitro* by employing an arginine bearing peptide sequence (CG(RHGH)₅RGC).⁶⁵ These encouraging results initiated the progress in guanidinium containing non-viral gene delivery systems.⁶⁶ Meanwhile, interdisciplinary investigations has been conducted on revealing peculiar characteristics of guanidinium group (**Figure 1.2**). The discoveries on guanidinium group were mainly on its physicochemical properties such as determination of pKa, interaction with water, aromatic groups and oxoanions. Such discoveries also aided to understand the role of guanidinium in non-viral gene delivery.

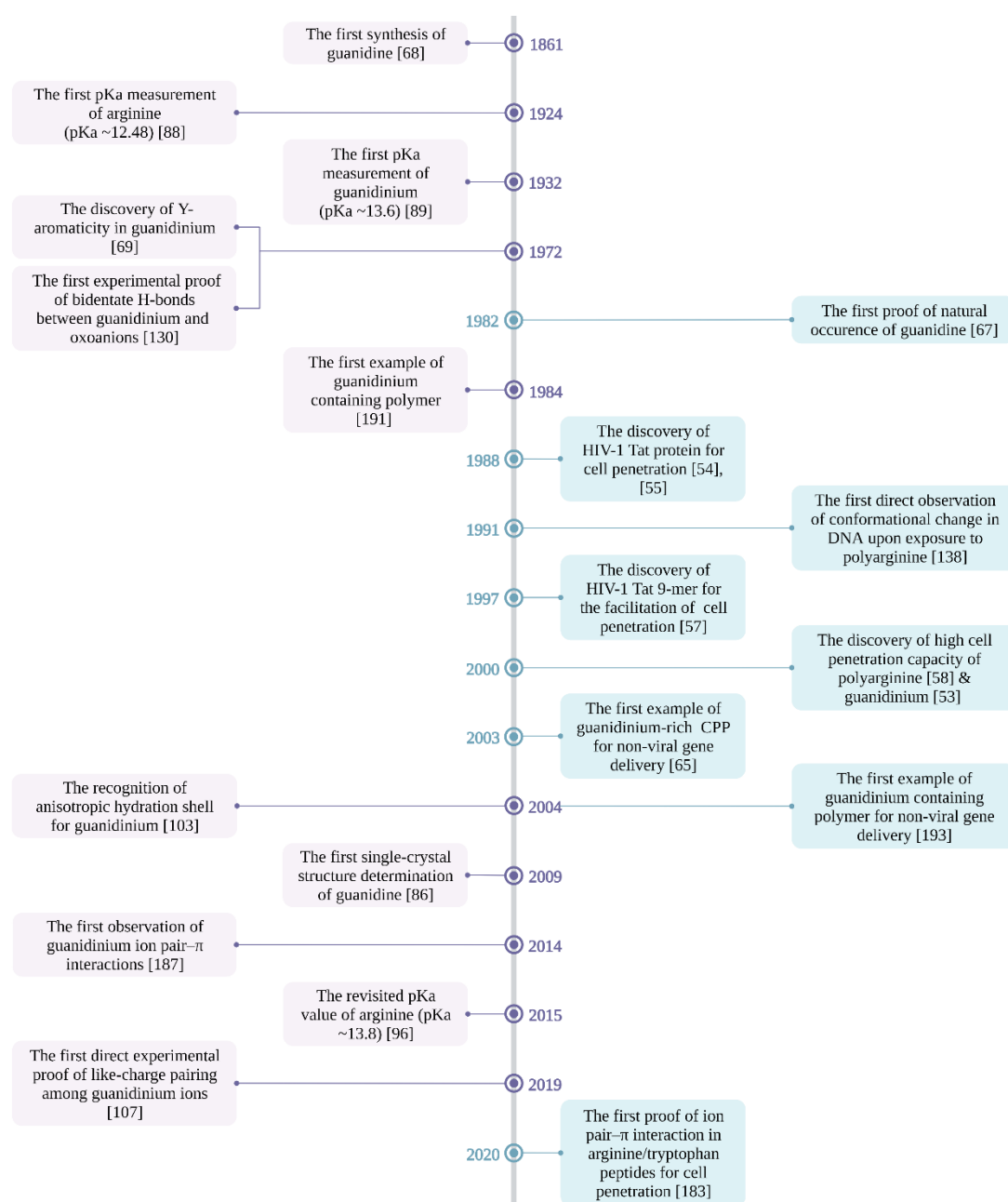


Figure 1.2 The breakthrough chemical and biological discoveries on guanidinium

1.3.1 History of guanidinium group

The discovery of creatine by Chevreul in 1835 is considered as the first appearance of a guanidine containing compound in the literature.⁶⁷ However, the simplest form of guanidine was synthesized by Strecker for the first time in 1861.⁶⁸ In 1982, Schulze isolated guanidine from a germ pea as the first proof of its natural occurrence.⁶⁷ Later on, more compounds bearing guanidinium (e.g., ethylguanidine, creatinine, arginine) were reported. In 1970s, guanidinium was recognized as highly basic (pKa ~13.6) and one of the most stable carbonium ions.⁶⁹ To address the high pKa and stability of guanidinium, quantum and chemical studies were employed primarily.

Different theoretical approaches were proposed to explain ‘aromatic’ stability of guanidinium yet not all the conclusions were in a common agreement. The first explanation for high stability was given by Pauling, who employed valence bond theory.⁷⁰ He gave the high resonance energy of guanidine (~47 kcal/mol), which is higher than the resonance energy of benzene (~35 kcal/mol), as the reason of the high stability. However, for Gund, this explanation was not enough by considering the exemplar of trimethylenemethane, an analogue to guanidine.⁶⁹ It has high resonance energy (~24.2 kcal/mol) yet low stability. By utilizing the perturbation theory, he concluded that the stability of guanidine was due to the closed-shell Y configuration of the 6π -electrons. This type of stability was also observed in benzene. Thus, Gund concluded that acyclic compounds could also be aromatic. This remarkable study also introduced a new terminology ‘Y-aromaticity’ in chemistry. The effect of Y-delocalization and 6π -electrons on guanidinium stability was also supported by other researchers who utilized different theoretical and experimental methods.⁷¹⁻⁷⁷ However, there were also contradictory findings.⁷⁸⁻⁷⁹ For instance, Wiberg claimed that the low resonance stabilization in guanidinium group was due to the small rotational barrier and protonation energy.⁸⁰ Therefore, there was no common agreement for the reason of high stability of guanidinium up to now but Gund’s argument has been recognized in most of the studies including guanidinium bearing compounds.

Until 1993, all the theoretical calculations were done by the assumption that guanidine and guanidinium have planar geometry. On the contrary, Gobbi and Frenking utilized non-planarity assumption and observed strongly pyramidal amino groups for guanidine.⁸¹ Sanna and co-workers supported non-planar geometry of guanidinium as well.⁸² In that period, the controversial theoretical studies were mainly due to the lack of experimental supports arising from the hurdles in guanidine synthesis and purification. In fact, the crystal structures of guanidinium chloride and guanidinium carbonate were already identified as planar in 1960s.⁸³⁻⁸⁴ Almost fifty years later, Göbel and Klapötke performed the first structural characterization of guanidine in solid-state by investigating co-crystal structures of guanidine and 2-amino-4,6-dimethyl-1,3,5-triazine with single-crystal X-ray diffraction.⁸⁵ The observation of pyramidal geometries for two amino groups of guanidine in gas phase was consistent with the theoretical calculation of Gobbi and Frenking.⁸¹ In 2009, Dronskowski and co-workers finally achieved the first single-crystal structure determination of guanidine and its hydrogen-bonded molecular network through single-crystal X-ray diffraction.⁸⁶ Similar non-planar geometry with pyramidal amino groups was detected. The experimental determination of guanidine structure in solid-state ended the ongoing controversial theoretical assumptions and paved the way for improved theoretical studies.⁸⁷

Another important feature of guanidinium is the high basicity. In 1932, the first pKa determination for a guanidinium ion, guanidinium hydrochloride, was performed *via* potentiometric titration against potassium hydroxide (KOH) by Hall and Sprinkle.⁸⁸ The pKa was measured to be ~13.6 at 25°C. In 1952, Angyal and Warburton obtained the similar pKa value by employing a glass electrode instead of a hydrogen electrode.⁸⁹

The reason of high basicity of guanidinium is a matter of considerable debate. In some studies, the reason of high basicity was given as the charge delocalization in Y-shaped geometry of guanidinium.^{74, 77, 90} In other studies, the capability of strong H bond formation for guanidinium in solution was proposed.⁸⁰⁻⁸¹ Nonetheless, it can be speculated that both factors play a crucial role.⁹¹ Interestingly, pKa measurement for arginine indicated much lower value, which was reported as 12.48 in 1924.⁹² Moreover, this value varied in the range of 11.43-12.48 in different studies.⁹³ The cause for the deviation was given as the response of glass electrode in highly basic solutions. For this reason, nuclear magnetic resonance (NMR)-pH titration was proposed as an alternative method to detect more precise pKa values in such conditions.⁹⁴ By employing this method, Orgován and Noszál determined pKa value of guanidinium side chain in arginine as 13.54.⁹⁵ Recently, McIntosh and co-workers revisited the pKa of arginine by combining potentiometric titration and NMR-monitored titration methods.⁹⁶ They reported pKa of guanidinium group in arginine as ~13.8. This value can also be supported by the protonation investigations on guanidinium, which indicated limited protonation of guanidinium even in superacid solutions under harsh conditions.⁹⁷⁻⁹⁸ In another study, protonation capability of arginine was investigated in the range of pH 1 and pH 13 by the aid of X-ray photoelectron spectroscopy of aqueous arginine nanoparticles.⁹⁹ At pH 13 guanidinium moieties remained protonated. The pKa revision was a turning point for a better understanding of physicochemical properties of guanidinium. For instance, it opened the way of performing more realistic theoretical estimations and revealing the role of guanidinium in chemical and biological processes further.¹⁰⁰

1.3.2 ‘Guanidinium magic’: special non-covalent interactions

The peculiar physicochemical features of guanidinium can be summarized as **Y-shaped geometry**, **high stability**, **charge delocalization**, and **high pKa value**. As a result of these properties, guanidinium can create various non-covalent interactions. These interactions are categorized as hydration shell, like-charge pairing, interaction with oxoanions, cation- π interactions, and ion pair- π interactions (**Figure 1.3**). The discovery of these interactions independently originated from guanidinium-rich transporters. However, as the time passed, the importance of these interactions has also been recognized in the efficient nucleic acid binding and cell penetration of guanidinium-rich transporters. Therefore, understanding these interactions is crucial to explain ‘guanidinium magic’ and to utilize them for non-viral gene delivery.

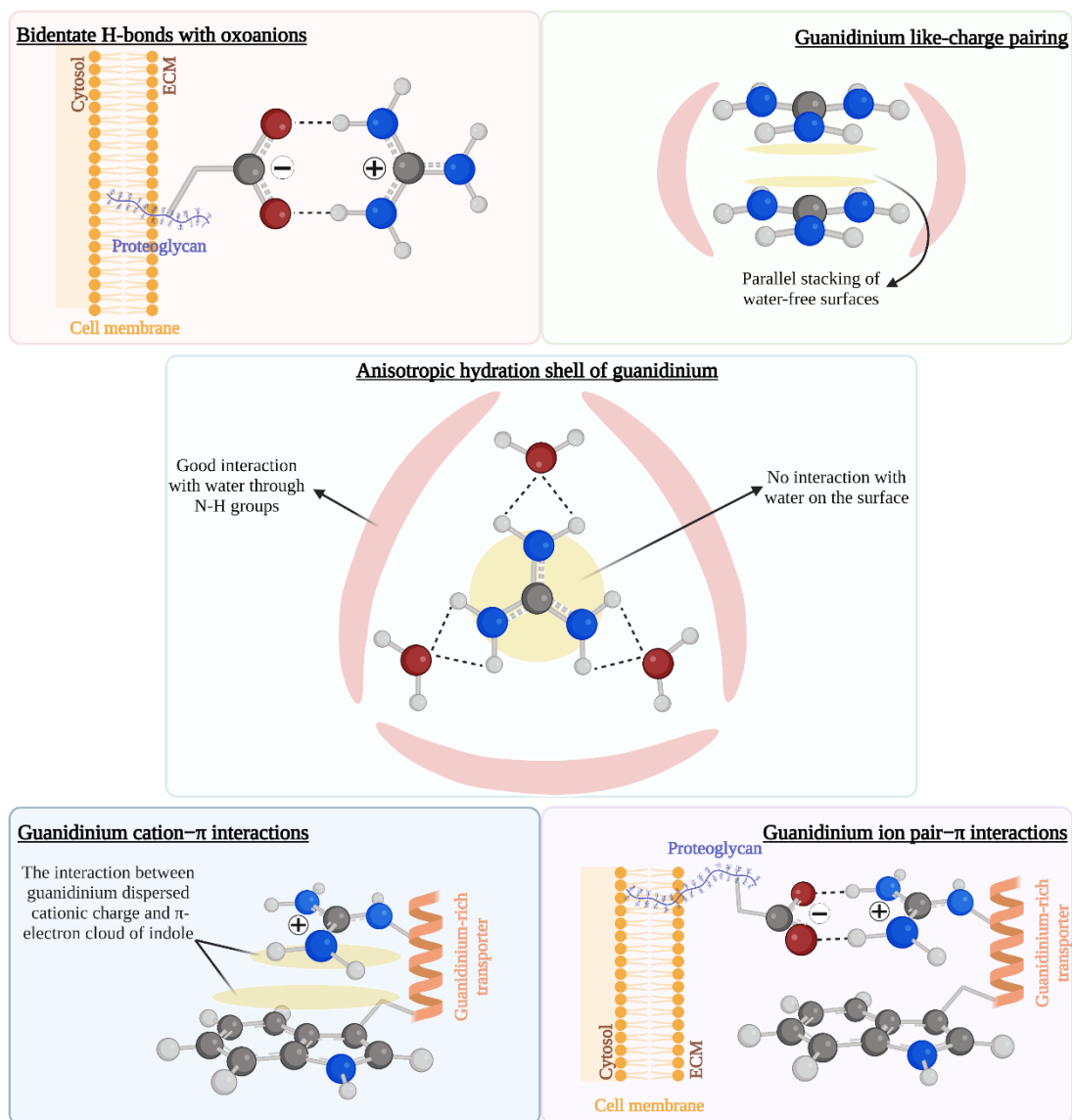


Figure 1.3 Schematic diagram for special non-covalent interactions of guanidinium

1.3.2.1 Impact of guanidinium hydration shell

The guanidinium/water interaction can be considered as the origin for the special behaviors of guanidinium in complex biological systems because most of biochemical processes occur in the presence of water. The first or the first few layers of water around biomolecules, where water dynamics are changed by the presence of biomolecule, is defined as hydration shell.¹⁰¹ The water dynamics in the hydration shell determines the structure and the biological activity of biomolecules by affecting hydrogen bond formation along with ionic, Coulombic, and hydrophobic interactions. Thus, there are various studies examined the hydration shell of guanidinium.

Neutron diffraction experiments, which was conducted by Cruickshank and co-workers, indicated no recognizable hydration shell of guanidinium in aqueous media.¹⁰² Brady and co-workers, investigated aqueous guanidinium chloride solution

via molecular dynamics (MD) simulations and neutron diffraction with isotopic substitution (NDIS) experiments.¹⁰³ They observed the good interaction with water molecules through N-H groups of guanidinium with a defined H-bond network. On the other hand, the planar surfaces of guanidinium were lack of any interaction with water. Hence, they defined an anisotropic (bimodal) hydration of the guanidinium ions. The anisotropic hydration of guanidinium was also supported by other studies¹⁰⁴⁻¹⁰⁷. Notwithstanding the results supporting the asymmetrical hydration of guanidinium, a direct experimental analysis of the hydration process has not achieved yet.

The role of water dynamics on intra- and intermolecular interactions was also explored in biological systems.¹⁰⁸ For example, hydration forces play a vital role in DNA condensation upon exposure to cationic complexes.¹⁰⁹⁻¹¹¹ On the other hand, the impact of hydration forces on nucleic acid condensation by guanidinium-rich transporters have not been examined yet. In the context of cell penetration, nonetheless, a few MD simulation studies in simplified models questioned the role of water and hydration forces on the direct translocation mechanism of guanidinium-rich transporters.¹¹²⁻¹¹⁸ It was concluded that translocation of guanidinium can occur by the formation of water-filled pores on the lipid membrane. As a result, guanidinium can be kept hydrated through the hydrophobic membrane. Nevertheless, most of the studies employed a single guanidinium analog. The translation of investigations based on guanidinium bearing macromolecules with the support of direct experimental observations is still missing to propose more realistic mechanisms.^{115, 119-121}

1.3.2.2 Impact of guanidinium interaction with oxoanions

Guanidinium group plays a vital role in the regulation of biochemical processes such as stabilization of protein tertiary structures and nucleic acids, recognition of enzymes and antibodies, etc.¹²² Such processes mostly rely on strong ion pair formation among guanidinium groups and oxoanions (e.g., phosphates, carboxylates, and sulfates).¹²³ High pKa (~13.8) of guanidinium with the positive charge delocalization on Y-shaped geometry makes these interactions distinct in comparison with other cations like ammonium.¹²⁴⁻¹²⁵

High pKa ensures the continuous protonated state of guanidinium in physiological conditions, which is not the case for ammonium.⁹⁶ Hence, guanidinium group creates easier electrostatic interactions with oxoanions in comparison to ammonium (pKa ~10.5). The pKa difference in guanidinium and ammonium has also impact in macromolecular level.⁶³ For polycations, the close proximity of cationic moieties in repeating units creates charge repulsion. Ammonium-rich transporters overcome this charge repulsion by deprotonation of ammonium groups leading to the decrease in pKa to ~7.0. On the contrary, guanidinium moieties cannot be deprotonated due to much higher pKa value. Therefore, the only way for overcoming the charge repulsion is to interact with the counter ions. As a result, guanidinium-rich transporters can create superior interactions with oxianions. This phenomenon was also observed in model

lipid membranes.¹²⁶⁻¹²⁸ Upon the interaction with phospholipids, guanidinium moieties could keep the protonated state while ammonium groups experienced deprotonation.

The delocalized positive charge over Y-shape geometry enables the formation of strong and efficient bidentate H-bonds between guanidinium molecules and oxoanions.¹²⁵ Due to the structural difference, ammonium can only form monodentate H-bond.¹²⁹ Therefore, **guanidinium has higher selectivity over ammonium for oxoanions**. Bidentate H-bonds were demonstrated *via* X-ray crystallography studies for the first time by employing phosphate ions and methylguanidinium¹³⁰ and propylguanidinium¹³¹ salts. The potentiometric titration experiments suggested that the primary force for the interaction of guanidinium ion with phosphate ion was electrostatic interaction.¹³² Action vibrational spectroscopy with quantum chemical computations studies revealed tweezer-like configurations of guanidinium cations for phosphate ions.¹³³ Each phosphate ion was trapped by two guanidinium molecules.

The guanidinium/phosphate interactions have a fundamental role on high selectivity of guanidinium for the ion pair formation with nucleic acids. Vasseur and co-workers employed matrix-assisted laser desorption/ionization coupled to time-of-flight (MALDI-TOF) mass spectrometry to reveal the high selectivity and specificity of guanidinium moieties for phosphate groups in ssDNA.¹³⁴ This specificity was also proposed as the reason for RNA recognition of HIV-1 Tat protein and the interaction was called as ‘arginine fork’ by Franke and co-workers.¹³⁵ Doi and co-workers utilized fluorescence microscopy and directly observed the biphasic conformational change of DNA for the first time upon exposure to polyarginine.¹³⁶ Guanidinium and ammonium groups were also compared regarding nucleic acid condensation efficiency by means of fluorescence microscopy¹³⁷, osmotic stressed technique coupled with X-ray scattering¹³⁸, and atomic force microscopy (AFM)¹³⁹ studies. Because of stronger and more selective interactions with phosphates, arginine homopeptides could condense DNA better than lysine counterparts.

The peculiar cell penetration ability of guanidinium-rich transporters indicated the influence of ion pair formation between guanidinium and phospholipid membrane. In 2003, Sakai and Matile proposed anion-mediated cell penetration of oligoarginine (R₆) and conducted phase-transfer experiments on model membranes.¹⁴⁰ They observed a decrease in polarity of guanidinium moieties upon the interactions with oxoanions, which led the phase transfer of polyarginine across both chloroform and lipid bilayers. The same phenomenon was also observed by Wender and co-workers.¹⁴¹ In octanol/water mixture, a phase transition from water to octanol was observed for fluorescein labeled oligoarginine (R₈) upon the addition of sodium laurate as a negatively charged mimic of cell membrane constitution. However, the same phase transfer did not occur for ammonium bearing ornithine counterparts. Moreover, monomethylated and asymmetrically dimethylated guanidinium bearing counterparts were tested with respect to cellular uptake efficiency in Jurkat cells. The increase in the degree of methylation caused the decrease in the cellular uptake, which proved the significance of bidentate H-bond formation of guanidinium groups for cell penetration.

Matile and co-workers investigated the intracellular release of such transporters in a reversed-phase transfer study by utilizing fluorescein-labelled oligoarginines; FL-R₈ and FL-R₁₆.¹⁴² The reversed-phase transfer from hydrophobic lipid bilayer domains to water took place only for FL-R₈ transporters. Cremer and co-workers compared the cell penetration ability of oligoarginine (R₉) and oligolysine (K₉) with respect to their binding strengths for a model lipid bilayer.¹⁴³ Fluorescence binding assays and MD simulations showed a stronger and cooperative binding for guanidinium moieties whereas for ammonium counterparts a weaker and anti-cooperative binding was observed because of the difference in ion pair formation. The role of guanidinium-oxoanion interactions on cell penetration was also investigated with other techniques such as MD simulations^{113, 128, 143-144}, confocal microscopy and synchrotron X-ray scattering (SAXS)¹⁴⁵, neutron diffraction¹⁴⁶, and solid-state NMR¹⁴⁷.

1.3.2.3 Impact of guanidinium like-charge pairing

Normally, Coulombic repulsion is expected between the molecules that carry the same charge. However, the investigations concerning the role of guanidinium in peptide/protein-protein interactions and protein denaturation led to a valuable question regarding the presence of attractive cation-cation interaction for guanidinium moieties.¹⁴⁸ Computer graphics analysis¹⁴⁹⁻¹⁵⁰, theoretical calculation¹⁵¹⁻¹⁵², Monte Carlo simulation¹⁵³, and MD simulation^{103, 154-161} studies indicated like-charge pairing of guanidinium groups in aqueous solution. On the contrary, such an interaction was not observed with ammonium in aqueous solution.^{155, 160} Like-charge pairing in guanidinium groups were also observed experimentally. For example, Brady and co-workers investigated aqueous guanidinium chloride solution by NDIS experiments as a complementary to MD simulations studies.¹⁰³ A tendency for parallel stacking of guanidinium molecules was observed. The same stacking effect was also detected through X-ray absorption spectroscopy by Saykally, Prendergast and co-workers.¹⁵⁹

The possible connection between higher cell penetration ability of guanidinium-rich transporters and the like-charge pairing of guanidinium moieties was proposed by Lazaradis and Yuzlenko.¹⁶² MD simulations represented the stacking arrangements of guanidinium groups of arginine at the interface of lipid and water. Further MD simulation studies were performed on oligoarginines in model phospholipid membranes.^{143, 163-164} All studies indicated the formation of strongly self-aggregated oligoarginines at the membrane surfaces. On the other hand, such an aggregation behavior was not detected for oligolysine counterparts. Hence, the formation of like-charge pairing for guanidinium molecules was proposed as an important factor for the direct translocation mechanism of guanidinium-rich transporters. Until 2019, the experimental approaches were not enough to get a direct proof of like-charge pairing among guanidinium molecules. The first direct experimental proof of the like-charge pairing was achieved *via* cryogenic ion mobility–mass spectrometry (cryo-IM–MS) by Hebert and Russel.¹⁰⁷ The charge delocalization on nearly planar guanidinium molecules with H-bonding network bridging between each other was shown as the

reason of the thermodynamically stable like-charged complex. Direct experimental demonstrations of like-charged pairing effect of guanidinium-rich transporters on biological membranes are expected in upcoming years to reveal its role in cell penetration.

1.3.2.4 Impact of guanidinium cation- π and ion pair- π interactions

Apart from the excellent interactions of guanidinium with oxoanions, guanidinium has the capability of creating cation- π interactions with aromatic compounds.¹⁶⁵⁻¹⁶⁷ The dispersed cationic charge on the Y-shaped structure of guanidinium enables a direct interaction with the π -electron cloud of aromatic groups. The physicochemical characteristics of cation- π interactions provide compatibility with both hydrophobic and hydrophilic environments. Therefore, cation- π interactions are fundamental for biochemical processes and biological constituents such as membrane proteins¹⁶⁸, peptide helix stability¹⁶⁹, protein-DNA interfaces¹⁷⁰, protein denaturation¹⁷¹⁻¹⁷², etc.¹⁶⁷

Cation- π interactions were detected for the first time in protein folding.¹⁷³⁻¹⁸⁰ Protein data bank was screened through geometrical analysis of the interactions between cationic amino acids (e.g., arginine, lysine, asparagine, glutamine, and histidine) and aromatic side chains of amino acids (e.g., phenylalanine, tyrosine and tryptophan) in proteins. A pronounced parallel stacking of guanidinium groups with the ring centroids of aromatic side chains was observed. In addition, a preferential interaction between guanidinium and indole (the side chain of tryptophan) was observed. Moreover, a favorable cation- π interaction for arginine over lysine was recognized. A recent theoretical calculation and MD simulations studies conducted by Subramanian and co-workers showed that the cation- π interaction tendency of guanidinium was the highest with tryptophan and followed by tyrosine and phenylalanine, respectively.¹⁷²

Cation- π interactions is also observed between arginine and tryptophan in α -helical secondary structures of amphiphilic CPPs.¹⁸¹⁻¹⁸³ For example, a theoretical investigation with the combination of circular dichroism (CD) and NMR spectroscopy experiments on model α -helical peptides showed that tryptophan/arginine sequences are responsible for the helix formation through cation- π interactions rather than phenylalanine/arginine counterparts.¹⁶⁹ One of the well-known amphiphilic CPPs 'Penetratin' also has α -helical secondary structure due to the presence of tryptophan and arginine residues.¹⁸⁴ This amphipathic peptide is highly efficient in cellular internalization similar to cationic guanidinium-rich CPPs.¹⁸⁵ Alves and co-workers proved the impact of the synergy between indole and guanidinium groups on the efficient cell penetration.¹⁸⁶ The conversion of three tryptophan residue into leucine in nine residue of arginine bearing peptide caused no cellular entry.

In 2014, Matile and co-workers proposed a revolutionary hypothesis which questioned the simultaneous formation of anion- π and cation- π interactions on the same aromatic surface.¹⁸⁷ A push-pull chromophore made of carboxylate-guanidinium ion pairs covalently located on the surface of 4-amino-1,8-naphthalimides was studied. In this

model, the simultaneous anion- π and cation- π interactions were observed by both absorption spectroscopy and ground-state modelling. This special interaction was named as ion pair- π interactions. After this significant finding, the same group conducted a more detailed study on ion pair- π interactions with the same system by covalent and semi-covalent attachment.¹⁸⁸ By means of ¹H NMR ion-exchange studies, parallel and anti-parallel ion pair- π interactions was also observed for the semi-covalent system in the ground state. Moreover, they investigated the possible biological impact of ion pair- π interactions especially for CPPs.¹⁸⁹ The utilization of push-pull aminonaphthalimides (ANIs) as CPP activators enabled the elimination of endosomal pathway and activation of the direct translocation by ion pair- π interactions in model membranes and Hela cells. In 2020, the influence of ion pair- π interactions on cell penetration of arginine and tryptophan containing peptides was experimentally proved by Sagan and co-workers for the first time.¹⁸³ For this purpose, a nonapeptide library containing various arginine and tryptophan sequences was prepared. Differential scanning calorimetry (DSC) experiments and theoretical studies suggested that ion pair- π interactions in tryptophan and arginine bearing peptides play the major role on the cell penetration through glycosaminoglycans (GAGs) bearing membranes.

Owing to above-mentioned findings on guanidinium, ‘guanidinium magic’ can be perceived in a better way. However, it is crucial to acknowledge the complexity of biological environment, where so many variables influence the fate of biomolecules and macromolecules. Hence, it is not possible to expect the same structure-function relationship for all guanidinium-rich transporters with different physicochemical features. Nevertheless, the peculiar physicochemical features of guanidinium make this group unique in regard of forming non-covalent interactions in comparison to other cationic functional groups such as ammonium, quaternary ammonium, and imidazolium. These interactions provide superiority of guanidinium for interactions with nucleic acids and penetration through phospholipid membranes. For this reason, guanidinium-rich transporters have a great potential for non-viral gene delivery. Although most of the guanidinium-rich transporters are based on CPPs, peptide chemistry comprises some limitations for their pharmaceutical applications such as limited synthetic approach and modification, laborious synthesis with high cost.¹⁹⁰ To overcome these hurdles, therefore, guanidinium containing polymers (GCPs) were proposed as the alternative of guanidinium-rich CPPs.

1.4 Guanidinium Containing Polymers for Non-viral Gene Delivery

The first appearance of GCPs occurred for the utilization of antibacterial activity in 1984¹⁹¹ whereas the potential of GCPs for non-viral gene delivery was recognized much later. In 2002, Wender and co-workers introduced guanidinium units into carbamate backbone to overcome the above-mentioned limitations in peptide chemistry.¹⁹² Guanidinium-rich oligocarbamates showed higher cellular uptake in Jurkat cells in comparison with oligoarginine counterparts. As a result, the potential of dissimilar backbone structures in guanidinium-rich transporters was proved for the

first time. Moreover, this study opened the path for the utilization of GPCs for non-viral gene delivery. In 2004, Hennink and co-workers showed that guanidinium bearing poly(methacrylate) homopolymer could efficiently condense DNA and transfect COS-7 cells.¹⁹³ Afterwards, a big effort was put on for the development of GCPs with different backbone structures (**Figure 1.4**). Guanidinium containing polyamidoamines, polyesteramides, polycarbonates, poly(oxanorbornene)s, bPEI, and poly(acrylate/methacrylate)s are the major polymer classes investigated for non-viral gene delivery. Additionally, guanidinium bearing chitosan¹⁹⁴⁻¹⁹⁵, polycaprolactone¹⁹⁶, polysuccinamides and polymalamides¹⁹⁷, polyvinylamine¹⁹⁸, polyguanidium¹⁹⁹⁻²⁰⁰, and polyaspartic acid²⁰¹ were tested for non-viral gene delivery. Most of the GCPs employed for non-viral gene delivery possessed linear, branch or graft polymer architectures. Nevertheless, there are also examples of guanidinium containing dendrimers²⁰²⁻²⁰⁴ and star polymers²⁰⁵, which are beyond the scope of this thesis. In each study the common aim was to enhance the performance of GCPs for nucleic acid delivery in the light of structure-activity investigations and different strategical approaches, which are explained in the following chapters accordingly.

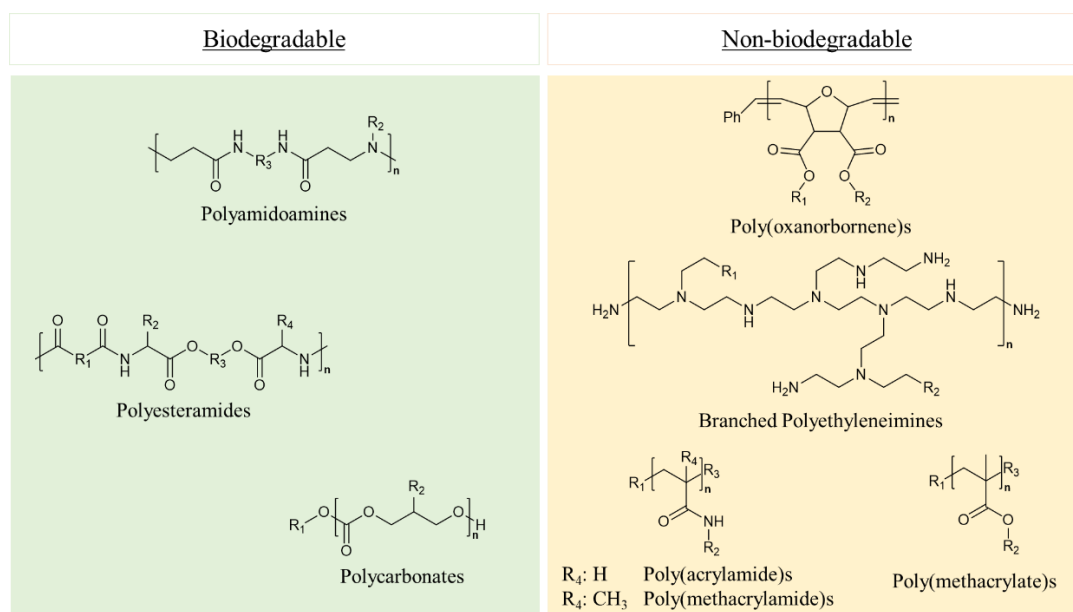


Figure 1.4 General chemical structures of commonly studied guanidinium containing polymers in non-viral gene delivery

1.4.1 Structure-activity investigations on guanidinium containing polymers

Polymer structure, cargo type, polyplex formulation and biophysical/mechanical features of target cells are fundamental decision points for the performance of polymeric vectors.³² These decision points had to be considered also for GCPs. For example, Reineke and co-workers tested cytotoxicity of DNA polyplexes made of guanidinium bearing poly(methacrylamide) homopolymer in HepG2 and HEK293T

cells.²⁰⁶ In HepG2 cells, apoptosis was triggered because of high toxicity aroused from the guanidinium groups although HEK293T showed lower toxicity with better transfection efficiency. Therefore, the structure-activity investigations are essential for the optimization of polyplex performance starting from the nucleic acid complexation *in situ* until *in vitro* release of the nucleic acid at the target site.

1.4.1.1 The comparison of cationic charge origin

Early structure-activity investigations on GCPs involved the comparison between guanidinium moiety and different nitrogen based cationic pendant groups. In most of the studies, primary amine group were employed as a counterpart due to the great potential of the first- and second-generation cationic polymers for nucleic acid delivery.²¹ Kim and co-workers compared the DNA transfection efficiency of primary amine and guanidinium bearing polyamidoamines in C2C12, NIH3T3, HEK293, and HepG2 cells.²⁰⁷⁻²⁰⁸ Guanidinium containing polyamidoamines performed better transfection than primary amine bearing counterparts. In addition, higher nuclear localization was observed for guanidinium containing counterparts.²⁰⁸ Guanylation of primary amines in chitosan resulted in higher DNA transfection efficiency in HEK293 cells.¹⁹⁴ In addition, the cellular uptake mechanism mainly transformed from clathrin-mediated endocytosis to caveolin-mediated endocytosis.¹⁹⁵ Pun, Horner and co-workers showed that guanidinium containing polycaprolactones performed higher DNA transfection than primary amine counterparts yet the presence of guanidinium increased toxicity.¹⁹⁶ Pun and co-workers observed higher DNA transfection for guanylated poly(methacrylamide) brush copolymers compared to primary amine counterparts in Hela cells.²⁰⁹ Liang, Tang and co-workers investigated primary amine or guanidinium bearing PEGylated poly(methacrylate) block copolymers for siRNA delivery both *in vitro* and *in vivo*.²¹⁰ Guanidinium containing block copolymers showed higher gene silencing accompanied by higher toxicity. Moreover, in the Hela-Luc xenograft murine model, higher siRNA accumulation was observed for guanidinium containing polymers at the target site. Traeger and co-workers investigated primary amine, tertiary amine and guanidinium bearing poly(acrylamide) homopolymers with respect to cellular uptake, transfection efficiency and toxicity.²¹¹ The highest cellular uptake and DNA transfection were observed for guanidinium containing counterparts in HEK293T cells. In addition, the presence of guanidinium moieties led to excellent endosomal escape of the polyplexes. However, the highest cytotoxicity was also observed for guanidinium bearing counterparts. Even though the above-mentioned studies indicated the increase in cytotoxicity upon guanidinium modification in polymers, Chandra and Nimesh observed improved cell viability in HEK293 cells for guanidinium grafted PEI.²¹² The reason for the higher cell viability was proposed as the presence of more delocalized charge upon guanidinium functionalization. Nevertheless, the presence of guanidinium groups in polymers generally improves transfection efficiency yet represents higher toxicity in comparison to other nitrogen-based cationic groups.

1.4.1.2 The comparison of backbone type, flexibility, and biodegradability

Other structure-activity investigations on GCPs focused on the influence of backbone structure on non-viral gene delivery. The difference in backbone type, flexibility and biodegradability were explored. Tew and co-workers compared the oxanorbornene and methacrylate backbone structures with similar guanidinium pendant groups regarding siRNA delivery efficiency in Jurkat T cells.²¹³ The dependency on backbone chemistry for siRNA internalization was insignificant. On the other hand, Chu and co-workers pointed out the importance of backbone flexibility for the performance of GCP vectors.²¹⁴ For this purpose, they incorporated oligoethylene glycol units with various lengths into guanidinium bearing polyesteramides. The higher flexibility resulted in a better DNA binding and transfection efficiency in primary rat smooth muscle cells. Similar effect was also observed with different cationic polymer systems.²¹⁵⁻²¹⁶ Concerning biodegradability, biodegradable polymers show superior biocompatibility while non-biodegradable polymers offer more freedom of structural control and modifications.²¹⁷⁻²¹⁸ The same phenomenon was also observed for GCPs. Guanidinium bearing biodegradable polymers own superior biocompatibility in comparison of non-biodegradable counterparts and commercially available standards; bPEI^{205, 207-208, 219-220}, SuperFect²²¹ and Lipofectamine^{TM214, 222-225}. However, degradable polymer backbones, alone, have not been enough to get the clinical approval for therapeutic applications thus far.²¹⁷ It is also important to state that biodegradable polymers with guanidinium and/or other cationic groups did not show any extraordinary transfection efficiency regarding non-biodegradable counterparts. Hence, beyond biodegradation, further chemical strategies for GCPs are necessary to overcome multiple extra- and intracellular barriers for successful non-viral gene delivery systems.

1.4.1.3 The role of guanidinium position in the polymer structure

Guanidinium can be incorporated in the backbone or side chains of polymers. The effect of guanidinium position in polyamidoamines was evaluated regarding DNA transfection efficiency²²⁶ and cellular uptake mechanism²²⁷ by Ding and co-workers. The polymers with guanidinium in the side chains improved the transfection efficiency in MCF-7 cells. In addition, changing the guanidinium position from backbone to side chain resulted in a change of the cellular uptake mechanism from clathrin-mediated endocytosis to endocytosis-independent pathway. Beside the positioning of guanidinium group, chemical structure of side chains has influence on nucleic acid complexation. Wender and co-workers showed that glycerol derived guanidinium side chains in oligocarbonates showed higher siRNA polyplex stability in comparison to methyl(trimethylene)carbonate derived counterparts.²²⁵

1.4.1.4 The impact of comonomer distribution

Synthetic polymers offer great structural variations on comonomer distributions (e.g., statistical, gradient, alternating, or block copolymers).³² In statistical copolymers, comonomers are arranged along the polymer chain depending on their reactivities. In alternating copolymers, comonomers are distributed in the alternating manner throughout the polymer chain. For gradient copolymers, the gradual increase of one comonomer along the polymer chain occurs. Finally, block copolymers are made of polymer blocks of each comonomer. For GCPs, the role of comonomer distribution on non-viral gene delivery efficiency was examined with free polymer chains. For example, Tew and co-workers synthesized a series of poly(oxanorbornene)s in the form of homopolymer, gradient and block copolymers by utilizing the comonomer bearing phenyl and guanidinium pendant groups.²²⁸ The cellular uptake performance of the polymers were studied in Jurkat T cells and HEK293T cells. The gradient copolymer with intermediate degree of hydrophobic functionalization performed the highest cellular uptake with low cytotoxicity. Perrier and co-workers prepared guanidinium and dimethyl or hydroxyethyl containing poly(acrylamide)s with homopolymer, statistical, diblock, and tetrablock copolymer structures.²²⁹ The effect of comonomer distribution on cellular uptake efficiency in MDA-MB-231 cells were examined. Polymers with the statistical comonomer distribution performed the best cellular uptake. The role of comonomer distribution on siRNA delivery was studied for guanidinium containing oligocarbonates by Wender and co-workers.²²⁴ Both statistical and block copolymer structures performed an efficient knockdown of the target protein depending on the hydrophobic comonomer pendant group. These studies indicated the importance of comonomer selection in addition to the comonomer distribution on non-viral gene delivery.

1.4.1.5 The impact of polymer chain length and charge density

For GCPs, the polymer chain length and charge density were examined to optimize the formation of stable polyplexes and an effective dissociation of the nucleic acid cargos at the target site.³² Montenegro, Trillo and co-workers prepared a library of guanidinium containing poly(acryloyl hydrazide) copolymers with different chain lengths to investigate DNA and siRNA delivery efficiency in HeLa cells.²³⁰ While 40 repeating units were enough for an efficient siRNA complexation and knockdown, more than 80 repeating units were necessary for an efficient DNA packing and transfection. Tew and co-workers explored the effect of chain length and charge density on siRNA knockdown efficiency for guanidinium containing poly(oxanorbornene)s homopolymers and block copolymers.²³¹ The increase in the cationic charge density improved the knockdown efficiency in Jurkat T cells. The same group also conducted a study to reveal the impact of cationic charge density on poly(oxanorbornene)s bearing one or two guanidinium moieties per unit.²³² The increase in number of cationic charges up to 40 showed the highest knockdown efficiency yet the further increase reduced the knockdown capability. Peneva, Potestio

and co-workers investigated a library of guanidinium bearing poly(methacrylamide) diblock copolymers with various cationic block lengths in regard of siRNA binding and knockdown efficiency.²³³ In addition, they proposed a computational approach for the structure-function investigation of siRNA binding and complexation for the first time. In the future, more complementary computational studies are expected for non-viral gene delivery investigation.

Many lessons could be learned by above-mentioned structure-activity studies to develop the next generations of GCPs for non-viral gene delivery applications. Guanidinium group has already proved the superior performance in comparison of other nitrogen based cationic groups. On the other hand, higher toxicity of guanidinium group should be overcome by further strategies. The chemical structure of polymer backbone has no significant effect on gene delivery efficiency yet biodegradable backbones with high flexibility can improve biocompatibility and transfection efficiency. Incorporation of guanidinium groups in the side chains of polymers also enhance the transfection efficiency. In addition, chemical structures of side chains also play an important role. Moreover, the charge density and polymer length should be adjusted carefully based on the selected cargo since nucleic acids morphologically show differences (**Table 1.1**). Furthermore, the comonomer content and its distribution should be selected carefully.

1.4.2 Strategies improving the nucleic acid delivery efficiency of guanidinium containing polymers

The structure-activity studies on GCPs gave an insight for enhancing the nucleic acid delivery performance. Additionally, further strategies were applied on GCPs to obtain the polymeric vectors with higher performance and biocompatibility. These strategies, which were also utilized for other cationic polymers, are the combination of different cationic groups, incorporation of hydrophobic comonomers, inclusion of neutral or negatively charged comonomers or polymers, incorporation of stimuli responsive groups, and ligand attachment.³²

1.4.2.1 Combination of different cationic pendant groups

Comonomers with different cationic pendant groups were incorporated into GCPs to improve nucleic acid delivery efficiency. Ding and co-workers showed that the polyplexes made up of primary amine and guanidinium containing polyamidoamine copolymer performed higher DNA transfection efficiency in comparison to the primary amine bearing homopolymer counterpart in NIH/3T3 and U87 MG cells.²³⁴ The same group also produced imidazole and guanidinium containing polyamidoamine copolymer with different comonomer content to analyze transfection efficiency in NIH/3T3.²³⁵ The optimum guanidinium content was determined as 80 mole percent (mol%). Peneva and co-workers investigated primary amine and guanidinium containing poly(methacrylamide) diblock copolymers to determine

siRNA complexation, binding strength and release of the cargo.²³⁶ Incorporation of guanidinium moieties as blocks into primary amine containing copolymers led to stable siRNA polyplexes at a lower nitrogen to phosphate ratio (N/P ratio). Mailänder, Peneva and co-workers prepared primary amine and guanidinium containing poly(methacrylamide) block copolymers and modified the primary amines with triphenylphosphonium (TPP) groups.²³⁷ They investigated the performance of siRNA delivery in CD8⁺ *T*-cells. Live cell imaging of the uptake into CD8⁺ *T*-cells by confocal laser scanning microscopy (cLSM) indicated that TPP modification enhanced cellular uptake and localization of polyplexes in the organelles close to the nucleus. However, primary amine counterparts accumulated on the cell membrane. Gao and co-workers prepared primary amine bearing poly(glycerol methacrylate)s which were functionalized with guanidinium groups to improve cellular uptake and Schiff-base linked imidazole moieties to ease endosomal escape.²³⁸ Primary amine bearing homopolymers showed the least DNA transfection in A549 cells while the highest transfection was observed with the polymers which combines primary amine, imidazole and guanidinium units with improved cell viability.

1.4.2.2 Inclusion of hydrophobic moiety

Incorporation of hydrophobic groups in polymer chains is a common strategy to promote gene delivery efficiency of cationic polymers.²³⁹ The reason can be the enhanced binding of genetic materials and cellular uptake due to the combination of electrostatic and hydrophobic interactions.²⁴⁰ The same strategy was also applied to GCPs and tested on free polymer chains and resulted polyplexes. Tew and co-workers substituted different alkyl groups into guanidinium containing poly(oxanorbornene)s.²⁴¹ The investigations on artificial phospholipid membranes indicated that the hydrophobic group substitution led to increase in penetration activity of the polymers. However, the higher degree of substitution caused reduction in solubility, and so the penetration activity. In addition, the same group observed higher transduction activity for aromatic group functionalized guanidinium containing poly(oxanorbornene)s in comparison to aliphatic group bearing counterparts.²⁴² Lienkamp, Tew and co-workers found out that the main driving force for the interaction between anionic phospholipid surfaces and poly(oxanorbornene)s with phenyl and guanidinium pendant groups is based on hydrophobicity.²⁴³ The electrostatic interactions were necessary for the initial recognition and the binding of the polymers on the membrane surface.

The influence of hydrophobic group functionalization on GCPs was also explored regarding the polyplex performance. Wu and co-workers synthesized guanidinium containing polyesteramides with various length of methylene groups in diacid and diol segments.²²³ The higher methylene substitution into the backbone caused decrease in DNA transfection and siRNA knockdown efficiencies because of lower solubility of the polymers in aqueous media. Wender and co-workers studied siRNA knockdown efficiency on guanidinium containing amphipathic oligocarbonates.²²⁴ At the same

N/P ratio, amphipathic polymer structures performed better knockdown efficiency in comparison to the guanidinium homooligomer counterparts. Tew and co-workers included phenyl and methyl segments into guanidinium bearing poly(oxanorbornene)s to test siRNA delivery performance.²³¹ Amphipathic block copolymers with an optimal cationic charge density enhanced the knockdown efficiency in comparison to guanidinium containing homopolymer.

Several studies revealed that the origin of hydrophobic groups determines the performance of amphipathic GCPs. For example, at the same N/P ratio in HaCaT cells and primary keratinocytes, dodecyl and guanidinium containing oligocarbonates showed the highest knockdown efficiency in comparison with hexyl and ethyl bearing counterparts.²²⁴ Tew and co-workers investigated siRNA delivery efficiency of a poly(oxanorbornene) library which comprises block copolymers with various hydrophobic pendant groups.²⁴⁴ Methyl phenyl, diisobutyl, and diphenyl containing polymers performed superior siRNA internalization in Jurkat T cells and Hela cells independent from the degree of hydrophobicity. Montenegro and co-workers incorporated isovaleraldehyde, hexanal, 2-naphthaldehyde, and benzaldehyde groups into guanidinium containing poly(acrylamide)s.²⁴⁵ Only isovaleraldehyde bearing polymers could execute efficient siRNA delivery in Hela cells. The same group also designed guanidinium containing poly(acrylamide)s with the substitution of different fatty acid and aldehyde chains to compare mRNA delivery efficiency in Hek293 cells.²⁴⁶ Myristoleic acid bearing polymers showed the best delivery performance while dodecanal counterparts could not transfect Hek293 cells. Moreover, transfection performance relied on degree of hydrophobic group substitution.

1.4.2.3 Incorporation of neutral or negatively charged groups

In terms of biocompatibility, *in vitro* cytotoxicity and blood compatibility are the two fundamental issues that are commonly investigated in polymeric vectors.²⁴⁷ Similar to other cationic polymers, the biocompatibility of GCPs may not be suitable for *in vivo* and clinical studies. For instance, Hennink and co-workers, on the contrary to the serum-free condition, could not observe the DNA transfection in the presence of serum proteins due to the unfavorable interactions of the polyplexes with those proteins.¹⁹³ In order to improve the biocompatibility of cationic polymers, one strategy is the combination of neutral charged polymers with cationic polymers. For example, the incorporation of polyethylene glycol (PEG) into cationic polymer structures, which is termed as PEGylation, has already given promising results.²⁴⁸

PEGylation was also employed for GCPs in several studies.^{206, 210, 214, 249-252} For instance, Piel and co-workers tested siRNA delivery both *in vivo* and *in vitro* by utilizing guanidinium and morpholine bearing polycarbonates with PEG₇₅₀ and PEG₂₀₀₀ blocks.²⁴⁹ *In vitro* studies showed that incorporation of PEG block reduces the rate of siRNA complexation and knockdown efficiency in Hela cells. On the other hand, *in vivo* studies on mice revealed that PEGylation changed the biodistribution of

polyplexes in the organs and reduced the accumulation of polyplexes in the lungs. Such a reduction in siRNA knockdown efficiency was also observed by Wender and co-worker for guanidinium-rich oligocarboxylates upon PEGylation.²²⁴ Recently, incorporation of PEG into nanoparticle formulations became controversial due to the observation of PEG immunogenicity in humans which can result in loss of therapeutic efficiency.²⁵³ For this reason, the incorporation of neutral charged carbohydrates was proposed as an alternative strategy. For example, neutral charged *N*-acetyl-D-galactosamine bearing poly(methacrylamide) block units were added to guanidinium bearing poly(methacrylamide) homopolymer by Reineke and co-workers.²⁰⁶ They observed higher biocompatibility in HepG2 cells for the block copolymer/DNA polyplexes in comparison with the guanidinium homopolymer counterparts.

In addition to the inclusion of neutral charged polymers, the monomers with negatively charged pendant groups can be incorporated into GCPs to improve biocompatibility. Stenzel and co-workers explored the impact of zeta potential on cellular uptake in A2780 cells for guanidinium functionalized poly(methacrylic acid)s.²⁵⁴ The presence of carboxylic acid group enhanced the biocompatibility while the higher guanidinium substitution improved the cellular uptake. Cavalli and co-workers investigated carboxylic acid and guanidinium bearing polyamidoamine copolymer for DNA delivery in HeLa cells and HT29 cells of rats. *In vitro* studies indicated that the polyplexes did not show either cytotoxic nor hemolytic activity.²⁵⁵ Ding and co-workers pointed out the importance of tuning the charge density in amphoteric polymers for an efficient gene delivery.²¹⁹ 80 mol% of guanidinium was necessary to obtain an efficient DNA transfection with an acceptable cytotoxicity for guanidinium and carboxylic acid bearing polyamidoamide copolymers in NIH/3T3 cells.

Employing zwitterionic monomers, which bear both negatively and positively charged pendant groups, is another strategy. For instance, Stenzel and co-workers designed micelles made of triblock poly(methacrylate) copolymer with a comonomer containing both carboxylic acid and guanidinium groups.²⁵⁶ The amphoteric micelles showed reduced zeta potential with an improved cell viability in OVCAR-3 cells while the cationic counterparts caused significant cell death. Ding and co-workers utilized zwitterionic guanidinium and carboxylic acid containing polyamidoamines for short hairpin RNA (shRNA) delivery to MCF7 cells.²²² The polyplexes of zwitterionic polymers showed higher cell viability and transfection efficiency in comparison with the cationic counterparts.

1.4.2.4 Inclusion of stimuli-responsive groups

The release of the cargo from polyplexes at the target site with a good timing is one of the most crucial requirements for the success of non-viral gene delivery. Incorporation of stimuli-responsive groups into cationic polymers can assist the desired release of nucleic acids.²⁵⁷ For this purpose, disulfide bonds are widely used. These bonds can be cleaved by thiol-disulfide exchange reaction with the aid of

glutathione (GSH). ~1000-fold higher GSH concentration in cytosol compared to the GSH concentration in blood plasma enables site-specific reduction of the disulfide bonds. Moreover, the presence of disulfide bonds in the structures of non-biodegradable cationic polymers can enhance their biocompatibility.²⁵⁸

Incorporation of disulfide bonds was also utilized for GCPs. The vast majority of guanidinium containing polyamidoamines was functionalized with disulfide bonds for non-viral gene delivery studies.^{205, 207-208, 219, 222, 234-235, 259-263} However, there is no exemplary study which directly investigates the impact of disulfide functionalization in these polymers. Apart from disulfide functionalization of GCPs, guanidinium containing poly(disulfide)s were synthesized by Matile and co-workers for the first time.²⁶⁴ Upon entering to Hela cells, depolymerization through the disulfide backbone and the cargo release occurred in less than 1 minute.²⁶⁵ Regarding polyarginine, guanidinium containing poly(disulfide)s showed higher biocompatibility. Xu and co-workers employed the same polymerization technique to obtain a library of PEGylated poly(disulfide)s with guanidinium moieties for DNA transfection in 4T1 cells and 4T1 tumor-bearing BALB/c nude mice.²⁶⁶ With the optimum degree of polymerization (DP), higher transfection efficiency and biocompatibility were observed in respect of bPEI.

Phenylboronic ester is another stimuli-responsive group that utilized in GCPs for non-viral gene delivery to cancer cells. For instance, Shi and co-workers synthesized guanidinium and phenylboronic ester bearing PEGylated poly(methacrylamide) diblock copolymer, which performed reactive oxygen species (ROS) dependent siRNA release.²⁵¹ During complex formation with siRNA, both hydrophilic and hydrophobic interactions played a role. However, at the tumor site of orthotopic U87MG-Luc human glioblastoma tumor-bearing nude mice, high concentration of ROS enabled conversion of phenylboronic ester into carboxylic acid groups. As a result of the change in hydrophobic/hydrophilic balance, siRNA release was more efficient than the guanidinium bearing counterpart. The same polymeric system was also efficient for microRNA (miRNA) delivery, which resulted in the inhibition of glioblastoma growth in similar animal model.²⁶⁷

1.4.2.5 Ligand attachment

Ligand attachment to cationic polymers promotes the specific delivery of polyplexes to the target tissues and cells.⁵² Ligand attachment to GCPs also improved gene delivery efficiency both *in vitro* and *in vivo*. For example, Ding and co-workers attached nuclear localization signal (NLS) peptide to disulfide functionalized polyamidoamine homopolymer.²⁶³ The NLS peptide attachment improved transfection efficiency and enhanced cell viability in NIH 3T3 cells. Shi and co-workers attached angiopep-2, a blood brain barrier (BBB) oligopeptide, to guanidinium and phenylboronic ester bearing PEGylated poly(methacrylamide) polymer. The cellular uptake of siRNA polyplexes in U87MG glioma cells was enhanced and an effective

suppression of tumor growth was observed in U87MG-Luc human glioblastoma tumor-bearing nude mice.²⁵¹ The same group studied siRNA delivery efficiency of guanidinium and tetrafluoropropyl bearing PEGylated poly(methacrylamide) polymers both in Neuro-2a cells and in mouse models.²⁵² Glycosylation of the polymers improved not only blood stability but also penetration of the polyplexes through BBB.

In summary, GCPs showed great potential in non-viral gene delivery yet the utilization of guanidinium groups for polymeric vectors has just started to evolve in comparison to well-known PLL, PEI, and PMAM polymers. Overall, the influence of above-mentioned strategies on GCPs are in accordance with the effects observed for other polymeric vectors.³² The combination of guanidinium moieties with cationic or hydrophobic groups enhanced the performance of nucleic acid delivery whereas these strategies negatively impact the biocompatibility of GCPs. During designing GCPs with such groups, the degree of substitution and the origin of comonomer pendant groups should be considered carefully. For instance, water solubility of the outcome polymers can dramatically reduce by incorporating hydrophobic moieties. Neutral, anionic, and zwitterionic pendant groups improved biocompatibility of GCPs. Nevertheless, the stability and transfection efficiency of polyplexes decreased significantly upon addition of such groups. Incorporation of stimuli-responsive groups and ligand attachment to GCPs increased transfection efficiency. Particularly for *in vivo* applications, these strategies should be used for GCPs to overcome extra- and intracellular barriers. Despite of encouraging results, the exemplary studies applying these strategies on GCPs are limited. Especially, the palette of hydrophobic, anionic, zwitterionic, and stimuli-responsive groups should be enlarged. Moreover, the investigations on GCPs with neutral charged groups should be performed in a more systematic way to obtain polyplexes with optimized stability and transfection efficiency. Therefore, there is still so much to discover on GCPs.

1.5 The Synthetic Approaches for Guanidinium Containing Polymers

Several polymer classes bearing guanidinium moieties were explored regarding their potential in non-viral gene delivery. Guanidinium group into polymer structures was incorporated either by polymerization of guanidinium containing monomers²⁶⁸⁻²⁶⁹ or by post-polymerization modifications²⁷⁰. The former method is more time efficient. Nonetheless, the selected polymerization method should be suitable for the presence of free or protected guanidinium groups. The later method is generally preferred for side specific grafting of guanidinium group. Additionally, it can be also a good alternative where free or protected guanidinium bearing monomer has low reactivity or leads to side reactions. For grafting of guanidinium groups on the side chains of polymers, different compounds were utilized such as arginine²⁰⁷, 1*H*-pyrazole-1-carboxamide hydrochloride^{208, 238, 250, 270-271}, dicyandiamide²³⁴, *O*-Methylisourea^{209, 212}, 2-ethyl-2-thiopseudourea hydrobromide²¹⁰, and guanidinium aldehyde^{230, 245-246}.

Post-polymerization modifications bring some drawbacks such as the hurdle in precise control over degree of substitution or the presence of side reactions leading to immature backbone degradation for degradable polymers.²⁷² Thus, guanidinium containing monomers are preferentially polymerized by different polymerization methods depending on the polymer backbone. For the selection of polymer class, certain features should be taken into account for non-viral gene delivery studies, such as good solubility in aqueous media, well-defined structure, feasibility for chemical modifications, no batch-to-batch variation, and biocompatibility.³² Hence, each polymer class and the polymerization method has its own advantages and disadvantages (**Table 1.2**).

Commonly investigated GCPs with biodegradable backbones are polyamidoamines, polyesteramides, and polycarbonates. Guanidinium containing polyamidoamines are synthesized by linear step growth Michael addition polymerization.²⁷³ This method has high functional group tolerance that enables the use of monomers bearing free guanidinium moieties. On the other hand, the long reaction time (up to 8 days), the lack of control on molar mass and molar mass distribution are the drawbacks of this polymerization method.²²² Guanidinium containing polyesteramides are prepared by solution polycondensation reaction.²⁷⁴ The monomers with free guanidinium groups can be directly polymerized by this method. A good control over molar mass and molar mass distribution can be achieved. However, the water solubility of these polymers is dramatically affected by the backbone chemistry. Moreover, the purification process for polyesteramides requires additional attention since the utilized solvent and by-products can be toxic for biological applications.²⁷⁴ Guanidinium containing polycarbonates are synthesized by organocatalytic ring-opening polymerization (ROP).²⁷⁵ For polymerization, cyclic carbonate monomers with protected guanidinium pendant groups are used. The protection of guanidinium groups is necessary to avoid immature termination because of side reactions. The use of metal free thiourea/amine catalyst helps to reduced cytotoxicity arising from catalysts residues. On the other hand, ROP demands high monomer purity and extreme dry conditions under inert environment.²⁷⁶ In addition, the monomer selection is limited because of the restricted tolerance of ROP to functional groups. For instance, some studies on guanidinium containing polycarbonates showed that the control over polymerization was highly affected by comonomer functional groups and degree of substitution.^{224-225, 249}

Guanidinium containing poly(oxanorbornene)s and poly(acrylate/methacrylate)s are non-biodegradable polymer classes that were investigated for non-viral gene delivery. Guanidinium containing poly(oxanorbornene)s are synthesized by ring-opening metathesis polymerization (ROMP)²⁷⁷. Boc-protected guanidinium bearing oxanorbornene monomers and Grubbs' third generation catalyst were utilized for the polymerization reactions.^{231, 244} ROMP provides a good control over molar mass and molar mass distribution. Nevertheless, in addition to non-degradable backbones, the reaction sensitivity and the use of a metal catalyst are the major drawbacks for the synthesis of poly(oxanorbornene)s. Guanidinium containing poly(acrylate/methacrylate)s were prepared by different polymerization techniques;

free-radical polymerization, atom transfer radical polymerization (ATRP), and reversible addition-fragmentation chain transfer (RAFT) polymerization.

Table 1.2 Guanidinium containing polymer classes for non-viral gene delivery regarding their advantages and disadvantages

Polymer class	Polymerization method	Advantages	Disadvantages	Ref.
Polyamidoamines	Linear step growth Michael addition polymerization	<ul style="list-style-type: none"> ✓ Biodegradable ✓ High tolerance to functional groups 	<ul style="list-style-type: none"> ○ Long reaction time ○ No control over molar mass and molar mass distribution 	205, 207-208, 219, 222, 234-235, 255, 259-263
Polyesteramides	Solution polycondensation	<ul style="list-style-type: none"> ✓ Biodegradable ✓ Good control over DP and molar mass distribution 	<ul style="list-style-type: none"> ○ Difficult purification process ○ Possibility of low biocompatibility due to the solvent residues and/or by-products 	214, 220-221, 223
Polycarbonates	Organocatalytic ROP	<ul style="list-style-type: none"> ✓ Biodegradable ✓ Good control over DP and molar mass distribution 	<ul style="list-style-type: none"> ○ Extremely sensitive reaction conditions ○ Restricted tolerance to functional groups ○ Limited monomer selection 	224-225, 249
Poly(oxanorbornene)s	ROMP	<ul style="list-style-type: none"> ✓ Good control over DP and molar mass distribution 	<ul style="list-style-type: none"> ○ Non-biodegradable ○ Extremely sensitive reaction conditions ○ The use of metal catalysts ○ Low tolerance to functional groups ○ Limited monomer selection 	231, 244
Poly(acrylate/methacrylate)s	Free-radical polymerization	<ul style="list-style-type: none"> ✓ High versatility with less sensitive reaction conditions ✓ High tolerance to functional groups 	<ul style="list-style-type: none"> ○ Non-biodegradable ○ No control over molar mass and molar mass distribution 	193
	ATRP	<ul style="list-style-type: none"> ✓ High versatility ✓ Less sensitive reaction conditions ✓ Good control over DP and molar mass distribution ✓ High tolerance to functional groups 	<ul style="list-style-type: none"> ○ Non-biodegradable ○ The use of transition metals 	210, 238, 270
	RAFT polymerization	<ul style="list-style-type: none"> ✓ High versatility ✓ Less sensitive reaction conditions ✓ Good control over DP and molar mass distribution ✓ High tolerance to functional groups 	<ul style="list-style-type: none"> ○ Non-biodegradable 	206, 209, 211, 213, 230, 233, 236-237, 245-246, 251-252

Free radical polymerization was the first method utilized for the synthesis of guanidinium containing poly(methacrylate) homopolymer.¹⁹³ This method can be conducted on the monomers with free guanidinium moieties in acidified water and the polymers can be purified simply by dialysis in water. However, a poor control on molar mass and molar mass distribution were the limiting factors for poly(acrylate/methacrylate)s in pharmaceutical applications.²⁷⁸ The discovery of reversible deactivation radical polymerization (RDRP) techniques (e.g., ATRP, nitroxide-mediated polymerization (NMP), and RAFT polymerization) removed this big hurdle by giving living characteristics to the radical propagation of vinyl-based monomers by minimizing premature termination.²⁷⁹ As a result, a good control over molar mass and molar mass distribution is provided for the monomers with various functionalities under mild reaction conditions. In regard of RDRP techniques, GCPs were typically prepared by either ATRP or RAFT polymerization. Although both techniques provide versatility, the use of transition metals in ATRP is a disadvantage for biological applications.²⁸⁰ Therefore, RAFT polymerization has a great potential for the synthesis of GCPs, which was also emphasized by Tew and co-workers.²¹³ No requirements of metal catalyst, less sensitive reaction conditions, and possibility of controlled polymerization of monomers with a bigger palette of functional groups make RAFT polymerization more versatile for pharmaceutical applications. The only drawback for guanidinium containing poly(acrylate/methacrylate)s is the non-degradable backbone structure. Nevertheless, this drawback can be minimized by the incorporation of bioreducible pendant groups.²⁸¹

1.5.1 RAFT polymerization

The non-viral gene delivery investigations of guanidinium containing poly(acrylate/methacrylate)s started in 2004¹⁹³ and gained acceleration after 2012²⁶⁹ by employing RDRP methods, especially RAFT polymerization. RAFT polymerization through thiocarbonylthio RAFT agents was introduced by Thang, Rizzardo, Moad, and co-workers in 1998.²⁸² At that time, existing living free-radical polymerization methods were not applicable for acid or protic monomers. In addition, the reagents utilized were expensive and hard to remove during the purification process. RAFT polymerization offered a high tolerance to both organic and protic solvents, except strong nucleophilic solvents. Beside solvent flexibility, the polymerization reactions can be conducted in bulk-, suspension-, emulsion-, mini-emulsion conditions.²⁸³ Consequently, both hydrophobic and hydrophilic monomers can be polymerized simultaneously without losing the control over polymerization. Moreover, it offers a straightforward synthesis and purification processes. Furthermore, the polymerization process keeps the character of living polymerization while taking the advantage of versatility of a radical process.²⁸⁴ As a result, various polymeric architectures can be obtained with a predictable molar mass with low dispersity index (\mathcal{D}), high end-group accuracy, and the possibility for regrowth of the

polymer chains. Various quantum-chemical studies on RAFT polymerization were conducted to reveal the reaction mechanism and kinetics.²⁸⁵

1.5.1.1 Mechanism of RAFT polymerization

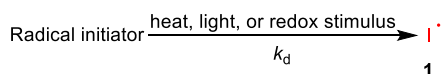
The generally accepted mechanism of RAFT polymerization relies on an equilibrium among active and dormant chain (**Scheme 1.1**).²⁸⁶ The major requirements for the RAFT polymerization are a radical initiator, a RAFT agent (typically a thiocarbonylthio group, $Z-C(=S)S-R$) and a monomer with vinyl group. The reaction mechanism can be divided into three main parts: RAFT pre-equilibrium, main RAFT equilibrium and termination. RAFT pre-equilibrium starts with the generation of primary radicals (**1**) from a radical source. The radical source can be created by thermal, redox, or light induced initiation.²⁸⁴ Among them, thermal initiation, which requires diazo compounds such as 4,4'-azobis(4-cyanovaleric acid) (ACVA), is used commonly.²⁸⁷ The process of radical generation determines high end-group fidelity, polymerization rate, and reaction conditions. After the radical generation, (**1**) can be added either to the RAFT agent (**3**) or to a monomer molecule to form the propagating radical (**2**) for the initiation of chain growth.

The first pathway occurs preferentially and starts with the addition of the generated radical to the RAFT agent (**3**). Consequently, the intermediate radical (**7**) forms. This reaction is reversible. To proceed in the forward direction, the R group of (**3**) should be a better free radical leaving group than (**1**). This step indicates the importance of radical source choice. As the reaction proceeds, the fragmentation of (**7**) into the new RAFT agent (**8**) and the radical (**6**) occurs. In the second pathway, the radicals (**1**) add to a monomer molecule. After addition of a few monomer molecules, the propagating radical (**2**) forms. Because of high-chain transfer constants of the RAFT agent, (**2**) can bear only a few monomer molecules. Afterwards, (**2**) adds to the RAFT agent (**3**) to form the intermediate radical (**4**). At this point, the process becomes reversible. With the correct choice for monomer/RAFT agent combination, (**4**) fragments into the new RAFT agent (**5**) and radical (**6**) favorably. At the end of both pathways, the generated new radicals (**6**) react with the monomer molecules to form the new propagating radicals (**9**), so the new oligomeric-type RAFT agents form. As a result, the RAFT pre-equilibrium is established by completing the steps (i), (ii) and (iii) (**Scheme 1.1**).

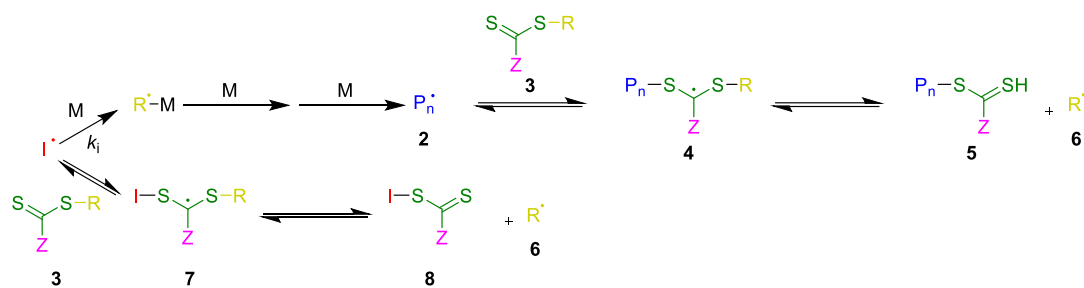
The next step is the formation of the main RAFT equilibrium (iv), where activation-deactivation process occurs. The main RAFT equilibrium is formed through degenerative chain transfer among propagating (**2**, **9**) and dormant chains (**5**, **11**). This degenerative transfer is controlled by the intermediate radical species (**10**). The last part of RAFT polymerization is termination (v). Since the polymerization process is mainly the insertion of monomers between the R- and $Z-C(=S)S$ groups of the RAFT agent, the majority of the synthesized polymers bear the α - and ω -end group.²⁸⁴ The presence of thiocarbonylthio end-group at the ω -end indicates the 'living' character of the polymers. This feature enables the further monomer addition to the polymer chain

that results in block copolymer structures. Beside the synthesis of block copolymer structures, the removal of thiocarbonylthio end-group at the ω -end by the reactions with nucleophiles, ionic reducing agents and oxidizing agents, UV irradiation, radical-induced reduction, or thermolysis enables further modifications of the polymer structure.²⁸⁸ The presence of α -end group is dictated by the nature of initiation.²⁸⁴ The α -end can be either an initiator fragment or R group of the RAFT agent. At the ω -end, dead polymer chains (inactive species) can also occur in the absence of thiocarbonylthio group because of the side reactions in radical process, which are combination, disproportionation and conventional chain transfer.²⁸⁵

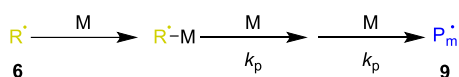
i) Radical generation



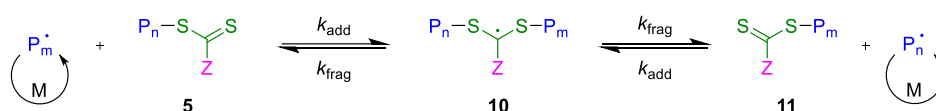
ii) RAFT agent activation/initialization



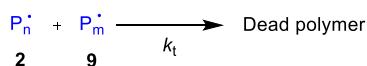
iii) Propagation



iv) The main RAFT equilibrium



v) Termination



Scheme 1.1 Generally accepted reaction mechanism of RAFT polymerization

1.5.1.2 Factors that determine the success of RAFT polymerization

The first factor is the careful selection of RAFT agent, which is also called as chain transfer agent (CTA).²⁸⁹ For an efficient RAFT polymerization, the RAFT agent should own a reactive C=S double bond for high k_{add} and a weak S-R bond for high k_{frag} without creating a side reaction (**Figure 1.5**). For the selection of RAFT agent, the utilized monomer should be considered thoroughly. The reason is that the C=S bond

in the RAFT agent should be more reactive to radical addition than the C=C bond in the monomer. This condition is regulated by the Z- and R group. Z groups in RAFT agent has a stabilizing effect on the intermediate radicals (**4**), (**7**) and (**10**). R groups should be a good homolytic leaving group. Moreover, the expelled radicals (**6**) should efficiently conduct the initialization and propagation steps. The high stability of (**6**) enable occurrence of the fragmentation step (homolytic dissociation).

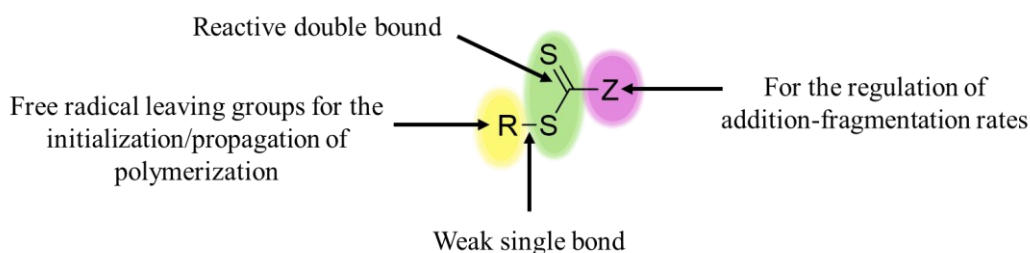


Figure 1.5 General structural properties of thiocarbonylthio RAFT agent

The monomers used in RAFT polymerization belong to the class of either more activated monomers (MAMs) or less activated monomers (LAMs) depending on their reactivity. In MAMs, the vinyl group can be conjugated to a double bond (e.g., butadiene, isoprene), an aromatic ring (e.g., styrene, vinylpyridine), a carbonyl group (e.g., methacrylates, methacrylamides, maleic anhydride, maleimide), or a nitrile (e.g., acrylonitrile). A double bond in LAMs can be conjugated to oxygen, nitrogen, halogen, sulfur lone pairs, or saturated carbons (e.g., vinyl acetate, *N*-vinylpyrrolidone, vinyl chloride, 1-alkenes). After myriads of investigations, guidelines for the selection of RAFT agent were prepared with respect to MAMs and LAMs (**Figure 1.6**).²⁹⁰

<u>Dithioesters</u>	<u>Trithiocarbonates</u>	<u>Xanthates</u>	<u>Dithiocarbamates</u>
<ul style="list-style-type: none"> ✓ A good control over molar mass distribution and end-group fidelity MAMs ○ Susceptibility to retardation at high concentration ○ Prone to hydrolysis and decomposition in the presence of Lewis acids ○ Not suitable for LAMs 	<ul style="list-style-type: none"> ✓ Easier synthesis in comparison to other RAFT agents ✓ A good control over molar mass distribution and end-group fidelity for MAMs ✓ Less susceptibility to retardation at high concentration ✓ Less prone to hydrolysis and decomposition in the presence of Lewis acids ○ Not suitable for LAMs 	<ul style="list-style-type: none"> ✓ More efficient with LAMs ○ Low transfer coefficients for styrenic and acrylic monomers ○ No control over molar mass distribution for methacrylic polymers 	<ul style="list-style-type: none"> ✓ A good control over molar mass distribution and end-group fidelity for both LAMs and MAMs ○ High activity dependency on the substituents for dithiocarbamate nitrogen ○ Less popular in comparison to other RAFT agents due to less commercial availability

Figure 1.6 General classes of RAFT agents and their advantages/disadvantages

RAFT agents are divided into four main classes, which are dithioesters²⁹¹, trithiocarbonates²⁹², xanthates²⁹³, and dithiocarbamates²⁹⁴. Each class has its own advantages and disadvantages. For example, when the propagating radicals (**2**) and (**9**) are with a terminal of MAMs, they show less reactivity in radical addition (lower k_p , lower k_{add}). Therefore, a more active RAFT agent (dithioesters, trithiocarbonates, and aromatic dithiocarbamates) should be employed for a good control on molar mass distribution. On the other hand, (**2**) and (**9**) with a terminal of LAMs have high reactivity in radical addition (higher k_p and higher k_{add}). For this reason, less active RAFT agents (dithiocarbamates and xanthates) are required.

Another important factor for an efficient RAFT polymerization is the selection of initiator²⁸⁹. For instance, the initiators such as dibenzoyl peroxide or potassium peroxydisulfate can oxidize RAFT agents to the sulfine and other side products. Therefore, it is crucial to find an initiator generating radicals, which do not cause the side reactions for the selected RAFT agent. Moreover, the generated radicals should be a good leaving group in comparison to the propagating radicals. The concentration of initiator and the rate of radical generation are also essential factors to consider. By keeping the initiator concentration lower than RAFT agent concentration, the ‘living’ character of the system can be adjusted.

Reaction time, temperature, pressure and solvent selection are the other factors that should be taken into account.²⁸⁹ The reaction time should be adjusted carefully by considering the monomer conversion. After full monomer conversion, prolongation of the reaction keeps further radical generation that causes the loss of thiocarbonylthio end-group at the ω -end of polymer chains, and so the loss of ‘living’ character occurs. Temperature for RAFT polymerization can vary from ambient to 140°C, which also depends on the selection of initiator. Optimization of reaction temperature is necessary for the regulation of the rate constants for fragmentation and transfer constants of RAFT agents. For example, the retardation problem in dithiobenzoates can be overcome by increasing the reaction temperature. The high pressure may play an important role to produce polymers with higher molar mass to minimize radical-radical termination. The solvent should be selected according to compatibility of RAFT agent, monomer, and initiator. Especially in aqueous solutions, the conditions for RAFT polymerization should be optimized carefully since RAFT agents are susceptible to hydrolysis due to their thiocarbonylthio group.²⁸⁶ The rate of hydrolysis can be avoided by conducting the reaction at acidic pH. Another challenge is the polymerization of monomers with nucleophilic substituents such as primary and secondary amines. Such groups can cause aminolysis of thiocarbonylthio group of RAFT agent and the activity loss. Therefore, a strategical approach such as protonation of amino groups should be considered.

1.5.1.3 Molar mass estimation in RAFT polymerization

In an optimum process for RAFT polymerization, the rate of addition/fragmentation equilibrium should be higher than the rate of propagation.²⁸⁴ In each activation cycle, less than one monomer unit should be inserted in R- and Z-C(=S)S groups of the RAFT agent. Hence, all chains can grow equally which gives similar DP and low D . By aiming higher DPs, nonetheless, the probability of termination and side reactions (e.g., loss of thiocarbonylthio group) increases. As a result, chain growth can stop and a smaller number of polymer chains with ‘living’ character are obtained. This phenomenon is considered as an advantage for the synthesis of oligomers and the polymers owning low molar mass ranging from 1 000 to 100 000 g mol⁻¹ with low D , which cannot be achieved with other RDRP techniques.

The addition of generated radicals to the RAFT agent is the preferential pathway. Moreover, the formation of dead chains is constant at a given concentration of radical source. Therefore, DP is influenced by the concentration of radical source insignificantly. It is rather influenced by the concentration of RAFT agent and can be calculated by (initial concentration of monomer)/(initial concentration of RAFT agent) ($[M]_0/[CTA]_0$). As a result, the theoretical number average molar mass ($M_{n,theory}$) can be estimated pre-polymerization by the equation 1.1:

$$M_{n,theory} = \frac{[M]_0 M_M \rho}{[CTA]_0 + 2f[I]_0(1 - e^{-k_d t})} + M_{CTA} \quad (1.1)$$

where $[I]_0$ is the initial concentration of initiator, ρ is the monomer conversion, M_M is the molar mass of monomer, M_{CTA} is the molar mass of RAFT agent, and k_d is the decomposition rate of initiator. Due to insignificant impact of the initiator concentration, the equation (1.1) can be simplified to equation (1.2):

$$M_{n,theory} = \frac{[M]_0 M_M \rho}{[CTA]_0} + M_{CTA} \quad (1.2)$$

In the previous section, the challenges of RAFT polymerization in aqueous medium and the use of monomers with nucleophilic pendant group was introduced. The determination of rate constants on the hydrolysis and aminolysis of RAFT agent was conducted by McCormick and co-workers to adopt the equation (1.2) for the polymerization conditions, where these side reactions can occur.²⁹⁵ The equation (1.3) is proposed for the hydrolysis of RAFT agent, which depicted pseudo-first-order rate in water. The rate of hydrolysis is also affected by M_{CTA} and pH.

$$-\frac{d[CTA]}{dt} = k_{hyd}CTA \quad (1.3)$$

In addition, because of both aminolysis and hydrolysis, the decrease in concentration of active RAFT agent is depicted in equation (1.4):

$$-\frac{d[CTA]}{dt} = k_{hyd}CTA + k_a[CTA][Amine]^2 \quad (1.4)$$

where k_a is the third-order rate constant for aminolysis derived from the study of Levesque and Del tre²⁹⁶ and $[Amine]$ is the concentration of amino groups of monomers in water. By considering a steady-state concentration of amino groups, the time-dependent concentration of RAFT agent can be shown as equation (1.5) by integrating the equation (1.4):

$$[CTA] = [CTA]_0 e^{-(k_{hyd}+k_a[Amine]^2)t} \quad (1.5)$$

During the RAFT pre-equilibrium, low molar mass of macro-RAFT agent is produced. This period is called as an induction period (t_{ind}), in which RAFT agent is more susceptible to hydrolysis and aminolysis. Therefore in t_{ind} , $[CTA]_0$ is reduced to $[CTA]_{ind}$. After t_{ind} is completed, the amount of RAFT agent left ($[CTA]_{ind}$) is calculated according to the equation (1.6):

$$[CTA] = [CTA]_0 e^{-(k_{hyd,CTA}+k_{a,CTA}[Amine]^2)t_{ind}} \quad (1.6)$$

In the main RAFT equilibrium, the rate of hydrolysis and aminolysis decreases significantly when the number of monomer units in the chain becomes higher than 9. In addition, most of the RAFT agents are converted into macro-RAFT agents. Hence the rate constants $k_{hyd,CTA}$ and $k_{a,CTA}$ are converted into $k_{hyd,macro}$ and $k_{a,macro}$, respectively. The concentration of RAFT agent during the main RAFT equilibrium is depicted in equation 1.7:

$$[CTA] = [CTA]_{ind} e^{-(k_{hyd,macro}+k_{a,macro}[Amine]^2)(t-t_{ind})} \quad (1.7)$$

where $(t - t_{ind})$ is the time for the main RAFT equilibrium. The equation (1.7) should be substituted into $[CTA]_0$ in equation (1.2) for the estimation of $M_{n,theory}$, which is represented in equation (1.8):

$$M_{n,theory} = \frac{M_M([M]_0 - [M]_0 e^{-k_{p^*}(t-t_{ind})})}{[CTA]_{ind} e^{-(k_{hyd,macro} + k_{a,macro}[Amine]^2)(t-t_{ind})}} + M_{CTA} \quad (1.8)$$

where $[M]_0\rho$ in equation (1.2) is substituted with the pseudo-first-order relationship for polymerization. The equation (1.8) estimates the molar mass of living chains for the RAFT polymerization where hydrolysis and aminolysis can occur as side reactions. Moreover, the applicability of this equation should fulfill the condition of $[M]_0/[CTA]_0 < 2000$, which ensures a constant propagation and higher polymerization rate in comparison to the rate of hydrolysis.

For RAFT polymerization of guanidinium containing vinyl monomers in aqueous solution, above-mentioned conditions should be considered carefully. Nevertheless, such limitations can be overcome by strategical optimization of the reaction conditions. Through RAFT polymerization, a good control over molar mass and molar mass distribution can be obtained. As a result, well-defined libraries can be prepared with a time-efficient way by minimizing batch-to-batch differences. In addition, different polymer architectures can be created efficiently. Moreover, the ‘living’ character of polymer chains enables further modifications in polymer structures such as conjugations of antibodies and/or chromophores. Furthermore, the synthesis of water-soluble polymers by RAFT polymerization in mild conditions without the need of transition metal or metal catalyst as well as easy purification steps make poly(acrylate/methacrylate)s a promising candidate for pharmaceutical applications including non-viral gene delivery. Following chapters represent the synthesis of different types of guanidinium containing poly(methacrylamide)s by RAFT polymerization in aqueous solutions for non-viral gene delivery.

2. Motivation

Each year millions of deaths are caused by the challenging diseases such as cancer, cardiovascular, infectious, and inflammatory diseases, etc.²⁹⁷ An enormous effort has been put to find treatments which can provide long term solutions with the least side effects for the patients. The breakthrough discoveries on nucleic acids provided a better understanding of diseases at the gene level as well as new treatment methodologies such as nucleic acid delivery. However, naked nucleic acids cannot systemically be administrated to the patients simply because they face with major physiological barriers during their travel starting from the blood circulation until their arrival to target cells. To overcome the barriers, viral and non-viral gene delivery systems were proposed.

Although viral gene delivery systems showed great transfection performance, low cargo capacity, susceptibility to inflammatory and immune reactions, and high production cost reduce their success of pharmaceutical implementation dramatically. Such drawbacks can efficiently be diminished by organic non-viral gene delivery systems, which employ lipid and/or polymeric biomaterials. Especially last three decades have witnessed an accelerated development of various lipid and polymeric vectors for non-viral gene delivery. In 2018, first lipid-based siRNA formulation was approved by FDA.³¹ In 2020, the great potential of non-viral gene delivery was recognized world-wide after the approval of lipid-based mRNA Covid 19 vaccine (BNT162b1) to overcome the global COVID-19 pandemic.²⁹⁸ To develop such efficient formulations, the aid of material science aiming functional lipid and polymer designs is incontrovertible.

In non-viral gene delivery, both lipidic and polymeric vectors possess advantages and disadvantages. Nevertheless, polymeric vectors show the superiority over lipidic vectors at certain points. Polymeric vectors are open to feasible chemical modifications, have structural and functional diversity, and offer precise control on particle features. The first polymer-based non-viral gene delivery was conducted by Vaheri and Pagano in 1965.³⁴ Afterwards, a plethora of studies were conducted on the various cationic polymers with primary, secondary, and tertiary amines, quaternary ammonium groups. On the other hand, the potential of GCPs for non-viral gene delivery had not been revealed until the discovery of guanidinium role on the excellent cellular uptake capability of HIV-1 Tat protein.⁵³ Therefore, the first example of GCPs for non-viral gene delivery appeared in the literature much later, in 2004.¹⁹³

After revealing the potential of GCPs as non-viral vectors, guanidinium containing polyamidoamines, polyesteramides, polycarbonates, poly(oxanorbornene)s, and poly(acrylate/methacrylate)s were investigated in regard of nucleic acid delivery efficiency. Depending on the backbone chemistry, GCPs were synthesized by various polymerization methods. Nevertheless, it is important to emphasize the importance of the utilized synthetic method in the pharmaceutical translation of polymers. Paul Wender defined an ideal synthesis as *‘those in which the target molecule is assembled*

*from readily available starting materials in one simple, safe, economical, and efficient operation that proceeds quickly and in quantitative yield.*²⁹⁹ By considering this fact, among all utilized polymerization methods, RAFT polymerization displays certain superiorities for the synthesis of GCPs such as the possibility of synthesis in water, no need of guanidinium protection, mild reaction conditions, good control over molar mass and molar mass distribution, easy purification, and the absence of toxic by-products or solvent residues.

Several investigations showed that GCPs performed better nucleic acid complexation/condensation and higher transfection in comparison to the polymers bearing other nitrogen based cationic moieties. The superior performance of GCPs relies on the peculiar physicochemical features of guanidinium group, which are positive charge delocalization on Y-shaped geometry and high pKa (~13.8). On the other hand, such properties are not observed for other nitrogen based cationic groups that are commonly employed in non-viral gene delivery. Moreover, the peculiarity of guanidinium provides the formation of special non-covalent interactions (e.g., like-charge pairing, bidentate H-bonding with oxoanions, cation- π interactions, and ion pair- π interactions) with other molecules in biological systems. Multiple studies revealed that these interactions together with the anisotropic hydration shell of guanidinium are strongly related to excellent cell penetration and binding to nucleic acids of guanidinium. For this reason, GCPs bear a great potential for non-viral gene delivery, which has not been completely revealed yet.

In light of the above-mentioned factors, innovative designs of guanidinium containing poly(methacrylamide)s are presented in the following chapters (**Figure 2.1**). Each polymer design was created with the motivation of achieving effective polymeric vectors, which surpass the already existing polymeric vectors for non-viral gene delivery systems. Because of the high correlation between the design and performance of polymeric vectors, the structure-activity studies were conducted with the help of an interdisciplinary collaboration by chemists, pharmaceutical technology scientists, and physicists. Each study aimed different strategies to fulfill fundamental requirements of effective polymeric vectors that are effective binding to nucleic acids, high transfection efficiency, and biocompatibility.

Chapter 3 explores guanidinium containing poly(methacrylamide) copolymers with respect to three fundamental factors influencing DNA binding affinity. The first factor is the polymer architecture, which are statistical and gradient comonomer distributions. For this purpose, a copolymer library was prepared by aiming similar molar mass for each copolymer sample. While statistical comonomer distribution provided random charge distribution in polymer chains, gradient counterparts offered a gradual increase of the cationic charge throughout the chains. The second factor is the cationic charge density, which ranged from 5 to 90 mol% of cationic comonomer content for each copolymer sample. As the final factor, the cationic charge origin and its impact on DNA binding were studied. Primary amine was selected as the second cationic charge source. A library of primary amine containing poly(methacrylamide)

copolymers were synthesized by achieving the similar features regarding the guanidinium bearing counterparts. As being the first investigation on the influence of gradient distribution on DNA binding affinity, this chapter provides a missing piece of information on GCPs for non-viral gene delivery.

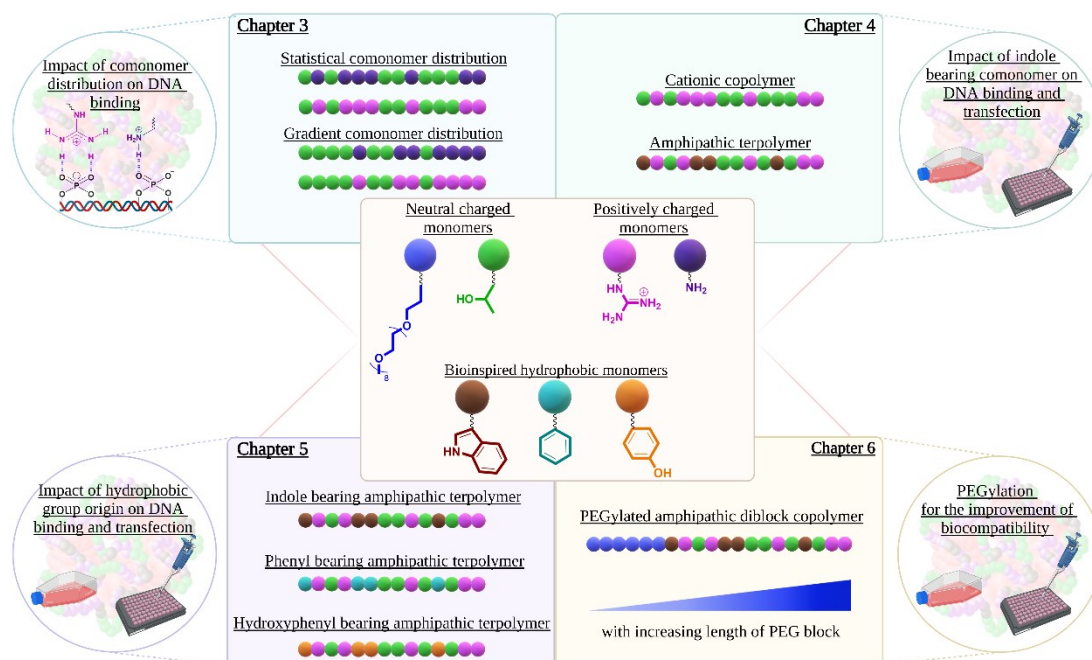


Figure 2.1 Innovative designs of guanidinium containing poly(methacrylamide)s

Nature is a powerful tool that can be synthetically mimicked to improve the performance of biomaterials. For example, the discovery of guanidinium power in HIV-1 Tat peptides led to implementation of guanidinium in CPPs and polymers for non-viral gene delivery systems. Another example is the recognition of excellent cell penetration ability of Penetratin due to the presence of indole moieties as the pendant group of tryptophan together with guanidinium groups of arginine. By considering the synergy between guanidinium and indole, **Chapter 4** represents the influence of indole inclusion in guanidinium containing poly(methacrylamide)s on pGL3 plasmid delivery efficiency. Additionally, incorporation of indole as a hydrophobic moiety switched cationic polymer structures to amphipathic counterparts, which was implemented as a strategy to improve DNA transfection efficiency of guanidinium containing poly(methacrylamide)s. This study is the first example of indole and guanidinium containing polymers for non-viral gene delivery.

The investigation on amphipathic GCPs indicated that the origin of hydrophobic pendant groups can dramatically affect the performance of polyplexes. Hence, in **Chapter 5**, phenyl and hydroxyphenyl bearing methacrylamide comonomers were selected as the mimic of phenylalanine and tyrosine, respectively. Indole, phenyl, hydroxyphenyl containing terpolymers were prepared with a comparable molar mass

Chapter 2

and comonomer content and tested for their pGL3 plasmid delivery efficiency. Exploration on the potential of indole, phenyl, and hydroxyphenyl pendant groups in guanidinium containing poly(methacrylamide)s, was conducted for the first time.

Chapter 6 depicts PEGylation of indole and guanidinium containing poly(methacrylamide) terpolymers to improve biocompatibility and applicability of the terpolymers for *in vivo* investigations. However, previous studies on polymeric vectors showed that the molar mass of PEG dictates the binding efficiency of polymers, colloidal stability, and transfection efficiency of polyplexes. Moreover, the optimum molar mass of PEG varies for each polymeric vector design. Hence, a library of diblock copolymers were prepared with poly(nona(ethylene glycol)methyl ether methacrylate) (P(MEO₉MA)) blocks as the PEG source. The molar mass of P(MEO₉MA) blocks increased gradually to decide the optimum P(MEO₉MA) length for the efficient pGL3 plasmid binding and transfection with the high colloidal stability. Such a systematic structure-function studies on PEGylation of GCPs was achieved for the first time. Apart from PEGylation, fluorescent labeling of the selected diblock copolymers was achieved.

Chapter 7 represents a transition of guanidinium containing poly(methacrylamide) copolymers illustrated in Chapter 1 into a different application. The versatility of these polymers enabled their utilization for the development of ultrasensitive aptasensor for arsenite (As⁺³) detection. The principle of the system is based on the competitive binding between As⁺³ ions and the polymers to the selected aptamer. As an alternative to the current complex and high-cost detection methods, this study provided a cost-effective system for the trace level detection of As⁺³ in real-world samples.

Chapter 8 summarizes the significant results of above-mentioned studies and outlines future design ideas on guanidinium containing poly(methacrylamide)s for non-viral gene delivery.

3. Impact of Comonomer Distribution on DNA Binding

Parts of this chapter was published in **P1**) Tabujew, I.; Cokca, C.; Zartner, L.; Schubert, U. S.; Nischang, I.; Fischer, D.; Peneva, K., The influence of gradient and statistical arrangements of guanidinium or primary amine groups in poly(methacrylate) copolymers on their DNA binding affinity. *J. Mater. Chem. B* **2019**, 7 (39), 5889-6066.

In the last six decades, an accelerated development on cationic polymers occurred for non-viral gene delivery in parallel with the advancement in macromolecular chemistry such as the discovery of RAFT polymerization.^{32, 284} Although polymeric vectors provide certain advantages (e.g., feasibility, versatility and multifunctionality), until now none of polymeric vectors could successfully pass the clinical trials. For tackling the clinical trials, the first criterion is the development of stable polyplex formulations, which can successfully pass through the extra- and intracellular barriers. The colloidal stability of polyplexes is highly dependent on physicochemical properties of the cationic polymers.²⁴⁰ Therefore, structure-activity investigations on the physicochemical properties of cationic polymers play an important role for the development of successful polymeric vectors.

Comonomer distribution belongs to those physicochemical properties. Nonetheless, for GCPs, there are limited number of structure-activity investigations on the impact of comonomer distribution for non-viral gene delivery.^{224, 228-229} Tew and co-workers showed that gradient comonomer distribution of guanidinium moieties in poly(oxanorbornene)s performed the optimum cellular uptake with low toxicity in Jurkat-T cells by comparison with homopolymer and block copolymer counterparts.²²⁸ In a study conducted by Perrier and co-workers, statistical distribution of guanidinium moieties in poly(acrylamide) accomplished better cellular uptake in MDA-MB-231 cells with respect to diblock and tetrablock counterparts.²²⁹ However, both studies were conducted by utilizing free polymer chains. In addition, the potential of gradient copolymers is mostly unrevealed for other polymeric vectors as well.³² The only example of gradient copolymers for non-viral gene delivery was depicted by Schubert and co-workers.³⁰⁰ They compared statistical and gradient comonomer distributions on DNA binding efficiency in amino functionalized poly(2-oxazoline)s. The polymers with gradient distribution showed higher polyplex stability. Therefore, this chapter discusses the first report of GCPs with gradient comonomer distribution for non-viral gene delivery.

The investigation was aimed at uncovering the impact of gradient comonomer distributions of guanidinium moieties on DNA binding affinity (**Figure 3.1**). For this purpose, a library of statistical and gradient poly(methacrylamide) copolymers was prepared with varying cationic comonomer contents ranging from 5 to 90 mol%. The molar mass of the copolymers was kept similar in order to eliminate the molar mass effect on DNA binding affinity. As a result, the impact of comonomer distribution on DNA binding was investigated in respect of various cationic charge densities. *N*-(3-guanidinopropyl)methacrylamide (GPMA) was selected as the guanidinium bearing monomer. *N*-(2-hydroxypropyl)methacrylamide (HPMA) was utilized as the

comonomer, which functioned as the inert “spacer-monomer” due to its neutral charge. It did not contribute to the binding of nucleic acids but it improved the colloidal stability of polyplexes.³⁰¹ The polymer library was extended by addition of the copolymers bearing *N*-(3-aminopropyl)methacrylamide (APMA) comonomer, which possess primary amine pendant groups. The library was prepared as the counterparts of guanidinium bearing copolymers to examine the relationship between the origin of cationic charge and comonomer distributions on DNA binding affinity.

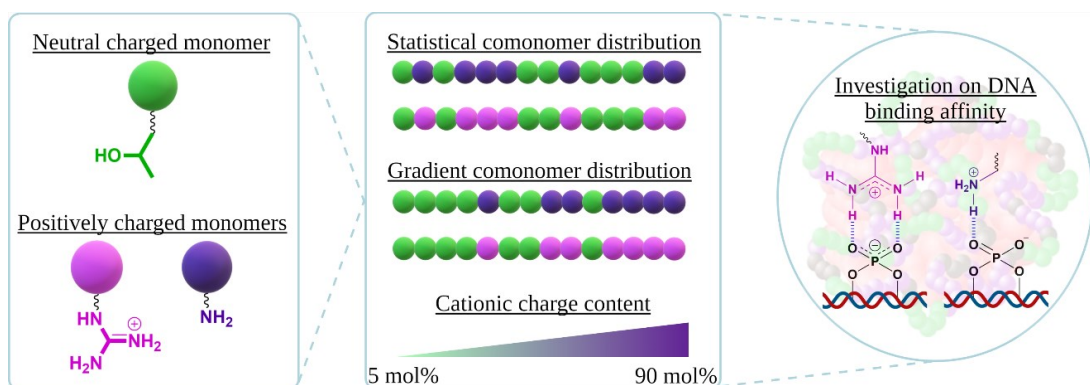
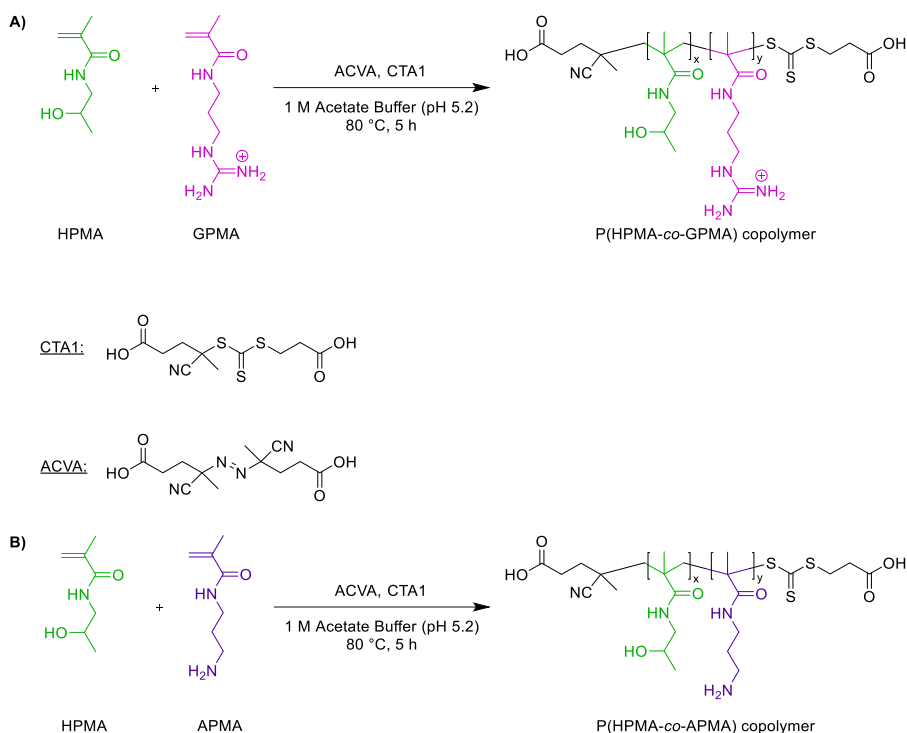


Figure 3.1 The general concept described in Chapter 3

3.1 Preparation and Physicochemical Characterization of the Polymer Library

For the preparation of copolymers, RAFT polymerization was utilized. However, the polymerization conditions had to be optimized carefully due to the presence of guanidinium and primary amine moieties, which could easily lead to aminolysis, especially for high nucleophilic comonomer contents. Moreover, an aqueous medium was used as the reaction solvent that could cause hydrolysis of the RAFT agent. Hence, the activity of the RAFT agent could be lost leading to interference in the control on molar mass and molar mass distribution.^{286, 295} Hydrolysis was minimized by selecting 4-(((2-carboxyethyl)thio)carbonothioyl)thio)-4-cyanopentanoic acid (CTA1) as the RAFT agent because it is less susceptible to hydrolysis and highly suitable for methacrylamides (**Scheme 3.1**).²⁹² Aminolysis of trithiocarbonate groups of CTA1 was minimized by conducting the reaction in 1M acetate buffer (pH 5.2), which assured the continuous protonation of guanidinium and primary amine groups in the time frame of polymerization. The thermal initiation of the polymerization was achieved by employing ACVA.



Scheme 3.1 RAFT polymerization of A) P(HPMA-*co*-GPMA) and B) P(HPMA-*co*-APMA) copolymers

The statistical copolymers were prepared *via* batch copolymerization, which provided variation in comonomer distributions in polymer chains depending on the reactivities of comonomers (**Figure 3.2**). Therefore, preliminary examinations were conducted on statistical copolymerization. A compositional drift was observed toward HPMA comonomer in both P(HPMA-*co*-APMA) and P(HPMA-*co*-GPMA) copolymers at low monomer conversion (<15%) (**Table 3.1**). This effect became more pronounced for the copolymer with high cationic charge content. In RAFT polymerization, such a drift at low monomer conversion can be the indication of preferential addition of the generated radicals by ACVA to HPMA monomers.³⁰² However, similar comonomer content can be observed as the polymerization proceeds if there is no significant difference in monomer reactivities. Therefore, further investigations on comonomer contents were conducted on P(HPMA-*stat*-APMA) and P(HPMA-*stat*-GPMA) copolymers during the polymerization timescale of 5 hours by aiming 80 mol% of APMA and GPMA comonomer contents (**Table 3.2**). Despite of the initial compositional drift for HPMA comonomer, the comonomer contents were similar for both P(HPMA-*stat*-APMA) and P(HPMA-*stat*-GPMA) copolymers as the chain propagation continued. Based on these preliminary examinations, the statistical copolymer libraries with desired comonomer compositions were prepared by further stoichiometric adjustments in comonomer compositions in feed.

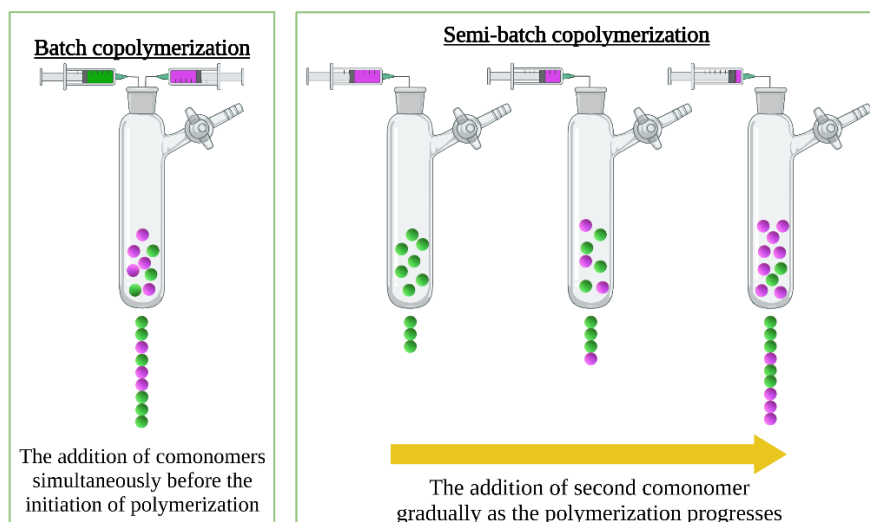


Figure 3.2 Schematic illustration of the synthetic approaches for statistical and gradient copolymers

Table 3.1 Preliminary investigations on comonomer content of P(HPMA-*stat*-APMA) and P(HPMA-*stat*-GPMA) copolymers at low monomer conversion (<15%)

Theoretical monomer composition (mol%)		Monomer in feed (mol%)		Monomer in composition (mol%)	
APMA	HPMA	APMA	HPMA	APMA	HPMA
90	10	91	9	79	21
70	30	67	33	58	42
60	40	59	41	44	56
50	50	52	48	43	57
40	60	40	60	29	71
GPMA	HPMA	GPMA	HPMA	GPMA	HPMA
90	10	93	7	85	15
70	30	64	36	54	47
50	50	47	53	58	42
40	60	40	60	38	66
30	70	32	68	28	72

* $[M]_0/[CTA]_0$ was 80/1 and $[CTA]_0/[I]_0$, was 3/1 with 1 M final monomer concentration. The comonomer contents were calculated by $^1\text{H-NMR}$ and trioxane used as the reference compound. The samples with high experimental error were discarded from the data set.

Table 3.2 Investigations on comonomer contents of P(HPMA-*stat*-APMA) and P(HPMA-*stat*-GPMA) copolymers during the polymerization timescale of 5 hours

Polymerization time (h)	HPMA (mol%)	APMA (mol%)
0	20	80
1	30	70
3	28	72
5	28	72
Polymerization time (h)	HPMA (mol%)	GPMA (mol%)
0	37	73
1	44	56
3	42	58
5	42	58

* $[M]_0/[CTA]_0$ was 80/1 and $[CTA]_0/[I]_0$, was 3/1 with 1 M final monomer concentration. The comonomer contents were calculated by $^1\text{H-NMR}$ and trioxane used as the reference compound.

The synthesis of gradient copolymers was achieved by a “forced” gradient copolymerization method: the semi-batch copolymerization (**Figure 3.2**). By the aid of a syringe pump at specified rates, 1 M buffered solution of the cationic comonomer was gradually added to the polymerization mixture containing 1 M HPMMA comonomer solution (**Table 3.3**). The addition rate was determined based on the cationic comonomer content in feed. In this way, the effect of monomer reactivity was minimized. As a result, a controlled synthesis of the gradient copolymers was achieved, which provided similar gradient behavior from chain to chain and batch to batch.³⁰³

Table 3.3 Cationic comonomer addition rate in semi-batch copolymerization

Cationic comonomer content (mol%)	Comonomer addition rate (mmol/h)
5	0.097
10	0.150
20	0.276
40	0.653
50	0.954
60	1.407
75	2.764
90	8.193

After successful preparation of cationic copolymer libraries, two different size exclusion chromatography (SEC) systems were utilized for the determination of apparent molar mass and dispersity indices (\bar{D}) of copolymers (**Table 3.4** and **3.5**). However, the determination of apparent molar mass was not possible for all copolymer samples for SEC_{DMAC} due to solubility problem of the copolymers with high cationic charge in dimethylacetamide (DMAC). The SEC_{DMAC} traces of statistical and gradient copolymers with APMA content exceeding 20 mol% were no longer detectable. For the GPMA counterparts, the statistical and gradient copolymers with 90 mol% GPMA content could not be measured. For this reason, SEC_{water} was additionally employed because all copolymers showed excellent solubility in water. However, the apparent molar mass in SEC_{DMAC} ($\sim 25\,000\text{ g mol}^{-1}$) and SEC_{water} ($\sim 6\,000\text{ g mol}^{-1}$) depicted big variation because of the difference in the utilized standards poly(methyl methacrylate) (PMMA) and poly(2-vinylpyridine) (P2VP). In addition, this variation was due to the difference in the cationic charge density of copolymers, which caused the changes in the hydrodynamic volume of the copolymers and/or interactions with the column materials in SEC_{DMAC} and SEC_{water}. Nevertheless, SEC_{DMAC} and SEC_{water} indicated low \bar{D} (~ 1.2) for the copolymers as a proof of good control over molar mass distribution by RAFT polymerization.

Table 3.4 Molar mass (in g mol^{-1}) and dispersity index (\mathcal{D}) for each P(HPMA-APMA) copolymer sample

Cationic comonomer content (mol%)	P(HPMA- <i>stat</i> -APMA)					P(HPMA- <i>grad</i> -APMA)				
	SEC _{DMAc} ^[a]		SEC _{water} ^[b]		HC ^[c]	SEC _{DMAc} ^[a]		SEC _{water} ^[b]		HC ^[c]
	M_n	\mathcal{D}	M_n	\mathcal{D}	$M_{s,f}^*$	M_n	\mathcal{D}	M_n	\mathcal{D}	$M_{s,f}^*$
5	28 500	1.08	5 300	1.18	11 500	25 000	1.10	6 100	1.06	11 400
10	28 000	1.09	6 000	1.18	12 400	25 500	1.08	7 300	1.04	12 100
20	28 000	1.05	7 000	1.18	11 700	22 000	1.11	8 000	1.06	12 500
40	Not applicable		7 800	1.18	11 600	Not applicable		8 300	1.19	9 100
50	Not applicable		8 500	1.18	10 800	Not applicable		8 100	1.08	9 400
60	Not applicable		8 000	1.17	10 500	Not applicable		8 000	1.21	9 800
75	Not applicable		9 000	1.17	11 200	Not applicable		8 500	1.30	10 000
90	Not applicable		11 000	1.05	10 700	Not applicable		11 000	1.05	10 400

[a] DMAc + 0.21% LiCl was used as the eluent and PMMA was employed as the standard.

[b] Water with 0.1% TFA and 0.1 M NaCl was used as the eluent and P2VP was employed as the standard.

[c] The absolute molar mass, $M_{s,f}$, was determined based on sedimentation-velocity experiments accompanied with sedimentation-diffusion analysis and density measurements in PBS.

Table 3.5 Molar mass (in g mol^{-1}) and dispersity index (\mathcal{D}) for each P(HPMA-GPMA) copolymer sample

Cationic comonomer content	P(HPMA- <i>stat</i> -GPMA)					P(HPMA- <i>grad</i> -GPMA)				
	SEC _{DMAc} ^[a]		SEC _{water} ^[b]		HC ^[c]	SEC _{DMAc} ^[a]		SEC _{water} ^[b]		HC ^[c]
	M_n	\mathcal{D}	M_n	\mathcal{D}	$M_{s,f}^*$	M_n	\mathcal{D}	M_n	\mathcal{D}	$M_{s,f}^*$
5	24 000	1.09	4 500	1.07	10 600	24 500	1.09	5 000	1.05	10 100
10	26 000	1.06	5 500	1.06	9 600	23 500	1.09	5 200	1.05	9 500
20	24 000	1.11	6 500	1.04	10 200	21 000	1.10	5 500	1.04	10 900
40	23 000	1.07	6 750	1.04	11 300	18 000	1.09	5 500	1.05	8 500
50	20 500	1.07	6 400	1.04	11 300	16 000	1.08	5 500	1.05	8 400
60	24 000	1.09	4 500	1.07	10 600	24 500	1.09	5 000	1.05	10 100
90	Not applicable		5 442	1.03	7 300	Not applicable		5 703	1.04	7 300

[a] DMAc + 0.21% LiCl was used as the eluent and PMMA was employed as the standard.

[b] Water with 0.1% TFA and 0.1 M NaCl was used as the eluent and P2VP was employed as the standard.

[c] The absolute molar mass, $M_{s,f}$, was determined based on sedimentation-velocity experiments accompanied with sedimentation-diffusion analysis and density measurements in PBS.

The significant difference in apparent molar mass for the copolymers obtained from SEC_{DMAc} and SEC_{water} was an obstacle for DNA binding investigations because the determination of nitrogen content in cationic pendant groups for the calculation of N/P ratio is strictly related to molar mass of the cationic polymers. For this reason, hydrodynamic characterization (HC) of the copolymers were additionally conducted in cooperation with Ivo Nischang (Institute of Organic Chemistry and Macromolecular Chemistry, Friedrich-Schiller-University Jena). HC method relies on physical principles in solution and does not require any calibration against standards.³⁰⁴ Therefore, in contrast to apparent molar mass detected by SEC systems, absolute molar mass of macromolecules can be determined. The absolute molar mass ($M_{s,f}$) is calculated by modified Svedberg equation depicted in equation 3.1:

$$M_{s,f} = 9\pi\sqrt{2}N_A \left([s] \left(f/f_{sph} \right)_0 \right)^{3/2} \sqrt{v} \quad (3.1)$$

where N_A is the Avogadro constant, $[s]$ stands for the intrinsic sedimentation coefficient, $(f/f_{sph})_0$ is the weight-average translational frictional ratio, and v is the partial specific volume. $[s]$, $(f/f_{sph})_0$ and v are determined by specific numerical and experimental methods. Therefore, molar mass determination of the copolymers by HC method required the combination of sedimentation velocity experiments with viscosity and density measurements. All these analytical procedures were performed in 0.01 M phosphate-buffered saline (PBS) to obtain the closest experimental conditions of DNA binding assays.

Sedimentation velocity experiments were performed by means of an analytical ultracentrifuge. The principle of sedimentation velocity experiments is based on the drift of macromolecules from meniscus to the bottom of centrifuge cell as a function of time under a strong gravitational field. The behavior of the macromolecules is dictated by the sedimentation and diffusion fluxes. Lamm equation (equation 3.2) describes the concentration change $c(r, t)$ of species at each radial position (r) and time (t) during the sedimentation process:

$$\frac{\partial c}{\partial t} = \frac{1}{r} \frac{\partial}{\partial r} \left[\left(D \frac{\partial c}{\partial r} - \omega^2 r s c \right) r \right] \quad (3.2)$$

where D is the diffusion coefficient, $\omega^2 r$ is the gravitational field with the angular velocity (ω), $\partial c/\partial r$ is the developed concentration gradient, and s is the sedimentation coefficient.

After completing sedimentation velocity experiments, the data were analyzed with SEDFIT and the $c(s)$ model with a maximum entropy regularization procedure, which is based on the numerical solution of equation 3.2. The resultant numerical values of s for the copolymers were used to estimate the sedimentation coefficients at infinite dilution (s_0) according to equation 3.3:

$$s^{-1} = s_0^{-1} (1 + k_s c) \quad (3.3)$$

where k_s is the concentration sedimentation coefficient (Gralen coefficient).

Afterwards, the estimated values of s_0 were employed for the calculation of $[s]$ by the equation 3.4:

$$[s] = \frac{s_0 \eta_0}{1 - v \rho_0} \quad (3.4)$$

where η_0 is the viscosity of the solvent (PBS) and $(1 - v \rho_0)$ is the buoyancy factor. η_0 was determined as 1.03 mPa.s by means of a viscometer. For the determination of $(1 - v \rho_0)$, a density-meter was utilized. The density increment measurements $(\rho_c - \rho_0)$ were conducted in the concentration range $0.1 \text{ w\%} \leq c \leq 1 \text{ w\%}$, where $\rho_0 = 1.0053 \text{ g cm}^{-3}$ (density of PBS). The slope of c vs $(\rho_c - \rho_0)$ plots gave the $(1 - v \rho_0)$. In addition, $(1 - v \rho_0)$ was used for the calculation of the partial specific volume (v) of each copolymer sample.

Viscosity measurements for the copolymers were conducted with the viscometer by aiming at relative viscosities of the copolymer as $1.2 < \eta_r < 2.5$. The obtained η_r values were used to plot copolymer concentration (c) vs $((\eta_r - 1)/c)$ graph for each copolymer sample. The intrinsic viscosity $[\eta]$ for each copolymer sample was calculated by the extrapolation to zero concentration. Moreover, Huggins constant (k_H) was calculated by the equation 3.5:

$$\frac{(\eta_r - 1)}{c} = [\eta] + k_H [\eta]^2 c \quad (3.5)$$

Numerical estimates of $[\eta]$ and k_H with (v) values for each copolymer were depicted in **Table 3.6**. Various interesting observations was made based on the increase in cationic charge content for both P(HPMA-APMA) and P(HPMA-GPMA) copolymers. The overall slight increase in $[\eta]$ and decrease in the apparent k_H , especially for P(HPMA-APMA) copolymers, indicated an improved solubility of the copolymers in PBS with the increase in charge density. Moreover, the higher charge content in the copolymers led to an apparent reduction in the values of v .

For the calculation of $M_{s,f}$, $(f/f_{sph})_0$ was the final value to determine. For this purpose, the weight-average f/f_{sph} values at different concentrations were utilized in equation 3.6:

$$\frac{f}{f_{sph}} = \left(\frac{f}{f_{sph}} \right)_0 (1 + k_f c) \quad (3.6)$$

where k_f is the concentration frictional ratio coefficient, f is the translation friction coefficient of the studied molecule, and f_{sph} is the translation frictional coefficient of an equivalent anhydrous sphere with the same mass and density. For both P(HPMA-APMA) and P(HPMA-GPMA) copolymers, f/f_{sph} values fluctuated around a mean with similar numerical values for each of the copolymers without any apparent concentration dependence. Hence, $(f/f_{sph})_0$ values for $M_{s,f}$ calculations were assumed as the average of frictional ratios at different concentrations. The estimated $M_{s,f}$ values were depicted in **Table 3.4** and **3.5**. Absolute molar mass values of the copolymers were mostly invariant ($\sim 11\,000\text{ g mol}^{-1}$), which were located between SEC_{DMAc} and SEC_{water} . Moreover, unimodal and narrow differential distributions of sedimentation coefficients (s) indicated low D for all copolymers (**Figure 3.3**), which was in agreement with the D values obtained from SEC_{DMAc} and SEC_{water} .

Table 3.6 The values of intrinsic viscosity ($[\eta]$), Huggins constants (k_H), and partial specific volume (v) for P(HPMA-APMA) and P(HPMA-GPMA) copolymers

APMA content (mol%)	P(HPMA- <i>stat</i> -APMA)			P(HPMA- <i>grad</i> -APMA)		
	$[\eta]$ (cm ³ g ⁻¹)	k_H	v (cm ³ g ⁻¹)	$[\eta]$ (cm ³ g ⁻¹)	k_H	v (cm ³ g ⁻¹)
5	7.6	1.8	0.78	7.2	1.8	0.80
10	7.5	1.8	0.81	7.7	1.4	0.80
20	8.2	1.7	0.79	8.1	1.5	0.79
40	7.8	1.6	0.80	7.7	1.5	0.76
50	9.0	1.3	0.77	7.4	1.4	0.77
60	9.4	1.1	0.75	8.0	1.3	0.76
75	9.7	1.1	0.74	8.6	1.2	0.73
90	9.7	1.0	0.73	8.6	1.1	0.74
GPMA content (mol%)	P(HPMA- <i>stat</i> -GPMA)			P(HPMA- <i>grad</i> -GPMA)		
	$[\eta]$ (cm ³ g ⁻¹)	k_H	v (cm ³ g ⁻¹)	$[\eta]$ (cm ³ g ⁻¹)	k_H	v (cm ³ g ⁻¹)
5	8.2	1.4	0.79	8.9	1.2	0.78
10	6.5	2.5	0.78	10.0	1.1	0.78
20	10.1	0.6	0.77	8.2	1.2	0.79
40	9.2	0.9	0.79	7.2	1.6	0.77
50	8.3	1.3	0.78	7.5	1.3	0.75
60	8.7	1.2	0.78	7.0	1.4	0.73
90	12.1	0.6	0.73	10.0	1.4	0.72

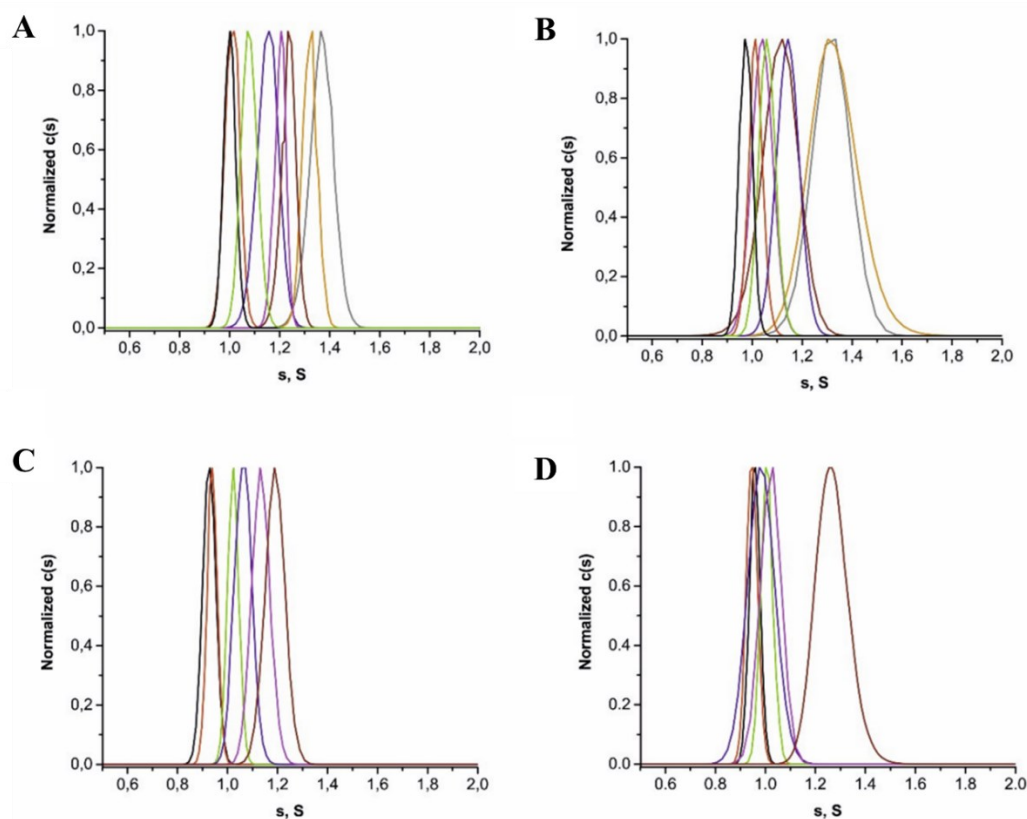


Figure 3.3 Example differential distributions of sedimentation coefficients, (s), of (A) P(HPMA-*stat*-APMA) copolymers (B) P(HPMA-*grad*-APMA) copolymers, (C) P(HPMA-*stat*-GPMA) copolymers, and (D) P(HPMA-*grad*-GPMA) copolymers. Trace color assignment: **black** Copolymers with 5 mol% cationic comonomer content; **red** Copolymers with 10 mol% cationic comonomer content; **green** Copolymers with 20 mol% cationic comonomer content; **blue** Copolymers with 40 mol% cationic comonomer content; **magenta** Copolymers with 50 mol% cationic comonomer content; **wine** Copolymers with 60 mol% cationic comonomer content; **orange** Copolymers with 75 mol% cationic comonomer content; **gray** Copolymers with 90 mol% cationic comonomer content

3.2 Biological Investigations on the Prepared Copolymers

Biological investigations were performed by Leon Zartner (Institute of Pharmacy, Friedrich-Schiller-University Jena).

The structure-activity studies on DNA binding affinity were conducted by the utilization of pGL3 plasmid. The quantitative detection of DNA binding ability of the copolymers was performed by means of AccuBlue™ assay, a type of fluorescence-based assays. Free DNA was employed as 100% control, which depicted the highest fluorescence intensity. Five copolymer quartets from the copolymer library were selected to be tested due to their comparable physicochemical properties. Overall, DNA binding efficiency of the copolymers was enhanced with the increase in N/P ratio independent from the cationic charge density and origin (**Figure 3.4**). This is a common observation for cationic polymers.^{32, 305}

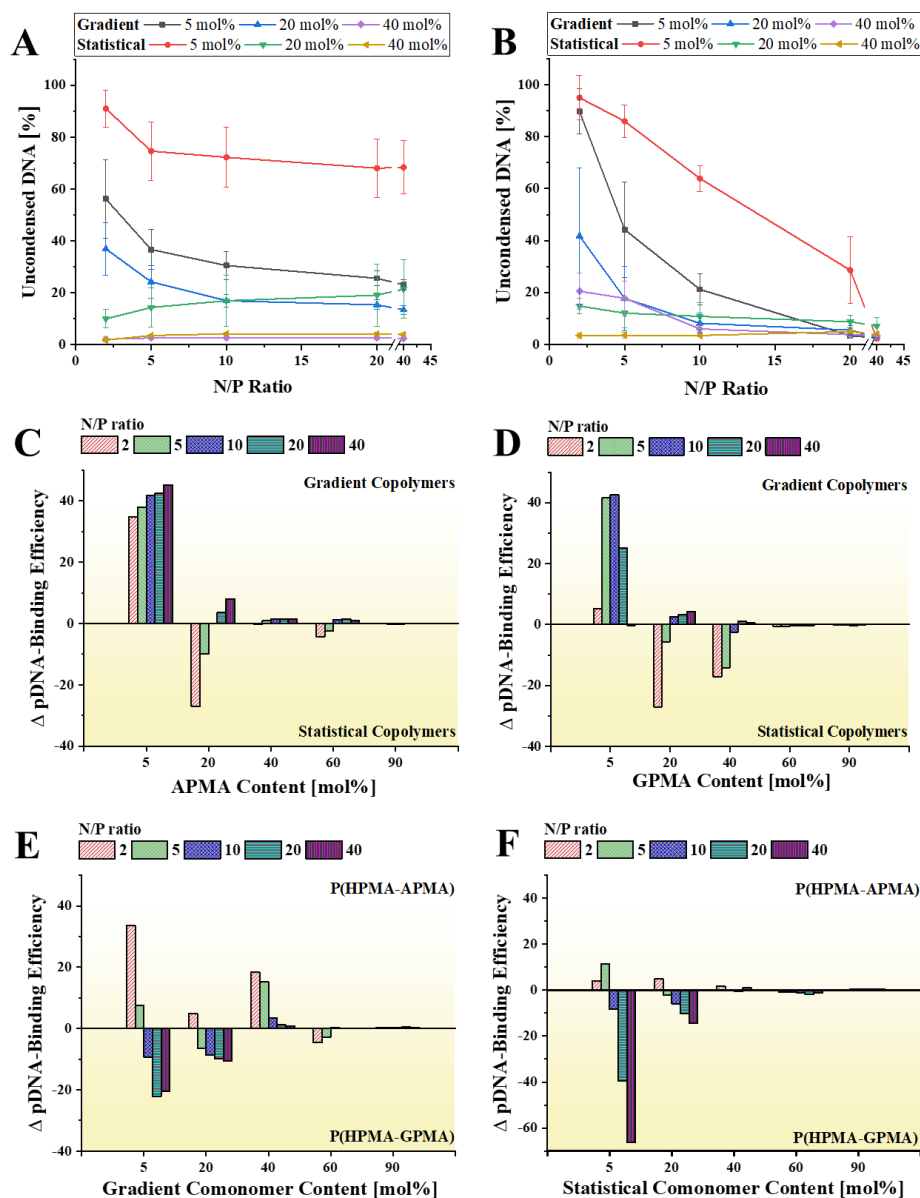


Figure 3.4 pGL3 DNA binding affinity of (A) P(HPMA-APMA) (B) and P(HPMA-GPMA) copolymers depending on the degree of substitution and N/P ratio ($n = 4$, mean \pm SD). The comparison of DNA binding affinity regarding the cationic comonomer content (C) APMA and (D) GPMA contents. The binding efficiency was calculated by subtracting the mean relative fluorescence unit (RFU) derived from the binding experiments from 100% binding efficiency. The efficiency of statistical copolymers was then subtracted from the binding efficiency of the gradient copolymers, leading to positive (superiority of gradient copolymers) or negative (superiority of statistical counterparts) values. The comparison of DNA binding affinity for (E) gradient and (F) statistical comonomer distribution. Positive values demonstrate a higher binding efficiency for P(HPMA-APMA) copolymers, negative values represent a more efficient binding of the P(HPMA-GPMA) copolymer counterparts. The binding efficiency was calculated by subtracting the mean RFU derived from the binding experiments from 100% binding efficiency. The efficiency of P(HPMA-GPMA) copolymers was then subtracted from the binding efficiency of the P(HPMA-APMA) copolymers, leading to positive (superiority of P(HPMA-APMA)) or negative (superiority of P(HPMA-GPMA)) values.

The influence of comonomer distribution on DNA binding was not recognizable for the copolymers with the cationic comonomer content of 60 and 90 mol%. The impact of comonomer distribution on DNA binding was more pronounced for the copolymers with cationic charge density 40 mol% or lower (**Figure 3.4-A** and **-B**). For both guanidinium and primary amine bearing copolymers, superior DNA binding was observed for gradient distribution with 5 mol% cationic comonomer content in comparison to statistical counterparts. Clustering of cationic charge locally in gradient copolymers could lead to this difference in the binding affinity.

The influence of comonomer distribution became less significant with the increase in cationic charge density because global charge distribution became more similar for both gradient and statistical counterparts (**Figure 3.4-C** and **-D**). The effect of cationic charge origin was observed for the copolymers with 5 mol% cationic comonomer content. At N/P ratio 40, both gradient and statistical P(HPMA-GPMA) copolymers with 5 mol% GPMA content could condense 95% of DNA while P(HPMA-APMA) copolymer counterparts could perform only 70% DNA condensation. This superior binding affinity of guanidinium containing copolymers can be because of more selective and stronger electrostatic interactions of guanidinium with the phosphate groups of nucleic acids.⁹⁶ In addition, guanidinium can form bidentate H-bonds with the phosphate groups of nucleic acids while primary amine can only form monodentate H-bonds.¹²⁵ The distinct DNA binding affinity of guanidinium containing copolymers was no longer observable for the 40 mol% comonomer content at N/P ratio 20 (**Figure 3.4-E** and **-F**).

Although the DNA binding studies provided valuable information on the impact of comonomer distribution, they were not sufficient to reveal the nucleic acid delivery performance of the copolymers. For example, the release of DNA from polyplexes cannot occur at the right time and place if the binding is too strong. Therefore, as a guideline for shaping the future polymer designs, preliminary transfection studies were conducted on the polyplexes at N/P ratio 20 in CHO-K1 cells by means of luciferase expression assay. The luciferase expression was calculated as relative light unit (RLU) per microgram protein. Overall, guanidinium containing copolymers performed better DNA transfection than the primary amine bearing counterparts (the data has not shown). In comparison with primary amine bearing counterparts, the higher transfection performance of GCPs was observed in other studies as well.^{194, 196, 207-211} The copolymers with 90 mol% cationic comonomer content depicted the highest transfection efficiency for both P(HPMA-APMA) and P(HPMA-GPMA) copolymers (**Figure 3.5-A**). The higher nucleic acid delivery efficiency with the increase in the cationic charge density was also observed for other polymeric vectors including GCPs.^{32, 231-232} The influence of comonomer distribution on transfection efficiency was more pronounced for primary amine containing copolymers. The polyplexes consisting of P(HPMA-*stat*-APMA) copolymers with 90 mol% primary amine content showed higher DNA transfection with respect to the gradient counterparts. The reason could be stronger DNA binding due to the more localized charge distribution in gradient copolymers resulting in harder DNA release from the polyplexes. For

P(HPMA-GPMA) copolymers with 90 mol% guanidinium content, comonomer distribution did not depict any significant effect on transfection efficiency.

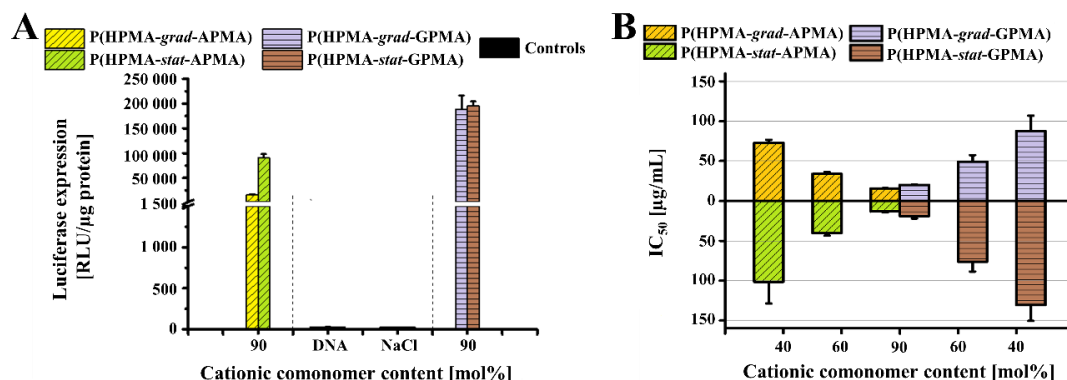


Figure 3.5 (A) *In vitro* luciferase reporter gene expression of pGL3 DNA/copolymer polyplexes at N/P ratio 20 in CHO-K1 cells compared to the negative controls; free DNA and sodium chloride (NaCl) (mean \pm SD). (B) Cationic comonomer content-dependent *in vitro* cell viability assay of P(HPMA-APMA) and P(HPMA-GPMA) copolymers in L-929 mouse fibroblasts (mean \pm SD).

Cationic polymers can cause toxic effects on biological membranes in various ways such as nanoscale pore formation, loss of membrane integrity, impairment of the metabolic activity, or change in the phospholipid composition of the lipid bilayer.³⁰⁶ Therefore, apart from the transfection studies, it was important to reveal the impact of comonomer distribution on cell viability. For this purpose, *in vitro* cell viability investigations on P(HPMA-APMA) and P(HPMA-GPMA) copolymers were conducted in L-929 mouse fibroblasts by 3-(4,5-dimethylthiazol-2-yl)-2,5-diphenyltetrazolium bromide (MTT) assay. The cells were incubated for 24 h in serum containing medium. Then, copolymer solutions with the concentrations ranging from 3.91 to 500 μ g/mL were added to the culture medium and the cells were further incubated for 24 h. Afterwards, the cells were treated with the MTT reagent for 4 h. Finally, half-maximal inhibitory concentration (IC₅₀) regarding the copolymer concentration were detected. For both P(HPMA-APMA) and P(HPMA-GPMA) with the cationic comonomer content lower than 40 mol%, IC₅₀ value could not be detected in the tested copolymer concentration range. Therefore, **Figure 3.5-B** illustrates the IC₅₀ values for the copolymers with equal to or higher than 40 mol% cationic comonomer content. Overall, the toxicity increased with the higher cationic charge content, which is commonly observed for cationic polymers.³² Higher cell viability was observed for guanidinium containing copolymers. This observation was opposite to the other studies on GCPs which compared the impact of cationic charge origin on cell viability.^{194, 196, 210-211} With respect to comonomer distribution, both guanidinium and primary amine containing copolymers with the statistical distribution showed lower toxicity in respect of gradient counterparts.

In conclusion, this study represents the first example of a comprehensive investigation on the impact of statistical and gradient comonomer distributions on DNA binding affinity for GCPs. Moreover, it utilizes valuable methodologies and results considering the synthesis, characterization of GCPs and their application for non-viral gene delivery. A facile synthesis of guanidinium and primary amine bearing poly(methacrylamide)s was achieved by RAFT polymerization. In addition to the utilization of batch- and semi-batch copolymerization techniques, the preliminary kinetical investigations on comonomer compositions helped to obtain the desired comonomer contents with statistical and gradient distributions. The hurdle in the determination of molar mass for the copolymers by SEC_{DMAc} and SEC_{water} was elegantly solved by HC method, which provided the absolute molar mass values of the copolymers. All copolymers showed a comparable absolute molar mass ($\sim 11\ 000\ \text{g mol}^{-1}$) with low dispersity indices ($D \sim 1.2$). DNA binding investigations revealed pronounced impact of comonomer distribution on the DNA binding affinity, especially for the copolymers with 5 mol% cationic comonomer content. Gradient comonomer distribution improved DNA binding affinity for both primary amine and guanidinium containing copolymers. Nevertheless, this effect was more pronounced for primary amine counterparts as the indication for the effect of cationic charge origin. In addition, cationic charge density influenced the impact of comonomer distribution on DNA binding affinity. As cationic comonomer content and N/P ratio increased, the the comonomer distribution related difference in DNA binding affinity became less significant. For the copolymers with 60 and 90 mol% cationic comonomer content, the difference in DNA binding was not recognizable with the utilized method. Preliminary transfection experiments in CHO-K1 cells showed that the polyplexes consisted of the copolymers with 90 mol% guanidinium performed higher transfection in comparison to primary amine counterparts at N/P ratio 20. The lower toxicity was observed for the statistical copolymers in L-929 mouse fibroblasts. These valuable observations opened the way of new polymer designs for guanidinium containing poly(methacrylamide)s by utilizing further strategies to improve nucleic acid delivery performance. Thus, the following chapter explains the influence of hydrophobic moieties, indole groups, in guanidinium containing poly(methacrylamide)s.

4. Impact of Indole Bearing Comonomer on DNA Delivery Efficiency

Parts of this chapter has been published in **P1**) Tabujew, I.; Cokca, C.; Zartner, L.; Schubert, U. S.; Nischang, I.; Fischer, D.; Peneva, K., The influence of gradient and statistical arrangements of guanidinium or primary amine groups in poly(methacrylate) copolymers on their DNA binding affinity. *J. Mater. Chem. B* **2019**, 7 (39), 5889-6066 and **P2**) Cokca, C.; Zartner, L.; Tabujew, I.; Fischer, D.; Peneva, K., Incorporation of Indole Significantly Improves the Transfection Efficiency of Guanidinium-Containing Poly(Methacrylamide)s. *Macromol. Rapid Commun.* **2020**, 41 (6), 1900668.

After revealing fundamental structure-activity relationships for guanidinium containing poly(methacrylamide) vectors, the focus was directed towards improving the transfection efficiency in comparison to current gold standards such as PEI^{205, 207-208, 219-220} and Lipofectamine^{TM214, 222-225}. For this purpose, viruses are good examples to mimic because they use the interplay of charge and polarity to cross extra- and intracellular barriers efficiently.³⁰⁷ The similar strategy has been applied for various cationic polymers (e.g., PEI, PLL, chitosan, polyamidoamines) by the inclusion of comonomers with a hydrophobic pendant groups to improve gene delivery efficiency.²³⁹ It was hypothesized that the increase in transfection efficiency of amphipathic polymeric vectors was a result of the enhanced binding of genetic materials and cellular uptake based on the combination of electrostatic and hydrophobic interactions.²⁴⁰

The same strategy has also been applied in a few studies on GCPs. Overall, inclusion of hydrophobic groups improved nucleic acid delivery efficiency in comparison to cationic counterparts.^{224, 231} In addition, it was shown that transfection efficiency is dependent on the origin of hydrophobic groups. For example, Wender and co-workers explored siRNA knockdown efficiency on guanidinium containing amphipathic oligocarbonates.²²⁴ Dodecyl and guanidinium containing oligocarbonates depicted the highest knockdown efficiency in comparison with hexyl and ethyl bearing counterparts at the same N/P ratio in HaCaT cells and primary keratinocytes. Tew and co-workers investigated siRNA delivery efficiency of a guanidinium containing poly(oxanorbornene) library with the block segments of dimethyl, methyl phenyl, diphenyl, diethyl, diisobutyl, or dicyclohexyl bearing hydrophobic comonomers.²⁴⁴ At the same N/P ratio, methyl phenyl, diisobutyl and diphenyl containing polymers performed superior siRNA internalization independent from the degree of hydrophobicity in Jurkat T cells and Hela cells. Montenegro and co-workers incorporated isovaleraldehyde, hexanal, 2-naphthaldehyde, and benzaldehyde groups into guanidinium containing poly(acrylamide)s.²⁴⁵ Only isovaleraldehyde bearing polymers could execute efficient siRNA knockdown in Hela cells. The same group also investigated guanidinium containing poly(acrylamide)s with the substitution of different fatty acid and aldehyde chains in respect of mRNA delivery efficiency in Hek293 cells.²⁴⁶ Myristoleic acid bearing polymers showed the best delivery performance while dodecanal counterparts could not transfect Hek293 cells.

In **Chapter 3.2**, it was shown that guanidinium containing poly(methacrylamide) copolymers with equal to or higher than 60 mol% guanidinium content could

efficiently bind to pGL3 plasmid independent from comonomer distribution. On the other hand, the preliminary transfection investigations depicted that these copolymers performed lower transfection efficiency in CHO-K1 cells in comparison to LPEI with similar molar mass. One possible reason could be the too tight binding of DNA due to high guanidinium content, which led to delayed release and/or poor translocation through the endosomal membrane. To overcome this challenge, an indole bearing methacrylamide comonomer, *N*-(2-indolethyl)methacrylamide (IEMA), was selected to prepare guanidinium containing amphipathic terpolymer (**Figure 4.1**). The selection of indole was based on its previously proved synergy with guanidinium. For instance, the amphipathic CPP ‘Penetratin’ can efficiently cross the cell membrane by means of indole and guanidinium groups.¹⁸⁶ The synthetic implication of guanidinium and indole bearing CPPs for siRNA delivery was achieved by Divita and co-workers.¹⁸¹ The transition of guanidinium and indole groups into synthetic polymers were done by Haeussler and co-workers in the form of poly(methacrylate)s for antimicrobial application.³⁰⁸ Hence, this study is the first example of indole and guanidinium containing polymeric vectors for non-viral gene delivery.

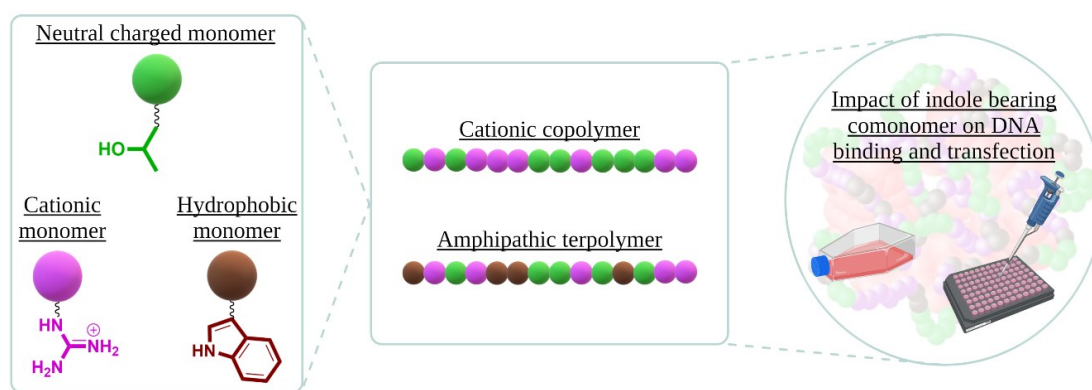


Figure 4.1 The general concept described in Chapter 4

4.1 Preparation and Physicochemical Characterization of Amphipathic Terpolymer

The amphipathic terpolymer containing guanidinium and indole groups was prepared by batch copolymerization. Nevertheless, RAFT polymerization of HPMA, GPMA and IEMA comonomers was challenging due to the poor solubility of IEMA in the aqueous reaction mixture. For this reason, preliminary studies on the reaction conditions were conducted to achieve well-defined P(HPMA-*co*-GPMA-*co*-IEMA) amphipathic terpolymer with equal to or higher than 60 mol% guanidinium content (**Table 4.1**). For all reactions, ACVA was employed as the initiator.

Table 4.1 Preliminary studies on polymerization of HPMA, GPMA, and IEMA comonomers

Polymerization Trails ^[a]	RAFT agent	Solvent [9:1 (v:v)]	Solubility of monomers			SEC _{DMAc} ^[b]	
			HPMA	GPMA	IEMA	<i>M_n</i> (g mol ⁻¹)	<i>Đ</i>
T1	CTA2	1 M Acetate Buffer/DMF	+	+	+	27 000	1.03
T2	CTA1	1 M Acetate Buffer/DMF	+	+	+	8 500	5.59
T3	CTA2	DMF/1 M Acetate Buffer	+	-	+	n.d.	n.d.
T4	CTA1	DMF/1 M Acetate Buffer	+	-	+	n.d.	n.d.
T5	CTA2	DMSO/ 4 M HCl in dioxane	+	+	+	n.d.	n.d.
T6	CTA1	DMSO/ 4 M HCl in dioxane	+	+	+	n.d.	n.d.

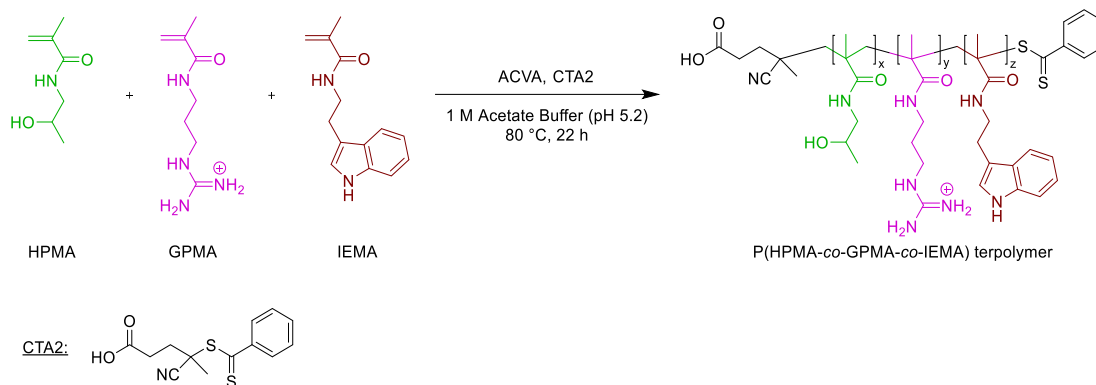
[a] $[M]_0/[CTA]_0$ was 200/1 and $[CTA]_0/[I]_0$, was 4/1 with 1 M final monomer concentration.

[b] DMAc + 0.21% LiCl was used as the eluent and PMMA was employed as the standard.

For achieving a successful RAFT polymerization, the selection of RAFT agent should be done carefully.²⁸⁴ In addition, it is important to find a proper solvent system where each reactant should have good solubility. For the trial reactions, two different RAFT agents were utilized: CTA1 and 4-cyano-4-(phenylcarbonothioylthio)pentanoic acid (CTA2) (**Scheme 4.1**). CTA1 is selected based on its compatibility for the polymerization of P(HPMA-*co*-GPMA) copolymers in the previous study while CTA2 was utilized for its more hydrophobic nature, which could ease the inclusion of IEMA comonomer by creating a hydrophobic microenvironment. Moreover, CTA2 is highly suitable for methacrylamide monomers. Apart from the selection of RAFT agent, different solvent systems were utilized to find the best solubility of each reactant. The trails T3 and T4 failed due to the precipitation of GPMA comonomer. Although each reactant depicted good solubility in the trials T5 and T6, the activity loss of CTA1 and CTA2 occurred because of hydrolysis and/or aminolysis. Thus, apparent molar mass and *Đ* values could not be determined (n.d.) for these trials. The best result was achieved in the trial T2. The reason could be a less polar microenvironment for IEMA provided by the presence of CTA2 and dimethylformamide (DMF) while 1 M acetate buffer (pH 5.2) helped to solubilize GPMA comonomer and kept the guanidinium moieties protonated to avoid the loss of CTA2 activity.

After finding the best reaction condition, P(HPMA-*co*-GPMA-*co*-IEMA) amphipathic terpolymer was synthesized by aiming at higher indole content (**Scheme 4.1**). P(HPMA-*co*-GPMA-*co*-IEMA) terpolymer was obtained with the comonomer content of 58 mol% GPMA, 16 mol% IEMA, and 26 mol% HPMA (**Table 4.2**). The attempt to increase the IEMA content higher than 20 mol% caused coagulation and precipitation during the polymerization reaction. As a result, the control over molar mass and molar mass distribution was lost. In addition, several studies on amphipathic GCPs indicated that the further increase in hydrophobic comonomer content can lead to low solubility of polymers in biological assays resulting in lower or loss of activity.^{223, 231, 241, 246} For the assessment of indole group impact on the DNA binding and transfection efficiency, P(HPMA-*co*-GPMA) copolymer with similar GPMA comonomer content was prepared. The synthesis of the copolymer was performed according to the previous study represented in **Chapter 3.1**. A comparable GPMA

comonomer content (53 mol%) was achieved (**Table 4.2**). Moreover, both polymer samples depicted comparable apparent molar mass ($\sim 20\,000\text{ g mol}^{-1}$) with low \mathcal{D} (~ 1.1).



Scheme 4.1 RAFT polymerization of P(HPMA-co-GPMA-co-IEMA) amphipathic terpolymers

Table 4.2 Overview of the selected physicochemical characteristics for P(HPMA-co-GPMA-co-IEMA) terpolymer and P(HPMA-co-GPMA) copolymer

Polymer samples	Comonomer content (mol%) ^[a]			SEC _{DMAc} ^[b]	
	HPMA	GPMA	IEMA	M_n (g mol ⁻¹)	\mathcal{D}
 P(HPMA-co-GPMA-co-IEMA)	26	58	16	19 000	1.13
 P(HPMA-co-GPMA)	47	53	-	18 000	1.09

[a] The comonomer contents were calculated by ¹H-NMR.

[b] DMAc + 0.21% LiCl was used as the eluent and PMMA was employed as the standard.

4.2 Biological Investigations on P(HPMA-co-GPMA-co-IEMA) Terpolymer and P(HPMA-co-GPMA) copolymer

Biological investigations were conducted by Leon Zartner (Institute of Pharmacy, Friedrich-Schiller-University Jena).

To reveal the impact of indole inclusion on cell viability, MTT assay was conducted on L-929 mouse fibroblasts for the polymer samples by increasing the polymer concentration (**Figure 4.2-A**). In comparison to the cationic copolymer counterpart, lower cell viability was observed for the amphipathic terpolymer at the concentrations

equal to or higher than $31.25 \mu\text{g mL}^{-1}$. The similar observation was also reported for indole bearing peptides.^{182, 309} For instance, Jobin et al. in 2015 synthesized arginine-rich peptide analogues.¹⁸² The change of phenylalanine residues into tryptophan resulted in higher cytotoxicity. For the assessment of cell death mechanism, cellular caspase 3/7 activity assay was performed as a measure for apoptosis following the incubation of L-929 mouse fibroblasts with the copolymer and terpolymer at various polymer concentrations (**Figure 4.2-B** and **-C**).²⁴⁷ Both P(HPMA-*co*-GPMA-*co*-IEMA) terpolymer and P(HPMA-*co*-GPMA) copolymer did not lead to any apoptotic events. Hence, this observation suggested that the cell death was probably the result of non-apoptotic pathway.

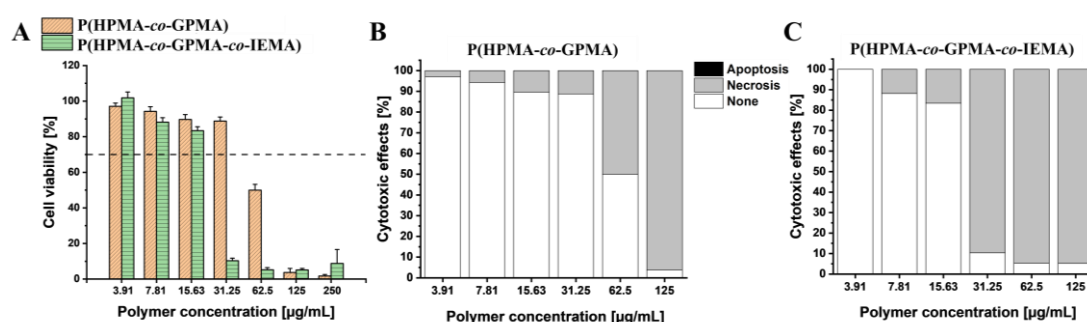


Figure 4.2 (A) Cell viability assay on L-929 mouse fibroblasts with increasing polymer concentrations ($n = 7 \pm \text{SD}$). Apoptosis versus necrosis and viability (B) for P(HPMA-*co*-GPMA) copolymer and (C) for P(HPMA-*co*-GPMA-*co*-IEMA) terpolymer determined by caspase activity Caspase-Glo 3/7 assay ($n = 3 \pm \text{SD}$).

The quantitative DNA binding for P(HPMA-*co*-GPMA-*co*-IEMA) terpolymer and P(HPMA-*co*-GPMA) copolymer was investigated by AccuBlue™ assay by employing pGL3 plasmid (**Figure 4.3-A**). For both polymer samples, more than 90% of DNA in the assay media could efficiently join to the polyplex formation even at N/P ratio 1. At N/P ratio 20, the copolymer and terpolymer depicted similar binding affinities in comparison to IPEI ($M_{n\text{IPEI}} \sim 2\,500 \text{ g mol}^{-1}$) under optimized conditions. The inclusion of hydrophobic groups into cationic polymers can affect hydrodynamic diameter (HD) and zeta potential (ZP) of polyplexes.²³⁹ Thus, HD and ZP of the polyplexes at N/P ratios ranging from 2 to 20 were measured through dynamic light scattering (DLS) and laser Doppler anemometry (LDA), respectively (**Figure 4.3-B**). The sizes of polyplexes varied between 75 and 200 nm independent from the polymer type. At N/P ratio 20, P(HPMA-*co*-GPMA-*co*-IEMA)/DNA polyplexes showed a slight trend to agglomeration. Both P(HPMA-*co*-GPMA-*co*-IEMA)/DNA and P(HPMA-*co*-GPMA)/DNA polyplexes showed similar trend regarding ZP. ZP values for the polyplexes rose from 30 mV to 60 mV with the increase in N/P ratio.

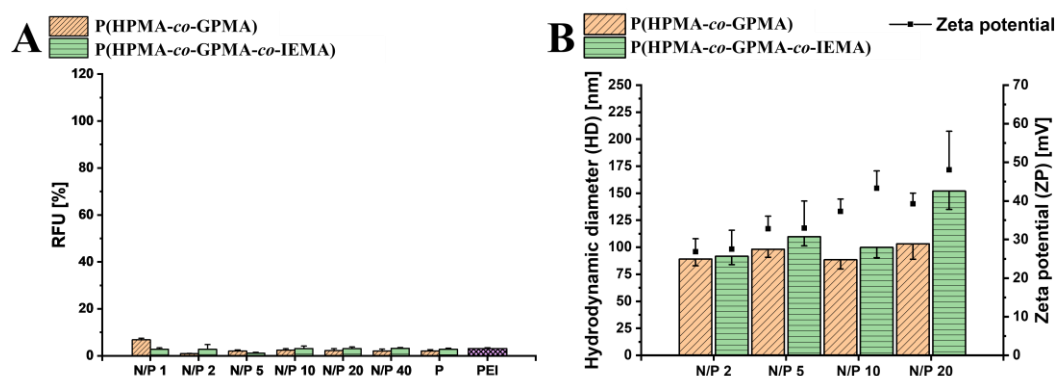


Figure 4.3 (A) Quantitative DNA binding assessment for P(HPMA-*co*-GPMA) copolymer and P(HPMA-*co*-GPMA-*co*-IEMA) terpolymer by AccuBlue™ assay including free polymers (P) and IPEI/DNA polyplexes (PEI) ($M_{nIPEI} \sim 2\,500\text{ g mol}^{-1}$, N/P 20) ($n = 4 \pm \text{SD}$) (B) Hydrodynamic diameters (HD) and zeta potentials (ZP) of P(HPMA-*co*-GPMA)/DNA and P(HPMA-*co*-GPMA-*co*-IEMA)/DNA polyplexes with a cumulative analysis of HD and ZP ($n = 4 \pm \text{SD}$).

Transfection studies were performed in CHO-K1 cells (**Figure 4.4-A** and **-B**). The reporter gene expression was calculated as RFU obtained by the bioluminescence measurements. Free DNA was used as a control, which did not show detectable gene expression. Both polyplexes could transfect CHO-K1 cells at N/P ratio equal to or lower than 20. At N/P ratio 20, nonetheless, they showed lower transfection efficiency in comparison with the positive control (IPEI/DNA polyplexes) under the selected conditions. At N/P ratio higher than 20, both polyplexes did not show any significant transfection ability either because of high toxicity or too strong binding to DNA. This reduction effect started to be recognized for P(HPMA-*co*-GPMA)/DNA polyplexes at N/P ratio 20. At the same N/P ratio, on the other hand, P(HPMA-*co*-GPMA-*co*-IEMA)/DNA polyplexes could induce ~ 200 times higher transgene expression in comparison with P(HPMA-*co*-GPMA)/DNA polyplexes. Such a big difference might be related to the better release of DNA upon the inclusion of indole as hydrophobic pendant groups. Moreover, the presence of indole and guanidinium groups in the polymer chains might ease the cellular uptake, which has been already shown in CPPs.^{182, 310} Furthermore, based on recent findings, it can be hypothesized that ion pair- π interactions play an important role on the higher transfection efficiency of P(HPMA-*co*-GPMA-*co*-IEMA)/DNA polyplexes.¹⁸³ P(HPMA-*co*-GPMA-*co*-IEMA)/DNA polyplexes could also transfect CHO-K1 cells in the presence of serum, which is generally not possible for the cationic polymers with very high charge density due to the interactions with serum proteins.¹⁹³

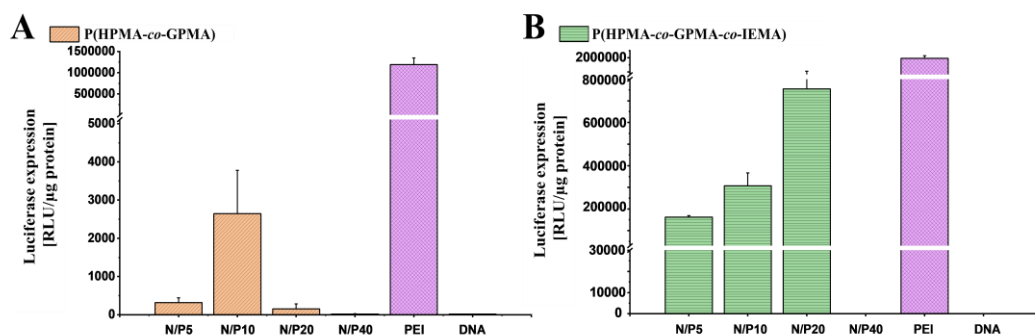


Figure 4.4 Transfection studies of (A) P(HPMA-co-GPMA) copolymer (B) P(HPMA-co-GPMA-co-IEMA) terpolymer in CHO-K1 cells (DNA: 4 μg pGL3 plasmid, PEI: $M_{\text{nPEI}} \sim 2\,500\text{ g mol}^{-1}$, N/P 20).

In summary, the incorporation of hydrophobic groups into cationic polymers is commonly used as a strategy to improve transfection efficiency. Based on this strategy, the first example of water-soluble poly(methacrylamide) containing indole and guanidinium moieties was synthesized by RAFT polymerization. The polymerization condition was adopted to achieve the inclusion of indole bearing comonomers into guanidinium containing poly(methacrylamide)s with high cationic charge content. The change in RAFT agent and the addition of small amount of DMF enabled to obtain well-defined terpolymer with apparent molar mass of $\sim 20\,000\text{ g mol}^{-1}$ and $D \sim 1.1$. To reveal the impact of indole incorporation, a guanidinium bearing copolymer counterpart was prepared by aiming similar apparent molar mass and guanidinium content. Biological investigations on the polymer samples indicated that the presence of indole decreased cell viability slightly in L-929 mouse fibroblasts but the transfection efficiency was improved over 200-fold in CHO-K1 cells. Based on the utilized methodologies, the explanation for the difference in transfection performance could not be explained directly. Nevertheless, by considering previous studies, it can be speculated that combination of hydrophobic and electrostatic interactions resulted in easier DNA release. In addition, the presence of ion pair- π interactions due to the presence of indole and guanidinium moieties could improve interaction with the cell membrane, which resulted in higher cellular uptake. However, the performance of amphipathic polymeric vectors is highly dependent on the origin of the utilized hydrophobic pendant groups. Hence, the next chapter depicts the investigations on other bioinspired hydrophobic groups in guanidinium containing amphipathic terpolymers.

5. The Impact of Hydrophobic Group Origin on DNA Delivery Efficiency

Parts of this chapter has been published in **P2)** [Cokca, C.](#); Zartner, L.; Tabujew, I.; Fischer, D.; Peneva, K., Incorporation of Indole Significantly Improves the Transfection Efficiency of Guanidinium-Containing Poly(Methacrylamide)s. *Macromol. Rapid Commun.* **2020**, *41* (6), 1900668 and **P3)** Hack, F. J.; [Cokca, C.](#); Städter, S.; Hülsmann, J.; Peneva, K.; Fischer, D., Indole, Phenyl, and Phenol Groups: The Role of the Comonomer on Gene Delivery in Guanidinium Containing Methacrylamide Terpolymers. *Macromol. Rapid Commun.* **2020**, *42* (8), 2000580.

In the previous chapter, indole bearing methacrylamide comonomer was selected to mimic of the tryptophan side chain to obtain guanidinium and indole containing amphipathic poly(methacrylamide) terpolymer. The inclusion of indole led to ~200-fold increase in DNA transfection efficiency in CHO-K1 cells by comparison with the guanidinium containing copolymer with a comparable guanidinium content. This increase could be related with higher cellular uptake by the ion pair- π interactions, which was discovered in CPPs.¹⁸³ However, to what extent indole, as the hydrophobic group, influenced the transfection efficiency in the amphipathic terpolymer was not clear. In different studies on GCPs, the importance of hydrophobic group origin was already emphasized.^{224, 244-246} Therefore, guanidinium containing poly(methacrylamide) terpolymers with different bioinspired hydrophobic comonomers were designed. In addition to indole containing comonomers described in the previous chapter, phenyl and hydroxyphenyl were selected as the side chains of the hydrophobic comonomers, which are the pendant groups of phenylalanine and tyrosine, respectively. Like indole, phenyl and hydroxyphenyl are commonly involved in various biochemical processes by creating cation- π interactions with guanidinium group of arginine.¹⁶⁷⁻¹⁷² Such a relationship between guanidinium and these hydrophobic groups could also influence the transfection efficiency. Therefore, this chapter reports the first comparison of DNA delivery efficiency for indole, phenyl, and hydroxyphenyl in guanidinium containing poly(methacrylamide) terpolymers.

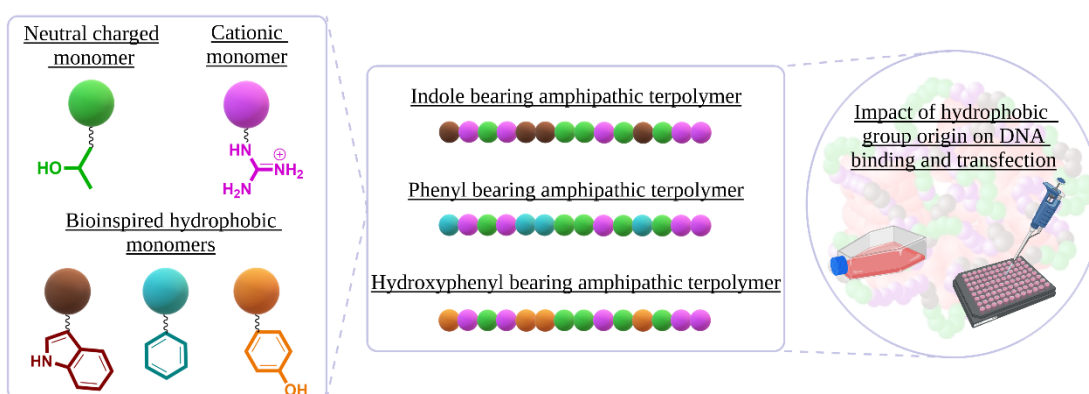
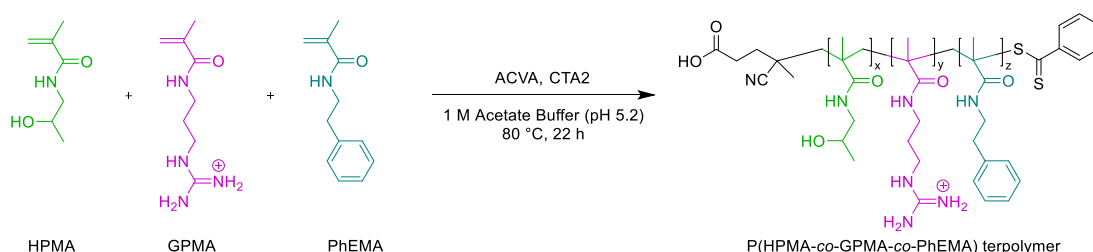


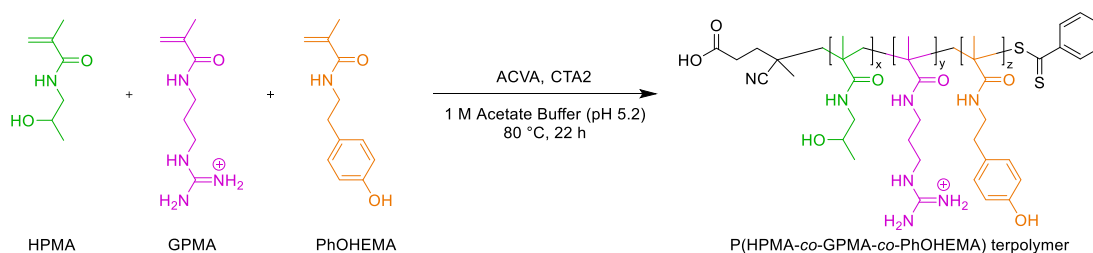
Figure 5.1 The general concept described in Chapter 5

5.1 Preparation and Physicochemical Characterization of Amphipathic Terpolymers

The synthesis of indole bearing terpolymer was achieved as stated in **Chapter 4.1**. For the synthesis of phenyl and hydroxyphenyl containing terpolymers *N*-Phenethylmethacrylamide (PhEMA) and *N*-(4-hydroxyphenethyl) methacrylamide (PhOHEMA) comonomers were employed, respectively (**Scheme 5.1** and **5.2**). The polymerization conditions for P(HPMA-*co*-GPMA-*co*-PhEMA) and P(HPMA-*co*-GPMA-*co*-PhOHEMA) terpolymers did not require further optimization. For each terpolymer sample the hydrophobic monomer content was aimed as 4 mol% in order to obtain more biocompatible terpolymers without losing the impact of hydrophobic comonomers on DNA binding and transfection efficiency. The reactions were conducted with 1 M final monomer concentration by aiming $[M]_0/[CTA]_0=200/1$ and $[CTA]_0/[I]_0=4/1$. Physicochemical characterization of the terpolymers were performed through $^1\text{H-NMR}$ spectroscopy and SEC_{DMAc} (**Table 5.1**). Well-defined terpolymers with comparable hydrophobic comonomer contents and apparent molar mass were successfully obtained.

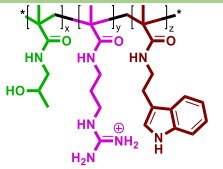
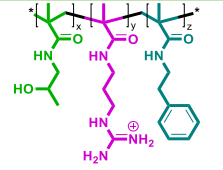
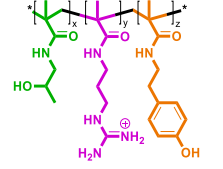


Scheme 5.1 RAFT polymerization of P(HPMA-*co*-GPMA-*co*-PhEMA) amphipathic terpolymer



Scheme 5.2 RAFT polymerization of P(HPMA-*co*-GPMA-*co*-PhOHEMA) amphipathic terpolymer

Table 5.1 Overview of the selected physicochemical characteristics for the prepared terpolymers

Polymer samples	Comonomer content (mol%) ^[a]					SEC _{DMAc} ^[b]	
	HPMA	GPMA	IEMA	PhEMA	PhOHEMA	<i>M_n</i> (g mol ⁻¹)	<i>D</i>
 <p>P(HPMA-co-GPMA-co-IEMA)</p>	21	75	4	-	-	23 000	1.07
 <p>P(HPMA-co-GPMA-co-PhEMA)</p>	12	84	-	4	-	15 000	1.14
 <p>P(HPMA-co-GPMA-co-PhOHEMA)</p>	12	85	-	-	3	15 000	1.07

[a] The comonomer contents were calculated by ¹H-NMR.

[b] DMAc + 0.21% LiCl was used as the eluent and PMMA was employed as the standard.

5.2 Biological Investigations on the Prepared Amphipathic Terpolymers

Biological investigations were conducted by Franz J. Hack (Institute of Pharmacy, Friedrich-Schiller-University Jena).

The toxicity assessment for the terpolymer samples were performed by means of CellTiter-Glo® luminescent cell viability assay on L-929 mouse fibroblasts for the terpolymer concentrations ranging from 3.9 to 500 µg mL⁻¹ over 24 h (**Figure 5.2-A**). The cells, which were not treated with the terpolymers, were set as 100% negative control. 0.02% thiomersal solution were used as the positive control. The three terpolymer samples depicted almost comparable IC₅₀ values: 28.1, 33.0, and 34.7 µg mL⁻¹ for P(HPMA-co-GPMA-co-IEMA), P(HPMA-co-GPMA-co-PhEMA), and P(HPMA-co-GPMA-co-PhOHEMA) terpolymers, respectively. With the selected hydrophobic comonomer content (4 mol%), therefore, there was no significant influence of hydrophobic comonomer origin on the cell viability. In addition to the cell viability assay, the hemocompatibility of terpolymers with erythrocytes was investigated (**Figure 5.2-B**). Sheep red blood cells were incubated for 1 h with varying concentration of the terpolymer samples. Afterwards, the hemoglobin release, the common indication for the membrane damage of erythrocytes, was detected by the spectrophotometric measurements. For all terpolymers, the mean values of hemolysis

were below 2%. The observed values can be considered as non-hemolytic based on the ASTM F756-08 standard.³¹¹

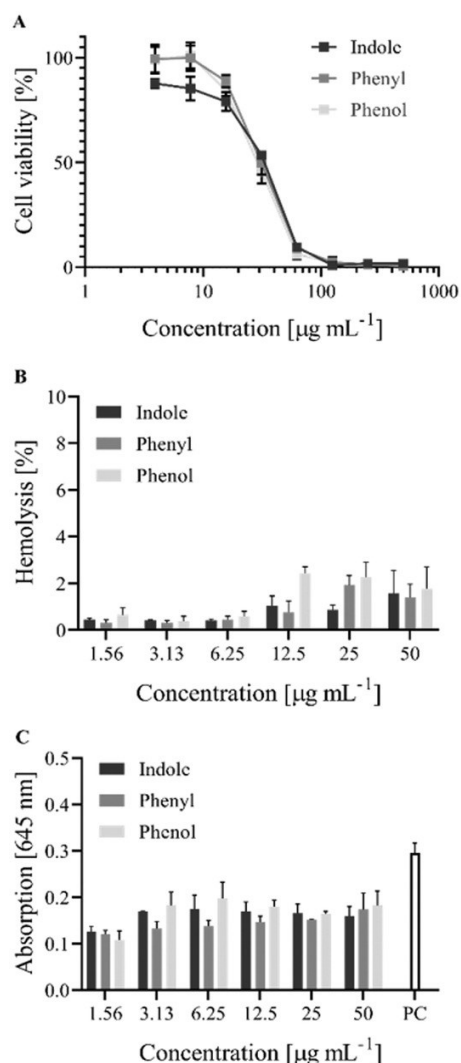


Figure 5.2 (A) Concentration-dependent *in vitro* cell viability assay of the terpolymers (named according to the pendant groups of the hydrophobic comonomers) in L-929 mouse fibroblasts after 24 h incubation by the CellTiter-Glo® luminescent cell viability assay ($n = 8$, mean \pm SD). (B) Dependency of hemolysis after 1 h incubation and (C) Polymer concentration dependent sheep erythrocyte aggregation after 2 h incubation induced by the terpolymers in comparison to $15 \mu\text{g mL}^{-1}$ bPEI ($M_n \sim 25\,000 \text{ g mol}^{-1}$) (PC) ($n = 6$, mean \pm SD).

The potential of terpolymer induced aggregation of erythrocytes was quantitatively investigated in sheep red blood cells by UV-Vis spectroscopy (**Figure 5.2-C**). A decrease in the UV-Vis absorption at 645 nm was expected upon the aggregation of erythrocytes. All terpolymer samples showed comparable absorption values to the negative control, hemoglobin (0.15). Therefore, the origin of hydrophobic

comonomers did not represent any significant impact on hemocompatibility profiles of indole, phenyl, and hydroxyphenyl bearing terpolymers.

The impact of hydrophobic pendant group origin on DNA binding was determined by AccuBlue™ assay (**Figure 5.3-A**). Naked DNA served as 100% control while DNA/IPEI polyplexes (LPEI) ($M_{n\text{IPEI}} \sim 2\,500\text{ g mol}^{-1}$, N/P ratio 20) was employed as positive control. The terpolymers in the absence of DNA (P) did not show any signals related to the non-specific polymer effects.

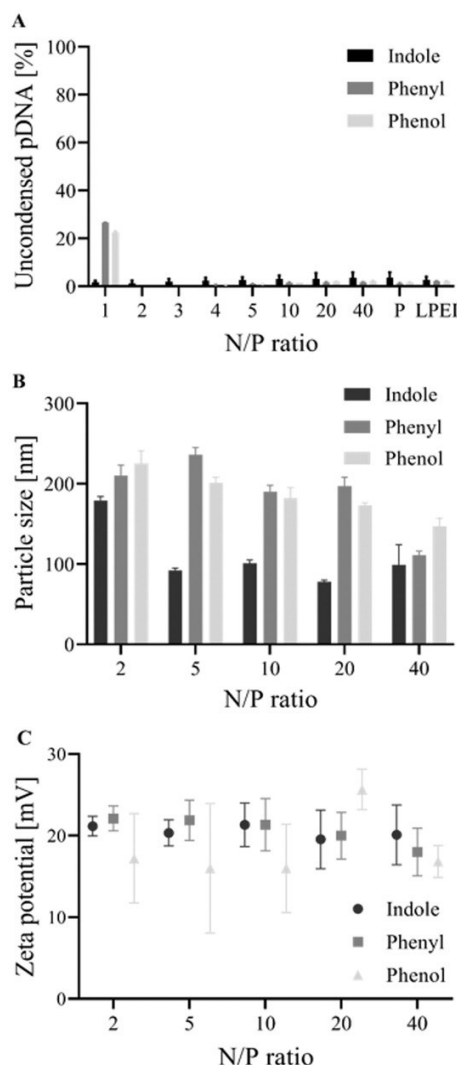


Figure 5.3 (A) N/P ratio dependent DNA binding capacity [%] of the terpolymers (named according to the pendant groups of the hydrophobic comonomers) determined by AccuBlue™ assay in comparison to DNA/IPEI polyplexes (LPEI) ($M_{n\text{IPEI}} \sim 2\,500\text{ g mol}^{-1}$, N/P ratio 20) and free polymers (P) ($n = 8$, mean \pm SD). (B) N/P ratio dependent particle size measurements of DNA/terpolymer polyplexes by nanoparticle tracking analysis (mean \pm SD measured in triplicates). (C) N/P ratio dependent zeta potential measurements of polyplexes by LDA (mean \pm SD measured in triplicates).

The influence of hydrophobic group origin on DNA binding was observed at N/P ratio 1. Although indole bearing terpolymer could provide an efficient DNA binding at all N/P ratios, phenyl and hydroxyphenyl containing terpolymers showed efficient DNA binding starting from N/P ratio 2. The better binding of indole containing terpolymer could be the result of the higher tendency for cation- π interaction of guanidinium with indole in comparison to phenyl and hydroxyphenyl.¹⁷² At N/P ratio equal to or higher than 2, all terpolymer samples showed similar DNA binding efficiency to the IPEI. Parallel increase in nucleic acid binding efficiency to the increase in N/P ratio is a well-known phenomenon for cationic polymers.³¹² Nanoparticle tracking analysis revealed the overall polyplex size reduction regarding the increase in N/P ratio (**Figure 5.3-B**). In comparison with phenyl and hydroxyphenyl bearing terpolymer/DNA polyplexes, indole bearing terpolymer/DNA polyplexes depicted the mean polyplex size below 100 nm by starting N/P ratio 5. Phenyl and hydroxyphenyl bearing terpolymer/DNA polyplexes represented mean particle sizes below 200 nm at N/P ratio starting from 10. As a result, all terpolymers formed nano-sized particles ranges below 200 nm, which is suitable for systemic delivery.³¹³ Zeta potentials of the polyplexes were around +20 mV independent from N/P ratio. The positive net charge can be considered as the indication of tightly packed DNA and high colloidal stability (**Figure 5.3-C**).³¹⁴

The influence of different hydrophobic side chains on transfection efficiency was investigated in eukaryotic CHO-K1 cells in the presence of serum using the pGL3 plasmid DNA/terpolymer polyplexes at N/P ratios ranging from 2 to 20 (**Figure 5.4**). Free DNA, as the negative control, did not show any specific reaction. N/P ratio dependent transfection efficiency was observed. At all N/P ratios, indole bearing polyplexes represented the highest transfection efficiency, which was followed by hydroxyphenyl and phenyl containing polyplexes, respectively. This result was parallel to the observation in binding studies, which could be related with the guanidinium tendency for cation- π interaction with indole, hydroxyphenyl and phenyl groups.¹⁷² In addition, it can be speculated that the special transfection performance of indole and guanidinium containing terpolymer could be related with their efficient ion pair- π interactions.¹⁸⁶ Nevertheless, under the chosen condition the positive control IPEI/DNA polyplexes at N/P ratio 20 (PC) performed 2-fold higher transfection in comparison to the indole containing terpolymer. In comparison to phenyl containing counterparts, the higher transfection efficiency by the hydroxyphenyl bearing terpolymer/DNA polyplexes could occur because of the additional polar interactions (e.g., the formation of counterions) or the formation of OH-related hydrogen bonds with DNA.³¹⁵ Moreover, the difference in transfection efficiency can be related with the hydrophobic group dependent dissimilarities in DNA release from the endosomal/lysosomal compartments.³¹⁶ However, proving these assumptions were not possible with the available physicochemical and biophysical characterization methods.

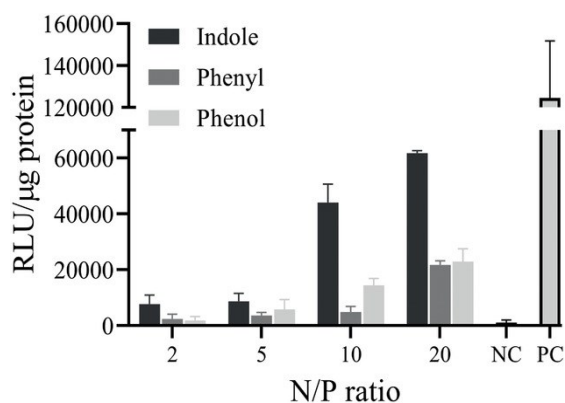


Figure 5.4 *In vitro* luciferase reporter gene expression of pGL3 plasmid DNA/terpolymer polyplexes at different N/P ratios in CHO-K1 cells compared to the positive control (PC) ($M_{n\text{IPEI}} \sim 2\,500\text{ g mol}^{-1}$, N/P ratio 20). Experiments were performed in quadruplicates and free DNA served as the negative control (NC) (mean \pm SD).

In summary, this study proved the versatility of RAFT polymerization by the preparation of well-defined guanidinium containing poly(methacrylamide) terpolymers, in which indole, phenyl, and hydroxyphenyl bearing methacrylamide comonomers were utilized. The selection of hydrophobic groups was done according to the bioinspired mimics for the pendant groups of tryptophan, phenylalanine, and tyrosine. The impact of hydrophobic group origin on DNA binding, transfection efficiency, and biocompatibility were investigated. Even at high concentrations, all terpolymers showed a marked cyto- and hemocompatibility independent from hydrophobic groups, which could happen due to low hydrophobic comonomer content ($\sim 4\text{ mol}\%$) in comparison to guanidinium content ($\sim 80\text{ mol}\%$). All terpolymers showed small particle size ($< 200\text{ nm}$) and comparable zeta potential ($+20\text{ mV}$), which were the indication for efficient polyplex formation. On the other hand, the impact of hydrophobic group origin was pronounced in transfection studies. Indole containing terpolymers showed the highest transfection performance in CHO-K1 cells. Explaining the effect of indole in comparison to phenyl and hydroxyphenyl was not possible with the available methods. Since indole bearing terpolymers performed the highest transfection efficiency among all prepared polymers, a further strategy for the improvement of biocompatibility were applied on indole bearing terpolymers, which is represented in the next chapter.

6. Improving the Biocompatibility of Guanidinium and Indole Containing Terpolymers

Parts of this chapter has been published in **P3**) Hack, F. J.; Cokca, C.; Städter, S.; Hülsmann, J.; Peneva, K.; Fischer, D., Indole, Phenyl, and Phenol Groups: The Role of the Comonomer on Gene Delivery in Guanidinium Containing Methacrylamide Terpolymers. *Macromol. Rapid Commun.* **2020**, *42* (8), 2000580 and **P4**) Cokca, C.; Hack, F. J.; Costabel, D.; Herwig, K.; Hülsmann, J.; Then, P.; Heintzmann, R.; Fischer, D.; Peneva, K., PEGylation of Guanidinium and Indole Bearing Poly(methacrylamide)s – Biocompatible Terpolymers for pDNA Delivery. *Macromol. Biosci.* **2021**, *21* (10), 2100146.

Despite of promising *in vitro* results, only a limited number of polymeric vectors is accepted for clinical studies.³² The most common bottleneck is the high cationic charge content, which creates safety and low performance issues after the systemic administration of polyplexes.^{305-306, 317} For instance, negatively charged proteins in the blood can interact with the positively charged polyplexes, which forms a protein corona leading to dramatic reduction in nucleic acid delivery efficiency. In addition, the high ionic strength of physiological environments can decrease the colloidal stability of polyplexes, which leads to aggregation of the particles, and thus fast clearance of the polyplexes from the blood stream. Beside undesired interactions with blood components, high cationic charge content can cause the disruption in physiological membranes. The most common strategy to overcome these limitations is the inclusion of neutral charged polymers into cationic polymers.^{248, 318-321} As a result, the cationic charges on the surface of polyplexes can be masked, which is so often called ‘the stealth effect’.

The ‘stealth effect’ of PEG was described for the first time by Davis and co-workers in 1977.³²² The inclusion of PEG into bioactive molecules and macromolecules was called as PEGylation.³²³ The impact of PEG has been widely investigated in different delivery systems including non-viral gene delivery.³² It was shown that the chain architecture and molar mass of PEG, density of PEG on the particle surface, the attachment way of PEG affect interactions of polyplexes with biological systems significantly.³²⁴⁻³²⁸ Most of the PEGylation studies for polymeric vectors were conducted on primary or tertiary amine bearing polymers such as PEI.³²⁹⁻³³³ On the other hand, this strategy was employed for GCPs only in very few studies.^{206, 210, 214, 249-252} The general observation for PEGylated GCPs was in accordance with other PEGylated polymeric vectors. Upon PEGylation, the biocompatibility of polyplexes increased while nucleic acid delivery efficiency of GCPs reduced.^{224, 249} Hence, structure-function optimizations for PEGylated GCPs are fundamental, which has not been studied thoroughly. This chapter depicts the first example of a systematic structure-activity study on PEGylated GCPs.

For this purpose, the best performing polymer, indole and guanidinium containing poly(methacrylamide) terpolymer, were selected to be PEGylated because the presence of high cationic charge content (≥ 60 mol%) and indole caused a significant decrease in the cell viability in L-929 cells at polymer concentrations equal to or higher than $31.25 \mu\text{g mL}^{-1}$ (**Chapter 5.2**). For the PEGylation a brush-type of PEG,

nona(ethylene glycol)methyl ether methacrylate (MEO₉MA) monomer, was selected. It bears multiple PEG chains as the pendant group which provides a higher PEG density comparing to linear PEG with the same DP. The higher PEG density on the nanoparticle surface can provide certain advantages such as smaller intermolecular spacing on the surface of polyplexes, denser hydration shell, better resistance to blood shear flow.³³⁴⁻³³⁸ Moreover, MEO₉MA bearing cationic polymers showed improved biocompatibility in the previous investigations.³³⁹⁻³⁴³ Furthermore, as a type of vinyl monomer, MEO₉MA monomer offers versatility because it can be incorporated into cationic polymers by RAFT polymerization.³⁴⁴⁻³⁴⁵ Therefore, the incorporation of MEO₉MA blocks with increasing length into indole and guanidinium containing terpolymer was performed by RAFT polymerization (**Figure 6.1**).

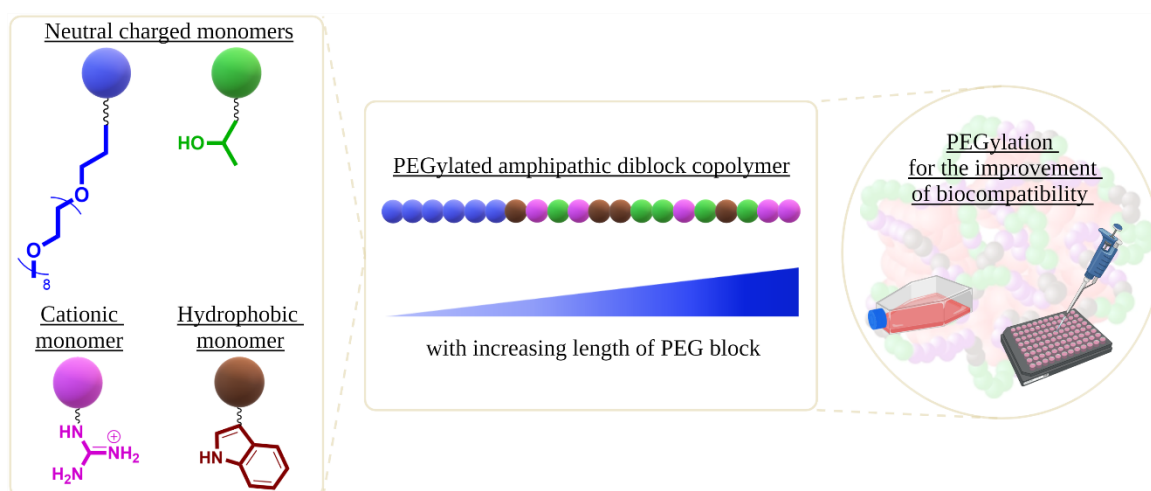


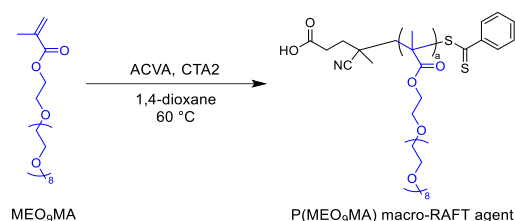
Figure 6.1 The general concept described in Chapter 6

6.1 Synthesis and Physicochemical Characterizations of Diblock Copolymers

RAFT polymerization is a versatile method for obtaining well-defined block copolymers because of its 'living character'. The presence of thiocarbonylthio end-group at the ω -end of the polymer chains enables the block extension by further monomer addition in sequential polymerization process.²⁸⁴ By taking the advantage of this phenomenon, PEGylated diblock copolymers were prepared by RAFT polymerization in two steps. The first step was the synthesis of P(MEO₉MA) macro-RAFT agents with different chain lengths, which served as the RAFT agent in the second step for the block extension with HPMA, GPMA and IEMA comonomers.

6.1.1 Synthesis and physicochemical characterization of P(MEO₉MA) macro-RAFT agents

For the polymerization reactions, the selection of RAFT agent was done based on its suitability with all incorporated monomers in order to achieve narrow molar mass distribution.³⁴⁶ The suitability of CTA2 for HPMA, GPMA and IEMA monomers was proved in **Chapter 4.1**. MEO₉MA monomer suitability for CTA2 was validated through the previous kinetic studies conducted by Jessica Tom (Institute of Organic Chemistry and Macromolecular Chemistry, Friedrich-Schiller-University Jena). Therefore, CTA2 was used for the synthesis of P(MEO₉MA) macro-RAFT agents. The polymerization reactions were carried out in 1,4-dioxane with the monomer concentration of 1 M (**Scheme 6.1**). The molar mass of P(MEO₉MA) macro-RAFT agents was aimed ranging from 3 000 to 40 000 g mol⁻¹, which was achieved by changing $[M]_0/[CTA]_0$ ratio while keeping $[CTA]_0/[I]_0$ ratio constant (**Table 6.1**). In order to diminish the formation of dead chain ends during the synthesis of P(MEO₉MA) macro-RAFT agents, monomer conversion was aimed to be kept below 70%.³⁴⁶ The reactions were monitored by ¹H-NMR spectroscopy. SEC_{DMAc} was utilized for the determination of apparent molar mass and \bar{D} (**Table 6.1**). The synthesized P(MEO₉MA) macro-RAFT agents was named according to the targeted molar mass in kg mol⁻¹. Overall, P(MEO₉MA) macro-RAFT agents displayed a good control over molar mass distribution ($\bar{D} \sim 1.2$), which were ready to be utilized for the block extension.



Scheme 6.1 RAFT polymerization of P(MEO₉MA) macro-RAFT agent

Table 6.1 Overview of reaction conditions and the selected physicochemical characteristics of P(MEO₉MA) macro-RAFT agents

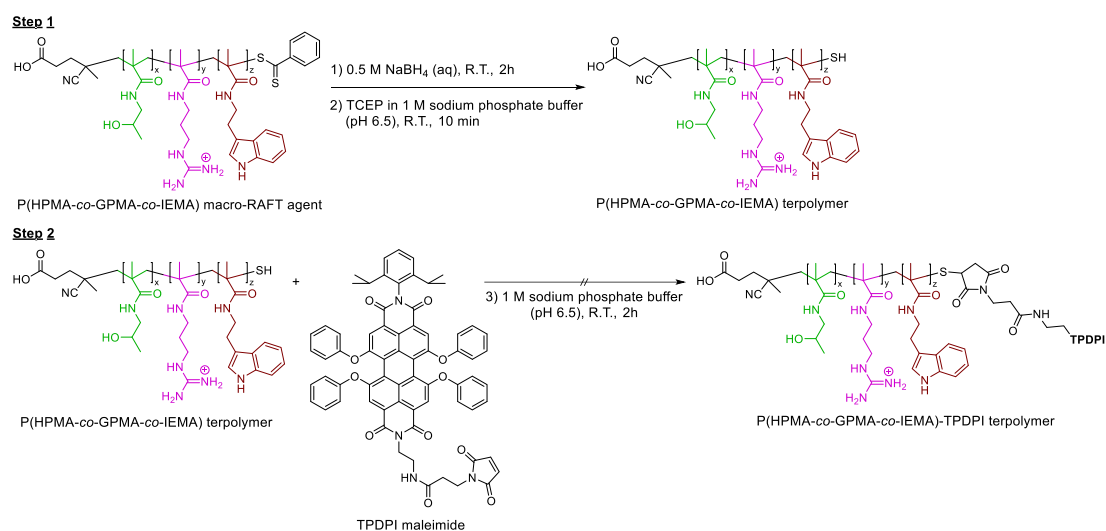
Polymer sample	$[M]_0/[CTA]_0/[I]_0$ ratio	T (°C)	t	SEC _{DMAc} ^[a]	
				M_n (g mol ⁻¹)	\bar{D}
P(MEO ₉ MA)3	15/1/0.25	60	200 min	3 000	1.22
P(MEO ₉ MA)6	25/1/0.25	60	200 min	6 500	1.13
P(MEO ₉ MA)10	53/1/0.25	60	200 min	10 000	1.18
P(MEO ₉ MA)15	85/1/0.25	60	200 min	15 000	1.17
P(MEO ₉ MA)20	110/1/0.25	60	200 min	20 000	1.22
P(MEO ₉ MA)30	220/1/0.25	60	200 min	31 000	1.28
P(MEO ₉ MA)40	320/1/0.25	60	200 min	44 000	1.40

[a] DMAc + 0.21% LiCl was used as the eluent and PMMA was employed as the standard.

6.1.2 Synthesis and Physicochemical Characterization of Fluorescently Labeled P(MEO₉MA-*co*-PMIM) Macro-RAFT Agents

Polymeric vectors with imaging capabilities can combine efficient nucleic acid delivery with tracking of the polyplexes through extra- and intracellular barriers by means of image-based systems such as fluorescence spectroscopy.³² In general, it is expected that chromophores should represent high extinction coefficient and quantum yield.³⁴⁷ In addition, for both *in vitro* and *in vivo* examinations, the chromophore should be selected by considering its spectral properties in aqueous media, its chemical stability regarding the cell metabolism, and its biocompatibility.³⁴⁸ Moreover, the chromophores with absorption and emission maxima above 500 nm in aqueous media can provide additional advantage on the elimination of the background noise coming from fluorescent impurities and the auto-fluorescence of the examined biological constitutions. However, finding a chromophore fulfilling all the mentioned criteria is quite difficult. For example, the chromophores with absorption and emission maxima above 500 nm (e.g., perylene, terylene) have further aromatic group extension in the main scaffold of naphthalene, which dramatically reduces the water-solubility. As a result, their utilization on biological applications is much harder although they represent excellent photochemical properties.

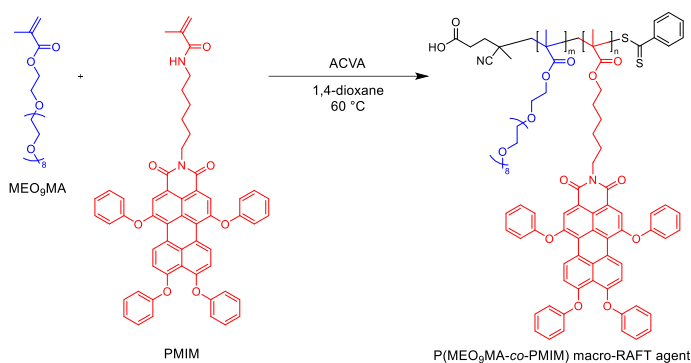
Hydrophobicity of the chromophore can also create hurdles in their conjugation to highly charged polymers due to their incompatible nature. For instance, indole and guanidinium containing poly(methacrylamide) terpolymer (with 75 mol% GPMA) was tested for the covalent labeling of a maleimide functionalized perylene diimide derivative (TPDPI maleimide) by a postpolymerization labelling method, which consisted of the reduction of RAFT agent and thiol-maleimide “click” reaction (Scheme 6.2).^{288, 349}



Scheme 6.2 Fluorescent labeling on P(HPMA-*co*-GPMA-*co*-IEMA) terpolymer by postpolymerization modification

Briefly, dithioester groups at the end of the polymer chains were reduced by utilization of 0.5 M aqueous sodium borohydride (NaBH_4) and dialyzed for two days.³⁵⁰ After freeze-drying of the reduced polymer, the sample was treated with 5 molar equivalents of tris(2-carboxyethyl)phosphine (TCEP) hydrochloride in 1 M sodium phosphate buffer (pH 6.5) in order to reduce possible disulfide bonds between polymer chains. Finally, 2 molar equivalents of TPDPI maleimide solution in DMSO was added dropwise under vigorous stirring and the reaction was conducted for 2 hours at room temperature. However, the chromophore in the reaction mixture precipitated which caused a dramatic decrease in the conjugation efficiency. Further optimization attempts for the reaction conditions did not improve the precipitation problem.

Nevertheless, postpolymerization modification is not the only approach for fluorescent labelling of polymers. RDRP methods enable chromophore inclusion into polymer chains by the functionalization of chromophores which can operate as an initiator, a RAFT agent, or a monomer.³⁵¹⁻³⁵² Due to the high compatibility of MEO₉MA monomer to both hydrophilic and hydrophobic solvents, in this study, it was hypothesized that the copolymerization of this monomer with a monomer bearing a perylene monoimide derivative (PMIM) could improve the solubility of the employed chromophore in aqueous media. In addition to hydrophilization, incorporation of dye molecules in the P(MEO₉MA) block could provide the positioning of the dye molecules in the outer shell of the polyplexes because P(MEO₉MA) block would not join for any interactions with DNA due to its neutral charge. PMIM monomer was prepared by Daniel Costabel (Institute of Organic Chemistry and Macromolecular Chemistry, Friedrich-Schiller-University Jena) (**Scheme 6.3**).³⁵³ The presence of vinyl group in the structure of PMIM monomer enabled its copolymerization with MEO₉MA monomer by RAFT polymerization.



Scheme 6.3 RAFT polymerization of P(MEO₉MA-co-PMIM) macro-RAFT agent

Since the synthesized P(MEO₉MA-co-PMIM) macro-RAFT agents were further intended to be utilized for the diblock formation with P(HPMA-co-GPMA-co-IEMA) terpolymer in acetate buffer, PMIM monomer content was aimed ~ 1 mol% to prevent the poor solubility of the perylene monoimide derivative in the reaction mixture.

Another reason of aiming at low content PMIM monomer is to prevent interference of the electrostatic interactions during polyplex formation as PMIM has a bulky perylene chromophore pendant group in comparison to other utilized comonomers which could cause steric hinderance for guanidinium groups in the polymer chain. The reaction conditions were optimized further by increasing the polymerization time to 24 h to counterbalance the lower PMIM monomer reactivity because of the bulky perylene moiety.³⁵¹ In addition, $[M]_0/[CTA]_0$ ratio had to be revisited to get the aimed molar mass (15 000 and 20 000 g mol^{-1}). The polymerization reactions were conducted in 1,4-dioxane with the monomer concentration of 1 M. The physicochemical characterizations of P(MEO₉MA-*co*-PMIM) macro-RAFT agents were performed by ¹H-NMR spectroscopy and SEC_{DMAc} (**Table 6.2**). Low \mathcal{D} indicated the success of the polymerization. The synthesized P(MEO₉MA-*co*-PMIM) macro-RAFT agents were ready to be employed for block copolymerization.

Table 6.2 Overview of reaction conditions and the selected physicochemical characteristics of P(MEO₉MA-*co*-PMIM) macro-RAFT agents

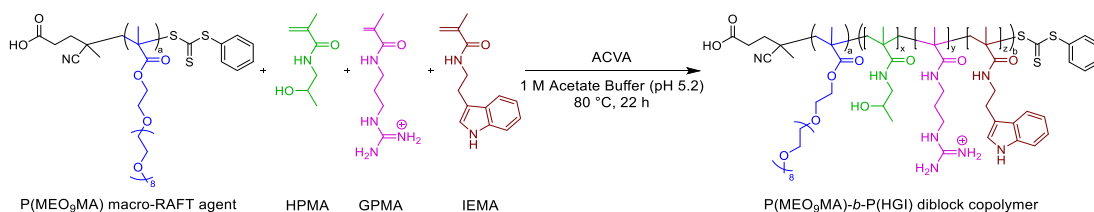
Polymer sample	$[M]_0/[CTA]_0/[I]_0$ ratio	T (°C)	t	Comonomer content (mol%) ^[a]		SEC _{DMAc} ^[b]	
				MEO ₉ MA	PMIM	M_n (g mol^{-1})	\mathcal{D}
P(MEO ₉ MA- <i>co</i> -PMIM)15	62/1/0.25	60	24 h	99	1	14 000	1.15
P(MEO ₉ MA- <i>co</i> -PMIM)20	62/1/0.25	60	24 h	98	2	23 000	1.20

[a] The comonomer contents were calculated by ¹H-NMR.

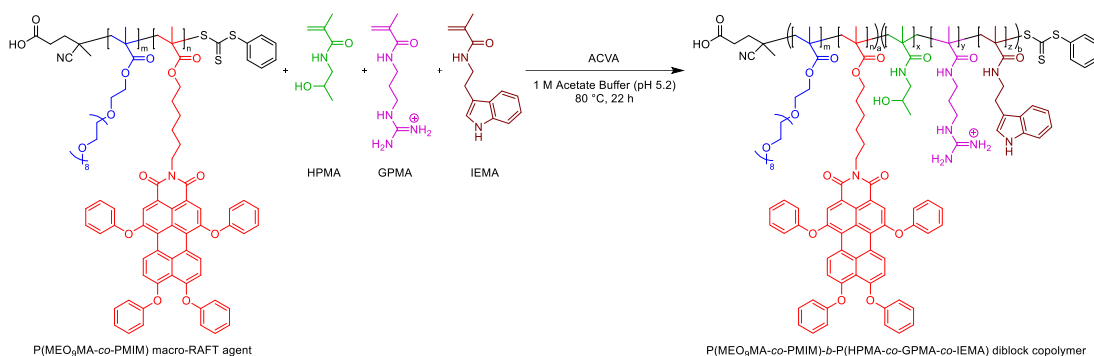
[b] DMAc + 0.21% LiCl was used as the eluent and PMMA was employed as the standard.

6.1.3 The preparation and physicochemical characterization of diblock copolymers

After successful preparation of P(MEO₉MA) and P(MEO₉MA-*co*-PMIM) macro-RAFT agents, block extension was performed by RAFT polymerization in 1 M acetate buffer with 1 M monomer concentration (**Scheme 6.4** and **6.5**). In order to avoid the imbalance between the initiator decomposition rate (k_d) and propagation rate (k_p), which can be observed in block extensions and causes high \mathcal{D} , $[CTA]_0/[INI]_0$ ratio was increased to 6.²⁸⁴ $[M]_0/[CTA]_0$ ratio was selected as 200, same as the ratio used in the synthesis of P(HPMA-*co*-GPMA-*co*-IEMA) terpolymer (P(HGI)) in **Chapter 5.1**. In addition to diblock copolymers, P(HGI) was selected as a reference polymer to reveal the effect of PEGylation on biocompatibility. The synthesis of P(HGI) was achieved in one step reaction based on the method represented in **Chapter 5.1**. For both diblock copolymers and terpolymer, GPMA and IEMA comonomer contents were aimed as ~75 mol% and ~5 mol%, respectively. Block extension for P(MEO₉MA-*co*-PMIM) macro-RAFT agents was conducted without any precipitation problem in the acetate buffer, which indicated the successful hydrophilization of the utilized chromophore by MEO₉MA moieties.



Scheme 6.4 RAFT polymerization of P(MEO₉MA)-*b*-P(HGI) diblock copolymers



Scheme 6.5 RAFT polymerization of P(MEO₉MA-co-PMIM)-*b*-P(HGI) diblock copolymers

¹H-NMR spectroscopy and SEC_{DMAc} were used for the physicochemical characterization of the synthesized polymers (**Table 6.3**). Molar mass of diblock copolymers showed gradual increase in increments of P(MEO₉MA) block molar mass. In addition, the diblock copolymers depicted moderately low \bar{D} (~1.3). The presence of PMIM comonomer did not interfere the block addition. The successful chain extension and moderately low \bar{D} were also observed for fluorescently labeled diblock copolymers.

Table 6.3 Overview of selected physicochemical characteristics for the prepared diblock copolymers and terpolymer

Polymer sample	Comonomer content (mol%) ^[a]					SEC _{DMAc} ^[b]	
	MEO ₉ MA	PMIM	HPMA	GPMA	IEMA	<i>M_n</i> (g mol ⁻¹)	\bar{D}
P(MEO ₉ MA)3- <i>b</i> -P(HGI)	4.3	-	27.9	65.6	2.2	26 000	1.26
P(MEO ₉ MA)6- <i>b</i> -P(HGI)	10.0	-	24.5	64	1.5	27 000	1.24
P(MEO ₉ MA)10- <i>b</i> -P(HGI)	13.2	-	23.4	60.7	2.7	33 000	1.40
P(MEO ₉ MA-co-PMIM)15- <i>b</i> -P(HGI)	17.4	0.6	20.6	59.8	1.6	37 000	1.27
P(MEO ₉ MA-co-PMIM)20- <i>b</i> -P(HGI)	27.4	1.2	17.6	51	2.8	44 000	1.41
P(MEO ₉ MA)30- <i>b</i> -P(HGI)	34.2	-	17.0	46.8	2.0	52 000	1.37
P(MEO ₉ MA)40- <i>b</i> -P(HGI)	38.2	-	15.9	44.7	1.2	69 000	1.59
P(HGI)	-	-	21	75	4	22 000	1.13

[a] The comonomer contents were calculated by ¹H-NMR.

[b] DMAc + 0.21% LiCl was used as the eluent and PMMA was employed as the standard.

The successful labelling was further proved by photophysical characterization of P(MEO₉MA-*co*-PMIM) macro-RAFT agent and P(MEO₉MA-*co*-PMIM)-*b*-P(HGI) diblock copolymer. The incorporation of the hydrophobic perylene monoimide derivative into P(MEO₉MA) chains enabled the observation of absorbance and emission spectra of PMIM in water. The labeled diblock copolymers showed maximum absorbance ($\lambda_{max,abs}$) at 540 nm and maximum emission ($\lambda_{max,em}$) at 638 nm at the polymer concentration of 10 mg mL⁻¹ in water (**Figure 6.2-A** and **-B**). The decrease in fluorescence intensity upon block copolymerization can be related to the decrease in PMIM mol% due to the increase in the polymer chain lengths.

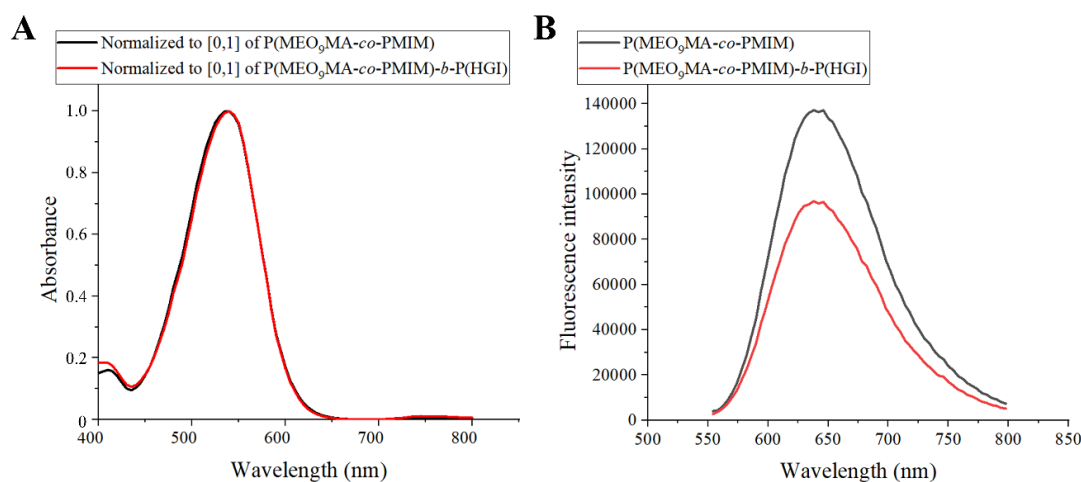


Figure 6.2 Photophysical characterization of P(MEO₉MA-*co*-PMIM) macro-RAFT agent and P(MEO₉MA-*co*-PMIM)-*b*-P(HGI) diblock copolymer at the polymer concentration of 10 mg mL⁻¹ in water (A) Normalized absorbance spectra and (B) Emission spectra of labelled polymers

6.2 Structured Illumination Microscopy Investigation on Fluorescently Labeled P(MEO₉MA-*co*-PMIM)-*b*-P(HGI) Diblock Copolymer

The applicability of the labeled polymers for biological investigations was tested by a proof-of-concept study, where structured illumination microscopy (SIM) was employed. SIM is a type of super-resolution fluorescence optical microscope that has a higher resolution (xy resolution: ~100-140 nm and z resolution: ~300 nm) in comparison to conventional microscopy techniques.³⁵⁴ This technique has been already utilized for the observation of cellular uptake and intracellular trafficking of polyplexes in different cellular compartments.³⁵⁵⁻³⁵⁶ SIM experiments were conducted by Patrick Then (Leibniz Institute of Photonic Technology, Jena). The polyplexes consisted of P(MEO₉MA-*co*-PMIM)20-*b*-P(HGI) diblock copolymer and pGL3 plasmid DNA at N/P ratio 10 were prepared by Franz J. Hack (Institute of Pharmacy, Friedrich-Schiller-University Jena). Before the image analysis, the polyplexes were incubated in HeLa cells for 1 and 4 h. After that, SIM investigation was performed by taking live images of the HeLa cells (**Figure 6.3**).

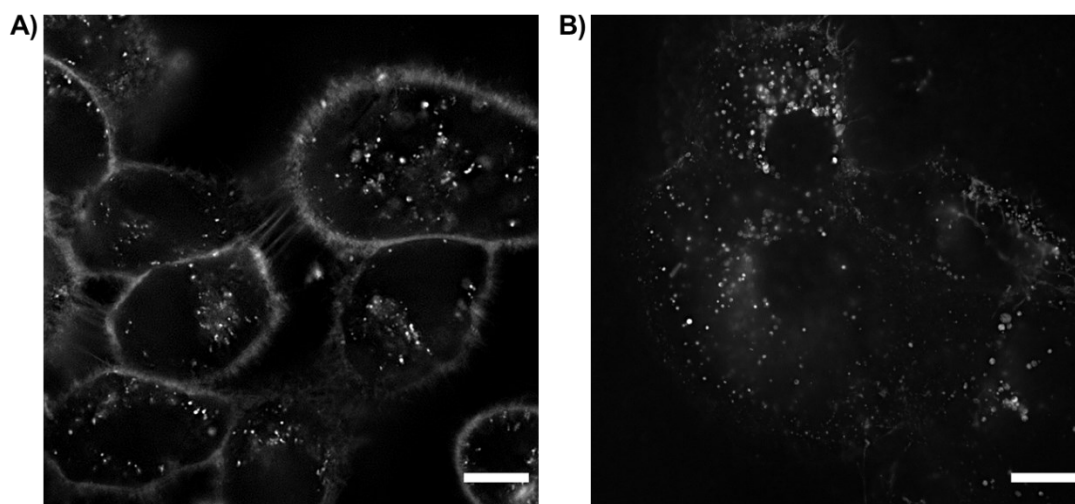


Figure 6.3 SIM live images of HeLa cells treated with P(MEO₉MA-*co*-PMIM)₂₀-*b*-P(HGI)/DNA polyplexes at N/P ratio 10 (A) after 1 h incubation and (B) after 4 h incubation. Optical magnification of the system in normal widefield fluorescence mode is ~100x (63x Objective + 1.6x Optovar for a total of 100.8x). The total area in the SIM-images is 76 x 76 μm, for a pixel size of 40 μm. The scalebar is 10 μm.

The fluorescent pattern was detected in the cellular membrane, cytoplasm, and perinuclear area after 1 h incubation and the fluorescence intensity increased after 4 h incubation. The observed fluorescent pattern was because of either the diblock copolymer/DNA polyplexes or free polymers. As a result, the success of the proposed labelling strategy was proved. Previously, the hydrophilization of such hydrophobic chromophores could be achieved by incorporation of hydrophilic polymers such as perylene functionalized dendrimers.^{347, 357} On the other hand, labeling cationic polymers by a perylene derivative *via* RAFT copolymerization for biological investigations was achieved for the first time.

6.3 Biological Investigations on P(MEO₉MA-*co*-PMIM)-*b*-P(HGI) Diblock Copolymers

Biological investigations were performed by Franz J. Hack (Institute of Pharmacy, Friedrich-Schiller-University Jena).

The impact of P(MEO₉MA) unit with different lengths on the *in vitro* biocompatibility was examined by means of CellTiter-Glo® luminescent cell viability assay (**Figure 6.4**). For this purpose, L-929 mouse fibroblasts were treated with P(HGI) and diblock copolymers with the concentration ranging from 3.9 to 500 μg mL⁻¹ over 24 h. Concentration and molar mass of P(MEO₉MA) block-dependent cell viability was observed. P(MEO₉MA) with molar mass equal to or higher than 6 000 g mol⁻¹ depicted higher IC₅₀ values in comparison to the non-shielded P(HGI) terpolymer at all tested polymer concentrations. The reason for such an effect can be due to the steric hinderance of cationic charges by P(MEO₉MA) blocks, which leads to lower cellular uptake of polyplexes and/or high cationic charge related reduction in cellular membrane disruption.³⁵⁸⁻³⁶⁰ Moreover, the inclusion of PMIM comonomer in P(MEO₉MA-*co*-PMIM)15-*b*-P(HGI) and P(MEO₉MA-*co*-PMIM)20-*b*-P(HGI) diblock copolymers did not influence cell viability significantly. On the other hand, P(MEO₉MA)3-*b*-P(HGI) reduced cell viability in a more pronounced way with respect to P(HGI) terpolymer. Such an impact of PEG derivatives with low molar mass can be explained according to the study conducted by Tao and co-workers.³⁶¹ MEO₉MA unit with *M_n* ~500 g mol⁻¹ led to higher toxicity in comparison to MEO₉MA unit with *M_n* ~950 g mol⁻¹ in L-929 mouse fibroblasts.

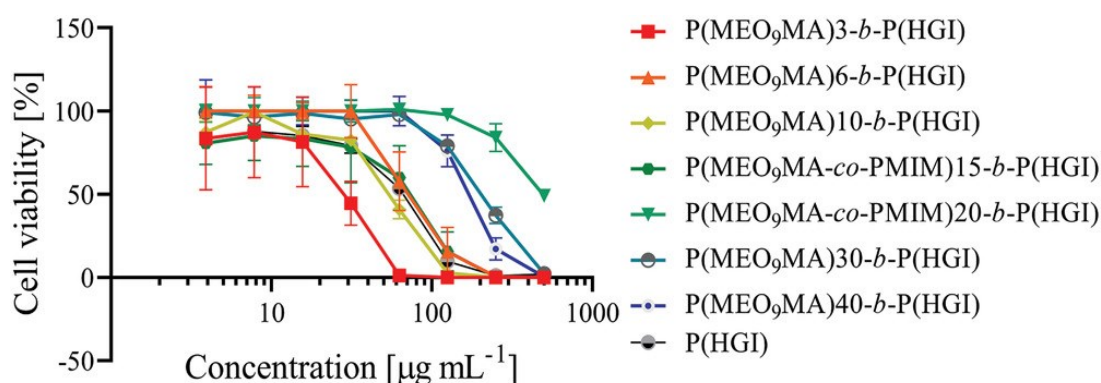


Figure 6.4 Concentration dependent *in vitro* cell viability assay of diblock copolymers and P(HGI) terpolymer in L-929 mouse fibroblasts after 24 h incubation using the CellTiter-Glo® luminescent cell viability assay (*eightfold*, mean ± SD).

The influence of P(MEO₉MA) units in guanidinium and indole containing terpolymers on pGL3 plasmid binding efficiency was investigated by the AccuBlue™ assay at N/P ratios ranging from 1 to 40 (**Figure 6.5**).³⁶² Free DNA was employed as 100% control and IPEI/DNA polyplexes (LPEI) (*M_n*_{IPEI} ~2 500 kg mol⁻¹, N/P ratio 20) were utilized as positive control.³⁶³ Starting from N/P ratio 2, all diblock copolymers, except P(MEO₉MA-*co*-PMIM)20-*b*-P(HGI) diblock copolymer, showed a comparably strong

DNA binding affinity with respect to the positive control. For P(MEO₉MA-*co*-PMIM)20-*b*-P(HGI) diblock copolymer, the complete DNA binding started from N/P ratio 5. On the other hand, P(MEO₉MA-*co*-PMIM)15-*b*-P(HGI) diblock copolymer (with 0.6 mol% PMIM comonomer content) followed a similar trend with other diblock copolymers. This binding difference can be related with the higher content of PMIM comonomer in P(MEO₉MA-*co*-PMIM)20-*b*-P(HGI) diblock copolymer (1.2 mol%). The bulky pendant groups of PMIM monomer could cause higher steric hinderance for the interactions of guanidinium and indole moieties with DNA, which is in accordance with the literature.³⁵¹ In general, chromophore comonomer content in the polymer chain is recommended below 1 mol% not to interfere with the general physicochemical properties of the polymer.

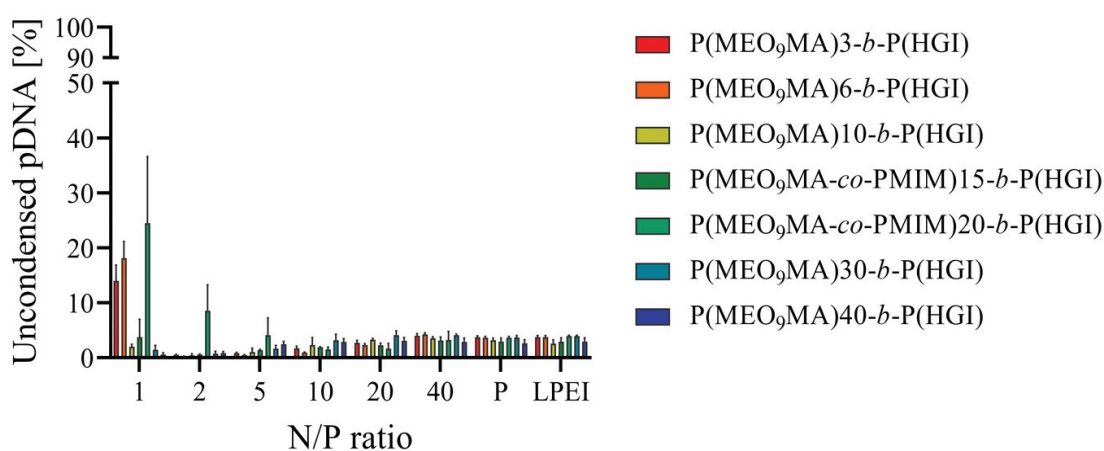


Figure 6.5 N/P ratio dependent pGL3 DNA binding capacity [%] of the diblock copolymers determined by the AccuBlue™ assay in comparison to LPEI/DNA polyplexes (LPEI) ($M_{n\text{LPEI}} \sim 2\,500\text{ g mol}^{-1}$, N/P ratio 20) and the free polymers (P) (eightfold, mean \pm SD).

The qualitative analysis of the polyplex stability was examined through agarose gel electrophoresis by applying harsh conditions.³⁶⁴ The polyplexes were prepared at N/P ratios ranging from 2 to 40 and incubated with DNase I. Then, DNA displacement from the polyplexes were performed by heparin. The stabilization of the polyplexes to protect from enzymatic degradation showed reduction upon the PEGylation (**Figure 6.6**). This observation can be explained by the steric hindrance of further electrostatic and hydrophobic interactions with DNA because of the brush architecture of P(MEO₉MA) with long PEG chains.³¹⁸ This hypothesis was supported by higher DNA retardation at the origin for the diblock copolymers with shorter lengths of P(MEO₉MA) blocks.

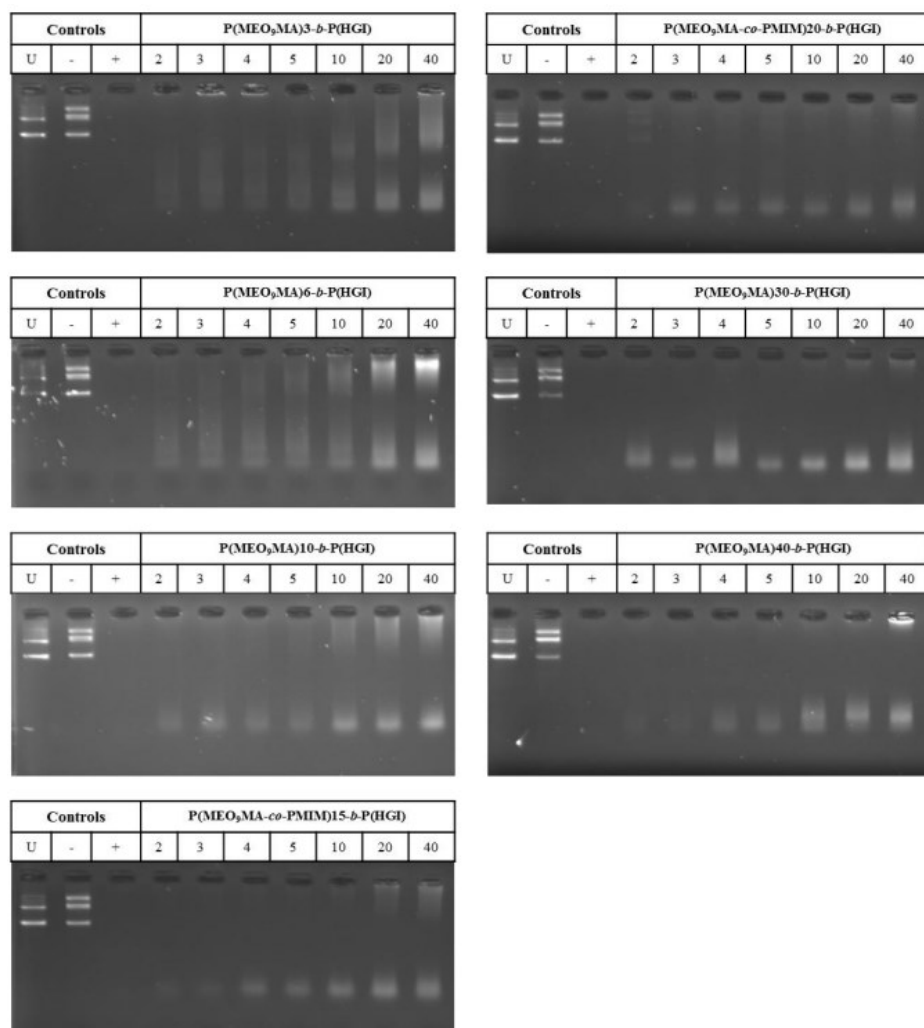


Figure 6.6 Stability of diblock copolymer/DNA polyplexes at different N/P ratios against enzymatic DNase I degradation (controls: untreated free DNA (U), free DNA treated in the same way as polyplexes but without enzyme (-), free DNA treated with enzyme (+))

The effect of increasing molar mass of P(MEO₉MA) blocks on the transfection efficiency for diblock copolymer/DNA polyplexes was investigated by a luminescence-based reaction in eukaryotic CHO-K1 cells in the presence of serum. The polyplexes were prepared at N/P ratios ranging from 2 to 40 (**Figure 6.7**). Due to lower PEG density in P(MEO₉MA)*3-b*-P(HGI) and P(MEO₉MA)*6-b*-P(HGI) diblock copolymers, their polyplexes at N/P ratio 20 performed higher transfection in comparison to higher molar mass counterparts. Polyplexes with P(MEO₉MA) blocks with the molar mass equal to or higher than 10 000 g mol⁻¹ showed insignificant transfection efficiency. Molar mass dependent reduction in nucleic acid delivery efficiency was also observed with the other PEGylated cationic polymers such as PEGylated PEI.³⁶⁵⁻³⁶⁸ It is very common to observe the reduction in nucleic acid delivery efficiency upon PEGylation, which is called as PEG dilemma.³² The lower cellular uptake and/or endosomal escape are the main reasons for this reduction.

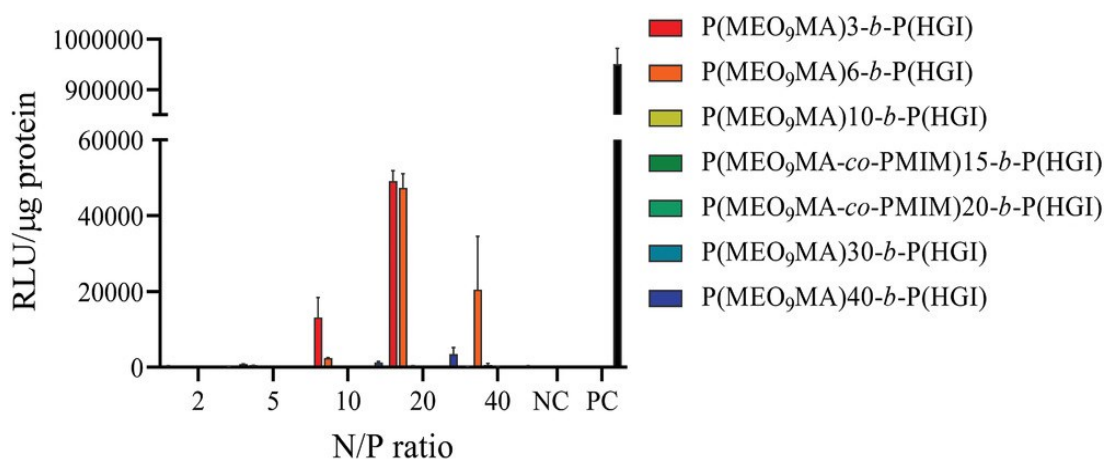


Figure 6.7 *In vitro* luciferase reporter gene expression of diblock copolymer/DNA polyplexes at different N/P ratios in CHO-K1 cells. Experiments were performed in quadruplicates with free DNA serving as negative control (NC) and lPEI/DNA polyplexes ($M_{n\text{PEI}} \sim 2\,500\text{ g mol}^{-1}$, N/P ratio 20) as positive control (PC) (mean \pm SD).

In summary, this chapter describes the PEGylation for indole and guanidinium containing poly(methacrylamide) terpolymer as an attempt to improve their biocompatibility. For this purpose, well-defined P(MEO₉MA) macro-RAFT agents with molar mass ranging from 3 000 to 40 000 g mol⁻¹ were synthesized through RAFT polymerization. ‘Living’ character of P(MEO₉MA) macro-RAFT agents enabled successful block copolymerization by addition of HPMA, GPMA, and IEMA comonomers with the contents of 21, 75, and 5 mol%, respectively. In order to reveal the impact of P(MEO₉MA) block with various molar mass on DNA delivery efficiency, the comonomer content of terpolymer were kept similar for each diblock copolymer structure. Overall, with the increase in molar mass of P(MEO₉MA) block an improved cell viability was observed. Although all diblock copolymers showed efficient DNA binding at N/P ratio equal to or higher than 2, the protection of DNA from enzymatic degradation was limited indicating the struggle in DNA condensation. At N/P ratio 20, DNA transfection was observed only for diblock copolymers bearing P(MEO₉MA) blocks with the molar mass of 3 000 and 6 000 g mol⁻¹. Apart from PEGylation studies, the presence of P(MEO₉MA) unit enabled the trial of a new labeling strategy, which was the inclusion of a perylene monoamide derivative, PMIM comonomer, by RAFT polymerization. The success of the labeling approach was tested by a proof-of-concept study, where Hela cells incubated with P(MEO₉MA-co-PMIM)20-*b*-P(HGI)/DNA polyplexes. The polyplexes and/or free polymer chains were successfully observed in different cell compartments by SIM. The studies represented in this chapter provided valuable information for both PEGylation and labeling of guanidinium and indole containing terpolymer to create better polymer designs.

7. Guanidinium Containing Poly(methacrylamide) Copolymer for Ultrasensitive Arsenic Detection

Parts of this chapter was published in **P1**) Tabujew, I.; [Cokca, C.](#); Zartner, L.; Schubert, U. S.; Nischang, I.; Fischer, D.; Peneva, K., The influence of gradient and statistical arrangements of guanidinium or primary amine groups in poly(methacrylate) copolymers on their DNA binding affinity. *J. Mater. Chem. B* **2019**, *7* (39), 5889-6066 and **P5**) Soni, G. K.; Wangoo, N.; [Cokca, C.](#); Peneva, K.; Sharma, R. K., Ultrasensitive aptasensor for arsenic detection using quantum dots and guanlylated Poly(methacrylamide). *Anal. Chim. Acta* **2022**, *1209*, 339854.

This chapter represents the applicability of guanidinium containing poly(methacrylamide)s for a different platform rather than non-viral gene delivery by collaborating with the Department of Chemistry and Centre of Advanced Studies in Chemistry, Panjab University, India. In the previous chapters, an evolution of guanidinium containing poly(methacrylamide)s were illustrated with respect to improving DNA binding, transfection efficiency and biocompatibility through different strategies step by step. After revealing DNA delivery potential of guanidinium and indole containing poly(methacrylamide) terpolymers in **Chapter 2**, the following studies mainly focused on guanidinium containing amphipathic terpolymers for DNA delivery. Nevertheless, the excellent DNA binding capacity of P(HPMA-*co*-GPMA) copolymers with high guanidinium content was considered as an advantage for its utilization in the development of an ultrasensitive aptasensor for arsenic detection.

Arsenic is naturally present in the crust of earth and it mainly exists in four oxidation states (-3, 0, +3, and +5).³⁶⁹ However, it is a big threat to human health and environment.³⁷⁰ One of the most common exposure sources for arsenic is the contaminated groundwater. This exposure can cause arsenic poisoning, cancer, cardiovascular diseases, diabetes, etc. For this reason, World Health Organization (WHO) and Environmental Protection Agency (EPA) determined the maximum permissible level of arsenic in useable water as 10 ppb.³⁷¹ One of the most common forms of arsenic in water is arsenite (As^{3+}) which shows high stability, high mobility for incorporation in food chain, and ability of enzyme activity inhibition.³⁷²⁻³⁷³ It is considered as the primary reason for arsenic poisoning and related diseases.³⁷⁴ Therefore, various conventional methods (e.g., high performance liquid chromatography, hydride generation atomic absorption spectroscopy, atomic fluorescence spectrometry, gas chromatography-mass spectrometry, etc.) are employed for As^{3+} detection but such methods are expensive, laborious and non-portable.³⁷⁴ Thus, optical based sensing strategies have been developed to overcome the drawbacks of the conventional methods because such systems can provide rapid, low-cost and quantitative detection of As^{3+} in water.

Herein, a three-component fluorometric aptasensing platform was proposed for As^{3+} detection in real-world samples (e.g., water, food, and soil) (**Figure 7.1**). The first component of this system is an aptamer as the As^{3+} recognition element, which provides low detection limit, high specificity, and fast response time.³⁷⁵ The second

component is semiconductor MPA-CdTe@CdS quantum dots (QDs), which was utilized for a sensitive quantitative detection of As^{3+} by fluorescence analysis. QDs are commonly utilized for the fabrication of sensors because they possess narrow and symmetric emission, unique brightness, high photostability, and large extinction coefficient in comparison to traditional fluorophores.³⁷⁴ The third component is P(HPMA-co-GPMA) copolymer with ~80 mol% guanidinium content, which acts as a quencher for the negatively charged MPA-CdTe@CdS QDs through electrostatic interactions. In the presence of As^{3+} ions, the aptamer specifically binds to the As^{3+} ions leading to the conformational change in aptamer.³⁷⁶ As a result, the binding of P(HPMA-co-GPMA) copolymer to the aptamer is not possible. The free polymers bind to MPA-CdTe@CdS QDs, which cause quenching of fluorescence signal. In the absence of As^{3+} ions, the polymers can bind to the aptamer, and therefore, fluorescence signal of MPA-CdTe@CdS QDs remains unaffected. As a result, a concentration dependent As^{3+} detection can be achieved depending on the change in the fluorescence signal.

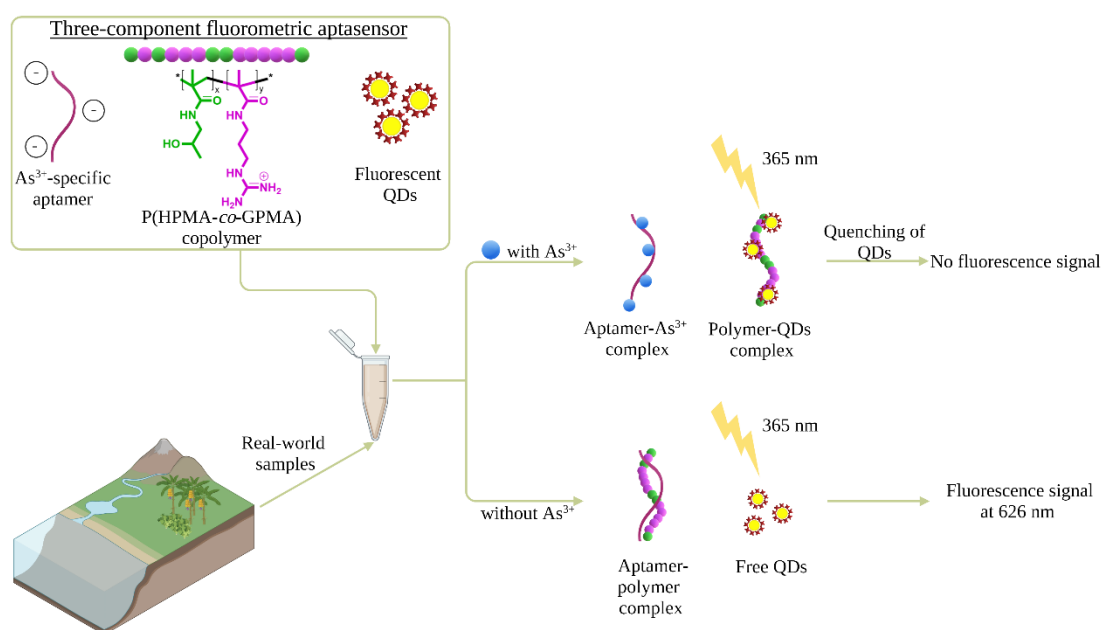
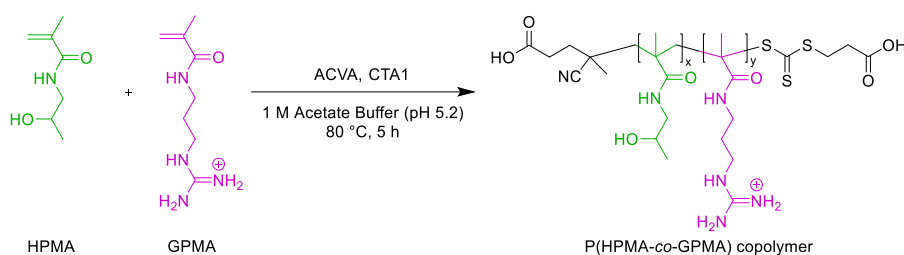


Figure 7.1 General description of Chapter 7

7.1 Synthesis and Physicochemical Characterization of P(HPMA-co-GPMA) Copolymer

The versatility of guanidinium group opens a broad application field for GCPs such as antimicrobial activity^{308, 377-379}, pest control³⁸⁰, and aptasensors³⁸¹ apart from non-viral gene delivery. Nevertheless, utilization of GCPs in aptasensors is not very common. In the previous study conducted by Sharma and co-workers, a guanidinium containing poly(methacrylamide) homopolymer was utilized for the detection of malathion by a QDs-based aptasensor for the first time.³⁸¹ The high specificity towards malathion

detection was obtained through this system. The distinctive binding ability of guanidinium toward nucleic acids contributed to the sensitivity of the aptasensor. Therefore, in this study, P(HPMA-*co*-GPMA) copolymer was statistically prepared *via* RAFT polymerization. With the incorporation of HPMA, the neutral charged comonomer, further colloidal stability was aimed upon binding of the copolymer to the aptamer.³² The similar reaction conditions represented in **Chapter 3.1** was applied by aiming $[M]_0/[CTA]_0/[I]_0 = 240/3/1$ (**Scheme 7.1**).



Scheme 7.1 RAFT polymerization of P(HPMA-*co*-GPMA) copolymer

The selected physicochemical characteristics of P(HPMA-*co*-GPMA) copolymer were shown in **Table 7.1**. The copolymer was obtained with 18 mol% HPMA and 82 mol% GPMA comonomer content, which was calculated by ¹H-NMR spectroscopy. The apparent molar mass of P(HPMA-*co*-GPMA) copolymer was calculated as 8 600 g mol⁻¹ with $D \sim 1.07$ by SEC_{water} system. Narrow molar mass distribution reflected the success of the RAFT polymerization. Additionally, the impact of high guanidinium content on the surface charge of the polymer was confirmed by zeta potential measurement, which showed a net positive charge of +51.3 mV.

Table 7.1 Overview of selected physicochemical characteristics for P(HPMA-*co*-GPMA) copolymer

Polymer sample	Comonomer content (mol%) ^[a]		SEC _{water} ^[b]	
	HPMA	GPMA	<i>M_n</i> (g mol ⁻¹)	<i>D</i>
P(HPMA- <i>co</i> -GPMA)	18	82	8 600	1.07

[a] The comonomer contents were calculated by ¹H-NMR.

[b] Water with 0.1% TFA and 0.1 M NaCl was used as the eluent and P2VP was employed as the standard.

7.2 Optimization, Selectivity Analysis, and Application of the Developed Aptasensor

The following experiments were conducted by Gurpreet K. Soni (Department of Chemistry and Centre of Advanced Studies in Chemistry, Panjab University, India).

Highly fluorescent core-shell MPA-CdTe@CdS QDs were synthesized by hot injection method.³⁸¹ The presence of mercaptopropionic acid (MPA) in the core of the synthesized QDs provided negative charge for further interactions with the positively

charged copolymer. Zeta potential measurement indicated a net negative charge of -40.4 mV for MPA-CdTe@CdS QDs. Cadmium sulfide (CdS) shell was utilized for improving the photostability and luminescence efficiency of MPA-CdTe@CdS QDs. CdTe- and CdTe@CdS QDs depicted fluorescence emission at 520 nm and 626 nm, respectively with the observed bathochromic shift (**Figure 7.2-a**). Similar trend was also recognized by means of UV-Vis spectrum in the range of 500-700 nm (**Figure 7.2-b**). High-resolution transmission electron microscopy (HR-TEM) examination illustrated monodispersed, spherical MPA-CdTe@CdS QDs with an average size of 4 nm (**Figure 7.2-c**).

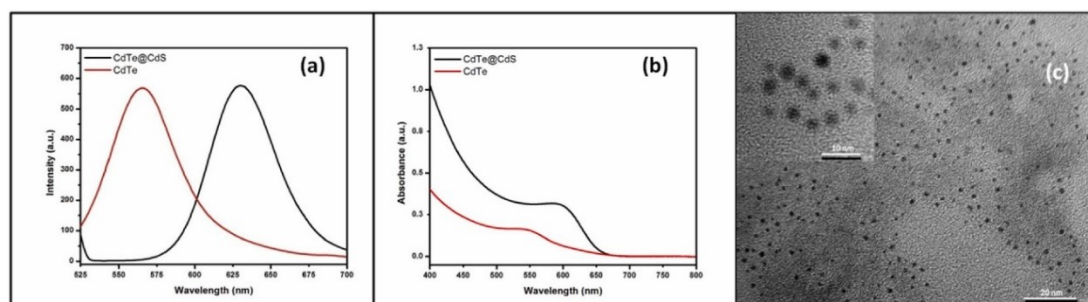


Figure 7.2 (a) Emission spectra of CdTe and CdTe@CdS QDs upon excitation at 365 nm and 357 nm, respectively, (b) Absorbance spectra of CdTe and CdTe@CdS QDs, (c) HR-TEM image of CdTe@CdS QDs at scale bar of 20 nm (inset HR-TEM image at the scale bar of 10 nm).

After successful synthesis of MPA-CdTe@CdS QDs, optimization experiments for As^{3+} detection were conducted based on the interactions between MPA-CdTe@CdS QDs/P(HPMA-co-GPMA) copolymer and P(HPMA-co-GPMA) copolymer/ As^{3+} -specific aptamer. For this purpose, concentration, volume, and incubation time were aimed to be optimized for achieving the best performance of the developed aptasensor. The studies on MPA-CdTe@CdS QDs/P(HPMA-co-GPMA) copolymer interaction depicted that 0.06 mg mL^{-1} copolymer concentration was sufficient to achieve the optimum quenching of fluorescence signal (**Figure 7.3-a**). As the second step, MPA-CdTe@CdS QDs were treated with different volumes of copolymer solution (at copolymer concentration of 0.06 mg mL^{-1}) ranging from 5 to 30 μL (**Figure 7.3-b**). The optimum volume required for quenching of MPA-CdTe@CdS QDs was decided as 25 μL . Finally, the optimum incubation time for MPA-CdTe@CdS QDs quenching in copolymer solution (0.06 mg mL^{-1} , 25 μL) was set as 30 min (**Figure 7.3-c**).

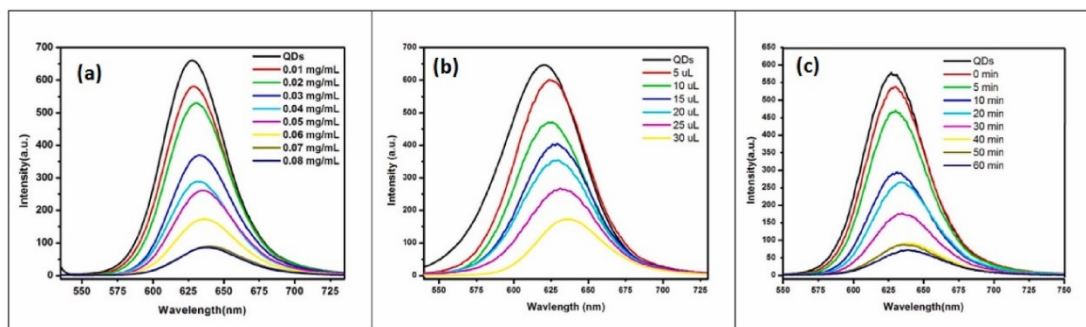


Figure 7.3 Influence of (a) the copolymer concentrations, (b) volume of the copolymer solution at 0.06 mg mL^{-1} copolymer concentration and (c) incubation time at 0.06 mg mL^{-1} copolymer concentration with $25 \text{ }\mu\text{L}$ copolymer solution on the fluorescence signal of MPA-CdTe@CdS QDs. The excitation wavelength was 357 nm with excitation and emission slit width 5 and 10 , respectively. All the samples were incubated in 1 M Tris buffer ($\text{pH } 7.0$) at R.T.

As the next step, optimum concentration, volume, and incubation time for the aptamer was decided in the presence of the copolymer solution (0.06 mg mL^{-1} , $25 \text{ }\mu\text{L}$) to obtain unaffected fluorescence intensity of MPA-CdTe@CdS QDs. The incubation of the aptamer solution ranging from 0.5 to $3.0 \text{ }\mu\text{M}$ with the copolymer solution indicated that the aptamer concentration below $3.0 \text{ }\mu\text{M}$ was not enough for the binding of all free copolymers (**Figure 7.4-a**). As a result, remaining free copolymers created interaction with the MPA-CdTe@CdS QDs, which caused the decrease in the fluorescence intensity. Therefore, $3.0 \text{ }\mu\text{M}$ was selected as the optimum aptamer concentration. In addition, $25 \text{ }\mu\text{L}$ aptamer solution with $3.0 \text{ }\mu\text{M}$ concentration was sufficient for the complete binding of free copolymers (**Figure 7.4-b**). Moreover, with the $3.0 \text{ }\mu\text{M}$, $25 \text{ }\mu\text{L}$ aptamer solution, the optimum incubation time was detected as 60 min (**Figure 7.4-c**).

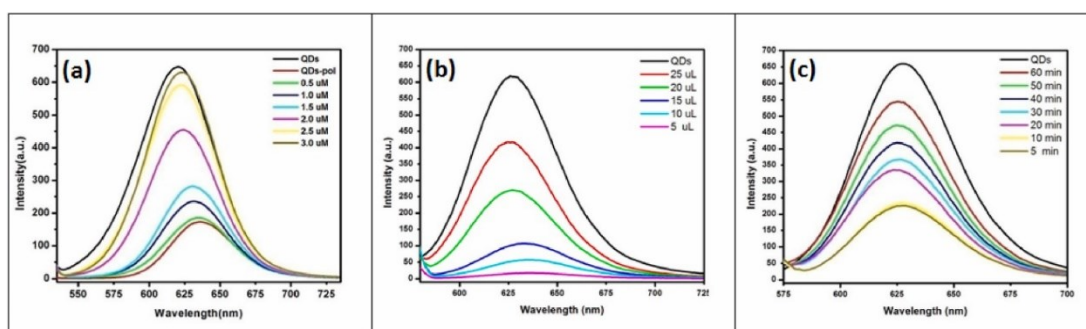


Figure 7.4 Influence of (a) aptamer concentration, (b) volume, and (c) incubation time on fluorescence intensity of MPA-CdTe@CdS QDs in the presence of P(HPMA-co-GPMA) copolymer solution (0.06 mg mL^{-1} , $25 \text{ }\mu\text{L}$). All the samples were incubated in 1 M Tris buffer ($\text{pH } 7.0$) at R.T.

After finalizing the optimization of the parameters for the three components, the limit of detection (LOD) was calculated for the developed As^{3+} aptasensor. For this purpose, sodium arsenite with various concentrations (ranging from 0.01 to 100 nM) was added to the optimized aptasensor and fluorescence intensity of each sample was measured. As As^{3+} concentration increased, the emission peak at 626 nm decreased because of the MPA-CdTe@CdS QDs aggregation upon free copolymer binding (**Figure 7.5-a**). This result proved the specific and competitive binding of As^{3+} ions to aptamer, which caused binding of the free copolymers to the MPA-CdTe@CdS QDs. The quantitative analysis of As^{3+} binding to aptamers were achieved with a calibration curve, where F_0 and F represents the fluorescence intensities in the absence and presence of As^{3+} ions, respectively (**Figure 7.5-b**). LOD was calculated to be 249.77 pM, which showed better sensitivity of the proposed aptasensor in comparison to other reported colorimetric methods for As^{3+} sensing (**Table 7.2**). The only sensing method, which showed higher sensitivity than the proposed aptasensor, was based on a water soluble Cu-polymer complex with LOD ~ 49.75 fM.³⁸² However, its applicability for further device fabrication is limited due to higher cost production and complicated synthetic protocol for Cu-polymer complex. On the other hand, the synthesis of P(HPMA-co-GPMA) copolymer by RAFT polymerization is quite facile and low cost. In addition, the combination of three components of the proposed aptasensor is straightforward.

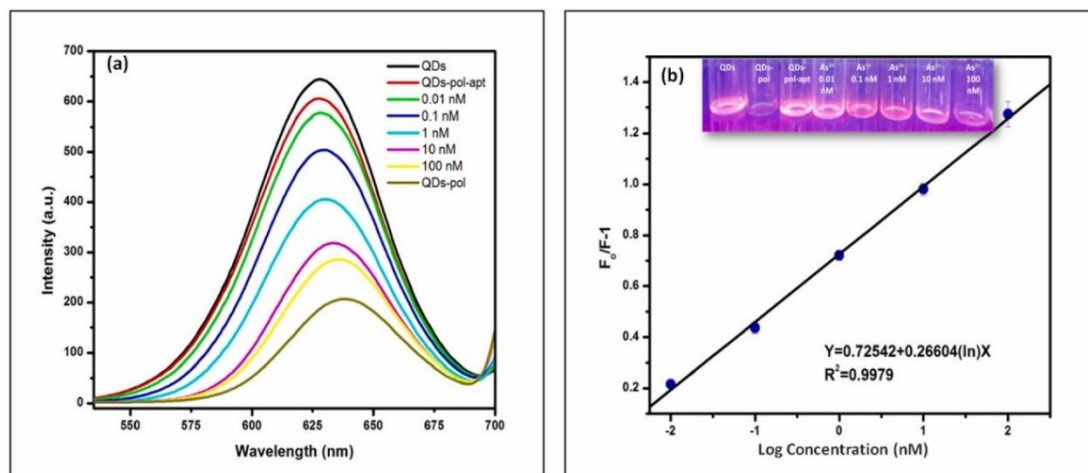


Figure 7.5 (a) Influence of As^{3+} ion concentration on the fluorescence signal of MPA-CdTe@CdS QDs in the presence of aptamer (3 μM) and copolymer (0.06 mg mL^{-1}), (b) Calibration curve of the aptasensor, where F_0 and F represent the fluorescence intensities in the absence and presence of As^{3+} ions, respectively. Inset shows the naked eye quenching of MPA-CdTe@CdS QDs in the presence of As^{3+} under a UV illuminator. For the detection of As^{3+} , the samples were incubated in 1 M Tris buffer (pH 7.0) at R.T.

Table 7.2 LOD values for As³⁺ detection based on previously reported sensing methods

Method of detection	LOD value	Ref.
Atomic absorption spectroscopy	3.20 nm	383
Neutron activation analysis	0.93 nM	384
Colorimetric	70.00 nM	385
High performance liquid chromatography & Inductively coupled plasma mass spectrometry	0.56 nM	386
Surface-enhanced Raman spectroscopy	23.06 nM	387
Impedimetry	0.80 μ M	388
Voltammetry	14.60 nM	389
Colorimetric	3.58 μ M	390
Fluorescence resonance energy transfer	6.00 nM	391
Fluorometric (SiNPs)	2.88 nm	392
Fluorometric (Cu-polymer)	49.75 fM	382
Fluorometric (QDs-polymer)	249.77 pM	Current method

The selectivity of the aptasensor for As³⁺ ions were tested by cross reactivity studies, which consists of other interfering metal ions; Hg²⁺, Cd²⁺, Na¹⁺, Pb²⁺, Cu²⁺, Ni²⁺, Zn²⁺, Mg²⁺, Co²⁺, Fe³⁺, and Ca²⁺ (**Figure 7.6**). The maximum quenching of MPA-CdTe@CdS QDs was obtained in the presence of As³⁺ ions, which proved the high specificity of the aptasensor for As³⁺ ions. In the presence of other tested metal ions, any significant quenching effect was not observed because the aptamer preferentially binds to the copolymer rather than other selected metal ions.

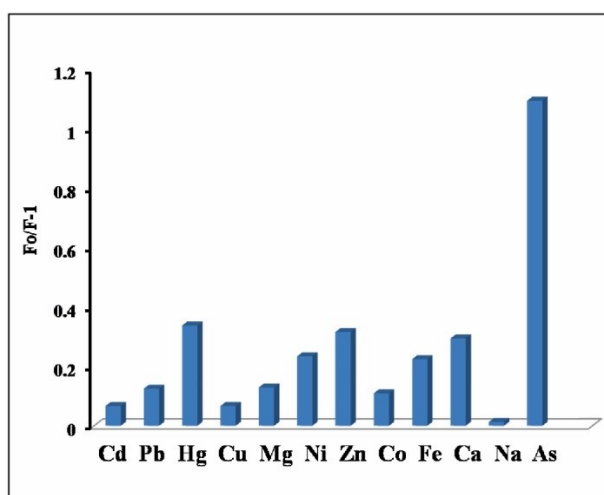


Figure 7.6 Fluorescence response of the aptasensor towards different non-target metal ions: 1 μ M As³⁺ ions and 1000 μ M non-target metal ions at the 0.06 mg mL⁻¹ copolymer concentration and 3 μ M aptasensor concentration, where F₀ and F represent the fluorescence intensities in the absence and presence of As³⁺ ions.

The applicability and relevance of the proposed aptasensor were investigated in real-world samples; mineral water, tap water, soil water, and apple juice after spiking with As^{3+} at different concentrations ranging from 0.01 to 100 nM. The As^{3+} amount found depicted similar values to the As^{3+} amount spiked with acceptable R^2 values for all samples (**Table 7.3**). Hence, the outstanding applicability of the aptasensor was proved for the tested real-world samples.

Table 7.3 Percentage recovery for detection of As^{3+} ions in spiked water, soil and food samples using the proposed assay

Sample	Regression Coefficient (R^2)	As^{3+} amount spiked (nm)	As^{3+} amount found (nm)	Recovery %
Mineral water	0.982	1	0.91	91.41
		100	99.89	99.89
Soil water	0.953	1	1.08	108.72
		100	107.92	107.92
Tap water	0.979	1	0.91	91.87
		100	101.03	101.03
Apple Juice	0.952	1	0.73	73.39
		100	102.11	102.11

In conclusion, excellent nucleic acid binding capability of guanidinium containing poly(methacrylamide) copolymer opened a new application platform; highly sensitive and selective fluorescent aptasensor for arsenic detection. For this purpose, well-defined P(HPMA-*co*-GPMA) copolymer was synthesized by RAFT polymerization with 82 mol% guanidinium content. In addition to guanidinium bearing copolymer, As^{3+} -specific aptamer and fluorescent MPA-CdTe@CdS QDs were the other components of the aptasensor. In the presence of As^{3+} ions, aptamer/ As^{3+} ions complexes are created leading to a conformational change in the aptamer. As a result, free copolymer in the aptasensor solution cannot bind to the aptamer, instead, it binds to the negatively charged MPA-CdTe@CdS QDs. Hence, P(HPMA-*co*-GPMA) copolymer/MPA-CdTe@CdS QDs complexes aggregate and fluorescence of MPA-CdTe@CdS QDs is quenched. It was shown that the sensitivity of the proposed aptasensor was higher than the majority of the other proposed methods for arsenic detection. LOD for the aptasensor was calculated as 246.77 pM indicating the trace level detection. In addition, the aptasensor depicted high selectivity for As^{3+} ions in the presence of other metal ions. Moreover, the performance of the proposed aptasensor was tested in real-world samples containing preservatives, metal ions, minerals, and other moieties. The As^{3+} amount found in the samples was almost same to the As^{3+} amount spiked into the sample, which indicated the suitability of the aptasensor for real-world samples. Furthermore, the proposed aptasensor was produced in a facile and cost-effective way, especially the synthesis of P(HPMA-*co*-GPMA) copolymer. Therefore, it can be easily applied to the fabrication of next level devices for on-site detection of arsenic in real-world samples.

8. Summary and Outlook

Guanidinium is one of the most fascinating molecules playing fundamental roles in various biochemical processes. The versatility of guanidinium comes from its peculiar physicochemical properties, which are charge delocalization on Y-shaped geometry, high pKa value (~13.8), and anisotropic hydration shell. Such properties lead to the formation of special non-covalent interactions (e.g., bidentate H-bonds with oxoanions, cation- π interactions, ion pair- π interactions, and like charge pairing) with other biomolecules. Nonetheless, guanidinium started to be recognized increasingly after the breakthrough discovery of its function in cell penetration of HIV-1 Tat protein. Hence, a new path for the development of guanidinium-rich transporters was opened. Apart from cell penetration capability, it was found that guanidinium can create special interactions with nucleic acids. Hence, guanidinium-rich transporters has been utilized for non-viral gene delivery.

Due to the structural and functional freedom of polymeric vectors, guanidinium groups were also incorporated into polymer chains and investigated for non-viral gene delivery in various studies. However, the potential of GCPs in non-viral gene delivery has not been completely revealed yet. Up to now, the most of designs for polymeric vectors involved primary, secondary and tertiary amine groups as the source of cationic charge. On the other hand, there is a lot more to be revealed for GCPs. Therefore, the presented thesis depicts prominent studies on GCPs for non-viral gene delivery. Starting from **Chapter 3**, an evolutionary process of guanidinium containing poly(methacrylamide)s was illustrated (**Figure 8.1**). Each chapter illustrated divergent polymer designs by emphasizing the versatility of RAFT polymerization. The polymer designs were created by utilizing methacrylamide monomers with bioinspired pendant groups to obtain the polymeric vectors with maximum performance.

Chapter 3 provided valuable information for poly(methacrylamide)s regarding the influence of comonomer distribution, charge density, and cationic charge origin on DNA binding affinity. The effect of comonomer distribution on DNA binding was more pronounced at low cationic comonomer content. Gradient copolymers with 5 mol% cationic comonomer content was more effective for DNA binding independent from origin of the cationic charge. Nevertheless, the more pronounced impact of comonomer distribution was observed for primary amine counterpart, which pointed out the influence of cationic charge source as well. The difference in DNA binding affinity in respect of comonomer distribution became less recognizable as the cationic charge density increased. Preliminary transfection experiments in CHO-K1 cells indicated higher transfection efficiency for the polyplexes with 90 mol% guanidinium content in comparison to the primary amine counterparts at N/P ratio 20. The impact of comonomer distribution on the transfection efficiency was insignificant for the polyplexes with 90 mol% guanidinium content. On the other hand, the statistical copolymers showed lower toxicity in L-929 mouse fibroblasts. These observations helped shaping the following desings of guanidinium containing

poly(methacrylamide)s by revealing the best comonomer distribution with optimum cationic charge density to achieve efficient transfection with high cell viability.

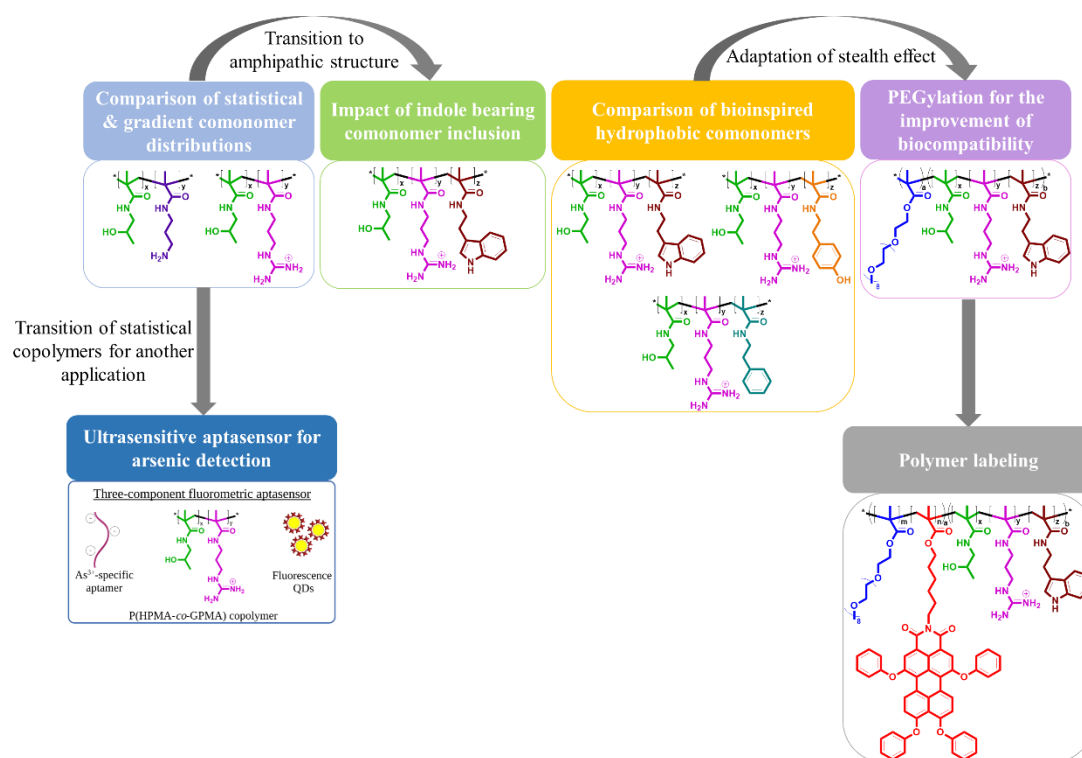


Figure 8.1 Evolutionary process of guanidinium containing poly(methacrylamide)s presented in this thesis

After revealing the optimum comonomer distribution and cationic charge density for guanidinium containing poly(methacrylamide)s, in **Chapter 4**, the focus was directed into the strategies to improve the transfection performance of these polymers. One strategy is the switching the cationic nature of the polymer into amphipathic one by the utilization of hydrophobic comonomers. The indole bearing methacrylamide monomer was selected as the mimic of tryptophan because of the synergy between indole and guanidinium, which is fundamental for different biochemical processes such as cell penetration. Hence, the first example of guanidinium and indole containing poly(methacrylamide) terpolymer for non-viral gene delivery was achieved. The indole bearing comonomer content was aimed as the maximum possible content (16 mol%) providing excellent solubility of the polymer in aqueous media apart from amphipathic nature. The guanidinium content was kept ~60 mol%. Inclusion of indole into guanidinium containing poly(methacrylamide) led to ~200-fold increase in DNA transfection efficiency in CHO-K1 cells despite of slight reduction in cell viability.

The extraordinary transfection result obtained with indole and guanidinium containing terpolymer stirred up the curiosity whether this effect was because of the synergy between guanidinium and indole or better effect could be obtained with other bioinspired hydrophobic groups. Thus, **Chapter 5** represented the investigations on

the impact of hydrophobic group origin on DNA delivery. Phenyl and hydroxyphenyl bearing bioinspired methacrylamide comonomers were selected as the mimics of phenylalanine and tyrosine side chains, respectively. The impact of indole, phenyl and hydroxyphenyl moieties in guanidinium containing terpolymers were explored in respect of DNA binding, transfection efficiency, and toxicity. Although cyto- and hemocompatibility investigations showed high biocompatibility independent from the origin of hydrophobic groups, indole containing terpolymers performed the highest transfection in CHO-K1 cells. As a result, it is concluded that the synergy between indole and guanidinium is special and the following studies focused on the indole and guanidinium containing terpolymer.

Despite of the promising *in vitro* transfection performance of indole and guanidinium containing terpolymers, the high guanidinium content is a limitation for the systemic administration of this polymeric vector for *in vivo* studies. To overcome this limitation, incorporation of neutral charged hydrophilic units is a common strategy providing 'stealth effect' against proteins in the blood. PEG is the most studied polymer for the stealth effect, yet its incorporation can reduce the nucleic acid delivery efficiency significantly. Particularly, molar mass of PEG plays a crucial role on the performance of polyplexes. Therefore, **Chapter 6** describes PEGylation of indole and guanidinium containing terpolymers. For this purpose, diblock copolymers consisted of P(MEO₉MA) homopolymer with molar mass ranging from 3 000 to 40 000 g mol⁻¹ were prepared. To reveal the optimum length of P(MEO₉MA) block, similar molar mass and comonomer content was aimed for the second block made of indole and guanidinium containing terpolymer. At N/P ratio 20, the diblock copolymers with 3 000 and 6 000 g mol⁻¹ of P(MEO₉MA) unit showed DNA transfection in CHO-K1 cells whereas the further increase in the P(MEO₉MA) length caused the loss of transfection performance. In addition, the presence of dense and long neutral charged units hindered efficient DNA condensation, and so a limited protection of DNA from enzymatic degradation was observed. Nevertheless, this study is the first example of systematic investigation on PEGylation of GCPs. Moreover, it provides practical information to enlighten the path for the biocompatibility improvement of indole and guanidinium containing terpolymers. In addition to PEGylation studies, this chapter illustrated a novel approach for fluorescent labeling of water-soluble polymers with hydrophobic chromophores. A perylene monoimide derivative, PMIM monomer was incorporated by RAFT polymerization by taking the advantage of the presence of P(MEO₉MA) block. The success of the labeling approach was observed in Hela cells by SIM studies proving the applicability of the proposed labeling approach.

Apart from non-viral gene delivery applications, the versatility of guanidinium containing poly(methacrylamide)s was shown in **Chapter 7**. P(HPMA-*co*-GPMA) copolymer was used as a component of a highly sensitive and selective fluorescent aptasensor for arsenic detection. P(HPMA-*co*-GPMA) copolymer binds selectively to the aptamer in the absence of As³⁺ ions by leaving MPA-CdTe@CdS QDs free. On the other hand, in the presence of As³⁺ ions, aptamer/As³⁺ ion complexes forms, which results in electrostatic interactions between free copolymers and MPA-CdTe@CdS

QDs. As a result, fluorescence of MPA-CdTe@CdS QDs is quenched. The presented aptasensor showed much higher sensitivity in comparison to other proposed As^{3+} detection methods. In addition, it was highly selective to As^{3+} in the presence of other metal ions. Its applicability was evaluated in real-world samples; mineral water, soil water, tap water, and apple juice which were spiked with As^{3+} . The recovery percentage of the aptasensor for each sample proved the efficiency of the method. In addition to facile and cost-effective preparation, the proposed aptasensor can deliver fast and on-site arsenic detection.

In conclusion, the presented thesis provided important results on guanidinium containing poly(methacrylamide)s from multiple aspects. The utilization of RAFT polymerization enabled incorporation of various monomers with arranged comonomer distribution, comonomer content, polymer architecture, and molar mass. Hydrodynamic characterization of the synthesized polymers for calculating absolute molar mass served as a suitable alternative for overcoming inconsistency in molar mass detection of cationic polymers *via* SEC systems. Moreover, copolymerization of both hydrophilic and hydrophobic monomers in aqueous reaction mixture in a controlled way provides valuable information for the synthesis of guanidinium containing amphipathic copolymers. Nature has been and still is the biggest inspiration source for scientists. In this thesis, the motivation was also the preparation of bioinspired guanidinium containing poly(methacrylamide) terpolymers. Side chains of tryptophane, phenylalanine, and tyrosine were selected as bioinspired hydrophobic comonomer pendant groups. The synergy between indole and guanidinium group for non-viral gene delivery was shown for the first time. The studies represented in **Chapter 3, 4 and 5** were also selected as cover pictures (**Figure 8.2**). In addition, the study depicted in **Chapter 4** was chosen as 'The Best of Healthcare' by Macromolecular Rapid Communication in 2020 as it increased the availability range of features and functions of polymer-based materials for healthcare. The fundamental investigation on the improvement of biocompatibility for indole and guanidinium containing terpolymers by PEGylation contributed to shaping the future polymer designs. Moreover, a new method for the inclusion of perylene monoimide derivative into the polymer helped to overcome the limitation in the biological application of perylene chromophores. Apart from the non-viral gene delivery potential, guanidinium containing poly(methacrylamide)s showed excellent performance as a component of aptasensor for arsenic detection.



Figure 8.2 Guanidinium containing poly(methacrylamide)s for non-viral gene delivery illustrated by cover pictures of publications represented in this thesis: **P1)** Journal of Materials Chemistry B, **P2)** Macromolecular Rapid Communications- selected as ‘Best of Healthcare’, and **P3)** Macromolecular Rapid Communications

Future research will be directed towards the application of further strategies to improve the performance of guanidinium and indole containing terpolymers. Incorporation of biodegradable bonds into the poly(methacrylamide)s will improve the biocompatibility. Utilization of stimuli responsive groups in the polymer structure can provide on-site nucleic acid release, which will enhance the transfection efficiency further. Moreover, attaching antibodies will help to increase the target specificity. Up to now, myriads of examples for polymeric vectors has been shown but the clinical success of polymeric vectors is still too low. This limitation can be overcome by further interdisciplinary collaborations. For this purpose, the scale of tested cell lines can be increased by including cellular uptake and endosomal escape studies. Theoretical and computational studies can be employed to reveal the synergy of indole and guanidinium groups in the terpolymers. In addition, such studies can provide information on polymer designs that can serve as a delivery platform compatible with different nucleic acids. Apart from all the offered strategies, the biggest lesson can be acquired from the success of lipid-based mRNA Covid 19 vaccine (BNT162b1). To achieve the optimum performance, multiple lipid structures with different properties were combined. So far, the approach for polymeric vectors has been the discovery of the simplest cationic polymer entity that can tackle extra- and intracellular barriers. It is time to change the strategy and change the direction into hybrid systems where each polymer entity bears a different function, yet together they efficiently and safely carry the nucleic acids to target sites.

9. Zusammenfassung und Ausblick

Guanidinium ist eines der faszinierendsten Moleküle, das eine grundlegende Rolle in verschiedenen biochemischen Prozessen spielt. Die Vielseitigkeit von Guanidinium ergibt sich aus seinen besonderen physikalisch-chemischen Eigenschaften, die eine Ladungsdelokalisierung in Y-förmiger Geometrie, ein hoher pKa-Wert (~13,8) und eine anisotrope Hydrathülle sind. Solche Eigenschaften führen zur Bildung spezieller nicht-kovalenter Wechselwirkungen (z. B. zweizählige H-Bindungen mit Oxoanionen, Kation- π -Wechselwirkungen, Ionenpaar- π -Wechselwirkungen und ähnliche Ladungspaarungen) mit anderen Biomolekülen. Nichtsdestotrotz wurde Guanidinium nach der bahnbrechenden Entdeckung seiner Funktion bei der Zellpenetration des Tat-Proteins von HIV-1 zunehmend anerkannt, was einen neuen Weg für die Entwicklung von Guanidinium-reichen Transportern eröffnete. Abgesehen von der Fähigkeit zur Zellpenetration wurde festgestellt, dass Guanidinium spezielle Wechselwirkungen mit Nukleinsäuren hervorrufen kann. Daher wurden Guanidinium-reiche Transporter für die nicht-virale Genübertragung verwendet.

Aufgrund der strukturellen und funktionellen Freiheit polymerer Vektoren wurden Guanidiniumgruppen auch in Polymerketten eingebaut und in verschiedenen Studien auf nicht-viralen Gentransport untersucht. Das Potenzial von GCPs für die nicht-virale Genübertragung wurde jedoch noch nicht vollständig aufgeklärt. Bisher umfassten die meisten Entwürfe für polymere Vektoren primäre, sekundäre und tertiäre Amingruppen als Quelle der kationischen Ladung. Auf der anderen Seite gibt es für GCPs noch viel mehr zu entdecken. Daher zeigt die vorgestellte Arbeit prominente Studien zu GCPs für den nicht-viralen Gentransfer. Beginnend mit Kapitel 3 wurde ein Evolutionsprozess von Guanidinium-haltigen Poly(methacrylamiden) dargestellt (**Abbildung 9.1**). Jedes Kapitel illustrierte unterschiedliche Polymerdesigns, indem es die Vielseitigkeit der RAFT-Polymerisation betonte. Die Polymerdesigns wurden unter Verwendung von Methacrylamid-Monomeren mit bioinspirierten Seitengruppen erstellt, um die Polymervektoren mit maximaler Leistung zu erhalten.

Kapitel 3 lieferte wertvolle Informationen für Poly(methacrylamide) bezüglich des Einflusses der Comonomerverteilung, der Ladungsdichte und des kationischen Ladungsursprungs auf die DNA-Bindungsaffinität. Die Auswirkung der Comonomerverteilung auf die DNA-Bindung war ausgeprägter bei niedrigem Gehalt an kationischem Comonomer. Gradientencopolymere mit einem Gehalt an kationischem Comonomer von 5 Mol-% waren effektiver für die DNA-Bindung, unabhängig vom Ursprung der kationischen Ladung. Nichtsdestotrotz wurde der ausgeprägtere Einfluss der Comonomerverteilung für das primäre Amingegenstück beobachtet, was auch auf den Einfluss der kationischen Ladungsquelle hinwies. Der Unterschied in der DNA-Bindungsaffinität bezüglich der Comonomerverteilung wurde mit zunehmender kationischer Ladungsdichte weniger erkennbar. Vorläufige Transfektionsexperimente in CHO-K1-Zellen zeigten eine höhere Transfektionseffizienz für die Polyplexe mit 90 Mol-% Guanidiniumgehalt im Vergleich zu den primären Amingegenständen bei einem N/P-Verhältnis von 20. Der

Einfluss der Comonomerverteilung auf die Transfektionseffizienz war für die Polyplexe mit unbedeutend 90 Mol-% Guanidiniumgehalt. Andererseits zeigten die statistischen Copolymere eine geringere Toxizität in L-929-Maus-Fibroblasten. Diese Beobachtungen trugen dazu bei, die folgenden Designs von Guanidinium enthaltenden Poly(methacrylamiden) zu formen, indem sie die beste Comonomerverteilung mit optimaler kationischer Ladungsdichte offenbarten, um eine effiziente Transfektion mit hoher Zellebensfähigkeit zu erreichen.

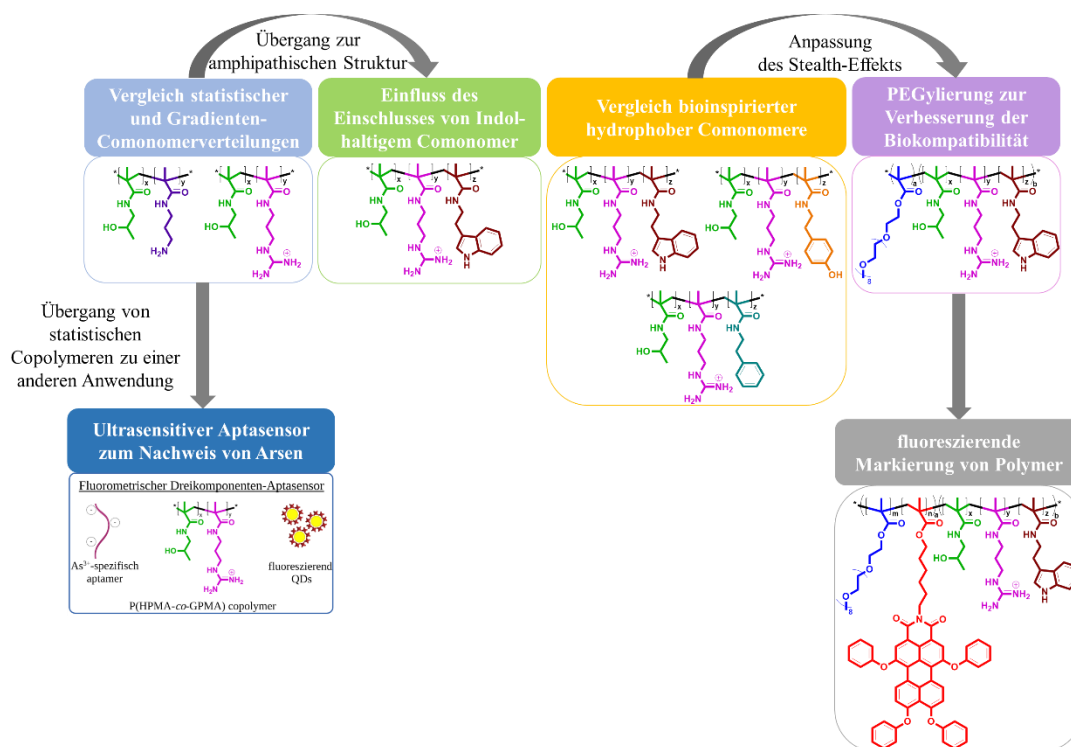


Abbildung 9.1 Der Evolutionsprozess von Guanidinium-haltigen Poly(methacrylamiden), der in dieser Dissertation vorgestellt wird

Nachdem die optimale Comonomerverteilung und kationische Ladungsdichte für Guanidinium-haltige Poly(methacrylamide) aufgezeigt wurden, richtete **Kapitel 4** den Fokus auf die Strategien zur Verbesserung der Transfektionsleistung dieser Polymere. Eine Strategie ist das Umschalten der kationischen Natur des Polymers in eine amphipathische durch die Verwendung von hydrophoben Comonomeren. Das bioinspirierte hydrophobe Comonomer, Indol-haltiges Methacrylamid-Monomer, wurde aufgrund der Synergie zwischen Indol und Guanidinium, die für verschiedene biochemische Prozesse wie die Zellpenetration von grundlegender Bedeutung ist, als Mimetikum von Tryptophan ausgewählt. Somit wurde das erste Beispiel eines Guanidinium- und Indol-haltigen Poly(methacrylamid)-Terpolymers für die nicht-virale Genübertragung erreicht. Der Gehalt an indolhaltigem Comonomer wurde als der maximal mögliche Gehalt (16 Mol-%) angestrebt, der eine ausgezeichnete Löslichkeit des Polymers in wässrigen Medien sowie eine amphipathische Natur

bereitstellt. Der Guanidiniumgehalt wurde bei ~60 Mol-% gehalten. Der Einschluss von Indol in Guanidinium enthaltendes Poly(methacrylamid) führte zu einer 200-fachen Steigerung der DNA-Transfektionseffizienz in CHO-K1-Zellen trotz einer leichten Verringerung der Zellebensfähigkeit.

Das außergewöhnliche Transfektionsergebnis, das mit Indol und Guanidinium enthaltendem Terpolymer erzielt wurde, weckte die Neugier, ob dieser Effekt auf die Synergie zwischen Guanidinium und Indol zurückzuführen ist oder ein besserer Effekt mit anderen bioinspirierten hydrophoben Gruppen erzielt werden könnte. Daher stellte **Kapitel 5** die Untersuchungen zum Einfluss des Ursprungs hydrophober Gruppen auf die DNA-Abgabe dar. Phenyl- und Hydroxyphenyl-tragende bioinspirierte Methacrylamid-Comonomere wurden als Mimetika von Phenylalanin- bzw. Tyrosin-Seitenketten ausgewählt. Der Einfluss von Indol-, Phenyl- und Hydroxyphenyleinheiten in Guanidinium enthaltenden Terpolymeren wurde im Hinblick auf DNA-Bindung, Transfektionseffizienz und Toxizität untersucht. Obwohl Zyto- und Hämokompatibilitätsuntersuchungen unabhängig vom Ursprung der hydrophoben Gruppen eine hohe Biokompatibilität zeigten, zeigten indolhaltige Terpolymere die höchste Transfektion in CHO-K1-Zellen. Als Ergebnis wird geschlussfolgert, dass die Synergie zwischen Indol und Guanidinium besonders ist, und die folgenden Studien konzentrieren sich auf das Indol und Guanidinium enthaltende Terpolymer.

Obwohl in-vitro-Studien von polymeren Vektoren vielversprechende Ergebnisse für die Nukleinsäureabgabe liefern können, verursacht die systemische Verabreichung von Polyplexen die signifikante Verringerung des Erfolgs der Nukleinsäureabgabe aufgrund der Wechselwirkungen von positiv geladenen Polyplexen mit negativ geladenen Proteinen im Blut. Um diese Einschränkung zu überwinden, ist der Einbau von neutral geladenen hydrophilen Einheiten in die polymeren Vektoren eine gängige Strategie, die einen „Stealth-Effekt“ gegen Proteine im Blut bietet. PEG ist das am besten untersuchte Polymer für den Stealth-Effekt, jedoch kann sein Einbau die Effizienz der Nukleinsäureabgabe erheblich verringern. Insbesondere die Molmasse von PEG spielt eine entscheidende Rolle für die Leistung von Polyplexen. Trotz der vielversprechenden In-vitro-Transfektionsleistung von Indol- und Guanidiniumhaltigen Terpolymeren ist der hohe Guanidiniumgehalt eine Einschränkung für die systemische Verabreichung dieses polymeren Vektors für In-vivo-Studien. Daher beschreibt **Kapitel 6** die PEGylierung von Indol- und Guanidiniumhaltigen Terpolymeren. Zu diesem Zweck wurden Diblockcopolymere bestehend aus P(MEO₉MA)-Homopolymer mit einer Molmasse im Bereich von 3 000 bis 40 000 g mol⁻¹ hergestellt. Um die optimale Länge des P(MEO₉MA)-Blocks aufzuzeigen, wurde für den zweiten Block aus Indol und Guanidinium enthaltendem Terpolymer eine ähnliche Molmasse und ein ähnlicher Comonomergehalt angestrebt. Bei einem N/P-Verhältnis von 20 zeigten die Diblockcopolymere mit 3 000 und 6 000 g mol⁻¹ P(MEO₉MA)-Einheit eine DNA-Transfektion in CHO-K1-Zellen, während die weitere Zunahme der P(MEO₉MA)-Länge den Verlust der Transfektion verursachte Leistung. Darüber hinaus verhinderte das Vorhandensein dichter und langer neutral

geladener Einheiten eine effiziente DNA-Kondensation, sodass ein begrenzter Schutz der DNA vor enzymatischem Abbau beobachtet wurde. Dennoch ist diese Studie das erste Beispiel einer systematischen Untersuchung zur PEGylierung von GCPs. Darüber hinaus liefert es praktische Informationen, um den Weg zur Verbesserung der Biokompatibilität von Indol- und Guanidinium-haltigen Terpolymeren aufzuzeigen. Neben PEGylierungsstudien veranschaulichte dieses Kapitel einen neuen Ansatz zur Fluoreszenzmarkierung von wasserlöslichen Polymeren mit hydrophoben Chromophoren. Ein Perylenmonoimid-Derivat, PMIM-Monomer, wurde durch RAFT-Polymerisation eingebaut, indem man sich die Anwesenheit des P(MEO₉MA)-Blocks zunutze machte. Der Erfolg des Markierungsansatzes wurde in HeLa-Zellen durch SIM-Studien beobachtet, die die Anwendbarkeit des vorgeschlagenen Markierungsansatzes bewiesen.

Abgesehen von nichtviralen Gentransportanwendungen wurde die Vielseitigkeit von Guanidinium-haltigen Poly(methacrylamiden) in **Kapitel 7** gezeigt. P(HPMA-co-GPMA)-Copolymer wurde als Komponente eines hochempfindlichen und selektiven fluoreszierenden Aptasensors für den Nachweis von Arsen verwendet. P(HPMA-co-GPMA)-Copolymer bindet in Abwesenheit von As³⁺-Ionen selektiv an das Aptamer, indem MPA-CdTe@CdS-QDs frei bleiben. Andererseits bilden sich in Gegenwart von As³⁺-Ionen Aptamer/As³⁺-Ionen-Komplexe, was zu elektrostatischen Wechselwirkungen zwischen freien Copolymeren und MPA-CdTe@CdS-QDs führt. Als Ergebnis wird die Fluoreszenz von MPA-CdTe@CdS-QDs gequenchet. Der vorgestellte Aptasensor zeigte eine viel höhere Empfindlichkeit im Vergleich zu anderen vorgeschlagenen As³⁺-Nachweismethoden. Außerdem war es in Gegenwart anderer Metallionen hochselektiv für As³⁺. Seine Anwendbarkeit wurde in realen Beispielen bewertet; Mineralwasser, Erdwasser, Leitungswasser und Apfelsaft, die mit As³⁺ versetzt wurden. Die prozentuale Wiederfindung des Aptasensors für jede Probe bewies die Effizienz des Verfahrens. Neben einer einfachen und kostengünstigen Vorbereitung kann der vorgeschlagene Aptasensor einen schnellen Arsennachweis vor Ort liefern.

Zusammenfassend lieferte die vorgestellte Dissertation in mehrfacher Hinsicht wertvolle Ergebnisse zu guanidiniumhaltigen Poly(methacrylamiden). Die Nutzung der RAFT-Polymerisation ermöglichte den Einbau verschiedener Monomere mit geordneter Comonomerverteilung, Comonomergehalt, Polymerarchitektur und Molmasse. Die hydrodynamische Charakterisierung der synthetisierten Polymere zur Berechnung der absoluten Molmasse diente als geeignete Alternative zur Überwindung von Inkonsistenzen bei der Molmassenbestimmung kationischer Polymere über SEC-Systeme. Darüber hinaus liefert die Copolymerisation von sowohl hydrophilen als auch hydrophoben Monomeren in einer wässrigen Reaktionsmischung auf kontrollierte Weise wertvolle Informationen für die Synthese von Guanidinium enthaltenden amphipathischen Copolymeren. Die Natur ist die größte Inspirationsquelle für Wissenschaftler. Auch in dieser Arbeit war die Motivation die Herstellung von bioinspirierten guanidiniumhaltigen Poly(methacrylamid)-Terpolymeren. Seitenketten von Tryptophan, Phenylalanin und Tyrosin wurden als

bioinspirierte hydrophobe Comonomer-Anhängergruppen ausgewählt. Die Synergie zwischen der Indol- und der Guanidinium-Gruppe für die nicht-virale Genübertragung wurde zum ersten Mal gezeigt. Die in den **Kapiteln 3, 4 und 5** dargestellten Studien wurden auch als Titelbilder ausgewählt (**Abbildung 8.2**). Darüber hinaus wurde die in **Kapitel 4** dargestellte Studie von Macromolecular Rapid Communication im Jahr 2020 als „The Best of Healthcare“ ausgewählt, da sie die Verfügbarkeit von Merkmalen und Funktionen von Materialien auf Polymerbasis für das Gesundheitswesen vergrößerte. Die grundlegende Untersuchung zur Verbesserung der Biokompatibilität von Indol- und Guanidinium-haltigen Terpolymeren durch PEGylierung trug zu zukünftigen Polymerdesigns bei, um das beobachtete Problem der Nukleinsäurekondensation zu überwinden. Darüber hinaus half die Einbettung eines Perylenmonoimidderivats in das Polymer, die Beschränkungen für die biologische Anwendung von Perylenchromophoren zu überwinden. Abgesehen von dem Potenzial für die Übertragung von nichtviralen Genen zeigten guanidiniumhaltige Poly(methacrylamide) eine hervorragende Leistung als Komponente eines Aptasensors für den Nachweis von Arsen.



Abbildung 9.2 Guanidiniumhaltige Poly(methacrylamide) für den nicht-viralen Gentransport illustriert durch Titelbilder der in dieser Arbeit vertretenen Publikationen: **P1)** Journal of Materials Chemistry B, **P2)** Macromolecular Rapid Communications– ausgewählt als „Best of Healthcare“ und **P3)** Macromolecular Rapid Communications

Zukünftige Forschung wird auf die Anwendung weiterer Strategien zur Verbesserung der Leistung von Guanidinium- und Indol-haltigen Terpolymeren gerichtet sein. Der Einbau biologisch abbaubarer Bindungen in die Poly(methacrylamide) verbessert die Biokompatibilität. Die Verwendung von auf Stimuli ansprechenden Gruppen in der Polymerstruktur wird eine Nukleinsäurefreisetzung vor Ort bereitstellen, was die Transfektionseffizienz weiter steigern wird. Darüber hinaus hilft das Anbringen von Antikörpern, die Zielspezifität zu erhöhen. Bisher wurden unzählige Beispiele für polymere Vektoren gezeigt, aber der klinische Erfolg von polymeren Vektoren ist noch zu gering. Diese Einschränkung kann durch weitere interdisziplinäre Kooperationen überwunden werden. Zu diesem Zweck kann der Umfang der getesteten Zelllinien erhöht werden, indem zelluläre Aufnahme- und endosomale Escape-Studien

eingeschlossen werden. Theoretische und rechnerische Studien können verwendet werden, um die Synergie von Indol- und Guanidiniumgruppen in den Terpolymeren aufzudecken. Darüber hinaus können solche Studien Informationen über Polymerdesigns liefern, die als Abgabepattform dienen können, die für mehrere Nukleinsäuren kompatibel ist. Abgesehen von all den angebotenen Strategien kann die größte Lehre aus dem Erfolg des lipidbasierten mRNA-Covid-19-Impfstoffs (BNT162b1) gezogen werden. Um die optimale Leistung zu erzielen, wurden mehrere Lipidstrukturen mit unterschiedlichen Eigenschaften zusammen verwendet. Bisher war der Ansatz für polymere Vektoren die Entdeckung der einfachsten kationischen Polymereinheit, die extra- und intrazelluläre Barrieren überwinden kann. Es ist an der Zeit, die Strategie zu ändern und die Richtung hin zu Hybridsystemen zu ändern, bei denen jede Polymereinheit eine andere Funktion trägt, aber zusammen die Nukleinsäuren effizient und sicher zu den Zielorten transportieren.

10. References

1. Dahm, R., Friedrich Miescher and the discovery of DNA. *Developmental Biology* **2005**, 278 (2), 274-288.
2. Avery, O. T.; MacLeod, C. M.; McCarty, M., Studies on the Chemical Nature of the Substance Inducing Transformation of Pneumococcal Types: Induction of Transformation by a Desoxyribonucleic Acid Fraction Isolated from Pneumococcus Type III. *Journal of Experimental Medicine* **1944**, 79 (2), 137-158.
3. Watson, J. D.; Crick, F. H. C., Molecular Structure of Nucleic Acids: A Structure for Deoxyribose Nucleic Acid. *Nature* **1953**, 171 (4356), 737-738.
4. Jackson, D. A.; Symons, R. H.; Berg, P., Biochemical method for inserting new genetic information into DNA of Simian Virus 40: circular SV40 DNA molecules containing lambda phage genes and the galactose operon of Escherichia coli. *Proceedings of the National Academy of Sciences of the United States of America* **1972**, 69 (10), 2904-2909.
5. Sanger, F.; Coulson, A. R., A rapid method for determining sequences in DNA by primed synthesis with DNA polymerase. *Journal of Molecular Biology* **1975**, 94 (3), 441-448.
6. Watson, J. D., The human genome project: past, present, and future. *Science* **1990**, 248 (4951), 44.
7. International Human Genome Sequencing, C., Finishing the euchromatic sequence of the human genome. *Nature* **2004**, 431 (7011), 931-945.
8. Eddy, S. R., Non-coding RNA genes and the modern RNA world. *Nature Reviews Genetics* **2001**, 2 (12), 919-929.
9. He, L.; Hannon, G. J., MicroRNAs: small RNAs with a big role in gene regulation. *Nature Reviews Genetics* **2004**, 5 (7), 522-531.
10. Wagner, E., Biomaterials in RNAi therapeutics: quo vadis? *Biomaterials Science* **2013**, 1 (8), 804-809.
11. Li, H.; Yang, Y.; Hong, W.; Huang, M.; Wu, M.; Zhao, X., Applications of genome editing technology in the targeted therapy of human diseases: mechanisms, advances and prospects. *Signal Transduction and Targeted Therapy* **2020**, 5 (1), 1.
12. Friedmann, T.; Roblin, R., Gene Therapy for Human Genetic Disease? *Science* **1972**, 175 (4025), 949.
13. Ginn, S. L.; Amaya, A. K.; Alexander, I. E.; Edelstein, M.; Abedi, M. R., Gene therapy clinical trials worldwide to 2017: An update. *The Journal of Gene Medicine* **2018**, 20 (5), e3015.
14. Brown, M. D.; Schätzlein, A. G.; Uchegbu, I. F., Gene delivery with synthetic (non viral) carriers. *International Journal of Pharmaceutics* **2001**, 229 (1), 1-21.
15. Hill, I. R. C.; Garnett, M. C.; Bignotti, F.; Davis, S. S., Determination of Protection from Serum Nuclease Activity by DNA-Polyelectrolyte Complexes Using an Electrophoretic Method. *Analytical Biochemistry* **2001**, 291 (1), 62-68.
16. Yang, Z.; Guo, Z.; Tian, H.; Chen, X., Enhancers in polymeric nonviral gene delivery systems. *View* **2021**, 2 (1), 20200072.
17. Jones, C. H.; Chen, C.-K.; Ravikrishnan, A.; Rane, S.; Pfeifer, B. A., Overcoming nonviral gene delivery barriers: perspective and future. *Molecular pharmaceutics* **2013**, 10 (11), 4082-4098.
18. van den Berg, A. I. S.; Yun, C.-O.; Schiffelers, R. M.; Hennink, W. E., Polymeric delivery systems for nucleic acid therapeutics: Approaching the clinic. *Journal of Controlled Release* **2021**, 331, 121-141.

References

19. Rosenberg, S. A.; Aebbersold, P.; Cornetta, K.; Kasid, A.; Morgan, R. A.; Moen, R.; Karson, E. M.; Lotze, M. T.; Yang, J. C.; Topalian, S. L.; Merino, M. J.; Culver, K.; Miller, A. D.; Blaese, R. M.; Anderson, W. F., Gene Transfer into Humans — Immunotherapy of Patients with Advanced Melanoma, Using Tumor-Infiltrating Lymphocytes Modified by Retroviral Gene Transduction. *New England Journal of Medicine* **1990**, *323* (9), 570-578.
20. Rubanyi, G. M., The future of human gene therapy. *Molecular Aspects of Medicine* **2001**, *22* (3), 113-142.
21. Lächelt, U.; Wagner, E., Nucleic Acid Therapeutics Using Polyplexes: A Journey of 50 Years (and Beyond). *Chemical Reviews* **2015**, *115* (19), 11043-11078.
22. Yahya, E. B.; Alqadhi, A. M., Recent trends in cancer therapy: A review on the current state of gene delivery. *Life Sciences* **2021**, *269*, 119087.
23. Felgner, P. L.; Gadek, T. R.; Holm, M.; Roman, R.; Chan, H. W.; Wenz, M.; Northrop, J. P.; Ringold, G. M.; Danielsen, M., Lipofection: a highly efficient, lipid-mediated DNA-transfection procedure. *Proceedings of the National Academy of Sciences* **1987**, *84* (21), 7413.
24. Zhi, D.; Zhang, S.; Cui, S.; Zhao, Y.; Wang, Y.; Zhao, D., The Headgroup Evolution of Cationic Lipids for Gene Delivery. *Bioconjugate Chemistry* **2013**, *24* (4), 487-519.
25. Dan, N.-D.; James, H.; Caroline, J. S., Structure-Activity Relationship in Cationic Lipid Mediated Gene Transfection. *Current Medicinal Chemistry* **2003**, *10* (14), 1233-1261.
26. Liu, Q.; Jiang, Q.-Q.; Yi, W.-J.; Zhang, J.; Zhang, X.-C.; Wu, M.-B.; Zhang, Y.-M.; Zhu, W.; Yu, X.-Q., Novel imidazole-functionalized cyclen cationic lipids: Synthesis and application as non-viral gene vectors. *Bioorganic & Medicinal Chemistry* **2013**, *21* (11), 3105-3113.
27. Buck, J.; Grossen, P.; Cullis, P. R.; Huwyler, J.; Witzigmann, D., Lipid-Based DNA Therapeutics: Hallmarks of Non-Viral Gene Delivery. *ACS Nano* **2019**, *13* (4), 3754-3782.
28. Rao, N. M., Cationic lipid-mediated nucleic acid delivery: beyond being cationic. *Chemistry and Physics of Lipids* **2010**, *163* (3), 245-252.
29. Freitag, F.; Wagner, E., Optimizing synthetic nucleic acid and protein nanocarriers: The chemical evolution approach. *Adv. Drug Deliv. Rev.* **2021**, *168*, 30-54.
30. Lee, E. R.; Marshall, J.; Siegel, C. S.; Jiang, C.; Yew, N. S.; Nichols, M. R.; Nietupski, J. B.; Ziegler, R. J.; Lane, M. B.; Wang, K. X.; Wan, N. C.; Scheule, R. K.; Harris, D. J.; Smith, A. E.; Cheng, S. H., Detailed Analysis of Structures and Formulations of Cationic Lipids for Efficient Gene Transfer to the Lung. *Human Gene Therapy* **1996**, *7* (14), 1701-1717.
31. Akinc, A.; Maier, M. A.; Manoharan, M.; Fitzgerald, K.; Jayaraman, M.; Barros, S.; Ansell, S.; Du, X.; Hope, M. J.; Madden, T. D.; Mui, B. L.; Semple, S. C.; Tam, Y. K.; Ciufolini, M.; Witzigmann, D.; Kulkarni, J. A.; van der Meel, R.; Cullis, P. R., The Onpattro story and the clinical translation of nanomedicines containing nucleic acid-based drugs. *Nature Nanotechnology* **2019**, *14* (12), 1084-1087.
32. Kumar, R.; Santa Chalarca, C. F.; Bockman, M. R.; Bruggen, C. V.; Grimme, C. J.; Dalal, R. J.; Hanson, M. G.; Hexum, J. K.; Reineke, T. M., Polymeric Delivery of Therapeutic Nucleic Acids. *Chemical Reviews* **2021**, *121* (18), 11527-11652.
33. Mitchell, M. J.; Billingsley, M. M.; Haley, R. M.; Wechsler, M. E.; Peppas, N. A.; Langer, R., Engineering precision nanoparticles for drug delivery. *Nature Reviews Drug Discovery* **2021**, *20* (2), 101-124.

34. Vaheri, A.; Pagano, J. S., Infectious poliovirus RNA: a sensitive method of assay. *Virology* **1965**, 27 (3), 434-436.
35. Wu, G. Y.; Wu, C. H., Receptor-mediated in vitro gene transformation by a soluble DNA carrier system. *The Journal of biological chemistry* **1987**, 262 (10), 4429-32.
36. Wu, G. Y.; Wu, C. H., Receptor-mediated gene delivery and expression in vivo. *Journal of Biological Chemistry* **1988**, 263 (29), 14621-14624.
37. Levine, A. S.; Levy, H. B., Phase I-II trials of poly IC stabilized with poly-L-lysine. *Cancer Treat Rep* **1978**, 62 (11), 1907-1912.
38. Luthman, H.; Magnusson, G., High efficiency polyoma DNA transfection of chloroquine treated cells. *Nucleic Acids Research* **1983**, 11 (5), 1295-1308.
39. Cotten, M.; Längle-Rouault, F.; Kirlappos, H.; Wagner, E.; Mechtler, K.; Zenke, M.; Beug, H.; Birnstiel, M. L., Transferrin-polycation-mediated introduction of DNA into human leukemic cells: stimulation by agents that affect the survival of transfected DNA or modulate transferrin receptor levels. *Proceedings of the National Academy of Sciences* **1990**, 87 (11), 4033.
40. Lopata, M. A.; Cleveland, D. W.; Sollner-Webb, B., High level transient expression of a chloramphenicol acetyl transferase gene by DEAE-dextran mediated DNA transfection coupled with a dimethyl sulfoxide or glycerol shock treatment. *Nucleic Acids Research* **1984**, 12 (14), 5707-5717.
41. Kawai, S.; Nishizawa, M., New procedure for DNA transfection with polycation and dimethyl sulfoxide. *Molecular and Cellular Biology* **1984**, 4 (6), 1172.
42. Zhang, X.; Sawyer, G. J.; Dong, X.; Qiu, Y.; Collins, L.; Fabre, J. W., The in vivo use of chloroquine to promote non-viral gene delivery to the liver via the portal vein and bile duct. *J Gene Med* **2003**, 5 (3), 209-18.
43. Haensler, J.; Szoka, F. C., Polyamidoamine cascade polymers mediate efficient transfection of cells in culture. *Bioconjugate Chemistry* **1993**, 4 (5), 372-379.
44. Zhang, P.; Wagner, E., History of Polymeric Gene Delivery Systems. *Topics in current chemistry (Cham)* **2017**, 375 (2), 26.
45. Boussif, O.; Lezoualc; h, F.; Zanta, M. A.; Mergny, M. D.; Scherman, D.; Demeneix, B.; Behr, J. P., A versatile vector for gene and oligonucleotide transfer into cells in culture and in vivo: polyethylenimine. *Proceedings of the National Academy of Sciences* **1995**, 92 (16), 7297.
46. Lungwitz, U.; Breunig, M.; Blunk, T.; Göpferich, A., Polyethylenimine-based non-viral gene delivery systems. *European Journal of Pharmaceutics and Biopharmaceutics* **2005**, 60 (2), 247-266.
47. Hsu, C. Y. M.; Uludağ, H., A simple and rapid nonviral approach to efficiently transfect primary tissue-derived cells using polyethylenimine. *Nature Protocols* **2012**, 7 (5), 935-945.
48. Funhoff, A. M.; van Nostrum, C. F.; Koning, G. A.; Schuurmans-Nieuwenbroek, N. M. E.; Crommelin, D. J. A.; Hennink, W. E., Endosomal Escape of Polymeric Gene Delivery Complexes Is Not Always Enhanced by Polymers Buffering at Low pH. *Biomacromolecules* **2004**, 5 (1), 32-39.
49. Benjaminsen, R. V.; Matthebjerg, M. A.; Henriksen, J. R.; Moghimi, S. M.; Andresen, T. L., The Possible “Proton Sponge ” Effect of Polyethylenimine (PEI) Does Not Include Change in Lysosomal pH. *Molecular Therapy* **2013**, 21 (1), 149-157.

References

50. Bieber, T.; Meissner, W.; Kostin, S.; Niemann, A.; Elsassner, H.-P., Intracellular route and transcriptional competence of polyethylenimine–DNA complexes. *Journal of Controlled Release* **2002**, *82* (2), 441-454.
51. Bus, T.; Traeger, A.; Schubert, U. S., The great escape: how cationic polyplexes overcome the endosomal barrier. *Journal of Materials Chemistry B* **2018**, *6* (43), 6904-6918.
52. Mintzer, M. A.; Simanek, E. E., Nonviral Vectors for Gene Delivery. *Chemical Reviews* **2009**, *109* (2), 259-302.
53. Mitchell, D. J.; Steinman, L.; Kim, D. T.; Fathman, C. G.; Rothbard, J. B., Polyarginine enters cells more efficiently than other polycationic homopolymers. *The Journal of Peptide Research* **2000**, *56* (5), 318-325.
54. Green, M.; Loewenstein, P. M., Autonomous functional domains of chemically synthesized human immunodeficiency virus tat trans-activator protein. *Cell* **1988**, *55* (6), 1179-1188.
55. Frankel, A. D.; Pabo, C. O., Cellular uptake of the tat protein from human immunodeficiency virus. *Cell* **1988**, *55* (6), 1189-1193.
56. Sternson, L. A., Obstacles to Polypeptide Delivery. *Annals of the New York Academy of Sciences* **1987**, *507* (1), 19-21.
57. Vivès, E.; Brodin, P.; Lebleu, B., A Truncated HIV-1 Tat Protein Basic Domain Rapidly Translocates through the Plasma Membrane and Accumulates in the Cell Nucleus*. *Journal of Biological Chemistry* **1997**, *272* (25), 16010-16017.
58. Wender, P. A.; Mitchell, D. J.; Pattabiraman, K.; Pelkey, E. T.; Steinman, L.; Rothbard, J. B., The design, synthesis, and evaluation of molecules that enable or enhance cellular uptake: Peptoid molecular transporters. *Proceedings of the National Academy of Sciences* **2000**, *97* (24), 13003.
59. Goun, E. A.; Pillow, T. H.; Jones, L. R.; Rothbard, J. B.; Wender, P. A., Molecular Transporters: Synthesis of Oligoguanidinium Transporters and Their Application to Drug Delivery and Real-Time Imaging. *ChemBioChem* **2006**, *7* (10), 1497-1515.
60. Wexselblatt, E.; Esko, J. D.; Tor, Y., On Guanidinium and Cellular Uptake. *The Journal of Organic Chemistry* **2014**, *79* (15), 6766-6774.
61. Pantos, A.; Tsogas, I.; Paleos, C. M., Guanidinium group: A versatile moiety inducing transport and multicompartimentalization in complementary membranes. *Biochimica et Biophysica Acta (BBA) - Biomembranes* **2008**, *1778* (4), 811-823.
62. Brock, R., The Uptake of Arginine-Rich Cell-Penetrating Peptides: Putting the Puzzle Together. *Bioconjugate Chemistry* **2014**, *25* (5), 863-868.
63. Gasparini, G.; Bang, E.-K.; Montenegro, J.; Matile, S., Cellular uptake: lessons from supramolecular organic chemistry. *Chemical Communications* **2015**, *51* (52), 10389-10402.
64. Stanzl, E. G.; Trantow, B. M.; Vargas, J. R.; Wender, P. A., Fifteen Years of Cell-Penetrating, Guanidinium-Rich Molecular Transporters: Basic Science, Research Tools, and Clinical Applications. *Accounts of Chemical Research* **2013**, *46* (12), 2944-2954.
65. Siphshvili, Z.; Scholl, F. A.; Oliver, S. F.; Adams, A.; Contag, C. H.; Wender, P. A.; Khavari, P. A., Gene Transfer via Reversible Plasmid Condensation with Cysteine-Flanked, Internally Spaced Arginine-Rich Peptides. *Human Gene Therapy* **2003**, *14* (13), 1225-1233.
66. Wender, P. A.; Galliher, W. C.; Goun, E. A.; Jones, L. R.; Pillow, T. H., The design of guanidinium-rich transporters and their internalization mechanisms. *Advanced Drug Delivery Reviews* **2008**, *60* (4), 452-472.

67. Mori, A., Biochemistry and neurotoxicology of guanidino compounds. *The Pavlovian Journal of Biological Science* **1987**, 22 (3), 85-94.
68. Strecker, A., Untersuchungen über die chemischen Beziehungen zwischen Guanin, Xanthin, Theobromin, Caffein und Kreatinin. *Justus Liebigs Annalen der Chemie* **1861**, 118 (2), 151-177.
69. Gund, P., Guanidine, trimethylenemethane, and "Y-delocalization." Can acyclic compounds have "aromatic" stability? *Journal of Chemical Education* **1972**, 49 (2), 100.
70. Pauling, L., *The Nature of the Chemical Bond*. Cornell University Press: Ithaca, New York, 1960.
71. Bally, T.; Diehl, P.; Haselbach, E.; Tracey, A. S., The Bond-Rotational Mobility of Guanidinium Ion. *Helvetica Chimica Acta* **1975**, 58 (8), 2398-2402.
72. Capitani, J. F.; Pedersen, L., Rotational barriers in the guanidinium ion: an ab initio study. *Chemical Physics Letters* **1978**, 54 (3), 547-550.
73. Ohwada, T.; Itai, A.; Ohta, T.; Shudo, K., Nitroethylene yields (N,N-dihydroxyiminium)methyl cation in trifluoromethanesulfonic acid. Dications stabilized by Y delocalization. *Journal of the American Chemical Society* **1987**, 109 (23), 7036-7041.
74. Sapse, A. M.; Massa, L. J., Guanidinium ion: SCF calculations. *The Journal of Organic Chemistry* **1980**, 45 (4), 719-721.
75. Tomohiko, O.; Hirotaka, K.; Hiroshi, I., π -Conjugation in Y-Shaped Configuration. Does a Special Stability Exist? *Bulletin of the Chemical Society of Japan* **1997**, 70 (10), 2411-2415.
76. Bharatam, P. V.; Iqbal, P.; Malde, A.; Tiwari, R., Electron Delocalization in Aminoguanidine: A Computational Study. *The Journal of Physical Chemistry A* **2004**, 108 (47), 10509-10517.
77. Kollman, P.; McKelvey, J.; Gund, P., Amino substituent effect on the properties of ionic compounds. *Journal of the American Chemical Society* **1975**, 97 (7), 1640-1645.
78. Rozas, I.; Sánchez-Sanz, G.; Alkorta, I.; Elguero, J., Solvent effects on guanidinium-anion interactions and the problem of guanidinium Y-aromaticity. *Journal of Physical Organic Chemistry* **2013**, 26 (5), 378-385.
79. Kleinpeter, E.; Koch, A., Y-aromaticity – existing: yes or no? An answer given on the magnetic criterion (TSNMRs). *Tetrahedron* **2016**, 72 (13), 1675-1685.
80. Wiberg, K. B., Resonance interactions in acyclic systems. 2. Y-Conjugated anions and cations. *Journal of the American Chemical Society* **1990**, 112 (11), 4177-4182.
81. Gobbi, A.; Frenking, G., Y-Conjugated compounds: the equilibrium geometries and electronic structures of guanidine, guanidinium cation, urea, and 1,1-diaminoethylene. *Journal of the American Chemical Society* **1993**, 115 (6), 2362-2372.
82. Caminiti, R.; Pieretti, A.; Bencivenni, L.; Ramondo, F.; Sanna, N., Amidine N-C(N)-N Skeleton: Its Structure in Isolated and Hydrogen-Bonded Guanidines from ab Initio Calculations. *The Journal of Physical Chemistry* **1996**, 100 (26), 10928-10935.
83. Haas, D. J.; Harris, D. R.; Mills, H. H., The crystal structure of guanidinium chloride. *Acta Crystallographica* **1965**, 19 (4), 676-679.
84. Adams, J. M.; Small, R. W. H., The crystal structure of guanidinium carbonate. *Acta Crystallographica Section B* **1974**, 30 (9), 2191-2193.

References

85. Göbel, M.; Klapötke, T. M., First structural characterization of guanidine, $\text{HN}\square\text{C}(\text{NH}_2)_2$. *Chemical Communications* **2007**, (30), 3180-3182.
86. Yamada, T.; Liu, X.; Englert, U.; Yamane, H.; Dronskowski, R., Solid-State Structure of Free Base Guanidine Achieved at Last. *Chemistry – A European Journal* **2009**, 15 (23), 5651-5655.
87. Deringer, V. L.; George, J.; Dronskowski, R.; Englert, U., Plane-Wave Density Functional Theory Meets Molecular Crystals: Thermal Ellipsoids and Intermolecular Interactions. *Accounts of Chemical Research* **2017**, 50 (5), 1231-1239.
88. Hall, N. F.; Sprinkle, M. R., Relations between the Structure and Strength of Certain Organic Bases in Aqueous Solution. *Journal of the American Chemical Society* **1932**, 54 (9), 3469-3485.
89. Angyal, S. J.; Warburton, W. K., 549. The basic strengths of methylated guanidines. *Journal of the Chemical Society (Resumed)* **1951**, (0), 2492-2494.
90. Sapse, A. M.; Snyder, G.; Santoro, A. V., Ab initio SCF study of guanidine and substituted guanidines. *International Journal of Quantum Chemistry* **1981**, 20 (3), 755-762.
91. Raczyńska, E. D.; Cyrański, M. K.; Gutowski, M.; Rak, J.; Gal, J.-F.; Maria, P.-C.; Darowska, M.; Duczmal, K., Consequences of proton transfer in guanidine. *Journal of Physical Organic Chemistry* **2003**, 16 (2), 91-106.
92. Hunter, A.; Borsook, H., The Dissociation Constants of Arginine. *Biochemical Journal* **1924**, 18 (5), 883-890.
93. Noszál, B.; Kassai-Tánczos, R., Microscopic acid—base equilibria of arginine. *Talanta* **1991**, 38 (12), 1439-1444.
94. Orgován, G.; Noszál, B., Electrodeless, accurate pH determination in highly basic media using a new set of ^1H NMR pH indicators. *Journal of Pharmaceutical and Biomedical Analysis* **2011**, 54 (5), 958-964.
95. Orgován, G.; Noszál, B., The complete microspeciation of arginine and citrulline. *Journal of Pharmaceutical and Biomedical Analysis* **2011**, 54 (5), 965-971.
96. Fitch, C. A.; Platzer, G.; Okon, M.; Garcia-Moreno E., B.; McIntosh, L. P., Arginine: Its pKa value revisited. *Protein Science* **2015**, 24 (5), 752-761.
97. Olah, G. A.; Burrichter, A.; Rasul, G.; Prakash, G. K. S., ^1H , ^{13}C , ^{15}N NMR and Ab Initio/IGLO/GIAO-MP2 Study of Mono-, Di-, Tri-, and Tetraprotonated Guanidine. *Journal of the American Chemical Society* **1997**, 119 (52), 12929-12933.
98. Olah, G. A.; Prakash, G. K. S.; Rasul, G., ^{13}C and ^{15}N NMR and ab Initio/GIAO-CCSD(T) Study of the Structure of Mono-, Di-, and Triprotonated Guanidine, Urea, and Thiourea. *The Journal of Physical Chemistry C* **2008**, 112 (21), 7895-7899.
99. Xu, B.; Jacobs, M. I.; Kostko, O.; Ahmed, M., Guanidinium Group Remains Protonated in a Strongly Basic Arginine Solution. *ChemPhysChem* **2017**, 18 (12), 1503-1506.
100. Fossat, M. J.; Zeng, X.; Pappu, R. V., Uncovering Differences in Hydration Free Energies and Structures for Model Compound Mimics of Charged Side Chains of Amino Acids. *The Journal of Physical Chemistry B* **2021**, 125 (16), 4148-4161.
101. Laage, D.; Elsaesser, T.; Hynes, J. T., Water Dynamics in the Hydration Shells of Biomolecules. *Chemical Reviews* **2017**, 117 (16), 10694-10725.
102. Mason, P. E.; Neilson, G. W.; Dempsey, C. E.; Barnes, A. C.; Cruickshank, J. M., The hydration structure of guanidinium and thiocyanate ions: Implications for

- protein stability in aqueous solution. *Proceedings of the National Academy of Sciences* **2003**, *100* (8), 4557.
103. Mason, P. E.; Neilson, G. W.; Enderby, J. E.; Saboungi, M.-L.; Dempsey, C. E.; MacKerell, A. D.; Brady, J. W., The Structure of Aqueous Guanidinium Chloride Solutions. *Journal of the American Chemical Society* **2004**, *126* (37), 11462-11470.
104. Wernersson, E.; Heyda, J.; Vazdar, M.; Lund, M.; Mason, P. E.; Jungwirth, P., Orientational Dependence of the Affinity of Guanidinium Ions to the Water Surface. *The Journal of Physical Chemistry B* **2011**, *115* (43), 12521-12526.
105. Cooper, R. J.; Heiles, S.; DiTucci, M. J.; Williams, E. R., Hydration of Guanidinium: Second Shell Formation at Small Cluster Size. *The Journal of Physical Chemistry A* **2014**, *118* (30), 5657-5666.
106. Werner, J.; Wernersson, E.; Ekholm, V.; Ottosson, N.; Öhrwall, G.; Heyda, J.; Persson, I.; Söderström, J.; Jungwirth, P.; Björneholm, O., Surface Behavior of Hydrated Guanidinium and Ammonium Ions: A Comparative Study by Photoelectron Spectroscopy and Molecular Dynamics. *The Journal of Physical Chemistry B* **2014**, *118* (25), 7119-7127.
107. Hebert, M. J.; Russell, D. H., Hydration of Guanidinium Ions: An Experimental Search for Like-Charged Ion Pairs. *The Journal of Physical Chemistry Letters* **2019**, *10* (6), 1349-1354.
108. S Leikin; V A Parsegian; D C Rau, a.; Rand, R. P., Hydration Forces. *Annual Review of Physical Chemistry* **1993**, *44* (1), 369-395.
109. Bloomfield, V. A., DNA condensation by multivalent cations. *Biopolymers* **1997**, *44* (3), 269-282.
110. Thomas, T. J.; Tajmir-Riahi, H. A.; Thomas, T., Polyamine–DNA interactions and development of gene delivery vehicles. *Amino Acids* **2016**, *48* (10), 2423-2431.
111. Osada, K., Structural Polymorphism of Single pDNA Condensates Elicited by Cationic Block Polyelectrolytes. *Polymers* **2020**, *12* (7), 1603.
112. MacCallum, J. L.; Bennett, W. F. D.; Tieleman, D. P., Transfer of Arginine into Lipid Bilayers Is Nonadditive. *Biophysical Journal* **2011**, *101* (1), 110-117.
113. Ou, S.; Lucas, T. R.; Zhong, Y.; Bauer, B. A.; Hu, Y.; Patel, S., Free Energetics and the Role of Water in the Permeation of Methyl Guanidinium across the Bilayer–Water Interface: Insights from Molecular Dynamics Simulations Using Charge Equilibration Potentials. *The Journal of Physical Chemistry B* **2013**, *117* (13), 3578-3592.
114. Hu, Y.; Ou, S.; Patel, S., Free Energetics of Arginine Permeation into Model DMPC Lipid Bilayers: Coupling of Effective Counterion Concentration and Lateral Bilayer Dimensions. *The Journal of Physical Chemistry B* **2013**, *117* (39), 11641-11653.
115. Herce, H. D.; Garcia, A. E.; Cardoso, M. C., Fundamental Molecular Mechanism for the Cellular Uptake of Guanidinium-Rich Molecules. *Journal of the American Chemical Society* **2014**, *136* (50), 17459-17467.
116. Hu, Y.; Liu, X.; Sinha, S. K.; Patel, S., Translocation Thermodynamics of Linear and Cyclic Nonaarginine into Model DPPC Bilayer via Coarse-Grained Molecular Dynamics Simulation: Implications of Pore Formation and Nonadditivity. *The Journal of Physical Chemistry B* **2014**, *118* (10), 2670-2682.
117. Hu, Y.; Sinha, S. K.; Patel, S., Reconciling Structural and Thermodynamic Predictions Using All-Atom and Coarse-Grain Force Fields: The Case of Charged Oligo-Arginine Translocation into DMPC Bilayers. *The Journal of Physical Chemistry B* **2014**, *118* (41), 11973-11992.

References

118. Sun, D.; Forsman, J.; Woodward, C. E., Evaluating Force Fields for the Computational Prediction of Ionized Arginine and Lysine Side-Chains Partitioning into Lipid Bilayers and Octanol. *Journal of Chemical Theory and Computation* **2015**, *11* (4), 1775-1791.
119. Allolio, C.; Magarkar, A.; Jurkiewicz, P.; Baxová, K.; Javanainen, M.; Mason Philip, E.; Šachl, R.; Cebecauer, M.; Hof, M.; Horinek, D.; Heinz, V.; Rachel, R.; Ziegler Christine, M.; Schröfel, A.; Jungwirth, P., Arginine-rich cell-penetrating peptides induce membrane multilamellarity and subsequently enter via formation of a fusion pore. *Proceedings of the National Academy of Sciences* **2018**, *115* (47), 11923-11928.
120. Verbeek, S. F.; Awasthi, N.; Teiwes, N. K.; Mey, I.; Hub, J. S.; Janshoff, A., How arginine derivatives alter the stability of lipid membranes: dissecting the roles of side chains, backbone and termini. *European Biophysics Journal* **2021**, *50* (2), 127-142.
121. Kanwa, N.; De, S. K.; Maity, A.; Chakraborty, A., Interaction of aliphatic amino acids with zwitterionic and charged lipid membranes: hydration and dehydration phenomena. *Physical Chemistry Chemical Physics* **2020**, *22* (6), 3234-3244.
122. Blondeau, P.; Segura, M.; Pérez-Fernández, R.; de Mendoza, J., Molecular recognition of oxoanions based on guanidinium receptors. *Chemical Society Reviews* **2007**, *36* (2), 198-210.
123. Schug, K. A.; Lindner, W., Noncovalent Binding between Guanidinium and Anionic Groups: Focus on Biological- and Synthetic-Based Arginine/Guanidinium Interactions with Phosph[on]ate and Sulf[on]ate Residues. *Chemical Reviews* **2005**, *105* (1), 67-114.
124. Ariga, K.; Kunitake, T., Molecular Recognition at Air–Water and Related Interfaces: Complementary Hydrogen Bonding and Multisite Interaction. *Accounts of Chemical Research* **1998**, *31* (6), 371-378.
125. Houk, R. J. T.; Tobey, S. L.; Anslyn, E. V., Abiotic Guanidinium Receptors for Anion Molecular Recognition and Sensing. In *Anion Sensing: -/-*, Stibor, I., Ed. Springer Berlin Heidelberg: Berlin, Heidelberg, 2005; pp 199-229.
126. Yoo, J.; Cui, Q., Does Arginine Remain Protonated in the Lipid Membrane? Insights from Microscopic pKa Calculations. *Biophysical Journal* **2008**, *94* (8), L61-L63.
127. Gleason Nicholas, J.; Vostrikov Vitaly, V.; Greathouse Denise, V.; Koeppe Roger, E., Buried lysine, but not arginine, titrates and alters transmembrane helix tilt. *Proceedings of the National Academy of Sciences* **2013**, *110* (5), 1692-1695.
128. Li, L.; Vorobyov, I.; Allen, T. W., The Different Interactions of Lysine and Arginine Side Chains with Lipid Membranes. *The Journal of Physical Chemistry B* **2013**, *117* (40), 11906-11920.
129. Mandell, D. J.; Chorny, I.; Groban, E. S.; Wong, S. E.; Levine, E.; Rapp, C. S.; Jacobson, M. P., Strengths of Hydrogen Bonds Involving Phosphorylated Amino Acid Side Chains. *Journal of the American Chemical Society* **2007**, *129* (4), 820-827.
130. Cotton, F. A.; Day, V. W.; Hazen, E. E.; Larsen, S., Structure of methylguanidinium dihydrogen orthophosphate. Model compound for arginine-phosphate hydrogen bonding. *Journal of the American Chemical Society* **1973**, *95* (15), 4834-4840.
131. S. Furberg, J. S., Crystal Structure of Propylguanidinium Diethyl Phosphate *Acta Chemica Scandinavica* **1972**, *26*, 3699-3707.

132. Springs, B.; Haake, P., Equilibrium constants for association of guanidinium and ammonium ions with oxyanions: The effect of changing basicity of the oxyanion. *Bioorganic Chemistry* **1977**, *6* (2), 181-190.
133. Avilés-Moreno, J. R.; Berden, G.; Oomens, J.; Martínez-Haya, B., Insights into the Recognition of Phosphate Groups by Peptidic Arginine from Action Spectroscopy and Quantum Chemical Computations. *The Journal of Physical Chemistry B* **2019**, *123* (35), 7528-7535.
134. Ohara, K.; Smietana, M.; Vasseur, J.-J., Characterization of Specific Noncovalent Complexes between Guanidinium Derivatives and Single-Stranded DNA by MALDI. *Journal of the American Society for Mass Spectrometry* **2006**, *17* (3), 283-291.
135. Calnan, B. J.; Tidor, B.; Biancalana, S.; Hudson, D.; Frankel, A. D., Arginine-Mediated RNA Recognition: the Arginine Fork. *Science* **1991**, *252* (5009), 1167-1171.
136. Minagawa, K.; Matsuzawa, Y.; Yoshikawa, K.; Matsumoto, M.; Doi, M., Direct observation of the biphasic conformational change of DNA induced by cationic polymers. *FEBS Letters* **1991**, *295* (1-3), 67-69.
137. Ito, M.; Sakakura, A.; Miyazawa, N.; Murata, S.; Yoshikawa, K., Nonspecificity Induces Chiral Specificity in the Folding Transition of Giant DNA. *Journal of the American Chemical Society* **2003**, *125* (42), 12714-12715.
138. DeRouchey, J.; Hoover, B.; Rau, D. C., A Comparison of DNA Compaction by Arginine and Lysine Peptides: A Physical Basis for Arginine Rich Protamines. *Biochemistry* **2013**, *52* (17), 3000-3009.
139. Mann, A.; Thakur, G.; Shukla, V.; Singh, A. K.; Khanduri, R.; Naik, R.; Jiang, Y.; Kalra, N.; Dwarakanath, B. S.; Langel, U.; Ganguli, M., Differences in DNA Condensation and Release by Lysine and Arginine Homopeptides Govern Their DNA Delivery Efficiencies. *Molecular Pharmaceutics* **2011**, *8* (5), 1729-1741.
140. Sakai, N.; Matile, S., Anion-Mediated Transfer of Polyarginine across Liquid and Bilayer Membranes. *Journal of the American Chemical Society* **2003**, *125* (47), 14348-14356.
141. Rothbard, J. B.; Jessop, T. C.; Lewis, R. S.; Murray, B. A.; Wender, P. A., Role of Membrane Potential and Hydrogen Bonding in the Mechanism of Translocation of Guanidinium-Rich Peptides into Cells. *Journal of the American Chemical Society* **2004**, *126* (31), 9506-9507.
142. Sakai, N.; Takeuchi, T.; Futaki, S.; Matile, S., Direct Observation of Anion-Mediated Translocation of Fluorescent Oligoarginine Carriers into and across Bulk Liquid and Anionic Bilayer Membranes. *ChemBioChem* **2005**, *6* (1), 114-122.
143. Robison, A. D.; Sun, S.; Poyton, M. F.; Johnson, G. A.; Pellois, J.-P.; Jungwirth, P.; Vazdar, M.; Cremer, P. S., Polyarginine Interacts More Strongly and Cooperatively than Polylysine with Phospholipid Bilayers. *The Journal of Physical Chemistry B* **2016**, *120* (35), 9287-9296.
144. Herce, H. D.; Garcia, A. E., Molecular dynamics simulations suggest a mechanism for translocation of the HIV-1 TAT peptide across lipid membranes. *Proceedings of the National Academy of Sciences* **2007**, *104* (52), 20805.
145. Mishra, A.; Gordon, V. D.; Yang, L.; Coridan, R.; Wong, G. C. L., HIV TAT Forms Pores in Membranes by Inducing Saddle-Splay Curvature: Potential Role of Bidentate Hydrogen Bonding. *Angewandte Chemie International Edition* **2008**, *47* (16), 2986-2989.
146. Chen, X.; Sa'adedin, F.; Deme, B.; Rao, P.; Bradshaw, J., Insertion of TAT peptide and perturbation of negatively charged model phospholipid bilayer revealed

References

- by neutron diffraction. *Biochimica et Biophysica Acta (BBA) - Biomembranes* **2013**, 1828 (8), 1982-1988.
147. Tang, M.; Waring, A. J.; Hong, M., Phosphate-Mediated Arginine Insertion into Lipid Membranes and Pore Formation by a Cationic Membrane Peptide from Solid-State NMR. *Journal of the American Chemical Society* **2007**, 129 (37), 11438-11446.
148. Vazdar, M.; Heyda, J.; Mason, P. E.; Tesei, G.; Allolio, C.; Lund, M.; Jungwirth, P., Arginine “Magic”: Guanidinium Like-Charge Ion Pairing from Aqueous Salts to Cell Penetrating Peptides. *Accounts of Chemical Research* **2018**, 51 (6), 1455-1464.
149. Magalhaes, A.; Maigret, B.; Hoflack, J.; Gomes, J. N. F.; Scheraga, H. A., Contribution of unusual Arginine-Arginine short-range interactions to stabilization and recognition in proteins. *Journal of Protein Chemistry* **1994**, 13 (2), 195-215.
150. Pednekar, D.; Tendulkar, A.; Durani, S., Electrostatics-defying interaction between arginine termini as a thermodynamic driving force in protein–protein interaction. *Proteins: Structure, Function, and Bioinformatics* **2009**, 74 (1), 155-163.
151. Inagaki, T.; Aono, S.; Nakano, H.; Yamamoto, T., Like-Charge Attraction of Molecular Cations in Water: Subtle Balance between Interionic Interactions and Ionic Solvation Effect. *The Journal of Physical Chemistry B* **2014**, 118 (20), 5499-5508.
152. No, K. T.; Nam, K.-Y.; Scheraga, H. A., Stability of Like and Oppositely Charged Organic Ion Pairs in Aqueous Solution. *Journal of the American Chemical Society* **1997**, 119 (52), 12917-12922.
153. Boudon, S.; Wipff, G.; Maigret, B., Monte Carlo simulations on the like-charged guanidinium-guanidinium ion pair in water. *The Journal of Physical Chemistry* **1990**, 94 (15), 6056-6061.
154. Soetens, J.-C.; Millot, C.; Chipot, C.; Jansen, G.; Ángyán, J. G.; Maigret, B., Effect of Polarizability on the Potential of Mean Force of Two Cations. The Guanidinium–Guanidinium Ion Pair in Water. *The Journal of Physical Chemistry B* **1997**, 101 (50), 10910-10917.
155. Vondrášek, J.; Mason, P. E.; Heyda, J.; Collins, K. D.; Jungwirth, P., The Molecular Origin of Like-Charge Arginine–Arginine Pairing in Water. *The Journal of Physical Chemistry B* **2009**, 113 (27), 9041-9045.
156. Kubíčková, A.; Křížek, T.; Coufal, P.; Wernersson, E.; Heyda, J.; Jungwirth, P., Guanidinium Cations Pair with Positively Charged Arginine Side Chains in Water. *The Journal of Physical Chemistry Letters* **2011**, 2 (12), 1387-1389.
157. Vazdar, M.; Vymětal, J.; Heyda, J.; Vondrášek, J.; Jungwirth, P., Like-Charge Guanidinium Pairing from Molecular Dynamics and Ab Initio Calculations. *The Journal of Physical Chemistry A* **2011**, 115 (41), 11193-11201.
158. Bandyopadhyay, D.; Bhanja, K.; Mohan, S.; Ghosh, S. K.; Choudhury, N., Effects of Concentration on Like-Charge Pairing of Guanidinium Ions and on the Structure of Water: An All-Atom Molecular Dynamics Simulation Study. *The Journal of Physical Chemistry B* **2015**, 119 (34), 11262-11274.
159. Shih, O.; England, A. H.; Dallinger, G. C.; Smith, J. W.; Duffey, K. C.; Cohen, R. C.; Prendergast, D.; Saykally, R. J., Cation-cation contact pairing in water: Guanidinium. *The Journal of Chemical Physics* **2013**, 139 (3), 035104.
160. Vazdar, M.; Uhlig, F.; Jungwirth, P., Like-Charge Ion Pairing in Water: An Ab Initio Molecular Dynamics Study of Aqueous Guanidinium Cations. *The Journal of Physical Chemistry Letters* **2012**, 3 (15), 2021-2024.

161. Mandal, M.; Mukhopadhyay, C., Concentration-dependent like-charge pairing of guanidinium ions and effect of guanidinium chloride on the structure and dynamics of water from all-atom molecular dynamics simulation. *Physical Review E* **2013**, *88* (5), 052708.
162. Yuzlenko, O.; Lazaridis, T., Interactions between Ionizable Amino Acid Side Chains at a Lipid Bilayer–Water Interface. *The Journal of Physical Chemistry B* **2011**, *115* (46), 13674-13684.
163. Vazdar, M.; Wernersson, E.; Khabiri, M.; Cwiklik, L.; Jurkiewicz, P.; Hof, M.; Mann, E.; Kolusheva, S.; Jelinek, R.; Jungwirth, P., Aggregation of Oligoarginines at Phospholipid Membranes: Molecular Dynamics Simulations, Time-Dependent Fluorescence Shift, and Biomimetic Colorimetric Assays. *The Journal of Physical Chemistry B* **2013**, *117* (39), 11530-11540.
164. Allolio, C.; Baxova, K.; Vazdar, M.; Jungwirth, P., Guanidinium Pairing Facilitates Membrane Translocation. *The Journal of Physical Chemistry B* **2016**, *120* (1), 143-153.
165. Dougherty, D. A., Cation- π Interactions in Chemistry and Biology: A New View of Benzene, Phe, Tyr, and Trp. *Science* **1996**, *271* (5246), 163-168.
166. Ma, J. C.; Dougherty, D. A., The Cation- π Interaction. *Chemical Reviews* **1997**, *97* (5), 1303-1324.
167. Mahadevi, A. S.; Sastry, G. N., Cation- π Interaction: Its Role and Relevance in Chemistry, Biology, and Material Science. *Chemical Reviews* **2013**, *113* (3), 2100-2138.
168. Infield, D. T.; Rasouli, A.; Galles, G. D.; Chipot, C.; Tajkhorshid, E.; Ahern, C. A., Cation- π Interactions and their Functional Roles in Membrane Proteins. *Journal of Molecular Biology* **2021**, *433* (17), 167035.
169. Shi, Z.; Olson, C. A.; Kallenbach, N. R., Cation- π Interaction in Model α -Helical Peptides. *Journal of the American Chemical Society* **2002**, *124* (13), 3284-3291.
170. Rومان, M.; Liévin, J.; Buisine, E.; Wintjens, R., Cation- π /H-bond Stair Motifs at Protein–DNA Interfaces. *Journal of Molecular Biology* **2002**, *319* (1), 67-76.
171. Duffy, E. M.; Kowalczyk, P. J.; Jorgensen, W. L., Do denaturants interact with aromatic hydrocarbons in water? *Journal of the American Chemical Society* **1993**, *115* (20), 9271-9275.
172. Balamurugan, K.; Prakash, M.; Subramanian, V., Theoretical Insights into the Role of Water Molecules in the Guanidinium-Based Protein Denaturation Process in Specific to Aromatic Amino Acids. *The Journal of Physical Chemistry B* **2019**, *123* (10), 2191-2202.
173. Warme, P. K.; Morgan, R. S., A survey of amino acid side-chain interactions in 21 proteins. *Journal of Molecular Biology* **1978**, *118* (3), 289-304.
174. Burley, S. K.; Petsko, G. A., Amino-aromatic interactions in proteins. *FEBS Letters* **1986**, *203* (2), 139-143.
175. Flocco, M. M.; Mowbray, S. L., Planar Stacking Interactions of Arginine and Aromatic Side-Chains in Proteins. *Journal of Molecular Biology* **1994**, *235* (2), 709-717.
176. Brocchieri, L.; Karlin, S., Geometry of interplanar residue contacts in protein structures. *Proceedings of the National Academy of Sciences* **1994**, *91* (20), 9297-9301.

References

177. Mitchell, J. B. O.; Nandi, C. L.; Ali, S.; McDonald, I. K.; Thornton, J. M.; Price, S. L.; Singh, J., Amino/aromatic interactions. *Nature* **1993**, *366* (6454), 413-413.
178. Mitchell, J. B. O.; Nandi, C. L.; McDonald, I. K.; Thornton, J. M.; Price, S. L., Amino/Aromatic Interactions in Proteins: Is the Evidence Stacked Against Hydrogen Bonding? *Journal of Molecular Biology* **1994**, *239* (2), 315-331.
179. Nandi, C. L.; Singh, J.; Thornton, J. M., Atomic environments of arginine side chains in proteins. *Protein Engineering, Design and Selection* **1993**, *6* (3), 247-259.
180. Gallivan, J. P.; Dougherty, D. A., Cation- π interactions in structural biology. *Proceedings of the National Academy of Sciences* **1999**, *96* (17), 9459-9464.
181. Crombez, L.; Aldrian-Herrada, G.; Konate, K.; Nguyen, Q. N.; McMaster, G. K.; Basseur, R.; Heitz, F.; Divita, G., A new potent secondary amphipathic cell-penetrating peptide for siRNA delivery into mammalian cells. *Molecular therapy : the journal of the American Society of Gene Therapy* **2009**, *17* (1), 95-103.
182. Jobin, M.-L.; Blanchet, M.; Henry, S.; Chaignepain, S.; Manigand, C.; Castano, S.; Lecomte, S.; Burlina, F.; Sagan, S.; Alves, I. D., The role of tryptophans on the cellular uptake and membrane interaction of arginine-rich cell penetrating peptides. *Biochimica et Biophysica Acta (BBA) - Biomembranes* **2015**, *1848* (2), 593-602.
183. Walrant, A.; Bauzá, A.; Girardet, C.; Alves, I. D.; Lecomte, S.; Illien, F.; Cardon, S.; Chaianantakul, N.; Pallerla, M.; Burlina, F.; Frontera, A.; Sagan, S., Ionpair- π interactions favor cell penetration of arginine/tryptophan-rich cell-penetrating peptides. *Biochimica et Biophysica Acta (BBA) - Biomembranes* **2020**, *1862* (2), 183098.
184. Derossi, D.; Joliot, A. H.; Chassaing, G.; Prochiantz, A., The third helix of the Antennapedia homeodomain translocates through biological membranes. *Journal of Biological Chemistry* **1994**, *269* (14), 10444-10450.
185. Dupont, E.; Prochiantz, A.; Joliot, A., Penetratin Story: An Overview. In *Cell-Penetrating Peptides: Methods and Protocols*, Langel, Ü., Ed. Humana Press: Totowa, NJ, 2011; pp 21-29.
186. Walrant, A.; Correia, I.; Jiao, C.-Y.; Lequin, O.; Bent, E. H.; Goasdoué, N.; Lacombe, C.; Chassaing, G.; Sagan, S.; Alves, I. D., Different membrane behaviour and cellular uptake of three basic arginine-rich peptides. *Biochimica et Biophysica Acta (BBA) - Biomembranes* **2011**, *1808* (1), 382-393.
187. Fujisawa, K.; Beuchat, C.; Humbert-Droz, M.; Wilson, A.; Wesolowski, T. A.; Mareda, J.; Sakai, N.; Matile, S., Anion- π and Cation- π Interactions on the Same Surface. *Angewandte Chemie International Edition* **2014**, *53* (42), 11266-11269.
188. Fujisawa, K.; Humbert-Droz, M.; Letrun, R.; Vauthey, E.; Wesolowski, T. A.; Sakai, N.; Matile, S., Ion Pair- π Interactions. *Journal of the American Chemical Society* **2015**, *137* (34), 11047-11056.
189. Chuard, N.; Fujisawa, K.; Morelli, P.; Saarbach, J.; Winssinger, N.; Metrangolo, P.; Resnati, G.; Sakai, N.; Matile, S., Activation of Cell-Penetrating Peptides with Ionpair- π Interactions and Fluorophiles. *Journal of the American Chemical Society* **2016**, *138* (35), 11264-11271.
190. deRonde, B. M.; Tew, G. N., Development of protein mimics for intracellular delivery. *Peptide Science* **2015**, *104* (4), 265-280.
191. Ikeda, T.; Yamaguchi, H.; Tazuke, S., New polymeric biocides: synthesis and antibacterial activities of polycations with pendant biguanide groups. *Antimicrob Agents Chemother* **1984**, *26* (2), 139-144.

192. Wender, P. A.; Rothbard, J. B.; Jessop, T. C.; Kreider, E. L.; Wylie, B. L., Oligocarbamate Molecular Transporters: Design, Synthesis, and Biological Evaluation of a New Class of Transporters for Drug Delivery. *Journal of the American Chemical Society* **2002**, *124* (45), 13382-13383.
193. Funhoff, A. M.; van Nostrum, C. F.; Lok, M. C.; Fretz, M. M.; Crommelin, D. J. A.; Hennink, W. E., Poly(3-guanidinopropyl methacrylate): A Novel Cationic Polymer for Gene Delivery. *Bioconjugate Chemistry* **2004**, *15* (6), 1212-1220.
194. Gao, Y.; Xu, Z.; Chen, S.; Gu, W.; Chen, L.; Li, Y., Arginine-chitosan/DNA self-assemble nanoparticles for gene delivery: In vitro characteristics and transfection efficiency. *International Journal of Pharmaceutics* **2008**, *359* (1), 241-246.
195. Zhang, H.; Zhu, D.; Song, L.; Liu, L.; Dong, X.; Liu, Z.; Leng, X., Arginine conjugation affects the endocytic pathways of chitosan/DNA nanoparticles. *Journal of Biomedical Materials Research Part A* **2011**, *98A* (2), 296-302.
196. Choi, J. L.; Tan, J.-K. Y.; Sellers, D. L.; Wei, H.; Horner, P. J.; Pun, S. H., Guanidinylated block copolymers for gene transfer: A comparison with amine-based materials for in vitro and in vivo gene transfer efficiency. *Biomaterials* **2015**, *54*, 87-96.
197. Zavrashvili, N.; Sarisozen, C.; Titvinidze, G.; Otinashvili, G.; Kantaria, T.; Tugushi, D.; Puiggali, J.; Torchilin, V. P.; Katsarava, R., Library of Cationic Polymers Composed of Polyamines and Arginine as Gene Transfection Agents. *ACS Omega* **2019**, *4* (1), 2090-2101.
198. Lin, M.; Lin, A.; Huang, S.; Liu, T.; Ke, F.; Qiu, D.; Lin, X.; Luo, D., Development of a novel vector for siRNA delivery based on arginine-modified polyvinylamine. *Polymer International* *n/a* (n/a).
199. Chen, Z.; Huang, W.; Zheng, N.; Bai, Y., Design and synthesis of a polyguanidium vector with enhanced DNA binding ability for effective gene delivery at a low N/P ratio. *Polymer Chemistry* **2020**, *11* (3), 664-668.
200. Taori, V. P.; Lu, H.; Reineke, T. M., Structure–Activity Examination of Poly(glycoamidoguanidine)s: Glycopolycations Containing Guanidine Units for Nucleic Acid Delivery. *Biomacromolecules* **2011**, *12* (6), 2055-2063.
201. Sarkar, A. K.; Debnath, K.; Arora, H.; Seth, P.; Jana, N. R.; Jana, N. R., Direct Cellular Delivery of Exogenous Genetic Material and Protein via Colloidal Nano-Assemblies with Biopolymer. *ACS Applied Materials & Interfaces* **2022**, *14* (2), 3199-3206.
202. Kretzmann, J. A.; Ho, D.; Evans, C. W.; Plani-Lam, J. H. C.; Garcia-Bloj, B.; Mohamed, A. E.; O'Mara, M. L.; Ford, E.; Tan, D. E. K.; Lister, R.; Blancafort, P.; Norret, M.; Iyer, K. S., Synthetically controlling dendrimer flexibility improves delivery of large plasmid DNA. *Chemical Science* **2017**, *8* (4), 2923-2930.
203. Okuro, K.; Nemoto, H.; Mogaki, R.; Aida, T., Dendritic Molecular Glues with Reductively Cleavable Guanidinium Ion Pendants: Highly Efficient Intracellular siRNA Delivery via Direct Translocation. *Chemistry Letters* **2018**, *47* (9), 1232-1235.
204. Chopra, M.; Sgro, A.; Norret, M.; Blancafort, P.; Iyer, K. S.; Evans, C. W., A peptide-functionalised dendronised polymer for selective transfection in human liver cancer cells. *New Journal of Chemistry* **2021**, *45* (41), 19315-19320.
205. Yang, W.; Yu, C.; Wu, C.; Yao, S. Q.; Wu, S., Cell-penetrating poly(disulfide)-based star polymers for simultaneous intracellular delivery of miRNAs and small molecule drugs. *Polymer Chemistry* **2017**, *8* (27), 4043-4051.
206. Tan, Z.; Dhande, Y. K.; Reineke, T. M., Cell Penetrating Polymers Containing Guanidinium Trigger Apoptosis in Human Hepatocellular Carcinoma

References

- Cells unless Conjugated to a Targeting N-Acetyl-Galactosamine Block. *Bioconjugate Chemistry* **2017**, *28* (12), 2985-2997.
207. Kim, T.-i.; Ou, M.; Lee, M.; Kim, S. W., Arginine-grafted bioreducible poly(disulfide amine) for gene delivery systems. *Biomaterials* **2009**, *30* (4), 658-664.
208. Kim, T.-i.; Lee, M.; Kim, S. W., A guanidinylated bioreducible polymer with high nuclear localization ability for gene delivery systems. *Biomaterials* **2010**, *31* (7), 1798-1804.
209. Carlson, P. M.; Schellinger, J. G.; Pahang, J. A.; Johnson, R. N.; Pun, S. H., Comparative study of guanidine-based and lysine-based brush copolymers for plasmid delivery. *Biomaterials Science* **2013**, *1* (7), 736-744.
210. Cheng, Q.; Huang, Y.; Zheng, H.; Wei, T.; Zheng, S.; Huo, S.; Wang, X.; Du, Q.; Zhang, X.; Zhang, H. Y.; Liang, X. J.; Wang, C.; Tang, R.; Liang, Z., The effect of guanidinylation of PEGylated poly(2-aminoethyl methacrylate) on the systemic delivery of siRNA. *Biomaterials* **2013**, *34* (12), 3120-31.
211. Richter, F.; Martin, L.; Leer, K.; Moek, E.; Hausig, F.; Brendel, J. C.; Traeger, A., Tuning of endosomal escape and gene expression by functional groups, molecular weight and transfection medium: a structure–activity relationship study. *Journal of Materials Chemistry B* **2020**, *8* (23), 5026-5041.
212. Nimesh, S.; Chandra, R., Guanidinium-grafted polyethylenimine: An efficient transfecting agent for mammalian cells. *European Journal of Pharmaceutics and Biopharmaceutics* **2008**, *68* (3), 647-655.
213. Sarapas, J. M.; Backlund, C. M.; deRonde, B. M.; Minter, L. M.; Tew, G. N., ROMP- and RAFT-Based Guanidinium-Containing Polymers as Scaffolds for Protein Mimic Synthesis. *Chemistry – A European Journal* **2017**, *23* (28), 6858-6863.
214. Wu, J.; Yamanouchi, D.; Liu, B.; Chu, C.-C., Biodegradable arginine-based poly(ether ester amide)s as a non-viral DNA delivery vector and their structure–function study. *Journal of Materials Chemistry* **2012**, *22* (36), 18983-18991.
215. Miyazaki, T.; Uchida, S.; Nagatoishi, S.; Koji, K.; Hong, T.; Fukushima, S.; Tsumoto, K.; Ishihara, K.; Kataoka, K.; Cabral, H., Polymeric Nanocarriers with Controlled Chain Flexibility Boost mRNA Delivery In Vivo through Enhanced Structural Fastening. *Advanced Healthcare Materials* **2020**, *9* (16), 2000538.
216. Grasso, G.; Deriu, M. A.; Patrulea, V.; Borchard, G.; Möller, M.; Danani, A., Free energy landscape of siRNA-polycation complexation: Elucidating the effect of molecular geometry, polymer flexibility, and charge neutralization. *PLOS ONE* **2017**, *12* (10), e0186816.
217. Ullah, I.; Muhammad, K.; Akpanyung, M.; Nejjari, A.; Neve, A. L.; Guo, J.; Feng, Y.; Shi, C., Bioreducible, hydrolytically degradable and targeting polymers for gene delivery. *Journal of Materials Chemistry B* **2017**, *5* (18), 3253-3276.
218. Zu, H.; Gao, D., Non-viral Vectors in Gene Therapy: Recent Development, Challenges, and Prospects. *The AAPS Journal* **2021**, *23* (4), 78.
219. Sun, Y.; Liu, H.; Yang, T.; Lang, L.; Cheng, L.; Xing, H.; Yang, L.; Ding, P., Amphoteric poly(amido amine)s with adjustable balance between transfection efficiency and cytotoxicity for gene delivery. *Colloids and Surfaces B: Biointerfaces* **2019**, *175*, 10-17.
220. Memanishvili, T.; Zavrashvili, N.; Kupatadze, N.; Tugushi, D.; Gverdsiteli, M.; Torchilin, V. P.; Wandrey, C.; Baldi, L.; Manoli, S. S.; Katsarava, R., Arginine-Based Biodegradable Ether–Ester Polymers with Low Cytotoxicity as Potential Gene Carriers. *Biomacromolecules* **2014**, *15* (8), 2839-2848.

221. Yamanouchi, D.; Wu, J.; Lazar, A. N.; Craig Kent, K.; Chu, C.-C.; Liu, B., Biodegradable arginine-based poly(ester-amide)s as non-viral gene delivery reagents. *Biomaterials* **2008**, *29* (22), 3269-3277.
222. Yu, J.; Zhang, J.; Xing, H.; Sun, Y.; Yang, Z.; Yang, T.; Cai, C.; Zhao, X.; Yang, L.; Ding, P., Novel guanidinylated bioresponsive poly(amidoamine)s designed for short hairpin RNA delivery. *International journal of nanomedicine* **2016**, *11*, 6651-6666.
223. You, X.; Gu, Z.; Huang, J.; Kang, Y.; Chu, C.-C.; Wu, J., Arginine-based poly(ester amide) nanoparticle platform: From structure–property relationship to nucleic acid delivery. *Acta Biomaterialia* **2018**, *74*, 180-191.
224. Geihe, E. I.; Cooley, C. B.; Simon, J. R.; Kiesewetter, M. K.; Edward, J. A.; Hickerson, R. P.; Kaspar, R. L.; Hedrick, J. L.; Waymouth, R. M.; Wender, P. A., Designed guanidinium-rich amphipathic oligocarbonate molecular transporters complex, deliver and release siRNA in cells. *Proc Natl Acad Sci U S A* **2012**, *109* (33), 13171-6.
225. Wender, P. A.; Huttner, M. A.; Staveness, D.; Vargas, J. R.; Xu, A. F., Guanidinium-Rich, Glycerol-Derived Oligocarbonates: A New Class of Cell-Penetrating Molecular Transporters That Complex, Deliver, and Release siRNA. *Mol. Pharm.* **2015**, *12* (3), 742-750.
226. Yu, J.; Zhang, J.; Xing, H.; Yang, Z.; Cai, C.; Zhang, C.; Zhao, X.; Wei, M.; Yang, L.; Ding, P., Guanidinylated bioresponsive poly(amido amine)s designed for intranuclear gene delivery. *International journal of nanomedicine* **2016**, *11*, 4011-4024.
227. Zhang, J.; Wang, C.; Lu, M.; Xing, H.; Yang, T.; Cai, C.; Zhao, X.; Wei, M.; Yu, J.; Ding, P., Intracellular distribution and internalization pathways of guanidinylated bioresponsive poly(amido amine)s in gene delivery. *Asian Journal of Pharmaceutical Sciences* **2018**, *13* (4), 360-372.
228. Sgolastra, F.; Minter, L. M.; Osborne, B. A.; Tew, G. N., Importance of Sequence Specific Hydrophobicity in Synthetic Protein Transduction Domain Mimics. *Biomacromolecules* **2014**, *15* (3), 812-820.
229. Martin, L.; Peltier, R.; Kuroki, A.; Town, J. S.; Perrier, S., Investigating Cell Uptake of Guanidinium-Rich RAFT Polymers: Impact of Comonomer and Monomer Distribution. *Biomacromolecules* **2018**, *19* (8), 3190-3200.
230. Priegue, J. M.; Lostalé-Seijo, I.; Crisan, D.; Granja, J. R.; Fernández-Trillo, F.; Montenegro, J., Different-Length Hydrazone Activated Polymers for Plasmid DNA Condensation and Cellular Transfection. *Biomacromolecules* **2018**, *19* (7), 2638-2649.
231. deRonde, B. M.; Torres, J. A.; Minter, L. M.; Tew, G. N., Development of Guanidinium-Rich Protein Mimics for Efficient siRNA Delivery into Human T Cells. *Biomacromolecules* **2015**, *16* (10), 3172-3179.
232. Caffrey, L. M.; deRonde, B. M.; Minter, L. M.; Tew, G. N., Mapping Optimal Charge Density and Length of ROMP-Based PTDMs for siRNA Internalization. *Biomacromolecules* **2016**, *17* (10), 3205-3212.
233. Tabujew, I.; Heidari, M.; Freidel, C.; Helm, M.; Tebbe, L.; Wolfrum, U.; Nagel-Wolfrum, K.; Koynov, K.; Biehl, P.; Schacher, F. H.; Potestio, R.; Peneva, K., Tackling the Limitations of Copolymeric Small Interfering RNA Delivery Agents by a Combined Experimental–Computational Approach. *Biomacromolecules* **2019**, *20* (12), 4389-4406.
234. Xing, H.; Cheng, L.; Lu, M.; Liu, H.; Lang, L.; Yang, T.; Zhao, X.; Xu, H.; Yang, L.; Ding, P., A biodegradable poly(amido amine) based on the antimicrobial

References

- polymer polyhexamethylene biguanide for efficient and safe gene delivery. *Colloids and Surfaces B: Biointerfaces* **2019**, *182*, 110355.
235. Sun, Y.; Liu, H.; Xing, H.; Lang, L.; Cheng, L.; Yang, T.; Yang, L.; Ding, P., Bioreducible poly(amido amine) copolymers derived from histamine and agmatine for highly efficient gene delivery. *Polymer International* **2019**, *68* (3), 447-455.
236. Tabujew, I.; Freidel, C.; Krieg, B.; Helm, M.; Koynov, K.; Müllen, K.; Peneva, K., The Guanidinium Group as a Key Part of Water-Soluble Polymer Carriers for siRNA Complexation and Protection against Degradation. *Macromolecular Rapid Communications* **2014**, *35* (13), 1191-1197.
237. Tabujew, I.; Willig, M.; Leber, N.; Freidel, C.; Negwer, I.; Koynov, K.; Helm, M.; Landfester, K.; Zentel, R.; Peneva, K.; Mailänder, V., Overcoming the barrier of CD8+ T cells: Two types of nano-sized carriers for siRNA transport. *Acta Biomater.* **2019**, *100*, 338-351.
238. Guo, P.; Gu, W.; Chen, Q.; Lu, H.; Han, X.; Li, W.; Gao, H., Dual functionalized amino poly(glycerol methacrylate) with guanidine and Schiff-base linked imidazole for enhanced gene transfection and minimized cytotoxicity. *Journal of Materials Chemistry B* **2015**, *3* (34), 6911-6918.
239. Liu, Z.; Zhang, Z.; Zhou, C.; Jiao, Y., Hydrophobic modifications of cationic polymers for gene delivery. *Progress in Polymer Science* **2010**, *35* (9), 1144-1162.
240. Nie, X.; Zhang, Z.; Wang, C.-H.; Fan, Y.-S.; Meng, Q.-Y.; You, Y.-Z., Interactions in DNA Condensation: An Important Factor for Improving the Efficacy of Gene Transfection. *Bioconjugate Chemistry* **2019**, *30* (2), 284-292.
241. Som, A.; Tezgel, A. O.; Gabriel, G. J.; Tew, G. N., Self-Activation in De Novo Designed Mimics of Cell-Penetrating Peptides. *Angewandte Chemie International Edition* **2011**, *50* (27), 6147-6150.
242. Som, A.; Reuter, A.; Tew, G. N., Protein Transduction Domain Mimics: The Role of Aromatic Functionality. *Angewandte Chemie International Edition* **2012**, *51* (4), 980-983.
243. Lis, M.; Dorner, F.; Tew, G. N.; Lienkamp, K., Anionic Lipid Content Presents a Barrier to the Activity of ROMP-Based Synthetic Mimics of Protein Transduction Domains (PTDMs). *Langmuir* **2016**, *32* (23), 5946-5954.
244. deRonde, B. M.; Posey, N. D.; Otter, R.; Caffrey, L. M.; Minter, L. M.; Tew, G. N., Optimal Hydrophobicity in Ring-Opening Metathesis Polymerization-Based Protein Mimics Required for siRNA Internalization. *Biomacromolecules* **2016**, *17* (6), 1969-1977.
245. Priegue, J. M.; Crisan, D. N.; Martínez-Costas, J.; Granja, J. R.; Fernandez-Trillo, F.; Montenegro, J., In Situ Functionalized Polymers for siRNA Delivery. *Angewandte Chemie International Edition* **2016**, *55* (26), 7492-7495.
246. Juanes, M.; Creese, O.; Fernández-Trillo, P.; Montenegro, J., Messenger RNA delivery by hydrazone-activated polymers. *MedChemComm* **2019**, *10* (7), 1138-1144.
247. Fischer, D.; Li, Y.; Ahlemeyer, B.; Krieglstein, J.; Kissel, T., In vitro cytotoxicity testing of polycations: influence of polymer structure on cell viability and hemolysis. *Biomaterials* **2003**, *24* (7), 1121-1131.
248. Knop, K.; Hoogenboom, R.; Fischer, D.; Schubert, U. S., Poly(ethylene glycol) in Drug Delivery: Pros and Cons as Well as Potential Alternatives. *Angew. Chem. Int. Ed.* **2010**, *49* (36), 6288-6308.
249. Frère, A.; Baroni, A.; Hendrick, E.; Delvigne, A.-S.; Orange, F.; Peulen, O.; Dakwar, G. R.; Diricq, J.; Dubois, P.; Evrard, B.; Remaut, K.; Braeckmans, K.; De Smedt, S. C.; Laloy, J.; Dogné, J.-M.; Feller, G.; Mespouille, L.; Mottet, D.; Piel, G.,

- PEGylated and Functionalized Aliphatic Polycarbonate Polyplex Nanoparticles for Intravenous Administration of HDAC5 siRNA in Cancer Therapy. *ACS Appl. Mater. Interfaces* **2017**, *9* (3), 2181-2195.
250. Sajeesh, S.; Choe, J. Y.; Lee, T. Y.; Lee, D.-k., Guanidine modified polyethyleneimine-g-polyethylene glycol nanocarriers for long interfering RNA (liRNA) based advanced anticancer therapy. *Journal of Materials Chemistry B* **2015**, *3* (2), 207-216.
251. Zheng, M.; Liu, Y.; Wang, Y.; Zhang, D.; Zou, Y.; Ruan, W.; Yin, J.; Tao, W.; Park, J. B.; Shi, B., ROS-Responsive Polymeric siRNA Nanomedicine Stabilized by Triple Interactions for the Robust Glioblastoma Combinational RNAi Therapy. *Adv. Mater.* **2019**, *31* (37), e1903277.
252. Zhou, Y.; Zhu, F.; Liu, Y.; Zheng, M.; Wang, Y.; Zhang, D.; Anraku, Y.; Zou, Y.; Li, J.; Wu, H.; Pang, X.; Tao, W.; Shimoni, O.; Bush, A. I.; Xue, X.; Shi, B., Blood-brain barrier-penetrating siRNA nanomedicine for Alzheimer's disease therapy. *Science Advances* **2020**, *6* (41), eabc7031.
253. Hoang Thi, T. T.; Pilkington, E. H.; Nguyen, D. H.; Lee, J. S.; Park, K. D.; Truong, N. P., The Importance of Poly(ethylene glycol) Alternatives for Overcoming PEG Immunogenicity in Drug Delivery and Bioconjugation. *Polymers* **2020**, *12* (2), 298.
254. Khine, Y. Y.; Callari, M.; Lu, H.; Stenzel, M. H., Direct Correlation Between Zeta Potential and Cellular Uptake of Poly(methacrylic acid) Post-Modified with Guanidinium Functionalities. *Macromolecular Chemistry and Physics* **2016**, *217* (20), 2302-2309.
255. Ferruti, P.; Franchini, J.; Bencini, M.; Ranucci, E.; Zara, G. P.; Serpe, L.; Primo, L.; Cavalli, R., Prevalingly Cationic Agmatine-Based Amphoteric Polyamidoamine as a Nontoxic, Nonhemolytic, and "Stealthlike" DNA Complexing Agent and Transfection Promoter. *Biomacromolecules* **2007**, *8* (5), 1498-1504.
256. Kim, Y.; Binauld, S.; Stenzel, M. H., Zwitterionic Guanidine-Based Oligomers Mimicking Cell-Penetrating Peptides as a Nontoxic Alternative to Cationic Polymers to Enhance the Cellular Uptake of Micelles. *Biomacromolecules* **2012**, *13* (10), 3418-3426.
257. Oupický, D.; Li, J., Bioreducible Polycations in Nucleic Acid Delivery: Past, Present, and Future Trends. *Macromol Biosci* **2014**, *14* (7), 908-922.
258. Cheng, R.; Feng, F.; Meng, F.; Deng, C.; Feijen, J.; Zhong, Z., Glutathione-responsive nano-vehicles as a promising platform for targeted intracellular drug and gene delivery. *Journal of Controlled Release* **2011**, *152* (1), 2-12.
259. Kim, S. H.; Jeong, J. H.; Kim, T.-i.; Kim, S. W.; Bull, D. A., VEGF siRNA Delivery System Using Arginine-Grafted Bioreducible Poly(disulfide amine). *Molecular Pharmaceutics* **2009**, *6* (3), 718-726.
260. Beloor, J.; Choi, C. S.; Nam, H. Y.; Park, M.; Kim, S. H.; Jackson, A.; Lee, K. Y.; Kim, S. W.; Kumar, P.; Lee, S.-K., Arginine-engrafted biodegradable polymer for the systemic delivery of therapeutic siRNA. *Biomaterials* **2012**, *33* (5), 1640-1650.
261. Ryu, J.-K.; Choi, M. J.; Kim, T.-I.; Jin, H.-R.; Kwon, K.-D.; Batbold, D.; Song, K.-M.; Kwon, M.-H.; Yin, G. N.; Lee, M.; Kim, S. W.; Suh, J.-K., A guanidinylated bioreducible polymer as a novel gene carrier to the corpus cavernosum of mice with high-cholesterol diet-induced erectile dysfunction. *Andrology* **2013**, *1* (2), 216-222.

References

262. Won, Y.-W.; Ankoné, M.; Engbersen, J. F. J.; Feijen, J.; Kim, S. W., Poly(Amido Amine)s Containing Agmatine and Butanol Side Chains as Efficient Gene Carriers. *Macromol Biosci* **2016**, *16* (4), 619-626.
263. Liu, H.; Sun, Y.; Lang, L.; Yang, T.; Zhao, X.; Cai, C.; Liu, Z.; Ding, P., Nuclear localization signal peptide enhances transfection efficiency and decreases cytotoxicity of poly(agmatine/N,N'-cystamine-bis-acrylamide)/pDNA complexes. *Journal of Cellular Biochemistry* **2019**, *120* (10), 16967-16977.
264. Bang, E.-K.; Gasparini, G.; Molinard, G.; Roux, A.; Sakai, N.; Matile, S., Substrate-Initiated Synthesis of Cell-Penetrating Poly(disulfide)s. *Journal of the American Chemical Society* **2013**, *135* (6), 2088-2091.
265. Gasparini, G.; Bang, E.-K.; Molinard, G.; Tulumello, D. V.; Ward, S.; Kelley, S. O.; Roux, A.; Sakai, N.; Matile, S., Cellular Uptake of Substrate-Initiated Cell-Penetrating Poly(disulfide)s. *Journal of the American Chemical Society* **2014**, *136* (16), 6069-6074.
266. Zhu, Y.; Lin, M.; Hu, W.; Wang, J.; Zhang, Z.-G.; Zhang, K.; Yu, B.; Xu, F.-J., Controllable Disulfide Exchange Polymerization of Polyguanidine for Effective Biomedical Applications by Thiol-Mediated Uptake. *Angewandte Chemie International Edition n/a* (n/a), e202200535.
267. Liu, Y.; Zheng, M.; Jiao, M.; Yan, C.; Xu, S.; Du, Q.; Morsch, M.; Yin, J.; Shi, B., Polymeric nanoparticle mediated inhibition of miR-21 with enhanced miR-124 expression for combinatorial glioblastoma therapy. *Biomaterials* **2021**, *276*, 121036.
268. Tezgel, A. Ö.; Telfer, J. C.; Tew, G. N., De Novo Designed Protein Transduction Domain Mimics from Simple Synthetic Polymers. *Biomacromolecules* **2011**, *12* (8), 3078-3083.
269. Treat, N. J.; Smith, D.; Teng, C.; Flores, J. D.; Abel, B. A.; York, A. W.; Huang, F.; McCormick, C. L., Guanidine-Containing Methacrylamide (Co)polymers via aRAFT: Toward a Cell-Penetrating Peptide Mimic. *ACS Macro Letters* **2012**, *1* (1), 100-104.
270. Buerkli, C.; Lee, S. H.; Moroz, E.; Stuparu, M. C.; Leroux, J.-C.; Khan, A., Amphiphatic Homopolymers for siRNA Delivery: Probing Impact of Bifunctional Polymer Composition on Transfection. *Biomacromolecules* **2014**, *15* (5), 1707-1715.
271. Bromberg, L.; Raduyk, S.; Hatton, T. A.; Concheiro, A.; Rodriguez-Valencia, C.; Silva, M.; Alvarez-Lorenzo, C., Guanidinylated Polyethyleneimine–Polyoxypropylene–Polyoxyethylene Conjugates as Gene Transfection Agents. *Bioconjugate Chemistry* **2009**, *20* (5), 1044-1053.
272. Patterson, D. M.; Nazarova, L. A.; Prescher, J. A., Finding the Right (Bioorthogonal) Chemistry. *ACS Chemical Biology* **2014**, *9* (3), 592-605.
273. Mather, B. D.; Viswanathan, K.; Miller, K. M.; Long, T. E., Michael addition reactions in macromolecular design for emerging technologies. *Progress in Polymer Science* **2006**, *31* (5), 487-531.
274. Fonseca, A. C.; Gil, M. H.; Simões, P. N., Biodegradable poly(ester amide)s – A remarkable opportunity for the biomedical area: Review on the synthesis, characterization and applications. *Progress in Polymer Science* **2014**, *39* (7), 1291-1311.
275. Kamber, N. E.; Jeong, W.; Waymouth, R. M.; Pratt, R. C.; Lohmeijer, B. G. G.; Hedrick, J. L., Organocatalytic Ring-Opening Polymerization. *Chemical Reviews* **2007**, *107* (12), 5813-5840.
276. Nuyken, O.; Pask, S. D., Ring-Opening Polymerization—An Introductory Review. *Polymers* **2013**, *5* (2), 361-403.

277. Slugovc, C., The Ring Opening Metathesis Polymerisation Toolbox. *Macromolecular Rapid Communications* **2004**, *25* (14), 1283-1297.
278. Peacock, A. J.; Calhoun, A., *Polymer Chemistry: properties and applications*. 1st ed.; Hanser Publishers: Munich, 2006.
279. *Fundamentals of Controlled/Living Radical Polymerization*. The Royal Society of Chemistry: Cambridge, UK, 2013.
280. Truong, N. P.; Jones, G. R.; Bradford, K. G. E.; Konkolewicz, D.; Anastasaki, A., A comparison of RAFT and ATRP methods for controlled radical polymerization. *Nature Reviews Chemistry* **2021**, *5* (12), 859-869.
281. Sui, B.; Cheng, C.; Xu, P., Pyridyl Disulfide Functionalized Polymers as Nanotherapeutic Platforms. *Advanced Therapeutics* **2019**, *2* (9), 1900062.
282. Chiefari, J.; Chong, Y. K.; Ercole, F.; Krstina, J.; Jeffery, J.; Le, T. P. T.; Mayadunne, R. T. A.; Meijs, G. F.; Moad, C. L.; Moad, G.; Rizzardo, E.; Thang, S. H., Living Free-Radical Polymerization by Reversible Addition–Fragmentation Chain Transfer: The RAFT Process. *Macromolecules* **1998**, *31* (16), 5559-5562.
283. McCormick, C. L.; Lowe, A. B., Aqueous RAFT Polymerization: Recent Developments in Synthesis of Functional Water-Soluble (Co)polymers with Controlled Structures. *Accounts of Chemical Research* **2004**, *37* (5), 312-325.
284. Perrier, S., 50th Anniversary Perspective: RAFT Polymerization—A User Guide. *Macromolecules* **2017**, *50* (19), 7433-7447.
285. *Handbook of RAFT Polymerization*. WILEY-VCH Verlag GmbH & Co. KGaA: Weinheim, 2008.
286. Lowe, A. B.; McCormick, C. L., RAFT Polymerization in Homogeneous Aqueous Media: Initiation Systems, RAFT Agent Stability, Monomers and Polymer Structures. In *Handbook of RAFT Polymerization*, 2008; pp 235-284.
287. Gody, G.; Maschmeyer, T.; Zetterlund, P. B.; Perrier, S., Exploitation of the Degenerative Transfer Mechanism in RAFT Polymerization for Synthesis of Polymer of High Livingness at Full Monomer Conversion. *Macromolecules* **2014**, *47* (2), 639-649.
288. Moad, G.; Rizzardo, E.; Thang, S. H., End-functional polymers, thiocarbonylthio group removal/transformation and reversible addition–fragmentation–chain transfer (RAFT) polymerization. *Polymer International* **2011**, *60* (1), 9-25.
289. Rizzardo, E.; Moad, G.; Thang, S. H., RAFT Polymerization in Bulk Monomer or in (Organic) Solution. In *Handbook of RAFT Polymerization*, 2008; pp 189-234.
290. Keddie, D. J.; Moad, G.; Rizzardo, E.; Thang, S. H., RAFT Agent Design and Synthesis. *Macromolecules* **2012**, *45* (13), 5321-5342.
291. Moad, G., Dithioesters in RAFT Polymerization. In *RAFT Polymerization*, 2021; pp 223-358.
292. Moad, G., Trithiocarbonates in RAFT Polymerization. In *RAFT Polymerization*, 2021; pp 359-492.
293. Wang, M.; Marty, J.-D.; Destarac, M., Xanthates in RAFT Polymerization. In *RAFT Polymerization*, 2021; pp 493-548.
294. Moad, G., Dithiocarbamates in RAFT Polymerization. In *RAFT Polymerization*, 2021; pp 549-610.
295. Thomas, D. B.; Convertine, A. J.; Hester, R. D.; Lowe, A. B.; McCormick, C. L., Hydrolytic Susceptibility of Dithioester Chain Transfer Agents and Implications in Aqueous RAFT Polymerizations. *Macromolecules* **2004**, *37* (5), 1735-1741.

References

296. Deletre, M.; Levesque, G., Kinetics and mechanism of polythioamidation in solution. 1. Reaction of mono- and bis(dithioester)s with excess amine. *Macromolecules* **1990**, *23* (22), 4733-4741.
297. WHO reveals leading causes of death and disability worldwide: 2000-2019. <https://www.who.int/news/item/09-12-2020-who-reveals-leading-causes-of-death-and-disability-worldwide-2000-2019> (accessed 06.06.2022).
298. Polack, F. P.; Thomas, S. J.; Kitchin, N.; Absalon, J.; Gurtman, A.; Lockhart, S.; Perez, J. L.; Pérez Marc, G.; Moreira, E. D.; Zerbini, C.; Bailey, R.; Swanson, K. A.; Roychoudhury, S.; Koury, K.; Li, P.; Kalina, W. V.; Cooper, D.; Frenck, R. W., Jr.; Hammitt, L. L.; Türeci, Ö.; Nell, H.; Schaefer, A.; Ünal, S.; Tresnan, D. B.; Mather, S.; Dormitzer, P. R.; Şahin, U.; Jansen, K. U.; Gruber, W. C., Safety and Efficacy of the BNT162b2 mRNA Covid-19 Vaccine. *The New England journal of medicine* **2020**, *383* (27), 2603-2615.
299. Wender, P. A., Toward the ideal synthesis and molecular function through synthesis-informed design. *Natural Product Reports* **2014**, *31* (4), 433-440.
300. Hertz, D.; Leiske, M. N.; Wloka, T.; Traeger, A.; Hartlieb, M.; Kessels, M. M.; Schubert, S.; Qualmann, B.; Schubert, U. S., Comparison of random and gradient amino functionalized poly(2-oxazoline)s: Can the transfection efficiency be tuned by the macromolecular structure? *Journal of Polymer Science Part A: Polymer Chemistry* **2018**, *56* (12), 1210-1224.
301. Johnson, R. N.; Chu, D. S. H.; Shi, J.; Schellinger, J. G.; Carlson, P. M.; Pun, S. H., HPMA-oligolysine copolymers for gene delivery: Optimization of peptide length and polymer molecular weight. *Journal of Controlled Release* **2011**, *155* (2), 303-311.
302. Madruga, E. L., From classical to living/controlled statistical free-radical copolymerization. *Progress in Polymer Science* **2002**, *27* (9), 1879-1924.
303. Sun, X.; Luo, Y.; Wang, R.; Li, B.-G.; Liu, B.; Zhu, S., Programmed Synthesis of Copolymer with Controlled Chain Composition Distribution via Semibatch RAFT Copolymerization. *Macromolecules* **2007**, *40* (4), 849-859.
304. Nischang, I.; Perevyazko, I.; Majdanski, T.; Vitz, J.; Festag, G.; Schubert, U. S., Hydrodynamic Analysis Resolves the Pharmaceutically-Relevant Absolute Molar Mass and Solution Properties of Synthetic Poly(ethylene glycol)s Created by Varying Initiation Sites. *Analytical Chemistry* **2017**, *89* (2), 1185-1193.
305. Schlenk, F.; Grund, S.; Fischer, D., Recent developments and perspectives on gene therapy using synthetic vectors. *Ther. Deliv.* **2013**, *4* (1), 95-113.
306. Hall, A.; Lächelt, U.; Bartek, J.; Wagner, E.; Moghimi, S. M., Polyplex Evolution: Understanding Biology, Optimizing Performance. *Mol. Ther.* **2017**, *25* (7), 1476-1490.
307. Ravindran, M. S.; Bagchi, P.; Cunningham, C. N.; Tsai, B., Opportunistic intruders: how viruses orchestrate ER functions to infect cells. *Nature Reviews Microbiology* **2016**, *14* (7), 407-420.
308. Locock, K. E. S.; Michl, T. D.; Stevens, N.; Hayball, J. D.; Vasilev, K.; Postma, A.; Griesser, H. J.; Meagher, L.; Haeussler, M., Antimicrobial Polymethacrylates Synthesized as Mimics of Tryptophan-Rich Cationic Peptides. *ACS Macro Letters* **2014**, *3* (4), 319-323.
309. Åmand, H. L.; Rydberg, H. A.; Fornander, L. H.; Lincoln, P.; Nordén, B.; Esbjörner, E. K., Cell surface binding and uptake of arginine- and lysine-rich penetratin peptides in absence and presence of proteoglycans. *Biochimica et Biophysica Acta (BBA) - Biomembranes* **2012**, *1818* (11), 2669-2678.

310. Kang, Z.; Ding, G.; Meng, Z.; Meng, Q., The rational design of cell-penetrating peptides for application in delivery systems. *Peptides* **2019**, *121*, 170149.
311. F756-13, A., Standard practice for assessment of hemolytic properties of materials. *Annual Book of ASTM Standards* **2013**.
312. Fischer, D.; Bieber, T.; Li, Y.; Elsässer, H.-P.; Kissel, T., A Novel Non-Viral Vector for DNA Delivery Based on Low Molecular Weight, Branched Polyethylenimine: Effect of Molecular Weight on Transfection Efficiency and Cytotoxicity. *Pharm. Res.* **1999**, *16* (8), 1273-1279.
313. Prabha, S.; Arya, G.; Chandra, R.; Ahmed, B.; Nimesh, S., Effect of size on biological properties of nanoparticles employed in gene delivery. *Artificial Cells, Nanomedicine, and Biotechnology* **2016**, *44* (1), 83-91.
314. Zelikin, A. N.; Putnam, D.; Shastri, P.; Langer, R.; Izumrudov, V. A., Aliphatic Ionenenes as Gene Delivery Agents: Elucidation of Structure–Function Relationship through Modification of Charge Density and Polymer Length. *Bioconjugate Chemistry* **2002**, *13* (3), 548-553.
315. Kono, K.; Akiyama, H.; Takahashi, T.; Takagishi, T.; Harada, A., Transfection Activity of Polyamidoamine Dendrimers Having Hydrophobic Amino Acid Residues in the Periphery. *Bioconjugate Chemistry* **2005**, *16* (1), 208-214.
316. Chang, H.; Zhang, J.; Wang, H.; Lv, J.; Cheng, Y., A Combination of Guanidyl and Phenyl Groups on a Dendrimer Enables Efficient siRNA and DNA Delivery. *Biomacromolecules* **2017**, *18* (8), 2371-2378.
317. Ita, K., Polyplexes for gene and nucleic acid delivery: Progress and bottlenecks. *Eur. J. Pharm. Sci.* **2020**, *150*, 105358.
318. Le Bohec, M.; Bonchouo Kenzo, K.; Piogé, S.; Mura, S.; Nicolas, J.; Casse, N.; Forcher, G.; Fontaine, L.; Pascual, S., Structure-pDNA complexation and structure–cytotoxicity relationships of PEGylated, cationic aminoethyl-based polyacrylates with tunable topologies. *Polym. Chem.* **2019**, *10* (15), 1968-1977.
319. Oupicky, D.; Ogris, M.; Howard, K. A.; Dash, P. R.; Ulbrich, K.; Seymour, L. W., Importance of Lateral and Steric Stabilization of Polyelectrolyte Gene Delivery Vectors for Extended Systemic Circulation. *Mol. Ther.* **2002**, *5* (4), 463-472.
320. Noga, M.; Edinger, D.; Rödl, W.; Wagner, E.; Winter, G.; Besheer, A., Controlled shielding and deshielding of gene delivery polyplexes using hydroxyethyl starch (HES) and alpha-amylase. *J. Control. Release* **2012**, *159* (1), 92-103.
321. Trützscher, A.-K.; Bus, T.; Sahn, M.; Traeger, A.; Weber, C.; Schubert, U. S., The Power of Shielding: Low Toxicity and High Transfection Performance of Cationic Graft Copolymers Containing Poly(2-oxazoline) Side Chains. *Biomacromolecules* **2018**, *19* (7), 2759-2771.
322. Abuchowski, A.; McCoy, J. R.; Palczuk, N. C.; van Es, T.; Davis, F. F., Effect of covalent attachment of polyethylene glycol on immunogenicity and circulating life of bovine liver catalase. *Journal of Biological Chemistry* **1977**, *252* (11), 3582-3586.
323. Harris, J. M.; Chess, R. B., Effect of pegylation on pharmaceuticals. *Nature Reviews Drug Discovery* **2003**, *2* (3), 214-221.
324. Suk, J. S.; Xu, Q.; Kim, N.; Hanes, J.; Ensign, L. M., PEGylation as a strategy for improving nanoparticle-based drug and gene delivery. *Adv. Drug Deliv. Rev.* **2016**, *99*, 28-51.
325. Freitag, F.; Wagner, E., Optimizing synthetic nucleic acid and protein nanocarriers: The chemical evolution approach. *Adv. Drug Deliv. Rev.* **2021**, *168*, 30-54.

References

326. Venkataraman, S.; Ong, W. L.; Ong, Z. Y.; Joachim Loo, S. C.; Ee, P. L.; Yang, Y. Y., The role of PEG architecture and molecular weight in the gene transfection performance of PEGylated poly(dimethylaminoethyl methacrylate) based cationic polymers. *Biomaterials* **2011**, *32* (9), 2369-78.
327. Dirisala, A.; Osada, K.; Chen, Q.; Tockary, T. A.; Machitani, K.; Osawa, S.; Liu, X.; Ishii, T.; Miyata, K.; Oba, M.; Uchida, S.; Itaka, K.; Kataoka, K., Optimized rod length of polyplex micelles for maximizing transfection efficiency and their performance in systemic gene therapy against stroma-rich pancreatic tumors. *Biomaterials* **2014**, *35* (20), 5359-5368.
328. Ozer, I.; Tomak, A.; Zareie, H. M.; Baran, Y.; Bulmus, V., Effect of Molecular Architecture on Cell Interactions and Stealth Properties of PEG. *Biomacromolecules* **2017**, *18* (9), 2699-2710.
329. Petersen, H.; Fechner, P. M.; Martin, A. L.; Kunath, K.; Stolnik, S.; Roberts, C. J.; Fischer, D.; Davies, M. C.; Kissel, T., Polyethylenimine-graft-Poly(ethylene glycol) Copolymers: Influence of Copolymer Block Structure on DNA Complexation and Biological Activities as Gene Delivery System. *Bioconjug. Chem.* **2002**, *13* (4), 845-854.
330. Brus, C.; Petersen, H.; Aigner, A.; Czubayko, F.; Kissel, T., Physicochemical and Biological Characterization of Polyethylenimine-graft-Poly(ethylene glycol) Block Copolymers as a Delivery System for Oligonucleotides and Ribozymes. *Bioconjug. Chem.* **2004**, *15* (4), 677-684.
331. Glodde, M.; Sirsi, S. R.; Lutz, G. J., Physicochemical Properties of Low and High Molecular Weight Poly(ethylene glycol)-Grafted Poly(ethylene imine) Copolymers and Their Complexes with Oligonucleotides. *Biomacromolecules* **2006**, *7* (1), 347-356.
332. Tang, G. P.; Zeng, J. M.; Gao, S. J.; Ma, Y. X.; Shi, L.; Li, Y.; Too, H. P.; Wang, S., Polyethylene glycol modified polyethylenimine for improved CNS gene transfer: effects of PEGylation extent. *Biomaterials* **2003**, *24* (13), 2351-2362.
333. Merdan, T.; Kunath, K.; Petersen, H.; Bakowsky, U.; Voigt, K. H.; Kopecek, J.; Kissel, T., PEGylation of Poly(ethylene imine) Affects Stability of Complexes with Plasmid DNA under in Vivo Conditions in a Dose-Dependent Manner after Intravenous Injection into Mice. *Bioconjug. Chem.* **2005**, *16* (4), 785-792.
334. Sofia, S. J.; Premnath, V.; Merrill, E. W., Poly(ethylene oxide) Grafted to Silicon Surfaces: Grafting Density and Protein Adsorption. *Macromolecules* **1998**, *31* (15), 5059-5070.
335. Tirosh, O.; Barenholz, Y.; Katzhendler, J.; Prievo, A., Hydration of Polyethylene Glycol-Grafted Liposomes. *Biophysical Journal* **1998**, *74* (3), 1371-1379.
336. Bhat, R. R.; Tomlinson, M. R.; Wu, T.; Genzer, J., Surface-Grafted Polymer Gradients: Formation, Characterization, and Applications. In *Surface-Initiated Polymerization II*, Jordan, R., Ed. Springer Berlin Heidelberg: Berlin, Heidelberg, 2006; pp 51-124.
337. Vonarbourg, A.; Passirani, C.; Saulnier, P.; Benoit, J.-P., Parameters influencing the stealthiness of colloidal drug delivery systems. *Biomaterials* **2006**, *27* (24), 4356-4373.
338. Tockary, T. A.; Osada, K.; Chen, Q.; Machitani, K.; Dirisala, A.; Uchida, S.; Nomoto, T.; Toh, K.; Matsumoto, Y.; Itaka, K.; Nitta, K.; Nagayama, K.; Kataoka, K., Tethered PEG Crowdedness Determining Shape and Blood Circulation Profile of Polyplex Micelle Gene Carriers. *Macromolecules* **2013**, *46* (16), 6585-6592.

339. Rungsardthong, U.; Deshpande, M.; Bailey, L.; Vamvakaki, M.; Armes, S. P.; Garnett, M. C.; Stolnik, S., Copolymers of amine methacrylate with poly(ethylene glycol) as vectors for gene therapy. *J. Control. Release* **2001**, *73* (2), 359-380.
340. Deshpande, M. C.; Garnett, M. C.; Vamvakaki, M.; Bailey, L.; Armes, S. P.; Stolnik, S., Influence of polymer architecture on the structure of complexes formed by PEG–tertiary amine methacrylate copolymers and phosphorothioate oligonucleotide. *J. Control. Release* **2002**, *81* (1), 185-199.
341. Deshpande, M. C.; Davies, M. C.; Garnett, M. C.; Williams, P. M.; Armitage, D.; Bailey, L.; Vamvakaki, M.; Armes, S. P.; Stolnik, S., The effect of poly(ethylene glycol) molecular architecture on cellular interaction and uptake of DNA complexes. *J. Control. Release* **2004**, *97* (1), 143-156.
342. Lutz, J.-F., Polymerization of oligo(ethylene glycol) (meth)acrylates: Toward new generations of smart biocompatible materials. *J. Polym. Sci., Part A: Polym. Chem.* **2008**, *46* (11), 3459-3470.
343. Chua, G. B. H.; Roth, P. J.; Duong, H. T. T.; Davis, T. P.; Lowe, A. B., Synthesis and Thermoresponsive Solution Properties of Poly[oligo(ethylene glycol) (meth)acrylamide]s: Biocompatible PEG Analogues. *Macromolecules* **2012**, *45* (3), 1362-1374.
344. Xu, F. J.; Yang, W. T., Polymer vectors via controlled/living radical polymerization for gene delivery. *Prog. Polym. Sci.* **2011**, *36* (9), 1099-1131.
345. Ahmed, M.; Narain, R., Progress of RAFT based polymers in gene delivery. *Prog. Polym. Sci.* **2013**, *38* (5), 767-790.
346. Keddie, D. J., A guide to the synthesis of block copolymers using reversible-addition fragmentation chain transfer (RAFT) polymerization. *Chem. Soc. Rev.* **2014**, *43* (2), 496-505.
347. Peneva, K. Design, Synthesis and Application of Ultrastable Rylene Dyes for Fluorescent Labeling of Biomolecules. Johannes Gutenberg-Universität Mainz, Mainz, 2008.
348. Weil, T.; Abdalla, M. A.; Jatzke, C.; Hengstler, J.; Müllen, K., Water-Soluble Rylene Dyes as High-Performance Colorants for the Staining of Cells. *Biomacromolecules* **2005**, *6* (1), 68-79.
349. Northrop, B. H.; Frayne, S. H.; Choudhary, U., Thiol–maleimide “click” chemistry: evaluating the influence of solvent, initiator, and thiol on the reaction mechanism, kinetics, and selectivity. *Polymer Chemistry* **2015**, *6* (18), 3415-3430.
350. Scales, C. W.; Convertine, A. J.; McCormick, C. L., Fluorescent Labeling of RAFT-Generated Poly(N-isopropylacrylamide) via a Facile Maleimide–Thiol Coupling Reaction. *Biomacromolecules* **2006**, *7* (5), 1389-1392.
351. Breul, A. M.; Hager, M. D.; Schubert, U. S., Fluorescent monomers as building blocks for dye labeled polymers: synthesis and application in energy conversion, biolabeling and sensors. *Chem. Soc. Rev.* **2013**, *42* (12), 5366-5407.
352. Beija, M.; Charreyre, M.-T.; Martinho, J. M. G., Dye-labelled polymer chains at specific sites: Synthesis by living/controlled polymerization. *Prog. Polym. Sci.* **2011**, *36* (4), 568-602.
353. Costabel, D.; Skabeev, A.; Nabiyan, A.; Luo, Y.; Max, J.; Rajagopal, A.; Kowalczyk, D.; Dietzek, B.; Wächtler, M.; Görls, H.; Ziegenbalg, D.; Zagranyski, Y.; Streb, C.; Schacher, F. H.; Peneva, K., 1,7,9,10-tetrasubstituted PMIs accessible via decarboxylative bromination: Synthesis, Characterization, Photophysical Studies and Hydrogen Evolution Catalysis. *Chem. Eur. J.* *n/a* (n/a).
354. Pujals, S.; Albertazzi, L., Super-resolution Microscopy for Nanomedicine Research. *ACS Nano* **2019**, *13* (9), 9707-9712.

References

355. Nomoto, T.; Fukushima, S.; Kumagai, M.; Machitani, K.; Arnida; Matsumoto, Y.; Oba, M.; Miyata, K.; Osada, K.; Nishiyama, N.; Kataoka, K., Three-layered polyplex micelle as a multifunctional nanocarrier platform for light-induced systemic gene transfer. *Nat. Commun.* **2014**, *5* (1), 3545.
356. Bus, T.; Englert, C.; Reifarth, M.; Borchers, P.; Hartlieb, M.; Vollrath, A.; Hoepfener, S.; Traeger, A.; Schubert, U. S., 3rd generation poly(ethylene imine)s for gene delivery. *J. Mater. Chem. B* **2017**, *5* (6), 1258-1274.
357. Golshan, M.; Rostami-Tapeh-Esmail, E.; Salami-Kalajahi, M.; Roghani-Mamaqani, H., A review on synthesis, photophysical properties, and applications of dendrimers with perylene core. *Eur. Polym. J.* **2020**, *137*, 109933.
358. Bauer, M.; Lautenschlaeger, C.; Kempe, K.; Tauhardt, L.; Schubert, U. S.; Fischer, D., Poly(2-ethyl-2-oxazoline) as Alternative for the Stealth Polymer Poly(ethylene glycol): Comparison of in vitro Cytotoxicity and Hemocompatibility. *Macromol. Biosci.* **2012**, *12* (7), 986-998.
359. Ogris, M.; Steinlein, P.; Carotta, S.; Brunner, S.; Wagner, E., DNA/polyethylenimine transfection particles: Influence of ligands, polymer size, and PEGylation on internalization and gene expression. *AAPS PharmSci* **2001**, *3* (3), 43.
360. Mishra, S.; Webster, P.; Davis, M. E., PEGylation significantly affects cellular uptake and intracellular trafficking of non-viral gene delivery particles. *European Journal of Cell Biology* **2004**, *83* (3), 97-111.
361. Liu, G.; Li, Y.; Yang, L.; Wei, Y.; Wang, X.; Wang, Z.; Tao, L., Cytotoxicity study of polyethylene glycol derivatives. *RSC Adv.* **2017**, *7* (30), 18252-18259.
362. Zink, M.; Hotzel, K.; Schubert, U. S.; Heinze, T.; Fischer, D., Amino Acid-Substituted Dextran-Based Non-Viral Vectors for Gene Delivery. *Macromol. Biosci.* **2019**, *19* (8), e1900085.
363. Fischer, D.; Dautzenberg, H.; Kunath, K.; Kissel, T., Poly(diallyldimethylammonium chlorides) and their N-methyl-N-vinylacetamide copolymer-based DNA-polyplexes: role of molecular weight and charge density in complex formation, stability, and in vitro activity. *Int. J. Pharm.* **2004**, *280* (1), 253-269.
364. Ochrimenko, S.; Vollrath, A.; Tauhardt, L.; Kempe, K.; Schubert, U. S.; Fischer, D., Dextran-graft-linear poly(ethylene imine)s for gene delivery: Importance of the linking strategy. *Carbohydr. Polym.* **2014**, *113*, 597-606.
365. Wei, H.; Pahang, J. A.; Pun, S. H., Optimization of Brush-Like Cationic Copolymers for Nonviral Gene Delivery. *Biomacromolecules* **2013**, *14* (1), 275-284.
366. Zhang, X.; Pan, S.-R.; Hu, H.-M.; Wu, G.-F.; Feng, M.; Zhang, W.; Luo, X., Poly(ethylene glycol)-block-polyethylenimine copolymers as carriers for gene delivery: Effects of PEG molecular weight and PEGylation degree. *J. Biomed. Mater. Res. A* **2008**, *84A* (3), 795-804.
367. Takeda, K. M.; Osada, K.; Tockary, T. A.; Dirisala, A.; Chen, Q.; Kataoka, K., Poly(ethylene glycol) Crowding as Critical Factor To Determine pDNA Packaging Scheme into Polyplex Micelles for Enhanced Gene Expression. *Biomacromolecules* **2017**, *18* (1), 36-43.
368. Tan, J. F.; Hatton, T. A.; Tam, K. C.; Too, H. P., Correlating Transfection Barriers and Biophysical Properties of Cationic Polymethacrylates. *Biomacromolecules* **2007**, *8* (2), 448-454.
369. Liang, R.-P.; Yu, L.-D.; Tong, Y.-J.; Wen, S.-H.; Cao, S.-P.; Qiu, J.-D., An ultratrace assay of arsenite based on the synergistic quenching effect of Ru(bpy)₃²⁺ and arsenite on the electrochemiluminescence of Au-g-C₃N₄ nanosheets. *Chemical Communications* **2018**, *54* (99), 14001-14004.

370. Arsenic. 15.02.2018 ed.; World Health Organization: 2018.
371. Drinking Water Arsenic Rule History. 22.01.2001 ed.; United States Environmental Protection Agency: 2001.
372. Jain, C. K.; Ali, I., Arsenic: occurrence, toxicity and speciation techniques. *Water Research* **2000**, *34* (17), 4304-4312.
373. Argos, M.; Kalra, T.; Rathouz, P. J.; Chen, Y.; Pierce, B.; Parvez, F.; Islam, T.; Ahmed, A.; Rakibuz-Zaman, M.; Hasan, R.; Sarwar, G.; Slavkovich, V.; van Geen, A.; Graziano, J.; Ahsan, H., Arsenic exposure from drinking water, and all-cause and chronic-disease mortalities in Bangladesh (HEALS): a prospective cohort study. *The Lancet* **2010**, *376* (9737), 252-258.
374. Devi, P.; Thakur, A.; Lai, R. Y.; Saini, S.; Jain, R.; Kumar, P., Progress in the materials for optical detection of arsenic in water. *TrAC Trends in Analytical Chemistry* **2019**, *110*, 97-115.
375. Liu, J.; Cao, Z.; Lu, Y., Functional Nucleic Acid Sensors. *Chemical Reviews* **2009**, *109* (5), 1948-1998.
376. Kaur, H.; Kumar, R.; Babu, J. N.; Mittal, S., Advances in arsenic biosensor development – A comprehensive review. *Biosensors and Bioelectronics* **2015**, *63*, 533-545.
377. Hae Cho, C. A.; Liang, C.; Perera, J.; Liu, J.; Varnava, K. G.; Sarojini, V.; Cooney, R. P.; McGillivray, D. J.; Brimble, M. A.; Swift, S.; Jin, J., Molecular Weight and Charge Density Effects of Guanidinylated Biodegradable Polycarbonates on Antimicrobial Activity and Selectivity. *Biomacromolecules* **2018**, *19* (5), 1389-1401.
378. Yang, C.; Lou, W.; Zhong, G.; Lee, A.; Leong, J.; Chin, W.; Ding, B.; Bao, C.; Tan, J. P. K.; Pu, Q.; Gao, S.; Xu, L.; Hsu, L. Y.; Wu, M.; Hedrick, J. L.; Fan, W.; Yang, Y. Y., Degradable antimicrobial polycarbonates with unexpected activity and selectivity for treating multidrug-resistant *Klebsiella pneumoniae* lung infection in mice. *Acta Biomaterialia* **2019**, *94*, 268-280.
379. Exley, S. E.; Paslay, L. C.; Sahukhal, G. S.; Abel, B. A.; Brown, T. D.; McCormick, C. L.; Heinhorst, S.; Koul, V.; Choudhary, V.; Elasmri, M. O.; Morgan, S. E., Antimicrobial Peptide Mimicking Primary Amine and Guanidine Containing Methacrylamide Copolymers Prepared by Raft Polymerization. *Biomacromolecules* **2015**, *16* (12), 3845-3852.
380. Parsons, K. H.; Mondal, M. H.; McCormick, C. L.; Flynt, A. S., Guanidinium-Functionalized Interpolyelectrolyte Complexes Enabling RNAi in Resistant Insect Pests. *Biomacromolecules* **2018**, *19* (4), 1111-1117.
381. Bala, R.; Swami, A.; Tabujew, I.; Peneva, K.; Wangoo, N.; Sharma, R. K., Ultra-sensitive detection of malathion using quantum dots-polymer based fluorescence aptasensor. *Biosensors and Bioelectronics* **2018**, *104*, 45-49.
382. Dey, B.; Mukherjee, P.; Mondal, R. K.; Chattopadhyay, A. P.; Hauli, I.; Mukhopadhyay, S. K.; Fleck, M., Femtomolar level sensing of inorganic arsenic(III) in water and in living-systems using a non-toxic fluorescent probe. *Chemical Communications* **2014**, *50* (96), 15263-15266.
383. Zhu, Z.; Zhang, S.; Lv, Y.; Zhang, X., Atomization of Hydride with a Low-Temperature, Atmospheric Pressure Dielectric Barrier Discharge and Its Application to Arsenic Speciation with Atomic Absorption Spectrometry. *Analytical Chemistry* **2006**, *78* (3), 865-872.
384. Paul, R. L., Evaluation of Radiochemical Neutron Activation Analysis Methods for Determination of Arsenic in Biological Materials. *Analytical Chemistry* **2011**, *83* (1), 152-156.

References

385. Wu, Y.; Zhan, S.; Wang, F.; He, L.; Zhi, W.; Zhou, P., Cationic polymers and aptamers mediated aggregation of gold nanoparticles for the colorimetric detection of arsenic(iii) in aqueous solution. *Chemical Communications* **2012**, *48* (37), 4459-4461.
386. Rodríguez, P. F.; Martín-Aranda, R. M.; López Colón, J. L.; de Mendoza, J. H., Ammonium acetate as a novel buffer for highly selective robust urinary HPLC-ICP-MS arsenic speciation methodology. *Talanta* **2021**, *221*, 121494.
387. Xu, S.; Sabino, F. P.; Janotti, A.; Chase, D. B.; Sparks, D. L.; Rabolt, J. F., Unique Surface Enhanced Raman Scattering Substrate for the Study of Arsenic Speciation and Detection. *The Journal of Physical Chemistry A* **2018**, *122* (49), 9474-9482.
388. Vega-Figueroa, K.; Santillán, J.; Ortiz-Gómez, V.; Ortiz-Quiles, E. O.; Quiñones-Colón, B. A.; Castilla-Casadio, D. A.; Almodóvar, J.; Bayro, M. J.; Rodríguez-Martínez, J. A.; Nicolau, E., Aptamer-Based Impedimetric Assay of Arsenite in Water: Interfacial Properties and Performance. *ACS Omega* **2018**, *3* (2), 1437-1444.
389. Sullivan, C.; Lu, D.; Brack, E.; Drew, C.; Kurup, P., Voltammetric codetection of arsenic(III) and copper(II) in alkaline buffering system with gold nanostar modified electrodes. *Analytica Chimica Acta* **2020**, *1107*, 63-73.
390. Motalebizadeh, A.; Bagheri, H.; Asiaei, S.; Fekrat, N.; Afkhami, A., New portable smartphone-based PDMS microfluidic kit for the simultaneous colorimetric detection of arsenic and mercury. *RSC Advances* **2018**, *8* (48), 27091-27100.
391. Tang, G.; Wang, J.; Li, Y.; Su, X., Determination of arsenic(iii) based on the fluorescence resonance energy transfer between CdTe QDs and Rhodamine 6G. *RSC Advances* **2015**, *5* (23), 17519-17525.
392. Oroval, M.; Coll, C.; Bernardos, A.; Marcos, M. D.; Martínez-Mañez, R.; Shchukin, D. G.; Sancenón, F., Selective Fluorogenic Sensing of As(III) Using Aptamer-Capped Nanomaterials. *ACS Applied Materials & Interfaces* **2017**, *9* (13), 11332-11336.

Selbständigkeitserklärung

Ich erkläre, dass ich die vorliegende Arbeit selbständig und unter Verwendung der angegebenen

Hilfsmittel, persönlichen Mitteilungen und Quellen angefertigt habe.

Ort, Datum

Unterschrift der Verfasserin

Acknowledgement

First and foremost, I wish to express my sincere gratitude to my supervisor Prof. Dr. Kalina Peneva for giving me the opportunity to be a part of her research team throughout my Ph.D. studies. I am very grateful for her professional supports and her unique guidance. Throughout my journey, she always trusted me and gave me the courage to go beyond my scientific and personal capabilities. Her endless kindness and understanding gave me the strength to go forward in difficult times. Her creative approach and strength were my biggest inspirations.

I sincerely acknowledge my co-supervisor Prof. Dr. Dagmar Fischer for her excellent guidance, critics, and the collaboration for our ‘PolyTarget - B03 - SFB 1278’ project. I gained precious experience regarding interdisciplinary way of thinking and presenting our work. During our formal and informal meetings, the fruitful scientific discussions nourished my research. With the valuable effort of her and her group members, especially Leon Zartner and Franz J. Hack, I was able to carry my research to the next step and we, together, could revealed more information with respect to the pharmaceutical potential of the guanidinium containing poly(methacrylamide)s presented in my dissertation.

Apart from my supervisor and co-supervisor, I would like to thank the German Research Foundation (DFG) for providing the funding to conduct my research with a limitless access to scientific resources and facilities. Moreover, DFG gave me the chance to meet excellent experts and colleagues, which enlarged my scientific vision. I could additionally improve my soft skills by attending to the training and activities supported by DFG. Especially, I collected so many special moments and valuable connections with my female colleagues through ‘Awesome Women in Science’ sessions, which was held by Dr. Anne-Christin Warskulat, Curiositas.

I am very grateful to Prof. Ulrich Schubert that he let me be a part of the PolyTarget project. It was a great time and sharing with all PolyTarget members with respect to their insightful comments and engrossing questions. In addition, I would like to thank for our collaboration to reveal the potential of gradient comonomer distribution of guanidinium bearing poly(methacrylamide)s for non-viral gene delivery. Thanks to Dr. Ivo Nischang, I gained deeper knowledge and hands-on laboratory experiences on the hydrodynamic characterization of polycations. I have special thanks to Dr. Grit Festag not only for our collaboration, but also her continuous support and kindness for the characterization of my polymers through size-exclusion chromatography. I am also grateful for other members of Schubert Group for their direct or indirect support throughout my research.

I would also like to express my gratitude to Prof. Dr. Felix Schacher for his kindness and support both scientifically and personally. By means of our fruitful discussions and his suggestions, I could critically consider my research projects from different point of views. I am so tankful to his former and current members of Schacher Group. Throughout my Ph.D. journey, together with my group, we evolved into a big family

where everyone showed kindness and support to each other. I would like to give my special thanks to Dr. Iuliia Romanenko. Her excellent work attitude always inspired. She always supports me as a close friend regardless of the distance. I am thankful to Dr. Jessica Tom for our collaboration and friendship.

I am very thankful to Prof. Dr. Rainer Heintzmann and Dr. Patrick Then for our fruitful collaboration to visualize our polyplexes through structured illumination microscopy. Our work became another example for the biological applicability of perylene chromophores.

I give special thanks to Asst. Prof. Rohit K. Sharma and his group members, especially Gurpreet K. Soni and Nishima Wangoo, for their precious efforts and support during our collaboration. We could remove the distance limit in our research and connect Germany and India.

The former and current members of Peneva group showed the warmest heart and endless support throughout my journey. I am very thankful to my group members. We supported each other both scientifically and personally. We had unforgettable memories together. We became a perfect example of an international group. Artem Skabeev worked as a catalyst all the time. His special sense of humor and connection skills bonded the group members strongly. I had great memories with Javier G. Lopez not only in Germany but also in Spain. At one point, his family became my family and his dog became my dog. I am very grateful for our collaboration with Daniel Costabel. His was a great example for productivity and proactivity. I have special thanks to Sebastian Städter. Without his efforts, we would not be able to achieve big things in a short time. He started as my bachelor student, yet he became a very good colleague and friend. He always supported me and showed kindness. I believe that I will be able to see him in very good positions and I will be always proud of him. The last but not the least, I would like to thank to Katja König. She was way beyond of a work friend. I will never forget our tea and coffee times together. She was so supportive and understanding. I apologize to people that I forgot to mention. All the people I met in Jena made me feel so lucky. Thank you for being beside me.

I am very grateful to Prof. Andreas Hochhaus for his precious effort. My family always supported me throughout my journey. Without them, I would not be able to come to Germany and gain such a great experience. I am so thankful to Pihlamägi family, especially to my husband, Tõnis Pihlamägi. He showed endless patience, support, and love.

Curriculum vitae

COKCA CEREN

Ebertstraße 1, 07743 Jena, Germany
0176/63182735

20.01.1986 in Adana/Türkei
Türkisch



Berufserfahrung

09/2016-09/2021

Wissenschaftliche Mitarbeiterin, Institut für Organische und Makromolekulare Chemie, *Friedrich-Schiller-Universität Jena, Deutschland*

- Kontrollierte Polymerisationsmethoden
- Polymercharakterisierung
- Herstellung von biokompatiblen Materialien für den Gentransport
- Markierung von Antikörpern und Polymeren mit Fluoreszenzfarbstoffen
- Betreuung Abschlussarbeiten (Master, Bachelor) und Praxisphase
- Vorträge halten und Publikationen schreiben

Ausbildung

Seit 10/2017

Doktorarbeit, Institut für Organische und Makromolekulare Chemie, *Friedrich-Schiller-Universität Jena, Deutschland*

Betreuung: Prof. Dr. Kalina Peneva, Institut für Organische und Makromolekulare Chemie, *Friedrich-Schiller-Universität Jena, Deutschland*

unterstützt von Deutsche Forschungsgemeinschaft (DFG) - **POLYTARGET** Project Nummer 316213987 - **SFB 1278**

Voraussichtlicher Zeitpunkt für den Abschluss: November 2022

2012 - 2015

M.Sc. in Biomedizinische Technik, *Middle East Technical University (METU), Turkey*

Abschlussarbeit: The Effects of Doxorubicin Containing Poly (Sebacic Anhydride) Nanocapsules on Glutathione S-Transferase Activity

Betreuung: Prof. Dr. Nesrin Hasirci, Fachbereich Chemie, *METU* und *BIOMATEN Center of Excellence in Biomaterials and Tissue Engineering, Ankara, Türkei*

2005 - 2010

B.Sc. in Biologie, *Middle East Technical University, Turkey*

Abschlussarbeit: The Effect of Etoposide on Doxorubicin Resistant MCF-7 Cells

Betreuung: Prof. Dr. Ufuk Gündüz, Fachbereich Biologische Wissenschaften, *METU*

2009	Praktikum, Hacettepe University Faculty of Medicine Department of Medical Oncology, Turkey
3 Monate	Betreuung: Prof. Dr. Dicle Güç and Prof. Dr. Güneş Esendağlı
2008	Praktikum, Çukurova University Department of Medical Biology, Turkey
2 Wochen	Betreuung: Prof. Dr. Osman Demirhan

Qualifikationen

Technische Fähigkeiten

Polymerchemie und Charakterisierung: Kondensationspolymerisation in Lösung und RAFT-Polymerisation, Größenausschlusschromatographie (SEC), Membranosmometrie, Viskosimeter, Densimeter, Kernspinresonanzspektroskopie (NMR), Fourier-Transformations-Infrarotspektrometer (FTIR), UV-VIS -Spektroskopie

Pharmazeutische Technologie: Zeta-Potential, Dynamische Lichtstreuung (DLS), Nanopartikel-Formulierung, Agarose-Gelelektrophorese, In-vitro-Zytotoxizitätsuntersuchungen

Sprachen

Türkisch	Muttersprache
Englisch	Verhandlungssicher
Deutsch	gute Kenntnisse

IT-Kenntnisse

MS Office		ChemDraw	
LaTeX		MestReNova	
GraphPad		EndNote	
Origin		WinGPC	
SciFinder			
C++			
MATLAB			

Konferenzen und Symposien

- Summerfest, Towards understanding polyplex mediated gene delivery, Jena/Germany (**13 August 2019**) – *Speaker*
- Innovative Polymers for the Nanomedicine of the 21st Century, Jena/Germany (**15th-17th July 2019**) - *Poster presentation*
- Nanomedicine Formulation, Characterization Translation Summer School (collaboration with Max Planck Institute for Polymer Research, Mainz), Fulda/Germany (**24th-28th June 2019**) - *Poster presentation and 3 min flash presentation*
- European Polymer Congress, Crete/Greece (**9th-14th June 2019**) - *Poster presentation*
- Biennial Meeting of the GDCh - Division of Macromolecular Chemistry, Karlsruhe/Germany (**24th-27th September 2018**) - *Poster presentation*
- Summerfest, NIR molecular probes for *in vivo* and *in vitro* imaging, Jena/Germany (**26 July 2018**) - *Speaker*

- 12th International Symposium on Polymer Therapeutics: from Laboratory to Clinical Practices, Valencia/Spain (28th-30th May 2018) - *Poster presentation and 3 min flash presentation*

Aktivitäten und Zertifikate

- 4th METU Science Exhibition (21st -22nd March 2009), Ankara/Turkey- *Kontribution-Zertifikat*
- Academic Writing Skill Course by Graduate Academy at Friedrich-Schiller-Universität Jena, Jena/Germany (16.11.2017) - *Teilnehmerzertifikat*
- Good Scientific Practice - Protecting Scientific Integrity by Graduate Academy at Friedrich-Schiller-Universität Jena, Jena/Germany (27th-28th January 2020) - *Teilnehmerzertifikat*
- Awesome Women in Science - Fundamentals of Productivity, Project Management, Scientific Leadership/ Supervision, Communication, Mental Health and Career Planning for Female Ph.D. Candidates by Curiositas at Friedrich-Schiller-Universität Jena, Jena/Germany (November 2019-June 2021) - *Teilnehmerzertifikat*
- Introduction to the GxPs - with special focus on GMP and GLP by Graduate Academy at Friedrich-Schiller-Universität Jena, Jena/Germany (14th-15th December2020) - *Teilnehmerzertifikat*

Publikationen

1. Fabrication of cell penetrating peptide labelled biodegradable poly(methacrylamide) nanoparticles for delivery of doxorubicin in HeLa cells: N. Devi; **C. Cokca**; R. Sharma; M. Kumar; K. Peneva; R. K. Sharma, *Materials Today Communications*, **2022**, 33, 104233.
2. Ultrasensitive Aptasensor for Arsenic Detection using Quantum dots and Guanylated Poly(methacrylamide): G. K. Soni; N. Wangoo; **C. Cokca**; K; Peneva; R. K. Sharma, *Analytica Chimica Acta*, **2022**, 1209, 339584.
3. PEGylation of Guanidinium and Indole Bearing Poly(methacrylamide)s – Biocompatible Terpolymers for pDNA Delivery: **C. Cokca**; F. J. Hack; D. Costabel; K. Herwig; J. Hülsmann; P. Then; R. Heintzmann; D. Fischer; K. Peneva, *Macromolecular Bioscience*, **2021**, 21(10), 2100146.
4. Indole, Phenyl, and Phenol Groups: The Role of the Comonomer on Gene Delivery in Guanidinium Containing Methacrylamide Terpolymers: F. J. Hack; **C. Cokca**; S. Städter; J. Hülsmann; K. Peneva; D. Fischer, *Macromolecular Rapid Communications*, **2020**, 42(8), 2000580. *Ausgewählt als Titelseite*
5. Incorporation of Indole Significantly Improves the Transfection Efficiency of Guanidinium-Containing Poly(Methacrylamide)s: **C. Cokca**; L. Zartner; I. Tabujew; D. Fischer; K. Peneva, *Macromolecular Rapid Communications*, **2020**, 41(9), 1900668. *Ausgewählt als 'Best of Healthcare from Macromolecular Rapid Communications' und Titelseite*
6. The influence of gradient and statistical arrangements of guanidinium or primary amine groups in poly(methacrylate) copolymers on their DNA binding affinity: I. Tabujew; **C. Cokca**; L. Zartner; U. S. Schubert; I. Nischang; D. Fischer; K. Peneva, *Journal of Materials Chemistry B*, **2019**, 7, 5920-5929. *Ausgewählt als Titelseite*

Interessen & Hobbys

Volleyball (Hochschulmannschaft)

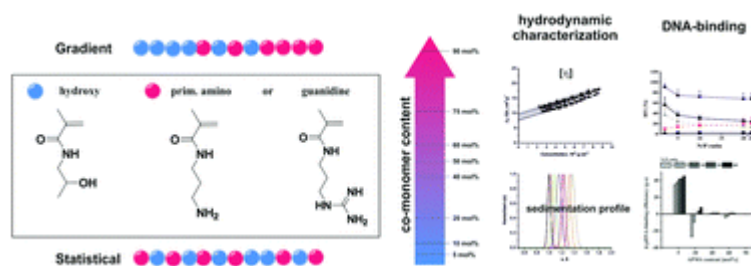
Tennis (Teilnahme an lokalen Wettbewerben)

Bogenschießen (Universitätsteam)

Zeichnen and Malen (Handgemachte Vorbereitung der Titelseite für das Journal of Materials Chemistry B)

Publication P1

The influence of gradient and statistical arrangements of guanidinium or primary amine groups in poly(methacrylate) copolymers on their DNA binding affinity



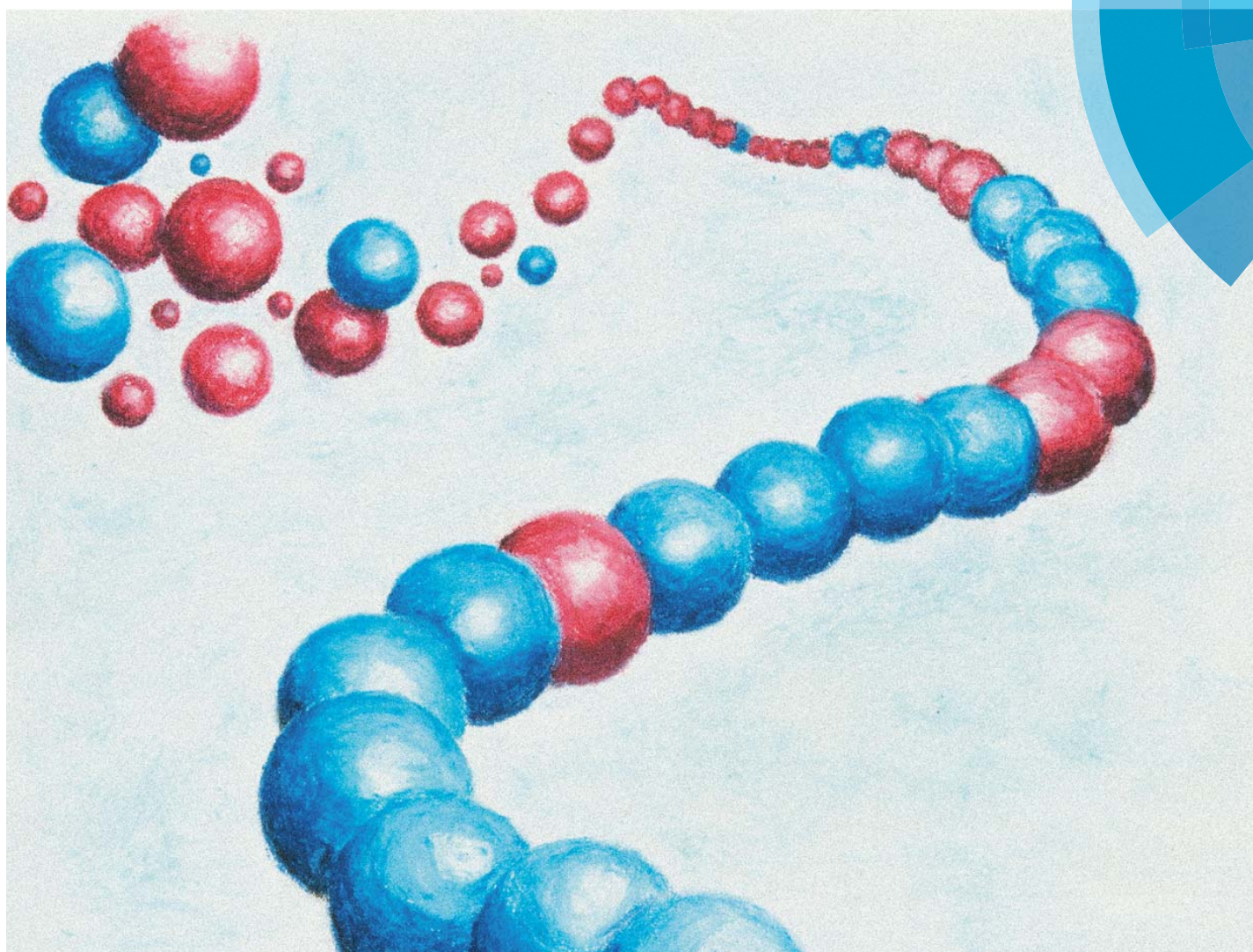
I. Tabujew, C. Cokca, L. Zartner, U. S. Schubert, I. Nischang, D. Fischer, K. Peneva

J. Mater. Chem. B **2019**, 7 (39), 5889-6066

Journal of Materials Chemistry B

Materials for biology and medicine

rsc.li/materials-b



ISSN 2050-750X



ROYAL SOCIETY
OF CHEMISTRY

Celebrating
IYPT 2019

PAPER

Kalina Peneva *et al.*

The influence of gradient and statistical arrangements of guanidinium or primary amine groups in poly(methacrylate) copolymers on their DNA binding affinity

Cite this: *J. Mater. Chem. B*, 2019,
7, 5920

The influence of gradient and statistical arrangements of guanidinium or primary amine groups in poly(methacrylate) copolymers on their DNA binding affinity†

Ilija Tabujew,^{‡a} Ceren Cokca,^{‡a} Leon Zartner,^b Ulrich S. Schubert,^{cd}
Ivo Nischang,^{cd} Dagmar Fischer^{b,c} and Kalina Peneva^{id *ac}

Herein, we report the first gradient guanidinium containing cationic copolymers and investigate their binding ability to plasmid DNA (pDNA). To understand the effect of different charge distributions and cationic charge sources (primary amines vs. guanidinium group) on (pDNA) binding affinity, we synthesized a library of well-defined statistical cationic copolymers comprising *N*-(2-hydroxy-propyl)methacrylamide (HPMA) and *N*-(3-aminopropyl)methacrylamide (APMA) or *N*-(3-guanidinopropyl)methacrylamide (GPMA) and compared them with gradient polymers containing the same monomers of similar composition. All copolymers were synthesized through aqueous reversible addition–fragmentation chain transfer (aRAFT) polymerization at various monomer ratios by aiming at similar molar masses with low dispersity indices. For the molar mass characterization, in addition to size exclusion chromatography with two different systems, hydrodynamic characterization utilizing analytical ultracentrifugation, viscometry, and accompanied density measurements was conducted. pDNA was used as a model drug to demonstrate the impact of copolymer architecture on binding efficiency. For both HPMA–APMA and HPMA–GPMA copolymers, the gradient distribution demonstrated superior binding and denser packing of pDNA than their statistical counterparts at 20% and lower cationic charge contents. With respect to charge origin, the guanidinium group represented a higher binding efficiency than primary amines with the same nitrogen to phosphate ratio (N/P ratio). Our study demonstrates the profound effect of gradient monomer arrangement on the ability of polyplex formation and reveals the potential for further investigation in gene delivery applications. Gradient guanidinium containing copolymers have great promise for gene delivery applications due to their high affinity toward pDNA even at very low degrees (<20%) of charged monomer content.

Received 24th June 2019,
Accepted 2nd September 2019

DOI: 10.1039/c9tb01269a

rsc.li/materials-b

1. Introduction

Cationic monomers and the development of their different copolymer structures are getting attention for gene delivery continuously.¹ All the efforts aim for the discovery of alternative polymer structures to improve the applicability of the cationic polymers in clinical studies for gene therapy.² Beside the discovery of new monomers, there is a high demand for a comprehensive investigation concerning the impact of physico-chemical properties of their polymers on the gene delivery efficiency. Since the approach relies on the reversible interaction between negatively charged nucleic acids and cationic macromolecules, the complex formation is one of the crucial points for the final success. In general, strong binding and stable complexes are demanded to secure the polyplex stability until reaching the release site. This can be promoted by using high local cationic charge densities throughout the polymer chains like in the case of block copolymers,^{3–5} stars⁶ or comb-shaped structures.⁷

^a Institute of Organic Chemistry and Macromolecular Chemistry, Friedrich Schiller University Jena, Lessingstraße 8, 07743 Jena, Germany. E-mail: kalina.peneva@uni-jena.de

^b Institute of Pharmacy, Friedrich Schiller University Jena, Lessingstraße 8, 07743 Jena, Germany

^c Jena Center of Soft Matter, Friedrich Schiller University Jena, Philosophenweg 7, 07743 Jena, Germany

^d Laboratory of Organic and Macromolecular Chemistry (IOMC), Humboldtstraße 10, 07743 Jena, Germany

† Electronic supplementary information (ESI) available: The synthesis pathways, the NMR spectra as well as the tables containing the desired, theoretical and experimental APMA or GPMA content in mol%, the intrinsic viscosity ($[\eta]$), the Huggins constant (k_H), partial specific volume (ν), the average total value of monomer units per polymer chain for each sample, and the monomer addition rates, which were used for the semi-batch polymerization of the gradient copolymers, are included. See DOI: 10.1039/c9tb01269a

‡ These authors contributed equally to the manuscript.

This strategy can nonetheless affect intracellular release of the polynucleotide cargo negatively if the interaction is overly strong. On the other hand, by statistical distribution of cationic units along the copolymer chain, the reduction in the local charge density can be achieved by stimulating a more responsive release; yet, the binding affinity is diminished.⁸ Based on these observations, the investigation of new co-monomer distributions is gaining attention.

Gradient cationic copolymers, which form a continuous pile-up of cationic monomer units and thereby cationic charge density along the chain, possess distinct properties in comparison to block- or statistical copolymers with analogous monomer compositions. However, the potential of gradient copolymers for gene delivery applications has not yet been understood completely and there are no documented studies on cationic gradient copolymers of guanidinium containing monomers in the literature. We believe that the examination of gradient copolymer structures regarding polyplex formation can open a new alternative way for optimizing the conditions leading to successful gene delivery applications. Considering that the efficacy of polyplex formation is influenced by factors like the molar mass, positive charge density, chain architecture, and shape of the particles,⁹ the gradient approach should also be investigated in detail. Up until now, the research on gradient copolymers has mostly focused on materials science-oriented applications, e.g. pressure sensitive adhesives,¹⁰ blend compatibilizers,¹¹ amphiphiles,¹² the backbone of hydrophobic polymer brushes^{13,14} and the corona of aluminum oxide particles, in order to improve the compatibility with organic solvents.¹⁵ These studies capitalized on the thermal and mechanical properties of gradient copolymers including glass transition temperature,¹⁶ morphology,^{17,18} surface activity,¹⁹ as well as their behavior in solution,²⁰ and micellization.^{21,22} The only literature example of gradient cationic copolymers is based on amino functionalized poly(2-oxazolines) for gene delivery where the influence of the cationic monomer distribution on the polyplex size was observed.²³ Utilizing gradient copolymers as gene delivery systems requires well-defined, water-soluble, and biocompatible structures. To fulfil such requirements, controlled polymerization techniques tolerating nucleophilic functional groups are necessary to be employed. Even though free radical polymerization is not affected by many of the functional groups, it is not a viable method for the synthesis of well-defined gradient copolymers. The reason is the dissimilarity in the monomer composition among the chains due to its initiation- and propagation kinetics. Utilizing reversible addition-fragmentation chain transfer (RAFT) polymerization, a controlled radical polymerization technique, can overcome this problem. Initiation kinetics of RAFT polymerization exceed the propagation speed and the reactive chain ends remain active during the polymerization. Since all chains propagate concertedly, near uniform polymer chains are expected,²⁴ yet the way of obtaining gradient copolymers through RAFT polymerization strongly depends on the reactivity ratios of monomers.²⁵ A gradient structure can form by one-pot (batch) copolymerization if the reactivities are significantly different from each other. For example, it is possible to promote the spontaneous formation of gradient copolymers by choosing

styrene and *n*-butyl acrylate or poly(ethylene glycol) methylether methacrylate and (2,2-dimethyl-1,3-dioxolane)methyl acrylamide that have notably different reactivity ratios.^{26–28} For monomers without remarkable differences in reactivity, on the contrary, the gradient formation through batch copolymerization is barely possible. Such circumstances require semi-batch copolymerization, as the influence of monomer reactivities can be diminished almost entirely. This method is based on the principle of continuous addition of the second monomer with a certain rate to the reaction mixture containing the first monomer.²⁹ It allows the gradient copolymerization of monomers over a broader range of conditions; even for monomers that tend to polymerize in an alternating fashion such as styrene and acrylonitrile.³⁰

Herein, we investigate the influence emerging from the change in the distribution of cationic co-monomer units through the linear copolymers on the polyplex formation. For this purpose, pGL3 plasmid was selected as a model polynucleotide cargo. The cationic units in the copolymers originate from the monomers *N*-(3-aminopropyl)methacrylamide (APMA) and *N*-(3-guanidinopropyl)methacrylamide (GPMA), which are the mimics of cell penetrating peptides containing lysine and arginine amino acid units, respectively, and they have already proven their efficiency in gene delivery.^{31,32} These monomers were copolymerized with the water-soluble *N*-(2-hydroxypropyl)methacrylamide (HPMA) monomer. HPMA, which is one of the most extensively studied monomers in gene and drug delivery,³³ was chosen as the inert “spacer-monomer”. It is not expected to contribute to the binding of polynucleotides even though it exhibits valuable properties such as low fouling in undiluted blood plasma.³⁴ The copolymerization reaction was performed through *a*RAFT polymerization, aiming at gradient and statistical copolymers that form two different charge distributions with respect to pDNA binding and condensation. Gradient copolymers were synthesized by means of semi-batch copolymerization while statistical analogs were obtained by batch copolymerization, which has already been conducted.^{35–39} To carry out a comprehensive study on the pDNA binding properties of these structures, we prepared a library of these copolymers with various monomer compositions, where the content of the cationic component ranges from 5 to 90 mol%, while keeping the molar mass of the copolymers similar to reduce the effect of increasing or decreasing molar mass on binding capacity. Furthermore, two distinct sources of cationic charges enabled us to compare their efficiency in polyplex formation since APMA relies on its primary amine group and GPMA possesses a permanently charged guanidinium group to bind pDNA. Following copolymer synthesis, monomer ratios of copolymers were calculated by means of nuclear magnetic resonance (NMR) spectroscopy. Size-exclusion chromatography (SEC) and analytical ultracentrifugation in combination with viscosity and density measurements to determine the molar mass of the copolymer samples were employed for elucidation of the copolymer structures with respect to the targeted molar mass and low dispersity ($D < 1.2$). The next step is the polyplex formation. For this purpose, we employed a fluorophore exclusion assay to investigate binding affinity and pDNA condensation properties

of the copolymers. As a result, we could elucidate the influence of the distinct copolymer architecture (gradient vs. statistical) and the different cationic groups (primary amine vs. guanidinium group) for the establishment of desired structure–activity relationships.

2. Experimental section

All chemicals were purchased from Sigma-Aldrich at the highest available purity and used as received unless mentioned otherwise. *N*-(3-Aminopropyl) methacrylamide hydrochloride (APMA) was purchased from PolySciences. 4,4'-Azobis(4-cyanovaleric acid) (ACVA) was recrystallized in methanol before use. The chain transfer agent 4-(((2-carboxyethyl)thio)carbonothioyl)thio-4-cyanopentanoic acid (CTA) was procured from Boron Molecular INC.

2.1. Synthesis

2.1.1 Monomers. *N*-(3-Guanidinopropyl)methacrylamide (GPMA) was synthesized in accordance with previous work.⁴⁰

N-(3-Hydroxypropyl)methacrylamide (HPMA) was prepared by utilizing Schotten–Baumann conditions: *N,N*-diisopropylethylamine (DIPEA) (18.55 g, 143.5 mmol) was dissolved under argon in 100 mL of dry dichloromethane (DCM) and the solution was cooled to $-10\text{ }^{\circ}\text{C}$, before 1-amino-2-propanol (10.78 g, 143.5 mmol) was added. Freshly distilled methacryloyl chloride (10.00 g, 95.66 mmol) dissolved in dry DCM was injected drop-wise under rigorous stirring to the reaction mixture over the time-scale of one hour. The solution was then allowed to reach ambient temperature and stirred for an additional 30 min. The precipitate was removed, and the filtrate was dried to give a crude product mixture, which was purified by means of silica gel column chromatography (200–400 mesh, 40–75 μm particle size) with DCM/ethanol in a ratio of 10:1 as the eluent. The NMR spectra of the obtained colorless powder were in agreement with the literature.⁴¹

2.1.2 Statistical copolymers. The statistical copolymers; P(HPMA-*stat*-APMA) and P(HPMA-*stat*-GPMA) with various monomer compositions of APMA or GPMA with mol%: 5, 10, 20, 40, 50, 60, 75, and 90 were prepared using *a*RAFT polymerization. The general procedure is described below based on an example for the composition P(HPMA-*stat*-APMA) with 10 mol% APMA.

The chain transfer agent (CTA), HPMA (0.50 g, 3.49 mmol, 90 mol%) and APMA (0.63 g, 0.35 mmol, 10 mol%) were added into a 50 mL Schlenk flask and dissolved in acetate buffer (pH = 5.2, 0.27 M acetic acid and 0.73 M sodium acetate) achieving a monomer concentration of 1 M. After addition of the initiator, ACVA, the reaction was carried out under argon at $80\text{ }^{\circ}\text{C}$ for 5 h. The initial monomer to CTA ratio, $[M]_0/[CTA]_0$, was 80/1 and the initial CTA to initiator ratio, $[CTA]_0/[I]_0$, was kept at 3/1. At the end of the reaction, dialysis in distilled water (at pH = 4) at $4\text{ }^{\circ}\text{C}$ was conducted, followed by lyophilization of the pure product. The compound was characterized regarding its monomer composition by using NMR spectroscopy. To analyze its apparent molar mass and D values, SEC and hydrodynamic characterization were performed.

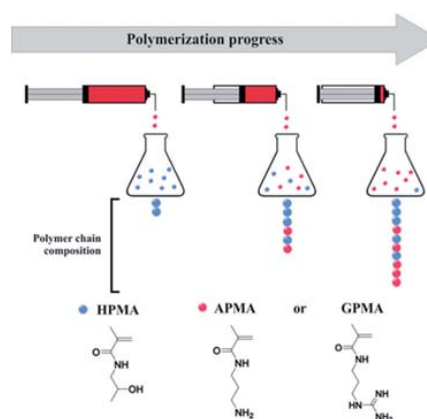


Fig. 1 Schematic illustration of the synthetic approach for gradient copolymers via the semi-batch copolymerization.

2.1.3 Gradient copolymers. A semi-batch copolymerization method through *a*RAFT was used for the synthesis of the gradient copolymer structures; P(HPMA-*grad*-APMA) and P(HPMA-*grad*-GPMA) with various monomer ratios in mol%: 5, 10, 20, 40, 50, 60, 75, and 90. This method relies on a continuous and rate-controlled monomer feed via a syringe pump into a polymerization mixture (Fig. 1). For the calculation of the desired molar mass and monomer composition, the co-monomers APMA or GPMA were treated as if fully present at the start of the reaction. The general procedure is shown below using the example of P(HPMA-*grad*-APMA) copolymer with 10 mol% of APMA.

A Schlenk flask was charged with HPMA (0.50 g, 3.49 mmol, 90 mol%) and acetate buffer (pH 5.2, 0.27 M acetic acid and 0.73 M sodium acetate) was added targeting a 1 M final monomer concentration. CTA and ACVA were added into the reaction mixture. APMA (0.63 g, 0.35 mmol, 10 mol%) was dissolved in the acetate buffer to get a 1 M solution and filled into a syringe, which was placed into the syringe pump. The polymerization was performed under argon at $80\text{ }^{\circ}\text{C}$ for 5 hours when the syringe pump was set to add the APMA monomer solution continuously into the reaction mixture over a certain period of time (Table S2, ESI[†]). The ratio of $[M]_0/[CTA]_0$ was adjusted as 80/1 and $[CTA]_0/[I]_0$ was 3/1. The obtained copolymer was purified via dialysis at $4\text{ }^{\circ}\text{C}$ at a pH of 4 and dried by means of lyophilization. The copolymer was characterized hydrodynamically and by NMR spectroscopy and SEC.

2.2. Polymer characterization

2.2.1 NMR spectroscopy. The monomer composition was determined using a Bruker WS 400 MHz spectrometer (controller: Bruker Avance III) in D_2O at 333 K. The integration of the intensities assigned to the methylene proton resonances of HPMA (3.92 ppm) and the methylene resonances of APMA or GPMA (3.08–3.21 ppm) enabled the estimation of the monomer compositions.

2.2.2 Size exclusion chromatography. The polymers were characterized using two different SEC systems (SEC_{DMAC} and SEC_{water}).

SEC_{DMAc}, running with dimethylacetamide (DMAc + 0.21% LiCl) as the eluent, was performed at 40 °C with the flow rate of 1 mL min⁻¹ using a PSS GRAM guard/1000/30 Å column (particle size: 10 μm). A refractive index detector (G1362A) and a UV Detector (G1315D, wavelength: 310 nm) were used to monitor the elution. The molar mass was calculated based on a calibration with poly(methyl methacrylate) (PMMA) standards. In the case of SEC_{water}, water with 0.1% TFA and 0.1 M NaCl was used as the eluent and AppliChrom ABOA CatPhil guard/200/350 Å was the column. The flow rate and the temperature were adjusted to 1 mL min⁻¹ and 30 °C, respectively. The elution was monitored through the refractive index (RI-930) and UV detection (UV-975, wavelength: 310 nm), and the apparent molar mass was calculated based on a poly(2-vinylpyridine) (P2VP) standard calibration.

2.2.3 Hydrodynamic characterization of the macromolecules.

The hydrodynamic properties of the macromolecules were investigated by utilizing a previously reported approach.^{42,43} In particular, we conducted viscometry and density measurements for the copolymers in addition to sedimentation velocity experiments by means of analytical ultracentrifugation. This characterization was performed in phosphate buffered saline (PBS with 0.138 M sodium chloride and 0.0027 M potassium chloride), a situation where the macromolecules are expected to carry various charges at physiological pH.

2.2.3.1 Viscosity measurements. The viscosity measurements were performed with an AMVn viscometer (Anton Paar, Graz, Austria) in analogy to that reported previously.^{42,43} The capillary/ball combination of the measurement system was used to determine the respective ball times for the solvent (0.01 M PBS), t_0 , and for macromolecule solutions of various concentrations, t_c , at a tilting angle of the capillary of 50°. The measurements were done at concentrations of the macromolecules resulting in relative viscosities, $1.2 < \eta_r = t_c/t_0 < 2.5$. The obtained values of $\eta_r - 1/c$ plotted against c were fitted linearly and the Huggins equation (eqn (1)) was used to calculate the Huggins constant, k_H , from the intrinsic viscosity ($[\eta]$) obtained from extrapolation to zero concentration:

$$\frac{\eta_r - 1}{c} = [\eta] + k_H[\eta]^2 c \quad (1)$$

Plots and fits according to eqn (1) for each of the studied macromolecules are shown in Fig. S5 (ESI†). Numerical estimates of $[\eta]$ and k_H are shown in Table S3 (ESI†). The viscosity of PBS was determined as $\eta_0 = 1.03$ mPa s.

2.2.3.2 Density measurements and partial specific volume (ν) of the macromolecules. The partial specific volume (ν) of a macromolecule is defined as the volume increase of a solution by addition of the macromolecule at constant temperature and pressure. ν of the macromolecules directly dissolved in the PBS solution was determined using a DMA4100 density-meter (Anton Paar, Graz, Austria) at $T = 20$ °C similar to the procedure utilized recently.^{42,43} The density increment ($\rho_c - \rho_0$) measurements were performed in the concentration range of $0.1 \text{ w\%} \leq c \leq 1 \text{ w\%}$. The resultant slope of the curves, *i.e.* the buoyancy

factor $(1 - \nu\rho_0)$, was used to calculate ν by using the measured PBS solvent density ($\rho_0 = 1.0053 \text{ g cm}^{-3}$).

2.2.3.3 Sedimentation velocity experiments. The experiments were performed using a ProteomeLab XL-I analytical ultracentrifuge (Beckman Coulter Instruments, Brea, CA) with an An-50 Ti eight-hole rotor. The ultracentrifuge cells were equipped with double-sector epon centerpieces with a 12 mm optical path length. One sector was filled with *ca.* 420 μL of the sample in PBS and the other with *ca.* 440 μL of PBS as the reference. The interference optic detection method was used for the observation of the sedimentation boundary with respect to time. The experiments were conducted at the rotor speed of 42 000 rpm for 24 h and at a temperature of $T = 20$ °C. The scans were acquired with 5 min intervals. Every fifth scan was used for the data evaluation.

2.2.3.4 Sedimentation-diffusion analysis. The sedimentation velocity data were analyzed with SEDFIT and the $c(s)$ model with a maximum entropy regularization procedure.⁴²⁻⁴⁴ This model is based on the numerical solution of the Lamm equation, assuming the same apparent weight-average translational frictional ratio f/f_{sph} of the sedimenting population of the copolymers. The sedimentation velocity experiments were performed with at least four of up to seven different concentrations. Example distributions of sedimentation coefficient, s , at the concentration of $c \approx 1 \text{ mg cm}^{-3}$ are depicted in Fig. S4 (ESI†). The resultant numerical values of s were obtained as the weight (signal) average of the distributions at various concentrations. These results were used to determine the value at infinite dilution (s_0) via extrapolation to zero concentration using the relationship $s^{-1} = s_0^{-1}(1 + k_s c)$ with k_s being the concentration-sedimentation coefficient, *i.e.* Gralen coefficient (Fig. S5, ESI†). f/f_{sph} values were observed to fluctuate around a mean with similar numerical values for each of the macromolecules and without any apparent concentration dependence. $(f/f_{\text{sph}})_0$ values for the molar mass calculations, therefore, were assumed as the average of frictional ratios at the different concentrations.

The molar mass ($M_{s,f}$) was calculated based on the modified Svedberg equation (eqn (2)), where N_A is the Avogadro constant and $[s] = s_0 \eta_0 / (1 - \nu\rho_0)$ stands for the intrinsic sedimentation coefficient:

$$M_{s,f} = 9\pi\sqrt{2}N_A \left([s] (f/f_{\text{sph}})_0 \right)^{3/2} \sqrt{\nu} \quad (2)$$

We note that this form of the Svedberg equation for the molar mass estimations relies on the values of the weight-average translational frictional ratios $(f/f_{\text{sph}})_0$ that are typically found adequate for narrow, unimodal dispersity macromolecules with a flexible backbone and random coil conformation.^{42,43} The molar masses of the copolymers were determined by applying this approach.

2.3. Biochemical methods

2.3.1 Preparation of plasmid DNA. The pGL3 plasmid (Promega, Madison, WI, USA) was amplified in *E. coli* DH5 α (kind gift of Hans-Knoell-Institute, Jena, Germany) and isolated

with an E.Z.N.A.[®] Plasmid DNA Maxi Kit (OMEGA bio-tek, GA, USA) according to the manufacturer's protocol.

2.3.2 Calculation of nitrogen to phosphate (N/P) ratios.

The amount of phosphate in pDNA was calculated as described in the literature by assuming an average molar mass per nucleotide of 330 g mol⁻¹ and 3.03 nmol phosphate per μg pDNA.⁴⁵ The nitrogen ratio was calculated based on the assumption that under physiological conditions, both the primary amino group of APMA and the guanidinium group of GPMA can only be protonated once. Hence, each of these functional groups was assumed to provide one basic nitrogen.

2.3.3 Preparation of polymer/DNA polyelectrolyte complexes.

Polyplexes were prepared as described in the literature.⁴⁶ 3 μg of pDNA and the appropriate amount of copolymer for the desired N/P ratio were separately diluted in 75 μL of saline (0.15 M sodium chloride, Carl Roth, Germany, in bi-distilled water, pH 7.4) and vortexed for 10 seconds. After equilibration for 10 minutes at room temperature, the copolymer solution was added to the pDNA solution and vortexed again for 10 seconds. Subsequently, the polyplex formation was allowed to take place for 10 minutes at room temperature, before further experiments were performed.

2.3.4 Fluorophore exclusion assay. To determine the pDNA binding ability of the polycations *via* fluorescence spectroscopy, free pDNA was quantified by using an AccuBlue™ high sensitivity dsDNA quantitation kit (Biotinum, Inc., Fremont, CA, USA), according to the manufacturer's protocol. On a black polystyrene microplate (FLUOROTRAC™ 200, Greiner Bio-One, Germany), 5 μL of polyplex solution, equivalent to 100 ng of pDNA, was added, followed by the addition of 200 μL of working solution (quantitation solution:enhancer = 50:1). Each well was pipetted, and the microplate was incubated in an orbital shaker (Titramax 100, Heidolph Instruments GmbH & Co. KG, Germany) at 450 rpm for 10 min. Fluorescence was measured at the wavelengths of 485 nm for the excitation and 530 nm for the emission (SPARK 10M, TECAN Group AG, Austria). As controls, polyplexes formed with linear polyethyleneimine (IPEI, 2500 g mol⁻¹, Polysciences Europe GmbH, Germany) and pDNA at N/P of 20 in addition to the pure polymer and pure pDNA diluted in saline were used. Relative fluorescence units (RFUs) were calculated with respect to the measured fluorescence intensity (F):

$$\text{RFU} = \frac{F(\text{sample}) - F(\text{blank})}{F(\text{pDNA}_{\text{only}}) - F(\text{blank})} \times 100$$

3. Results and discussion

3.1. The synthesis of HPMA-APMA and HPMA-GPMA copolymers and their characterization

The statistical and gradient copolymers consisting of HPMA and APMA or GPMA were synthesized by aRAFT polymerization (Schemes S2 and S3, ESI†). The reaction temperature was set to 80 °C and the polymerization took place in 5 hours.³⁷ Although this study mainly aimed at the comparison of two different cationic monomer distributions, we expected that the amount

of cationic charge in the copolymer can amplify or diminish the effect of monomer distribution on the efficiency of polyplex formation. For the proof of this presumption, we had to remove the effect of molar mass by keeping the theoretical molar mass ($M_{n,\text{theo}}$) constant at 12 000 g mol⁻¹ for both gradient and statistical samples, while changing the molar percentage of the cationic monomers from 10 to 90% in the copolymers by adjusting the monomer stoichiometry during the polymerization step. At this point, the selection of the chain transfer agent (CTA) was very critical, since the unwanted hydrolysis and aminolysis of thiocarbonylthio groups is more probable as the concentration of APMA or GPMA increases. Such side-reactions have a detrimental effect on the control of molar mass and dispersity (*D*) of polymers.⁴⁷ Taking this fact into account, we selected a hydrolytically more stable CTA: 4-(((2-carboxyethyl)thio)carbonothioyl)thio-4-cyanopentanoic acid.

The statistical copolymers were prepared through batch copolymerization in accordance to the literature,^{36,37} whereas the gradient copolymers were synthesized by a "forced" gradient copolymerization method, the semi-batch copolymerization. By this method, 1 M buffered solutions of the cationic co-monomers were continuously added to the polymerization mixture, containing 1 M HPMA monomer *via* a syringe pump at specified rates. The addition rate varied, depending on the amount of cationic co-monomer. This approach, in combination with a controlled polymerization technique, allowed us a controlled synthesis of the gradient copolymers by minimizing the monomer reactivity effect.⁴⁸ In the literature, there are also examples of gradient distributions formed spontaneously during batch copolymerization.⁴⁹ In this case, however, the utilized monomers are consumed unequally due to the absence of the control of the monomer addition rate that is pronouncedly affected by the steric and electronic properties of the monomers. Consequently, the consistency in the distribution of monomers cannot be achieved; so, the gradient behavior exhibits differences from chain-to-chain and batch-to-batch, unless the monomer reactivities show significant differences. This variation generates a big obstacle for a proper analysis of the structural effect on polyplex formation. On the contrary, semi-batch copolymerization enables the preparation of well-defined gradient copolymers with monomers, which usually show alternating sequences in polymers by batch copolymerization.⁵⁰ Overall, semi-batch gradient copolymerization appeared to be the most suitable method to accomplish the desired structures.

The monomer composition of gradient and statistical copolymers was investigated by using ¹H-NMR. For the statistical copolymerization, the co-monomer content (mol%) was calculated by using ¹H-NMR, indicating that the content is similar for both P(HPMA-APMA) and P(HPMA-GPMA) during the polymerization timescale of 5 hours (Table S1, ESI†). However, we observed differences between the reactivities of HPMA, APMA, and GPMA monomers due to a lower final molar ratio of APMA and GPMA monomers than expected. This can be explained by a compositional drift. To eradicate this drift and reach the aimed final monomer contents, there was a need for correction of the stoichiometry. The desired statistical

Table 1 Molar mass (in g mol^{-1}) and dispersity (D) for each P(HPMA-APMA) prepared by aRAFT polymerization

Cationic monomer content (mole%)	P(HPMA- <i>stat</i> -APMA)					P(HPMA- <i>grad</i> -APMA)				
	SEC _{DMAC}		SEC _{water}		HC	SEC _{DMAC}		SEC _{water}		HC
	M_n	D	M_n	D	$M_{s,f}^a$	M_n	D	M_n	D	$M_{s,f}^a$
5	28 500	1.08	5300	1.18	11 500	25 000	1.10	6100	1.06	11 400
10	28 000	1.09	6000	1.18	12 400	25 500	1.08	7300	1.04	12 100
20	28 000	1.05	7000	1.18	11 700	22 000	1.11	8000	1.06	12 500
40	Not applicable		7800	1.18	11 600	Not applicable		8300	1.19	9100
50	Not applicable		8500	1.18	10 800	Not applicable		8100	1.08	9400
60	Not applicable		8000	1.17	10 500	Not applicable		8000	1.21	9800
75	Not applicable		9000	1.17	11 200	Not applicable		8500	1.30	10 000
90	Not applicable		11 000	1.05	10 700	Not applicable		11 000	1.05	10 400

^a The molar mass, $M_{s,f}$, was determined *via* hydrodynamic characterization (HC) based on sedimentation-velocity experiments accompanied with sedimentation-diffusion analysis and density measurements, all performed in PBS.

copolymer compositions were achieved by adjusting the initial monomer ratios (Table S3, ESI[†], co-monomer content).

The synthesized polymers were obtained with low dispersities ($D < 1.2$), which were determined by SEC utilizing either water or DMAc as the eluent (Tables 1 and 2, D). Determination of the molar mass, on the other hand, was challenging due to the cationic nature of the copolymers. Statistical and gradient polymers with APMA content exceeding 20 mol% were no longer soluble in salt-containing DMAc. In case of the GPMA-containing copolymers, the solubility in DMAc was reduced at high GPMA-contents (≥ 20 mol%) as well. However, it was still possible to perform size-exclusion chromatography (SEC_{DMAC}) to obtain an estimation of apparent molar masses against the reference standard (PMMA) except for the 90% statistical and gradient samples. Moreover, the molar mass values showed an inversely proportional correlation to the co-monomer content since it steadily decreased at increasing GPMA ratios. This behavior is an indicator of pronounced structural changes among the copolymer chains due to the increase in the charge content with higher APMA or GPMA content and the inappropriate reference standard. Nevertheless, by using RAFT polymerization, we expected an efficient control of the molar mass and dispersity. The low D values obtained from SEC_{DMAC} supported this argument.

For this reason, SEC_{water} was used to investigate the DMAc-insoluble structures knowing the divergence in the apparent molar masses. However, for this system, another inappropriate

standard was available (P2VP). Hence, the SEC_{water}-determined data were not in agreement with the results of SEC_{DMAC} ($\sim 6000 \text{ g mol}^{-1}$ instead of $\sim 28000 \text{ g mol}^{-1}$). This analytical approach also indicated the change of the molar mass with different co-monomer contents (APMA or GPMA). In the case of increasing APMA-ratios, the SEC_{water}-estimated molar mass ranged from 5300 g mol^{-1} (5 mol% of APMA) to 11000 g mol^{-1} (90 mol% of APMA). The GPMA-containing copolymers did not exhibit any proportionality in the molar mass taking into account the co-monomer content. They had similar apparent molar masses but with significant fluctuations based on SEC_{water}. However, the changes were not pronounced compared to APMA-based copolymers. Overall, these observations for APMA- and GPMA-based copolymers indicate that it is not the chain architecture of the linear copolymers but the various cationic charge densities causing the differences in hydrodynamic volume and/or interactions with the column material generated these deviations in SEC_{DMAC} and SEC_{water}.

However, the pDNA binding capacity is strongly affected by the change in molar mass and if we could not keep the molar mass similar, we would not observe the charge density and charge distribution effects on the binding capacity without the unwanted molar mass influence. Therefore, it was necessary to prove, beyond any doubt, that all synthesized copolymers have similar molar masses for an accurate and representative comparison of their physicochemical properties and their binding affinity toward polynucleotides. To achieve this goal,

Table 2 Molar mass (in g mol^{-1}) and dispersity (D) for each P(HPMA-GPMA) prepared by aRAFT polymerization

Cationic monomer content (mole%)	P(HPMA- <i>stat</i> -GPMA)					P(HPMA- <i>grad</i> -GPMA)				
	SEC _{DMAC}		SEC _{water}		HC	SEC _{DMAC}		SEC _{water}		HC
	M_n	D	M_n	D	$M_{s,f}^a$	M_n	D	M_n	D	$M_{s,f}^a$
5	24 000	1.09	4500	1.07	10 600	24 500	1.09	5000	1.05	10 100
10	26 000	1.06	5500	1.06	9600	23 500	1.09	5200	1.05	9500
20	24 000	1.11	6500	1.04	10 200	21 000	1.10	5500	1.04	10 900
40	23 000	1.07	6750	1.04	11 300	18 000	1.09	5500	1.05	8500
50	20 500	1.07	6400	1.04	11 300	16 000	1.08	5500	1.05	8400
60	24 000	1.09	4500	1.07	10 600	24 500	1.09	5000	1.05	10 100
90	Not applicable		5442	1.03	7300	Not applicable		5703	1.04	7300

^a The molar mass, $M_{s,f}$, was determined *via* hydrodynamic characterization (HC) based on sedimentation-velocity experiments accompanied with sedimentation-diffusion analysis and density measurements, all performed in PBS.

we utilized hydrodynamic characterization methods including viscometry together with sedimentation velocity experiments in an analytical ultracentrifuge. Additional density measurements were utilized for partial specific volume estimations, and consequently the molar mass.

In contrast to other approaches, this approach relies on physical principles in solution and does not require any calibration against standards, typically utilized in SEC systems as described above. Moreover, we expected to track potential effects of charge density and hydrodynamic volume associated with the molar mass, in the hope of a smaller bias toward expected results. To achieve this and be the closest to desired solution conditions used for pDNA binding studies, all analytical procedures for the hydrodynamic characterization were performed in PBS; experimental conditions that are close to pDNA binding assays. Several interesting observations could be made with increasing content of either APMA or GPMA in the polymer backbone. We observed an overall slight increase in the intrinsic viscosity ($[\eta]$) and a decrease in the apparent Huggins constant (k_H) (particularly for the APMA co-monomer) supporting the idea of an improved overall solubility of the polymers in the buffer at an increased amount of ionizable groups. This was accompanied with an apparent reduction of the partial specific volume with the higher content of the charged monomers in the polymer backbone. The observed higher density increased the weight-average sedimentation coefficients of the respective copolymer populations (Fig. S4, ESI[†]), as expected. Notwithstanding, the calculated molar masses based on the modified Svedberg equation (eqn (2)) remained largely invariant. The estimated molar masses of the copolymer chains were located between the two SEC methods (on average $\sim 11\,000\text{ g mol}^{-1}$), a value very close, though smaller, to the theoretical molar mass.

Additionally, the fluctuations of the determined molar masses between statistical and gradient and among different charge contents are found to be much lower than in SEC. The employed hydrodynamic methods also confirmed our hypothesis concerning the variance in the SEC data arising from the difference in the charge density. The molar mass values determined *via* the hydrodynamic characterization were used to calculate the monomer composition of the respective copolymer chains by taking the NMR-estimated monomer content (mol%) into account. This approach revealed the charge distribution in a more transparent manner in each case since the maximum possible amount of positive charges as well as their distribution along the linear copolymer chains (statistical or gradient) became accessible (Tables 1 and 2, Table S3, ESI[†]). Based on the molar masses derived from hydrodynamic studies, we observed slight differences in the maximum possible amount of positive charges even though we aimed at the same charge content, *e.g.* P(HPMA-*stat*-APMA_{5%}) *vs.* P(HPMA-*grad*-GPMA_{5%}) (Table S3, ESI[†]).

3.2. Interaction of P(HPMA-APMA) and P(HPMA-GPMA) copolymers with polyanions

To simulate the interaction of the modified HPMA derivatives with polyanions and to obtain a quantitative insight into the

electrostatic interactions between the oppositely charged binding partners for the establishment of structure-activity relationships, pGL3 plasmid was selected as a model drug. The binding ability of the copolymers to pDNA was determined by a fluorescence-based assay that depends on the exclusion of a fluorophore from its DNA binding sites by the copolymers. The intercalative dye in the AccuBlue™ assay only exhibits pronounced fluorescent signals upon binding to double stranded nucleic acids, while in its unbound state, the fluorescence is negligible.

The formation of polyplexes from cationic copolymers and polyanionic DNA is driven by the electrostatic attraction of oppositely charged polyions and a gain in entropy due to the release of relatively large numbers of small counter ions.^{51,52} Depending on the magnitude of interaction, the copolymers are able to displace the utilized dye from its DNA binding sites or inhibit dye-DNA interactions, thereby decreasing the fluorescence signal. Free DNA demonstrated the highest fluorescence (100% control). The copolymers *per se* gave no signals and, therefore, did not non-specifically interfere with the assay (data not shown). As positive control, polyplexes of pDNA and 2500 g mol⁻¹ IPEI at N/P = 20 demonstrated a strong binding capacity with only 5% uncondensed pDNA. In order to carry out a comprehensive study on the pDNA binding capacity that we proposed to originate from the strong dependency on the architecture of copolymers, we selected five copolymer quartets from our library (Table 2) exhibiting comparable molar masses and similar degrees of substitution of APMA and GPMA for both the gradient and statistical counterparts. All polyplexes were formed at physiological pH 7.4, which represents the conditions during preparation and storage.

For all copolymers, the pDNA binding capability was related to the co-monomer content, the organization in the monomer distributions: statistical *vs.* gradient, and the N/P ratio. As documented in the literature for a vast number of cationic polymers designed for gene delivery, an increase in the N/P ratio is correlated with more effective binding of polyanions, especially for polymers with lower cationic charge density.^{52,53} For our case, a quantitative pDNA binding was achieved at all tested N/P ratios for copolymers exhibiting 60 and 90 mol% cationic moieties, regardless of their compositional architecture. On the other hand, the copolymers with co-monomer contents below or equal to 40 mol% represented distinct differences between gradient and statistical APMA/GPMA compositions (Fig. 2A and B). For copolymers with 5 mol% cationic co-monomers, gradient copolymers demonstrated superior pDNA binding for both APMA and GPMA derivatives. This result shows that the gradient copolymer structure providing locally high cationic charge densities is the most probable cause for the observed differences in the binding affinity.

This structural influence, however, diminished upon increasing the amount of APMA or GPMA content due to the fact that the higher overall abundance of cationic moieties in the chains results in a more similar global charge distribution in the gradient and statistical counterparts (Fig. 2C and D).

Additionally, the increase in N/P ratio also reduced the differences between gradient and statistical structures, apart

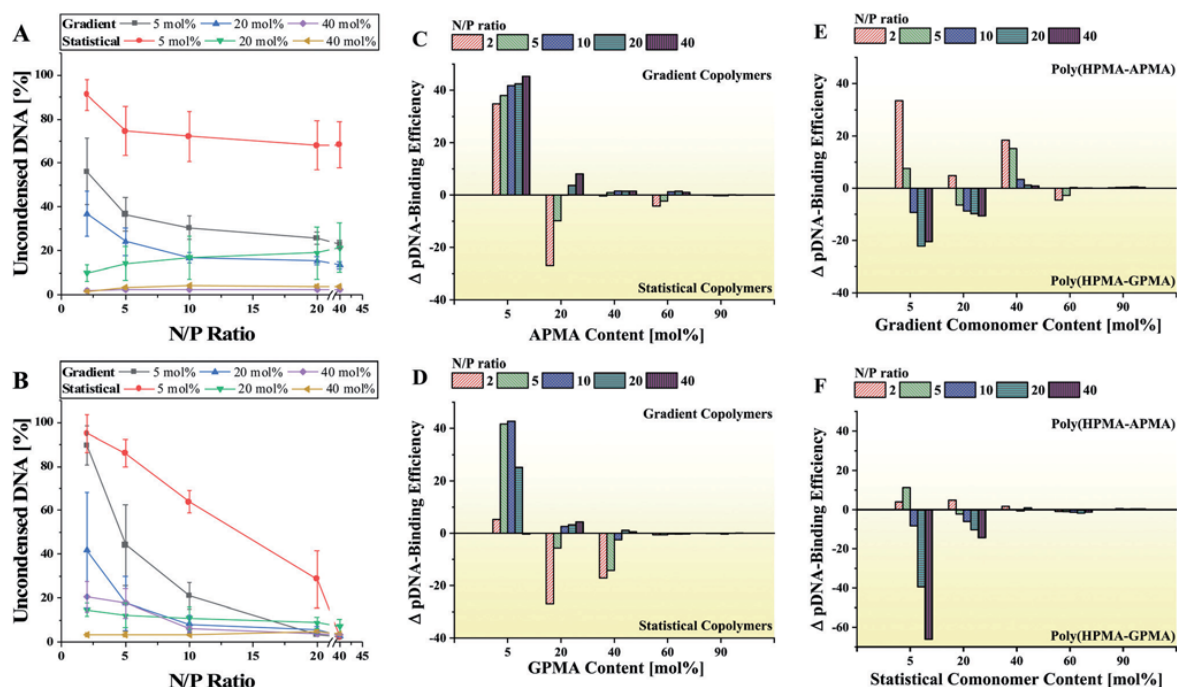


Fig. 2 The pDNA binding efficiency of (A) P(HPMA-APMA) (B) and P(HPMA-GPMA) copolymers depending on the degree of substitution and the copolymer concentration (shown as N/P ratio) was determined by an AccuBlue™ assay (mean \pm SD, $n = 4$). The comparison of the pDNA binding efficiency regarding the mol% content of (C) APMA and (D) GPMA monomers. Positive values illustrate a superior binding efficiency for the gradient copolymers; negative values indicate a more efficient binding of the statistical derivatives. The binding efficiency was calculated by subtracting the mean RFU derived from the binding experiments from 100% binding efficiency. The efficiency of statistical copolymers was then subtracted from the binding efficiency of the gradient copolymers, leading to positive (superiority of gradient) or negative (superiority of statistical) values. The comparison of the pDNA binding efficiency of HPMA-APMA and HPMA-GPMA copolymers with (E) gradient and (F) statistical architecture. Positive values demonstrate a higher binding efficiency for APMA copolymers, negative values represent a more efficient binding of the GPMA derivatives. The binding efficiency was calculated by subtracting the mean RFU derived from the binding experiments from 100% binding efficiency. The efficiency of GPMA copolymers was then subtracted from the binding efficiency of the APMA copolymers, leading to positive (superiority of APMA) or negative (superiority of GPMA) values.

from P(HPMA-APMA_{5%}), for which the statistical counterpart failed to achieve equal binding capabilities as the gradient structure. In this case, the difference between gradient and statistical architecture was even more significant at high N/P ratios.

On the contrary, increasing the N/P ratio led to comparable pDNA binding capabilities for P(HPMA-GPMA_{5%}) copolymers. Furthermore, gradient and statistical P(HPMA-GPMA_{5%}) polymers were able to reduce the residual fluorescence to levels of the positive control of approximately 5% uncondensed pDNA at N/P 40, comparable to the values of the positive control, which indicated complete pDNA binding, although we calculated a slightly lower cationic monomer content based on hydrodynamic characterization (Table S3, ESI†).

On the other hand, P(HPMA-grad-APMA_{5%}) could not reduce the residual fluorescence below 20% uncondensed pDNA and P(HPMA-stat-APMA_{5%}) only showed a weak binding capability, plateauing at approximately 70% uncondensed pDNA. This superior binding efficiency of GPMA copolymers can be attributed to the unique architecture of the guanidinium group that facilitates not only electrostatic interactions with the polyanionic pDNA, but also up to five hydrogen bonds with energetically

favorable steric orientations, unlike the primary amine groups in APMA monomer.^{54,55}

The basicity of the functional groups may also play a secondary role in the affinity toward pDNA since the guanidinium group is a strong base with a pK_a of around 13, contrary to the primary amine group of APMA having a lower pK_a around 11.^{56,57} At 40% co-monomer content and the N/P ratio of 20, the copolymer/pDNA interactions of APMA copolymers enhanced, and the distinct binding affinity of HPMA-GPMA copolymers was no longer detectable with our experimental setup (Fig. 2E and F).

4. Conclusions

In conclusion, statistical and gradient copolymers were successfully synthesized at various monomer ratios. Hydrodynamic characterization of the copolymers indicates the similar molar mass of polymers with varied physicochemical properties, which was impossible to show with SEC using various calibration standards. Increasing the content of the cationic co-monomers in macromolecules decreased their apparent partial specific volume in PBS and the apparently

higher density led to changes in the sedimentation coefficient distributions to larger values. Although the detailed physico-chemical properties of the macromolecules appear distinct, their actual molar masses determined by means of sedimentation-diffusion analysis of analytical ultracentrifugation experiments indicated the same value, which emphasizes the potency of the synthetic approach. The low dispersity and the similarity in the molar masses of the copolymers can be assumed as indicators of well-defined structures, which were necessary for the pDNA binding investigation. All tested macromolecules showed interaction potential with pDNA to various extents. The gradient copolymers demonstrated higher binding affinity, remarkably, in comparison to their statistical counterparts for both APMA and GPMA copolymers to a certain degree of charge and N/P ratio. In addition, we demonstrated the influence of the origin of cationic charges on the pDNA binding capacity by comparing primary amine and guanidinium group containing copolymers. Even a very low amount of the pendant guanidinium group enabled highly efficient binding of pDNA, while it was not possible to achieve similar results by using the primary amine as the source of cationic charge. The reason for this observation is the unique geometry of the guanidinium group with permanent charge based on high basicity that also establishes strong hydrogen bonds with DNA molecules adding up to more efficient interactions. Nonetheless, this strong binding affinity became less significant upon increasing the content of the charged monomers based on our observation.

Conclusively, we proved our claim that the cationic monomer distribution and the origin of cationic charge in water-soluble methacrylamide copolymers strongly affect their utility for pDNA binding. Gradient copolymers have great promise for gene delivery applications due to their high affinity toward pDNA even at extremely low degrees of charged monomer content. Furthermore, the excellent pDNA binding capabilities of our copolymers create great potential for utilizing them as non-viral vectors for nucleic acid delivery, which will be investigated in future studies.

Funding sources

The authors acknowledge support of this study from the Thüringer Ministerium für Wirtschaft, Wissenschaft und Digitale Gesellschaft (TMWWDG, ProExzellenz II, NanoPolar) for funding the Solution Characterization Group (SCG) at the Jena Center for Soft Matter (JCSM), Friedrich Schiller University Jena. Furthermore, this work was supported by the DFG-funded Collaborative Research Center PolyTarget (SFB 1278, projects B03 and Z01).

Conflicts of interest

There are no conflicts to declare.

References

- 1 E. L. Tatum, *Perspect. Biol. Med.*, 1966, **10**, 19–32.
- 2 D. Stone, *Viruses*, 2010, **2**, 1002–1007.
- 3 R. Kalinova, J. A. Doumanov, K. Mladenova, D. Janevska, M. Georgieva, G. Miloshev, T. Topouzova-Hristova and I. Dimitrov, *ChemistrySelect*, 2017, **2**, 12006–12013.
- 4 P. Singhsa, D. Diaz-Dussan, H. Manuspiya and R. Narain, *Biomacromolecules*, 2018, **19**, 209–221.
- 5 T.-I. Kim, H. J. Seo, J. S. Choi, H.-S. Jang, J. Baek, K. Kim and J.-S. Park, *Biomacromolecules*, 2004, **5**, 2487–2492.
- 6 F. J. Xu, Z. X. Zhang, Y. Ping, J. Li, E. T. Kang and K. G. Neoh, *Biomacromolecules*, 2009, **10**, 285–293.
- 7 F. J. Xu, Y. Ping, J. Ma, G. P. Tang, W. T. Yang, J. Li, E. T. Kang and K. G. Neoh, *Bioconjugate Chem.*, 2009, **20**, 1449–1458.
- 8 B. Krieg, M. Hirsch, E. Scholz, L. Nuhn, I. Tabujew, H. Bauer, S. Decker, A. Khobta, M. Schmidt, W. Tremel, R. Zentel, K. Peneva, K. Koynov, A. J. Mason and M. Helm, *Pharm. Res.*, 2015, **32**, 1957–1974.
- 9 H. Lv, S. Zhang, B. Wang, S. Cui and J. Yan, *J. Controlled Release*, 2006, **114**, 100–109.
- 10 O. Guerret, Gradient copolymers that are as soluble or at least as dispersible in water as in organic solvents, FR2848557A1, 2004.
- 11 J. Kim, M. K. Gray, H. Zhou, S. T. Nguyen and J. M. Torkelson, *Macromolecules*, 2005, **38**, 1037–1040.
- 12 S. Qin, J. Pyun, J. Saget, S. Jia, T. Kowalewski and K. Matyjaszewski, *Polym. Prepr. (Am. Chem. Soc., Div. Polym. Chem.)*, 2002, **43**, 235–236.
- 13 H. G. Boerner, D. Duran, K. Matyjaszewski, M. da Silva and S. S. Sheiko, *Macromolecules*, 2002, **35**, 3387–3394.
- 14 G. T. Pickett, *J. Chem. Phys.*, 2003, **118**, 3898–3903.
- 15 B. Gu and A. Sen, *Macromolecules*, 2002, **35**, 8913–8916.
- 16 M. K. Gray, H. Zhou, S. T. Nguyen and J. M. Torkelson, *Macromolecules*, 2004, **37**, 5586–5595.
- 17 K. Karaky, L. Billon, C. Pouchan and J. Desbrières, *Macromolecules*, 2007, **40**, 458–464.
- 18 M. D. Lefebvre, M. Olvera de la Cruz and K. R. Shull, *Macromolecules*, 2004, **37**, 1118–1123.
- 19 M. D. Lefebvre, C. M. Dettmer, R. L. McSwain, C. Xu, J. R. Davila, R. J. Composto, S. T. Nguyen and K. R. Shull, *Macromolecules*, 2005, **38**, 10494–10502.
- 20 J.-S. Park and K. Kataoka, *Macromolecules*, 2006, **39**, 6622–6630.
- 21 C. L. H. Wong, J. Kim, C. B. Roth and J. M. Torkelson, *Macromolecules*, 2007, **40**, 5631–5633.
- 22 T. Pakula and K. Matyjaszewski, *Macromol. Theory Simul.*, 1996, **5**, 987–1006.
- 23 D. Hertz, M. N. Leiske, T. Wloka, A. Traeger, M. Hartlieb, M. M. Kessels, S. Schubert, B. Qualmann and U. S. Schubert, *J. Polym. Sci., Part A: Polym. Chem.*, 2018, **56**, 1210–1224.
- 24 P. Gaspard, *Philos. Trans.: Math., Phys. Eng. Sci.*, 2016, **374**, 20160147.
- 25 *Polymer Handbook*, ed. J. Brandrup, E. H. Immergut and E. A. Grulke, 4th edn, 2003, 2 Volumes Set, ISBN: 978-0-471-47936-9.
- 26 C. M. Dettmer, M. K. Gray, J. M. Torkelson and S. T. Nguyen, *Macromolecules*, 2004, **37**, 5504–5512.
- 27 G. Chambard and B. Klumperman, *Controlled/Living Radical Polymerization*, American Chemical Society, 2000, ch. 14, vol. 768, pp. 197–210.

- 28 N. A. A. Rossi, Y. Zou, M. D. Scott and J. N. Kizhakkedathu, *Macromolecules*, 2008, **41**, 5272–5282.
- 29 K. Matyjaszewski, M. J. Ziegler, S. V. Arehart, D. Greszta and T. Pakula, *J. Phys. Org. Chem.*, 2000, **13**, 775–786.
- 30 D. Greszta, K. Matyjaszewski and T. Pakula, *Polym. Prepr. (Am. Chem. Soc., Div. Polym. Chem.)*, 1997, **38**, 709–710.
- 31 S. Jung, T. P. Lodge and T. M. Reineke, *J. Phys. Chem. B*, 2018, **122**, 2449–2461.
- 32 K. H. Parsons, M. H. Mondal, C. L. McCormick and A. S. Flynt, *Biomacromolecules*, 2018, **19**, 1111–1117.
- 33 R. Duncan, *Nat. Rev. Cancer*, 2006, **6**, 688.
- 34 C. Rodriguez-Emmenegger, E. Brynda, T. Riedel, M. Houska, V. Šubr, A. B. Alles, E. Hasan, J. E. Gautrot and W. T. S. Huck, *Macromol. Rapid Commun.*, 2011, **32**, 952–957.
- 35 L. Lybaert, N. Vanparijs, K. Fierens, M. Schuijs, L. Nuhn, B. N. Lambrecht and B. G. De Geest, *Biomacromolecules*, 2016, **17**, 874–881.
- 36 A. W. York, F. Huang and C. L. McCormick, *Biomacromolecules*, 2010, **11**, 505–514.
- 37 N. J. Treat, D. Smith, C. Teng, J. D. Flores, B. A. Abel, A. W. York, F. Huang and C. L. McCormick, *ACS Macro Lett.*, 2012, **1**, 100–104.
- 38 A. C. Holley, W. Wan, G. R. Bishop, F. Huang and C. L. McCormick, From Abstracts of Papers, 247th ACS National Meeting & Exposition, Dallas, TX, United States, 2014, POLY-641.
- 39 A. W. York, Y. Zhang, A. C. Holley, Y. Guo, F. Huang and C. L. McCormick, *Biomacromolecules*, 2009, **10**, 936–943.
- 40 I. Tabujew, C. Freidel, B. Krieg, M. Helm, K. Koynov, K. Müllen and K. Peneva, *Macromol. Rapid Commun.*, 2014, **35**, 1191–1197.
- 41 C. W. Scales, Y. A. Vasilieva, A. J. Convertine, A. B. Lowe and C. L. McCormick, *Biomacromolecules*, 2005, **6**, 1846–1850.
- 42 I. Nischang, I. Perevyazko, T. Majdanski, J. Vitz, G. Festag and U. S. Schubert, *Anal. Chem.*, 2017, **89**, 1185–1193.
- 43 M. Grube, M. N. Leiske, U. S. Schubert and I. Nischang, *Macromolecules*, 2018, **51**, 1905–1916.
- 44 P. Schuck, *Biophys. J.*, 2000, **78**, 1606–1619.
- 45 P. L. Felgner, Y. Barenholz, J. P. Behr, S. H. Cheng, P. Cullis, L. Huang, J. A. Jessee, L. Seymour, F. Szoka, A. R. Thierry, E. Wagner and G. Wu, *Hum. Gene Ther.*, 1997, **8**, 511–512.
- 46 D. Fischer, H. Dautzenberg, K. Kunath and T. Kissel, *Int. J. Pharm.*, 2004, **280**, 253–269.
- 47 D. B. Thomas, A. J. Convertine, R. D. Hester, A. B. Lowe and C. L. McCormick, *Macromolecules*, 2004, **37**, 1735–1741.
- 48 X. Sun, Y. Luo, R. Wang, B.-G. Li, B. Liu and S. Zhu, *Macromolecules*, 2007, **40**, 849–859.
- 49 Y. Chen, H. Chen, M. Feng and Y. Dong, *Eur. Polym. J.*, 2016, **85**, 489–498.
- 50 T. Bronich, A. V. Kabanov and L. A. Marky, *J. Phys. Chem. B*, 2001, **105**, 6042–6050.
- 51 I. Insua, A. Wilkinson and F. Fernandez-Trillo, *Eur. Polym. J.*, 2016, **81**, 198–215.
- 52 F. Schlenk, S. Grund and D. Fischer, *Ther. Delivery*, 2013, **4**, 95–113.
- 53 H. Hosseinkhani, F. Abedini, K.-L. Ou and A. J. Domb, *Polym. Adv. Technol.*, 2015, **26**, 198–211.
- 54 D. M. Perreault, L. A. Cabell and E. V. Anslyn, *Bioorg. Med. Chem.*, 1997, **5**, 1209–1220.
- 55 N. M. Luscombe, R. A. Laskowski and J. M. Thornton, *Nucleic Acids Res.*, 2001, **29**, 2860–2874.
- 56 A. Albert, R. Goldacre and J. Phillips, *J. Chem. Soc.*, 1948, 2240–2249, DOI: 10.1039/jr9480002240.
- 57 H. K. Hall, *J. Am. Chem. Soc.*, 1957, **79**, 5441–5444.

Supporting Information

The influence of gradient and statistical arrangements of guanidinium or primary amine groups in poly(methacrylate) copolymers on their DNA binding affinity

‡Ilja Tabujew^a, ‡Ceren Cokca^a, Leon Zartner^b, Ulrich S. Schubert^{c,d}, Ivo Nischang^{c,d}, Dagmar Fischer^b and Kalina Peneva^{a,c}*

^a Institute of Organic Chemistry and Macromolecular Chemistry, Friedrich Schiller University Jena, Lessingstraße 8, 07743 Jena, Germany

^b Institute of Pharmacy, Friedrich Schiller University Jena, Lessingstraße 8, 07743 Jena, Germany

^c Jena Center of Soft Matter, Friedrich Schiller University Jena, Philosophenweg 7, 07743 Jena, Germany

^d Laboratory of Organic and Macromolecular Chemistry (IOMC), Humboldtstraße 10, 07743 Jena, Germany

[‡] the authors contributed equally to the manuscript

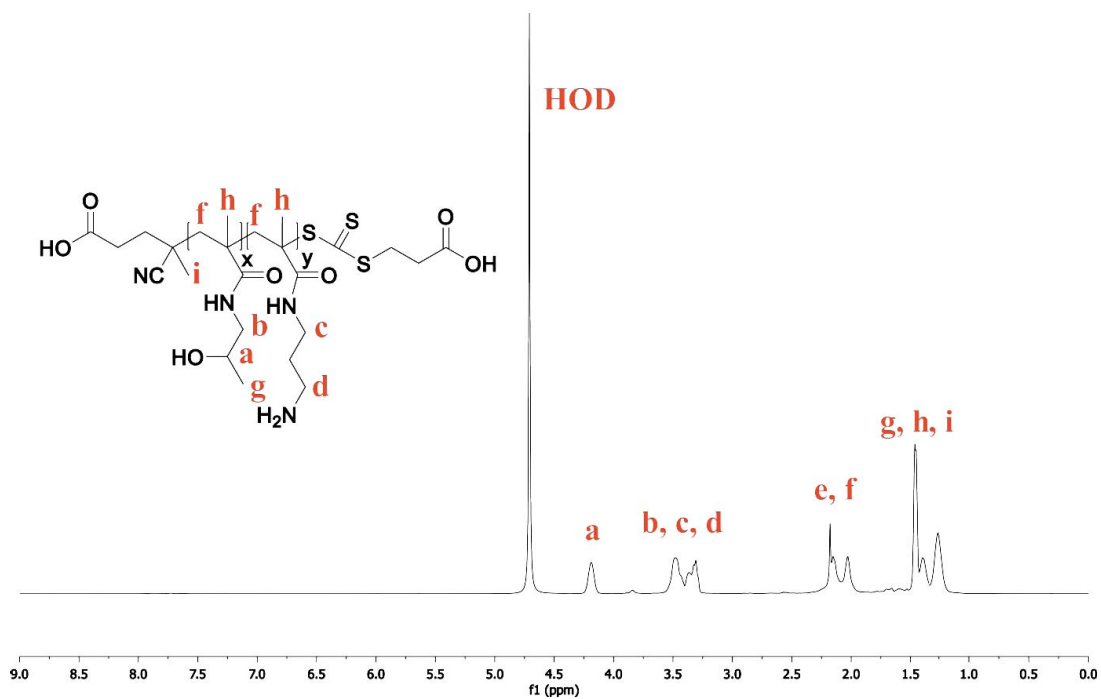


Figure S1. ¹H-NMR spectrum of (HPMA_{90%}-s-APMA_{10%}) in D₂O at 333 K (400 MHz)

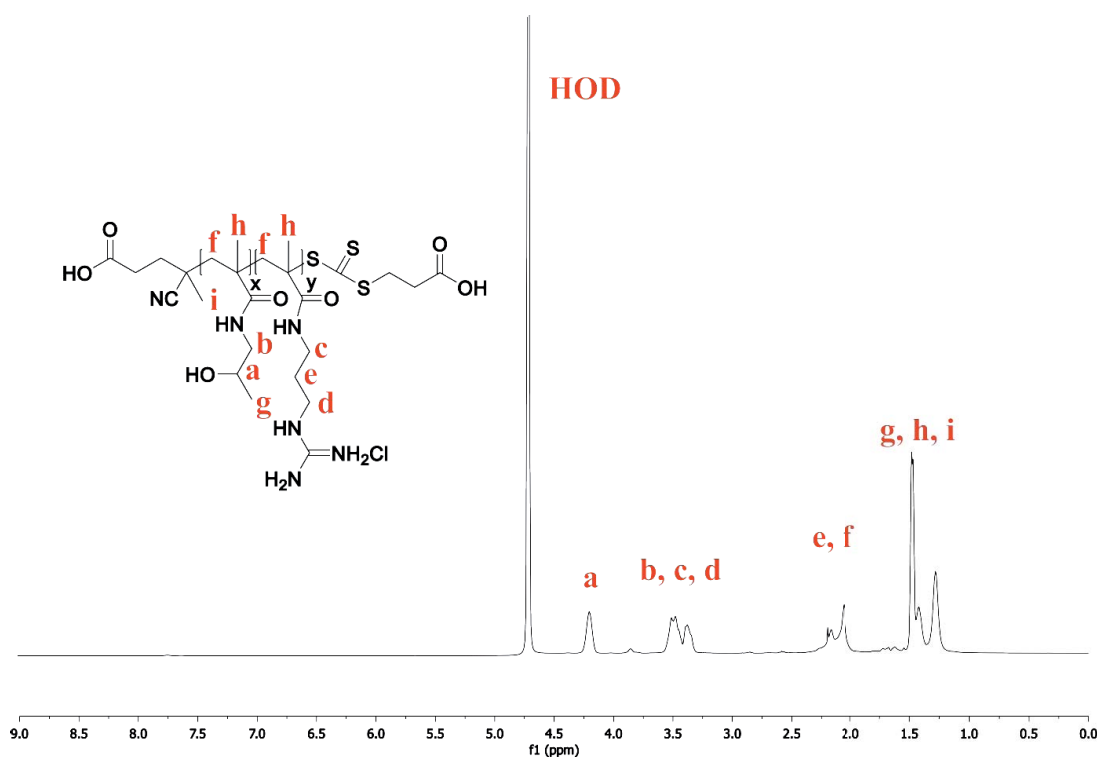


Figure S2. ¹H-NMR spectrum of (HPMA_{90%}-s-GPMA_{10%}) in D₂O at 333 K (400 MHz)

Table S1. Comonomer content (mol%) for P(HPMA-APMA) and P(HPMA-GPMA) copolymers during statistical copolymerization with aimed 40% HPMA and 60% APMA or GPMA mole content.

Polymerization Time (h)	HPMA (mol%)	APMA (mol%)
0	33.78	66.22
1	32.68	67.32
3	32.78	67.21
5	32.68	67.32
Polymerization Time	HPMA (mol%)	GPMA (mol%)
0	44.68	55.36
1	44.05	55.95
3	44.05	55.95
5	43.86	56.14

Table S2. Monomer addition rates in [mmol/h] of APMA and GPMA throughout the semi-batch copolymerization

Gradient copolymer with x mol% APMA/GPMA	monomer addition rate [mmol/h]
5%	0.097
10%	0.150
20%	0.276
40%	0.653
50%	0.954
60%	1.407
75%	2.764
90%	8.193

Table S3. The desired, theoretical and experimental APMA- or GPMA content in mole%, intrinsic viscosity ($[\eta]$), Huggins constants (k_H), partial specific volumes (v) and the average total value of monomer units per polymer chain for each sample

Polymer	$M_{n,theo}^a$	Co-monomer content			$[\eta]$ $cm^3 g^{-1}$	k_H	v $cm^3 g^{-1}$	Monomers	
		desired	Theo ^b	Exp ^c				APMA or GPMA	HPMA
HPMA- <i>stat</i> -APMA _{5%}	12100	5	12.0	8.9	7.6	1.8	0.78	7	72
HPMA- <i>stat</i> -APMA _{10%}	12096	10	17.1	14.2	7.5	1.8	0.81	12	71
HPMA- <i>stat</i> -APMA _{20%}	12095	20	27.3	23.4	8.2	1.7	0.79	18	59
HPMA- <i>stat</i> -APMA _{40%}	12115	40	46.9	44.0	7.8	1.6	0.80	32	41
HPMA- <i>stat</i> -APMA _{50%}	12134	50	56.4	54.1	9.0	1.3	0.77	36	31
HPMA- <i>stat</i> -APMA _{60%}	12158	60	65.5	63.2	9.4	1.1	0.75	40	23
HPMA- <i>stat</i> -APMA _{75%}	12203	75	78.8	77.6	9.7	1.1	0.74	51	15
HPMA- <i>stat</i> -APMA _{90%}	12258	90	91.7	87.9	9.7	1.0	0.73	54	7
HPMA- <i>grad</i> -APMA _{5%}	11907	5	18.8	6.7	7.2	1.8	0.80	5	73
HPMA- <i>grad</i> -APMA _{10%}	11843	10	26.4	15.1	7.7	1.4	0.80	12	69
HPMA- <i>grad</i> -APMA _{20%}	11767	20	39.7	25.8	8.1	1.5	0.79	21	60
HPMA- <i>grad</i> -APMA _{40%}	11760	40	60.9	41.3	7.7	1.5	0.76	25	36
HPMA- <i>grad</i> -APMA _{50%}	11805	50	69.5	47.7	7.4	1.4	0.77	28	31
HPMA- <i>grad</i> -APMA _{60%}	11874	60	77.0	58.0	8.0	1.3	0.76	35	25
HPMA- <i>grad</i> -APMA _{75%}	12010	75	86.8	80.6	8.6	1.2	0.73	47	11
HPMA- <i>grad</i> -APMA _{90%}	12176	90	95.1	89.1	8.6	1.1	0.74	53	6
HPMA- <i>stat</i> -GPMA _{5%}	11762	5	12.0	5.7	8.2	1.4	0.79	4	68
HPMA- <i>stat</i> -GPMA _{10%}	11759	10	17.1	9.9	6.5	2.5	0.78	6	57
HPMA- <i>stat</i> -GPMA _{20%}	11759	20	27.3	18.5	10.1	0.6	0.77	12	53
HPMA- <i>stat</i> -GPMA _{40%}	11782	40	46.9	35.1	9.2	0.9	0.79	23	43
HPMA- <i>stat</i> -GPMA _{50%}	11804	50	56.4	40.7	8.3	1.3	0.78	26	38
HPMA- <i>stat</i> -GPMA _{60%}	11884	75	78.8	52.8	8.7	1.2	0.78	33	29
HPMA- <i>stat</i> -GPMA _{90%}	11946	90	91.7	83.2	12.1	0.6	0.73	35	5
HPMA- <i>grad</i> -GPMA _{5%}	11541	5	18.8	5.0	8.9	1.2	0.78	3	65
HPMA- <i>grad</i> -GPMA _{10%}	11468	10	26.4	10.5	10.0	1.1	0.78	7	56
HPMA- <i>grad</i> -GPMA _{20%}	11384	20	39.7	14.9	8.2	1.2	0.79	10	60
HPMA- <i>grad</i> -GPMA _{40%}	11380	40	60.9	34.4	7.2	1.6	0.77	17	33
HPMA- <i>grad</i> -GPMA _{50%}	11433	50	69.5	41.5	7.5	1.3	0.75	20	28
HPMA- <i>grad</i> -GPMA _{60%}	11667	75	86.8	60.8	7.0	1.4	0.73	32	21
HPMA- <i>grad</i> -GPMA _{90%}	11854	90	95.1	84.4	10.0	1.4	0.72	35	5

a) The theoretical molar mass was calculated using the Formula $M_{n,th} = ([M]_0/[CTA]_0)M_{w,monomer}\rho + M_{w,CTA}$ while the conversion ρ was near quantitative ($\geq 95\%$);
 b) according to the used stoichiometry; c) determined via $^1\text{H-NMR}$.

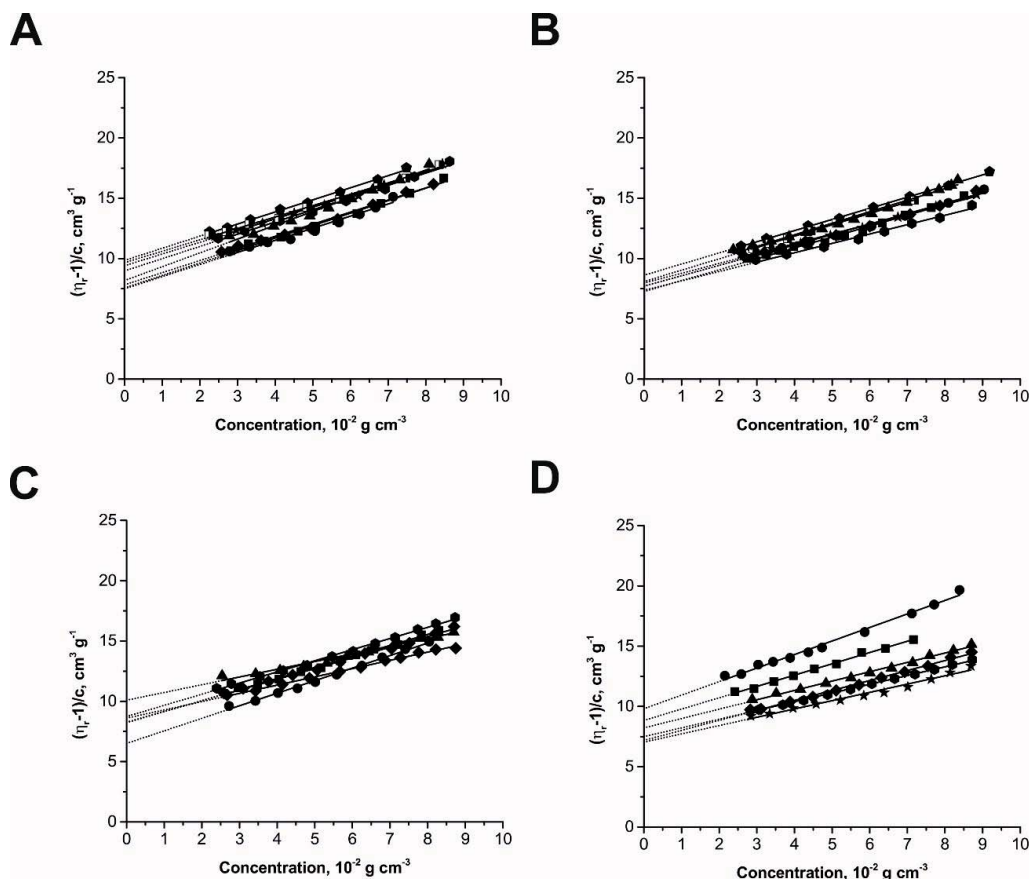


Figure S3. Plots to determine intrinsic viscosities, $[\eta]$, and Huggins constant, k_H , after eq. 1 of (A) statistical copolymers of HPMA and APMA, (B) the gradient copolymers of HPMA and APMA, (C) the statistical copolymers of HPMA and GPMA, and (D) the gradient copolymers of HPMA and GPMA. Fits to eq 1 are shown as solid lines and extrapolations to determine $[\eta]$ as dotted lines. Symbol assignment for polymers: **Squares** HPMA_{95%}-s-APMA_{5%} HPMA_{95%}-g-APMA_{5%} / HPMA_{95%}-s-GPMA_{5%} / HPMA_{95%}-g-GPMA_{5%}; **circles** HPMA_{90%}-s-APMA_{10%} / HPMA_{90%}-g-APMA_{10%} / HPMA_{90%}-s-GPMA_{10%} / HPMA_{90%}-g-GPMA_{10%}; **triangles** HPMA_{80%}-s-APMA_{20%} / HPMA_{80%}-g-APMA_{20%} / HPMA_{80%}-s-GPMA_{20%} / HPMA_{80%}-g-GPMA_{20%}; **diamonds** HPMA_{60%}-s-APMA_{40%} / HPMA_{60%}-g-APMA_{40%} / HPMA_{60%}-s-GPMA_{40%} / HPMA_{60%}-g-GPMA_{40%}; **hexagons** HPMA_{50%}-s-APMA_{50%} / HPMA_{50%}-g-APMA_{50%} / HPMA_{50%}-s-GPMA_{50%} / HPMA_{50%}-g-GPMA_{50%}; **stars** HPMA_{40%}-s-APMA_{60%} / HPMA_{40%}-g-APMA_{60%}; **pentagons** HPMA_{25%}-s-APMA_{75%} / HPMA_{25%}-g-APMA_{75%} /

HPMA_{25%}-s-GPMA_{75%} / HPMA_{25%}-g-GPMA_{75%}; **half-filled squares** HPMA_{10%}-s-APMA_{90%} / HPMA_{10%}-g-APMA_{90%} / HPMA_{10%}-s-GPMA_{90%} / HPMA_{10%}-g-GPMA_{90%}.

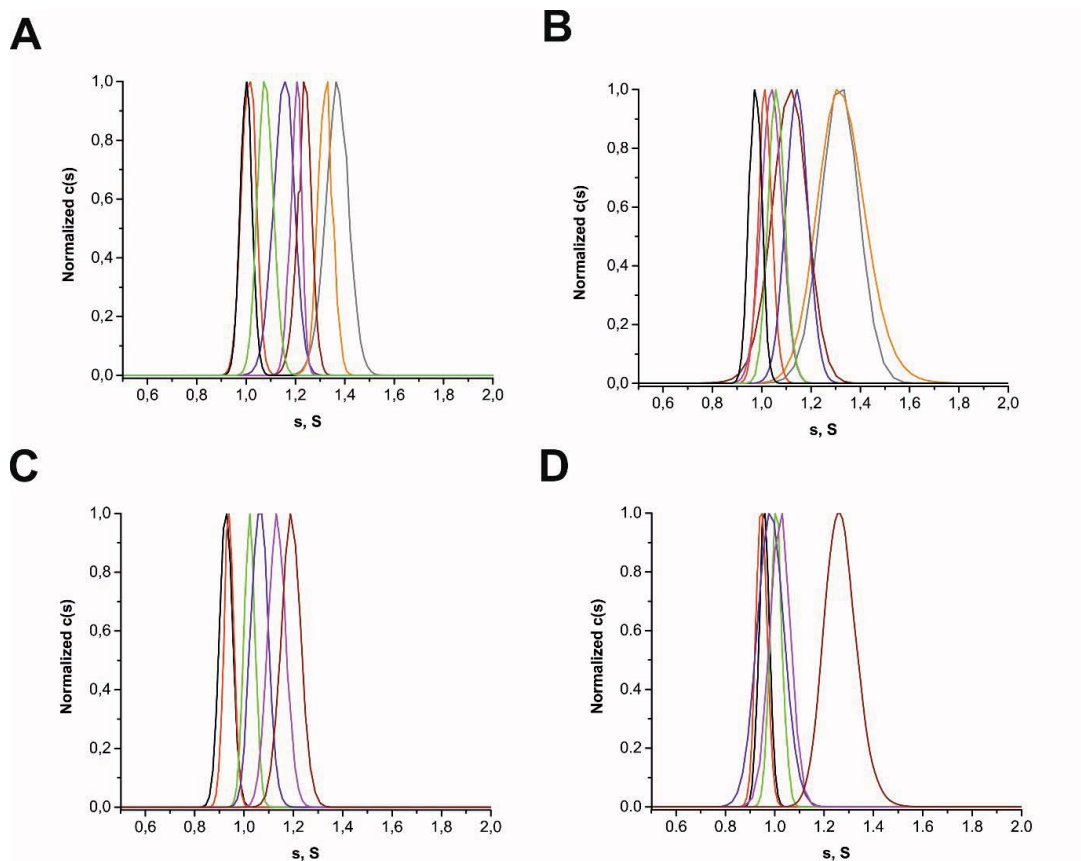


Figure S4. Example differential distributions of sedimentation coefficients, s , of (A) statistical copolymers of HPMA and APMA, (B) the gradient copolymers of HPMA and APMA, (C) the statistical copolymers of HPMA and GPMA, and (D) the gradient copolymers of HPMA and GPMA. Trace color assignment: **black** HPMA_{95%}-s-APMA_{5%} / HPMA_{95%}-g-APMA_{5%} / HPMA_{95%}-s-GPMA_{5%} / HPMA_{95%}-g-GPMA_{5%}; **red** HPMA_{90%}-s-APMA_{10%} / HPMA_{90%}-g-APMA_{10%} / HPMA_{90%}-s-GPMA_{10%} / HPMA_{90%}-g-GPMA_{10%}; **green** HPMA_{80%}-s-APMA_{20%} / HPMA_{80%}-g-APMA_{20%} / HPMA_{80%}-s-GPMA_{20%} / HPMA_{80%}-g-GPMA_{20%}; **blue** HPMA_{60%}-s-APMA_{40%} / HPMA_{60%}-g-APMA_{40%} / HPMA_{60%}-s-GPMA_{40%} / HPMA_{60%}-g-GPMA_{40%}; **magenta** HPMA_{50%}-s-APMA_{50%} / HPMA_{50%}-g-APMA_{50%} / HPMA_{50%}-s-GPMA_{50%} / HPMA_{50%}-g-GPMA_{50%}; **wine** HPMA_{40%}-s-APMA_{60%} / HPMA_{40%}-g-APMA_{60%}; **orange** HPMA_{25%}-s-APMA_{75%} / HPMA_{25%}-g-APMA_{75%} / HPMA_{25%}-s-GPMA_{75%} / HPMA_{25%}-g-GPMA_{75%}; **gray** HPMA_{10%}-s-APMA_{90%} / HPMA_{10%}-g-APMA_{90%} / HPMA_{10%}-s-GPMA_{90%} / HPMA_{10%}-g-GPMA_{90%}.

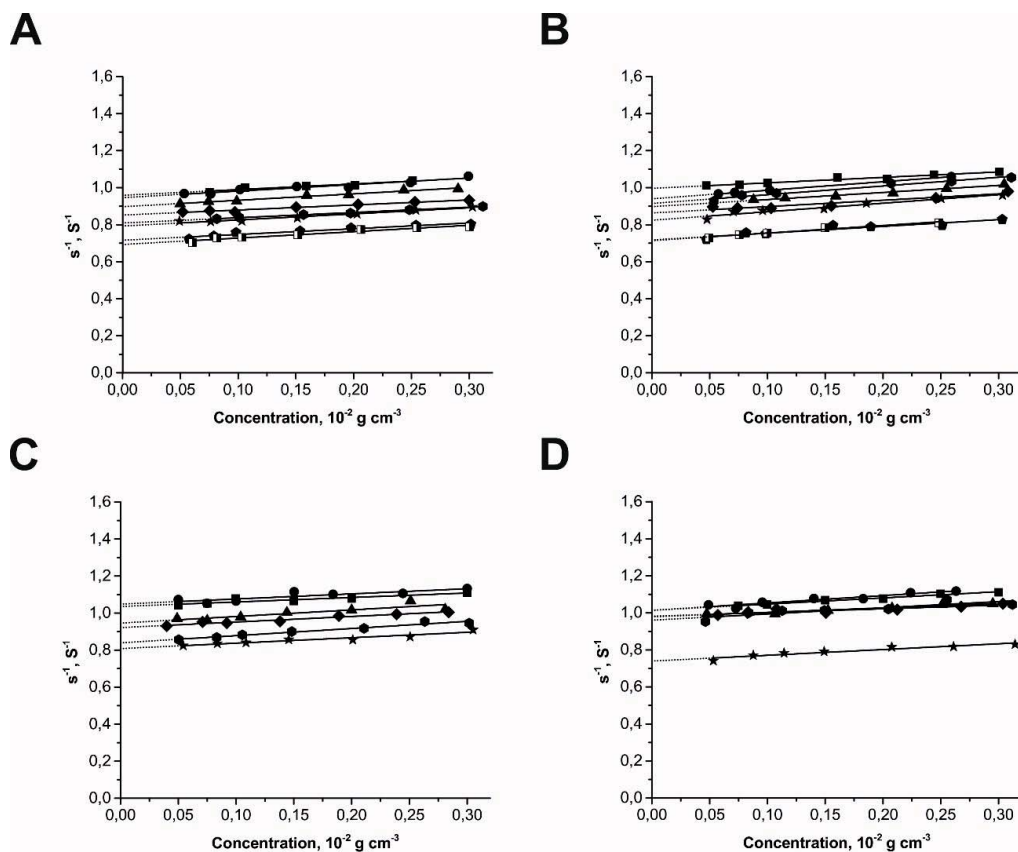
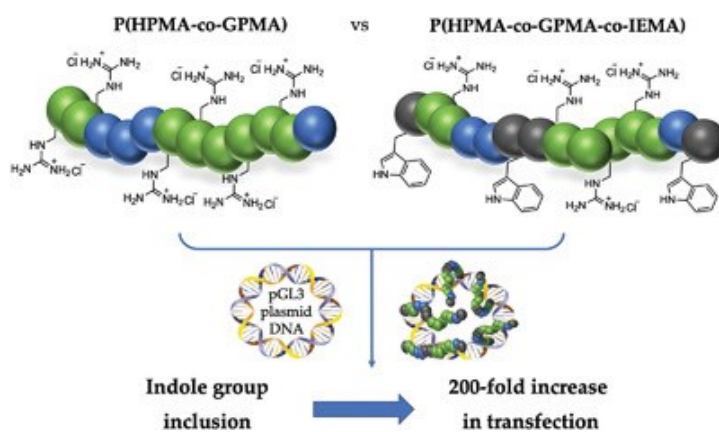


Figure S5. Plots of inverse sedimentation coefficients, s^{-1} , against macromolecule solution concentration with linear fits (solid lines) and extrapolations to zero concentration (dotted lines) to determine s_0 for of (A) statistical copolymers of HPMA and APMA, (B) the gradient copolymers of of HPMA and APMA, (C) the statistical copolymers of HPMA and GPMA, and (D) the gradient copolymers of HPMA and GPMA. Symbol assignment for polymers: **Squares** HPMA_{95%}-s-APMA_{5%} / HPMA_{95%}-g-APMA_{5%} / HPMA_{95%}-s-GPMA_{5%} / HPMA_{95%}-g-GPMA_{5%}; **circles** HPMA_{90%}-s-APMA_{10%} / HPMA_{90%}-g-APMA_{10%} / HPMA_{90%}-s-GPMA_{10%} / HPMA_{90%}-g-GPMA_{10%}; **triangles** HPMA_{80%}-s-APMA_{20%} / HPMA_{80%}-g-APMA_{20%} / HPMA_{80%}-s-GPMA_{20%} / HPMA_{80%}-g-GPMA_{20%}; **diamonds** HPMA_{60%}-s-APMA_{40%} / HPMA_{60%}-g-APMA_{40%} / HPMA_{60%}-s-GPMA_{40%} / HPMA_{60%}-g-GPMA_{40%}; **hexagons** HPMA_{50%}-s-APMA_{50%} / HPMA_{50%}-g-APMA_{50%} / HPMA_{50%}-s-GPMA_{50%} / HPMA_{50%}-g-GPMA_{50%}; **stars** HPMA_{40%}-s-APMA_{60%} / HPMA_{40%}-g-APMA_{60%}; **pentagons** HPMA_{25%}-s-APMA_{75%} / HPMA_{25%}-g-APMA_{75%} / HPMA_{25%}-s-GPMA_{75%} / HPMA_{25%}-g-GPMA_{75%}; **half-filled squares** HPMA_{10%}-s-APMA_{90%} / HPMA_{10%}-g-APMA_{90%} / HPMA_{10%}-s-GPMA_{90%} / HPMA_{10%}-g-GPMA_{90%}.

Publication P2

Incorporation of Indole Significantly Improves the Transfection Efficiency of Guanidinium-Containing Poly(Methacrylamide)s



C. Cokca, L. Zartner, I. Tabujew, D. Fischer, K. Peneva

Macromol. Rapid Commun. **2020**, *41* (6), 1900668.



Incorporation of Indole Significantly Improves the Transfection Efficiency of Guanidinium-Containing Poly(Methacrylamide)s

Ceren Cokca, Leon Zartner, Ilja Tabujew, Dagmar Fischer,* and Kalina Peneva*

A highly efficient transfection agent is reported that is based on terpolymer consisting of *N*-(2-hydroxypropyl)methacrylamide (HPMA), *N*-(3-guanidinopropyl)methacrylamide (GPMA), and *N*-(2-indolethyl)methacrylamide monomers (IEMA) by analogy to the amphipathic cell-penetrating peptides containing tryptophan and arginine residues. The incorporation of the indole-bearing monomer leads to successful plasmid DNA condensation even at a nitrogen-to-phosphate (N/P) ratio of 1. The hydrodynamic diameter of polyplexes is determined to be below 200 nm for all N/P ratios. The transfection studies demonstrate a 200-fold increase of the transgene expression in comparison to P(HPMA-co-GPMA) with the same guanidinium content. This study reveals the strong potential of the indole group as a side-chain pendant group that can increase the cellular uptake of polymers and the transfection efficiency of the respective polyplexes.

Viruses often use the interplay of charge and polarity to efficiently cross biological barriers like the cell membrane.^[1] The same principle has been widely applied to enhance the internalization of cell-penetrating peptides (CPPs), for example, by the incorporation of hydrophobic residues such as phenylalanine or tyrosine.^[2,3] Ever since the first report of gene therapy by Merrill et al. in 1971, one of the pressing challenges we still face is the invention of an efficient non-viral delivery vector that can trans-

port genetic materials inside living cells.^[4] The design of such synthetic vectors is often inspired by nature and it is frequently based on cationic macromolecules with well-defined molecular weight, dispersity, and functionality.^[5,6] However, positive charge is only one important fragment that is needed to ensure efficient binding to the negatively charged nucleic acids.^[7,8] The second crucial step that determines the efficiency of many gene delivery agents is the release of the intact genetic material inside the cell. At this stage of intracellular transport, a rather subtle balance between charge and hydrophobicity has proven to be vitally important. For example, the translocation of CPP such as Pep-1 and MPG could be improved by the incorporation of hydrophobic residues.^[9] Similar design principle was applied to polymeric siRNA carriers where the incorporation of segregated hydrophobic monomers demonstrated that a hydrophobic block is required to reach an improved internalization.^[10,11]

Recently, we demonstrated that guanidinium-containing methacrylamides with guanidinium monomer content equal to or higher than 60% can efficiently bind plasmid DNA (pDNA), regardless of whether gradient or statistical copolymers were prepared.^[12] However, a high percentage of guanidinium monomers in the copolymers shows lower transfection efficiency compared to linear poly(ethylene imine) polymers with similar molar mass due to delayed release and poor translocation through the endosomal membrane. To address this challenge, we incorporated *N*-(2-indolethyl)methacrylamide (IEMA) and copolymerized it with methacrylamide monomers. Inspired by the amino acid tryptophan, we report the first terpolymer that contains *N*-(2-hydroxypropyl)methacrylamide (HPMA), *N*-(3-guanidinopropyl)methacrylamide (GPMA), and their indole counterpart IEMA. Transfection studies using pDNA demonstrated a 200-fold increase of the transgene expression in comparison to a P(HPMA-co-GPMA) copolymer with comparable guanidinium content. Probing the effect of the insertion of indole monomers could pave the way to better design of non-viral delivery agents.

The synthesis of HPMA, GPMA, and IEMA monomers was performed in a one-step process (Schemes S1, S2, and S3, Supporting Information). To be able to determine the influence of the indole group over the binding and transfection of pDNA, we selected a high-performing P(HPMA-co-GPMA) copolymer from our previous study and conducted a direct comparison with the terpolymer counterpart. Their most important physicochemical

C. Cokca, Dr. I. Tabujew, Prof. K. Peneva
Institute of Organic Chemistry and Macromolecular Chemistry (IOMC)
Friedrich Schiller University Jena
Lessingstraße 8, 07743 Jena, Germany
E-mail: kalina.peneva@uni-jena.de

L. Zartner, Prof. D. Fischer
Institute of Pharmacy, Pharmaceutical Technology and Biopharmacy
Friedrich Schiller University Jena
Lessingstraße 8, 07743 Jena, Germany
E-mail: dagmar.fischer@uni-jena.de

Prof. D. Fischer, Prof. K. Peneva
Jena Center of Soft Matter
Friedrich Schiller University Jena
Philosophenweg 7, 07743 Jena, Germany

The ORCID identification number(s) for the author(s) of this article can be found under <https://doi.org/10.1002/marc.201900668>.

© 2020 The Authors. Published by WILEY-VCH Verlag GmbH & Co. KGaA, Weinheim. This is an open access article under the terms of the Creative Commons Attribution-NonCommercial-NoDerivs License, which permits use and distribution in any medium, provided the original work is properly cited, the use is non-commercial and no modifications or adaptations are made.

DOI: 10.1002/marc.201900668

Table 1. Monomer contents, molar masses, and dispersity indices of copolymer and terpolymer samples.

Polymer samples	Experimental [mol%]			$M_{n, \text{experimental}}$ [g mol ⁻¹]	\mathcal{D}
	HPMA	IEMA	GPMA		
 P(HPMA-co-GPMA) ^{a)}	47	—	53	18 000	1.09
 P(HPMA-co-GPMA-co-IEMA) ^{b)}	26	16	58	19 000	1.13

characteristics are summarized in **Table 1**. The polymers were synthesized via aqueous reversible addition–fragmentation chain transfer polymerization with some modification of previously reported polymerization procedures (Scheme S4, Supporting Information).^[12–14] Two different chain transfer

agents were utilized during the synthesis of the copolymer and the terpolymer due to the difference in solubility and reactivity of the indole monomer. The guanidinium content was kept around 60 mol% for both copolymers, whereas HPMA monomer, used as spacer unit, was lower in content due to the IEMA monomer inclusion (16 mol%) in the terpolymer structure. Our attempts to increase the IEMA content higher than 20% led to coagulation and precipitation during the polymerization reaction, which in turn increased the dispersity of the resulting terpolymers. All polymer samples showed molar masses $\approx 20\,000$ g mol⁻¹ as well as a low dispersity index (\mathcal{D}) < 1.2. P(HPMA-co-GPMA) and P(HPMA-co-GPMA-co-IEMA) were compared with respect to their biocompatibility, toxicity, and performance as gene carriers side by side, to understand to what extent the addition of the indole comonomer can improve the transfection efficiency of guanidinium-containing polymers.

Cationic polymers are known to cause toxic effects on biological membranes in different ways, for example, nanoscale pore formation, loss of membrane integrity, impairment of the metabolic activity, or change in the phospholipid composition of the lipid bilayer.^[15] To assess the cell viability, the 3-(4,5-dimethylthiazol-2-yl)-2,5-diphenyltetrazolium bromide assay was performed on L-929 mouse fibroblasts compared to the negative control (untreated cells, 100%) and the positive control (0.2% thiomersal, <3% viability) (**Figure 1A**). Increased toxicity was observed from the terpolymer at concentrations

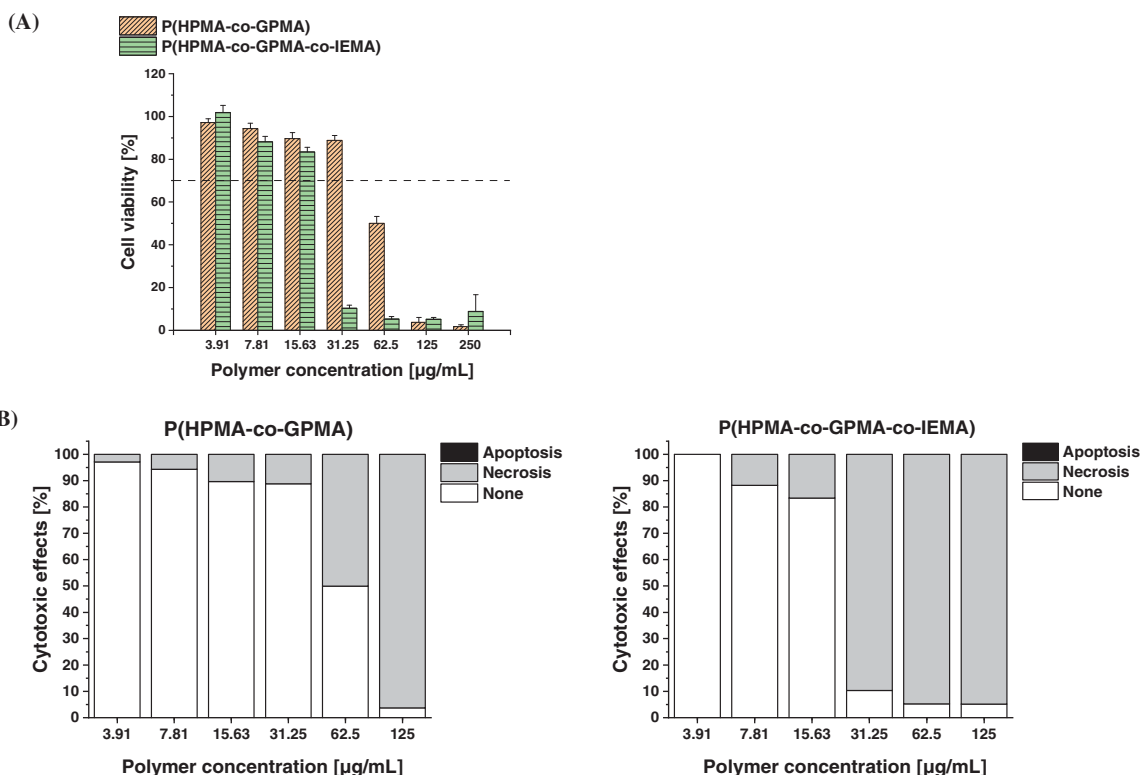


Figure 1. A) Cell viability assay performed on L-929 mouse fibroblasts with increasing polymer concentrations ($n = 7 \pm \text{SD}$). B) Apoptosis determined by caspase activity Caspase-Glo 3/7 assay ($n = 3 \pm \text{SD}$) versus necrosis and viability.

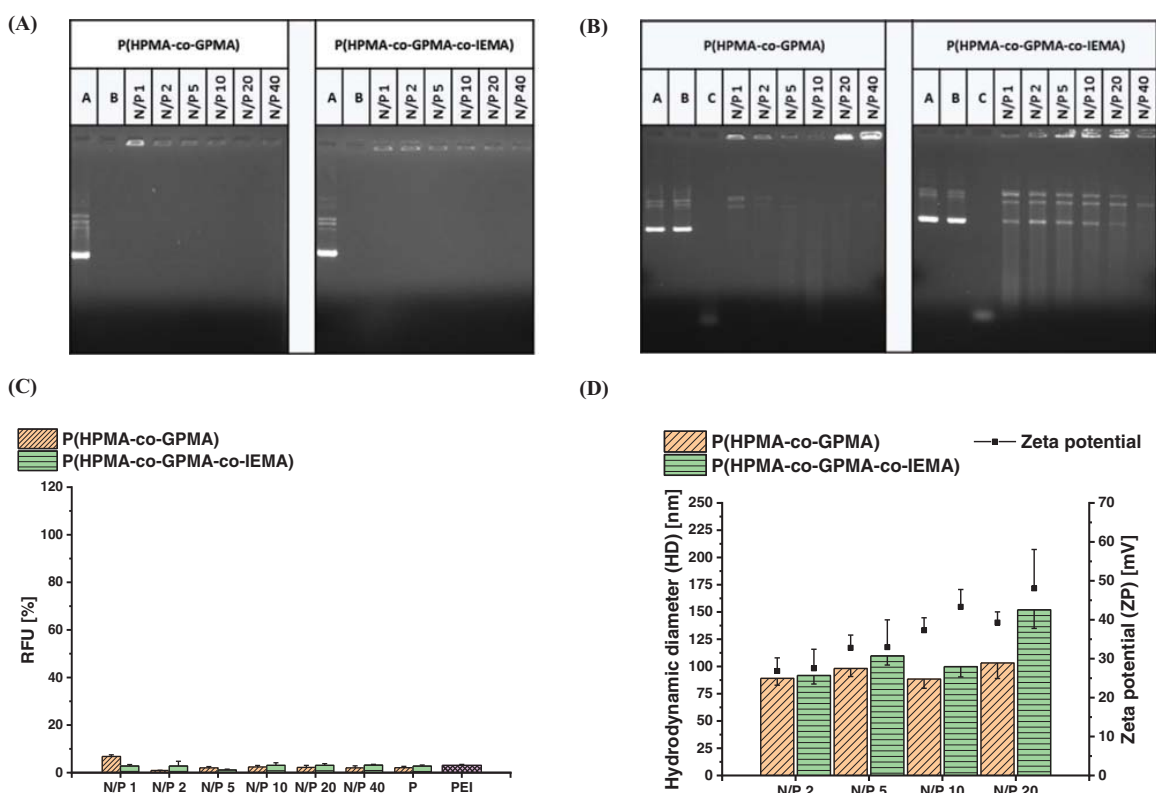


Figure 2. Physicochemical characterization of the polyplexes: A) pDNA binding of P(HPMA-co-GPMA) and P(HPMA-co-GPMA-co-IEMA) determined by horizontal agarose gel electrophoresis with pDNA (Lane A) and polymer (Lane B) controls. B) Protection from enzymatic degradation and polyplex dissociation visualized by horizontal agarose gel electrophoresis with untreated pDNA (Lane A), heat-treated pDNA without DNase I (Lane B), and pDNA treated with DNase I (Lane C). C) Fluorophore exclusion assay with the polymers (P) and IPEI 2.5 kDa/pDNA N/P 20 (PEI) controls ($n = 4 \pm \text{SD}$). D) Hydrodynamic diameters (HD) and zeta potentials (ZP) of P(HPMA-co-GPMA) and P(HPMA-co-GPMA-co-IEMA) polyplexes with a cumulative analysis of HD and ZP ($n = 4 \pm \text{SD}$).

higher than $31.25 \mu\text{g mL}^{-1}$. This was in accordance with the literature, where increased cell toxicity of indole containing peptides has been reported earlier.^[16] For instance, Jobin et al. in 2015 synthesized arginine-rich seven peptide analogues where they changed phenylalanine residue into tryptophan to systematically explore cellular uptake. In their study, all indole-bearing peptides showed higher cytotoxicity.^[17] To gain better insights into the cell death mechanism, cellular caspase 3/7 activity assay following the polymer treatment was performed as a measure for apoptosis (Figure 1B).^[18] Both polymers did not show any apoptotic events measured by the caspase 3/7 activity assay, which suggested a non-apoptotic cell death pathway could be responsible for the cell death.

The binding ability of the polymers to pDNA was assessed qualitatively by horizontal gel electrophoresis and quantitatively by the AccuBlue dye exclusion assay. In agarose gel electrophoresis (Figure 2A), naked pDNA displayed the typical band pattern of nicked circular, linear, and supercoiled plasmid conformations while the polymer alone did not exhibit any signal. Upon polyplex formation, the migration of the negatively charged plasmid toward the anode was impeded due to the charge compensation (complexation) and/or the formation of large complexes of several

hundred nanometers unable to migrate through the gel.^[19–21] The electrophoresis assay demonstrated efficient pDNA binding at all tested N/P ratios with complete retardation of the plasmid for both P(HPMA-co-GPMA) and P(HPMA-co-GPMA-co-IEMA). In addition to the immobilization of pDNA, an N/P ratio-dependent fluorescence quenching was observed for both polymers, which was interpreted as molecular collapse of the plasmid (condensation) and displacement of the nucleic acid stain from the double helix. The AccuBlue assay supported the successful pDNA condensation quantitatively (Figure 2C). Even at the lowest tested N/P ratio of 1, for both polymers, more than 90% pDNA were no longer accessible for the intercalation of the fluorescent dye. Consequently, the polymers reached binding affinities comparable to the pDNA polyplexes (N/P 20) with 2.5 kDa PEI under optimized conditions.

To understand whether the two polymers can protect pDNA against enzymatic degradation, a stability assay was performed using the enzyme DNase I, followed by removal of pDNA from the polyplexes with heparin and separation with agarose gel electrophoresis. Although untreated intact pDNA as well as pDNA treated without enzyme revealed the typical band pattern excluding any unspecific degradation effect, after 45 min treatment with DNase I, all bands disappeared, indicating the

degradation to smaller fragments with lower molar masses (Figure 2B). Polyplexes of P(HPMA-co-GPMA) and P(HPMA-co-GPMA-co-IEMA) represented intact bands at all tested N/P ratios from 1 to 40 as an evidence of protected pDNA payload from enzymatic degradation. However, displacement of pDNA payload from the polyplexes by heparin decreased with increasing N/P ratios. Additionally, the release of pDNA from the polyplexes was found to be more efficient for the P(HPMA-co-GPMA-co-IEMA) than for the P(HPMA-co-GPMA) where most of the pDNA was still located at the beginning of the gel, starting at N/P 10. Significantly higher heparin affinity was observed in several amphipathic peptides which can explain the easier pDNA release from the P(HPMA-co-GPMA-co-IEMA)/pDNA polyplexes.^[22]

The hydrodynamic diameter (HD) and zeta potential (ZP) of polyplexes can impact their uptake and intracellular distribution. For this reason, HD and ZP of the polyplexes were

measured through dynamic light scattering and laser Doppler anemometry (Figure 2D). The sizes of polyplexes at N/P ratios 2–20 were between 75 and 200 nm independent from the polymer type with a slight trend to agglomeration for p(HPMA-co-GPMA-co-IEMA) at N/P 20. ZP measurements indicated an increase of the ZP values from about 30 to 60 mV with the increase in N/P ratio comparable for both polymers.

Transfection studies of the P(HPMA-co-GPMA)/pDNA and P(HPMA-co-GPMA-co-IEMA)/pDNA polyplexes containing 4 µg pGL3 pDNA, which encodes for the luciferase gene under a SV40 promoter, were conducted on CHO-K1 cells (Figure 3A,B). Reporter gene expression was presented as relative light units quantified by bioluminescence measurements. Naked pDNA served as control and failed the production of detectable expression signals. Both polymer/pDNA polyplexes transfected CHO-K1 cells and induced an N/P-dependent

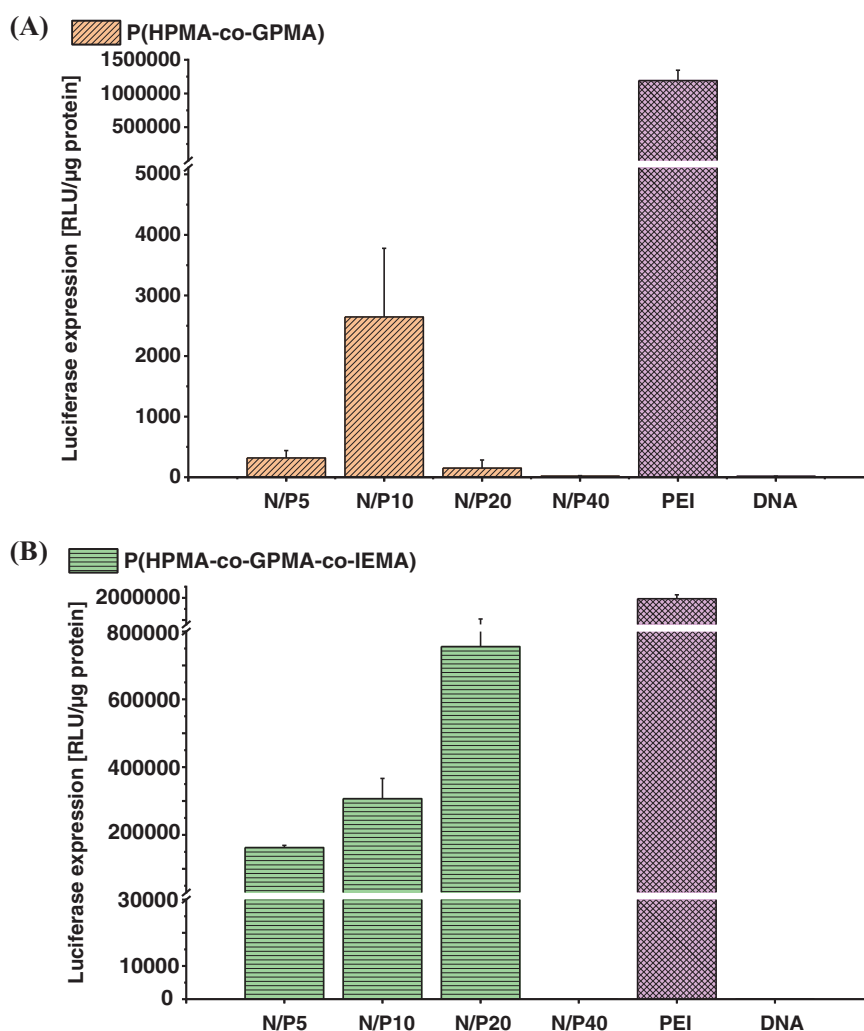


Figure 3. Transfection studies of A) P(HPMA-co-GPMA) and B) P(HPMA-co-GPMA-co-IEMA) on CHO-K1 cells (DNA: 4 µg pDNA, PEI: 2.5 kDa linear PEI at N/P 20).



luciferase transgene expression, although they did not reach the values of the positive control PEI/pDNA polyplexes under the chosen conditions. As a major difference, the P(HPMA-co-GPMA-co-IEMA) polyplexes induced over 200 times higher transgene expression than P(HPMA-co-GPMA) polyplexes. In both cases, N/P > 20 did not increase the transfection ability either because of high toxicity or too strong binding of the pDNA. The higher transfection efficacy might be related on the one hand to the better release of pDNA by the indole-containing polymer as shown above in the electrophoresis experiments. On the other hand, guanidinium has already proven its cell-penetrating efficiency due to its ability to form bidentate hydrogen bonds with anionic groups or self-aggregation for effective translocation in the cell membrane.^[23] However, it has been shown that hydrophobic residues in vectors containing also guanidinium groups improved cell translocation dramatically due to the interaction with the cell membrane.^[7] Especially, the indole group of tryptophan has the ability of π - π stacking with aromatic parts of membrane proteins.^[24,25] It should be mentioned that the polyplexes were able to transfect cells even in the presence of serum. As a result, the positive charges of the polyplexes can be shielded further and membrane translocation can occur more efficiently.

In summary, we report the first example of a water-soluble terpolymer containing HPMA, GPMA, and IEMA monomers and its successful application in gene delivery. Although the presence of indole group increased the toxicity after a certain N/P ratio, the synergy between indole and guanidinium group proved to significantly increase the transfection efficiency. This study reveals the strong potential of the indole group as side-chain pending group that increases the cellular uptake of polymers and the transfection efficiency of the respective polyplexes. Further investigations in more complex biological models as well as in vivo experiments will follow.

Supporting Information

Supporting Information is available from the Wiley Online Library or from the author.

Acknowledgements

C.C. and L.Z. contributed equally to this work. The authors would like to thank the Deutsche Forschungsgemeinschaft (DFG, German Research Foundation)—project number 316213987—SFB 1278 (projects B03 and Z01) for funding and Angela Herre for excellent technical support.

Conflict of Interest

The authors declare no conflict of interest.

Keywords

gene delivery, guanidinium, indole, methacrylamide

Received: December 29, 2019

Revised: February 3, 2020

Published online: February 19, 2020

- [1] M. S. Ravindran, P. Bagchi, C. N. Cunningham, B. Tsai, *Nat. Rev. Microbiol.* **2016**, *14*, 407.
- [2] E. Wesselblatt, J. D. Esko, Y. Tor, *J. Org. Chem.* **2014**, *79*, 6766.
- [3] Y. Li, Y. Li, X. Wang, R. J. Lee, L. Teng, *Int. J. Pharm.* **2015**, *495*, 527.
- [4] C. R. Merrill, M. R. Geier, J. C. Petricciani, *Nature* **1971**, *233*, 398.
- [5] I.-K. Park, K. Singha, R. B. Arote, Y.-J. Choi, W. J. Kim, C.-S. Cho, *Macromol. Rapid Commun.* **2010**, *31*, 1122.
- [6] K. Klinker, K. Klinker, M. Barz, *Macromol. Rapid Commun.* **2015**, *36*, 1943.
- [7] I. Tabujew, M. Lelle, K. Peneva, *BioNanomaterials* **2015**, *16*, 59.
- [8] I. Tabujew, C. Freidel, B. Krieg, M. Helm, K. Koynov, K. Mullen, K. Peneva, *Macromol. Rapid Commun.* **2014**, *35*, 1191.
- [9] M. C. Morris, S. Deshayes, F. Heitz, G. Divita, *Biol. Cell* **2008**, *100*, 201.
- [10] C. Buerkli, S. H. Lee, E. Moroz, M. C. Stuparu, J.-C. Leroux, A. Khan, *Biomacromolecules* **2014**, *15*, 1707.
- [11] C. Wang, L. Du, J. Zhou, L. Meng, Q. Cheng, C. Wang, X. Wang, D. Zhao, Y. Huang, S. Zheng, H. Cao, J. Zhang, L. Deng, Z. Liang, A. Dong, *ACS Appl. Mater. Interfaces* **2017**, *9*, 32463.
- [12] I. Tabujew, C. Cokca, L. Zartner, U. S. Schubert, I. Nischang, D. Fischer, K. Peneva, *J. Mater. Chem. B* **2019**, *7*, 5920.
- [13] N. J. Treat, D. Smith, C. Teng, J. D. Flores, B. A. Abel, A. W. York, F. Huang, C. L. McCormick, *ACS Macro Lett.* **2012**, *1*, 100.
- [14] I. Tabujew, C. Freidel, B. Krieg, M. Helm, K. Koynov, K. Mullen, K. Peneva, *Macromol. Rapid Commun.* **2014**, *35*, 1191.
- [15] A. Hall, U. Lächelt, J. Bartek, E. Wagner, S. M. Moghimi, *Mol. Ther.* **2017**, *25*, 1476.
- [16] H. L. Aamand, H. A. Rydberg, L. H. Fornander, P. Lincoln, B. Norden, E. K. Esbjornner, *Biochim. Biophys. Acta, Biomembr.* **2012**, *1818*, 2669.
- [17] M.-L. Jobin, M. Blanchet, S. Henry, S. Chaignepain, C. Manigand, S. Castano, S. Lecomte, F. Burlina, S. Sagan, I. D. Alves, *Biochim. Biophys. Acta, Biomembr.* **2015**, *1848*, 593.
- [18] D. Fischer, Y. X. Li, B. Ahlemeyer, J. Kriegelstein, T. Kissel, *Biomaterials* **2003**, *24*, 1121.
- [19] D. Fischer, H. Dautzenberg, K. Kunath, T. Kissel, *Int. J. Pharm.* **2004**, *280*, 253.
- [20] J. Narayanan, J.-Y. Xiong, X.-Y. Liu, *J. Phys.: Conf. Ser.* **2006**, *28*, 83.
- [21] F. Schlenk, S. Grund, D. Fischer, *Ther. Delivery* **2013**, *4*, 95.
- [22] Ü. Langel, in *CPP, Cell-Penetrating Peptides* (Ed: Ü. Langel), Springer, Singapore **2019**, p. 359.
- [23] C. L. Hannon, E. V. Anslyn, in *Bioorganic Chemistry Frontiers* (Eds: H. Dugas, F. P. Schmidtchen), Springer, Berlin **1993**, p. 193.
- [24] M. L. Jobin, M. Blanchet, S. Henry, S. Chaignepain, C. Manigand, S. Castano, S. Lecomte, F. Burlina, S. Sagan, I. D. Alves, *Biochim. Biophys. Acta* **2015**, *1848*, 593.
- [25] Z. Kang, G. Ding, Z. Meng, Q. Meng, *Peptides* **2019**, *121*, 170149.



Supporting Information

for *Macromol. Rapid Commun.*, DOI: 10.1002/marc.201900668

Incorporation of Indole Significantly Improves the
Transfection Efficiency of Guanidinium-Containing
Poly(Methacrylamide)s

Ceren Cokca, Leon Zartner, Ilja Tabujew, Dagmar Fischer,*
and Kalina Peneva*

Supporting Information

Incorporation of indole significantly improves the transfection efficiency of guanidinium-containing poly(methacrylamide)s

[‡]*Ceren Cokca*^a, [‡]*Leon Zartner*^b, *Ilja Tabujew*^a, *Dagmar Fischer*^{b,c,*} and *Kalina Peneva*^{a,c,*}

[‡]*The authors contributed equally to the manuscript.*

*Corresponding authors: dagmar.fischer@uni-jena.de, kalina.peneva@uni-jena.de

^a Institute of Organic Chemistry and Macromolecular Chemistry (IOMC), Friedrich Schiller University Jena, Lessingstraße 8, 07743 Jena, Germany

^b Institute of Pharmacy, Pharmaceutical Technology and Biopharmacy, Friedrich Schiller University Jena, Lessingstraße 8, 07743 Jena, Germany

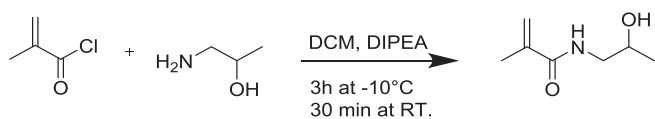
^c Jena Center of Soft Matter, Friedrich Schiller University Jena, Philosophenweg 7, 07743 Jena, Germany

1. Materials and Methods

All chemicals were purchased from SIGMA-Aldrich at the highest available purity and used as received unless mentioned otherwise. *N*-(3-aminopropyl) methacrylamide hydrochloride (APMA) was purchased from PolySciences. 4,4'-Azobis(4-cyanovaleric acid) (ACVA) was recrystallized in methanol before use. The chain transfer agent 4-(((2-carboxyethyl)thio)carbonothioyl)thio)-4-cyanopentanoic acid (CTA1) was procured from Boron Molecular INC.

1.1 Synthesis of Monomers

***N*-(3-hydroxypropyl)methacrylamide (HPMA):** The synthesis was conducted based on literature.^[1] *N,N*-diisopropylethylamine (DIPEA) (18.55 g, 143.5 mmol) was mixed with 100 mL of dry dichloromethane (DCM) under argon flow and the temperature was adjusted to -10 °C. Then, 1-amino-2-propanol (10.78 g, 143.5 mmol) was added. Methacryloyl chloride (10.00 g, 95.66 mmol) was distilled and mixed with dry DCM (1:1 volume ratio). It was slowly dropped into the reaction mixture by means of a dropping funnel. The reaction continued for 3 hours at -10 °C and then at room temperature for 30 min. After reaction was stop, the precipitate was removed and the filtrate was dried through sodium sulfate (Na₂SO₄). The solvent was evaporated and the crude product was purified by means of silica gel column chromatography (200-400 mesh, 40-75 μm) with DCM/ethanol in a ratio of 10:1 as the eluent. The solvent was removed and semi-transparent white crystals were obtained (78% yield). The NMR analysis was conducted to analyze the pure product. ¹H NMR (300 MHz, D₂O, 298K) δH (ppm) = 1.18 (dd, 3H, CH- CH₃), 1.96 (s, 3H, C-CH₃), 3.29 (m, 1H, NH-CH₂), 3.98 (m, 2H, CH-CH₃), 5.47 (s, 1H, C=CH₂), 5.72 (s, 1H, C=CH₂).



Scheme S1. Synthesis of *N*-(3-hydroxypropyl)methacrylamide (HPMA)

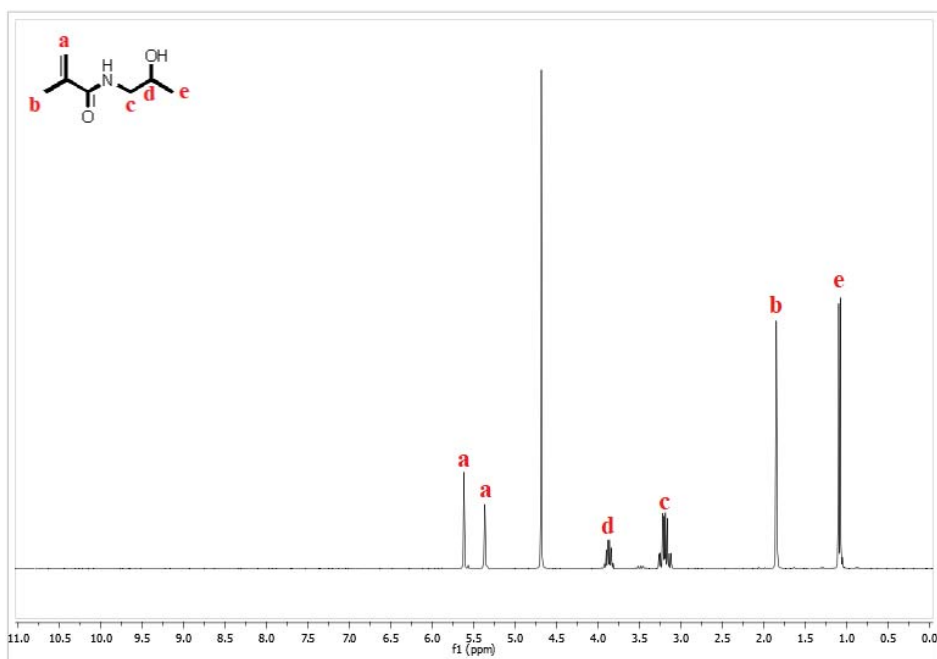
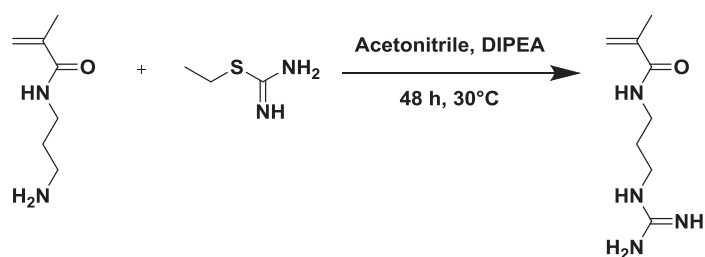


Figure S1. ^1H NMR spectrum of *N*-(3-hydroxypropyl)methacrylamide (HPMA) in D_2O at 333 K (300 MHz)

***N*-(3-guanidinopropyl)methacrylamide (GPMA):** It was synthesized according to a literature work.^[2] A small Erlenmeyer flask was charged with *N*-(3-aminopropyl)methacrylamide hydrochloride (0.641 g, 3.63 mmol). It was dissolved in distilled water (dH_2O). pH of the solution was adjusted into 11 by adding 50 wt% sodium hydroxide (NaOH) solution to deacidify APMA. This solution was placed in a separator funnel and it was washed for 6 times with dichloromethane (DCM). Each time the organic fraction was collected. At the end, the water residue was removed by means of (Na_2SO_4). DCM was removed by means of

vacuum evaporator. At the end a transparent, yellow colored oil was obtained. During solvent evaporation, a round bottom flask was prepared for the reaction by adding S-ethylisothiurea hydrobromide (0.743 g, 3.99 mmol) and DIPEA (0.469 g, 3.63 mmol) by dissolving in acetonitrile. Then, the deprotonated APMA was added dropwise into this mixture. The reaction was vigorously stirred at 30°C for 48 hours. When the reaction finished, acetonitrile was removed via cold distillation. The product was purified by column chromatography with 50:50 ethanol: ethyl acetate. Transparent yellow viscous oil was obtained (30% yield). ¹H NMR (300 MHz, D₂O, 298 K): δH (ppm)= 1.63 (m, 2H), 1.71 (s, 3H), 3.02 (t, 2H), 3.12 (t, 2H), 5.24 (s, 1H), 5.49 (s, 1H).



Scheme S2. Synthesis of *N*-(3-guanidinopropyl)methacrylamide (GPMA)

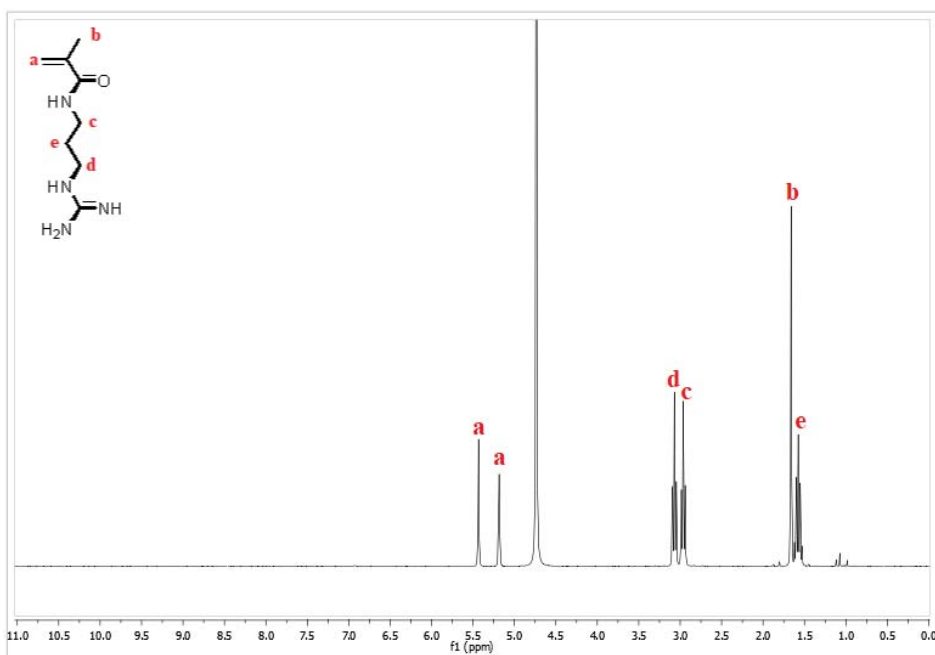
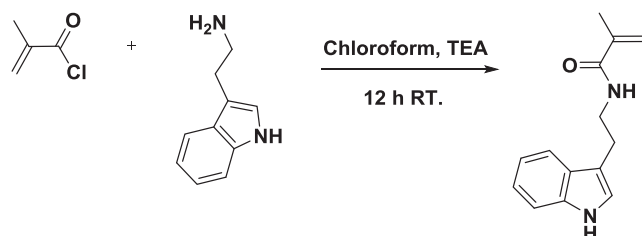


Figure S2. ¹H NMR spectrum of *N*-(3-guanidinopropyl)methacrylamide (GPMA) in D₂O at 333 K (300 MHz)

***N*-(2-indolethyl)methacrylamide (IEMA):** Trypamine (2 g, 12.48 mmol) and triethylamine (TEA) (1.39 g, 13.72 mmol) were dissolved in 30 mL dry chloroform and cooled to 0 °C. Distilled methacryloyl chloride (1.44 g, 13.73 mmol) in 2 mL chloroform was added dropwise to the solution very slowly while keeping the temperature at 0 °C. It was then allowed to warm to room temperature and continued stirring for 12 h. The reaction mixture was washed with sodium bicarbonate (NaHCO₃) solution (3x50 mL) followed by brine (2x50 mL) and water (1x50 mL). The organic phase was then dried over Na₂SO₄ and the solvent was removed through vacuum evaporator before it was purified by means of column chromatography using ethyl acetate:n-hexane (2:1) as the eluent mixture. The obtained yellow colored oil was crystallized overnight in the refrigerator. ¹H NMR (300 MHz, CHCl₃, 298 K):

δ H (ppm)= 8.31 (br s, NH), 7.64 (dd, 1H⁶), 7.40 (t, 1H⁹), 7.26-7.13 (m, 2H^{7,8}), 7.04 (d, 1H⁵), 5.92 (br s, NH-CO), 5.60 (t, 1H²), 5.27 (m, 1H²), 3.65 (td 2H³), 3.02 (m, 2H⁴), 1.90 (t, 3H¹).



Scheme S3. Synthesis of *N*-(2-Indolethyl)methacrylamide (IEMA)

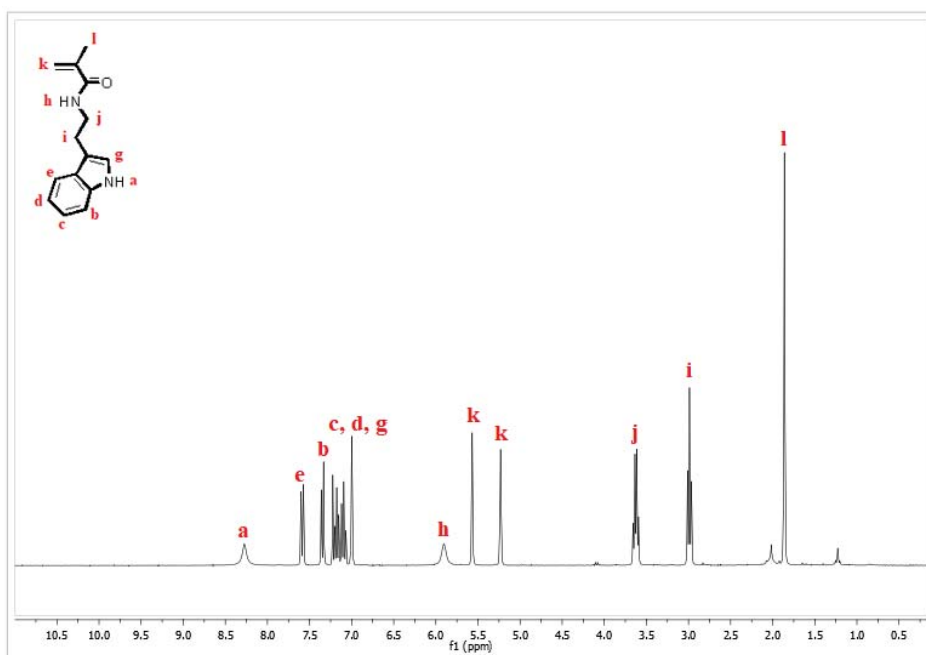
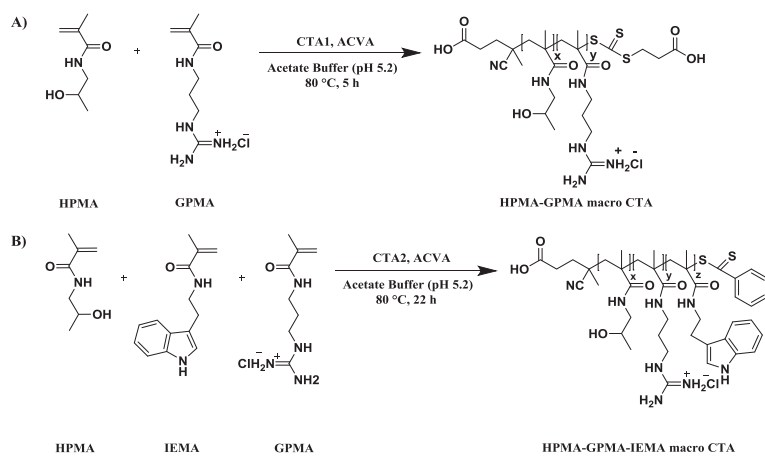


Figure S3. ¹H NMR spectrum of *N*-(2-Indolethyl)methacrylamide (IEMA) in CHCl₃ at 333 K (300 MHz)

1.2 Polymer Synthesis

Synthesis of P(HPMA-co-GPMA): The copolymer structures of P(HPMA-co-GPMA) with 60% monomer compositions of GPMA were prepared by *a*RAFT polymerization described below:

The chain transfer agent CTA1, HPMA (0.150 g, 1.1 mmol) and GPMA (0.762 g, 2.37 mmol) were added into a 25 mL Schlenk flask and dissolved in 1 M degassed acetate buffer (pH 5.2) achieving a monomer concentration of 1 M. After addition of the initiator, ACVA, the reaction was carried out under argon at 80 °C for 5 h. The initial monomer to CTA1 ratio, $[M]_0/[CTA1]_0$ ratio, was 80/1 and the initial CTA1 to initiator ratio, $[CTA1]_0/[I]_0$, was kept at 3/1. At the end of the reaction, the dialysis was conducted for the reaction mixture in dH₂O (pH 4) at 4 °C and then the lyophilization of the pure product was performed. The compound was characterized regarding its monomer composition by using ¹H NMR spectroscopy. The molar mass and dispersity index were analysed by SEC_{DMAc}.



Scheme S4. *a*RAFT Polymerization of **A)** P(HPMA-co-GPMA) copolymers **B)** P(HPMA-co-GPMA-co-IEMA) terpolymers

Field Code Changed

Synthesis of P(HPMA-co-GPMA-co-IEMA): The copolymer structures of P(HPMA-co-GPMA-co-IEMA) with 60% monomer compositions of GPMA was prepared by *a*RAFT polymerization which is explained below:

The chain transfer agent 4-Cyano-4-(phenylcarbonothioylthio)pentanoic acid (CTA2), HPMA (0.083 g, 0.58 mmol), GPMA (0.3 g, 1.62 mmol), and IEMA (0.026 g, 0.12 mmol) were added into a 25 mL Schlenk flask and dissolved in 1 M degassed acetate buffer (pH 5.2) achieving a monomer concentration of 1 M. To increase the solubility of IEMA monomer, 2% DMF was additionally involved. Following the addition of ACVA, the reaction was performed under argon at 79 °C for 22 h. The initial monomer to CTA2 ratio, $[M]_0/[CTA2]_0$ ratio, was 200/1 and the initial CTA2 to initiator ratio, $[CTA2]_0/[I]_0$, was 3/1. When the reaction completed, the dialysis was conducted in dH₂O (pH 4) at 4 °C for the purification of the compound. After that, the polymer samples were dried through lyophilization. The monomer content was analysed by ¹H NMR spectroscopy. The molar mass and dispersity index were detected by means of SEC_{DMAC}.

1.3 NMR Characterization of Polymers

The monomer compositions in the polymer samples were analyzed through a Bruker WS 400 MHz spectrometer (controller: Bruker Avance III) in D₂O at 333 K. The integration of the intensities assigned to the methylene proton resonances of HPMA (3.92 ppm), IEMA (7.0-7.8 ppm) and the methylene resonances of APMA or GPMA (3.08-3.21 ppm) enabled the estimation of the monomer compositions.

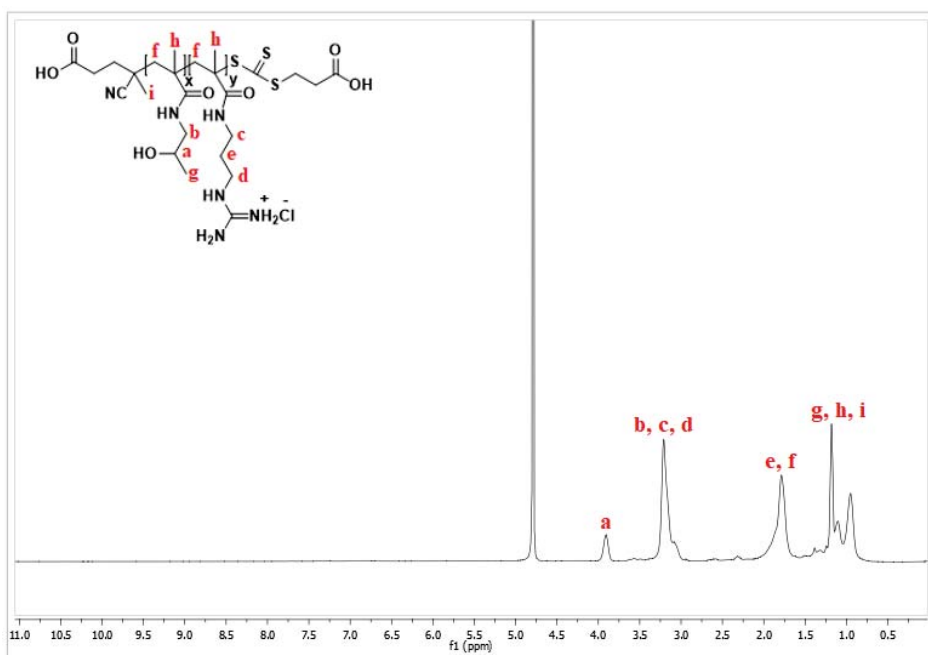


Figure S4. ¹H-NMR spectrum of P(HPMA-co-GPMA) in D₂O at 333 K (400 MHz)

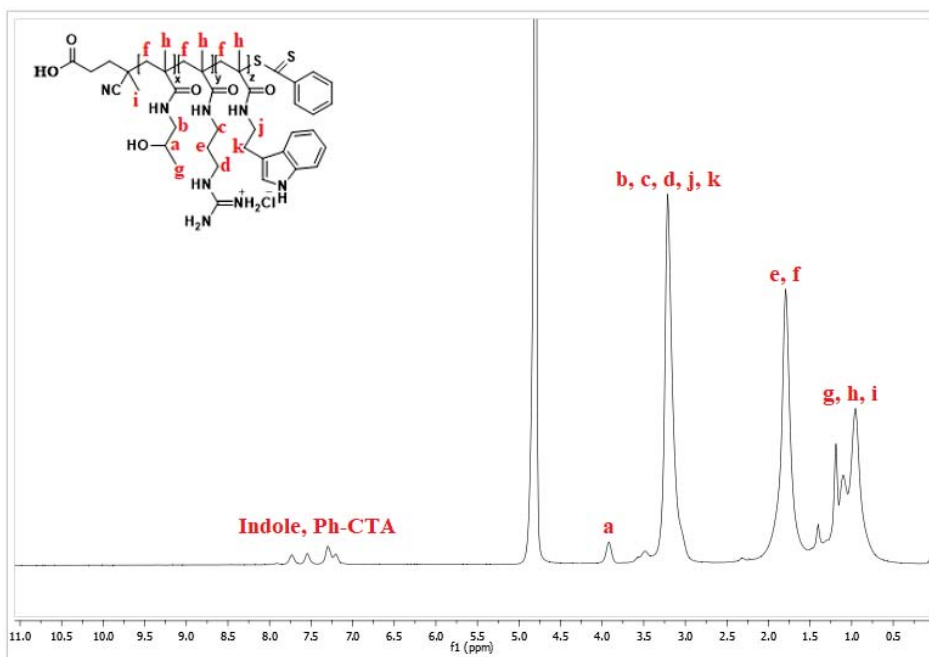


Figure S5. ¹H-NMR spectrum of P(HPMA-co-GPMA-co-IEMA) in D₂O at 333 K (400 MHz)

1.4 Size Exclusion Chromatography

The polymers were characterized through SEC_{DMAc} that was conducted with dimethylacetamide and lithium chloride (DMAc + 0.21% LiCl) as the eluent at 40 °C with the flow rate of 1 mL/min using a PSS GRAM guard/1000/30 Å column (particle size: 10 μm). The refractive index detector (G1362A) and the UV Detector (G1315D, wavelength: 310 nm) were used to monitor the elution. The molar mass was calculated based on a calibration with poly (methyl methacrylate) (PMMA) standards.

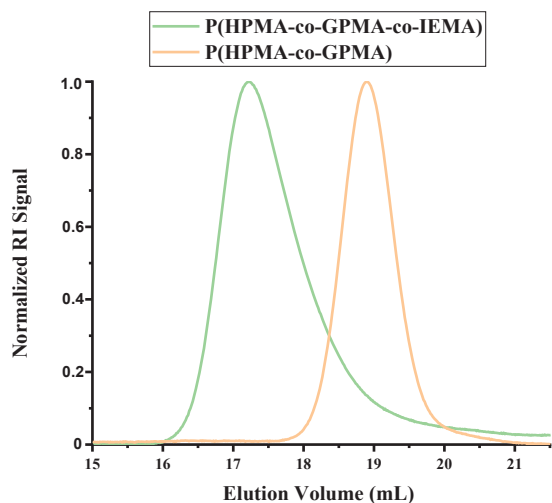


Figure S6. SEC_{DMAc} traces of P(HPMA-co-GPMA-co-IEMA) terpolymer and P(HPMA-co-GPMA) copolymer

2. Biological Studies

2.1 Cell Viability Assay

The cell viability was determined by 3-(4,5-dimethylthiazol-2-yl)-2,5-diphenyltetrazolium bromide (MTT, Carl Roth) assay in L929 murine fibroblast cells (ACC 2, German Collection of Microorganisms and Cell Cultures, DSMZ). Cells were seeded on transparent 96-well polystyrene microplates (CELLSTAR[®], Greiner Bio-One) with a density of 8,500 cells per well and incubated for 24 hours in cell culture medium (RPMI 1640 medium supplemented with L-glutamine, CLS Cell Lines Service GmbH, supplemented with 10 vol% fetal bovine serum, FBS, GE Healthcare Europe GmbH) at 37° C, 5% CO₂ and 95% relative humidity. Subsequently, the culture medium was aspirated and replaced by serial dilutions of polymer in cell culture medium (3.91 µg/mL – 500 µg/mL). As positive and negative controls, 0.02 wt·vol⁻¹% thiomersal (Carl Roth) diluted in medium and pure medium were used, respectively. After 24 hours of incubation, medium was replaced by cell culture medium

Field Code Changed

containing 0.5 mg/mL MTT and incubation was continued for four hours. Subsequently, medium was removed, and the blue formazan crystals were dissolved at 600 rpm orbital agitation for 30 minutes in 200 μ L dimethyl sulfoxide (DMSO) containing 5 vol% of an aqueous 0.1 M sodium hydrogen carbonate solution (both Carl Roth). Sample absorbance was measured at 570 nm (SPARK 10M, Tecan Austria GmbH) and relative cell viability was calculated (**Equation 1**). The inhibitory concentrations were calculated by nonlinear dose-response analysis of the average cell viabilities of two individual experiments. Additionally, cell morphology was examined by light microscopy (Primovert, Carl Zeiss Microscopy GmbH).

$$\text{Relative viability [\%]} = \frac{A(\text{sample}) - A(\text{blank})}{A(\text{negative control}) - A(\text{blank})} \times 100\% \quad (1)$$

2.2 Apoptosis Assay

Caspase activity was quantified as a marker for apoptosis by Caspase-Glo[®] 3/7 Assay (Promega). L929 cells were cultivated in 96 well polystyrene plates (μ Clear[®] 96) at a density of 8,500 cells/well for 24 hours in cell culture medium (RPMI 1640 medium supplemented with L-glutamine and 10 vol% FBS) at 37[°] C, 5% CO₂ and 95% relative humidity. Subsequently, the culture medium was aspirated and replaced by serial dilutions of the polymer in cell culture medium (3.91-125 μ g/mL). As positive and negative controls, cells treated for 48 hours with camptothecin sodium (5 μ M, Sigma Aldrich) and cells only treated with culture medium were used, respectively, while culture medium without cells served as blank. Luminescence was quantified according to the manufacturer's protocol (SPARK 10M). All samples were prepared in triplicates and measured three times. The experiment was repeated once. Relative light units (RLUs) were calculated as mean of three individual wells \pm standard deviation.

2.3 Preparation of plasmid DNA

Amplification of the pGL3 reporter plasmid (Promega) was performed in *Escherichia coli* DH5 α (a kind gift from Hans-Knoell-Institute) at 37 °C for 16 hours in lysogeny broth (Carl Roth). Subsequently, the plasmid was isolated using the E.Z.N.A.® Plasmid DNA Maxi Kit (OMEGA bio-tek) according to the manufacturer's protocol. Plasmid concentration and purity were determined by ultraviolet spectroscopy at 230 nm, 260 nm and 280 nm (SPARK 10M). Additionally, plasmid purity and topology were confirmed by horizontal agarose gel electrophoresis, as described in section 2.5.

2.4 Preparation of Polyplexes

Polyplexes were prepared as previously reported.^[3] In brief, the desired amount of polymer and pDNA stock solution in bidistilled water (ddH₂O) were diluted in equivalent volumes of saline (0.15 M sodium chloride, Carl Roth, in ddH₂O, pH 7.4), vortexed for 10 seconds and incubated at room temperature for 10 minutes. Subsequently, the polymer solution was added to the pDNA solution, vortexed for 10 seconds and incubated again for further 10 minutes prior to use. Unless stated otherwise, the final pDNA concentration was kept at 20 μ g/mL. The polyplex dispersions were classified according to their cationic polymer nitrogen (N) to anionic DNA phosphate (P) ratio (N/P ratio).

2.5 Horizontal Agarose Gel Electrophoresis

To evaluate the pDNA binding ability of polymers and to confirm the plasmid integrity and topology, the polyplex or plasmid dispersion were mixed with loading buffer (10 μ L+ 1 μ L, 40 mM Tris-hydroxymethyl-aminomethane, Tris-base, 1 mM ethylenediaminetetraacetic acid, EDTA, all Carl Roth, 50 vol% glycerol, Caesar & Loretz GmbH, pH 7.4). Ten μ L mixture

were loaded onto a 1 wt·vol⁻¹% agarose gel (peqGOLD universal agarose, PEQLAB Biotechnologie GmbH) containing 0.125 µg/mL ethidium bromide (SERVA Electrophoresis GmbH). Pure plasmid and bromophenol blue (SERVA) were utilized as negative control and running control, respectively. Electrophoresis was performed in a horizontal chamber (Biometra GmbH) at 80 V (Biorad PowerPac 1000, Bio-Rad Laboratories) for 60 minutes in Tris-acetate-EDTA (TAE) buffer (40 mM Tris-base, 20 mM acetic acid, Merck KGaA, 1 mM EDTA). Gels were photographed (DOC-PRINT VX5, Vilber Lourmat) under UV transillumination (Intas Science Imaging Instruments GmbH) at 312 nm.

2.6 Fluorophore Exclusion Assay

To determine the amount of free pDNA in the polyplex dispersions as a measure for pDNA binding capability, the AccuBlue™ High Sensitivity dsDNA Quantitation Kit (Biotinum, Inc.) was used. Five µL polyplex dispersion was added in a black polystyrene microplate (FLUOROTRAC™ 200, Greiner) followed by addition of 200 µL of working solution (quantitation solution/enhancer 50:1). After incubation at 450 rpm under orbital agitation (Titramax 100) for 10 minutes, sample fluorescence was measured at 485 nm excitation wavelength and 530 nm emission wavelength (SPARK 10M). Polyplexes formed with linear poly(ethylene imine) (PEI, 2,500 g/mol, Polysciences Europe GmbH) and pDNA at N/P ratio 20, pure polymer in saline and free pDNA in saline were used as controls. Furthermore, a mixture of 200 µL working solution and 5 µL saline solution served as blank. Based on the measured sample fluorescence (F), the relative fluorescence units (RFU) were calculated (**Equation 2**).

$$RFU = \frac{F(sample) - F(blank)}{F(pDNA_{only}) - F(blank)} \times 100\% \quad (2)$$

2.7 Size and Zeta Potential of Polyplexes

Hydrodynamic diameter and zeta potential of polyplexes were measured with the Zetasizer nano ZS (4 mW HeNe Laser, 633 nm, 173° backscatter, Malvern Instruments) at 25 °C. For all samples, the refractive index (1.33) and viscosity (0.8872 mPa·s) of dH₂O at 25 °C were used. The hydrodynamic diameter was determined in a micro cuvette (ZEN0040, Malvern) and the zeta potential in a high concentration cell (ZEN1010, Malvern), without dilution of the polyplex dispersions. Results were calculated using the Malvern Zetasizer software 7.11.

2.8 Protection against Enzymatic Degradation

To assess the protection ability of polymers for the pDNA against enzymatic degradation, 100 µL polyplex dispersion was treated with 2 µL deoxyribonuclease I (DNase I, 1.5 U/µg pDNA, AppliChem GmbH) solution (2.5 U/µL, 0.15 M NaCl, 20 mM MgCl₂, all Carl Roth) for 45 minutes at 37 °C. Subsequently, the enzyme was heat inactivated at 70 °C for 35 minutes, followed by the addition of 20 µL heparin solution (500 U/mL, 0.005 U/µg pDNA, AppliChem GmbH) and incubation for 20 minutes at 37 °C. As controls, pDNA with and without DNase I as well as untreated pDNA were used. Dissociation of polyplexes and structural integrity of pDNA were evaluated by horizontal agarose gel electrophoresis as described above.

2.9 In Vitro Transfection of Eukaryotic Cells

The transfection efficiency was determined based on a previous study.^[4] Chinese hamster ovary cells (CHO-K1, ACC 110, DSMZ) were seeded on 12-well polystyrene plates with 50,000 cells per well and incubated in cell culture medium (Hams F12 medium supplemented with L-glutamine, CLS, supplemented with 10 vol% FBS) at 37° C, 5% CO₂ and 95% relative

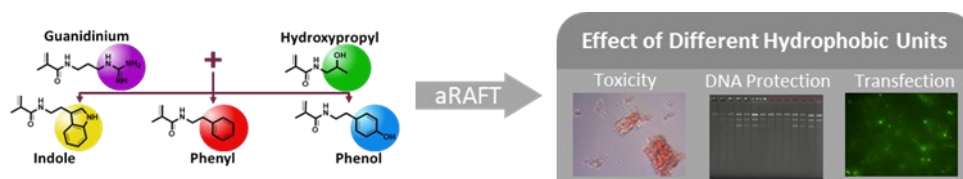
humidity for 24 hours. Subsequently, cells were washed with phosphate buffered saline (PBS pH 7.4, Carl Roth), and treated with 2 mL fresh cell culture medium and 200 μ L polyplex dispersion equivalent to 4 μ g pDNA. As controls, 200 μ L saline solution, 4 μ g free plasmid in saline, and IPEI/pDNA polyplexes at N/P ratio 20 were added to the cells. After four hours of incubation, cells were washed once with PBS, 2 mL fresh medium were added, and the incubation was continued for 44 hours. Afterwards, the cells were washed twice with PBS followed by lysis of the cells and performance of the luciferase assay (Luciferase Assay System, Promega). Protein amount in the cell lysate was quantified by the bicinchoninic acid assay (Pierce BCA Protein Assay Kit, Thermo Fisher) according to the manufacturer's protocol. To inactivate dithiothreitol (DTT) in the lysis reagent, 25 μ L of the cell lysate were treated with 10 μ L (0.05 M) iodoacetamide (AppliChem GmbH) for 20 minutes at 37° C. Both, the measurements for the luciferase expression assay and the BCA assay were carried out on a microplate reader (FLUOstar OPTIMA, BMG LABTECH GmbH). The luciferase expression was calculated as relative light units (RLU) per microgram protein.

References

- [1] C. W. Scales, Y. A. Vasilieva, A. J. Convertine, A. B. Lowe, C. L. McCormick, *Biomacromolecules* **2005**, *6*, 1846.
- [2] I. Tabujew, C. Freidel, B. Krieg, M. Helm, K. Koynov, K. Müllen, K. Peneva, *Macromolecular Rapid Communications* **2014**, *35*, 1191.
- [3] D. Fischer, H. Dautzenberg, K. Kunath, T. Kissel, *Int J Pharm* **2004**, *280*, 253.
- [4] S. Ochrimenko, A. Vollrath, L. Tauhardt, K. Kempe, S. Schubert, U. S. Schubert, D. Fischer, *Carbohydr Polym* **2014**, *113*, 597.

Publication P3

Indole, Phenyl, and Phenol Groups: The Role of the Comonomer on Gene Delivery in Guanidinium Containing Methacrylamide Terpolymers



F. J. Hack, C. Cokca, S. Städter, J. Hülsmann, K. Peneva, D. Fischer

Macromol. Rapid Commun. **2020**, *42* (8), 2000580



Indole, Phenyl, and Phenol Groups: The Role of the Comonomer on Gene Delivery in Guanidinium Containing Methacrylamide Terpolymers

Franz J. Hack, Ceren Cokca, Sebastian Städter, Juliana Hülsmann, Kalina Peneva,* and Dagmar Fischer*

This report highlights the importance of hydrophobic groups mimicking the side chains of aromatic amino acids, which are tryptophan, phenylalanine, and tyrosine, in guanidinium bearing poly(methacrylamide)s for the design of non-viral gene delivery agents. Guanidinium containing methacrylamide terpolymers are prepared by aqueous reversible addition–fragmentation chain transfer (aRAFT) polymerization with different hydrophobic monomers, *N*-(2-indolethyl) methacrylamide (IEMA), *N*-phenethylmethacrylamide (PhEMA), or *N*-(4-hydroxyphenethyl)methacrylamide (PhOHEMA) by aiming similar contents. The well-defined polymers are obtained with a molar mass of $\approx 15\,000\text{ g mol}^{-1}$ and ≈ 1.1 dispersity. All terpolymers demonstrate almost comparable *in vitro* cell viability and hemocompatibility profiles independent of the type of side chain. Although they all form positively charged, enzymatically stable polyplexes with plasmid DNA smaller than 200 nm, the incorporation of the IEMA monomer improve these parameters by demonstrating a higher DNA binding affinity and forming nanoassemblies of about 100 nm. These physicochemical characteristics are correlated with increased transfection rates in CHO-K1 cells dependent on the type of the monomer and the nitrogen to phosphate (N/P) ratio of the polyplexes, as determined by luciferase reporter gene assays.

The guanidinium group is composed of three amino groups bound to a central carbon atom and it is a planar Y-shaped quasi aromatic structure with a pK_a value of 13.6 in water, which is fully protonated in biological media.^[1,2] It acts as a hydrogen bond donor and strongly interacts with water molecules in the plane of guani-

dinium ion, while its π -faces remain hydrophobic as suggested by neutron diffraction and molecular dynamics simulations.^[3,4] Recently, the first experimental observation demonstrated that guanidinium ions form stable dimeric complexes in aqueous solution.^[5] These distinctive properties are sometimes referred to as “arginine” magic, in particular with regard to polyarginines or arginine-rich peptides such as HIV-1 transactivator of transcription (TAT) that can cross the cell membrane and have generated a lot of interest in the field of drug delivery.^[1–6] The strategy of incorporating guanidinium moieties to favorably influence the properties of a material is not limited to the field of peptide-mediated intracellular delivery, but it has also been exploited for the preparation of polymeric carriers for cell transfection, antimicrobial activity, and cell penetration.^[7–11] Many recent reports have shown that the addition of hydrophobic counterions or the incorporation of hydrophobic groups into peptides can improve membrane translocation, cellular uptake, polyplex stability, and mRNA or siRNA delivery.^[12,13] The cation- π interactions between the side chains of arginine and tryptophan, tyrosine, or phenylalanine play an important role in these processes.^[14,15] Considering the hydrophobic nature of the π -faces in guanidinium ions, such

F. J. Hack, J. Hülsmann, Prof. D. Fischer
Pharmaceutical Technology and Biopharmacy
Institute of Pharmacy
Friedrich Schiller University Jena
Lessingstrasse 8, Jena D-07743, Germany
E-mail: dagmar.fischer@uni-jena.de

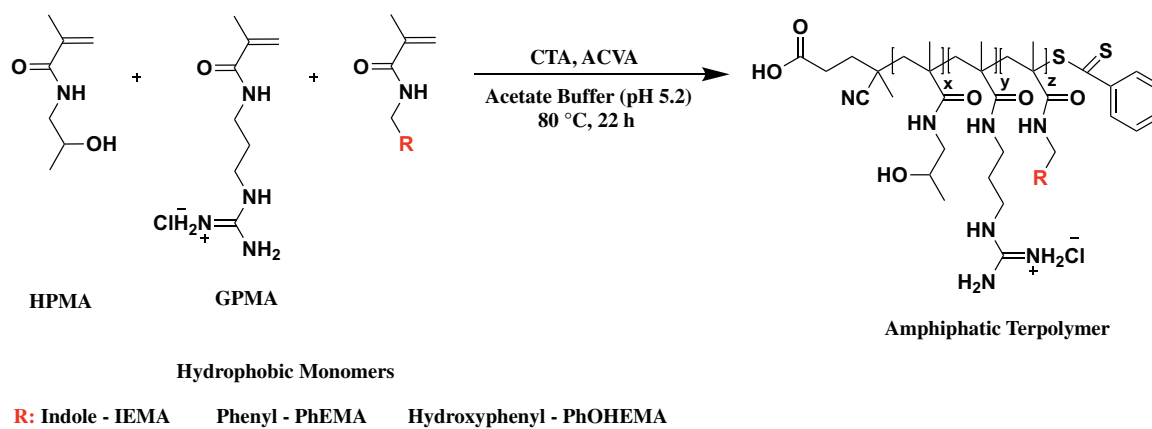
The ORCID identification number(s) for the author(s) of this article can be found under <https://doi.org/10.1002/marc.202000580>.

© 2020 The Authors. Macromolecular Rapid Communications published by Wiley-VCH GmbH. This is an open access article under the terms of the Creative Commons Attribution-NonCommercial-NoDerivs License, which permits use and distribution in any medium, provided the original work is properly cited, the use is non-commercial and no modifications or adaptations are made.

The copyright line for this article was changed on 14 January 2021 after original online publication.

DOI: 10.1002/marc.202000580

C. Cokca, S. Städter, Prof. K. Peneva
Institute of Organic Chemistry and Macromolecular Chemistry (IOMC)
Friedrich Schiller University Jena
Lessingstrasse 8, Jena D-07743, Germany
E-mail: kalina.peneva@uni-jena.de
Prof. K. Peneva, Prof. D. Fischer
Jena Center for Soft Matter (JCSM)
Friedrich Schiller University Jena
Philosophenweg 7, Jena D-07743, Germany



Scheme 1. aRAFT polymerization of guanidinium containing terpolymers with different hydrophobic monomers.

stacking against hydrophobic side chain in a protein could reduce the entropic cost of hydrophobic hydration. Jobin et al. showed that not only the number but also the nature and positioning of the hydrophobic residues are important for membrane translocation in arginine-rich cell-penetrating peptides.^[16] We recently reported that poly(methacrylamide)s with the content of guanidinium bearing monomers of 60% or higher can efficiently bind plasmid DNA (pDNA).^[17] Moreover, we revealed that the incorporation of indole comonomer mimicking the side chain of the amino acid tryptophan, leads to a 200-fold increase of the transgene expression in comparison to a copolymer with comparable guanidinium content.^[18] To understand to what extent the origin of the hydrophobic residue influences the internalization, complexation of pDNA, and the ability of the polymers to act as gene carriers, we designed terpolymers that contain side chains mimicking hydrophobic residues found in the side chains of amino acids.

Well-defined guanidinium containing methacrylamide terpolymers were prepared with different hydrophobic monomers, *N*-(2-indolethyl)methacrylamide (IEMA), *N*-Phenethylmethacrylamide (PhEMA) or *N*-(4-hydroxyphenethyl)methacrylamide (PhOHEMA), through aqueous reversible addition-fragmentation chain transfer (aRAFT) polymerization while keeping the hydrophobic monomer contents similar (≈ 4 mol%)

in each polymer structure (**Scheme 1**). The synthesis of monomers, polymers, and their physicochemical characterizations are described in detail in the supporting information. Briefly, predetermined amounts of HPMA and GPMA were placed in a 25 mL Schlenk flask and dissolved in degassed aqueous acetate buffer. The hydrophobic monomer was dissolved in DMF separately and slowly added to the reaction mixture followed by slow addition of 4-cyano-4-(phenylcarbonothioylthio) pentanoic acid (CTA) and 4,4'-azobis (4-cyano-pentanoic acid) (ACVA) solutions in DMF. The reaction was carried out at ≈ 80 °C for 22 h under argon. The resulting polymer was purified by dialysis in distilled water (dH₂O, pH 4) at 4 °C and dried by lyophilization. The monomer composition of the polymeric product was measured by ¹H NMR spectroscopy while the molar mass and dispersity index were determined by size exclusion chromatography (SEC_{DMAC}). The data are summarized in **Table 1**.

The safe and biocompatible application of the prepared terpolymers for gene delivery was investigated using the luminescence-based CellTiter-Glo assay on L-929 mouse fibroblasts as a standard cell line for toxicity testing, in concentrations ranging from 3.9 to 500 $\mu\text{g mL}^{-1}$ over 24 h (**Figure 1A**).^[19] Untreated cells were set as 100% negative control, whereas 0.02% thiomersal solution acted as the positive control reducing the

Table 1. Monomer contents, molar masses, and dispersity indices of the terpolymer samples.

	Poly(HPMA-co-GPMA-co-IEMA)	Poly(HPMA-co-GPMA-co-PhEMA)	Poly(HPMA-co-GPMA-co-PhOHEMA)
M_n Experimental [g mol^{-1}]	23 000	15 000	15 000
\bar{D}	1.07	1.14	1.07
HPMA [mol%]	21	12	12
GPMA [mol%]	75	84	85
IEMA [mol%]	4	–	–
PhEMA [mol%]	–	4	–
PhOHEMA [mol%]	–	–	3

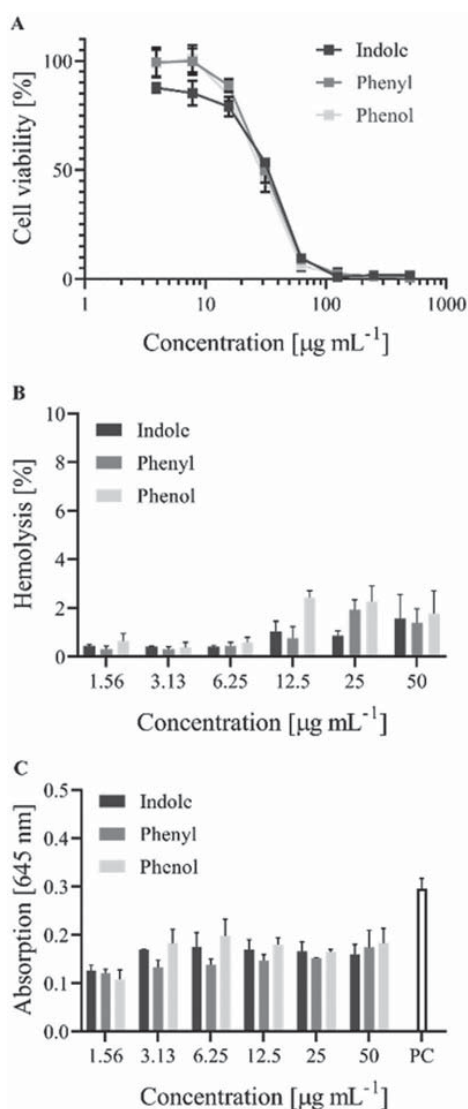


Figure 1. A) Concentration-dependent in vitro cell viability assay of the terpolymers (named according to their side chains) in L-929 mouse fibroblasts after 24 h using the CellTiter-Glo assay ($n = 8$, mean \pm SD). B) Dependency of hemolysis after 1 h incubation and C) sheep erythrocyte aggregation after 2 h incubation induced by the terpolymers on polymer concentration compared to 25 000 BPEI ($15 \mu\text{g mL}^{-1}$) (PC) ($n = 6$, mean \pm SD).

metabolic activity of the cells to $<1\%$. The three terpolymers revealed semilogarithmic curves with sigmoidal profiles and almost comparable IC_{50} values of 28.1, 33.0, and 34.7 $\mu\text{g mL}^{-1}$ for poly(HPMA-co-GPMA-co-IEMA), poly(HPMA-co-GPMA-co-PhEMA), and poly(HPMA-co-GPMA-co-PhOHEMA) terpolymers, respectively. The comparison of these data suggested no relevant influence of the type of the hydrophobic side chains.

Since the prepared terpolymers are intended for systemic administration, their compatibility with erythrocytes as the

most abundant particular component in the bloodstream was investigated. After 1 h, incubation of sheep red blood cells in the presence of terpolymers in varying concentrations of up to $50 \mu\text{g mL}^{-1}$, the spectrophotometric measurements of the hemoglobin release, a common marker for the damage of the erythrocyte membranes due to electrostatic interactions with the cationic polymers, revealed that mean values of hemolysis did not exceed 2% (Figure 1B). This can be categorized as non-hemolytic according to the ASTM F756-08 standard and these results reflect the data previously published for indole derivatives.^[18,19] The data were comparable to the HEPES buffered glucose (HBG) solution pH 7.4 which was set as a negative control (0.1%), whereas a Triton X-100 solution was used as a positive control (100%). Moreover, to avoid systemic complications like thrombosis and embolism due to a polycation induced aggregation of erythrocytes, the potential of the terpolymers to aggregate sheep red blood cells was investigated qualitatively by light microscopy including a classification in three stages, as well as quantitatively by UV-vis spectroscopy. As illustrated by light microscopic evaluation (Figure S12, Supporting Information), the negative control (HBG pH 7.4) did not cause any cell cluster formation (stage 1), whereas the positive control (25000 g mol^{-1} branched poly(ethylene imine), BPEI, $15 \mu\text{g mL}^{-1}$) induced the formation of large aggregates (stage 3).^[20,21] After a 2 h treatment, none of the terpolymers induced relevant red blood cell aggregating effects as indicated by a stage 1 classification in the light microscopy even at the highest tested concentration of $50 \mu\text{g mL}^{-1}$. This quantitative measurement is based on the principle that the diffuse light scattered at the cell membrane of free erythrocytes is reduced with increasing red blood cell aggregation, which leads to a decrease in the UV-vis absorption. Absorption values comparable to the negative control (absorption values of 0.15) were obtained for the terpolymers (Figure 1C). In all cyto- and hemocompatibility tests, the application of polymer controls excluded nonspecific polymer related effects.

To determine the optimal composition of the terpolymer with polyanionic pDNA in the polyplexes, the binding efficacy of the polymers driven by electrostatic interactions was determined by fluorescent dye exclusion measurement using the AccuBlue Quantification kit (Figure 2A) as well as by horizontal agarose gel electrophoresis (Figure S13).^[22] Naked pDNA demonstrated the highest fluorescence signals serving as 100% control representing the full accessibility of the pDNA for the intercalating dye, whereas polyplexes with linear PEI (LPEI; 2500 g mol^{-1}) at N/P ratio 20 acted as positive control with high binding affinities. The terpolymers in the absence of pDNA revealed no signals excluding non-specific polymer related effects. Although poly(HPMA-co-GPMA-co-IEMA) terpolymer was able to bind pDNA completely already at N/P ratio 1, the other terpolymers demonstrated a full dye exclusion at N/P ratio 2 with an efficacy comparable to the LPEI control. These findings correlate well with the results obtained from the gel electrophoresis experiments. The characteristic band pattern of pDNA with the most prominent open circular and supercoiled form disappeared at N/P ratio 1 for poly(HPMA-co-GPMA-co-IEMA) whereas at N/P ratio 2 for poly(HPMA-co-GPMA-co-PhEMA) and poly(HPMA-co-GPMA-co-PhOHEMA) terpolymers as a result of a completely inhibited movement in the electric

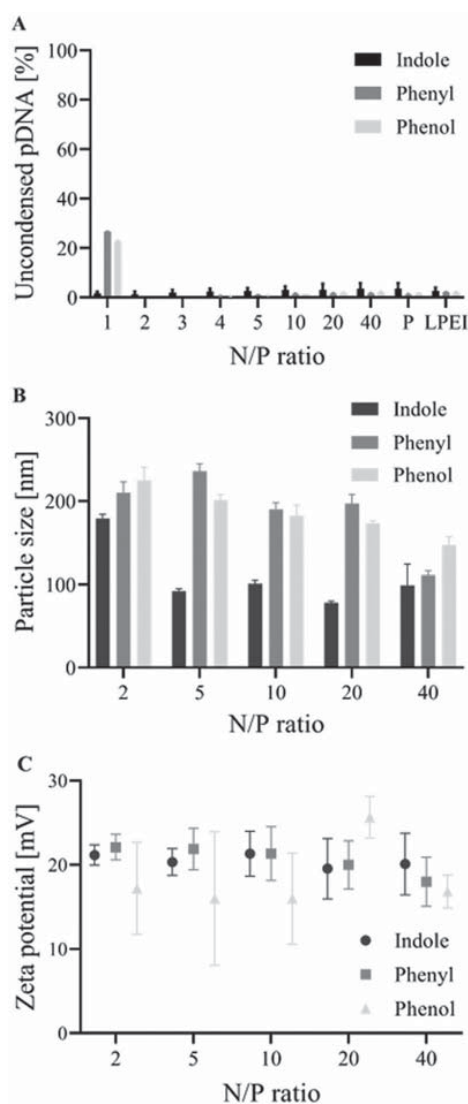


Figure 2. Physicochemical characterization of the polyplexes: A) Binding capacity [%] of the terpolymers (named according to their side chains) for pDNA depending on the N/P ratio determined by the AccuBlue Quantification in comparison to linear PEI (LPEI; 2500 g mol⁻¹, N/P 20) and free polymers (P) (*n* = 8, mean ± SD). B) Particle size measurements of the pDNA/terpolymer polyplexes using nanoparticle tracking analysis (mean ± SD measured in triplicates). C) Zeta potentials of polyplexes formed at different N/P ratios in water (WFI) and measured by laser Doppler anemometry in triplicates (mean ± SD).

field either by the increase in size and/or masking the anionic charge of pDNA due to the formation of polyplexes. The increase in N/P ratio is known to be correlated with more effective binding of genetic materials through cationic polymers.^[23] Additionally, the better binding performance of indole containing terpolymer is in good agreement with the reported data that show that indole modified low molecular

weight PEI has higher pDNA binding ability compared to its phenyl containing counterpart.^[24]

These binding characteristics of the terpolymers were also reflected in the reduction of the polyplex size as a function of N/P ratio in the range 2 to 40, as measured by nanoparticle tracking analysis (Figure 2B). The three terpolymers were able to form stable and nano-scaled polyplexes. Under comparable conditions, the indole containing terpolymer was characterized by the smallest polyplexes with mean particle sizes below 100 nm already at N/P 5, whereas the phenyl and phenol bearing terpolymers demonstrated a decrease in their sizes at higher N/P ratios. Conclusively, all terpolymers formed nanoassemblies in suitable size ranges below 200 nm for an efficient cell uptake and an intracellular processing of nanomaterials.^[25,26] Up to N/P ratio 10, the phenol bearing terpolymer was characterized by the lowest and highly variable cationic surface charges determined via zeta potential (Figure 2C) in contrast to the indole and phenyl containing terpolymers with zeta potentials around +20 mV independent of the N/P ratio, indicating an efficient electrostatic polyplex repulsion and inhibition in particle agglomeration.

The compact binding of pDNA by the terpolymers is a prerequisite to protect the polyplexes against in vivo enzymatic hydrolysis by the formation of an electrostatic and physical barrier.^[27] Using agarose gel electrophoresis, the stability of pDNA complexed with the prepared terpolymers at N/P ratios from 2 to 40 was confirmed after incubation with DNase I and displacement by heparin (Figure S14, Supporting Information). Even though untreated pDNA and pDNA treated without enzyme remained intact excluding unspecific degradation or destruction by the treatment per se, enzyme-treated free pDNA was completely degraded as shown by the disappearance of the characteristic bands. All terpolymers displayed protection of the pDNA against enzymatic hydrolysis already at N/P ratio 2 where a complete binding was shown in the assays described above. At N/P ratios 20 and 40, only a partial pDNA release from the complexes was observed as demonstrated by the fluorescence in the gel slot which is typical for polymers with a very high binding affinity. Changes in the topology of the pDNA are common for such procedures as reported in many other studies.^[27–29]

The influence of different side chains on transfection efficacy was determined by a luminescence-based reaction in eukaryotic CHO-K1 cells in the presence of serum using pGL3 pDNA/polyplexes with N/P ratios from 2 to 20 (Figure 3). No specific reaction was detected for free pDNA and the solvent 0.9% NaCl which were used as controls. The transfection efficacy increased with higher N/P ratios with poly(HPMA-co-GPMA-co-IEMA) > poly(HPMA-co-GPMA-co-PhOHEMA) > poly(HPMA-co-GPMA-co-PhEMA). By far the highest transfection potential was observed for the indole containing terpolymer corresponding to the highest binding activity and the smallest polyplex size as described above. For comparison, the positive control consisting of 2500 g mol⁻¹ linear PEI and pDNA at N/P ratio 20 was used as gold standard for gene transfection^[27] and reached a 2-fold higher transfection efficiency compared to the best performing indole-based terpolymer under the chosen conditions. The improved performance of the indole containing terpolymers is in a good agreement with the data reported

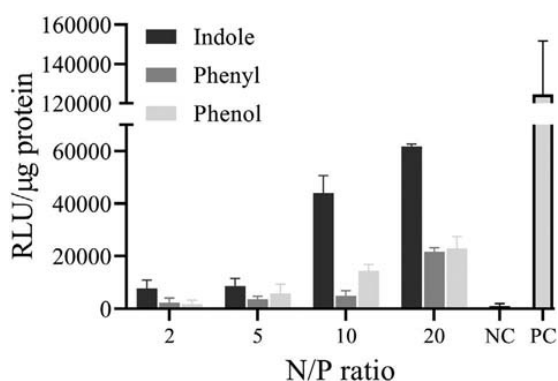


Figure 3. In vitro luciferase reporter gene expression of pGL3 DNA/terpolymer polyplexes at different N/P ratios in CHO-K1 cells compared to the positive control (PC) linear PEI (LPEI; 2500 g mol⁻¹, N/P 20). Experiments are performed in quadruplicates with free pDNA serving as a negative control (NC) (mean ± SD).

previously for tryptophane containing cell-penetrating peptides or indole-functionalized PEI polymers.^[30,31] The better transfection induced by the phenol bearing terpolymer compared to its phenyl counterpart can be related to the additional polar interactions (like the formation of counterions) or to the formation of OH-related hydrogen bonds with pDNA.^[31] More efficient release from the endosomal/lysosomal compartment as described by Chang et al.^[32] could be at play, as well. Further investigation is necessary to support either of these hypotheses.

In summary, well-defined guanidinium containing methacrylamide terpolymers were synthesized by *a*RAFT polymerization with comparable contents (≈4 mol%) of indole, phenyl, and phenol bearing methacrylamide monomers mimicking the hydrophobic residues of tryptophan, phenylalanine, and tyrosine and used to evaluate to what extent the identity of these hydrophobic groups can influence their pDNA binding, transfection, and polyplex toxicity. For all terpolymers, a marked cyto- and hemocompatibility was demonstrated even at high concentrations. Since all terpolymers gave comparable results in cell viability and hemotoxicity tests, with low content of hydrophobic groups compared to the content of guanidinium groups, the cationic residues appear to have a more pronounced effect on the toxicity than the identity of hydrophobic side chains. However, the transfection data highlighted the importance of the type of the side chain for effective gene transfer with indole bearing terpolymers, which performed the best. The physicochemical characteristics of the polyplexes revealed the formation of polyplexes with important small particle size, high positive surface charge, and the ability of efficient and protective pDNA binding. Conclusively, the careful selection of the type of side chains mimicking hydrophobic residues found in the side chains of tryptophan, phenylalanine, and tyrosine revealed a strong potential for the design of non-viral gene delivery agents. Future studies will focus on more detailed investigations of effects that different residues have on the interactions with cell membranes, endosomal/lysosomal pDNA release, and the intracellular behavior of the polyplexes.

Supporting Information

Supporting Information is available from the Wiley Online Library or from the author.

Acknowledgements

F.J.H. and C.C. contributed equally to this work. The authors would like to thank the Deutsche Forschungsgemeinschaft (DFG, German Research Foundation) – project number 316213987 – SFB 1278 (projects B03, Z01) and Angela Herre for her excellent technical support. The authors are grateful to Juliane Müller, Tina Liebernickel, and Alayham Mahfoud for helpful discussions. Correction added on 14 January 2021, after first online publication: Projekt Deal funding statement has been added.

Open access funding enabled and organized by Projekt DEAL.

Conflict of Interest

The authors declare no conflict of interest.

Keywords

gene delivery, guanidinium groups, hydrophobic groups, methacrylamide terpolymers

Received: October 1, 2020

Revised: October 28, 2020

Published online: December 4, 2020

- [1] M. Vazdar, J. Heyda, P. E. Mason, G. Tesei, C. Allolio, M. Lund, P. Jungwirth, *Acc. Chem. Res.* **2018**, *51*, 1455.
- [2] B. Xu, M. I. Jacobs, O. Kostko, M. Ahmed, *ChemPhysChem* **2017**, *18*, 1503.
- [3] J. B. Rothbard, T. C. Jessop, R. S. Lewis, B. A. Murray, P. A. Wender, *J. Am. Chem. Soc.* **2004**, *126*, 9506.
- [4] P. E. Mason, G. W. Neilson, C. E. Dempsey, A. C. Barnes, J. M. Cruickshank, *Proc. Natl. Acad. Sci. U. S. A.* **2003**, *100*, 4557.
- [5] M. J. Hebert, D. H. Russell, *J. Phys. Chem. Lett.* **2019**, *10*, 1349.
- [6] M. Green, P. M. Loewenstein, *Cell* **1988**, *55*, 1179.
- [7] K. Koschek, M. Dathe, J. Rademann, *ChemBioChem* **2013**, *14*, 1982.
- [8] L. Martin, R. Peltier, A. Kuroki, J. S. Town, S. Perrier, *Biomacromolecules* **2018**, *19*, 3190.
- [9] B. M. deRonde, G. N. Tew, *Biopolymers* **2015**, *104*, 265.
- [10] J. M. Sarapas, C. M. Backlund, B. M. deRonde, L. M. Minter, G. N. Tew, *Chemistry* **2017**, *23*, 6858.
- [11] Z. Tan, Y. Jiang, W. Zhang, L. Karls, T. P. Lodge, T. M. Reineke, *J. Am. Chem. Soc.* **2019**, *141*, 15804.
- [12] B. M. deRonde, N. D. Posey, R. Otter, L. M. Caffrey, L. M. Minter, G. N. Tew, *Biomacromolecules* **2016**, *17*, 1969.
- [13] C. M. Backlund, L. Parhamifar, L. Minter, G. N. Tew, T. L. Andresen, *Mol. Pharmaceutics* **2019**, *16*, 2462.
- [14] H. J. Kim, S. Ogura, T. Otabe, R. Kamegawa, M. Sato, K. Kataoka, K. Miyata, *ACS Cent. Sci.* **2019**, *5*, 1866.
- [15] K. Kempe, A. Vollrath, H. W. Schaefer, T. G. Poehlmann, C. Biskup, R. Hoogenboom, S. Hornig, U. S. Schubert, *Macromol. Rapid Commun.* **2010**, *31*, 1869.
- [16] M.-L. Jobin, M. Blanchet, S. Henry, S. Chaignepain, C. Manigand, S. Castano, S. Lecomte, F. Burlina, S. Sagan, I. D. Alves, *Biochim. Biophys. Acta, Biomembr.* **2015**, *1848*, 593.
- [17] I. Tabujew, C. Cokca, L. Zartner, U. S. Schubert, I. Nischang, D. Fischer, K. Peneva, *J. Mater. Chem. B* **2019**, *7*, 5920.



- [18] C. Cokca, L. Zartner, I. Tabujew, D. Fischer, K. Peneva, *Macromol. Rapid Commun.* **2020**, *41*, 1900668.
- [19] ASTM F756, *Annual Book of ASTM Standards*, Vol. 13. 01, ASTM, Philadelphia **2013**.
- [20] M. Bauer, C. Lautenschlaeger, K. Kempe, L. Tauhardt, U. S. Schubert, D. Fischer, *Macromol. Biosci.* **2012**, *12*, 986.
- [21] DIN EN ISO 10993-5:2009-10, Biological evaluation of medical devices - Part5: Test for in vitro cytotoxicity, *European Standard EN ISO 10993-5, Brussels* **2009**.
- [22] M. Zink, K. Hotzel, U. S. Schubert, T. Heinze, D. Fischer, *Macromol. Biosci.* **2019**, *19*, 1900085.
- [23] D. Fischer, T. Bieber, Y. Li, H.-P. Elsässer, T. Kissel, *Pharm. Res.* **1999**, *16*, 1273.
- [24] Q.-Y. Yu, Y.-R. Zhan, J. Zhang, C.-R. Luan, B. Wang, X.-Q. Yu, *Polymers* **2017**, *9*, 362.
- [25] Z. Chen, W. Huang, N. Zheng, Y. Bai, P. Chem, *Polym. Chem.* **2020**, *11*, 664.
- [26] R. Bhattacharya, B. Osburg, D. Fischer, U. Bickel, *Pharm. Res.* **2008**, *25*, 605.
- [27] S. Ochrimenko, A. Vollrath, L. Tauhardt, K. Kempe, S. Schubert, U. S. Schubert, D. Fischer, *Carbohydr. Polym.* **2014**, *113*, 597.
- [28] D. Fischer, H. Dautzenberg, K. Kunath, T. Kissel, *Int. J. Pharm.* **2004**, *280*, 253.
- [29] C. L. Gebhart, S. Sriadibhatla, S. Vinogradov, P. Lemieux, V. Alakhov, A. V. Kabanov, *Bioconjugate Chem.* **2002**, *13*, 937.
- [30] Z. Kang, G. Ding, Z. Meng, Q. Meng, *Peptides* **2019**, *121*, 170149.
- [31] K. Kono, H. Akiyama, T. Takahashi, T. Takagishi, A. Harada, *Bioconjugate Chem.* **2005**, *16*, 208.
- [32] H. Chang, J. Zhang, H. Wang, J. Lv, Y. Cheng, *Biomacromolecules* **2017**, *18*, 2371.

Ä!"#Ä\$%&'(Ä)*+Ä,-.+



/011234%56Ä75823-94%25

823Ä Macromol. Rapid Commun., ;7<Ä#=#""!>-93?=!""@A"

75B2&'CÄDE'5(&CÄ95BÄDE'52&Ä,3201F<ÄGE'ÄH2&'Ä28
4E'Ä*2-252-'3Ä25Ä,'5'Ä:'&%I'3(Ä%5Ä,095%B%5%0-
*2549%5%564E9?3(&9-%BG312&(-'3F

K395LÄM=Ä+9?NCÄ*'3'5Ä*2N?9CÄ/'.9F4%95Ä/4OB4'3CÄM0&%959
+P&F-955CÄQ9&%59ÄD'5'I9CRÄ95BÄ:96-93ÄK%F?E'3R

Copyright WILEY-VCH Verlag GmbH & Co. KGaA, 69469 Weinheim, Germany, 2018.

Supporting Information

Indole, Phenyl and Phenol Groups - the Role of the Comonomer on Gene Delivery in Guanidinium Containing Methacrylamide Terpolymers

Franz J. Hack; Ceren Cokca; Sebastian Städter; Juliana Hülsmann; Kalina Peneva and Dagmar Fischer**

1. Materials and Methods

All chemicals were purchased from SIGMA-Aldrich at the highest available purity and used as received unless mentioned otherwise. 4,4'-azobis(4-cyanovaleric acid) (ACVA) was recrystallized in methanol before use. The chain transfer agent 4-(((2-carboxyethyl)thio)carbonothioyl)thio)-4-cyanopentanoic acid (CTA) was purchased from Boron Molecular INC.

1.1 Synthesis of the Monomers

N-(3-guanidinopropyl)methacrylamide (GPMA):

The synthesis has already been shown in our previous work.^[1] ¹H NMR (300 MHz, D₂O, 298 K): δH (ppm)= 1.63 (m, 2H); 1.71 (s, 3H); 3.02 (t, 2H); 3.12 (t, 2H); 5.23 (s, 1H); 5.49 (s, 1H).

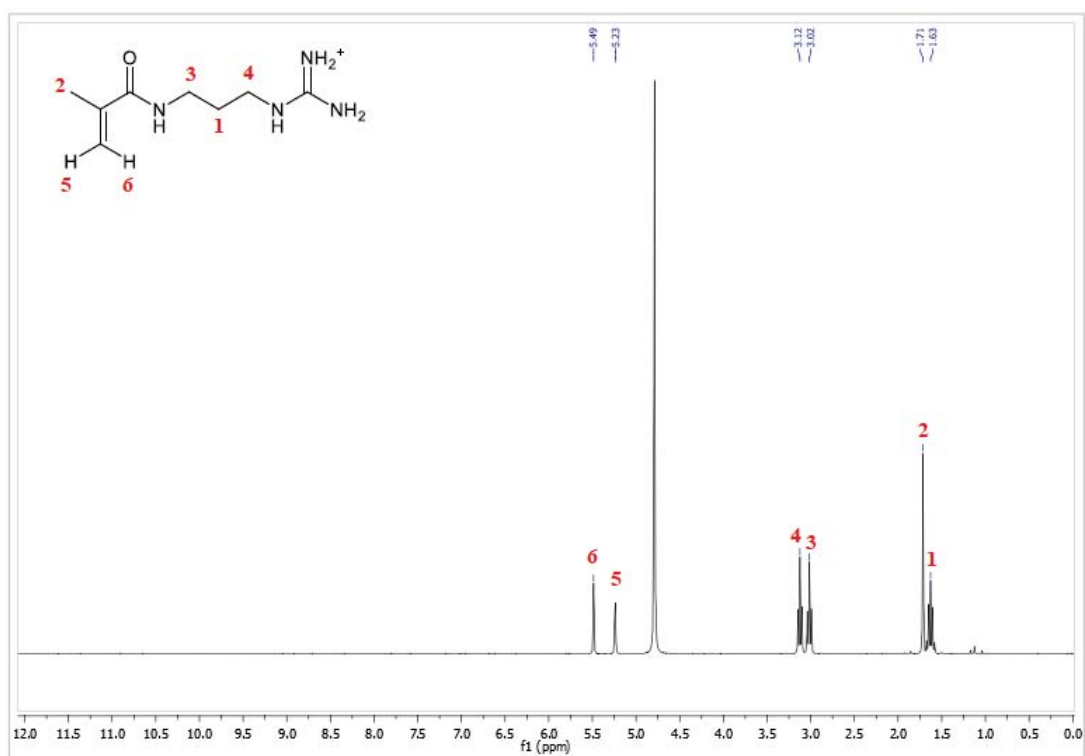
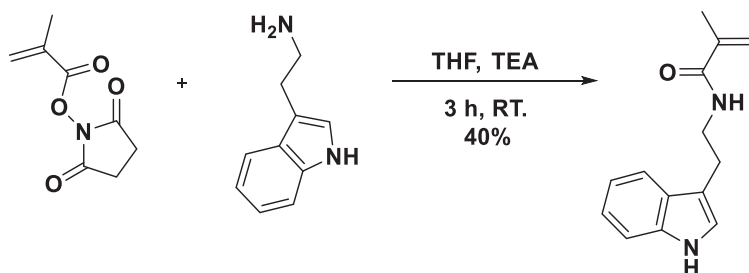


Figure S1. ¹H NMR spectrum of *N*-(3-guanidinopropyl)methacrylamide (GPMA) (300 MHz, D₂O, 298 K)

***N*-(2-indolethly)methacrylamide (IEMA):**

The synthesis was carried out under protective gas using dry solvents. 1.76 g (10.97 mmol) tryptamine was dissolved in 40 mL dry tetrahydrofuran (THF) and 1.17 g (1.60 mL; 11.54 mmol) triethylamine (TEA) was added. After that, a solution of 10 mL dry THF and 2.01 g (10.97 mmol) *N*-succinimidyl methacrylate were added dropwise to the reaction mixture and stirred for 3 hours at room temperature under inert atmosphere. Afterwards, the solvent was removed by cold distillation and the product was purified by column chromatography (n-Hexane/ EtOAc: 1/2). The product was isolated as an orange solid. Isolated yield: 0.70 g (4.39 mmol, 40 %). ¹H NMR (250 MHz, d₆-DMSO, 298 K): δH (ppm)= 10.79 (s, 1H); 8.02 (t, 1H); 7.53 (d, 1H); 7.31 (d, 1H); 7.14 (d, 1H); 7.06 (t, 1H); 6.97 (t, 1H); 5.64 (s, 1H); 5.31 (s, 1H); 3.43 (m, 2H); 2.85 (t, 2H); 1.85 (s, 3H).



Scheme S1. Synthesis of *N*-(2-indolethly)methacrylamide (IEMA)

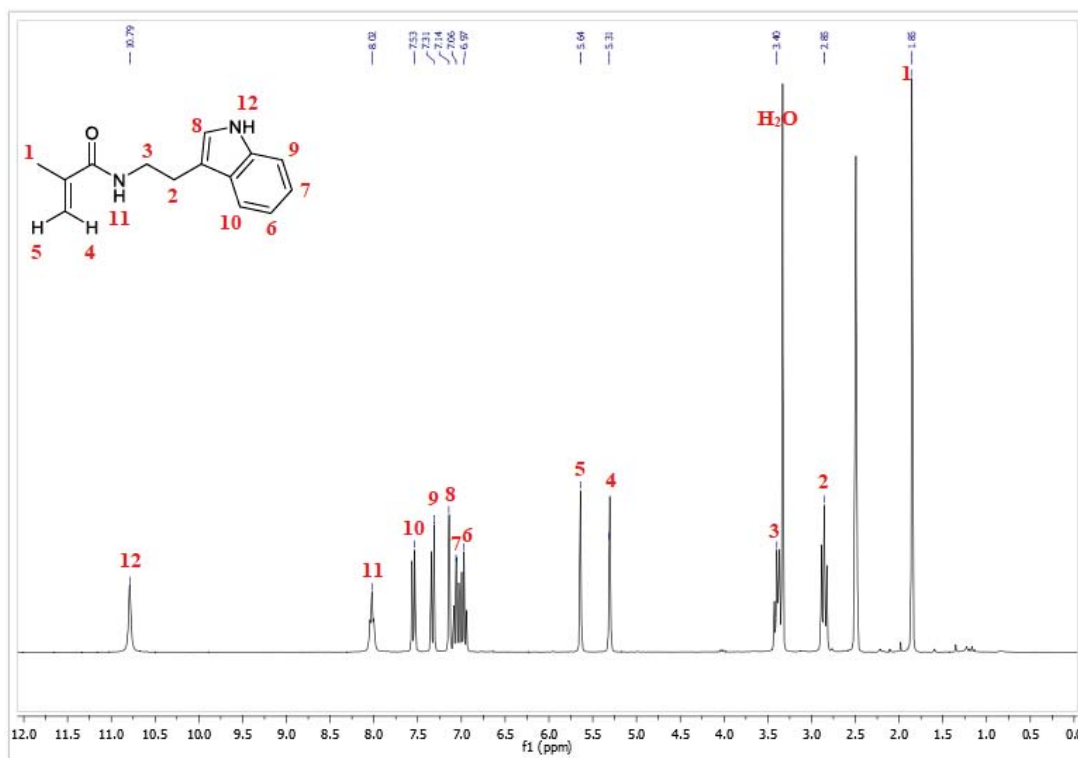


Figure S2. ^1H NMR spectrum of *N*-(2-indolethyl)methacrylamide (IEMA) (250 MHz, d_6 -DMSO, 298 K)

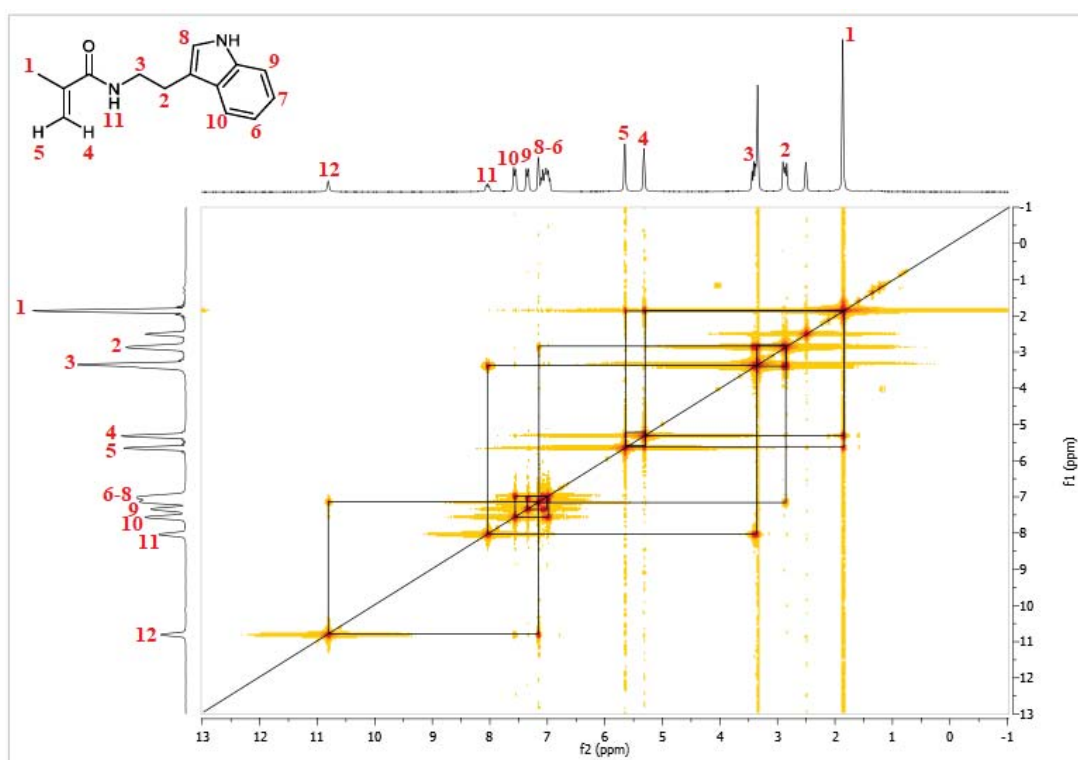
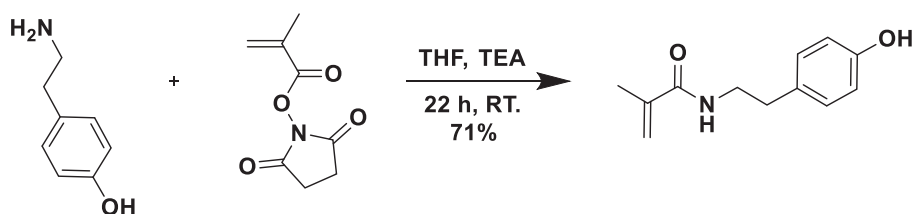


Figure S3. ^1H , ^1H -COSY-Spectrum of IEMA (250 MHz, d_6 -DMSO, 298 K)

***N*-(4-Hydroxyphenethyl)methacrylamide (PhOHEMA):**

0.38 g (2.74 mmol) of tyramine was dissolved in 20 mL of dry THF and 0.28 g (0.38 mL, 2.74 mmol) of TEA was added. In a separate flask, a solution of 4 mL of dry THF and 0.50 g (2.73 mmol) of *N*-succinimidyl methacrylate was prepared. Afterwards, this solution was added dropwise to tyramine and TEA containing solution and the reaction mixture was stirred at room temperature for 22 hours under argon flow. The solvent was removed by cold distillation and the product was purified by column chromatography (DCM/ EtOAc: 7/10). The product was obtained as dark yellow solid. Isolated yield: 0.27 g (1.95 mmol, 71%). ¹H NMR (250 MHz, d₆-DMSO, 298 K): δH (ppm)= 9,15 (s, 1H); 7,93 (t, 1H); 6,95 (d, 2H); 6,68 (d, 2H); 5,60 (s, 1H); 5,28 (s, 1H); 3,26 (m, 2H); 2,61 (t, 2H); 1,82 (s, 3H).



Scheme S2. Synthesis of *N*-(4-hydroxyphenethyl)methacrylamide (PhOHEMA)

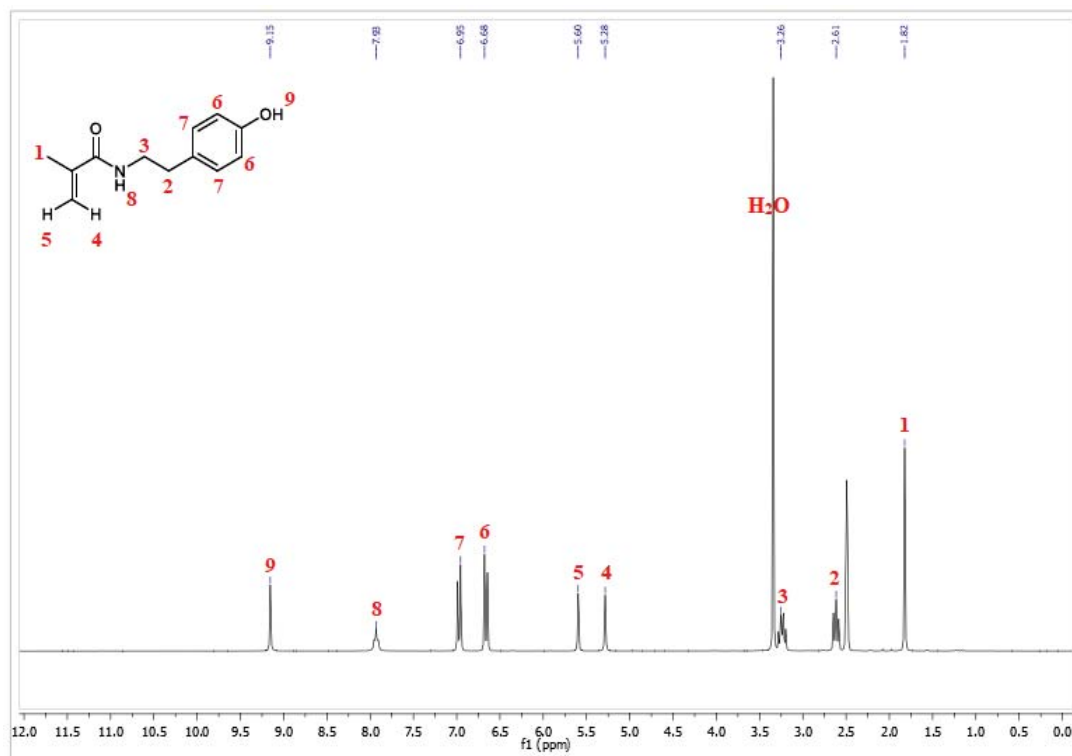


Figure S4. ^1H NMR spectrum of *N*-(4-hydroxyphenethyl)methacrylamide (PhOHEMA) (250 MHz, d_6 -DMSO, 298 K)

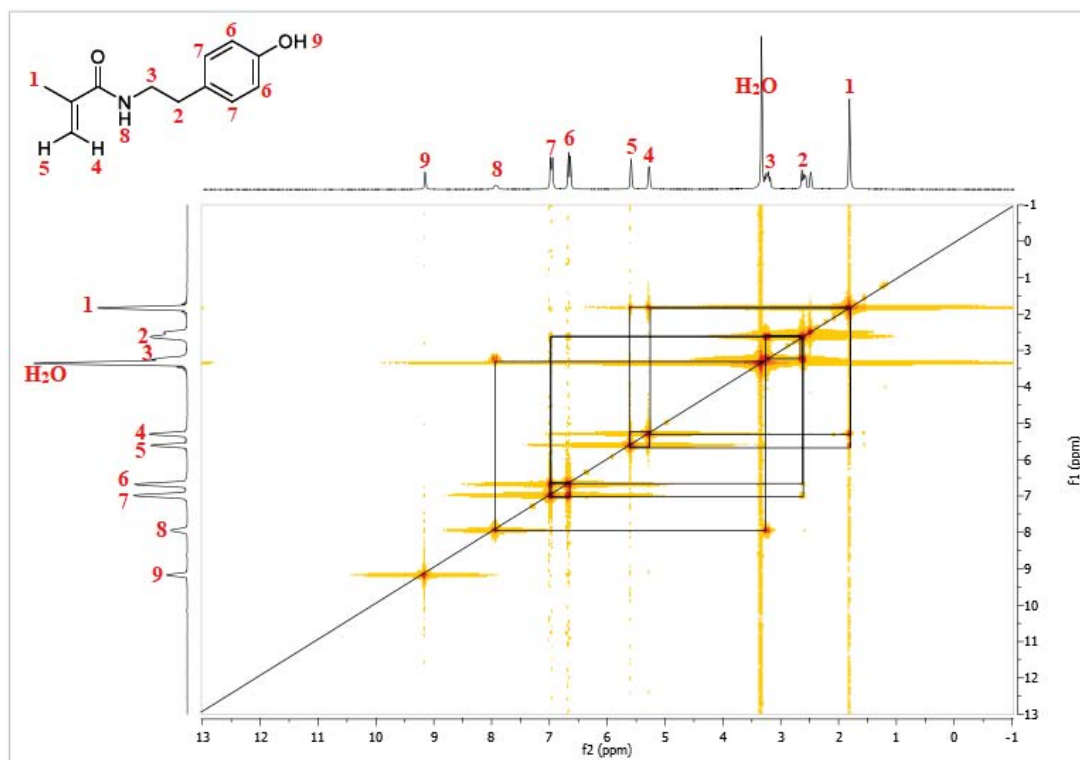
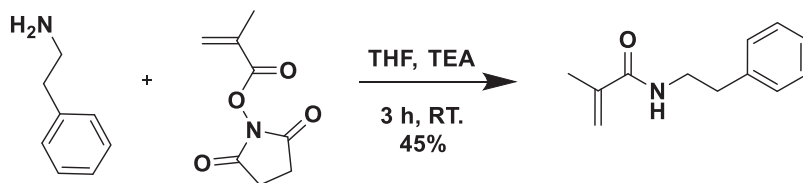


Figure S5. ^1H , ^1H -COSY-Spectrum of PhOHEMA (250 MHz, d_6 -DMSO, 298 K)

***N*-Phenethylmethacrylamide (PhEMA):**

1.64 g (1.7 mL, 13.53 mmol) of phenethylamine was added to 40 mL of dry THF. Then, 1.31 g (1.8 mL, 12.99 mmol) of TEA was put in this mixture. After that, separately prepared a solution of 10 mL of dry THF and 2.48 g (13.54 mmol) of *N*-succinimidyl methacrylate was added dropwise into the reaction mixture. The reaction was stirred at room temperature under argon flow for 3 hours. The solvent was removed by cold distillation, next 50 mL dichloromethane (DCM) was added and the solution was washed 3 times with 0.03 M hydrochloric acid (HCl), 2 times with saturated sodium carbonate (Na₂CO₃), and 2 times with distilled water (dH₂O). The solution was dried over sodium sulphate (Na₂SO₄) and the solvent was removed under vacuum. The product was obtained as white solid. Isolated yield: 0.74 g (6.09 mmol, 45%). ¹H NMR (250 MHz, d6-DMSO, 298 K): δH (ppm)= 8.00 (s, 1H); 7.27 (d, 2H); 7.22 (t, 2H); 7.20 (t, 1H); 5.62 (s, 1H); 5.31 (s, 1H); 3.31 (m, 2H); 2.76 (t, 2H); 1.84 (s, 3H).



Scheme S3. Synthesis of *N*-phenethylmethacrylamide (PhEMA)

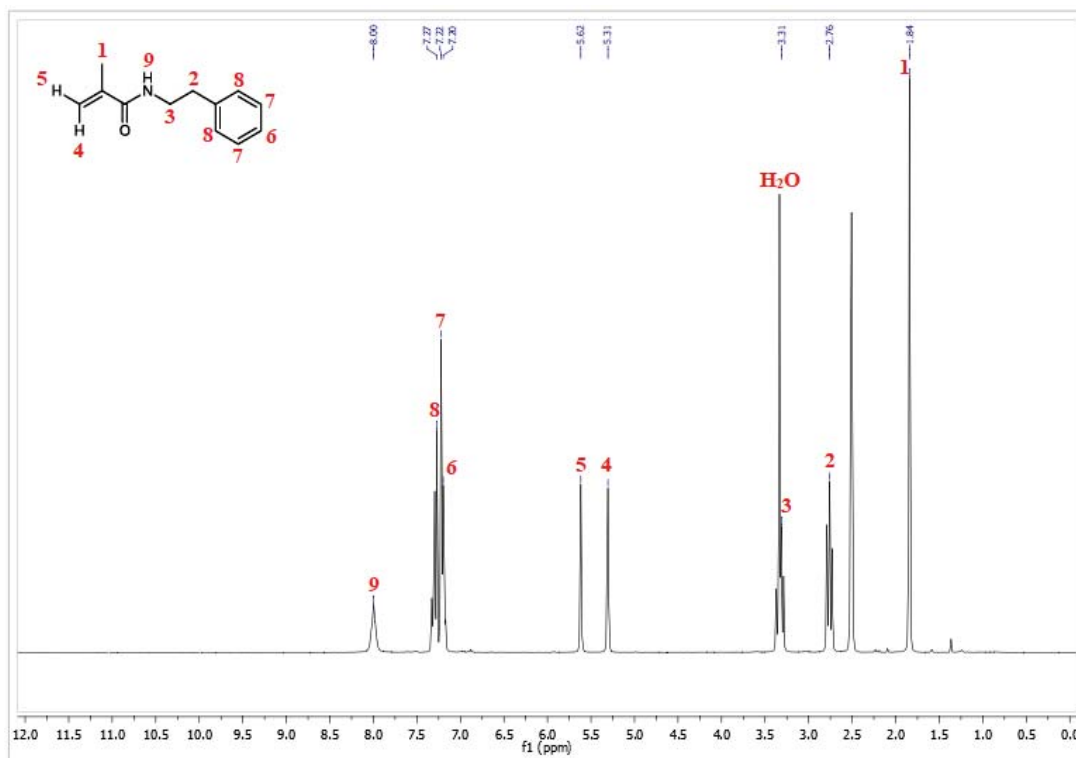


Figure S6. ^1H NMR spectrum of *N*-phenethylmethacrylamide (PhEMA) (250 MHz, d_6 -DMSO, 298K)

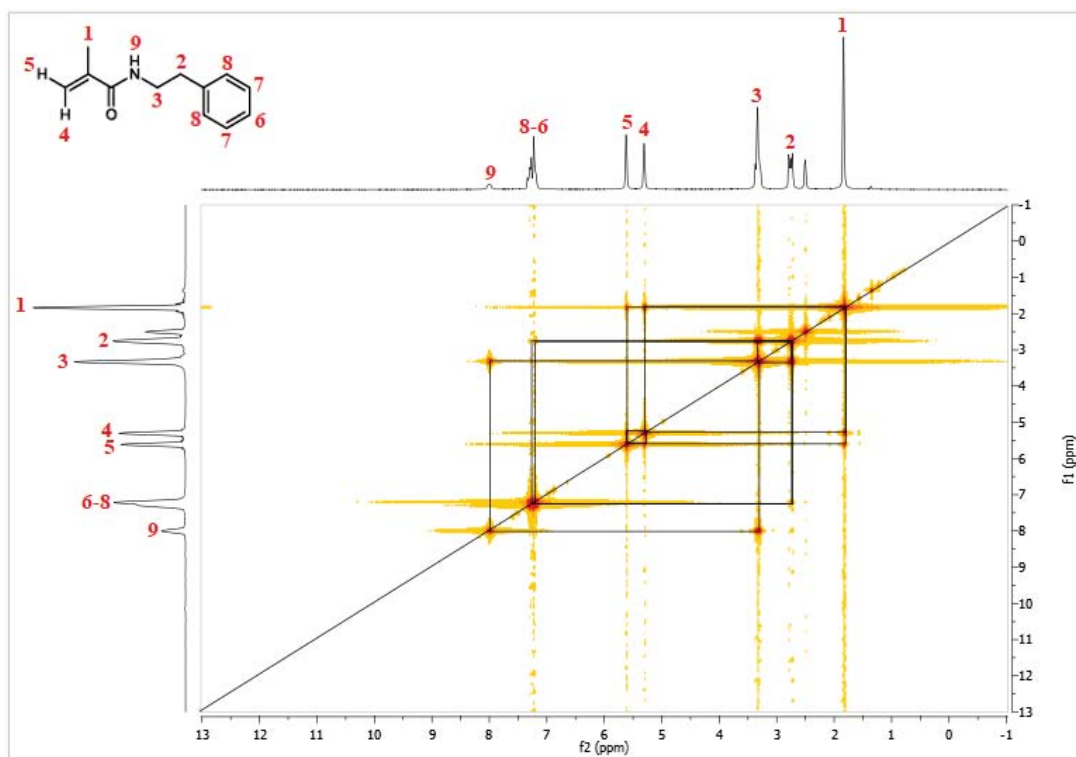


Figure S7. ^1H , ^1H -COSY-Spectrum of PhEMA (250 MHz, d_6 -DMSO, 298 K)

1.2 Synthesis and Characterization of the Polymers

1.2.1 Synthesis of Amphipathic Terpolymers

The polymers were synthesized through aqueous reversible addition-fragmentation chain-transfer (*a*RAFT) polymerization. Predetermined amount of HPMA and GPMA were placed in a 25 mL Schlenk flask and dissolved in degassed acetate buffer. The hydrophobic monomer was dissolved in DMF separately and slowly added to the reaction mixture. After that, 4-cyano-4-(phenylcarbonothioylthio) pentanoic acid (CTA) and then 4,4'-azobis (4-cyano-pentanoic acid) (ACVA) dissolved in DMF were slowly added. The reaction was conducted at 80 °C for 22 hours under argon. The product was then purified by dialysis in distilled water (dH₂O) (pH 4) at 4 °C. Finally, the polymer samples were dried through lyophilization. The monomer content was analysed by ¹H NMR spectroscopy. The molar mass and dispersity index were detected by means of SEC_{DMAC}.

Table 1: The amounts used for polymerization reactions

	Poly(HPMA-co-GPMA-co-IEMA)	Poly(HPMA-co-GPMA-co-PhEMA)	Poly(HPMA-co-GPMA-co-PhOHEMA)
Acetate Buffer (1M, pH 5.2)	1.16 mL	1.10 mL	1.10 mL
CTA	1.67 mg 5.98 μmol	1.3 mg 4.66 μmol	1.3 mg 4.66 μmol
ACVA	0.56 mg 2.00 μmol	0.98 mg 3.50 μmol	0.46 mg 1.64 μmol
HPMA	12.0 mg 83.80 μmol	8.0 mg 55.87 μmol	7.5 mg 52.38 μmol
GPMA	220 mg 742.59 μmol	225 mg 752.63 μmol	233 mg 786.4 μmol
IEMA	8.35 mg 36.57 μmol 45 $\mu\text{L DMF}$	-	-
PhEMA	-	4.40 mg 23.25 μmol 45 $\mu\text{L DMF}$	-
PhOHEMA	-	-	4.70 mg 22.90 μmol 45 $\mu\text{L DMF}$

1.2.2 ^1H NMR Characterization of Polymers

The monomer compositions of the polymer samples were determined by a Bruker WS 400 MHz spectrometer (controller: Bruker Avance III) in D_2O at 298 K.

Poly(HPMA-co-GPMA-co-IEMA)

^1H NMR (400 MHz, D_2O , 298 K): δH (ppm)= 8.00-7.11 (5H from indole group; 5H from phenyl group of CTA), 3.92 (1H from the side chain of the HPMA), 3.64-2.88 (2H from HPMA, 4H from IEMA, 4H from GPMA side chains), 2.11-1.50 (6H from the backbone, 2H from the side chain of the GPMA); 1.40-0.40 (12H from the backbone, 3H from the side chain of the HPMA).

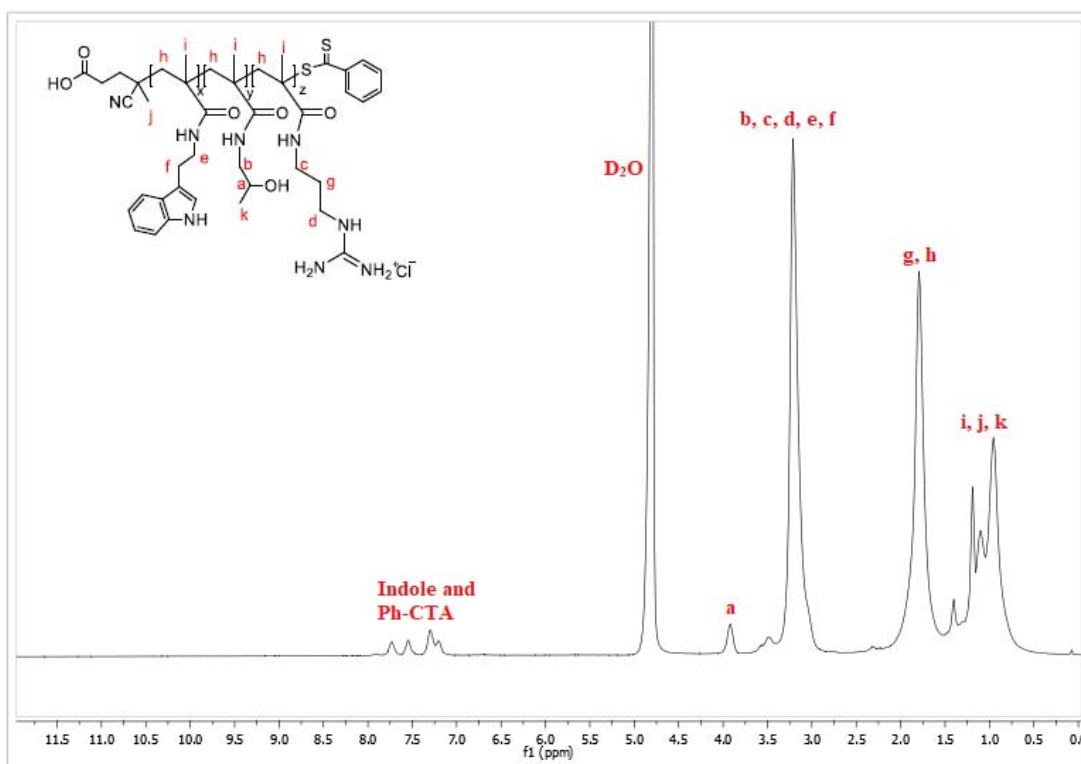


Figure S8. ^1H NMR spectrum of Poly(HPMA-co-GPMA-co-IEMA) (400 MHz, D_2O , 298 K)

Poly(HPMA-co-GPMA-co-PhEMA)

^1H NMR (400 MHz, D_2O , 298 K): δH (ppm)= 7.43-7.16 (5H from the phenyl group of the PhEMA), 3.83 (1H from the side chain of the HPMA), 3.50-2.65 (2H from HPMA, 4H from PhEMA, 4H from GPMA side chains), 2.11-1.39 (6H from the backbone, 2H from the side chain of the GPMA), 1.21-0.40 (12H from the backbone, 3H from the side chain of the HPMA).

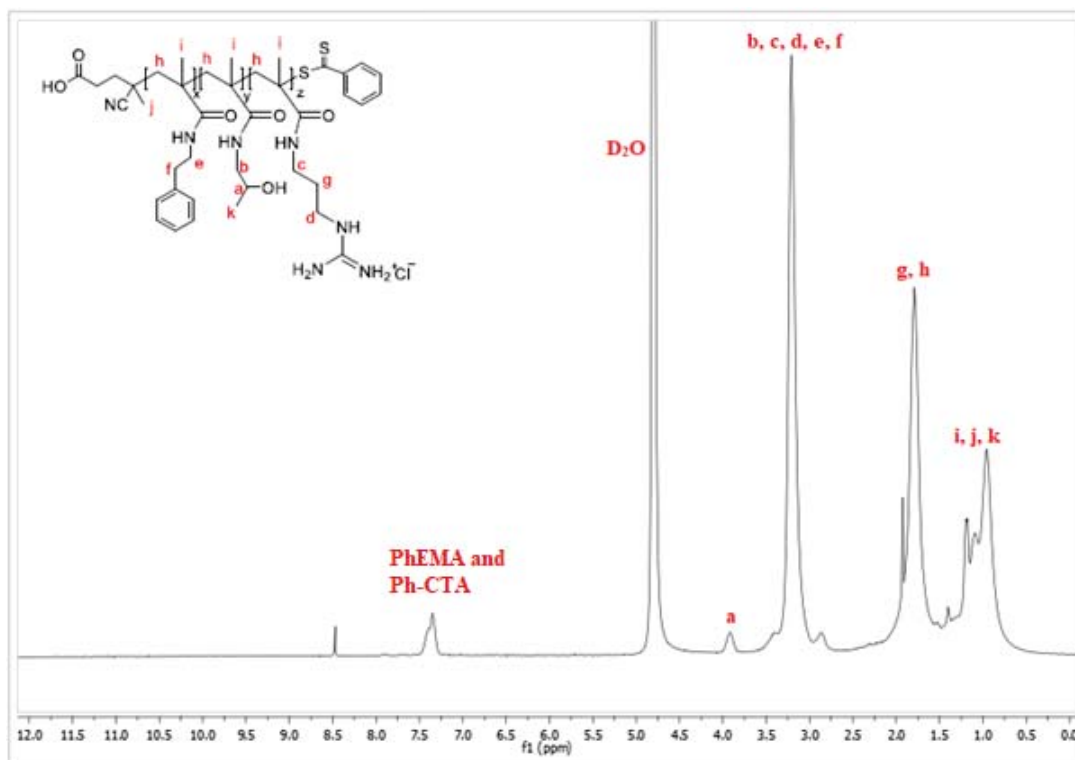


Figure S9. ^1H NMR spectrum of Poly(HPMA-co-GPMA-co-PhEMA) (400 MHz, D_2O , 298 K)

Poly(HPMA-co-GPMA-co-PhOHEMA)

^1H NMR (400 MHz, D_2O , 298 K): δH (ppm)= 7.11 (2H from the aromatic of PhOHEMA), 6.82 (2H from the aromatic of PhOHEMA), 3.83 (1H from the side chain of the HPMA), 3.45-2.59 (2H from HPMA, 4H from PhOHEMA, 4H from GPMA side chains), 2.03-1.49 (6H from the backbone, 2H from the side chain of the GPMA), 1.27-0.47 (12H from the backbone, 3H from the side chain of the HPMA).

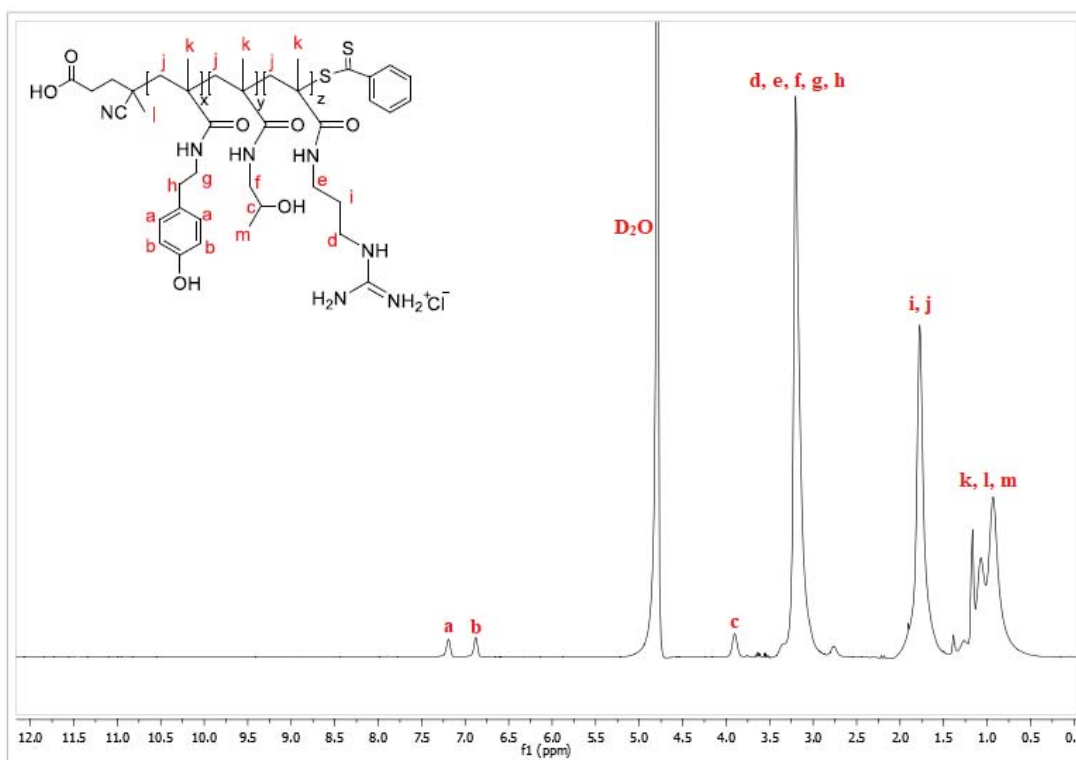


Figure S10. ^1H NMR spectrum of Poly(HPMA-co-GPMA-co- PhOHEMA) (400 MHz, D_2O , 298 K)

1.2.3 Size Exclusion Chromatography

The molar mass of terpolymers were characterized by SEC_{DMAc} conducted with dimethylacetamide and lithium chloride (DMAc + 0.21% LiCl) as the eluent at 40 °C with the flow rate of 1 mL/min using a PSS GRAM guard/1000/30 Å column (particle size: 10 µm). The refractive index detector (G1362A) and the UV Detector (G1315D, wavelength: 310 nm) were used to monitor the elution. The molar mass was determined in comparison of a calibration with poly(methyl methacrylate) (PMMA) standards.

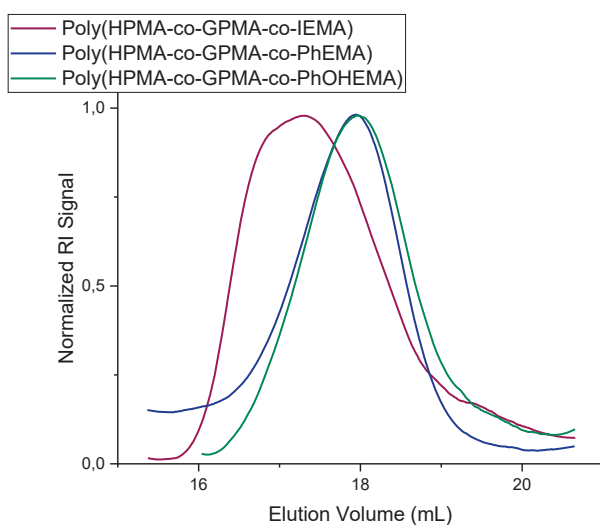


Figure S11. SEC_{DMAc} Traces of the Polymers

1.3 *In Vitro* Cytotoxicity

The *in vitro* cytotoxicity of the polymers was tested using the CellTiter-Glo[®] Luminescent Cell Viability Assay (Promega Corporation, Madison, USA) following the manufacturer's instructions. The assay was performed with 8 500/ well L-929 mouse fibroblasts (ACC 2, DSMZ-German Collection of Microorganisms and Cell Cultures GmbH, Braunschweig, Germany) in 96-well plates after 24 h pre-incubation in Roswell Park Memorial Institute (RPMI) cell culture medium supplemented with 1% L-glutamine and 10% fetal bovine serum (FBS) (Gibco, ThermoFisher[™] Scientific, Darmstadt, Germany). Cells were treated with 100 μL polymer solution with concentrations ranging from 3.9 to 500 $\mu\text{g mL}^{-1}$ in cell culture medium. 100 μL of the CellTiter-Glo[®] reagent were added after 24 h followed by 10 min incubation. Afterwards, luminescence was measured using the Tecan Spark M20 (Tecan Group AG, Männedorf, Switzerland). Thiomersal (0.02%, Caelo, Hilden, Germany) was used as positive control, whereas non-treated cells were considered as negative control. Cell culture medium without cells was treated as blank and RPMI medium with polymer only was performed as control to exclude unspecific reactions between the polymer and the assay. Cell viability was calculated as percentage of the negative control after subtraction of the blank values from all values measured and calculated as mean \pm SD.^[2] A cell viability \leq 70% was considered as toxic according to DIN EN ISO 10993-5.^[3]

1.4 *In Vitro* Hemocompatibility

Hemolysis and red blood cell (RBC) aggregation were tested following the methods of Bauer et al.^[2] Fresh heparinized full blood from sheep was pooled and centrifuged 3x at 2 880x g for 7 min to isolate the RBC's. All procedures with the sheep blood were approved by the Department for Animal Welfare of the Thuringian State Authority in compliance with the National Animal Protection Act (registration number: UKJ-18-101). A stock solution of 1.8 Mio RBC μL^{-1} with HEPES buffered glucose (HBG) solution containing 5% glucose and

10 mM HEPES (both Carl Roth, Karlsruhe, Germany) at pH 7.4 was prepared. To quantify hemolysis, polymers in concentrations between 1.56 and 50 $\mu\text{g mL}^{-1}$ were added to 200 μL of 1.8 Mio RBC μL^{-1} in 96-deepwell plates (Greiner bio-one) at 37 °C under shaking conditions (450 rpm) for 1 h. Triton X-100 (0.1%, Ferak, Berlin, Germany) was used as positive control and HBG buffer as negative control. After centrifugation (2880 x g, 7 min) supernatants were collected and measured at 544 nm using the Tecan Spark M20.

Following the ASTM F756-08 standard, values < 2% were considered as non-hemolytic, 2 to 5% as slightly hemolytic, and values > 5% as hemolytic.^[4] Results were calculated as percentage of the positive control after subtraction of the blank according to the following equation:

$$\text{Hemolysis [\%]} = \frac{(Abs_{\text{sample}} - Abs_{\text{sample control}}) - (Abs_{\text{negative control}} - Abs_{\text{blank}})}{Abs_{\text{positive control}} - Abs_{\text{blank}}} \times 100$$

For RBC aggregation testing 20×10^6 erythrocytes per mL were treated with polymer solutions in serial dilutions (1.56 to 50 $\mu\text{g mL}^{-1}$) compared to 25 000 g mol^{-1} branched poly(ethylene imine) (BPEI, 15 $\mu\text{g mL}^{-1}$, as a kind gift from BASF Corporation, Ludwigshafen, Germany) as positive control (PC) and HBG as negative control.^[5] Samples and controls were incubated for 2 h at 37 °C while shaking. Absorbance was measured using the Tecan Spark M20 at 645 nm. Erythrocyte aggregation was calculated according to Bauer et al. using the following equation:^[2]

$$\text{Absorption} = (Abs_{\text{sample}} - Abs_{\text{blank}}) - (Abs_{\text{sample control}} - Abs_{\text{blank}})$$

1.5 Formation of Polyplexes

Polyplexes were formed using the respective polymer and the luciferase reporter gene plasmid DNA (pGL3 pDNA, Promega, Madison, USA). The plasmid was transferred to competent *E. coli* TG1 (Hans-Knoell-Institute, Jena, Germany) using heat shock and afterwards

amplified. For isolation of pDNA and quality control the E.Z.N.A. Plasmid Maxi Kit (OMEGA bio-tek, Norcross, USA) was used following the manufacturer's protocol.

For the formation of polyplexes the pDNA to polymer ratio was calculated as the ratio of cationic polymer nitrogen (N) to anionic pDNA phosphate (P) as so called N/P ratio. The required volumes of polymer stock solution (5 mg mL^{-1}) and $4 \text{ }\mu\text{g}$ pDNA were each diluted in equivalent volumes of saline buffer (150 mM NaCl and 10 mM HEPES buffer, pH 7.4). The solutions were vortexed for 10 s and incubated at room temperature (RT) for 10 min. Afterwards the polymer solution was pipetted to the pDNA solution, vortexed for 10 s and incubated again for 10 min before use.^[6]

1.6 Horizontal Agarose Gel Electrophoresis

$50 \text{ }\mu\text{L}$ polyplex solution containing $1 \text{ }\mu\text{g}$ pDNA were mixed with $5 \text{ }\mu\text{L}$ loading buffer (40 mM Tris , 50% glycerol 85% , $1 \text{ mM ethylenediaminetetraacetic acid (EDTA)}$ pH 7.4 and loaded on an agarose gel (1%) (peqGold Universal Agarose, Peqlab Biotechnology, Erlangen, Germany) containing $0.125 \text{ }\mu\text{g mL}^{-1}$ ethidium bromide (SERVA Electrophoresis GmbH, Heidelberg, Germany). Plasmid DNA and bromophenol blue (Serva Electrophoresis GmbH) were used as positive and running control, respectively. Electrophoretic separation at 80 V was performed in an electrophoresis chamber (Biometra, Goettingen, Germany) for 1 h with TAE running buffer (40 mM Tris , 1 mM EDTA , 1% acetic acid, all Carl Roth). Gels were photographed under UV transillumination (Inas GmbH, Goettingen, Germany) at 312 nm and analyzed using the BioVision gel documentation software (VILBER, Collegien, France).

To determine the protection abilities of the polyplexes to prevent enzymatic degradation, complexes were treated with $2 \text{ }\mu\text{L}$ of DNase I with an activity of $5 \text{ Kunitz units }\mu\text{g}^{-1}$ pDNA (Amersham Biosciences, Piscataway, USA) at $37 \text{ }^\circ\text{C}$ for 45 min. Afterwards, the enzyme was inactivated by heating ($70 \text{ }^\circ\text{C}$, 35 min) and the was pDNA released from the polyplexes by heparin treatment (20 I.U.) at $37 \text{ }^\circ\text{C}$ for 20 min followed by agarose gel electrophoresis as

described above. As controls free pDNA, pDNA equally treated but without addition of DNase I, and free pDNA treated under the same conditions with DNase I were used.

1.7 pDNA Binding Assay

The binding efficacy of the polymers for pDNA was quantified using the AccuBlue[®] Quantification kit (Biotium, Hayward, USA) according to the manufacturer's protocol. Samples were mixed in black 96-well plates (Fluotrac 200, Greiner bio-one) with 200 μ L of a freshly prepared mixture of 100X enhancer and quantification solution (1:100) followed by incubation under shaking (450 rpm) for 10 min at RT in the dark. The fluorescence measurements were performed using the Tecan[®] Spark M20 (485 nm excitation, 530 nm emission). Plasmid DNA without polymer was used as 100% reference, a mixture of 150 mM NaCl and 10 mM HEPES solution pH 7.4 as blank which was subtracted from all measured values. Polyplexes of pDNA and linear poly(ethylene imine) (LPEI, 2 500 g mol⁻¹; Polysciences, Warrington, PA, USA) at N/P 20 were used as positive control. The results were calculated as mean \pm SD as percentage of the pDNA reference.

1.8 Particle Size and Zeta Potential Measurements

The NanoSight[®] LM10 (Malvern Instruments GmbH, Herrenberg, Germany) was used to perform nanoparticle tracking analysis (NTA) utilizing the red laser light at 638 nm. Polyplex solutions were diluted 1:1 before measuring with bidistilled water to a final volume of 200 μ L. Measurements were performed at 25 °C with a tracking time of 30 s with 5 captures per sample.

A Zetasizer Nano ZS (Malvern Instruments GmbH, Herrenberg, Germany) was used to investigate the zeta potential of the polyplexes in bidistilled water. Zeta potential was determined in high concentration cells (ZEN1010, Malvern Instruments) by analyzing the electrophoretic mobility at 25 °C. The results were calculated with the Malvern software 6.20.

1.9 *In Vitro* Transfection Efficacy using Luciferase Reporter Gene

Transfection efficacy was tested in CHO-K1 cells (ACC 110, DSMZ-German Collection of Microorganisms and Cell Cultures GmbH) using 50 000 cells/well in 12-well plates.^[7] Cells were cultured in Ham's F12 medium supplemented with 1 mM L-glutamine and 10% fetal bovine serum (Gibco, Darmstadt, Germany) at 37 °C, 5% CO₂ and 95% relative humidity. Polyplexes containing 4 µg pDNA in 200 µL buffer (150 mM NaCl and 10 mM HEPES, pH 7.4)/well were added to the cells in serum containing medium, incubated for 4 h before medium change and further incubation for 44 h. Cells only treated with 200 µL of NaCl/HEPES-buffer served as solvent control and polyplexes formed with pDNA and 2 500 g mol⁻¹ LPEI at a N/P ratio 20 as positive control. As negative control (NC), free pDNA was used. Transfection efficacy was determined by the Luciferase Assay System (Promega) following the manufacturer's instructions using the microplate reader Tecan Spark M20. Results were given as relative light units (RLUs) µg⁻¹ protein.

The protein amount was quantified using the bicinchoninic acid (BCA) assay kit (PierceTM BCA Protein Assay Kit, ThermoFisherTM) following the manufacturer's protocol. Briefly, 25 µL cell lysate were treated with 10 µL 0.05 M iodoacetamide (Applichem, Darmstadt, Germany) solution at 37 °C for 20 min. Afterwards, BCA assay reagent was added and the samples were incubated at 37 °C for 40 min. BCA assay results were calculated in relation to a bovine serum albumin (BSA) standard curve and were spectrophotometrically measured (Tecan Spark M20) at 570 nm.

2. Results

2.3 *In Vitro* Erythrocyte Aggregation Tests

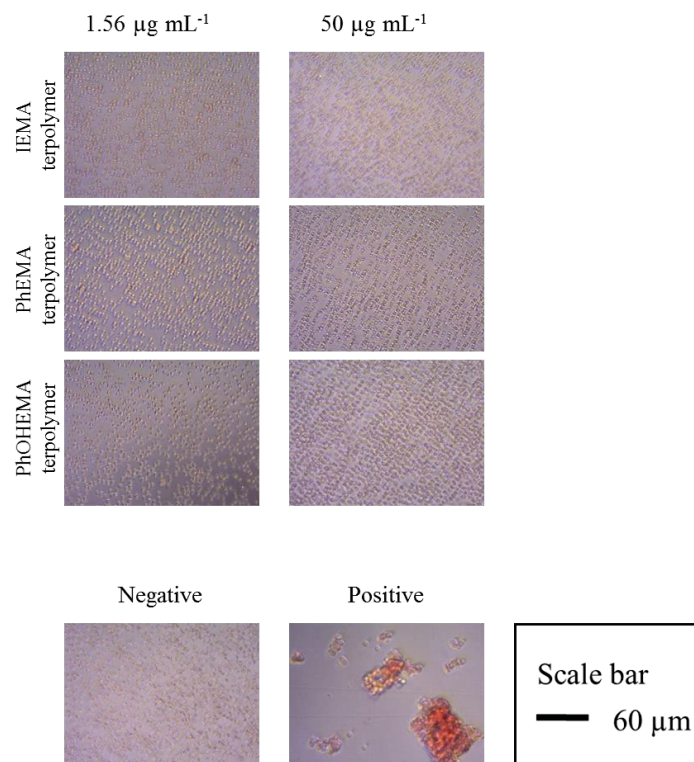


Figure S12. Microscopic evaluation of the aggregation potential of sheep red blood cells after incubation of the methacrylamide terpolymers at different concentrations (shown are the lowest and highest concentration). Buffer treated sheep red blood cells served as negative control, whereas 25 000 g mol⁻¹ branched PEI served as positive control.

2.1 Determination of the pDNA Binding Capacity by Agarose Gel Electrophoresis

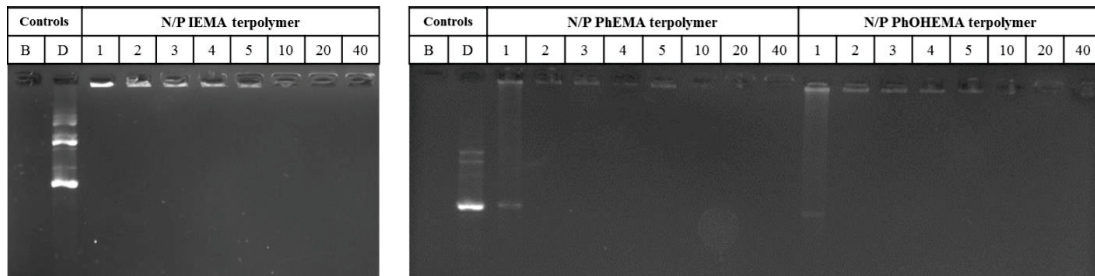


Figure S13. pDNA binding capacity of the terpolymers at different N/P ratios tested by horizontal agarose gel electrophoresis compared to free pDNA (D) (Bromophenolblue (B) served as running control).

2.2 Enzymatic Stability Testing

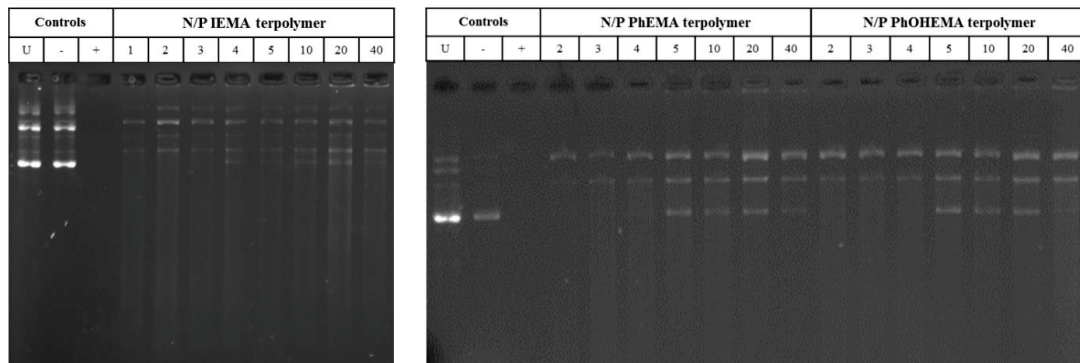


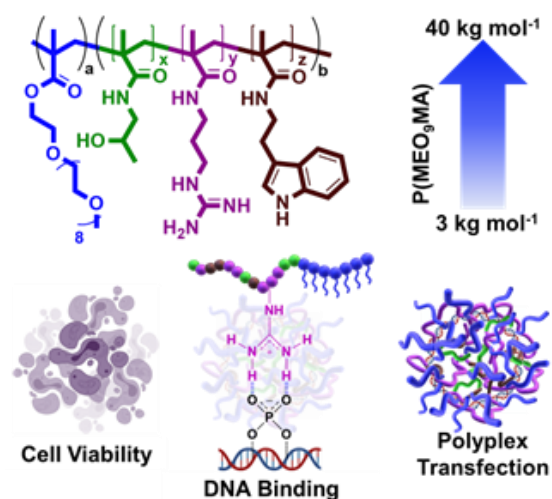
Figure S14. Stability of the polyplexes with pDNA against enzymatic degradation by DNase I at different N/P ratios (controls: untreated free plasmid (U); free plasmid treated in the same way as polyplexes but without enzyme (-); free plasmid treated with enzyme (+)).

References

- [1] C. Cokca, L. Zartner, I. Tabujew, D. Fischer, K. Peneva, *Macromol. Rapid Commun.* **2020**, 1900668.
- [2] M. Bauer, C. Lautenschlaeger, K. Kempe, L. Tauhardt, U. S. Schubert, D. Fischer, *Macromol. Biosci.* **2012**, 12, 986.
- [3] DIN EN ISO 10993-5:2009-10, Biological evaluation of medical devices - Part5: Test for in vitro cytotoxicity, in *European Standard EN ISO 10993-5, Brussels*.
- [4] ASTM F756, "Standard practice for assessment of hemolytic properties of materials", in *Annual Book of ASTM Standards, Vol. 13. 01, ASTM, Philadelphia*.
- [5] H. Petersen, P. M. Fechner, A. L. Martin, K. Kunath, S. Stolnik, C. J. Roberts, D. Fischer, M. C. Davies, T. Kissel, *Bioconjug Chem* **2002**, 13, 845.
- [6] D. Fischer, T. Bieber, Y. Li, H.-P. Elsässer, T. Kissel, *Pharm. Res.* **1999**, 16, 1273.
- [7] M. Zink, K. Hotzel, U. S. Schubert, T. Heinze, D. Fischer, *Macromol. Biosci.* **2019**, 1900085.

Publication P4

PEGylation of Guanidinium and Indole Bearing Poly(methacrylamide)s - Biocompatible Terpolymers for pDNA Delivery



C. Cokca, F. H. Hack, D. Costabel, K. Herwig, J. Hülsmann, P. Then, R. Heintzmann, D. Fischer, K. Peneva

Macromol. Biosci. **2021**, *21* (10), 2100146

PEGylation of Guanidinium and Indole Bearing Poly(methacrylamide)s – Biocompatible Terpolymers for pDNA Delivery

Ceren Cokca, Franz J. Hack, Daniel Costabel, Kira Herwig, Juliana Hülsmann, Patrick Then, Rainer Heintzmann, Dagmar Fischer, and Kalina Peneva*

This study describes the first example for shielding of a high performing terpolymer that consists of *N*-(2-hydroxypropyl)methacrylamide (HPMA), *N*-(3-guanidinopropyl)methacrylamide (GPMA), and *N*-(2-indolethyl)methacrylamide monomers (IEMA) by block copolymerization of a polyethylene glycol derivative – poly(nona(ethylene glycol)methyl ether methacrylate) (P(MEO₉MA)) via reversible addition–fragmentation chain transfer (RAFT) polymerization. The molecular weight of P(MEO₉MA) is varied from 3 to 40 kg mol⁻¹ while the comonomer content of HPMA, GPMA, and IEMA is kept comparable. The influence of P(MEO₉MA) block with various molecular weights is investigated over cytotoxicity, plasmid DNA (pDNA) binding, and transfection efficiency of the resulting polyplexes. Overall, the increase in molecular weight of P(MEO₉MA) block demonstrates excellent biocompatibility with higher cell viability in L-929 cells and an efficient binding to pDNA at N/P ratio of 2. The significant transfection efficiency in CHO-K1 cells at N/P ratio 20 is obtained for block copolymers with molecular weight of P(MEO₉MA) up to 10 kg mol⁻¹. Moreover, a fluorescently labeled analogue of P(MEO₉MA), bearing perylene monoimide methacrylamide (PMIM), is introduced as a comonomer in RAFT polymerization. Polyplexes consisting of labeled block copolymer with 20 kg mol⁻¹ of P(MEO₉MA) and pDNA are incubated in HeLa cells and investigated through structured illumination microscopy (SIM).

1. Introduction

A plethora of positively charged polymers is already used for binding and protection of genetic materials like plasmid DNA (pDNA) for non-viral gene delivery. However, only a limited number of such polymers reached clinical applications since their high content of cationic charges hampers therapeutic use due to biocompatibility and safety issues, unspecific interactions with blood components and cell membranes as well as a fast clearance of polyplexes from the blood stream.^[1–4] One approach to overcome these limitations is the shielding with neutral polymers such as polyethylene glycol (PEG),^[5,6] poly(*N*-(2-hydroxypropyl)methacrylamide),^[7] hydroxyethyl starch,^[8] or poly(oxazolines)^[9] which are attached via covalent bonds or non-covalent interactions to mask the cationic charges resulting in the so called “stealth effect”. PEG has been widely investigated regarding its chain architecture, molecular weight, density on the particle surface, linking technology, and its interactions

C. Cokca, D. Costabel, K. Herwig, K. Peneva
Institute of Organic Chemistry and Macromolecular Chemistry (IOMC)
Friedrich Schiller University Jena
Lessingstrasse 8, Jena 07743, Germany
E-mail: kalina.peneva@uni-jena.de

F. J. Hack, J. Hülsmann
Pharmaceutical Technology and Biopharmacy
Institute of Pharmacy
Friedrich Schiller University Jena
Lessingstrasse 8, Jena 07743, Germany
P. Then, R. Heintzmann
Leibniz Institute of Photonic Technology
Albert Einstein Str. 9, Jena 07745, Germany
R. Heintzmann
Institute of Physical Chemistry and Abbe Center of Photonics
Friedrich Schiller University Jena
Helmholtzweg 4, Jena 07743, Germany
D. Fischer
Department of Chemistry and Pharmacy
Pharmaceutical Technology
Friedrich-Alexander-University Erlangen-Nürnberg
Cauerstrasse 4, Erlangen 91058, Germany
D. Fischer, K. Peneva
Jena Center for Soft Matter (JCSM)
Friedrich Schiller University Jena
Philosophenweg 7, Jena 07743, Germany

 The ORCID identification number(s) for the author(s) of this article can be found under <https://doi.org/10.1002/mabi.202100146>

© 2021 The Authors. Macromolecular Bioscience published by Wiley-VCH GmbH. This is an open access article under the terms of the Creative Commons Attribution-NonCommercial-NoDerivs License, which permits use and distribution in any medium, provided the original work is properly cited, the use is non-commercial and no modifications or adaptations are made.

DOI: 10.1002/mabi.202100146

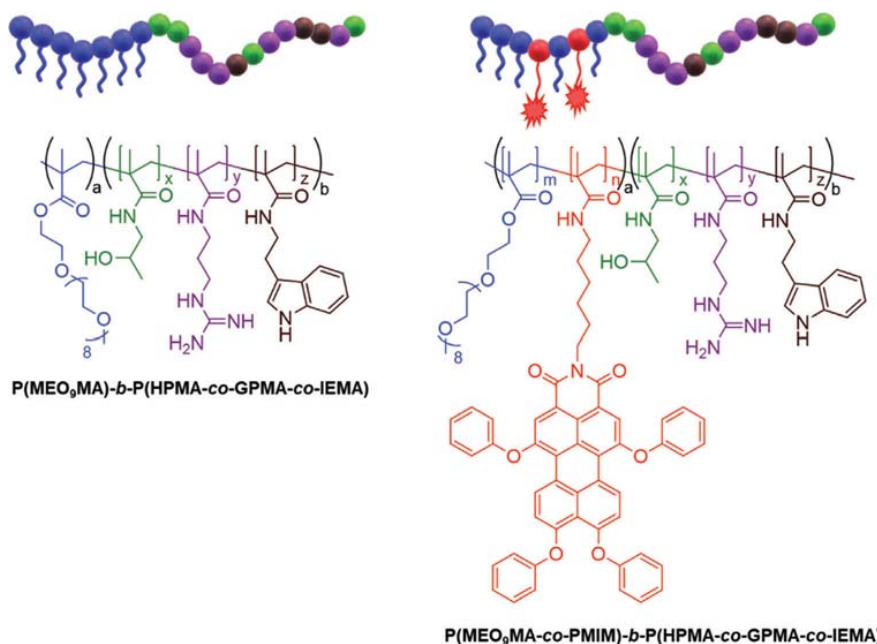


Figure 1. Graphical representation and chemical structures of P(MEO₉MA)-*b*-P(HPMA-*co*-GPMA-*co*-IEMA) and P(MEO₉MA-*co*-PMIM)-*b*-P(HPMA-*co*-GPMA-*co*-IEMA) polymers.

with biological systems.^[10–14] Most of the shielding studies with PEG derivatives were conducted on primary or tertiary amine bearing polymers such as poly(ethylene imine) (PEI)^[15–19] and only very few examples of PEGylated guanidinium containing polymers or polyplexes were reported in the literature. Additionally, most of these works did not examine the physicochemical properties of the shielding moieties systematically.^[20–25]

Recently, we showed that guanidinium and indole bearing methacrylamide based terpolymers possess excellent pDNA transfection ability. We investigated monomers with different hydrophobic groups – indole, phenyl, and phenol – in guanidylated terpolymers and identified that the indole containing terpolymer has the highest performance in pDNA transfection.^[26] Nevertheless, the presence of the high cationic charge (>60 mol%) caused a significant decrease in the cell viability in L-929 cells at polymer concentrations $\geq 31.25 \mu\text{g mL}^{-1}$. To address this drawback and to improve the biocompatibility of this class of terpolymers, we prepared copolymers consisting of nona(ethylene glycol)methyl ether methacrylate (MEO₉MA), *N*-(2-hydroxypropyl)methacrylamide (HPMA), *N*-(3-guanidinopropyl)methacrylamide (GPMA), and *N*-(2-indolethyl)methacrylamide (IEMA) monomers by reversible addition–fragmentation chain transfer (RAFT) polymerization. MEO₉MA monomer is a brush-type of PEG bearing multiple oligo(ethylene glycol) chains and it is utilized as a shielding moiety due to its versatile way of polymerization with different monomers and high biocompatibility.^[27–30] Moreover, its efficiency in shielding of cationic polymers for non-viral gene delivery has previously been demonstrated.^[31–34] We introduced poly(nona(ethylene glycol)methyl ether methacrylate) (P(MEO₉MA)) in the polymer

chains with increasing molecular weight from 3 to 40 kg mol⁻¹ of the P(MEO₉MA) block, representing^[35] Keeping the apparent molecular weight of the terpolymer similar ($\approx 22 \text{ kg mol}^{-1}$) with the content of HPMA ($\approx 20\%$), GPMA ($\approx 75\%$), and IEMA ($\approx 5\%$) (Figure 1, Table 1), the molecular weight of P(MEO₉MA) block was varied to select an optimal block size regarding cytotoxicity, pDNA binding, and transfection efficacy. Moreover, a fluorescent methacrylamide monomer, *N*-(6-methacrylamidylhexyl)-1,6,9,10-tetraphenoxyperylene-3,4-monoimide (PMIM), was synthesized and employed as comonomer by RAFT polymerization to produce the fluorescently labeled P(MEO₉MA-*co*-PMIM) macro-RAFT agent with molecular weight of 15 and 20 kg mol⁻¹. After successful block copolymerization with HPMA, GPMA, and IEMA, pDNA polyplexes of block copolymers with $M_n = 20 \text{ kg mol}^{-1}$ of P(MEO₉MA-*co*-PMIM) block were examined under structured illumination microscopy (SIM) to reveal the potential of this novel fluorescence labeling approach for cationic polymers.

2. Results and Discussion

The synthesis of GPMA and IEMA was performed following the procedure described previously.^[26] GPMA was utilized due to the excellent ability of the guanidinium group to interact with genetic material, while HPMA was selected as a spacer unit to ensure the colloidal stability of the polyplexes.^[26,36–39] IEMA was included to allow hydrophobic interactions with pDNA and cell membranes, to improve the cellular uptake and the transfection efficiency of the polyplexes.^[26,36]

Table 1. Monomer contents, apparent molecular weight, and dispersity indices of the (block) copolymers.

	M_n , Experimental [kg mol ⁻¹] ^{a)}	\bar{D}	MEO ₉ MA ^{b)} [mol%]	PMIM ^{b)} [mol%]	HPMA ^{b)} [mol%]	GPMA ^{b)} [mol%]	IEMA ^{b)} [mol%]
P(MEO ₉ MA)3	3	1.22	100	—	—	—	—
P(MEO ₉ MA)3- <i>b</i> -P(HGI)	26	1.26	4.3	—	27.9	65.6	2.2
P(MEO ₉ MA)6	6.5	1.13	100	—	—	—	—
P(MEO ₉ MA)6- <i>b</i> -P(HGI)	27	1.24	10.1	—	24.5	64	1.5
P(MEO ₉ MA)10	10	1.18	100	—	—	—	—
P(MEO ₉ MA)10- <i>b</i> -P(HGI)	33	1.40	13.2	—	23.4	60.7	2.7
P(MEO ₉ MA)15	14	1.15	99	1	—	—	—
P(MEO ₉ MA)15- <i>b</i> -P(HGI)	37	1.27	17.4	0.6	20.6	59.8	1.6
P(MEO ₉ MA)20	23	1.20	98	2	—	—	—
P(MEO ₉ MA)20- <i>b</i> -P(HGI)	44	1.41	27.4	1.2	17.6	51.0	2.8
P(MEO ₉ MA)30	31	1.28	100	—	—	—	—
P(MEO ₉ MA)30- <i>b</i> -P(HGI)	52	1.37	34.2	—	17.0	46.8	2.0
P(MEO ₉ MA)40	44	1.40	100	—	—	—	—
P(MEO ₉ MA)40- <i>b</i> -P(HGI)	69	1.59	38.2	—	15.9	44.7	1.2
P(HGI)	22	1.13	—	—	21	75	4

^{a)} Apparent molecular weight determined by SEC_{DMAC}; ^{b)} Calculated via ¹H NMR spectroscopy by considering whole polymer chain.

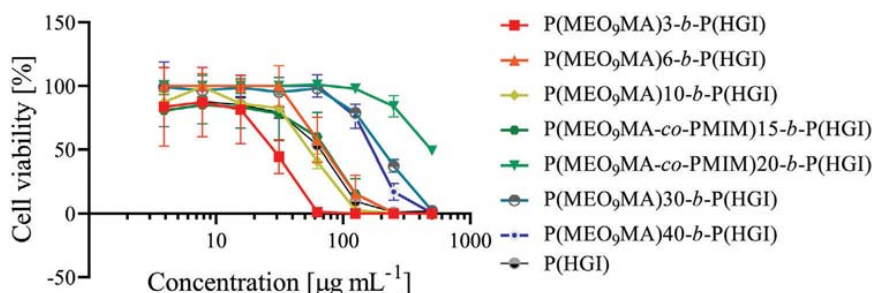


Figure 2. Concentration dependent in vitro cell viability assay of block copolymers in L-929 mouse fibroblasts after 24 h incubation using the CellTiter-Glo assay (eightfold, mean \pm SD).

P(HPMA-*co*-GPMA-*co*-IEMA) (P(HGI)) terpolymer was synthesized as a reference polymer to evaluate the shielding effect based on our previous work.^[26] The monomer contents and molecular weights with dispersity index are depicted in Table 1; Figure S16, Supporting Information. For the synthesis of P(MEO₉MA) macro-RAFT agents, the same CTA (4-Cyano-4-(phenylcarbonothioylthio)pentanoic acid) was used due to its proven suitability with the employed monomers.^[40,41] Molecular weights from 3 to 40 kg mol⁻¹ were targeted by changing the $[M]_0/[CTA]_0$ ratios while keeping the $[CTA]_0/[INI]_0$ ratio constant. The nomenclature of the P(MEO₉MA)-based macro-RAFT agents was chosen according to the targeted molecular weight (Scheme S2 and Table S1, Supporting Information; Table 1). The reaction was monitored by ¹H NMR spectroscopy (Figure S12, Supporting Information), followed by apparent molecular weight (M_n , Experimental) and dispersity indices (\bar{D}) determination via SEC_{DMAC} (Table 1; Figure S16, Supporting Information). Due to the high water solubility of P(MEO₉MA),^[30] block addition with HPMA, GPMA, and IEMA monomers in acetate buffer was possible but to avoid the imbalance between the monomer de-

composition rate (k_d) and propagation rate (k_p), which can be observed in block extensions, the $[CTA]_0/[INI]_0$ ratio was increased to six while keeping $[M]_0/[CTA]_0 = 200$ (Scheme S4 and Table S2, Supporting Information).^[42] The block copolymers depicted unimodal SEC_{DMAC} traces with moderately low dispersity indices (Figures S14 and S16, Supporting Information; Table 1).

The influence of the P(MEO₉MA) unit on the in vitro biocompatibility of the polymers was investigated via luminescence-based CellTiter-Glo assay on L-929 mouse fibroblasts with polymer concentration ranging from 3.9 to 500 μ g mL⁻¹ over 24 h (Figure 2). A cell viability $\leq 70\%$ was considered as toxic according to DIN EN ISO 10993-5.^[43] Untreated cells were utilized as 100% negative control and 0.02% thiomersal solution was employed as the positive control reducing the metabolic activity of the cells to $<1\%$ (data not shown). After incubation for 24 h, a concentration and PEG molecular weight-dependent effect on cell viability was observed. Overall, higher IC₅₀ values were determined for the polymers with $M_n \geq 6$ kg mol⁻¹ of P(MEO₉MA) block in respect of the non-shielded terpolymer. Although a higher biocompatibility was observed for P(MEO₉MA)30-*b*-P(HGI) and

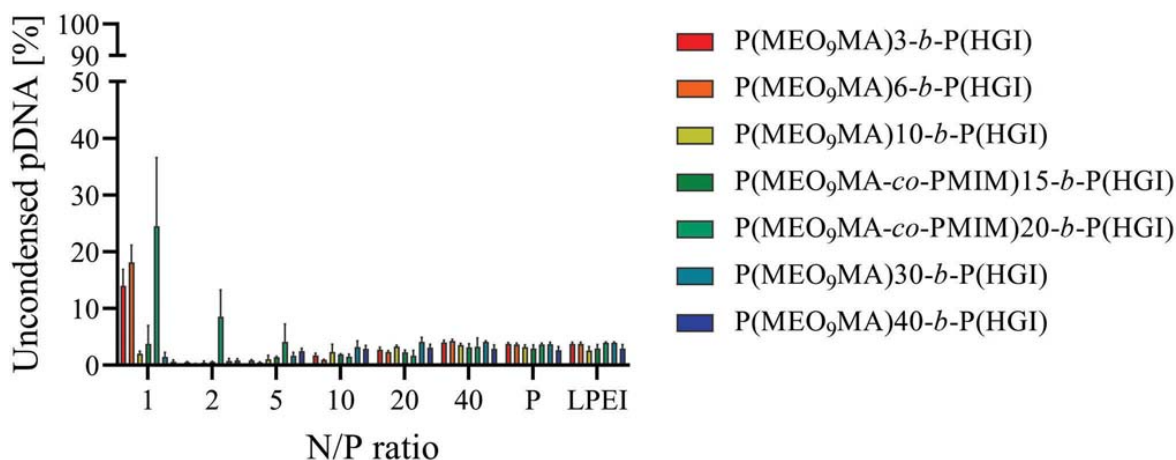


Figure 3. Binding capacity [%] of the block copolymers for pDNA depending on the N/P ratio determined by the AccuBlue assay in comparison to linear PEI polyplexes (LPEI; 2.5 kg mol⁻¹, N/P 20) and the free polymers (P) (eightfold, mean ± SD).

P(MEO₉MA)40-*b*-P(HGI) especially at higher polymer concentrations, P(MEO₉MA)3-*b*-P(HGI) showed more pronounced damaging effects on the viability of the fibroblasts in comparison of P(HGI). Comparable effects were observed in the study of Bauer et al. which indicates a less efficient uptake of PEG with increasing molecular weight into cells; and therefore, less toxic effects were observed.^[44] The pronounced cytotoxicity of P(MEO₉MA)3-*b*-P(HGI) compared to P(HGI) can also be explained according to the study of Liu et al. on the cytotoxicity of PEG oligomers.^[45] A MEO₉MA unit with $M_n = 500 \text{ g mol}^{-1}$ caused higher toxicity than MEO₉MA unit with $M_n = 950 \text{ g mol}^{-1}$ in L-929 cells.

To investigate the influence of the P(MEO₉MA) shielding on the electrostatic interaction of the cationic polymers with the anionic pDNA, the DNA binding capability was quantified by the AccuBlue high sensitivity fluorescent dsDNA quantitation assay after electrostatic formation of polyplexes at different N/P ratios from 1 to 40 (Figure 3).^[46] Naked pDNA was used as 100% control representing the maximum accessibility of the pDNA for the intercalating dye with the highest fluorescence signals. Polyplexes with linear PEI (LPEI; 2.5 kg mol⁻¹) at N/P ratio 20 were employed as positive control due to the well-established high binding affinity of LPEI.^[47] All shielded block copolymers except P(MEO₉MA)20-*b*-P(HGI) demonstrated a comparably strong binding affinity starting from N/P ratio 2 similar to the LPEI control and to our previous study.^[26] The qualitative binding results were obtained by horizontal agarose gel electrophoresis (Figure S19, Supporting Information). The typical band pattern of pDNA due to the most prominent open circular and supercoiled structure started to disappear at a N/P ratio of 2 for the shielded polymers as an indicator of polyplex formation.

The polyplex stability that arises from the compact binding of shielded polymers to pDNA was investigated by means of agarose gel electrophoresis by applying harsh conditions.^[48] The polyplexes were prepared at N/P ratios from 2 to 40 and incubated with DNase I followed by displacement of the pDNA from the polyplexes by heparin (Figure S20, Supporting Information). Although we observed efficient pDNA binding even at low N/P ratios, stabilization of the polyplexes to protect from enzymatic

degradation seems to be reduced by the PEGylation. A possible explanation can be the brush architecture of P(MEO₉MA) which can cause steric hinderance and reduce the accessibility of the cationic charges to the pDNA.^[5] Moreover, pDNA release can be followed during the enzymatic stability tests indirectly when the pDNA was released by heparin. As a result, the smaller the PEGs are, the more pDNA seemed to be retarded at the origin which could be interpreted as a more efficient interaction between polymer and DNA.

The influence of the increasing molecular weight of P(MEO₉MA) on the transfection efficacy was determined through a luminescence-based reaction in eukaryotic CHO-K1 cells in the presence of serum by employing pGL3 DNA/polyplexes at N/P ratios from 2 to 40 (Figure 4). Free pDNA and the solvent 0.9% NaCl (data not shown) were used as controls without gene transfer activity determined by negligible luminescence signals. For P(MEO₉MA)3-*b*-P(HGI) and P(MEO₉MA)6-*b*-P(HGI), a weaker shielding effect compared to their higher molecular weight counterparts was suggested. As a result, we observed a more pronounced transfection efficacy at an N/P ratio of 20 for these polymers. Polyplexes with P(MEO₉MA) blocks of $M_n \geq 10 \text{ kg mol}^{-1}$ showed almost no transfection efficiency. Lower transfection efficiency was also observed with the increase in molecular weight of the shielding unit in other systems such as PEGylated PEI as a consequence of lower cellular uptake and/or endosomal escape.^[49–52] In a follow up experiment, the intracellular uptake of polyplexes was examined to understand the reasons of molecular weight of P(MEO₉MA)-dependent decrease in transfection efficiency for guanidinium and indole containing terpolymers.

Block copolymers with P(MEO₉MA)15 and P(MEO₉MA)20 units were labeled with a perylene monoimide derivative, PMIM, where PMIM was incorporated along the polymer chain by RAFT polymerization as a comonomer of MEO₉MA. The synthesis of PMIM was achieved in five steps starting from dibutyl-1,6,9,10-tetrabromoperylene 3,4-dicarboxylate (Compound 1 in Scheme S1, Supporting Information).^[53] Nucleophilic aromatic substitution with phenol resulted in dibutyl-1,

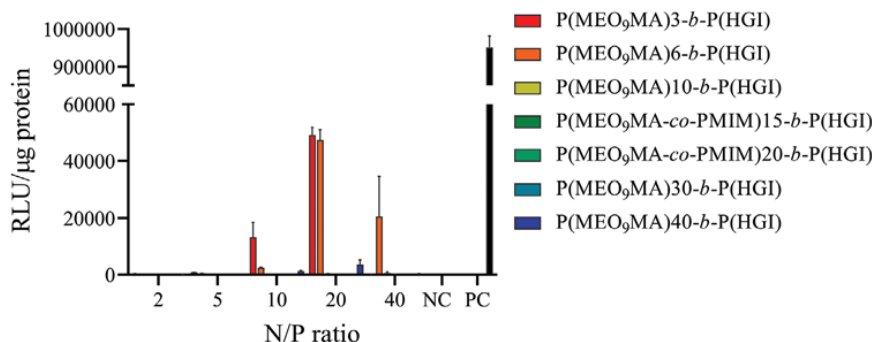


Figure 4. In vitro luciferase reporter gene expression of pGL3 DNA/block copolymer polyplexes at different N/P ratios in CHO-K1 cells. Experiments were performed in quadruplicates with free pDNA serving as negative control (NC) and polyplexes of IPEI and pDNA at N/P ratio 20 as positive control (PC) (mean \pm SD).

6,9,10-tetraphenoxyperylene 3,4-dicarboxylate (**2**) and acidic ester hydrolysis afforded perylene monoanhydride (**3**). For the imidization involving *N*-Boc-1,6-hexanediamine, imidazole was used as solvent with catalytic amounts of zinc acetate to give the respective perylene monoimide (**4**). Following deprotection of the amine group, **5** was converted to PMIM via Schotten–Baumann reaction. The chemical structure and purity of compounds **1–6** were confirmed by ^1H and ^{13}C NMR spectroscopy and mass spectrometry (Figures S1–S11, Supporting Information).

P(MEO₉MA-*co*-PMIM) macro-RAFT agents were prepared (Scheme S3 and Table S1, Supporting Information) to obtain fluorescently labeled macro-RAFT agents not only for the control over number of dye units in the polymer chain,^[54,55] but also to overcome the poor water solubility of the PMIM monomer.^[56] The increase in polymerization time was required to counterbalance the lower monomer reactivity caused by the bulky perylene moiety of PMIM.^[54] The labeled polymer was characterized by ^1H NMR spectroscopy and SEC_{DMAc} (Table 1; Figures S13 and S16, Supporting Information). Block extension of P(MEO₉MA-*co*-PMIM) units (Table 1; Scheme S5, Figures S15 and S16, Supporting Information) was achieved by RAFT polymerization in aqueous media. The labeled block copolymers showed maximum absorbance at 540 nm and emission at 638 nm at polymer concentration of 10 mg mL⁻¹ in water (Figures S17 and S18, Supporting Information).

The applicability of the proposed labeling strategy and the choice of chromophore for SIM were investigated by a proof-of-concept study. SIM has a higher resolution ($\alpha\gamma$ resolution: ≈ 100 – 140 nm and z resolution: ≈ 300 nm) in comparison to conventional microscopy techniques^[57] which enables the observation of cellular uptake of polyplexes and their intracellular trafficking in different cellular compartments.^[58,59] For SIM investigation, the polyplexes formed by P(MEO₉MA-*co*-PMIM)20-*b*-P(HGI) block copolymer and pDNA at N/P ratio of 10 were incubated in HeLa cells for 1 and 4 h. Afterward, SIM was performed receiving live images of the HeLa cells (Figure S21, Supporting Information). The fluorescent pattern of the P(MEO₉MA-*co*-PMIM)20-*b*-P(HGI) block copolymer/pDNA polyplex was observed in the cellular membrane, cytoplasm and perinuclear area after 1 h incubation and its intensity increased after 4 h incubation.

The labeled block copolymers with P(MEO₉MA-*co*-PMIM)15 and P(MEO₉MA-*co*-PMIM)20 units were also investigated with respect to cell viability, pDNA binding (Figure S20, Supporting Information), polyplex stability, and transfection efficiency. The inclusion of PMIM monomer did not influence the cell viability in L-929 cells compared to the non-labeled copolymers (Figure 2). Even though pDNA binding for P(MEO₉MA-*co*-PMIM)15-*b*-P(HGI) followed a similar trend with other shielded block copolymers and P(HGI), P(MEO₉MA-*co*-PMIM)20-*b*-P(HGI) showed a weaker interaction with pDNA and complete binding started from N/P ratio 5 instead of 2 (Figure 3). The higher content of the bulky chromophore in the PMIM monomer can lead to higher steric hinderance which can in turn interfere with the electrostatic and hydrophobic interactions of the polymer chain with pDNA.

3. Conclusion

Well-defined copolymers consisting of P(MEO₉MA) as a shielding unit and HPMA, GPMA, and IEMA monomers were successfully synthesized by RAFT polymerization. The molecular weight of the shielding unit was varied between 3 and 40 kg mol⁻¹ with comparable mol% of HPMA, GPMA, and IEMA monomers in each polymer structure. The block copolymers containing P(MEO₉MA) showed increase in cell viability with increasing molecular weight of the P(MEO₉MA) unit in comparison with the non-shielded terpolymer. All block copolymers demonstrated effective binding starting from N/P ratio equal to or higher than 2 yet the protection of pDNA from enzymatic degradation was limited for all samples. The transfection efficiency of the block copolymers with 3 and 6 kg mol⁻¹ of P(MEO₉MA) unit remained unchanged, while a decrease in transfection efficiency was observed for the polymers with ≥ 10 kg mol⁻¹ of P(MEO₉MA) block. This decrease could be due to the lower cellular uptake and/or endosomal escape of polyplexes resulting from the increase in stealth capability. Labeling the block copolymers by the inclusion of a methacrylamide monomer bearing perylene chromophore as a comonomer of MEO₉MA did not interfere with the cell viability and pDNA binding. P(MEO₉MA-*co*-PMIM)20-*b*-P(HGI) polyplexes which were incubated with HeLa cells were studied by SIM. The fluorescent pattern in the images of live cells proved the

efficiency of labeling approach by the employment of RAFT polymerization. Overall, the biocompatibility of guanidinium and indole bearing terpolymers was successfully improved by shielding with P(MEO₂MA) and polyplexes. The stability and release of pDNA from polyplexes inside the cell will be investigated in more detail; future studies will also include chemical modifications such as inclusion of cleavable bonds and attachment of targeting ligands.

Supporting Information

Supporting Information is available from the Wiley Online Library or from the author.

Acknowledgements

C.C. and F.J.H. contributed equally to this work. This research was supported by the German Research Foundation (DFG, Deutsche Forschungsgemeinschaft) – POLYTARGET project number 316213987 – SFB 1278 (Projects B03, A03, C04 and Z01) and “Catalight” project number 364549901 – SFB TRR 234 (Project A3). The authors would like to thank Felix H. Schacher, Jessica Tom, and Javier G. Lopez for useful discussions as well as Angela Fischer for her excellent technical support.

Open access funding enabled and organized by Projekt DEAL.

Conflict of Interest

The authors declare no conflict of interest.

Data Availability Statement

Research data are not shared.

Keywords

gene delivery, guanidinium, indole, methacrylamides, poly(ethylene glycol) methacrylate

Received: April 8, 2021
Revised: June 28, 2021
Published online: July 26, 2021

- [1] A. Hall, U. Lächelt, J. Bartek, E. Wagner, S. M. Moghimi, *Mol. Ther.* **2017**, *25*, 1476.
- [2] S. V. Vinogradov, T. K. Bronich, A. V. Kabanov, *Bioconjugate Chem.* **1998**, *9*, 805.
- [3] K. Ita, *Eur. J. Pharm. Sci.* **2020**, *150*, 105358.
- [4] F. Schlenk, S. Grund, D. Fischer, *Theor. Delivery* **2013**, *4*, 95.
- [5] M. Le Bohec, K. Bonchouo Kenzo, S. Piogé, S. Mura, J. Nicolas, N. Casse, G. Forcher, L. Fontaine, S. Pascual, *Polym. Chem.* **2019**, *10*, 1968.
- [6] K. Knop, R. Hoogenboom, D. Fischer, U. S. Schubert, *Angew. Chem., Int. Ed.* **2010**, *49*, 6288.
- [7] D. Oupicky, M. Ogris, K. A. Howard, P. R. Dash, K. Ulbrich, L. W. Seymour, *Mol. Ther.* **2002**, *5*, 463.
- [8] M. Noga, D. Edinger, W. Rödl, E. Wagner, G. Winter, A. Besheer, *J. Controlled Release* **2012**, *159*, 92.
- [9] A.-K. Trützscher, T. Bus, M. Sahn, A. Traeger, C. Weber, U. S. Schubert, *Biomacromolecules* **2018**, *19*, 2759.
- [10] J. S. Suk, Q. Xu, N. Kim, J. Hanes, L. M. Ensign, *Adv. Drug. Delivery Rev.* **2016**, *99*, 28.
- [11] F. Freitag, E. Wagner, *Adv. Drug. Delivery Rev.* **2021**, *168*, 30.
- [12] S. Venkataraman, W. L. Ong, Z. Y. Ong, S. C. Joachim Loo, P. L. Rachel Ee, Y. Y. Yang, *Biomaterials* **2011**, *32*, 2369.
- [13] A. Dirisala, K. Osada, Q. Chen, T. A. Tockary, K. Machitani, S. Osawa, X. Liu, T. Ishii, K. Miyata, M. Oba, S. Uchida, K. Itaka, K. Kataoka, *Biomaterials* **2014**, *35*, 5359.
- [14] I. Ozer, A. Tomak, H. M. Zareie, Y. Baran, V. Bulmus, *Biomacromolecules* **2017**, *18*, 2699.
- [15] H. Petersen, P. M. Fechner, A. L. Martin, K. Kunath, S. Stolnik, C. J. Roberts, D. Fischer, M. C. Davies, T. Kissel, *Bioconjugate Chem.* **2002**, *13*, 845.
- [16] C. Brus, H. Petersen, A. Aigner, F. Czubyko, T. Kissel, *Bioconjugate Chem.* **2004**, *15*, 677.
- [17] M. Glodde, S. R. Sirsi, G. J. Lutz, *Biomacromolecules* **2006**, *7*, 347.
- [18] G. P. Tang, J. M. Zeng, S. J. Gao, Y. X. Ma, L. Shi, Y. Li, H.-P. Too, S. Wang, *Biomaterials* **2003**, *24*, 2351.
- [19] T. Merdan, K. Kunath, H. Petersen, U. Bakowsky, K. H. Voigt, J. Kopecek, T. Kissel, *Bioconjugate Chem.* **2005**, *16*, 785.
- [20] Q. Cheng, Y. Huang, H. Zheng, T. Wei, S. Zheng, S. Huo, X. Wang, Q. Du, X. Zhang, H.-Y. Zhang, X.-J. Liang, C. Wang, R. Tang, Z. Liang, *Biomaterials* **2013**, *34*, 3120.
- [21] M. Zheng, Y. Liu, Y. Wang, D. Zhang, Y. Zou, W. Ruan, J. Yin, W. Tao, J. B. Park, B. Shi, *Adv. Mater.* **2019**, *31*, 1903277.
- [22] J. Zhou, Y. Chau, *Biomater. Sci.* **2016**, *4*, 1462.
- [23] E. I. Geihe, C. B. Cooley, J. R. Simon, M. K. Kiesewetter, J. A. Edward, R. P. Hickerson, R. L. Kaspar, J. L. Hedrick, R. M. Waymouth, P. A. Wender, *Proc. Natl. Acad. Sci. U.S.A.* **2012**, *109*, 13171.
- [24] P. A. Wender, M. A. Huttner, D. Staveness, J. R. Vargas, A. F. Xu, *Mol. Pharmaceutics* **2015**, *12*, 742.
- [25] A. Frère, A. Baroni, E. Hendrick, A.-S. Delvigne, F. Orange, O. Peulen, G. R. Dakwar, J. Diricq, P. Dubois, B. Evrard, K. Remaut, K. Braeckmans, S. C. De Smedt, J. Laloy, J.-M. Dogné, G. Feller, L. Mespouille, D. Mottet, G. Piel, *ACS Appl. Mater. Interfaces* **2017**, *9*, 2181.
- [26] F. J. Hack, C. Cokca, S. Stadter, J. Hulsmann, K. Peneva, D. Fischer, *Macromol. Rapid Commun.* **2021**, *42*, e2000580.(8).
- [27] F. J. Xu, W. T. Yang, *Prog. Polym. Sci.* **2011**, *36*, 1099.
- [28] S. d. Á. Gonçalves, R. P. Vieira, *React. Funct. Polym.* **2020**, *147*, 104453.
- [29] M. Ahmed, R. Narain, *Prog. Polym. Sci.* **2013**, *38*, 767.
- [30] G. B. H. Chua, P. J. Roth, H. T. T. Duong, T. P. Davis, A. B. Lowe, *Macromolecules* **2012**, *45*, 1362.
- [31] U. Rungsardthong, M. Deshpande, L. Bailey, M. Vamvakaki, S. P. Armes, M. C. Garnett, S. Stolnik, *J. Controlled Release* **2001**, *73*, 359.
- [32] M. C. Deshpande, M. C. Garnett, M. Vamvakaki, L. Bailey, S. P. Armes, S. Stolnik, *J. Controlled Release* **2002**, *81*, 185.
- [33] M. C. Deshpande, M. C. Davies, M. C. Garnett, P. M. Williams, D. Armitage, L. Bailey, M. Vamvakaki, S. P. Armes, S. Stolnik, *J. Controlled Release* **2004**, *97*, 143.
- [34] J.-F. Lutz, *J. Polym. Sci., Part A: Polym. Chem.* **2008**, *46*, 3459.
- [35] J. J. F. Verhoef, T. J. Anchordoquy, *Drug Delivery Transl. Res.* **2013**, *3*, 499.
- [36] C. Cokca, L. Zartner, I. Tabujew, D. Fischer, K. Peneva, *Macromol. Rapid Commun.* **2020**, *41*, 1900668.
- [37] I. Tabujew, C. Cokca, L. Zartner, U. S. Schubert, I. Nischang, D. Fischer, K. Peneva, *J. Mater. Chem. B* **2019**, *7*, 5920.
- [38] I. Tabujew, M. Heidari, C. Freidel, M. Helm, L. Tebbe, U. Wolfrum, K. Nagel-Wolfrum, K. Koynov, P. Biehl, F. H. Schacher, R. Potestio, K. Peneva, *Biomacromolecules* **2019**, *20*, 4389.
- [39] I. Tabujew, M. Willig, N. Leber, C. Freidel, I. Negwer, K. Koynov, M. Helm, K. Landfester, R. Zentel, K. Peneva, V. Mailänder, *Acta Biomater.* **2019**, *100*, 338.

- [40] D. J. Keddie, *Chem. Soc. Rev.* **2014**, *43*, 496.
- [41] C. Cokca, L. Zartner, I. Tabujew, D. Fischer, K. Peneva, *Macromol. Rapid Commun.* **2020**, *41*, 1900668.
- [42] S. Perrier, *Macromolecules* **2017**, *50*, 7433.
- [43] “D. I. N. E. N. I. S. O. 10993–5:2009-10, Biological Evaluation of Medical Devices-Part 5: Test for In Vitro Cytotoxicity”, in European Standard EN ISO 10993–5, Brussels.
- [44] M. Bauer, C. Lautenschlaeger, K. Kempe, L. Tauhardt, U. S. Schubert, D. Fischer, *Macromol. Biosci.* **2012**, *12*, 986.
- [45] G. Liu, Y. Li, L. Yang, Y. Wei, X. Wang, Z. Wang, L. Tao, *RSC Adv.* **2017**, *7*, 18252.
- [46] M. Zink, K. Hotzel, U. S. Schubert, T. Heinze, D. Fischer, *Macromol. Biosci.* **19**, **2019**, 1900085.
- [47] D. Fischer, H. Dautzenberg, K. Kunath, T. Kissel, *Int. J. Pharm.* **2004**, *280*, 253.
- [48] S. Ochrimenko, A. Vollrath, L. Tauhardt, K. Kempe, S. Schubert, U. S. Schubert, D. Fischer, *Carbohydr. Polym.* **2014**, *113*, 597.
- [49] H. Wei, J. A. Pahang, S. H. Pun, *Biomacromolecules* **2013**, *14*, 275.
- [50] X. Zhang, S.-R. Pan, H.-M. Hu, G.-F. Wu, M. Feng, W. Zhang, X. Luo, *J. Biomed. Mater. Res., Part A* **2008**, *84A*, 795.
- [51] K. M. Takeda, K. Osada, T. A. Tockary, A. Dirisala, Q. Chen, K. Kataoka, *Biomacromolecules* **2017**, *18*, 36.
- [52] J. F. Tan, T. A. Hatton, K. C. Tam, H. P. Too, *Biomacromolecules* **2007**, *8*, 448.
- [53] D. Costabel, A. Skabeev, A. Nabiyan, Y. Luo, J. B. Max, A. Rajagopal, D. Kowalczyk, B. Dietzek, M. Wächter, H. Görls, D. Ziegenbalg, Y. Zagranjarski, C. Streb, F. H. Schacher, K. Peneva, *Chemistry* **2021**, *27*, 4081.
- [54] A. M. Breul, M. D. Hager, U. S. Schubert, *Chem. Soc. Rev.* **2013**, *42*, 5366.
- [55] M. Beija, M.-T. Charreyre, J. M. G. Martinho, *Prog. Polym. Sci.* **2011**, *36*, 568.
- [56] M. Golshan, E. Rostami-Tapeh-Esmail, M. Salami-Kalajahi, H. Roghani-Mamaqani, *Eur. Polym. J.* **2020**, *137*, 109933.
- [57] S. Pujals, L. Albertazzi, *ACS Nano* **2019**, *13*, 9707.
- [58] T. Nomoto, S. Fukushima, M. Kumagai, K. Machitani, Arnida, Y.u Matsumoto, M. Oba, K. Miyata, K. Osada, N. Nishiyama, K. Kataoka, *Nat. Commun.* **2014**, *5*, 3545.
- [59] T. Bus, C. Englert, M. Reifarth, P. Borchers, M. Hartlieb, A. Vollrath, S. Hoepfner, A. Traeger, U. S. Schubert, *J. Mater. Chem. B* **2017**, *5*, 1258.

Supporting Information

PEGylation of Guanidinium and Indole Bearing Poly(methacrylamide)s - Biocompatible Terpolymers for pDNA Delivery

*Ceren Cokca, Franz J. Hack, Daniel Costabel, Kira Herwig, Juliana Hülsmann, Patrick Then, Rainer Heintzmann, Dagmar Fischer and Kalina Peneva**

C. Cokca, D. Costabel, K. Herwig, Prof. K. Peneva
Institute of Organic Chemistry and Macromolecular Chemistry (IOMC), Friedrich Schiller
University Jena, Lessingstrasse 8, D-07743 Jena, Germany
E-mail: kalina.peneva@uni-jena.de

F. J. Hack, J. Hülsmann
Pharmaceutical Technology and Biopharmacy, Institute of Pharmacy, Friedrich Schiller
University Jena, Lessingstrasse 8, D-07743 Jena, Germany

Prof. R. Heintzmann
Institute of Physical Chemistry and Abbe Center of Photonics, Helmholtzweg 4, D-07743
Jena, Germany

Prof. R. Heintzmann and Dr. P. Then
Leibniz Institute of Photonic Technology, Albert Einstein Str. 9, 07745 Jena, Germany

Prof. D. Fischer
Department of Chemistry and Pharmacy, Pharmaceutical Technology, Friedrich-Alexander-
University Erlangen-Nürnberg, Cauerstrasse 4, D-91058 Erlangen, Germany

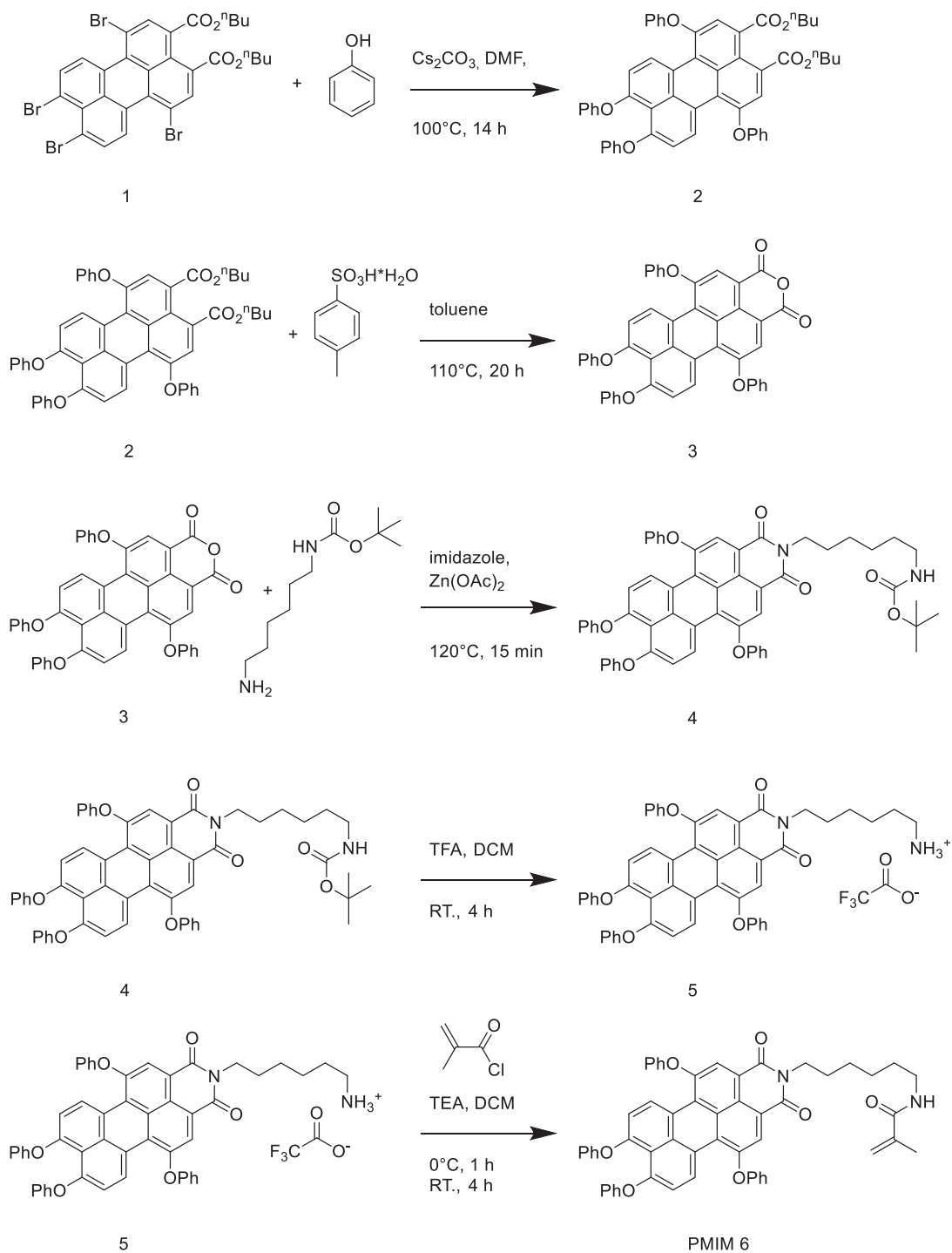
Prof. K. Peneva, Prof. D. Fischer
Jena Center for Soft Matter (JCSM), Friedrich Schiller University Jena, Philosophenweg 7, D-
07743 Jena, Germany

1. Materials and Methods for Chemical Experiments

All chemicals were purchased from SIGMA-Aldrich at the highest available purity and used as received unless mentioned otherwise. 4,4'-azobis(4-cyanovaleric acid) (ACVA) was recrystallized in methanol (MeOH) before the use. The chain transfer agent 4-Cyano-4-(phenylcarbonothioylthio)pentanoic acid (CTA) was purchased from Boron Molecular INC. The synthesis of *N*-(3-guanidinopropyl)methacrylamide (GPMA), *N*-(2-indolethyl)methacrylamide (IEMA) and P(HPMA-*co*-GPMA-*co*-IEMA) (P(HGI)) terpolymer was accomplished according to our previous study.^[1]

1.1 Synthesis of *N*-(6-methacrylamidylhexyl)-1,6,9,10-tetraphenoxyperylene-3,4-monoimide (PMIM)

The synthetic pathway to prepare *N*-(6-methacrylamidylhexyl)-1,6,9,10-tetraphenoxyperylene-3,4-monoimide (PMIM) is depicted in **Scheme S1**.



Scheme S1: Synthesis of *N*-(6-methacrylamidylhexyl)-1,6,9,10-tetraphenoxyperylene-3,4-monoimide

1.1.1 Dibutyl-1,6,9,10-tetrabromoperylene 3,4-dicarboxylate (1)

The compound was prepared as described earlier and the analytical data corresponds to the data reported before.^[2]

¹H NMR (300 MHz, CDCl₃, δ): 8.66 (d, *J* = 8.3 Hz, 2H), 8.27 (s, 2H), 8.04 (d, *J* = 8.3 Hz, 2H), 4.32 (t, *J* = 6.8 Hz, 4H), 1.72-1.83 (m, 4H), 1.40-1.52 (m, 4H), 0.99 (t, *J* = 7.4 Hz, 6H) ppm.

¹³C NMR (100 MHz, CDCl₃, δ): 168.3, 167.4, 141.3, 136.8, 134.7, 134.2, 132.3, 131.7, 131.6, 129.9, 129.8, 129.3, 129.2, 129.0, 128.6, 128.2, 127.1, 126.5, 121.6, 120.8, 119.8, 117.5, 65.9, 65.7, 30.8, 30.7, 19.4, 19.4, 13.9 ppm.

APCI-MS (neg.) *m/z* (%): calcd for C₃₀H₂₄Br₄O₄, 767.837; found, 767.844 (100) [M⁻].

1.1.2 Dibutyl-1,6,9,10-tetraphenoxyperylene 3,4-dicarboxylate (2)

To a solution of compound **1** (500 mg, 6.5 x 10⁻¹ mmol) in and caesium carbonate (2.55 g, 7.8 mmol) in DMF (25 mL) phenol (490 mg, 5.2 mmol) was added. The reaction mixture was stirred at 100°C for 14 h. After cooling to room temperature, DCM (250 mL) and water (250 mL) were added. The organic layer was separated, dried over sodium sulfate, filtered and the solvent was evaporated under reduced pressure. The product was purified *via* column chromatography (*n*-hexane: ethyl acetate 6:1). **Yield: 85%** (450 mg, 5.5 x 10⁻¹ mmol)

¹H NMR (300 MHz, CDCl₃, δ): 9.01 (d, *J* = 8.7 Hz, 2H), 7.75 (s, 2H), 6.75-7.41 (m, 22H), 4.30 (t, *J* = 6.8 Hz, 4H), 1.63-1.81 (m, 4H), 1.34-1.48 (m, 4H), 0.95 (t, *J* = 7.3 Hz, 6H).

¹³C NMR (75 MHz, CDCl₃, δ): 168.3, 167.4, 141.3, 136.8, 134.7, 134.2, 132.3, 131.7, 131.6, 129.9, 129.8, 129.3, 129.2, 129.0, 128.6, 128.2, 127.1, 126.5, 121.6, 120.8, 119.8, 117.5, 65.9, 65.7, 30.8, 30.7, 19.4, 19.4, 13.9 ppm.

APCI-MS (neg.) *m/z* (%): calcd for C₅₄H₄₄O₈, 820.304; found, 820.309 (100) [M⁻].

1.1.3 1,6,9,10-tetraphenoxyperylene 3,4-dicarboxylic monoanhydride (3)

To a solution of compound **2** (450 mg, 5.5×10^{-1} mmol) in toluene (50 mL), *p*-toluenesulfonic acid monohydrate (625 mg, 3.3 mmol) was added. The reaction mixture was stirred at 110°C for 20 h. After cooling to room temperature, ethyl acetate (100 mL) and 0.05 M hydrochloric acid (in water, 150 mL) were added. The organic layer was separated, dried over sodium sulfate, filtered and the solvent was evaporated under reduced pressure. The crude product was purified *via* column chromatography (*n*-hexane: dichloromethane 1:2). **Yield: 95%** (360 mg, 5.2×10^{-1} mmol)

^1H NMR (300 MHz, CDCl_3 , δ): 9.30 (d, $J = 8.9$ Hz, 2H), 8.20 (s, 2H), 7.37-7.45 (m, 4H), 7.17-7.32 (m, 6H), 7.01-7.13 (m, 8H), 6.77-6.85 (m, 4H) ppm.

^{13}C NMR (75 MHz, CDCl_3 , δ): 168.3, 167.4, 141.3, 136.8, 134.7, 134.2, 132.3, 131.7, 131.6, 129.9, 129.8, 129.3, 129.2, 129.0, 128.6, 128.2, 127.1, 126.5, 121.6, 120.8, 119.8, 117.5, 65.9, 65.7, 30.8, 30.7, 19.4, 19.4, 13.9 ppm.

APCI-MS (neg.) m/z (%): calcd for $\text{C}_{46}\text{H}_{26}\text{O}_7$, 690.168; found, 690.173 (100) [M^-].

1.1.4 *N*-(6-*tert*-butylcarbamoyl-hexyl)-1,6,9,10-tetraphenoxyperylene-3,4-monoimide (4)

A mixture of compound **3** (360 mg, 5.2×10^{-1} mmol), *N*-Boc-1,6-hexanediamine (990 mg, 4.6 mmol), zinc acetate (10 mg, 5.5×10^{-2} mmol) and imidazole (5 g, 73.5 mmol) was melted under stirring and heating at 120°C for 15 minutes. The reaction mixture was allowed to cool to room temperature and subsequently dissolved in dichloromethane (300 mL). The solution was washed with water (2 x 300 mL) and the organic layer was separated, dried over sodium sulfate, and filtered. The solvent was evaporated under reduced pressure. The crude product was purified *via* column chromatography (dichloromethane). **Yield: 75%** (350 mg, 4.9×10^{-1} mmol)

^1H NMR (300 MHz, CDCl_3 , δ): 9.25 (d, $J = 8.8$ Hz, 2H), 8.21 (s, 2H), 6.76-7.41 (m, 22H), 4.52 (broad s, 1H), 4.09 (t, $J = 7.5$ Hz, 2H), 3.09 (m, 2H), 1.63-1.74 (m, 2H), 1.38-1.52 (m, 15H).

^{13}C NMR (75 MHz, CDCl_3 , δ): 163.3, 157.6, 156.1, 154.6, 152.5, 133.7, 131.1, 130.7, 130.4, 129.8, 127.4, 125.6, 124.3, 123.6, 123.2, 122.9, 120.9, 120.1, 118.9, 118.5, 117.0, 77.4, 43.9, 40.5, 29.9, 28.6, 26.9, 26.5, 26.5 ppm.

1.1.5 *N*-(6-aminohexyl) 1,6,9,10-tetraphenoxyperylene-3,4-monoimide trifluoroacetat (5)

Compound 4 (350 mg, 4.9×10^{-1} mmol) was dissolved in dichloromethane (150 mL). Trifluoroacetic acid (40 mL) was added and the reaction mixture was stirred at room temperature for 4 hours before dichloromethane (150 mL) was added. The solution was washed with water (2 x 300 mL), the organic layer was separated, dried over sodium sulfate, filtered and the solvent was evaporated under reduced pressure. The crude product was purified *via* column chromatography dichloromethane: methanol 19:1). **Yield: 60%** (220 mg, 2.4×10^{-1} mmol)

^1H NMR (300 MHz, CDCl_3 , δ): 9.09 (d, $J = 8.9$ Hz, 2H), 8.04 (s, 2H), 7.29-7.38 (m, 4H), 7.09-7.25 (m, 6H), 6.92-7.06 (m, 8H), 6.72-6.80 (m, 4H), 4.03 (t, $J = 7.5$ Hz, 2H), 2.89 (t, $J = 7.4$ Hz, 2H), 1.30-1.67 (m, 8H).

No ^{13}C -NMR due to poor solubility.

1.1.6 *N*-(6-methacrylamidylhexyl)-1,6,9,10-tetraphenoxyperylene-3,4-monoimide (PMIM, 6)

Compound 5 (220 mg, 2.9×10^{-1} mmol) was dissolved in dry dichloromethane (15 mL) under argon. Triethylamine (70 mg, 6.9×10^{-1} mmol) was added and the reaction mixture was stirred at 0°C for 10 minutes. Methacroyl chloride (35 mg, 3.3×10^{-1} mmol) were dissolved in dry dichloromethane under argon and the resulting solution was added to the reaction mixture. The solution was stirred at 0°C for 1 hour and was allowed to warm to room temperature over 4 hours. Dichloromethane (50 mL) was added and the solution was washed with water (2 x

150 mL). The organic layer was separated, dried over sodium sulfate, filtered, and the solvent was evaporated under reduced pressure. The crude product was purified *via* column chromatography (dichloromethane: methanol 19: 1). **Yield: 60%** (125 mg, 1.5×10^{-1} mmol) ^1H NMR (300 MHz, CDCl_3 , δ): 9.27 (d, $J = 8.8$ Hz, 2H), 8.23 (s, 2H), 7.34-7.43 (m, 4H), 7.00-7.28 (m, 14H), 6.75-6.81 (m, 4H), 5.89 (broad s, 1H), 5.65 (s, 1H), 5.26 (s, 1H), 4.12 (t, $J = 7.4$ Hz, 2H), 3.28 (m, 2H), 1.93 (s, H), 1.30-1.67 (m, 8H).

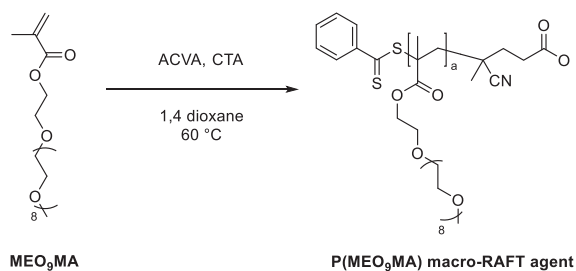
^{13}C NMR (75 MHz, CDCl_3 , δ) 163.4, 157.6, 156.1, 154.6, 152.5, 130.7, 130.4, 129.7, 127.5, 124.6, 124.4, 123.6, 123.2, 119.2, 118.9, 118.5, 117.0, 39.6, 29.9, 29.5, 27.9, 26.6, 26.5, 18.9 ppm.

APCI-MS (neg.) m/z (%): calcd for $\text{C}_{56}\text{H}_{44}\text{N}_2\text{O}_7$, 856.315; found, 856.315 (100) [M].

1.2 Synthesis of P(MEO₉MA) macro-RAFT agent

Predetermined amounts of MEO₉MA ($M_n = 500 \text{ g mol}^{-1}$), CTA, and ACVA were placed in a 25 mL Schlenk flask with a magnetic stir bar and dissolved in 1,4-dioxane by aiming 1 M final monomer concentration (**Table S1**). Then, the flask was sealed with a rubber septum and the solution was deoxygenated by purging with argon for 40 min. Following the deoxygenation process, the polymerization was started by placing the flask into a thermostated oil bath which was preheated to 60 °C. After completing the predetermined reaction time, the reaction was quenched by freezing in liquid nitrogen and then, the reaction mixture was diluted with dichloromethane (DCM). The diluted mixture was precipitated into a mixture of *n*-hexane and diethyl ether (1:1 (v/v)) 3 times. The solvent was removed *in vacuo* and a pink viscous liquid product was obtained. P(MEO₉MA) polymers were analysed by ^1H NMR spectroscopy. The molar mass (M_n) and dispersity index (D) determination was done by means of SEC_{DMAC}.

^1H NMR (300 MHz, CDCl_3 , 300 K): δH (ppm)= 4.21–3.94 (–OCH₂CH₂–(EO)₈–), 3.80–3.49 (–CH₂–(EO)₈–), 3.37 (–O–CH₃), 2.3–0.5 (4H from the backbone).

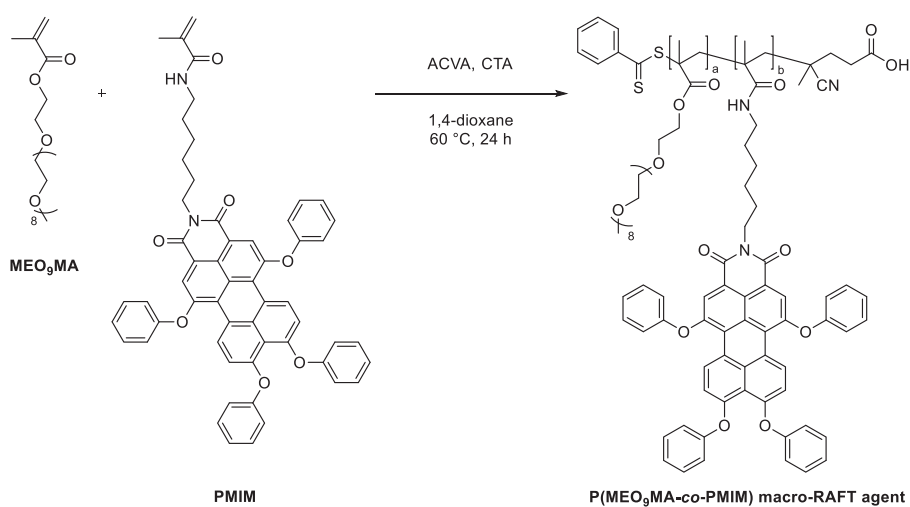


Scheme S2: RAFT polymerization of P(MEO₉MA) macro-RAFT agent

1.3 Synthesis of P(MEO₉MA-*co*-PMIM) macro-RAFT agents

P(MEO₉MA-*co*-PMIM) macro-RAFT agents (P(MEO₉MA)₁₅ and P(MEO₉MA)₂₀) were synthesized, purified and characterized by following the same route explained in section 1.2 and additionally PMIM monomer was included to the reaction. In addition, to get rid of PMIM impurity, the precipitation repeated 6 times. The reaction conditions are stated in **Table S1**.

¹H NMR (300 MHz, CDCl₃, 300 K): δH (ppm)= 9.25-6.72 (6H from PMIM; 5H from CTA), 4.23-3.80 (2H from MEO₉MA side chain; 2H from PMIM side chain), 3.72-3.40 (6H from MEO₉MA side chain), 3.38-3.28 (3H from MEO₉MA side chain; 2H from PMIM side chain), 2.05-0.60 (4H from the backbone).



Scheme S3: RAFT polymerization of P(MEO₉MA-*co*-PMIM) macro-RAFT agent

Table S1: Amounts used for the synthesis of P(MEO₉MA) macro-RAFT agents with different*M_n*

	MEO ₉ MA	PMIM	1,4-dioxane	CTA	ACVA	Reaction Duration
P(MEO₉MA)3	1.85 mL 4.1 mmol	-	1.85 mL	42.8 mg 1.5×10^{-1} mmol	10.7 mg 3.8×10^{-2} mmol	200 min
P(MEO₉MA)6	1.85 mL 4.1 mmol	-	1.85 mL	20.8 mg 7.4×10^{-2} mmol	5.21 mg 1.8×10^{-2} mmol	200 min
P(MEO₉MA)10	1.85 mL 4.1 mmol	-	1.85 mL	10.2 mg 3.6×10^{-2} mmol	2.6 mg 9.2×10^{-3} mmol	200 min
P(MEO₉MA-co-PMIM)15	1.85 mL 4.1 mmol	35 mg 4.1×10^{-2} mmol	1.9 mL	18.8 mg 6.7×10^{-2} mmol	4.7 mg 1.6×10^{-3} mmol	24 h
P(MEO₉MA-co-PMIM)20	1.85 mL 4.1 mmol	80 mg 9.3×10^{-2} mmol	2.5 mL	19.2 mg 6.8×10^{-2} mmol	4.8 mg 1.7×10^{-3} mmol	24 h
P(MEO₉MA)30	2.8 mL 6 mmol	-	2.8 mL	20.5 mg 7.3×10^{-1} mmol	5.2 mg 1.8×10^{-2} mmol	120 min
P(MEO₉MA)40	2.8 mL 6 mmol	-	2.8 mL	5.2 mg 1.8×10^{-1} mmol	1.31 mg 1.3×10^{-2} mmol	200 min

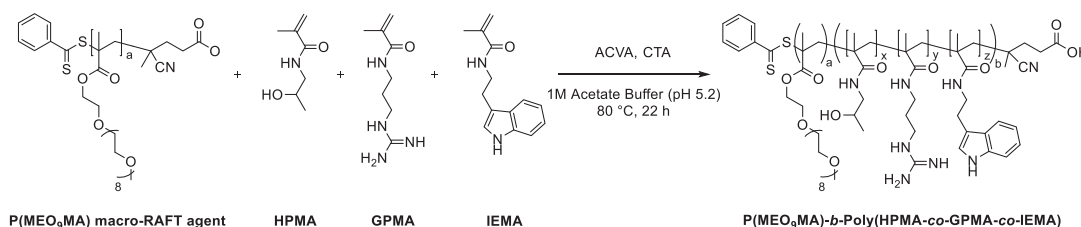
1.4 Synthesis of P(MEO₉MA)-*b*-Poly(HPMA-co-GPMA-co-IEMA) block copolymers

The terpolymer block additions with various P(MEO₉MA) units were achieved by aiming similar HPMA (21 mol%), GPMA (75 mol%), and IEMA (4 mol%) contents with comparable molar masses through reversible addition–fragmentation chain transfer (RAFT) polymerization. The details regarding the reaction contents were summarized in **Table 2S**. The reaction technique for each polymer is same and for explained below based on P(MEO₉MA)10-*b*-P(HGI):

HPMA (19.0 mg, 1.3×10^{-1} mmol) and GPMA (300 mg, 1.6 mmol) were placed in a 25 mL Schlenk flask and dissolved in degassed acetate buffer (1.2 mL) by aiming 1 M final monomer concentration. IEMA (34.7 mg, 1.5×10^{-1} mmol) in 50 μ L DMF and P(MEO₉MA) macro-RAFT agent (95.1 mg, 9.5×10^{-3} mmol) were dissolved and slowly added to the reaction

mixture. For ACVA, a stock solution (w/v) was prepared in DMF and added into reaction mixture based on precalculated amount (4.4×10^{-1} mg, 1.5×10^{-3} mmol). Then, the flask was closed with a rubber septum and the reaction mixture was purged with argon for 15 min. After that, the reaction was conducted at 80 °C for 22 hours. The product was then purified by dialysis in distilled water (dH₂O) (pH 4) at 4 °C. Finally, the sample was dried through lyophilization. The block copolymers were analyzed by ¹H NMR spectroscopy. *M_n* and *D* of the samples were detected by means of SEC_{DMAC}.

¹H NMR (300 MHz, (CD₃)₂SO, 300 K): δH (ppm)= 10.86 (1H from indole group), 8.25-6.55 (5H from indole group; 5H from phenyl group of CTA), 4.85 (1H from the side chain of the HPMA), 4.21-3.83 (2H from MEO₉MA side chain), 3.78-3.40 (1H from the side chain of the HPMA; 6H from MEO₉MA side chain), 3.29-2.59 (3H from MEO₉MA side chain; 2H from HPMA, 4H from IEMA, 4H from GPMA side chains), 2.21-0.33 (16H from the backbone, 2H from the side chain of the GPMA; 3H from the side chain of the HPMA).



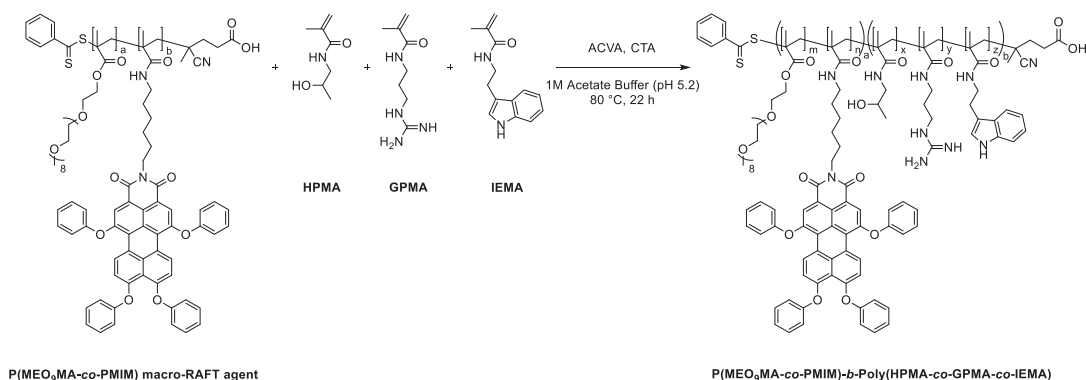
Scheme S4: RAFT polymerization of P(MEO₉MA)-*b*-Poly(HPMA-*co*-GPMA-*co*-IEMA) block copolymers

1.5 Synthesis of P(MEO₉MA-*co*-PMIM)-*b*-Poly(HPMA-*co*-GPMA-*co*-IEMA) block copolymers

The synthesis of P(MEO₉MA-*co*-PMIM)-*b*-Poly(HPMA-*co*-GPMA-*co*-IEMA) was conducted similar to section 1.4 with some changes. The reaction technique is described for P(MEO₉MA)₂₀-*b*-P(HGI) block copolymer below:

HPMA (19.0 mg, 1.3×10^{-1} mmol) and GPMA (300 mg, 1.6 mmol) were placed in a 25 mL Schlenk flask and dissolved in degassed acetate buffer (1.2 mL) by aiming 1 M final monomer concentration. IEMA (34.7 mg, 1.5×10^{-1} mmol) in 50 μ L and P(MEO₉MA)₂₀ macro-RAFT agent (209.3 mg, 9.5×10^{-3} mmol) in 60 μ L DMF were dissolved and slowly added to the reaction mixture. For ACVA, 4.4×10^{-1} mg, 1.5×10^{-3} mmol was used from the stock solution. Then, the flask was closed with a rubber septum and the reaction mixture was purged with argon for 15 min. After that, the reaction was done at 80 °C for 22 hours. At the end of the reaction, the product was purified by dialysis in distilled water (dH₂O) (pH 4) at 4 °C was dried through lyophilization. Following lyophilization, the product was washed with acetone several times to get rid of P(MEO₉MA)₂₀ residue in the sample and dried *in vacuo* overnight. The block copolymers were analyzed via ¹H NMR spectroscopy. *M_n* and *D* of the samples were detected through SEC_{DMAC}.

¹H NMR (300 MHz, (CD₃)₂SO, 300 K): δ H (ppm)= 10.85 (1H from indole group), 9.43-6.55 (6H from PMIM; 5H from indole group; 5H from phenyl group of CTA), 4.87 (1H from the side chain of the HPMA), 4.25-3.83 (2H from MEO₉MA side chain), 3.80-3.40 (1H from the side chain of the HPMA; 6H from MEO₉MA side chain), 3.29-2.62 (3H from MEO₉MA side chain; 2H from PMIM side chain; 2H from HPMA, 4H from IEMA, 4H from GPMA side chains), 2.04-0.24 (20H from the backbone, 2H from the side chain of the GPMA; 3H from the side chain of the HPMA).



Scheme S5: RAFT polymerization of P(MEO₉MA-*co*-PMIM)-*b*-Poly(HPMA-*co*-GPMA-*co*-HEMA) block copolymers

Table S2: The amounts used for synthesis of P(MEO₉MA)-*b*-P(HGI) block copolymers

	HPMA	GPMA	HEMA	P(MEO ₉ MA)	ACVA
P(MEO₉MA)3-<i>b</i>-P(HGI)	19.0 mg 1.3 × 10 ⁻¹ mmol	300 mg 1.6 mmol	34.7 mg 1.5 × 10 ⁻¹ mmol in 50 μL DMF	33.3 mg 9.5 × 10 ⁻³ mmol in 5 μL DMF	4.4 × 10 ⁻¹ mg 1.5 × 10 ⁻³ mmol
P(MEO₉MA)6-<i>b</i>-P(HGI)	19.0 mg 1.3 × 10 ⁻¹ mmol	300 mg 1.6 mmol	34.7 mg 1.5 × 10 ⁻¹ mmol in 50 μL DMF	57.0 mg 9.5 × 10 ⁻³ mmol in 10 μL DMF	4.4 × 10 ⁻¹ mg 1.5 × 10 ⁻³ mmol
P(MEO₉MA)10-<i>b</i>-P(HGI)	19.0 mg 1.3 × 10 ⁻¹ mmol	300 mg 1.6 mmol	34.7 mg 1.5 × 10 ⁻¹ mmol in 50 μL DMF	95.1 mg 9.5 × 10 ⁻³ mmol in 15 μL DMF	4.4 × 10 ⁻¹ mg 1.5 × 10 ⁻³ mmol
P(MEO₉MA-<i>co</i>-PMIM)15-<i>b</i>-P(HGI)	19.0 mg 1.3 × 10 ⁻¹ mmol	300 mg 1.6 mmol	34.7 mg 1.5 × 10 ⁻¹ mmol in 50 μL DMF	147.4 mg 9.5 × 10 ⁻³ mmol in 60 μL DMF	4.4 × 10 ⁻¹ mg 1.5 × 10 ⁻³ mmol
P(MEO₉MA-<i>co</i>-PMIM)20-<i>b</i>-P(HGI)	19.0 mg 1.3 × 10 ⁻¹ mmol	300 mg 1.6 mmol	34.7 mg 1.5 × 10 ⁻¹ mmol in 50 μL DMF	209.3 mg 9.5 × 10 ⁻³ mmol in 60 μL DMF	4.4 × 10 ⁻¹ mg 1.5 × 10 ⁻³ mmol
P(MEO₉MA)30-<i>b</i>-P(HGI)	19.0 mg 1.3 × 10 ⁻¹ mmol	300 mg 1.6 mmol	34.7 mg 1.5 × 10 ⁻¹ mmol in 50 μL DMF	294.9 mg 9.5 × 10 ⁻³ mmol in 40 μL DMF	4.4 × 10 ⁻¹ mg 1.5 × 10 ⁻³ mmol
P(MEO₉MA)40-<i>b</i>-P(HGI)	19.0 mg 1.3 × 10 ⁻¹ mmol	300 mg 1.6 mmol	34.7 mg 1.5 × 10 ⁻¹ mmol in 50 μL DMF	371 mg 9.5 × 10 ⁻³ mmol in 50 μL DMF	4.4 × 10 ⁻¹ mg 1.5 × 10 ⁻³ mmol

1.6 ^1H NMR and ^{13}C NMR spectra of the compounds

The synthesized compounds were characterized by a Bruker WS 300 MHz spectrometer (controller: Bruker Avance III) in CDCl_3 and $(\text{CD}_3)_2\text{SO}$ at 300 K.

1.6.1 Dibutyl-1,6,9,10-tetrabromoperylene-3,4-dicarboxylate (1)

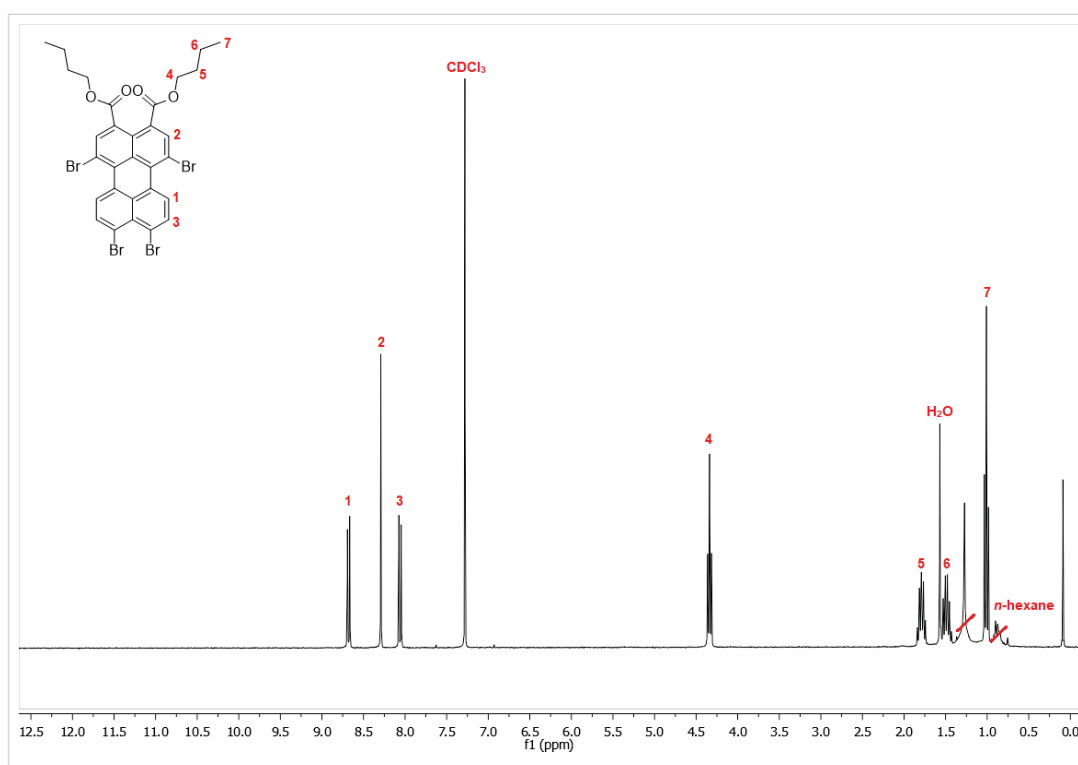


Figure S1. ^1H NMR spectrum of dibutyl-1,6,9,10-tetrabromoperylene-3,4-dicarboxylate (300 MHz, CDCl_3 , 300 K)

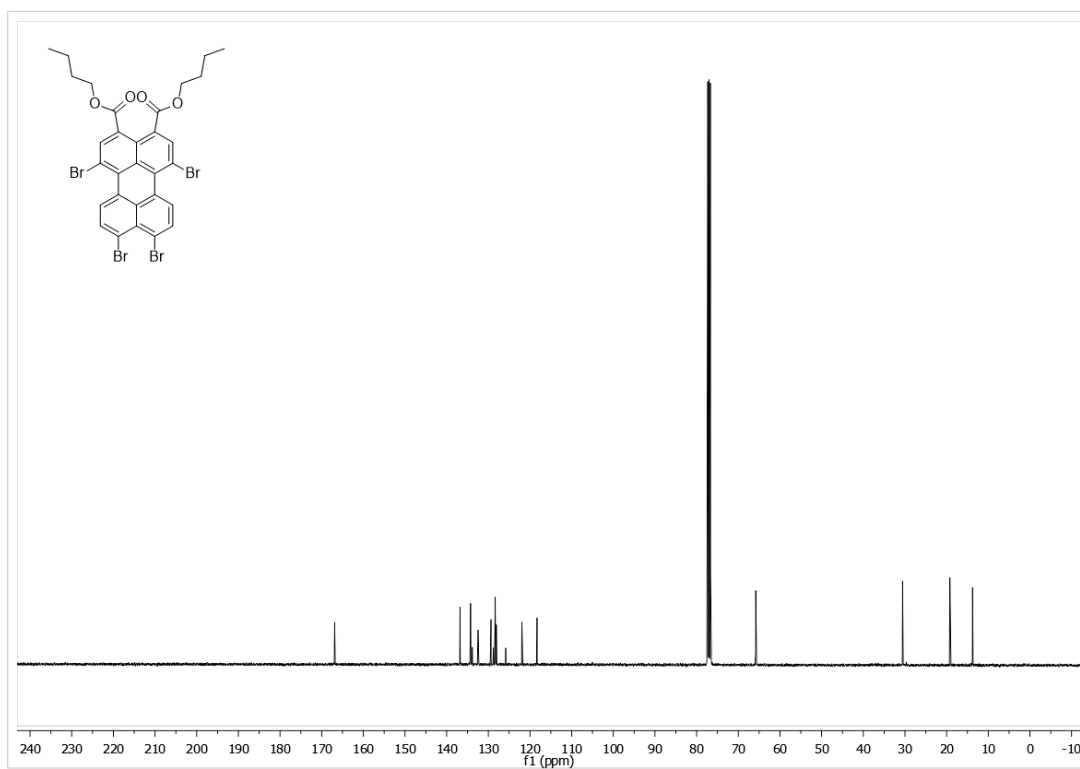


Figure S2. ¹³C NMR spectrum of dibutyl-1,6,9,10-tetrabromoperylene-3,4-dicarboxylate (100 MHz, CDCl₃, 300 K)

1.6.2 Dibutyl-1,6,9,10-tetraphenoxyperylene 3,4-dicarboxylate (2)

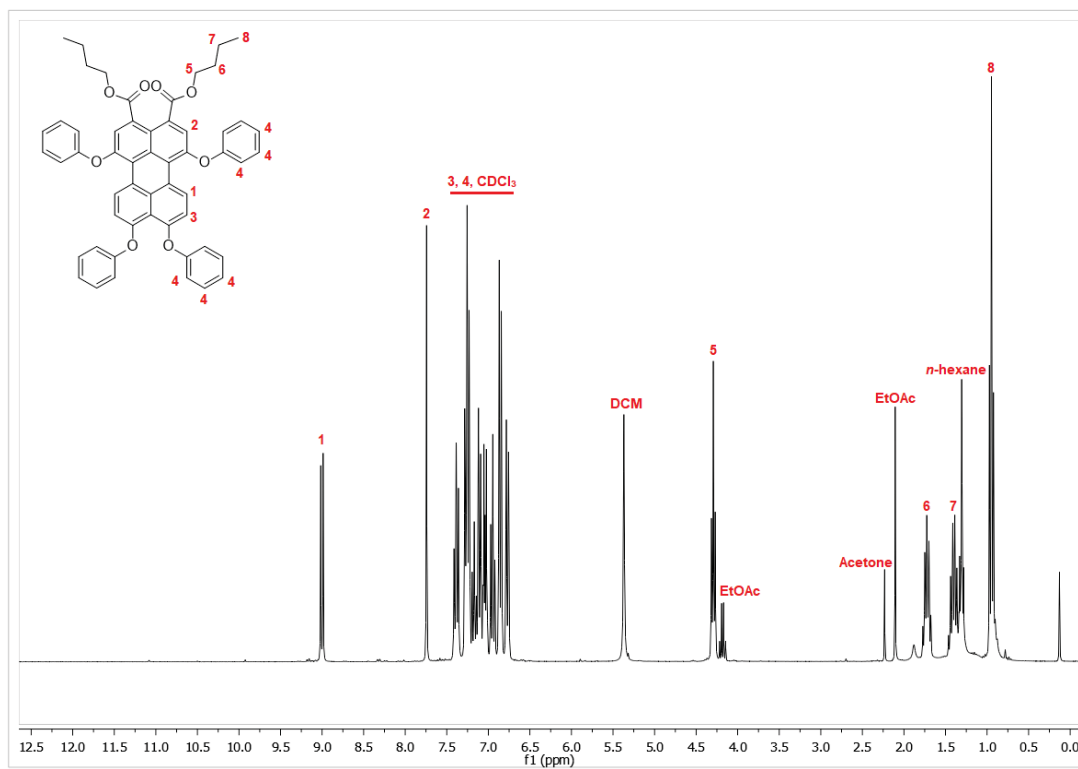


Figure S3. ^1H NMR spectrum of dibutyl-1,6,9,10-tetraphenoxyperylene 3,4-dicarboxylate (300 MHz, CDCl_3 , 300 K)

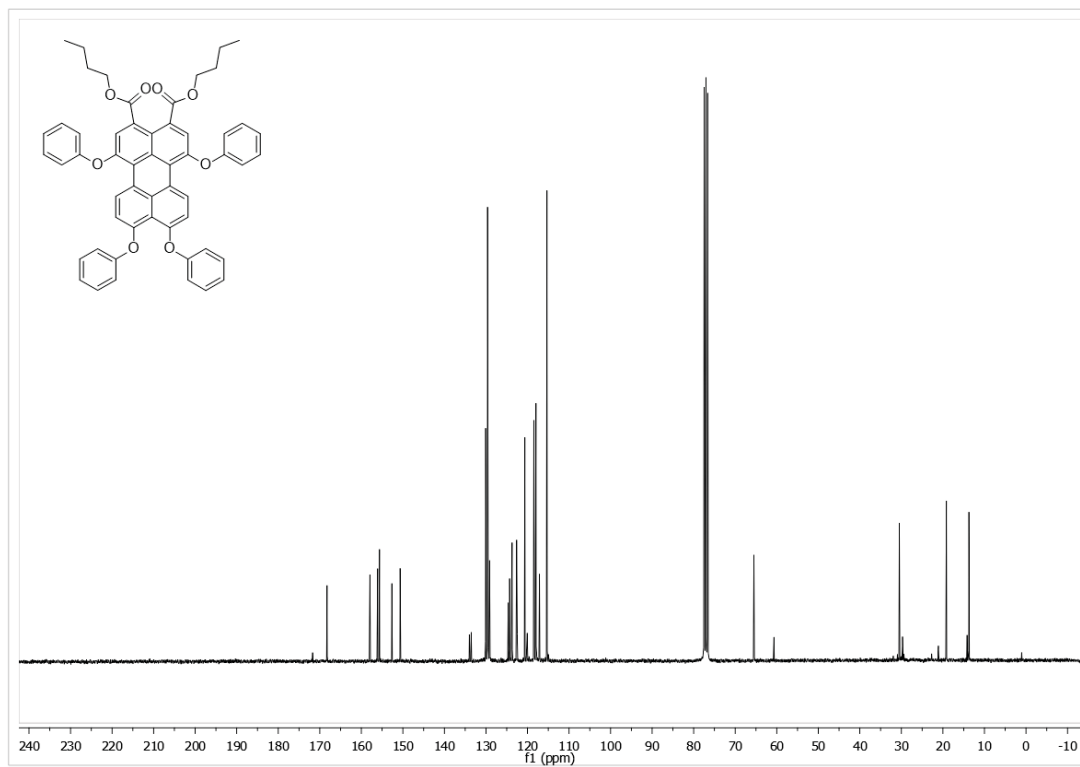


Figure S4. ^{13}C NMR spectrum of dibutyl-1,6,9,10-tetraphenoxyperylene 3,4-dicarboxylate (75 MHz, CDCl_3 , 300 K)

1.6.3 1,6,9,10-tetraphenoxyperylene 3,4-dicarboxylic monoanhydride (3)

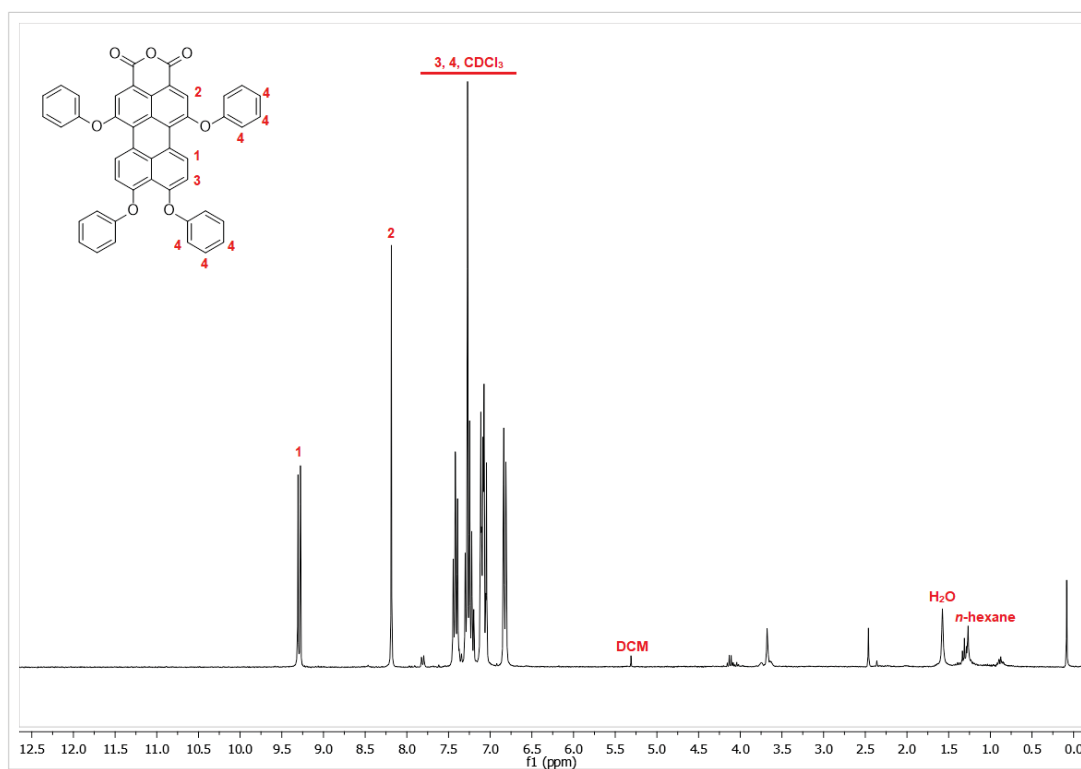


Figure S5. ¹H NMR spectrum of 1,6,9,10-tetraphenoxyperylene 3,4-dicarboxylic monoanhydride (300 MHz, CDCl₃, 300 K)

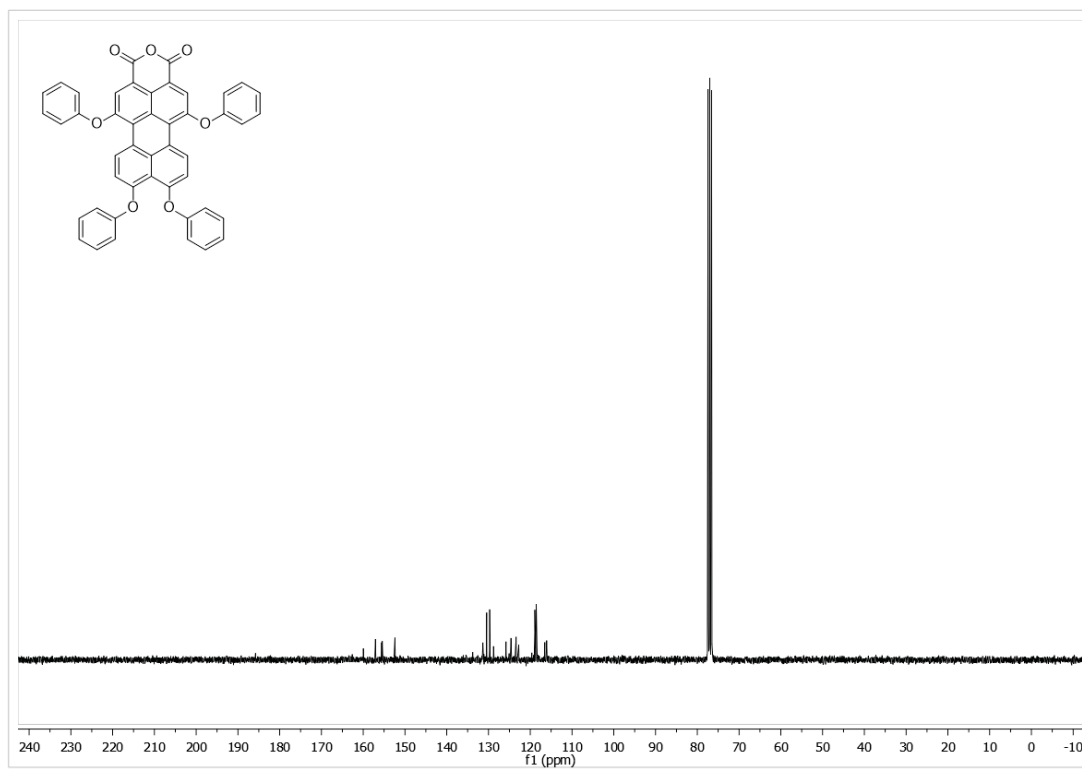


Figure S6. ^{13}C NMR spectrum of 1,6,9,10-tetraphenoxyperylene 3,4-dicarboxylic monoanhydride (75 MHz, CDCl_3 , 300 K)

1.6.4 *N*-(6-*tert*-butylcarbamate-yl-hexyl)-1,6,9,10-tetraphenoxyperylene-3,4-monoimide

(4)

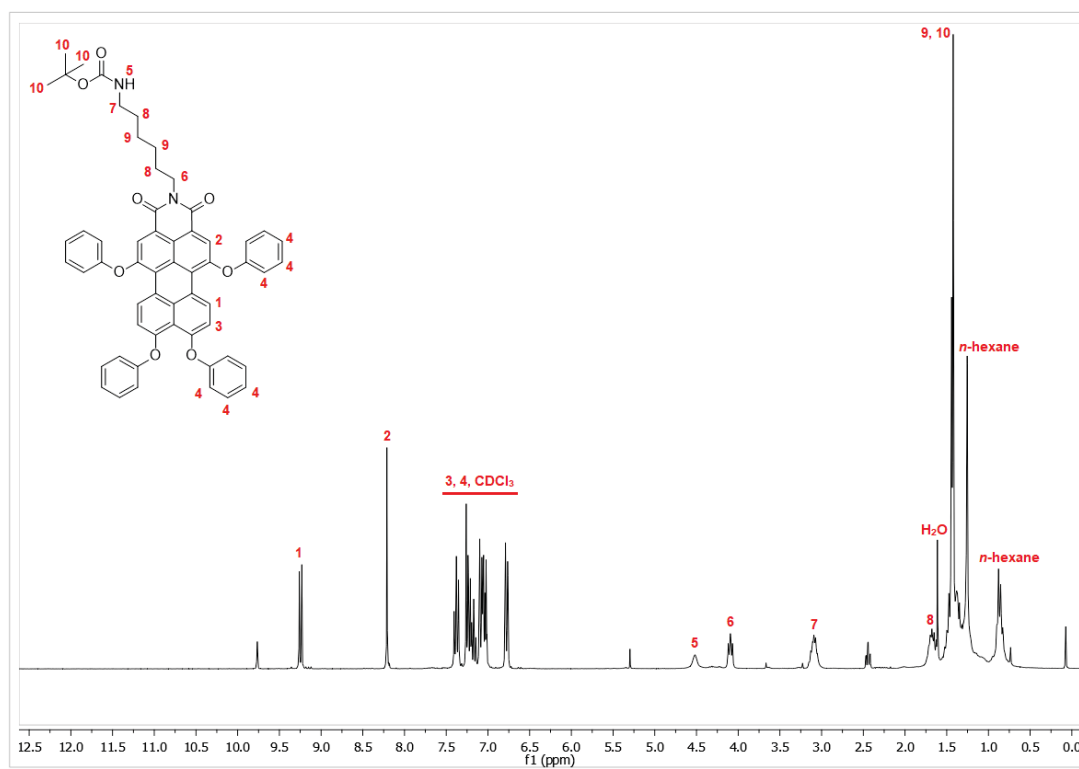


Figure S7. ¹H NMR spectrum of *N*-(6-*tert*-butylcarbamate-yl-hexyl)-1,6,9,10-tetraphenoxyperylene-3,4-monoimide (300 MHz, CDCl₃, 300 K)

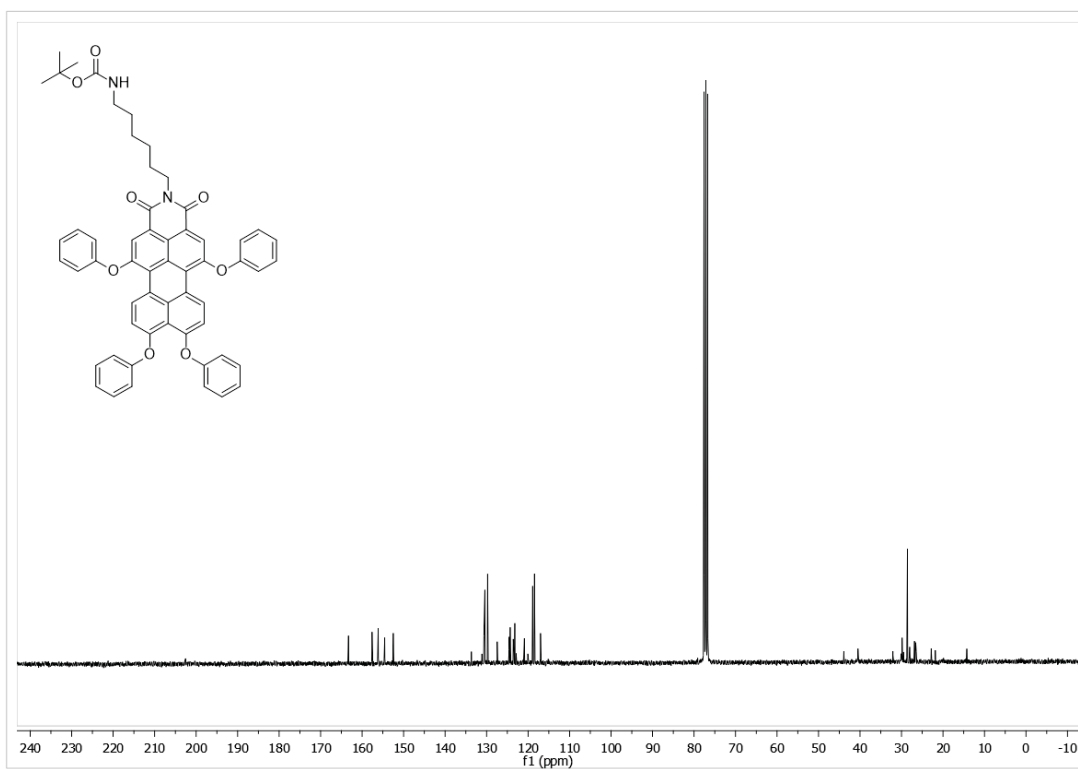


Figure S8. ¹³C NMR spectrum of *N*-(6-*tert*-butylcarbamoyl-hexyl)-1,6,9,10-tetraphenoxyperylene-3,4-monoimide (75 MHz, CDCl₃, 300 K)

1.6.5 *N*-(6-aminohexyl) 1,6,9,10-tetraphenoxyperylene-3,4-monoimide trifluoroacetate (5)

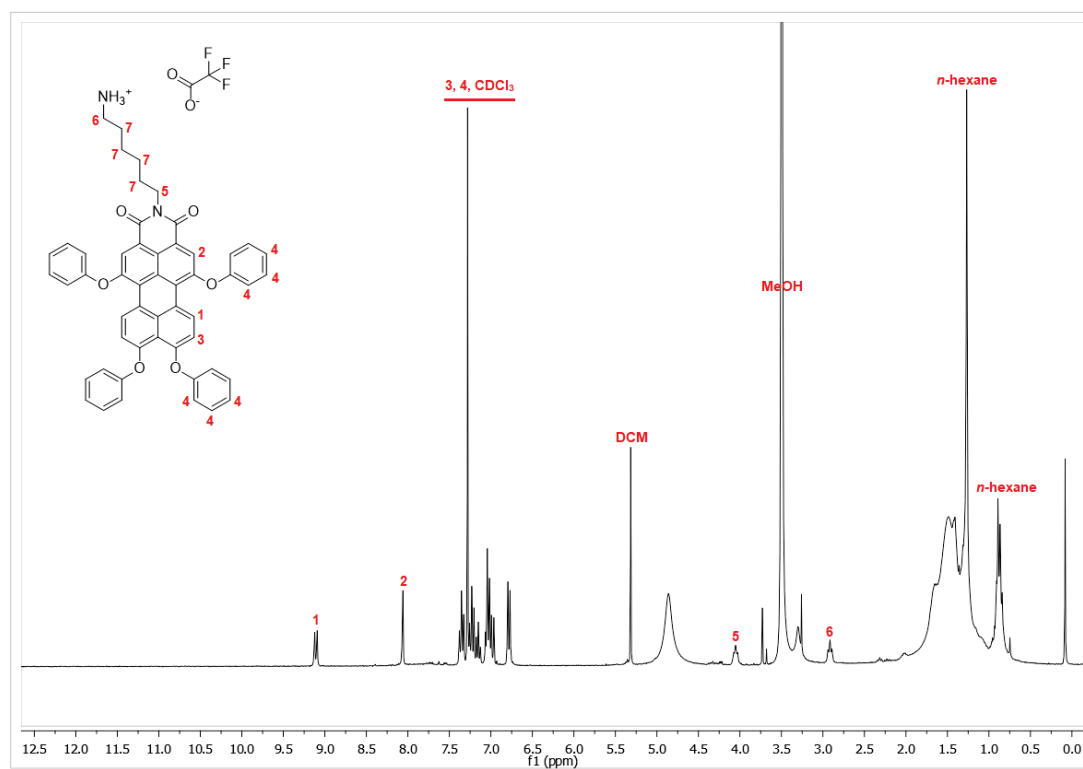


Figure S9. ¹H NMR spectrum of *N*-(6-aminohexyl) 1,6,9,10-tetraphenoxyperylene-3,4-monoimide trifluoroacetate (300 MHz, CDCl₃, 300 K)

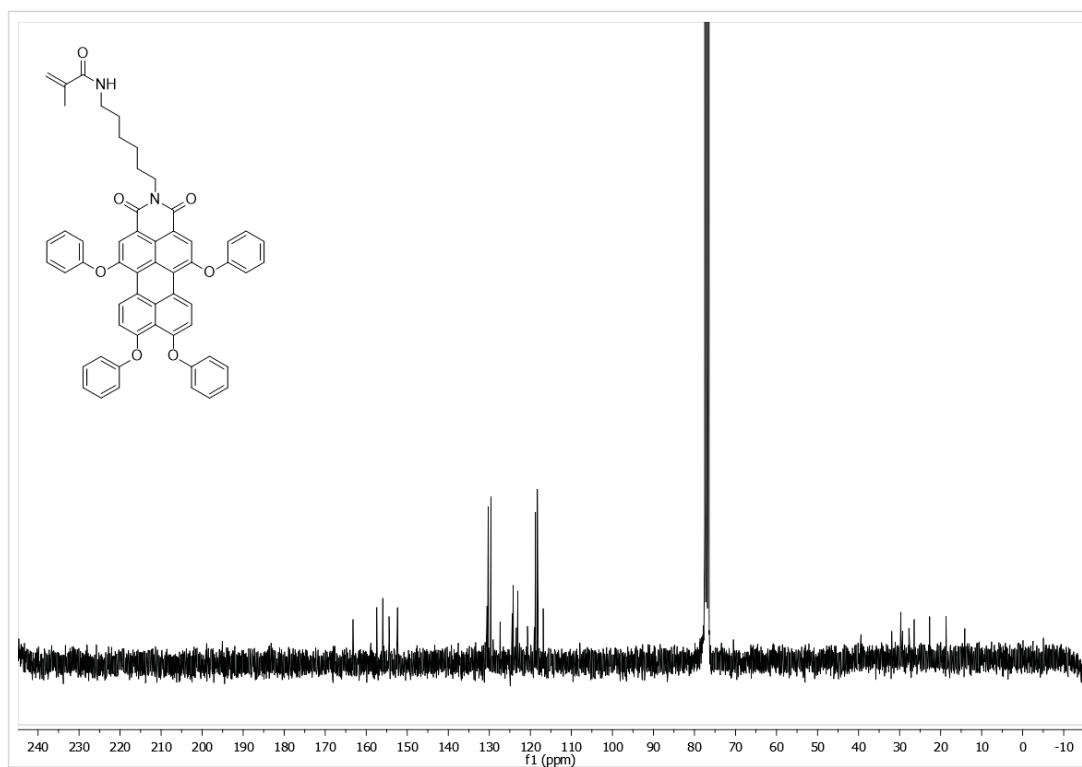


Figure S11. ¹³C NMR spectrum of *N*-(6-methacrylamidylhexyl)-1,6,9,10-tetraphenoxyperylene-3,4-monoimide (75 MHz, CDCl₃, 300 K)

1.6.7 P(MEO₉MA)₁₀ macro-RAFT agent

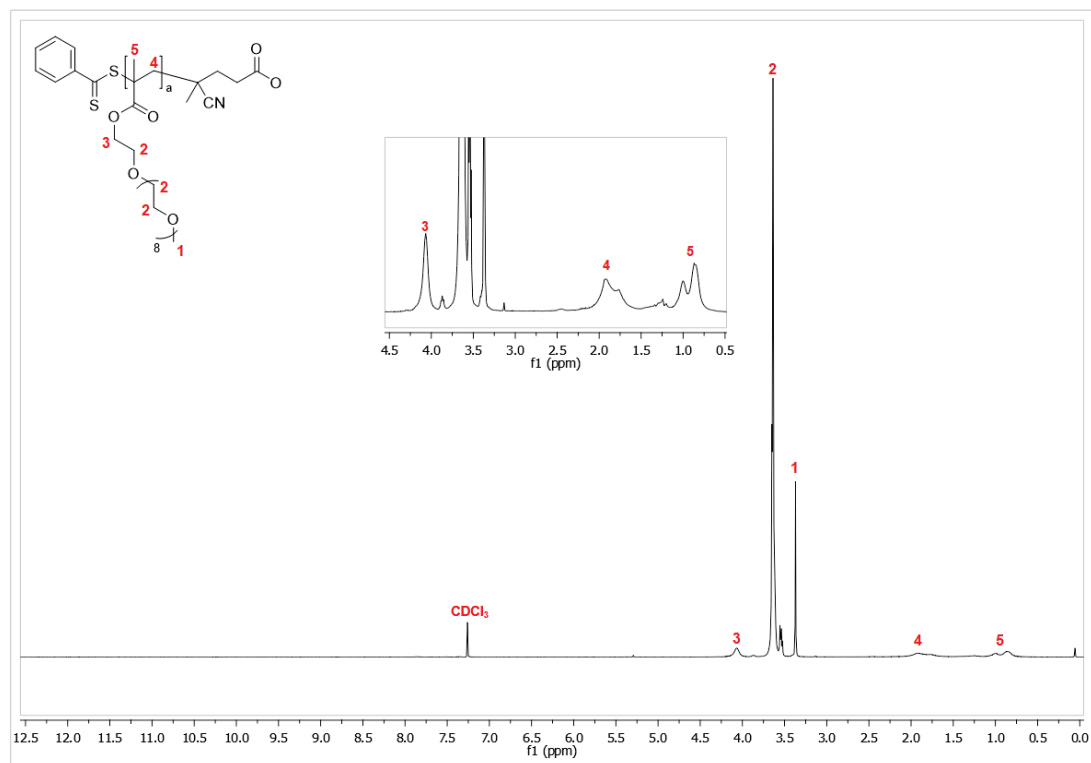


Figure S12. ¹H NMR spectrum of P(MEO₉MA)₁₀ macro-RAFT agent (300 MHz, CDCl₃, 300 K)

1.6.8 P(MEO₉MA)20 macro-RAFT agent

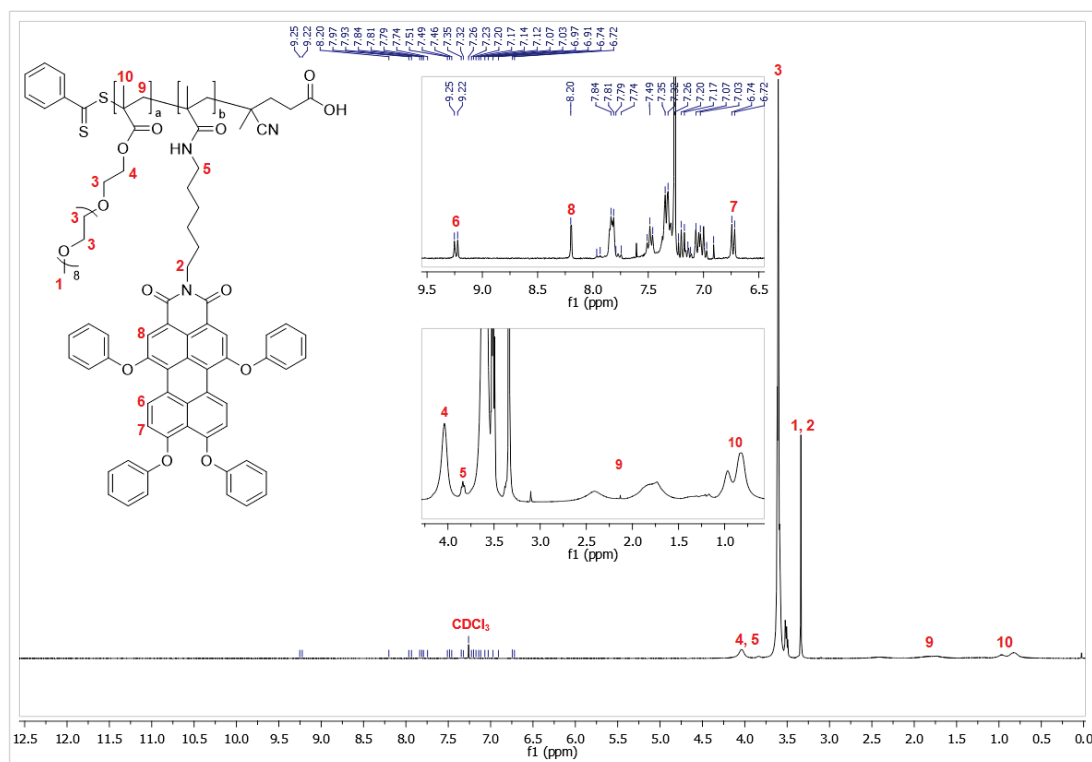


Figure S13. ¹H NMR spectrum of P(MEO₉MA-co-PMIM)₂₀ macro-RAFT agent (300 MHz, CDCl₃, 300 K)

1.6.9 P(MEO₉MA)10-*b*-P(HGI) block copolymer

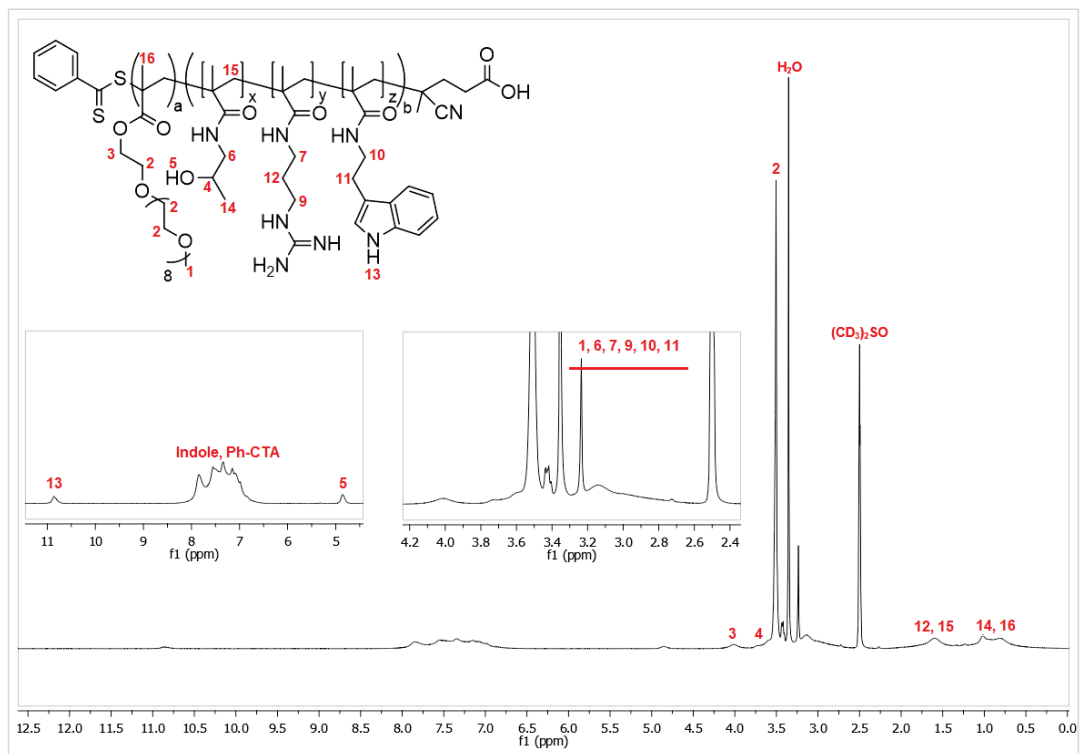


Figure S14. ¹H NMR spectrum of P(MEO₉MA)10-*b*-P(HGI) block copolymer (300 MHz, (CD₃)₂SO, 300 K)

1.6.10 P(MEO₉MA)₂₀-*b*-P(HGI) block copolymer

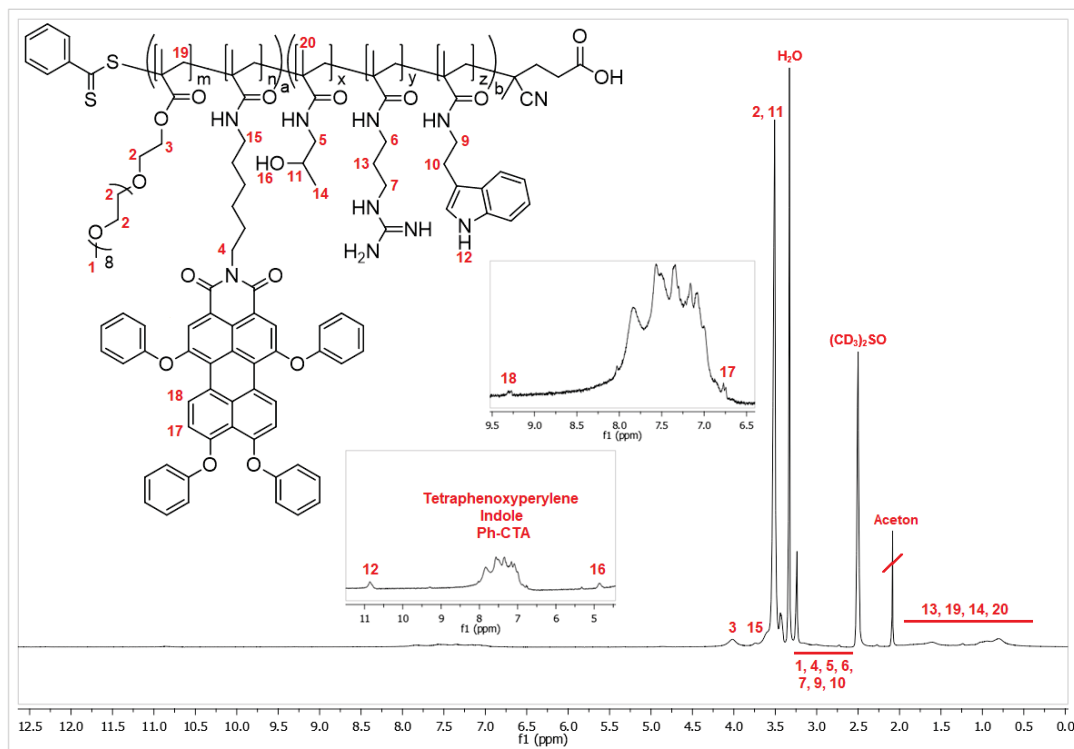


Figure S15. ¹H NMR spectrum of P(MEO₉MA-*co*-PMIM)₂₀-*b*-P(HGI) block copolymer (300 MHz, (CD₃)₂SO, 300 K)

1.7 Size Exclusion Chromatography

The molar mass of polymers were characterized by SEC_{DMAc} conducted with dimethylacetamide and lithium chloride (DMAc + 0.21% LiCl) as the eluent at 40 °C with the flow rate of 1 mL/min using a PSS GRAM guard/1000/30 Å column (particle size: 10 μm). The refractive index detector (G1362A) and the UV Detector (G1315D, wavelength: 310 nm) were used to monitor the elution. The molar mass was determined in comparison of a calibration with poly(methyl methacrylate) (PMMA) standards.

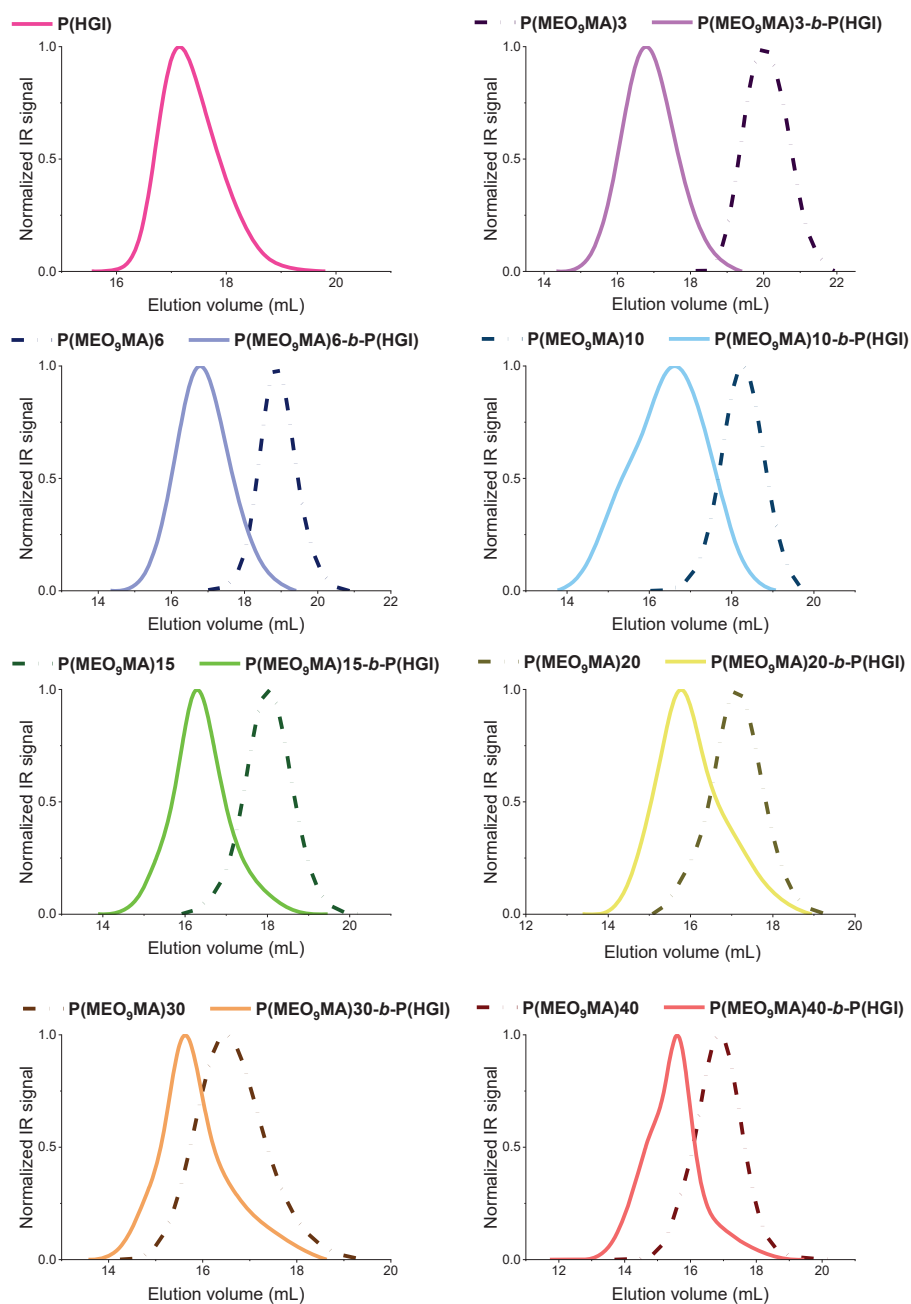


Figure S16. SEC_{DMAc} traces of P(MEO₉MA) macro-RAFT agents and P(MEO₉MA)-*b*-P(HGI) block copolymers

1.8 Absorbance and emission spectra of labeled polymers

Absorbance and emission spectra were recorded by means of Tecan Infinite 200 PRO at room temperature.

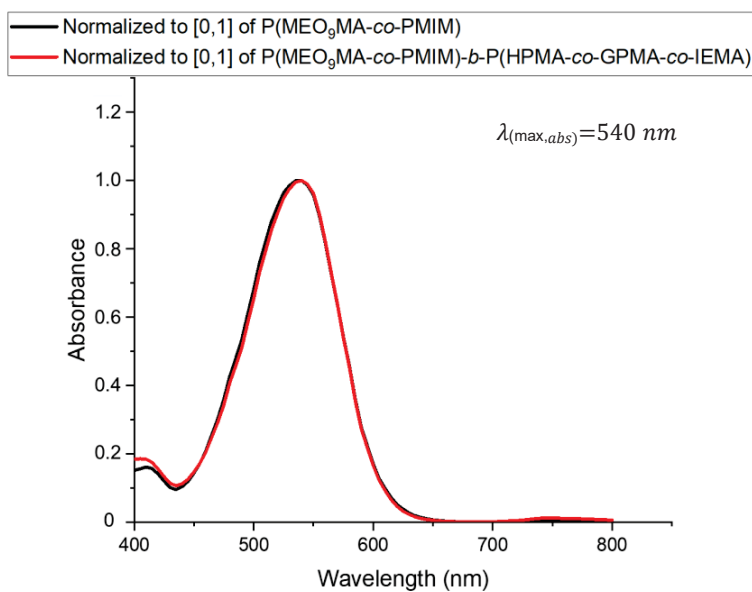


Figure S17. Absorbance spectra of P(MEO₉MA-co-PMIM) macro-RAFT agent and P(MEO₉MA-co-PMIM)-b-Poly(HPMA-co-GPMA-co-IEMA) block copolymer (10 mg mL⁻¹ polymer solution in water)

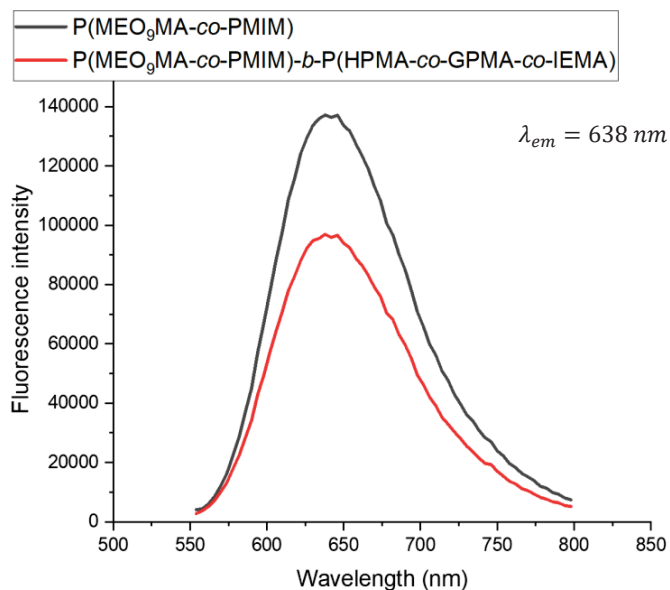


Figure S18. Emission spectra of P(MEO₉MA-*co*-PMIM) macro-RAFT agent and P(MEO₉MA-*co*-PMIM)-*b*-Poly(HPMA-*co*-GPMA-*co*-IEMA) block copolymer (10 mg mL⁻¹ polymer solution in water)

2. Biological Studies

2.1 *In vitro* cytotoxicity assay

Cell viability of L-929 mouse fibroblasts (ACC 2, DSMZ-German Collection of Microorganisms and Cell Cultures GmbH, Braunschweig, Germany) was investigated using the CellTiter-Glo[®] Luminescent Cell Viability Assay (Promega Corporation, Madison, USA) following the manufacturer's instructions. L-929 cells were seeded into 96-well plates (8,500 cells/well) in 100 μ L Roswell Park Memorial Institute (RPMI) cell culture medium supplemented with 1% L-glutamine and 10% fetal bovine serum (FBS) (all Gibco, ThermoFisher[™] Scientific, Darmstadt, Germany) and incubated for 24 h. Afterwards, polymers (100 μ L/well) were dissolved in the same medium with concentrations ranging from 3.9 to 500 μ g mL⁻¹ and after further 24 h 100 μ L CellTiter-Glo[®] reagent were added.

Luminescence was measured using the Tecan Spark 20M (Tecan Group AG, Männedorf, Switzerland). Thiomersal (0.02%) treated cells were considered as positive control whereas non-treated cells were used as negative control (100%). Medium and polymer containing medium without cells were referred to as blank and polymer control, respectively. Polymer containing medium control was subtracted from the measured values. The experiment was repeated once (n = 8) giving results in mean \pm SD. A cell viability \leq 70% was considered as toxic according to DIN EN ISO 10993-5.^[3]

2.2 Preparation of plasmid/polymer polyplexes

pGL3 plasmid DNA (pDNA) (Promega, Madison, USA) encoding for the luciferase reporter gene was transferred to competent *E. coli* TG1 (Hans-Knoell-Institute, Jena, Germany) and isolated and purified using the E.Z.N.A. Plasmid Maxi Kit (OMEGA bio-tek, Norcross, USA) as described in details earlier.^[4] The formation of polyplexes made of PEGylated polymers and plasmid DNA at different N/P ratios (i.e. the ratio of cationic polymer nitrogen (N) to anionic pDNA phosphate (P)) from 2 to 40 was achieved by adding the required volumes of polymer stock solution (5 mg mL⁻¹) to an equal volume of pDNA solution in 150 mM NaCl with 10 mM HEPES ((4-(2-hydroxyethyl)-1-piperazineethanesulfonic acid)) buffer, pH 7.4 (both Carl Roth, Karlsruhe, Germany). After vortexing for 10 s and incubation at room temperature for 10 min, polyplexes were used in experiments.^[5]

2.3 pDNA binding assay

The AccuBlue[®] High Sensitivity dsDNA Quantitation Kit (Biotium, Hayward, USA) was used to quantify the pDNA binding efficacy of the polymers following the manufacturer's protocol. Five microliters of polyplex solution per well were mixed in black 96-well plates (Fluotrac 200, Greiner bio-one) with 200 μ L of a mixture of 100X enhancer and quantification solution (1:100). After 10 min incubation time under shaking (450 rpm) at room temperature in the dark

fluorescence was measured using the Tecan Spark 20M (485 nm excitation, 530 nm emission). The 100% reference was determined from free pDNA without polymer whereas a mixture of 150 mM NaCl and 10 mM HEPES solution pH 7.4 served as blank control. Polyplexes of pDNA with linear poly(ethylene imine) (lPEI, 2,500 g mol⁻¹; Polysciences Europe GmbH, Eppelheim, Germany) at N/P 20 served as positive control. The experiment was independently repeated once (n = 8) giving results in percent as mean ± SD.

2.4 Horizontal agarose gel electrophoresis

Agarose gel electrophoresis of polyplexes was performed with 10 µL polyplex solution containing 200 ng pDNA at different N/P ratios. Samples were mixed with 1 µL loading buffer (Carl Roth) and loaded on an agarose gel (1%) (peqGold Universal Agarose, Peqlab Biotechnology, Erlangen, Germany) gel containing 0.125 µg mL⁻¹ ethidium bromide (SERVA Electrophoresis GmbH, Heidelberg, Germany). Free pDNA (200 ng) was used as positive control whereas bromophenol blue (SERVA Electrophoresis GmbH) served as running control. Polymer without pDNA was considered as negative control. Electrophoretic separation was performed at 80 V in an electrophoresis chamber (Biometra, Goettingen, Germany) for 30 min using TAE solution (40 mM Tris, 1 mM EDTA, 1% acetic acid, all Carl Roth) as running buffer. Afterwards, gels were photographed under UV transillumination (Inas GmbH, Goettingen, Germany) at 312 nm. Analysis and gel evaluation was performed using the BioVision gel documentation software (VILBER, Collegien, France).

To evaluate the ability to protect the pDNA from enzymatic degradation by nucleases, the polyplex solution was treated with 2 µL of DNase I (activity of 5 Kunitz units µg⁻¹ pDNA, Amersham Biosciences, Piscataway, USA) at 37 °C for 45 min. Inactivation of the enzyme after the incubation time was performed at 70 °C for 35 min. Afterwards, the pDNA was released from the polyplexes by heparin treatment (20 I.U., Carl Roth) at 37 °C for 20 min followed by agarose gel electrophoresis as described above. Free untreated pDNA served as pDNA control,

whereas pDNA treated under the same conditions but without the enzyme was used as negative control. pDNA treated with DNase I served as positive control to proof efficient enzymatic degradation.

2.5 *In vitro* transfection efficacy using luciferase reporter gene

Transfection efficacy was investigated in CHO-K1 cells (ACC 110, DSMZ-German Collection of Microorganisms and Cell Cultures GmbH) and quantified by luciferase reporter gene expression (Luciferase Assay System (Promega)) following the manufacturer's protocol using the microplate reader Tecan Spark 20M.^[4] CHO-K1 cells were seeded into a 12-well plate with 50,000 cells/well in 1 mL Ham's F12 medium supplemented with 1 mM L-glutamine and 10% fetal bovine serum (Gibco) at 37 °C, 5% CO₂ and 95% relative humidity. After 24 h incubation cells were incubated with polyplexes (N/P 2 to 40) containing 4 µg pDNA in 200 µL buffer (150 mM NaCl and 10 mM HEPES, pH 7.4)/well. The medium was changed after 4 h followed by 44 h of further incubation. Cells treated with free pDNA (4 µg) only as well as cells treated with buffer solution (200 µL) and cells treated with 2,500 g mol⁻¹ IPEI and pDNA at a N/P ratio of 20 were used as controls. Transgene expression was quantified by the luciferase assay after cell lysis and results were given as relative light units (RLUs) µg⁻¹ protein. The protein amount was quantified using the bicinchoninic acid (BCA) assay kit (PierceTM BCA Protein Assay Kit, ThermoFisherTM) following the manufacturer's instructions. Thus, 25 µL cell lysate were treated with 10 µL 0.05 M iodoacetamide (Applichem, Darmstadt, Germany) solution at 37 °C for 20 min and incubated at 37 °C for 40 min. BCA assay results were calculated in relation to a bovine serum albumin (BSA) standard curve after spectrophotometric quantification (Tecan Spark 20M) at 570 nm. The experiment was performed twice (n = 8) giving results in mean ± SD.

3. Biological Results

3.1 Determination of the pDNA binding by agarose gel electrophoresis

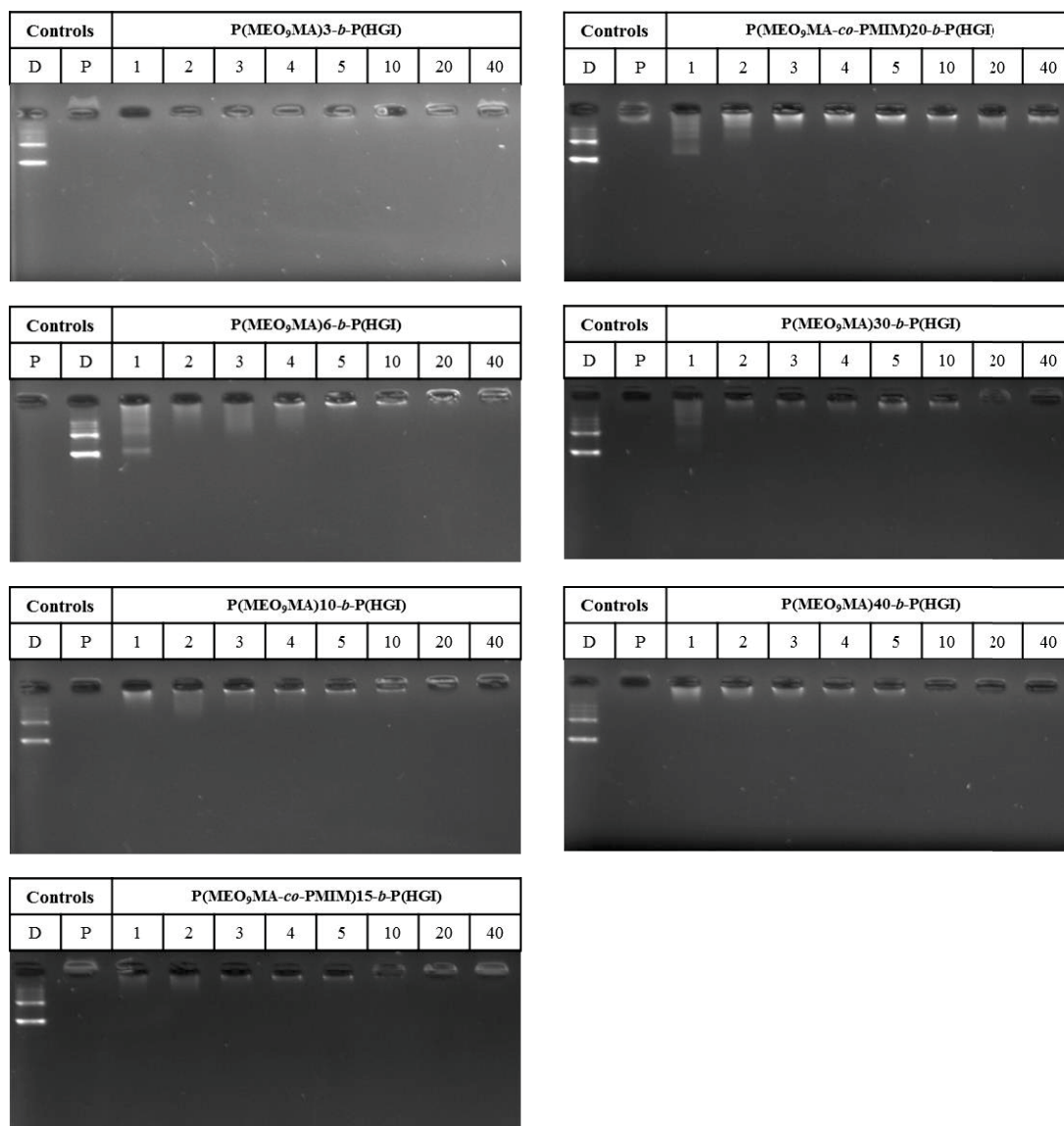


Figure S19. pDNA binding of the block copolymers with varying PEG content at different N/P ratios determined by horizontal agarose gel electrophoresis compared to free pDNA (D) and free polymer (P).

3.2 Enzymatic stability testing

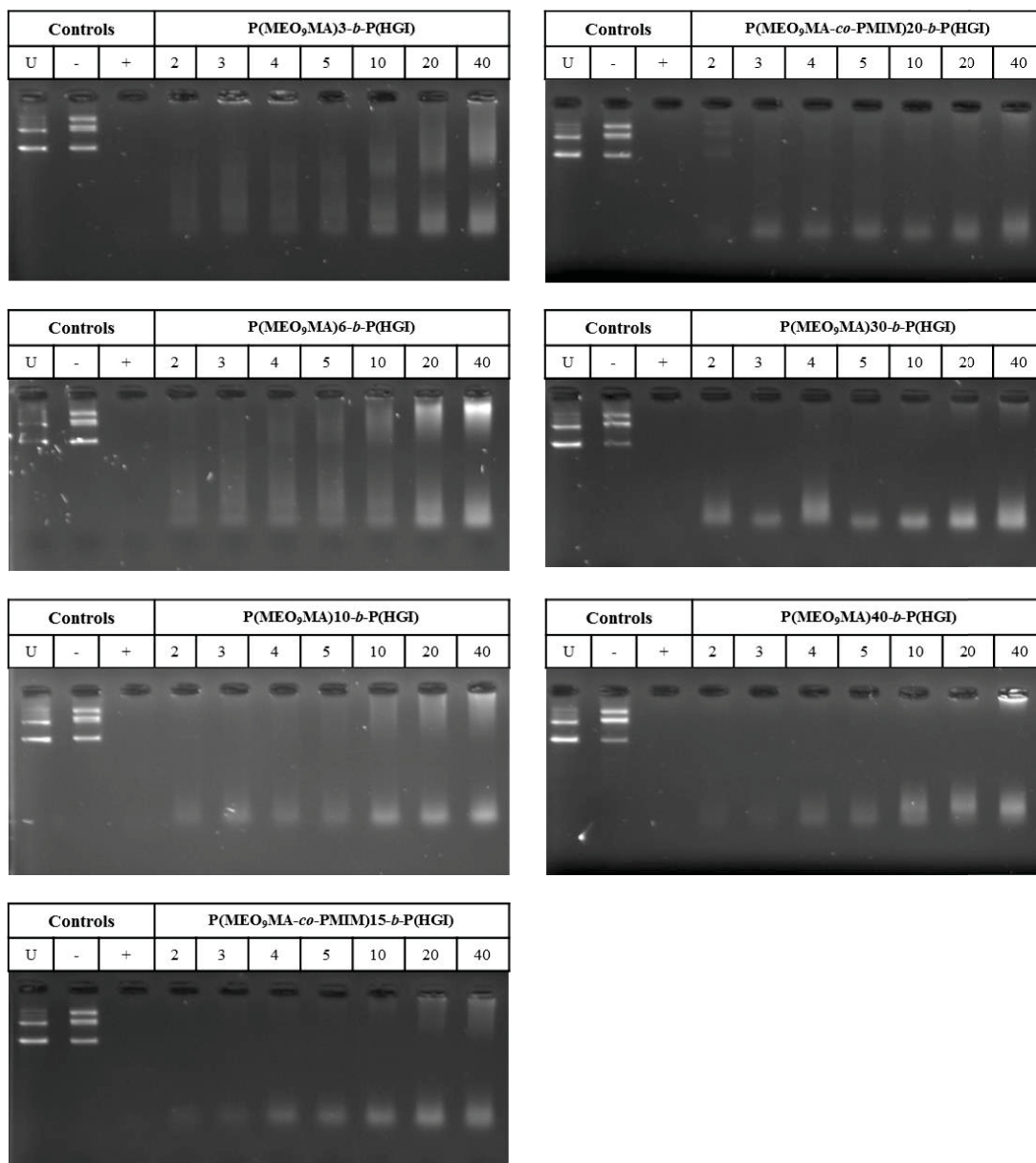


Figure S20. Stability of the terpolymer based polyplexes with pDNA at different N/P ratios, against enzymatic DNaseI degradation (controls: untreated free plasmid (U); free plasmid treated in the same way as polyplexes but without enzyme (-); free plasmid treated with enzyme (+)).

4. Structured illumination microscopy (SIM)

For structured illumination microscopy (SIM) experiments HeLa cells (ATCC CCL-2) were cultured at 37 °C and 5% CO₂ in standard tissue culture flasks using Dulbecco's Modified Eagle's Medium (DMEM) cell culture medium (containing no phenol red to reduce unspecific fluorescence) supplemented with 10 % FBS and 1 % penicillin/streptomycin (Pen/Strep). One day prior to imaging, cells have been transferred to 8-well chambered cover slips (ibidi μ -Slide with Glass Bottom #1.5H, ibidi GmbH, Graefeling Germany) in 100 μ L cell culture medium. Staining was performed by replacing the medium in the respective wells with polyplex solution prepared as described earlier and diluted in cell culture medium. Incubation was performed for 1 h and 4 h. Directly prior to imaging, the medium was aspirated, wells have been washed twice with PBS and refilled with fresh cell culture medium. All structured illumination microscopy images have been acquired using a commercial Zeiss Elyra S.1 system (Zeiss, Jena, Germany), equipped with a Zeiss plan-apochromat 63 \times /1.40 Oil DIC objective (Zeiss) and an Andor iXon 885 emCCD (Andor-Oxford Instruments, Belfast, UK). The Zeiss "Zen" software (version 2.1, Zeiss, Germany) was used for image acquisition and reconstruction of SIM images. The Elyra's 561 nm (100 mW) laser line has been used for excitation of the dyes.

Exposure time and laser intensity were adjusted to utilize the full dynamic range of the emCCD when possible. An exposure time of 100 ms and an em-gain of 20 were selected, together with a laser power of 35% for samples with 1h incubation time. For the samples incubated for 4h, laser power was set to 45% at 150 ms exposure time and no em-gain.

The raw SIM data was then reconstructed with ZEN software in manual mode using standard settings and „baseline shift“ for conservation of full dynamic range in the final SIM images.

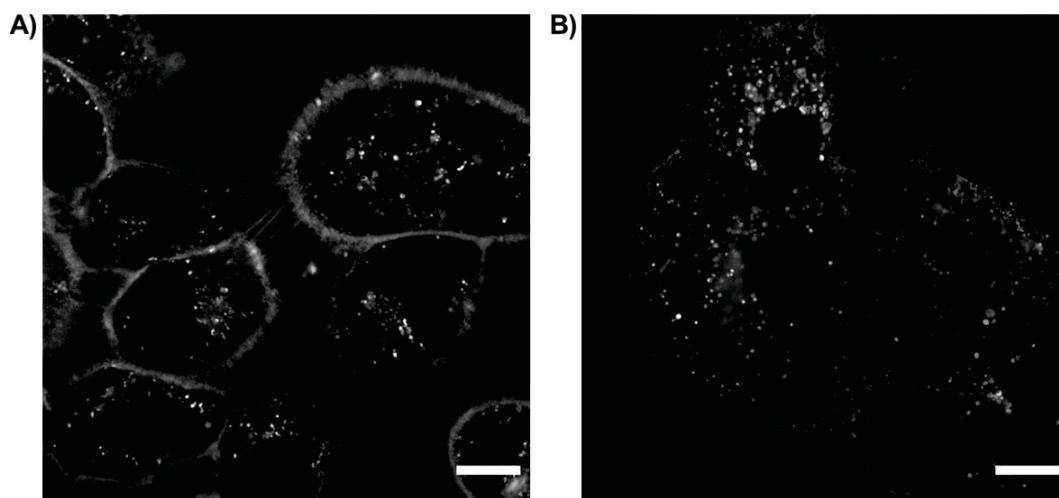


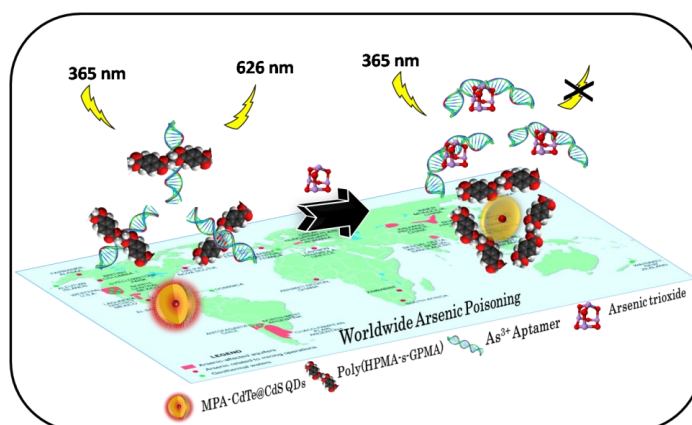
Figure S21. SIM live images of HeLa cells treated with P(MEO₉MA-*co*-PMIM)₂₀-*b*-P(HGI) polyplexes at N/P ratio 10 A) after 1 h incubation B) after 4 h incubation. Optical magnification of the system in normal widefield fluorescence mode is ~100x (63x Objective + 1.6x Optovar for a total of 100.8x). The total area in the SIM-images is 76x76μm, for a pixel size of 40 μm. The scale bar is 10 μm.

References:

- [1] F. J. Hack, C. Cokca, S. Stadter, J. Hulsmann, K. Peneva, D. Fischer, *Macromol. Rapid Commun.* **2020**, e2000580.
- [2] D. Costabel, A. Skabeev, A. Nabiyan, Y. Luo, J. Max, A. Rajagopal, D. Kowalczyk, B. Dietzek, M. Wächtler, H. Görls, D. Ziegenbalg, Y. Zagranjarski, C. Streb, F. H. Schacher, K. Peneva, *Chem. Eur. J.*, *n/a*.
- [3] "DIN EN ISO 10993-5:2009-10, Biological evaluation of medical devices-Part5: Test for in vitro cytotoxicity", in *European Standard EN ISO 10993-5, Brussels*.
- [4] M. Zink, K. Hotzel, U. S. Schubert, T. Heinze, D. Fischer, *Macromol. Biosci.* **2019**, *19*, e1900085.
- [5] D. Fischer, T. Bieber, Y. Li, H.-P. Elsässer, T. Kissel, *Pharm. Res.* **1999**, *16*, 1273.

Publication P5

Ultrasensitive aptasensor for arsenic detection using quantum dots and grafted Poly(methacrylamide)



G. K. Soni, N. Wangoo, C. Cokca, K. Peneva, R. K. Sharma

Anal. Chim. Acta **2022**, 1209, 339854



Contents lists available at ScienceDirect

Analytica Chimica Acta

journal homepage: www.elsevier.com/locate/aca

Ultrasensitive aptasensor for arsenic detection using quantum dots and guanylated Poly(methacrylamide)

Gurpreet K. Soni^a, Nishima Wangoo^b, Ceren Cokca^{c,d}, Kalina Peneva^{c,d,**}, Rohit K. Sharma^{a,*}

^a Department of Chemistry and Centre of Advanced Studies in Chemistry, Panjab University, Sector-14, Chandigarh, 160014, India

^b Department of Applied Science, University of Engineering and Technology (U.I.E.T.), Panjab University, Sector-25, Chandigarh, 160025, India

^c Institute of Organic Chemistry and Macromolecular Chemistry (IOMC), Friedrich Schiller University Jena, Lessingstrasse, 8 Jena D, 07743, Germany

^d Jena Center for Soft Matter (JCSM), Friedrich Schiller University Jena, Philosophenweg 7 Jena D, 07743, Germany

ARTICLE INFO

Keywords:

Arsenic detection
Guanylated poly(methacrylamide)
Fluorometric
Aptasensor
Quantum dots
Picomolar detection

ABSTRACT

The present study demonstrate the first time usage of poly (HPMA-s-GPMA) copolymer for the fabrication of three-component based aptasensor for simple, selective, rapid and label free detection of arsenite (As^{3+}). For this purpose, guanidinium bearing poly (HPMA-s-GPMA) copolymer and MPA-CdTe@CdS quantum dots (QDs) was employed in conjunction with As^{3+} specific aptamer. This protocol utilizes the quenching phenomena displayed by QDs due to the competitive binding of As^{3+} ions and cationic copolymer to the aptamer. In particular, the As^{3+} bind to the specific aptamer, leaving poly (HPMA-s-GPMA) freely available for its electrostatic intercalations with QDs, which quenches the fluorescent signal. Contrarily, in the absence of As^{3+} ions, the aptamer can electrostatically bind to poly (HPMA-s-GPMA); making copolymer inactive to affect the fluorescence signal of the QDs. The efficiency of the proposed fluorescence nanoprobe was further tested using linear calibration curves. The obtained data in the range of 0.01-100 nM showed excellent specificity for As^{3+} ions with the limit of detection (LOD) of 246.77 pM. Moreover, the "on-off" fluorescent aptasensor is highly selective for As^{3+} ions in the presence of other interfering metal ions by utilizing As^{3+} specific aptamer. Furthermore, the reported study showed outstanding applicability in the real-world samples (water, food and soil) containing preservatives, metal ions, minerals, and other moieties. The proposed sensing platform not only exhibits the trace level detection of As^{3+} ions in cost-effective manner but also opens a pathway for the development of state-of-art device fabrication for on-site detection of arsenic.

1. Introduction

Arsenic is found in earth's crust as naturally occurring metalloid and known to be a serious threat to human health and environment [1]. It exists in various forms mainly comprising of four oxidation states (-3, 0, +3, +5). Owing to the high stability of As^{3+} , it is specifically known to get incorporated into the food chain, therefore, As^{3+} has been labeled as one of the environmentally hazardous moieties [2,3]. Consequently, World Health Organization (WHO) and Environmental Protection Agency (EPA) have recommended maximum permissible level of arsenic in useable water at 10 ppb [4]. The contaminated water containing arsenic is a result of both anthropogenic and natural processes such as mining, disposal of industrial waste, usage of arsenical pesticides/insecticides, volcanic eruptions, erosion, and weathering [5].

Furthermore, the long term exposure of arsenic in human body from contaminated water results in a chronic illness called as arsenicosis or arsenic poisoning [6]. It has been reported that exposure to arsenic through contaminated water leads to serious and/or fatal diseases such as skin pigmentation, melanosis, respiratory failure, neurological disorder, vascular diseases (Blackfoot disease and hypertension), diabetes mellitus, keratosis, cardiovascular disease, anemia, and tumorigenesis to millions worldwide [7,8]. Considering these harmful effects, it is highly desirable to devise a selective and highly sensitive method for on-site monitoring of arsenic.

At present, most of the methods for sensitive detection of arsenic employ standard conventional techniques such as high performance liquid chromatography (HPLC), hydride generation atomic absorption spectroscopy (HG-AAS), atomic fluorescence spectrometry (AFS), gas

* Corresponding author.

** Corresponding author.

E-mail addresses: kalina.peneva@uni-jena.de (K. Peneva), rohitksg@pu.ac.in (R.K. Sharma).

<https://doi.org/10.1016/j.aca.2022.339854>

Received 20 January 2022; Received in revised form 4 April 2022; Accepted 16 April 2022

Available online 23 April 2022

0003-2670/© 2022 Elsevier B.V. All rights reserved.

chromatography–mass spectrometry (GC-MS), inductively coupled plasma mass spectrometry (ICP-MS), neutron activation analysis (NAA), and inductively coupled plasma atomic emission spectrometry (ICP-AES) [9–15]. However, these techniques are often expensive, laborious, non-portable, and require stringent safety standards in laboratories. To overcome these drawbacks, sensing strategies have continuously been developed for switching the conventional methods to more rapid and low-cost absorption, emission and electrochemical based techniques for quantitative detection of As^{3+} ions.

Out of multiple detection strategies, fluorescence analysis of chemical and biochemical analytes, in particular, has proven to be significantly more sensitive than other techniques [16]. Among the utilized fluorophores so far, quantum dots represent an excellent alternative over conventional fluorophores, such as organic dyes or fluorescent proteins, due to their superior physical properties [17]. QDs are known to have better resistance toward photobleaching, sharp emission peak, size-tunable emission, large Stokes shift, bright emission, and high signal-to-noise ratio compared to organic dyes [18–22].

Alongside QDs as a nanoprobe, polymers have shown various applications in the fabrication of sensors [23,24]. Molecularly imprinted polymers with different functional groups have been conjugated with various nanomaterials and used for the detection of variety of biological molecules, explosives and other analytes [25–27]. In the same context, our group earlier reported detection of malathion using QDs-polymer based fluorescent aptasensor [28]. The designed aptasensor comprised of *N*-(3-guanidinopropyl)methacrylamide based homopolymer (GPMA) and QDs, where the polymer acts as a quencher for QDs via electrostatic interactions [29,30]. Similar to this approach, ultrasensitive detection of As^{3+} ions and malathion have been reported based on a cationic polymer, polydiallyldimethylammonium chloride (PDDA), gold nanoparticles (AuNPs) and analyte specific aptamer [31,32]. Aptamers have been employed as a promising molecular recognition element over antibodies primarily due to easier modification, smaller size, strong target affinity, high thermal stability, and low production cost [33,34]. As compared to classical target receptors such as antibodies and enzymes, aptamers can be constructed against wide variety of targets including toxic and non-toxic immunogens, metal ions, bacteria, viruses, proteins, peptides and tissues [35,36].

We propose a copolymer poly (HPMA-*s*-GPMA) and mercaptopropionic acid capped CdTe@CdS QDs (MPA-CdTe@CdS) based fluorescent probe in conjunction with As^{3+} specific aptamer as recognition element for simple, selective, rapid and label-free detection of As^{3+} ions. This three component (QDs, copolymer and aptamer) fluorescence nanoprobe is based on quenching of fluorescent intensity of QDs bound to the guanidinium bearing copolymer-poly (HPMA-*s*-GPMA). In the presence of As^{3+} ions, aptamer recognizes its target and binds to As^{3+} ions, leaving the cationic copolymer free in the solution which quenches the fluorescence signal of QDs via electrostatic interactions. However, in the absence of As^{3+} ions negatively charged aptamer electrostatically binds to the cationic copolymer and as a result, the polymer can no longer affect the fluorescent signal of the QDs. The reported on-off fluorescence strategy is highly effective in the presence of various metal ions as well as in the analysis of real-world samples. Moreover, it provides a major advantage of allowing rapid and on-site sensing of As^{3+} ions by overcoming disadvantages of the conventional systems. This is the first report on the fabrication of an ultra-sensitive aptasensor for fluorometric detection of As^{3+} ions in combination with arsenic ($\bar{A}\bar{A}$) specific aptamer and MPA-CdTe@CdS QDs that includes cationic guanylated poly (methacrylamide).

2. Experimental details

2.1. Chemicals and reagents

Cadmium bromide tetrahydrate (98%) ($CdBr_2 \cdot 4H_2O$), tellurium powder (200 mesh, 99.8% trace metal basis), sodium arsenite ($NaAsO_2$)

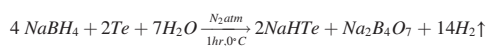
and sodium borohydride (>96%) ($NaBH_4$) were purchased from Sigma Aldrich, India. Thiourea ($SC(NH_2)_2$), 2-mercaptopropionic acid (>95%) (2-MPA) and sodium hydroxide (NaOH) were purchased from SRL, India for the synthesis of quantum dots. The aptamer with sequence (5'-GGTAATACGACTCACTATAGGGGATACCAGCTTATCAATTTTACAGAACAACCAACGTCGCTCCGGTACTTCTTCATCGAGATAGTAAGTGC AATCT-3') was received from Sigma Aldrich, India [31]. For polymerization reaction, all the chemicals were purchased from Sigma-Aldrich at the highest available purity and used as received. 4,4'-azobis (4-cyanovaleic acid) (ACVA) was recrystallized in methanol (MeOH) before the use. The chain transfer agent 4-(((2-carboxyethyl)thio)carbonothioyl)thio-4-cyanopentanoic acid (CTA) was purchased from Boron Molecular INC. All other chemicals were purchased from Sigma Aldrich, India and used without any further purification. All the experimental work was carried out using ultrapure water with resistivity of 18.2 M Ω cm which was procured using Direct-Q3 system (Merck Millipore, India).

2.2. Equipments

The fluorometric assay was recorded on Carry Eclipse fluorescence spectrophotometer Agilent. The ultracentrifugation of QDs was carried out using Optima XPN-100 ultracentrifuge. The size characterization (HRTEM) and charge analysis of QDs were carried out using Hitachi (H-7500) microscope and Malvern zetasizer nano s90, respectively. Elemental analysis was carried on JSM-6100 microscope.

2.3. Synthesis of MPA-CdTe@CdS QDs

The controlled aqueous synthesis of ultrasmall MPA-CdTe@CdSQDs was carried out as per a previously reported method [28]. Initially, the dissolution of 0.02 mol of $NaBH_4$ was carried out in 10 mL double distilled water (ddH_2O) under nitrogen atmosphere for 30 min, followed by the addition of 0.005 mol of tellurium powder. The reaction mixture was stirred for 1 h at 0 °C provided the purple colored NaHTe precursor with $Na_2B_4O_7$ as side product.



Further, cadmium bromide salt (0.0028 mol) was added into 100 mL DI water along with thiol stabilizer i.e. 2-mercaptopropionic acid (0.0037 mol) and pH of resultant mixture was set to 11.5 using 1 M sodium hydroxide (NaOH). The molar ratio of Cd:MPA:Te was kept at 1:1.33:1.66, respectively. Then, the reaction mixture was transferred to a three necked flask and refluxed at 100 °C for 1 h under the N_2 atmosphere. The drop-wise addition of NaHTe via injection led to immediate formation of red colored MPA-CdTe QDs. Surface passivation of prepared quantum dots was done via formation of CdS shell on MPA-CdTe core. In the typical synthesis of MPA-CdTe@CdS QDs, excessive amount of thiourea added to the boiling solution of prepared QDs in an inert atmosphere. The reaction was run for 1.5 h yielding the core shell QDs which were purified using an ultracentrifugation at 70,000 rpm and stored at 4 °C. In order to check the stability of MPA-CdTe@CdS quantum dots effect of pH was studied by varying it from 4.0 to 12.4. The results demonstrated that synthesized QDs were highly stable between pH 5–12.4 (Fig. S1).

2.4. Synthesis of poly(HPMA-*s*-GPMA) copolymer

The synthesis of *N*-(3-guanidinopropyl)methacrylamide (GPMA) was conducted according to our previous study [29]. The chain transfer agent (CTA), *N*-(2-Hydroxypropyl)methacrylamide (HPMA) (0.017 g, 0.000118 mol, 5 mol%) and GPMA (0.423 g, 0.00228 mol, 95 mol%) were added into a 25 mL schlenk flask and dissolved in acetate buffer (pH = 5.2, 0.27 M acetic acid and 0.73 M sodium acetate) achieving a monomer concentration of 1 M. After the addition of ACVA, the reaction

was conducted at 80 °C for 5 h in inert atmosphere. The initial monomer to CTA ratio, $[M]_0/[CTA]_0$, was 145/1 and the initial CTA to initiator ratio, $[CTA]_0/[I]_0$, was kept at 3/1. At the end of the reaction, dialysis in distilled water (at pH = 4) at 4 °C was carried out which was followed by lyophilization. The compound was characterized with respect to its co-monomer composition by using 1H NMR spectroscopy. To analyze its apparent molar mass and D values, SEC_{Water} was performed.

2.5. 1H NMR spectroscopy

The monomer compositions of poly (HPMA-*s*-GPMA) were determined using a Bruker WS 300 MHz spectrometer (controller: Bruker-Avance III) in D₂O at 333 K (Fig. S2). The integration of the intensities assigned to the methylene proton resonances of HPMA (3.84 ppm) and the methylene resonances of GPMA (2.89–3.30 ppm) enabled the estimation of the monomer compositions (Fig. S2).

2.6. Size exclusion chromatography

Poly (HPMA-*s*-GPMA) was characterized by SEC_{Water}. Water with 0.1% TFA and 0.1 M NaCl was used as the eluent and AppliChrom ABOA CatPhil guard/200/350 Å was the column (Fig. S3). The flow rate and the temperature were adjusted to 1 mL min⁻¹ and 30 °C, respectively. The elution was monitored by the refractive index (RI-930) and UV detection (UV-975, wavelength: 310 nm). Poly (2-vinylpyridine) (P2VP) was employed as the standard calibration to calculate the relative molar mass.

2.7. Fluorometric assay for As³⁺

The stock solution of arsenic was prepared by dissolution of sodium arsenite (NaAsO₂) in de-ionized water and preserved with 2% (v/v) nitric acid. The prepared solution was stored in amber bottle with parafilm on it to provide dark and dry condition at 6 °C. For the detection of As³⁺ ions, 3 μM of arsenic specific aptamer (25 μL) was mixed with various concentrations of sodium arsenite (100 μL), diluted with Tris buffer (100 μL) and incubated at room temperature for 30 min. In the next step, 0.6 mg mL⁻¹ aqueous polymer solution (25 μL) were added into reaction mixture and incubated for 60 min. At last, 25 μL of MPA-CdTe@CdS QDs were added and after 30 min incubation fluorescence spectra was recorded. To check the specificity of aptasensor other metal ions such as mercury (Hg²⁺), cadmium (Cd²⁺), sodium (Na⁺), lead (Pb²⁺), copper (Cu²⁺), nickel (Ni²⁺), zinc (Zn²⁺), magnesium (Mg²⁺), aluminium (Al³⁺), gold (Au³⁺), bismuth (Bi³⁺), chromium (Cr³⁺) etc. were added as a substitute of As³⁺ followed by fluorometric measurements.

2.8. Determination of As³⁺ in spiked samples

The real life usefulness of the proposed aptasensor was evaluated by performing the experiment in real-world samples such as water and food. Tap water and soil water was filtered using 0.4 μm filter to remove suspended impurities whereas mineral water used in its native form. Apple juice was chosen as food matrix, for that apple was crushed and grinded to form a homogenate mixture followed by the extraction using methanol/water (50% (v/v), 5 times) at room temperature. After that sample was filtered using 0.22 μm filter and methanol was evaporated followed by the dilution with de-ionized water. All the real-world samples were further spiked with a known amount of sodium arsenite and detected using proposed aptasensor.

Caution: Due to the harmful effects of arsenite ions to human health, all the safety precautions were taken during the experimentation work.

3. Results and discussion

3.1. Synthesis and characterization of MPA-CdTe@CdS QDs

Recently, semiconductor QDs have envisioned to be a potential substrate for the fabrication of sensing techniques owing to their narrow and symmetric emission, unique brightness, high photostability, and large extinction coefficient as compared to traditional fluorophores [17, 18]. Keeping this in mind, highly fluorescent core-shell MPA-CdTe@CdS QDs were synthesized using hot injection method [28]. Initially, tellurium powder was reduced using NaBH₄ in an inert environment which led to the formation of NaHTe precursor. The purple colored NaHTe precursor was added dropwise to the hot solution of cadmium bromide and 2-MPA at basic pH (11.5) yielding bright red colored MPA-CdTe QDs. An important consideration for QD synthesis is that the Cd²⁺ and Te²⁻ ions should aptly react followed by nucleation of crystalline seeds in the presence of MPA via epitaxial process [37,38]. MPA molecules play a significant role in the synthesis by controlling the size and shape of QDs via newly formed Cd-S bond. In addition, MPA molecules are responsible for overall negative surface charge of these QDs due to presence of free carboxylate groups at basic pH.

Additionally, the photostability and luminescence efficiency of MPA-CdTe QDs were enhanced by using surface passivation of dangling bonds through the introduction of a cadmium sulfide shell. The core-shell QDs were synthesized by addition of thiourea as sulfur source into the hot solution of CdTe QDs. The thiourea undergoes decomposition producing S²⁻ anions which amalgamate with excessive Cd²⁺ cations from the initial solution leading to the formation of MPA-CdTe@CdS core-shell QDs. These synthesized CdTe@CdS QDs exhibited a band gap of 1.98 eV which was marked lower than 2.25 eV as exhibited by CdTe QDs, in alignment with the inverse trend observed for the size of these QDs (Fig. 1a). The CdTe and CdTe@CdS QDs showed fluorescence emission at 520 nm and 626 nm, respectively with the observed bathochromic shift confirming the quantum confinement effect in QDs (Fig. 1a). Similar trend was observed in the UV-Vis spectrum in the range of 500–700 nm (Fig. 1b). The synthesized MPA-CdTe@CdS QDs were monodispersed with spherical morphology and average size of 4 nm as illustrated in the HR-TEM images (Fig. 1c). The hydrodynamic radius of MPA-CdTe@CdS QDs was determined to be about 7.6 nm (Fig. S4) with a net negative charge of -40.4 mV (Fig. S5). The presence of cadmium (Cd), tellurium (Te) and sulfur (S) ion peaks in the energy dispersive X-ray (EDX) spectrum confirmed the formation of MPA-CdTe@CdS QDs (Fig. S6).

3.2. Synthesis and characterization of poly(HPMA-*s*-GPMA)

Guanidinium bearing polymers have been receiving an increasing attention in various applications such as non-viral gene delivery, antimicrobial activity, pest control, aptasensors [28,39–47]. This versatility comes from the unique chemical properties of the guanidinium group which possess a Y-shaped quasi aromatic structure where the charge is delocalized [48]. Its pKa value is ~13.6 in water which renders it fully protonated in a wide pH range [49,50]. This protonated state at physiological pH provides an excellent multivalent salt-bridge formation with oxyanions, which is much stronger than the case for ammonium group [51]. Therefore, guanidinium group shows a distinctive binding ability toward nucleic acids which bear phosphate groups. In a previous study, a guanidinium bearing homopolymer, Poly (*N*-(3-guanidinopropyl) methacrylamide), was applied for the first time in the detection of malathion by utilizing the quantum dots-polymer based fluorescent aptasensor [28]. Considering the strong binding of guanidinium group to the selected aptamer, in this study, poly (HPMA-*s*-GPMA) copolymer

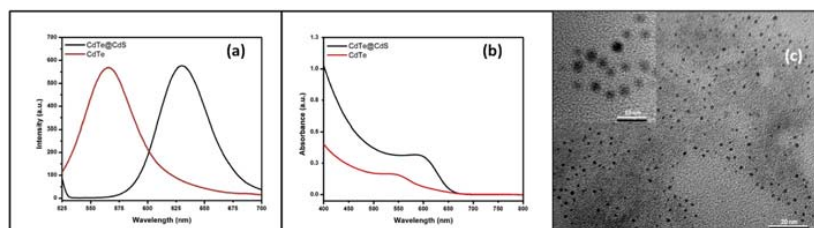


Fig. 1. (a) Emission spectra of CdTe and CdTe@CdS QDs upon excitation at 365 nm and 357 nm, respectively, (b) Absorbance spectra of CdTe and CdTe@CdS QDs, (c) HR-TEM image of CdTe@CdS QDs at scale bar of 20 nm (inset HR-TEM image at the scale bar of 10 nm).

composed of *N*-(2-Hydroxypropyl)methacrylamide (HPMA) and *N*-(3-guanidinopropyl)methacrylamide (GPMA) monomers was used. HPMA was selected as a spacer unit for further colloidal stability and GPMA was employed as a binding unit for the aptamer. Poly (HPMA-*s*-GPMA) was synthesized via aqueous reversible addition-fragmentation chain transfer (aRAFT) polymerization (Fig. 2a). The copolymer was characterized by ^1H NMR spectroscopy which indicated an excellent purity of the polymer (Fig. 2b). The integration of intensities coming from 1H from the side chain of HPMA (3.84 ppm) with 2H from the side chain of HPMA and 4H from the side chain of GPMA (2.89–3.30 ppm) enabled the calculation of comonomer content which is 18 mol% of HPMA and 82 mol% of GPMA (Fig. 2c). A water-based size exclusion chromatography (SEC_{Water}) system depicted that the molar mass of poly (HPMA-*s*-GPMA) was 8600 g mol^{-1} with a dispersity index of 1.07 (Fig. 2c). Furthermore, the surface charge investigation by zeta potential confirms the positive nature of poly (HPMA-*s*-GPMA) (Fig. S7).

3.3. Mechanistic principle of sensing scheme

The mechanistic principle of As^{3+} ions for the detection of fluorometric aptasensor is based on an alteration in the fluorescence intensity of synthesized MPA-CdTe@CdS QDs (Scheme 1). The proposed nanoprobe is based on the three-component system which incorporate As^{3+} binding aptamer, guanidinium containing copolymer and CdTe@CdS derived QDs. The overall strategy of the proposed fluorescence nanoprobe for As^{3+} ions is based on preferable electrostatic interactions among negatively charged QDs and aptamer with positively charged guanidinium bearing copolymer at different stages of the detection scheme. For the fabrication of aptasensor, guanylated poly (methacrylamide) copolymer acts as a quencher of the negatively charged QDs through electrostatic interactions. The detection scheme for As^{3+} ions sensing broadly consists of two distinct pathways depending on the presence or absence of the target ions. Specifically, these pathways have mentioned as Path I (in the absence of As^{3+} ions) and Path II (in the

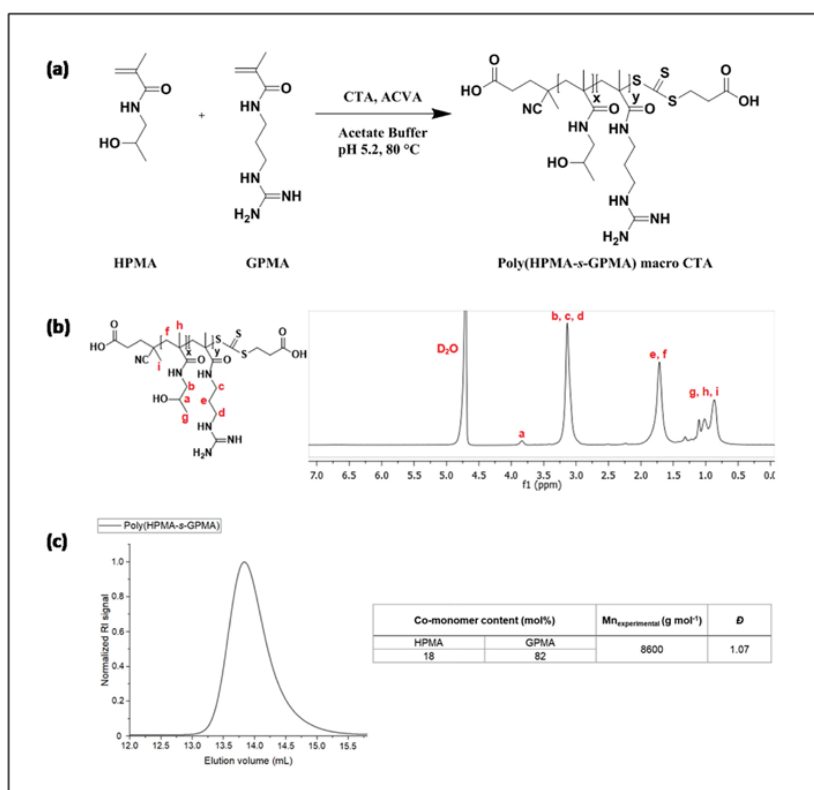


Fig. 2. (a) Synthesis of poly (HPMA-*s*-GPMA), (b) ^1H NMR spectrum of poly (HPMA-*s*-GPMA) copolymer, (c) SEC_{Water} trace of poly (HPMA-*s*-GPMA) copolymer with co-monomer content, $M_{n, \text{experimental}}$ and \bar{D} .

presence of As^{3+} ions (Scheme 1). In path I, the aptamer was made to interact directly with the copolymer in the absence of As^{3+} ions. The phosphate groups present in the aptamer backbone electrostatically interact with guanidinium moieties of poly (HPMA-s-GPMA). This interaction results in the formation of aptamer-poly (HPMA-s-GPMA) complex which inhibits the interaction of any free polymer with the QDs; and as a consequence, fluorescence intensity of QDs remains unaffected (Scheme 1). However, the As^{3+} ions are initially present in the aptamer solution in Path II. Therefore, the aptamer specifically binds to the As^{3+} ions resulting in the conformation change of aptamer [52]. The plausible mechanism for aptamer- As^{3+} complex formation involves the association between nucleotide bases and As^{3+} ions via hydrogen bonding and electrostatic interactions, which provides the specific binding site for arsenite [53]. As a result, quenching of QDs fluorescence signal was observed due to further interaction of free poly (HPMA-s-GPMA) copolymers with QDs.

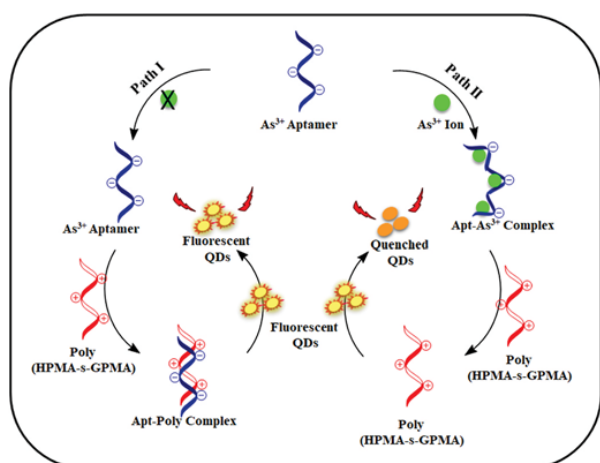
The extent of fluorescence quenching is directly proportional to the availability of the poly (HPMA-s-GPMA) copolymer which further depends upon the concentration of As^{3+} ions conjugating with the aptamer in the sample. Path I and II, therefore, allow an 'on-off' type of fluorescent sensor for a reliable detection of As^{3+} ions with a relatively simple and easy approach. The optimization of various reaction parameters for the construction of proposed fluorescent nanoprobe have been carried out which have been discussed in the subsequent sections.

3.4. Optimization of the reaction parameters for As^{3+} detection

The analytical performance of any sensor depends on the optimization of the reaction parameters such as concentration, volume and incubation time, all of which need to be analyzed carefully. Thus, the above-mentioned reaction parameters were sequentially optimized for the three components namely poly (HPMA-s-GPMA) copolymer, aptamer and the target (As^{3+} ions) as discussed below.

3.4.1. Interaction of MPA-CdTe@CdS QDs with poly(HPMA-s-GPMA) copolymer

First and foremost, the concentration of poly (HPMA-s-GPMA)



Scheme 1. Schematic representation of the mechanistic principle of the As^{3+} ions detecting fluorometric aptasensor. The fluorescence signal of QDs is quenched in the presence of As^{3+} ions due to free copolymer while in the absence of As^{3+} ions, poly (HPMA-s-GPMA) copolymer bound to aptamer and fluorescence intensity of QDs retained.

copolymer needed to quench fluorescent signal was investigated. For this reason, the concentration of poly (HPMA-s-GPMA) was varied from 0.01 mg mL^{-1} to 0.08 mg mL^{-1} in Tris buffer (Fig. 3a). It was observed that the quenching of the QDs fluorescence increased with the increase of the copolymer concentration. The addition of poly (HPMA-s-GPMA) copolymer to the solution containing QDs led to the electrostatic interactions among the guanidinium moieties of copolymer and carboxylate groups of QDs (Fig. S8) [28]. These interactions narrowed the interparticle distance which further induced the aggregation of QDs [54, 55]. As the concentration of the copolymer was further increased, the extent of these intermolecular electrostatic interactions also expanded resulting in an additional formation of QDs aggregations. As evident in Figs. 3a, 0.06 mg mL^{-1} poly (HPMA-s-GPMA) concentration was sufficient for an optimum signal quenching.

Similarly, the effect of copolymer volume on the fluorescent signal of QDs was also studied by varying the volume sequentially from 5 to 30 μL at concentration of poly (HPMA-s-GPMA) equal to 0.06 mg mL^{-1} . As visible in Fig. 3b, 25 μL copolymer solution was found to be best for quenching of the QDs. In the same context, the variation in the incubation time was noted at fixed polymer concentration and volume within the time frame of 0–60 min (Fig. 3c). It was observed that 30 min incubation time was sufficient for signal quenching. The optimized parameters for poly (HPMA-s-GPMA) including 0.06 mg mL^{-1} copolymer concentration, 25 μL volume of copolymer solution and 30 min of incubation time were used for further experiments.

3.4.2. Interaction of poly(HPMA-s-GPMA) with arsenic (As^{3+}) specific aptamer

In the next step, the concentration of aptamer was optimized in order to understand its interaction with evaluated concentration of copolymer above so that the fluorescent intensity of QDs remains unaffected. For this purpose, the aptamer concentration was incrementally varied between 0.5 and 3.0 μM and incubated with poly (HPMA-s-GPMA) solution (0.06 mg mL^{-1} , 25 μL) at R.T. followed by the addition of QDs. The fluorescence intensity of QDs augmented with increasing the aptamer concentrations due to selective electrostatic binding of aptamer with copolymer chains as compared to QDs (Fig. 4a) [56]. Furthermore, the emission spectra of QDs revealed that at comparatively lower concentrations of the aptamer (0.5–2 μM), the amount of aptamer was not enough to completely bind with the copolymer resulting the remaining copolymer to aggregate QDs. However, 3 μM concentration of aptamer was observed to be enough to regain the quenched fluorescence signal of QDs, therefore, it was chosen as the optimum aptamer concentration. Moreover, these results were supported by analysis of zeta potential in which surface charge of aptamer changes with the addition of the polymer (Figs. S9 and S10). Alteration of the volume of aptamer between 5 and 25 μL , showed that 25 μL aptamer is sufficient to ensure interaction with polymer, while at the same time the fluorescence of QDs remains unaffected (Fig. 4b). Similarly, the incubation time was incrementally increased (Figs. 4c) and 60 min incubation time was observed to be optimum for the signal retention.

3.5. Detection of As^{3+} ions and calculation of LOD

The proposed aptasensor for As^{3+} ions was validated through treatment with sodium arsenite concentrations ranging from 0.01 to 100 nM followed by the fluorescence measurements. The fluorescence spectra of QDs (Fig. 5a) revealed that with the increase in As^{3+} concentration, the characteristic emission peak at 626 nm decreased due to the aggregation of QDs. These results showed that the specific binding of aptamer increased with the augmentation in As^{3+} ions, and available free copolymer in the solution leads to quenching of fluorescence signal. In order to quantitative analyze As^{3+} ions, a calibration curve between F_0/F

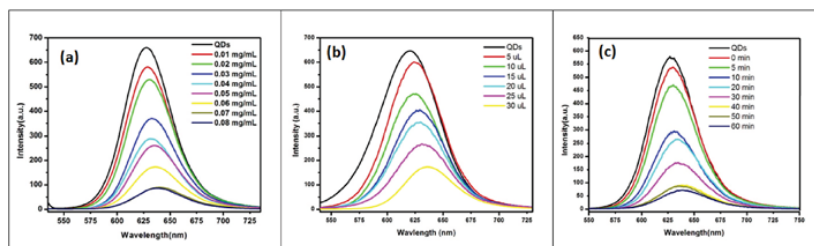


Fig. 3. Influence of poly (HPMA-s-GPMA) copolymer concentrations (a), volume of copolymer solution at 0.06 mg mL^{-1} concentration (b) and incubation time (c) on the fluorescence signal of QDs. The excitation wavelength was 357 nm with excitation and emission slit width 5 and 10 , respectively. All the samples were incubated at R.T. ($\text{pH} = 7.0$, 1.0 M Tris buffer).

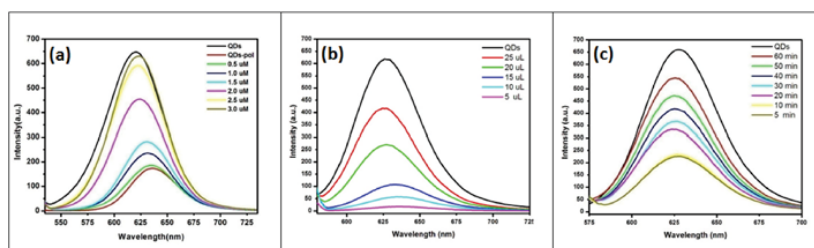


Fig. 4. Influence of aptamer concentration (a), volume (b), and incubation time (c) on fluorescence intensity of QDs in the presence of poly (HPMA-s-GPMA) copolymer. The concentration and volume of copolymer was kept constant (0.06 mg mL^{-1} , $25 \mu\text{L}$). All these experiments were carried out at R.T. ($\text{pH} = 7.0$, 1.0 M Tris buffer).

$F-1$ (where F_0 and F represent the fluorescence intensities in the absence and presence of As^{3+} ions) and logarithmic concentration of As^{3+} ions were plotted, which increases linearly as the concentration of As^{3+} ions changes from 0.01 nM to 100 nM . The regression coefficient (R^2) was calculated using origin lab 6.0 software and found to be 0.9979 (Fig. 5b). The limit of detection (LOD) of proposed aptasensor for As^{3+} ions was calculated to be 249.77 pM using formula $3\alpha/\text{slope}$, where the slope is obtained from linear plot and α represent the standard deviation of the instrument (Cal S1) [57]. It should be noted that this LOD value for the proposed aptasensor is far less than the lower permissible limit of As^{3+} ions which is $10 \mu\text{g/L}$ [58].

3.6. Selectivity analysis of the developed aptasensor

From the perspective of qualitative analysis, the selectivity of any sensor is one of the most important aspects due to the existence of different metal ions in the environment. Therefore, cross reactivity studies using other interfering metal ions such as Hg^{2+} , Cd^{2+} , Na^+ , Pb^{2+} , Cu^{2+} , Ni^{2+} , Zn^{2+} , Mg^{2+} , Co^{2+} , Fe^{3+} , Ca^{2+} were carried out to evaluate the selectivity of proposed aptasensor (Fig. 6). The results demonstrated that presence of As^{3+} ions led to the maximum quenching of fluorescence signal and corresponding to this resulted high $F_0/F-1$ value. In comparison to this, other tested metal ions did not effect the fluorescence spectra of QDs because aptamer is specific for As^{3+} ions only. In the presence of other metal ions, the aptamer bind preferentially to the guanidinium containing copolymer and as a result, the fluorescence

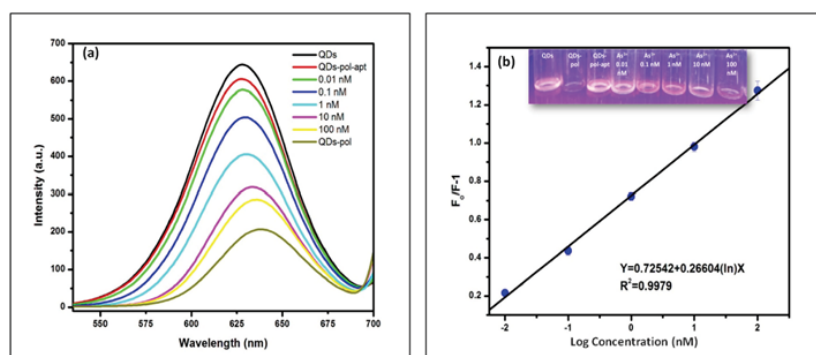


Fig. 5. (a) Influence of As^{3+} ions concentrations (0.01 nM - 100 nM) on the fluorescence signal of QDs in the presence of aptamer and copolymer. The concentration of the poly (HPMA-s-GPMA) copolymer (0.06 mg mL^{-1}) and aptamer ($3 \mu\text{M}$) were kept constant, (b) Calibration curve of the aptasensor, where F_0 and F represent the fluorescence intensities in the absence and presence of As^{3+} ions. Inset shows the naked eye quenching of QDs in the presence of arsenic under UV illuminator. For the detection of As^{3+} , samples were incubated at R.T. ($\text{pH} = 7.0$, 1.0 M Tris buffer).

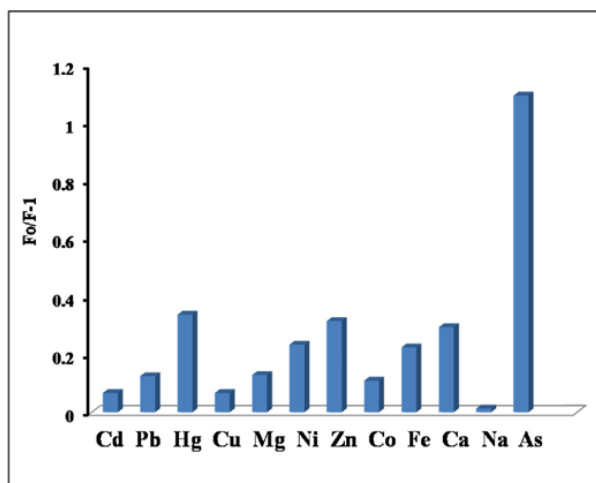


Fig. 6. Fluorescence response of the aptasensor towards different non-target metal ions: 1 μM As^{3+} ions and 1000 μM other metal ions. Poly (HPMA-*s*-GPMA) copolymer (0.06 mg mL^{-1}) and aptamer (3 μM) concentrations were kept constant, where F_0 and F represent the fluorescence intensities in the absence and presence of As^{3+} ions.

intensity of QDs remains unchanged, thereby resulting in relative lower $F_0/F-1$ value (Fig. 6). The proposed aptasensor exhibited three-fold selectivity over other tested metal ions and the above results confirmed the specificity for As^{3+} ions. In this context we also studied

the effect other tri-valent metal ions such as Al^{3+} , Cr^{3+} , Au^{3+} , Bi^{3+} and Fe^{3+} on the selectivity of proposed fluorescent aptasensor in the absence and presence of As^{3+} ions (Fig. S13). The results demonstrated that this aptasensor is highly specific for As^{3+} ions as compared to other tri-valent metal ions.

3.7. Application of developed aptasensor in real-world sample analysis

The applicability and relevance of the proposed aptasensor in real-world samples was verified by analysing the samples from different sources such as mineral water, tap water, soil water and apple juice after spiking with As^{3+} . For this purpose, mineral water (Fig. 7a and S14a), tap water (Fig. 7b and S14b), soil water (Fig. 7c and S14c) were chosen as water matrix where apple juice (Fig. 7d and S14d) was selected as food matrix. Firstly for water matrix, the samples were filtered to remove the suspended impurities followed by spiking with a known amount of As^{3+} ions in incremental concentrations (0.01–100 nM). After that to check the viability of the proposed sensor for food samples apple juice was extracted, filtered and spiked with similar concentrations of As^{3+} ions. The results obtained from the spiked samples were analyzed by using the regression curve and it was observed that the added amount of As^{3+} ions was in a good correlation with the amount detected with acceptable R^2 value (Table 1). Thus, the proposed aptasensing platform showed outstanding applicability in case of apple juice, mineral water, tap water and soil water. Overall, these results demonstrated the excellent applicability of the proposed aptasensor in terms of recovery percentage and real-world sample analysis of the As^{3+} ions.

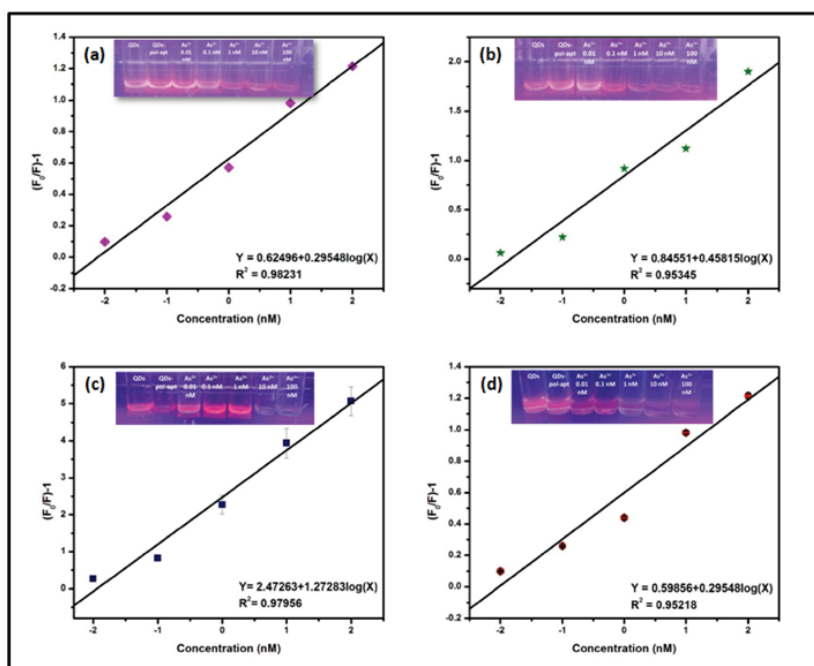


Fig. 7. Calibration curve response to different As^{3+} ions concentrations in mineral water (a), soil water (b), tap water (c), and apple juice (d), respectively. Inset shows the change in fluorescence intensity of QDs under UV illuminator.

Table 1
Percentage recovery for detection of As³⁺ ions in spiked water, soil and food samples using the proposed assay.

Sample	Regression Coefficient (R ²)	Amount Spiked (nM)	Amount Found (nM)	Recovery %
Mineral Water	0.982	1	0.91	91.41
		100	99.89	99.89
Soil Water	0.953	1	1.08	108.72
		100	107.92	107.92
Tap Water	0.979	1	0.91	91.87
		100	101.03	101.03
Apple Juice	0.952	1	0.73	73.39
		100	102.11	102.11

Table 2
LOD values for As³⁺ ion detection based on already reported methods/techniques as compared to the present method.

S. No	Method of Detection	LOD	References
1.	AAS	3.20 nM	[10]
2.	NAA	0.93 nM	[14]
3.	Colorimetric	70 nM	[31]
4.	HPLC ICP-MS	0.56 nM	[59]
5.	SERS	23.06 nM	[60]
6.	Impedimetry	0.80 μM	[61]
7.	Voltammetry	14.60 nM	[62]
8.	Colorimetric	3.58 μM	[63]
9.	FRET	6.00 nM	[64]
10.	Fluorometric (SiNPs)	2.88 nM	[65]
11.	Fluorometric (Cu-polymer)	49.75 fM	[66]
12.	Fluorometric using QDs	249.77 pM	Present method

3.8. Comparison of proposed LOD with existing strategies

The proposed aptasensor showed high sensitivity with LOD value of 249.77 pM for As³⁺ ions along with excellent R² value of 0.9979. It is pertinent to mention that this LOD obtained from the developed aptasensor makes the proposed sensing platform more sensitive compared to the previously reported arsenite sensing schemes based on conventional methods (Table 2). In particular, the presently proposed aptasensor was observed to be much more sensitive (LOD 249.77 pM) in comparison with already reported colorimetric method which used As³⁺ aptamer, PDDA polymer and AuNPs displaying LOD value of 70 nM [31]. The high specificity of aptamer for As³⁺ ions and the good binding affinity among guanidinium moieties to the phosphate groups of aptamer have resulted in high sensitivity of the developed sensing platform. Moreover, addition of HPMA in the copolymer improved colloidal stability and avoided unwanted aggregation during the polymer-aptamer binding. Recently, fluorometric detection of inorganic arsenic (As³⁺) has been carried out using water soluble Cu(II) complex with LOD of 49.75 fM [66]. Although this method depicted better sensitivity, it has limited applicability for further device fabrication owing to higher cost and requirement of complicated expertise synthetic protocol for [Cu(n-BuM)(DEA)]_n complex.

4. Conclusions

A highly sensitive and selective fluorescent aptasensor for arsenic with a complete interference profile and real-world sample analysis is reported. Specifically, the sensing strategy utilized the fluorescence response of MPA-CdTe@CdS quantum dots for testing various concentrations of As³⁺ ions. Apart from MPA-CdTe@CdS QDs, arsenic specific aptamer and guanidinium rich positively poly (methacrylamide) copolymer were employed to complete the three-component fluorescence nanoprobe for detection of As³⁺ ions. The basic sensing scheme is based on the alteration of fluorescence intensity of prepared QDs. In the absence of As³⁺ ions, arsenic specific aptamer binds electrostatically

with poly (HPMA-s-GPMA) copolymer and QDs remains unaffected in the reaction mixture. However, in the presence of target ions aptamer specifically binds to As³⁺ ions leaving the poly (HPMA-s-GPMA) copolymer free in the solution which further alters the fluorescence intensity of QDs via electrostatic interaction. The proposed sensing platform based on three-component system showed excellent specificity for As³⁺ ions with LOD of 246.77 pM. The “on-off” fluorescent aptasensor is highly selective for the target ions in the presence of other metal ions owing to the binding of arsenic specific aptamer with As³⁺ ions. Moreover, the reported study demonstrated excellent results in the real-world samples containing preservatives, metal ions, minerals and other moieties. The authors would like to emphasize that the proposed sensing platform not only exhibited the trace level detection of As³⁺ ions in rapid, selective, and cost-effective manner but also opens a pathway for next level device fabrication for on-site detection of arsenic in real-world samples. As a future goal, this may include the opto-electronic response based portable kit, smartphone-based sensors, chip-based sensors, paper strip-based sensors and wearable sensors for heavy metal ions.

CRedit authorship contribution statement

Gurpreet K. Soni: Investigation, experimentation, Writing – original draft, preparation. **Nishima Wangoo:** Conceptualization, Research support. **Ceren Cokca:** Experimentation, Writing – original draft. **Kalina Peneva:** Supervision, Conceptualization, Writing – review & editing. **Rohit K. Sharma:** Supervision, Conceptualization, Manuscript writing, Writing – review & editing, Overall.

Declaration of competing interest

The authors declare the following financial interests/personal relationships which may be considered as potential competing interests: Rohit K. Sharma reports financial support was provided by Department of Science and Technology India.

Acknowledgements

G.K.S. thanks University grant commission (UGC), India for her respective research fellowship. R.K.S. acknowledges the support of the Department of Science and Technology (DST), India-Project No. DST/TDT/AGRO-10/2019. C.C. and K.P. would like to acknowledge the support of the Deutsche Forschungsgemeinschaft (DFG, German Research Foundation) – project number 316213987 – SFB 1278 (Project B03).

Appendix A. Supplementary data

Supplementary data to this article can be found online at <https://doi.org/10.1016/j.aca.2022.339854>.

References

- [1] R.P. Liang, L.D. Yu, Y.J. Tong, S.H. Wen, S.P. Cao, J.D. Qiu, An ultratrace assay of arsenite based on the synergistic quenching effect of Ru(Bpy)₃²⁺ and arsenite on the electrochemiluminescence of Au-G-C₃N₄ nanosheets, *Chem. Commun.* 54 (2018) 14001–14004.
- [2] C.K. Jain, I. Ali, Arsenic: occurrence, toxicity and speciation techniques, *Wat. Res.* 34 (2000) 4304–4312.
- [3] M. Argos, T. Kalra, P.J. Rathouz, Y. Chen, B. Pierce, F. Parvez, T. Islam, A. Ahmed, M.R. Zaman, R. Hasan, G. Sarwar, V. Slavkovich, A. Geen, J. Graziano, H. Ahsan, Arsenic exposure from drinking water, and all-cause and chronic-disease mortalities in Bangladesh (HEALS): a prospective cohort study, *Lancet* 376 (2010) 252–258.
- [4] United States Environmental Protection Agency, Drinking Water Arsenic Rule History, 2016. November 2, <https://www.epa.gov/dwreginfo/drinking-water-arsenic-rule-history#Review>.
- [5] N. Soleja, O. Manzoor, P. Khan, M. Mohsin, Engineering genetically encoded FRET-based nanosensors for real time display of arsenic (As³⁺) dynamics in living cells, *Sci. Rep.* 9 (2019) 11240–11254.

- [6] B.K. Datta, A. Mishra, A. Singh, T.K. Sar, S. Sarkar, A. Bhattacharya, A. K. Chakraborty, T.K. Mandal, Chronic arsenicosis in cattle with special reference to its metabolism in arsenic endemic village of nadia district West Bengal India, *Sci. Total Environ.* 409 (2010) 284–288.
- [7] Y. Chen, F. Wu, M. Liu, F. Parvez, V. Slavkovich, M. Eunos, A. Ahmed, M. Argos, T. Islam, M.R. Zaman, R. Hasan, G. Sarwar, D. Levy, J. Graziano, H. Ahsan, A prospective study of arsenic exposure, arsenic methylation capacity, and risk of cardiovascular disease in Bangladesh, *Environ. Health Perspect.* 121 (2013) 832–838.
- [8] S.L. Chen, S.R. Dzung, M.H. Yang, Arsenic species in groundwaters of the Blackfoot disease area, Taiwan, *Environ. Sci. Technol.* 28 (1994) 877–881.
- [9] S.N. Ronkart, V. Laurent, P. Carbonnelle, N. Mabon, A. Copin, J.P. Barthelemy, Speciation of five arsenic species (arsenite, arsenate, MMAAV, DMAAV and asbet) in different kind of water by HPLC-ICP-MS, *Chemosphere* 66 (2007) 738–745.
- [10] Z. Zhu, S. Zhng, Y. Lv, X. Zhng, Atomization of hydride with a low-temperature, atmospheric pressure dielectric barrier discharge and its application to arsenic speciation with atomic absorption spectrometry, *Anal. Chem.* 78 (2006) 865–872.
- [11] K. Marschner, S. Musil, J. Dedina, Achieving 100% efficient post column hydride generation for arsenic speciation analysis by atomic fluorescence spectrometry, *Anal. Chem.* 88 (2016) 4041–4047.
- [12] J. Richter, S. Lischka, C. Piechotta, Analysis of arsenic species in fish after derivatization by GC-MS, *Talanta* 101 (2012) 524–529.
- [13] B. Klauke, J.D. Blum, Trace analyses of arsenic in drinking water by inductively coupled plasma mass spectrometry: high resolution versus hydride generation, *Anal. Chem.* 71 (1999) 1408–1414.
- [14] R.L. Paul, Evaluation of radiochemical neutron activation analysis methods for determination of arsenic in biological materials, *Anal. Chem.* 83 (2011) 152–156.
- [15] S. Karthikeyan, S. Hirata, Simultaneous determination of arsenic (III) and arsenic (V) by flow injection-inductively coupled plasma-atomic emission spectrometry (ICP-AES) with ultrasonic nebulization, *Anal. Bioanal. Chem.* 375 (2003) 139–144.
- [16] Fluorescence sensing, in: J.R. Lakowicz (Ed.), *Principles of Fluorescence Spectroscopy*, Springer, Boston, MA, 2006, https://doi.org/10.1007/978-0-387-46312-4_19.
- [17] U.R. Genger, M. Grabolle, S.C. Jaricot, R. Nitschke, T. Nann, Quantum dots versus organic dyes as fluorescent labels, *Nat. Methods* 5 (2008) 763–775.
- [18] H.K. Jun, M.A. Careem, A.K. Arof, Quantum dot-sensitized solar cells-perspective and recent developments: a review of Cd chalcogenide quantum dots as sensitizers, *Renew. Sustain. Energy Rev.* 22 (2013) 148–167.
- [19] S.K. Panda, S.G. Hickey, C. Waurisch, A. Eychmuller, Gradated alloyed CdZnSe nanocrystals with high luminescence quantum yields and stability for optoelectronic and biological applications, *J. Mater. Chem.* 21 (2011) 11550–11555.
- [20] J. Zieqler, A. Merkulov, M. Grabolle, U.R. Genger, T. Nann, High-quality ZnS shells for CdSe nanoparticles: rapid microwave synthesis, *Langmuir* 23 (2007) 7751–7759.
- [21] S. Melle, O.G. Calderon, M. Laurenti, D.M. Gonzalez, A.E. Gomez, E.L. Cabarcos, E. C. Granada, E. Díaz, J.R. Retama, FÄRster resonance energy transfer distance dependence from upconverting nanoparticles to quantum dots, *J. Phys. Chem. C* 122 (2018) 18751–18758.
- [22] Q. Zhang, S.P. Morgan, M.L. Mater, Nanoscale ultrasound-switchable FRET-based liposomes for near-infrared fluorescence imaging in optically turbid media, *Small* 13 (2017) 1602895–1602905.
- [23] B. Adhikari, S. Majumdar, Polymers in sensor applications, *Prog. Polym. Sci.* 29 (2004) 699–766.
- [24] F. Zhng, E. Lees, F. Amin, P.R. Gil, F. Yang, P. Mulvaney, W.J. Parak, Polymer-coated nanoparticles: a universal tool for biolabelling experiments, *Small* 7 (2011) 3113–3127.
- [25] A.A. Ensafi, P.N. Eshfahani, B. Rezaei, Synthesis of molecularly imprinted polymer on carbon quantum dots as an optical sensor for selective fluorescent determination of promethazine hydrochloride, *Sensor. Actuator. B Chem.* 257 (2018) 889–896.
- [26] S. Xu, H. Lu, J. Li, X. Song, A. Wang, L. Chen, S. Han, Dummy molecularly imprinted polymers-capped CdTe quantum dots for the fluorescent sensing of 2,4,6-trinitrotoluene, *ACS Appl. Mater. Interfaces* 16 (2013) 8146–8154.
- [27] S.E. Diltemiz, R. Say, S. Buyuktiyaki, D. Hur, A. Denizli, A. Ersoz, Quantum dot nanocrystals having guanosine imprinted nanoshell, *Talanta* 75 (2008) 890–896.
- [28] R. Bala, A. Swami, I. Tabujew, K. Peneva, N. Wangoo, R.K. Sharma, Ultra-sensitive detection of malathion using quantum dots-polymer based fluorescence aptasensor, *Biosens. Bioelectron.* 104 (2018) 45–49.
- [29] I. Tabujew, C. Cokca, L. Zartner, U.S. Schubert, I. Nisxhang, D. Fischer, K. Peneva, The influence of gradient and statistical arrangements of guanidinium or primary amine groups in poly(methacrylate) copolymers on their DNA binding affinity, *J. Mater. Chem. B* 7 (2019) 5920–5929.
- [30] F.J. Hack, C. Cokca, S. Stadter, J. Hulsmann, K. Peneva, D. Fischer, Indole, phenyl, and phenol groups: the role of the comonomer on gene delivery in guanidinium containing methacrylamide polymers, *Macromol. Rapid Commun.* (2020), e2000580.
- [31] Y. Wu, S. Zhan, F. Wang, L. He, W. Zhi, P. Zhou, Cationic polymer and aptamers mediated aggregation of gold nanoparticles for the colorimetric detection of arsenic (III) in aqueous solution, *Chem. Commun.* 48 (2012) 4459–4461.
- [32] R. Bala, M. Kumar, K. Bansal, R.K. Sharma, N. Wangoo, Ultrasensitive aptamer biosensor for malathion detection based on cationic polymer and gold nanoparticles, *Biosens. Bioelectron.* 85 (2016) 445–449.
- [33] E.M. McConnell, J. Nguyen, Y. Li, Aptamer-based biosensors for environmental monitoring, *Front. Chem.* 8 (2020) 1–24.
- [34] J. Zhou, J. Rossi, Aptamers as targeted therapeutics: current potential and challenges, *Nat. Rev. Drug Discov.* 16 (2017) 181–202.
- [35] C.L.L. Justino, A.C. Freitas, R. Pereira, A.C. Duarte, T.A.P.R. Santos, Recent developments in recognition elements for chemical sensors and biosensors, *Trends Anal. Chem.* 68 (2015) 2–17.
- [36] S.D. Jayasena, Aptamers: an emerging class of molecules that rival antibodies in diagnostics, *Clin. Chem.* 45 (1999) 1628–1650.
- [37] A. Francesc, E. Turrillas, A.A. Fuentes, Applications of quantum dots as probes in immunosensing of small-sized analytes, *Biosens. Bioelectron.* 14 (2013) 12–29.
- [38] R. Gui, X. An, Layer-by-layer aqueous synthesis, characterization and fluorescent properties of type-II CdTe/CdS core/shell quantum dots with near-infrared emission, *RSC Adv.* 3 (2013) 20959–20969.
- [39] C. Cokca, L. Zartner, I. Tabujew, D. Fischer, K. Peneva, Incorporation of indole significantly improves the transfection efficiency of guanidinium-containing poly(methacrylamide)s, *Macromol. Rapid Commun.* 41 (2020), e1900668.
- [40] I. Tabujew, M. Heidari, C. Freidel, M. Helm, L.U.K. Koynov, P. Biehl, F.H. Schacher, R. Postesio, K. Peneva, Tackling the limitations of copolymeric small interfering RNA delivery agents by a combined experimental–computational approach, *Biomacromolecules* 12 (2019) 4389–4406.
- [41] I. Tabujew, M. Willig, N. Leber, C. Freidel, I. Negwer, K. Koynov, M. Helm, K. Landfester, R. Zentel, K. Peneva, V. Mailänder, Overcoming the barrier of CD8⁺ T cells: two types of nano-sized carriers for siRNA transport, *Acta Biomater.* 100 (2019) 338–351.
- [42] C.A. Hae Cho, C. Liang, J. Perera, J. Liu, K.G. Varnava, V. Sarojini, R.P. Cooney, D. J. McGillivray, M.A. Brimble, S. Swift, J. Jin, Molecular weight and charge density effects of guanidylated biodegradable polycarbonates on antimicrobial activity and selectivity, *Biomacromolecules* 19 (2018) 1389–1401.
- [43] C. Yang, W. Lou, G. Zhong, A. Lee, J. Leong, W. Chin, B. Ding, C. Bao, J.P.K. Tan, Q. Pu, S. Gao, L. Xu, L.Y. Hsu, M. Wu, J.L. Hedrick, W. Fan, Y.Y. Yang, Degradable antimicrobial polycarbonates with unexcited activity and selectivity for treating multidrug-resistant klebsiellapneumoniae lung infection in mice, *Acta Biomater.* 94 (2019) 268–280.
- [44] K.E.S. Locoock, T.D. Michl, N. Stevens, J.D. Hayball, K. Vasilev, A. Postma, H. J. Griesser, L. Meagher, M. Haussler, Antimicrobial polymethacrylates synthesized as mimics of tryptophan-rich cationic peptides, *ACS Macro Lett.* 3 (2014) 319–323.
- [45] S.E. Exley, L.C. Paslay, G.S. Sahukhal, B.A. Abel, T.D. Brown, C.L. McCormick, S. Heinhorst, V. Koul, V. Choudhary, M.O. Elasri, S.E. Morgan, Antimicrobial peptide mimicking primary amine and guanidine containing methacrylamide copolymers prepared by raft polymerization, *Biomacromolecules* 12 (2015) 3845–3852.
- [46] K.H. Parsons, M.H. Mondal, C.L. McCormick, A.S. Flynt, Guanidinium-functionalized interpolyelectrolyte complexes enabling RNAi in resistant insect pests, *Biomacromolecules* 19 (2018) 1111–1117.
- [47] S. Li, C. Liu, B. Han, J. Luo, G. Yin, An electrochemiluminescence aptasensor switch for aldicarb recognition via ruthenium complex-modified dendrimers on multiwalled carbon nanotubes, *Microchim. Acta* 184 (2017) 1669–1675.
- [48] P. Gund, Guanidine, trimethylenemethane, and “Y-delocalization.” can acyclic compounds have “aromatic” stability? *J. Chem. Educ.* 49 (1972) 100.
- [49] B. Xu, M.L. Jacobs, O. Kostko, M. Ahmed, Guanidinium group remains protonated in a strongly basic arginine solution, *ChemPhysChem* 18 (2017) 1503–1506.
- [50] C.A. Fitch, G. Platzter, M. Okon, B. Garcia-Moreno, McIntosh, L.P. Arginine, Its pK_a value revisited, *Protein Sci.* 24 (2015) 752–761.
- [51] R. Mogaki, P.K. Hashim, K. Okuro, T. Aida, Guanidinium-based “molecular glues” for modulation of biomolecular functions, *Chem. Soc. Rev.* 46 (2017) 6480–6491.
- [52] S.M. Taghdisi, N.M. Danesh, M. Ramezani, A.S. Emrani, K. Abnous, A simple and rapid fluorescent aptasensor for ultrasensitive detection of arsenic based on target-induced conformational change of complementary strand of aptamer and silica nanoparticles, *Biosens. Bioelectron.* 256 (2018) 472–478.
- [53] H. Kaur, R. Kumar, J.N. Babu, S. Mittal, Advances in arsenic biosensor development- A comprehensive review, *Biosens. Bioelectron.* 63 (2015) 533–545.
- [54] A.N. Muttathukattil, S. Srinivasan, A. Haldar, G. Reddy, Role of guanidinium-carboxylate ion interaction in enzyme inhibition with implications for drug design, *J. Phys. Chem. B* 44 (2019) 9302–9311.
- [55] C.T. Armstrong, P.E. Mason, J.L.R. Anderson, C.E. Dempsey, Arginine side chain interactions and the role of arginine as a gating charge carrier in voltage sensitive ion channels, *Sci. Rep.* 6 (2016), 21759.
- [56] K. Ohara, M. Smietana, J.J. Vasseur, Characterization of specific noncovalent complexes between guanidinium derivatives and single-stranded DNA by MALDI, *J. Am. Soc. Mass Spectrom.* 17 (2006) 283–291.
- [57] D. Sharma, N. Wangoo, R.K. Sharma, Sensing platform for pico-molar level detection of ethyl parathion using Au-Ag nanoclusters based enzymatic strategy, *Talanta* 221 (2021) 121267–121275.
- [58] https://www.who.int/ipcs/assessment/public_health/arsenic/en/.
- [59] P.F. Rodríguez, R.M. Martín-Aranda, J.L. LópezColón, J.H. Mendoza, Ammonium acetate as a novel buffer for highly selective robust urinary HPLC-ICP-MS arsenic speciation methodology, *Talanta* 221 (2021), 221494.
- [60] S. Xu, F.P. Sabino, A. Janotti, D.B. Chase, D.L. Sparks, Unique surface enhanced Raman scattering substrate for the study of arsenic speciation and detection, *J. Phys. Chem. C* 122 (2018) 9474–9482.
- [61] K. Vega-Figueroa, J. Santillán, V. Ortiz-Gómez, E.O. Ortiz-Quiles, B.A. Quiñones-Colón, D.A. Castilla-Casadio, J. Almodovar, M.J. Bayro, J.A. Rodríguez-Martínez, E. Nicolau, Aptamer-based impedimetric assay of arsenite in water: interfacial properties and performance, *ACS Omega* 3 (2018) 1437–1444.
- [62] C. Sulliván, D. Lu, E. Brack, C. Drew, P. Kurup, Voltammetric codetection of arsenic (III) and copper(II) in alkaline buffering system with gold nanostar modified electrodes, *Anal. Chim. Acta* 1107 (2020) 63–73.

- [63] A. Motalebizadeh, H. Bagheri, S. Asiaei, N. Fekrat, A. Afkhami, New portable smartphone-based PDMS microfluidic kit for the simultaneous colorimetric detection of arsenic and mercury, *RSC Adv.* 8 (2018) 27091–27100.
- [64] G. Tang, J. Wangb, Y. Lia, Y. Su, Determination of arsenic (III) based on the fluorescence resonance energy transfer between CdTe QDs and rhodamine 6G, *RSC Adv.* 5 (2015) 17519–17525.
- [65] M. Oroval, C. Coll, A. Bernardos, M.D. Marcos, R. Martínez-Máñez, D.G. Shchukin, F. Sancenón, Selective fluorogenic sensing of as(III) using aptamer-capped nanomaterials, *ACS Appl. Mater. Interfaces* 9 (2017) 11332–11336.
- [66] B. Dey, P. Mukherjee, R.K. Mondal, A.P. Chattopadhyay, I. Hauli, S. K. Mukhopadhyay, M. Fleck, Femtomolar level sensing of inorganic arsenic(III) in water and in living-systems using a non-toxic fluorescent probe, *Chem. Commun.* 50 (2014) 15263–15266.

Ultrasensitive Aptasensor for Arsenic Detection using Quantum Dots and Guanylated Poly(methacrylamide)

Gurpreet K. Soni^a, Nishima Wangoo^b, Ceren Cokca^{c,d}, Kalina Peneva^{c,d,*}, Rohit K. Sharma^{a,*}

^aDepartment of Chemistry and Centre of Advanced Studies in Chemistry, Panjab University, Sector-14, Chandigarh 160014, India. Email: rohiksg@pu.ac.in

^bDepartment of Applied Science, University of Engineering and Technology (U.I.E.T.), Panjab University, Sector-25, Chandigarh 160025, India.

^cInstitute of Organic Chemistry and Macromolecular Chemistry (IOMC), Friedrich Schiller University Jena, Lessingstrasse 8, Jena D-07743, Germany. Email: kalina.peneva@uni-jena.de

^dJena Center for Soft Matter (JCSM), Friedrich Schiller University Jena, Philosophenweg 7, Jena D-07743, Germany.

Table of Contents

Fig. No.	Caption
Fig. S1	Effect of pH on the stability of MPA-CdTe@CdS QDs
Table S1	List of buffer used to check the stability of MPA-CdTe@CdS QDs
Fig. S2	¹ H NMR spectrum of Poly(HPMA- <i>s</i> -GPMA) copolymer (300 MHz, D ₂ O, 300 K)
Fig. S3	SEC _{Water} trace of Poly(HPMA- <i>s</i> -GPMA) copolymer
Fig. S4	Size distribution of MPA-CdTe@CdS QDs by number
Fig. S5	Surface charge of MPA-CdTe@CdS QDs determination by zeta potential
Fig. S6	Elemental analysis of MPA-CdTe@CdS QDs using energy dispersive X-ray spectroscopy (EDX)
Fig. S7	Surface charge of Poly(HPMA- <i>s</i> -GPMA) determination by zeta potential
Fig. S8	Zeta potential of MPA-CdTe@CdS QDs-Poly(HPMA- <i>s</i> -GPMA) complex
Fig. S9	Surface charge of arsenic aptamer determination by zeta potential
Fig. S10	Zeta potential of arsenic aptamer-Poly(HPMA- <i>s</i> -GPMA) complex
Fig. S11	Comparison of Zeta potential of QDs, Poly(HPMA- <i>s</i> -GPMA) and QDs-Poly(HPMA- <i>s</i> -GPMA) complex
Fig. S12	Comparison of Zeta potential of Aptamer, Poly(HPMA- <i>s</i> -GPMA) and Aptamer-Poly(HPMA- <i>s</i> -GPMA) complex
Fig. S13	Fluorescence response of the aptasensor towards different trivalent metal ions: 1 μM As ³⁺ ions and 1000 μM other metal ions. Poly(HPMA- <i>s</i> -GPMA) copolymer (0.06 mg mL ⁻¹) and aptamer (3 μM) concentrations were kept constant, where F ₀ and F represent the fluorescence intensities in the absence and presence of As ³⁺ ions.
Fig. S14	Fluorescent spectra of QDs having different concentration of As ³⁺ ions in mineral water (a), soil water (b), tap water (c) and apple juice (d) respectively.
Cal S1	Calculations-Limit of detection

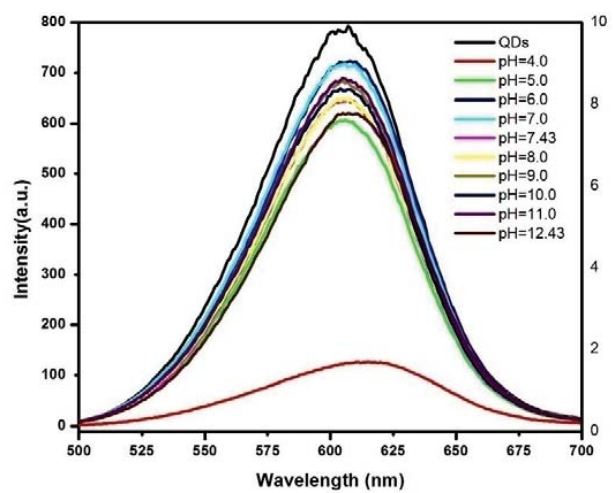


Fig. S1 Effect of pH on the stability of MPA-CdTe@CdS QDs

Table S1 List of buffers used to check the stability of MPA-CdTe@CdS QDs

S.No.	Buffer	pH
1.	Citrate	4.0
2.	Citrate phosphate	5.0
3.	2-(<i>N</i> -morpholino)ethanesulfonicacid (MES)	6.0
4.	Tris	7.0
5.	Phosphate(PB)	7.4
6.	Phosphate buffer saline(PBS)	8.0
7.	Carbonate/Bicarbonate	9.0
8.	Glycine/NaOH	10.0
9.	Sodium Bicarbonate/NaOH	11.0
10.	Potassium chloride/NaOH	12.4

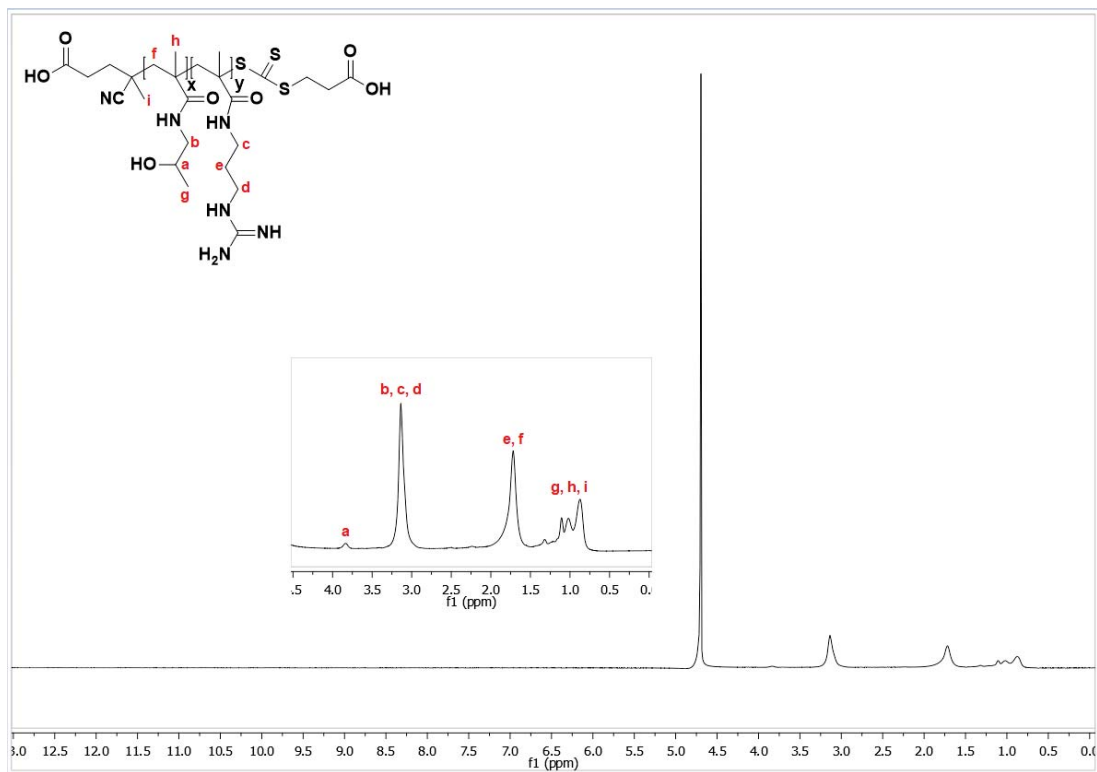


Fig. S2 ¹H NMR spectrum of Poly(HPMA-*s*-GPMA) copolymer (300 MHz, D₂O, 300 K)

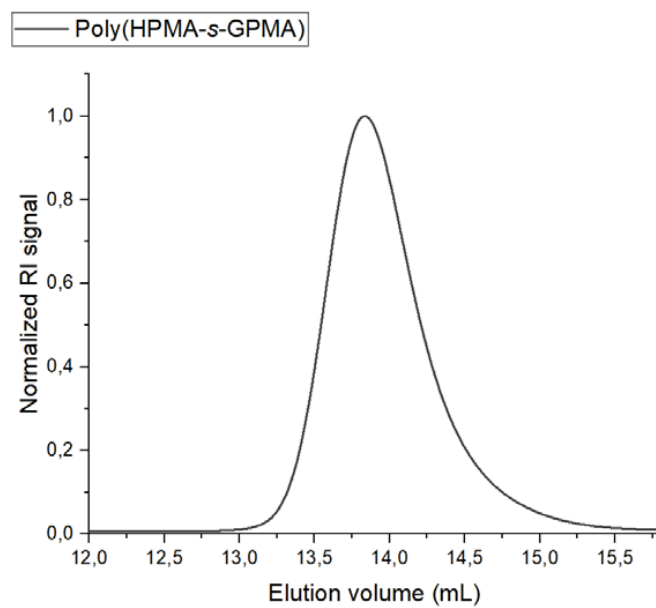


Fig. S3 SEC_{Water} trace of Poly(HPMA-s-GPMA) copolymer

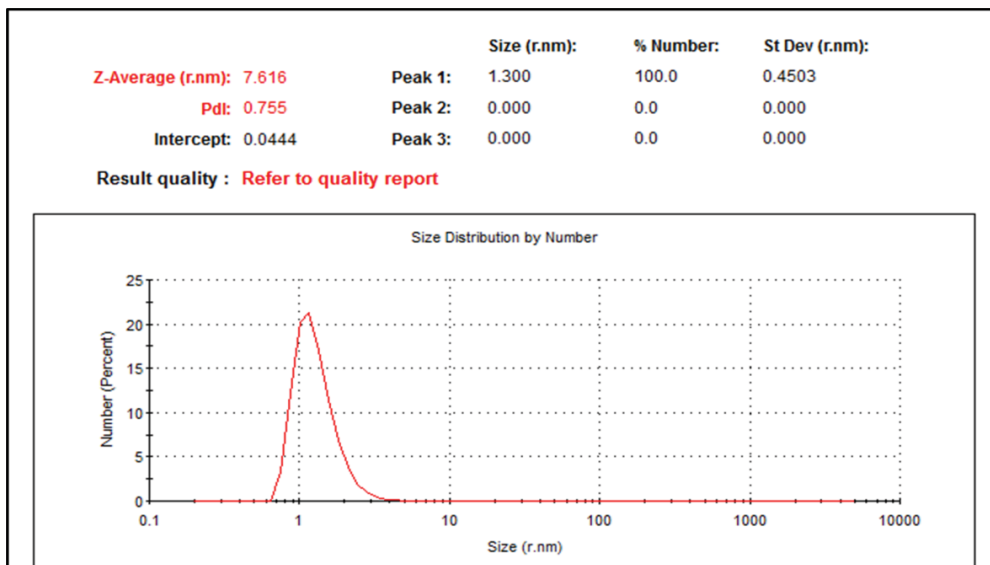


Fig. S4 Size distribution of MPA-CdTe@CdS QDs by number

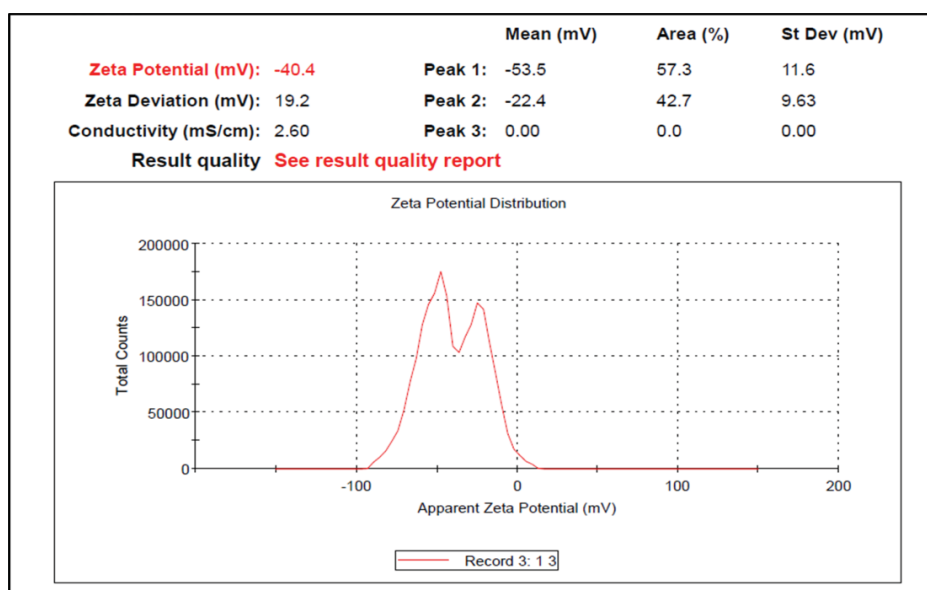


Fig. S5 Surface charge of MPA-CdTe@CdS QDs determination by zeta potential

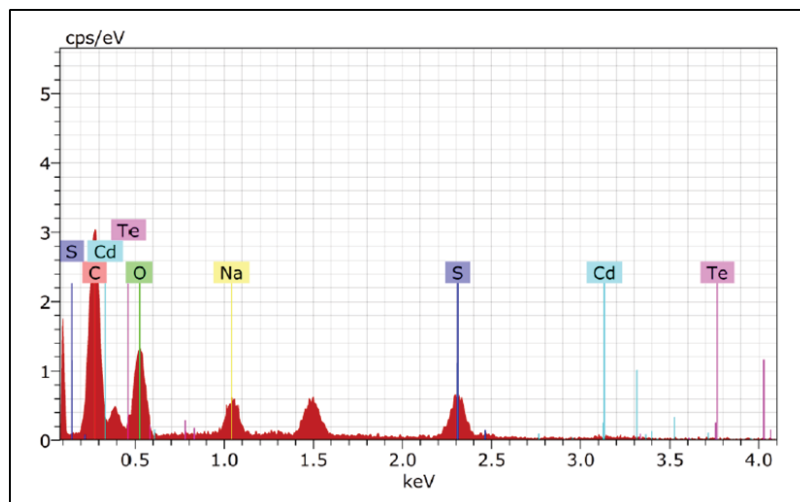


Fig. S6 Elemental analysis of MPA-CdTe@CdS QDs using energy dispersive X-ray spectroscopy (EDX) confirms the presence of Cd, Te, S, C, O elements

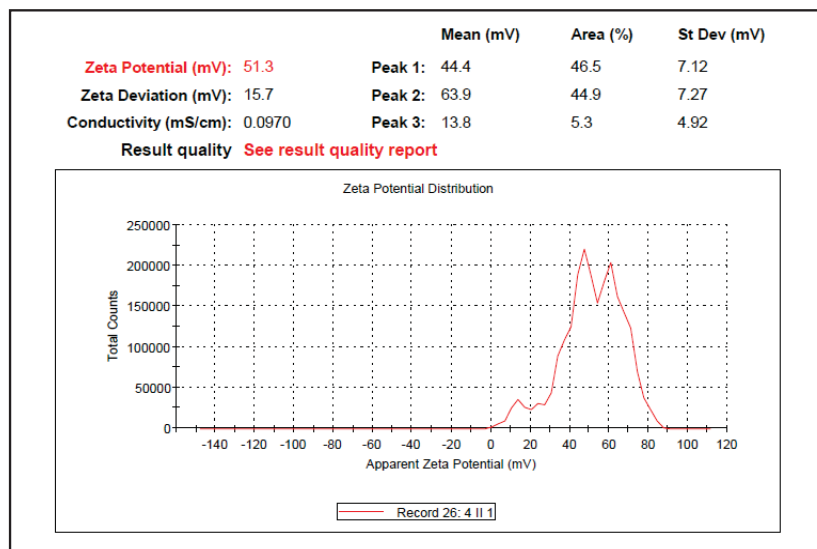


Fig. S7 Surface charge of Poly(HPMA-s-GPMA) determination by zeta potential

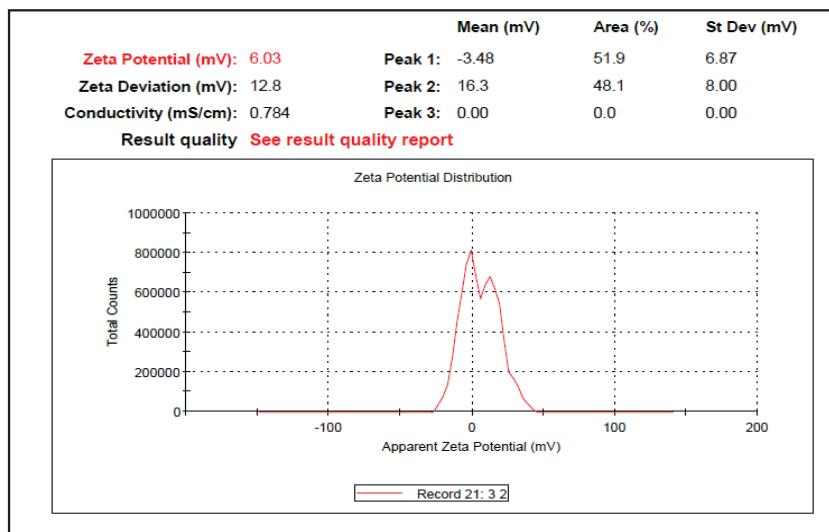


Fig. S8 Zeta potential of MPA-CdTe@CdS QDs-Poly(HPMA-s-GPMA) complex

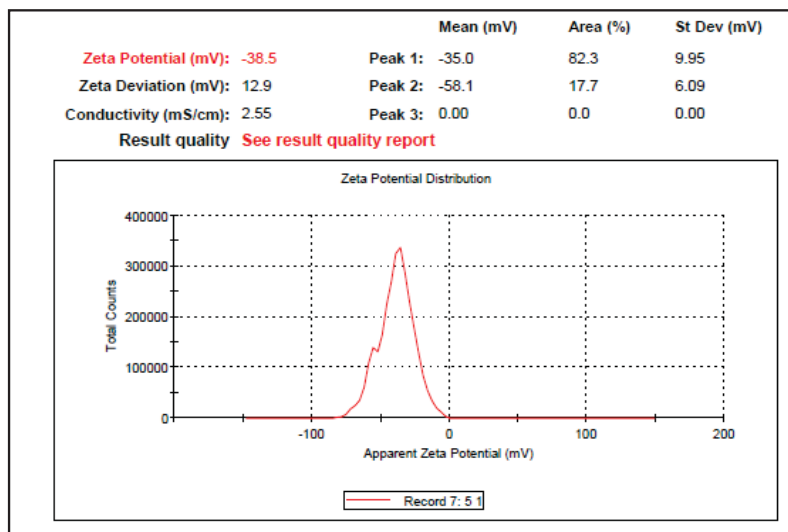


Fig. S9 Surface charge of arsenic aptamer determination by zeta potential

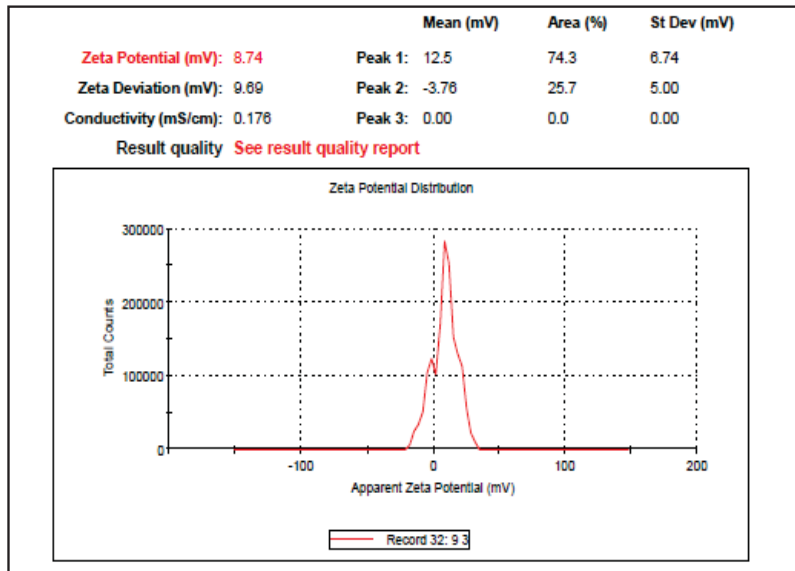


Fig. S10 Zeta potential of arsenic aptamer-Poly(HPMA-s-GPMA) complex

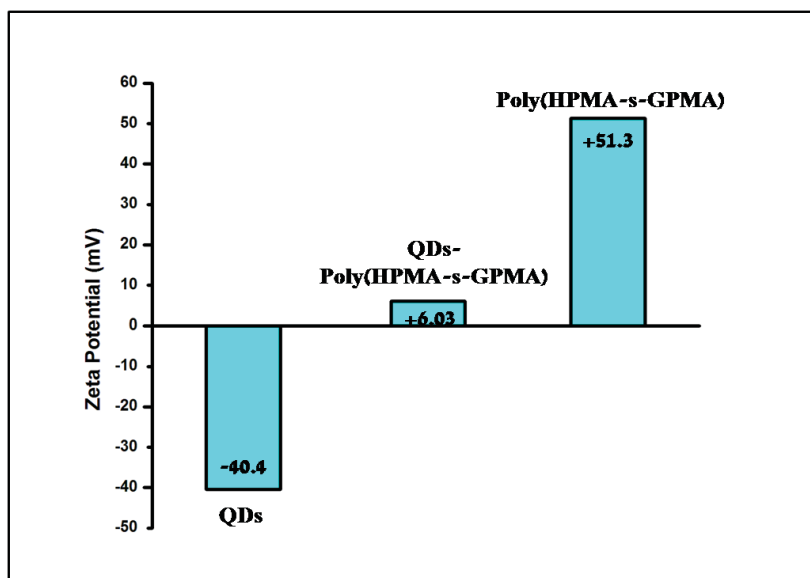


Fig. S11 Comparison of Zeta potential of QDs, Poly(HPMA-s-GPMA) and QDs- Poly(HPMA-s-GPMA) complex

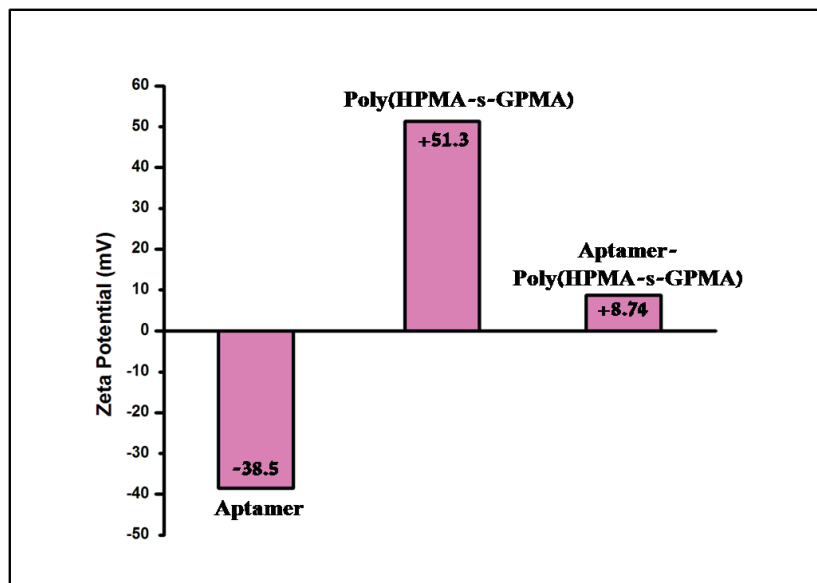


Fig. S12 Comparison of Zeta potential of Aptamer, Poly(HPMA-s-GPMA) and Aptamer- Poly(HPMA-s-GPMA) complex

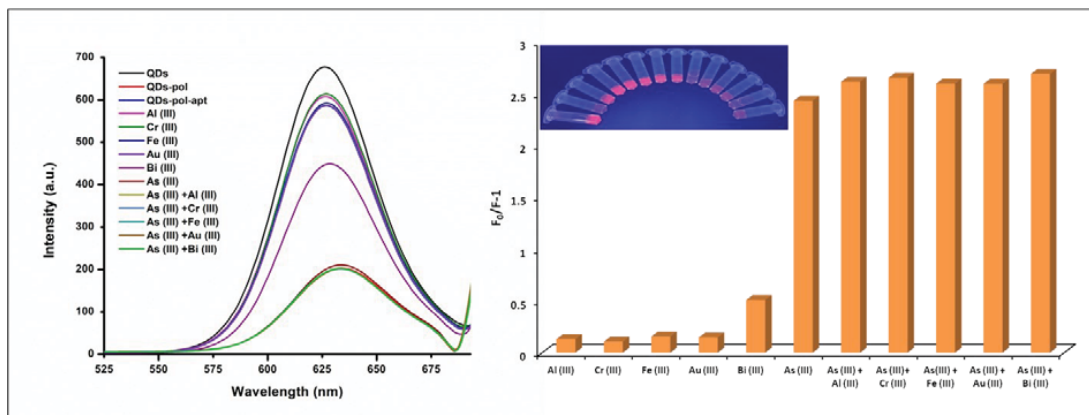


Fig. S13 Fluorescence response of the aptasensor towards different tri-valent metal ions: $1\mu\text{M}$ As^{3+} ions and $1000\mu\text{M}$ other metal ions. Poly(HPMA-*s*-GPMA) copolymer (0.06 mg mL^{-1}) and aptamer ($3\mu\text{M}$) concentrations were kept constant, where F_0 and F represent the fluorescence intensities in the absence and presence of As^{3+} ions.

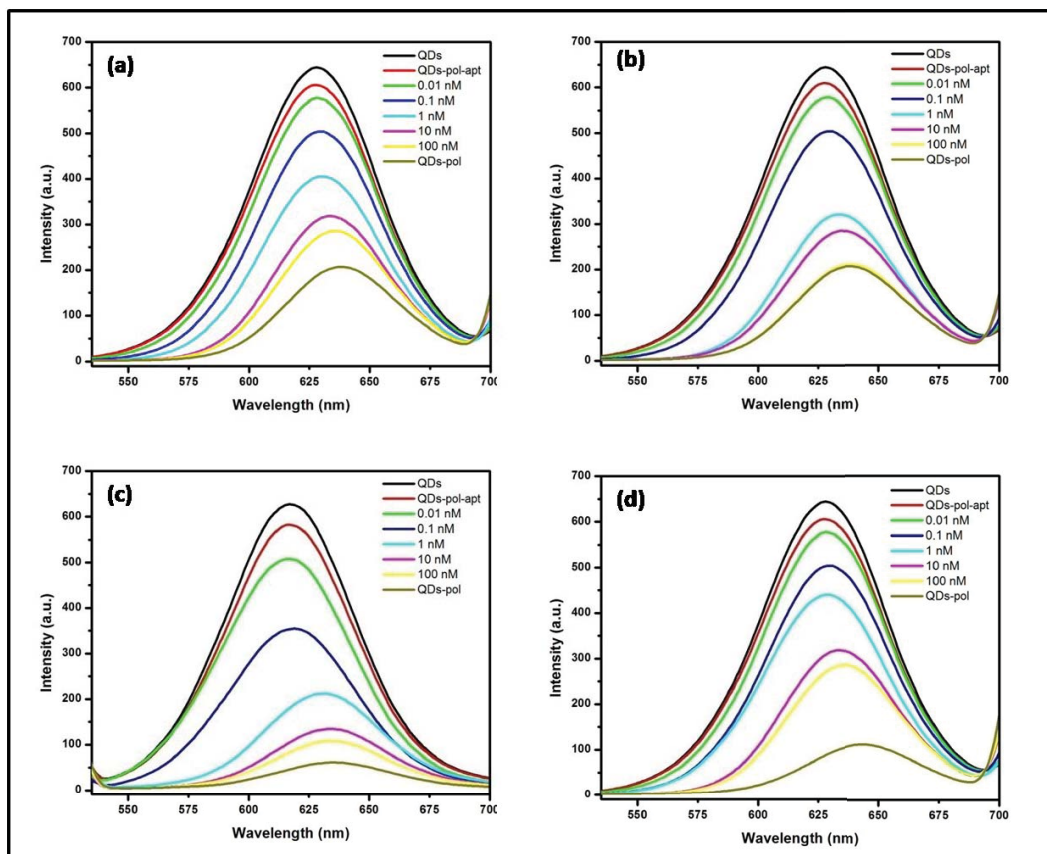


Fig. S14 Fluorescent spectra of QDs having different concentration of As^{3+} ions in mineral water (a), soil water(c), tap water (c) and apple juice (d) respectively.

Cal S1

Limit of Detection

$$\text{LOD} = 3\alpha/m$$

α = standard deviation

m = slope

$$y = mx + c$$

$$\text{LOD} = (3 \times 0.02215)/0.26604$$

$$= 0.24977$$

Y = A + B * X			
Parameter	Value	Error	
A	0.72542	0.00991	
B	0.26604	0.00701	
R	SD	N	P
0.99896	0.02215	5	<0.0001